The effect of ageing on the blood-brain barrier: The potential of nanoparticle drug delivery systems to target cerebrovascular changes

JESSICA BATES

A thesis submitted in partial fulfilment of the

requirements of Nottingham Trent University

for the degree of Doctor of Philosophy

This research programme was carried out

in collaboration with University of Nottingham Doctoral Training Programme

September 2024

Contents

Acknowledgements

Firstly, I would like to thank my supervisors, Dr Zahraa Al-Ahmady and Professor Claire Gibson, without who this project would not have been possible. It has been a pleasure to work with both of you, growing as a person and scientist over the years together and I wish you both the best. I also thank my supervisory support team, Dr Richard Hulse and Dr Craig Doig, for all their support over the years and letting me know I am on track.

I would like to thank the doctoral training programme and BBSRC for funding this PhD and providing invaluable opportunities for learning within a cohort system. I also thank the behavioural support facility at NTU, Andy, Joe, Lou, Gemma, and Adam for all your help with the *in vivo* work. For my imaging studies, Dr Graham Hickman, Dr Dominic Craske, Dr Rob Harris and Jim Hall were pivotal in my understanding of all microscope and MRI work, thank you.

My two lab groups; NTU (Asif and Satinder) and UoN (Melissa, Sakaorna, Gabe and Mitch) thank you for helping me through the project, you made my PhD journey better by being in it. My ISTeC friends; Jade, Lydia, Awais, Alice, Arnold, Nikky and Cristina, thank you for always being there through the tough times and being around for a coffee break- I could not have got through this without you. Special shout out to Rhianna, my DTP friend, who I could not have seen the last 4 years without.

To my friends, the Hunz, Fab five and Charlotte, the support you all gave me encouraging me to go on this journey will never be forgotten, neither will your abilities to make me smile even through the hardest times. To my family, I know this has not been the easiest journey, but I appreciate everything you have and continue to do for me. Science is not your thing but thank you for listening to me when I have needed you the most. Finally, to James, without you this would not have been possible you are my rock. You have made sacrifices for me to be able to do this PhD and I will never be able to repay you.

Abbreviations

ABCC9	ATP-Binding Cassette, Sub-Family C Member 9
AD	Alzheimer's Disease
AMT	Adsorptive-Mediated Transcytosis
ANOVA	Analysis Of Variance
APOE	Apolipoprotein E
AQP4	Aquapourin-4
ARRIVE	Animal Research: Reporting of *In Vivo* Experiments
ARHGAP25	Rho GTPase Activating Protein 25
ASL	Arterial Spin Labelling
ATP11B	ATPase Phospholipid Transporting 11B
AuNP	Silver Nanoparticles
Aβ	Amyloid Beta
BBB	Blood-Brain Barrier
BCA	Bicinchoninic Acid
BDNF	Brain-Derived Neurotrophic Factor
BEC	Brain Endothelial Cell
BM	Basement Membrane
BSF	Barrier Support Facility
CA1	Cornu Ammonis 1
CA3	Cornu Ammonis 2
CAPS	Cryopyrin-Associated Autoinflammatory Syndromes
CD31	Cluster Of Differentiation 31
CLP	Caecal Ligation and Puncture
CMT	Caveolae-Mediated Transcytosis
CNS	Central Nervous System
COVID	Coronavirus
CRTC1	CREB-Regulated Transcription Coactivator 1
CT	Computed Tomography
CX3CX1	CX3C Motif Chemokine Receptor 1
CXCL1	Chemokine (C-X-C Motif) Ligand 1
DAB	3, 3'-Diaminobenzidine
DCE-MRI	Dynamic Contrast-Enhanced Magnetic Resonance Imaging
dd H_20	Distilled Water
DII-LIP	DiI-Liposome
DLS	Dynamic Light Scattering
DP-PCASL	Diffusion Prepared Pseudo-Continuous Arterial Spin Labelling
DSPE	1, 2-Distearoyl-sn-glycero-3-phosphoethanolamine
EBD	Evans Blue Dye
EC	Endothelial Cell
ECM	Extra Cellular Matrix
EDTA	Ethylenediaminetetraacetic Acid
ELISA	Enzyme-Linked Immunosorbent Assay:
ESP8	Epidermal Growth Factor Receptor Kinase Substrate 8
FFPE	Formalin-Fixed Paraffin Embedded
FMR1	Fragile X Syndrome
GAG	Glycosaminoglycan
GBCA	Gadolinium Based Contrast Agent
GC	Glucocorticoid
GDNF	Glial Cell Line-Derived Neurotrophic Factor

GFAP	Glial Fibrillary Acidic Protein
GLUT-1	Glucose Transporter 1
H_20	Water
H_20_2	Hydrogen Peroxide
HA	Hyaluronan
HA-PLGA	Hyaluronic Acid-Conjugated Poly(Lactic-Co-Glycolic Acid)
HEPES	4-(2-Hydroxyethyl)-1-Piperazineethanesulfonic Acid
HIF-1α	Hypoxia Inducing Factor-1 Alpha
HIV	Human Immunodeficiency Virus
HSPC	Hydrogenated Soybean Phosphatidylcholine
IBA-1	Ionized Calcium-Binding Adaptor Molecule 1
ICAM-1	Intercellular Adhesion Molecule 1
ICV	Intracerebroventricular
IFIT3	Interferon-Induced Protein with Tetratricopeptide Repeats 3
IGG	Immunoglobulin G
IL	Interleukin
IL-1B	Interleukin-1 Beta
IL1-RA	Interleukin 1 Receptor Antagonist
IL1-RA-LIP	Interleukin-1 Receptor Antagonist Liposome
IP	Intraperitoneal
IPA	Ingenuity Pathway Analysis
iPSC	Induced Pluripotent Stem Cell
IV	Intravenous
IVIS	In Vivo Imaging System
LAMP2	Lysosome-Associated Membrane Glycoprotein 2
LDAM	Lipid Droplet Accumulating Microglia
LPS	Lipopolysaccharide
LTP	Long Term Potentiation
MAPK	Mitogen-Activated Protein Kinase
MHC-II	Major Histocompatibility Complex II
MMP	Matrix Metalloproteinase
MPIO	Microparticles Of Iron Oxide
MSF2DA	Major Facilitator Super Family Domain Containing 2a
MW	Molecular Weight
MYD88	Myeloid Differentiation Primary Response 88
NACL	Sodium Chloride
NAD	Nicotinamide Adenine Dinucleotide
NF-KB	Nuclear Factor Kappa-Light-Chain-Enhancer of Activated B Cells
NG2	Nerve/Glial-Antigen 2
NLRP3	NLR Family Pyrin Domain Containing 3
NOL	Novel Object Location
NOR	Novel Object Recognition
NSAIDS	Nonsteroidal Anti-Inflammatory Drugs
NVU	Neurovascular Unit
OCT	Optical Coherence Tomography
OCT	Optimal Cutting Temperature Compound
OPC	Oligodendrocyte Precursor Cells
PAMAM	Poly(Amidoamine)
PBS	Phosphate Buffered Saline

PCI	Peritoneal Contamination and Infection Model
PDGFRB	Platelet-Derived Growth Factor Receptor Beta
PECAM-1	Platelet Endothelial Cell Adhesion Molecule
PEG	Polyethylene Glycol
PET	Positron Emission Tomography
P-gP	P-Glycoprotein 1
PMI	Post-Mortem Interval
QPCR	Quantitative Polymerase Chain Reaction
RAB6A	Ras-Related Protein Rab-6A
RGB	Red Green Blue
RIPA	Radioimmunoprecipitation Assay
RMT	Receptor Mediated Transcytosis
RNA	Ribonucleic Acid
ROS	Reactive Oxygen Species
RPM	Revolutions Per Minute
RT	Room Temperature
S100A9	S100 Calcium-Binding Protein A9
S100β	S100 calcium-binding protein B
SEM	Standard Error of Mean
SAMP8	Senescence Accelerated Mice 8
SERPIN3N	Serine Protease Inhibitor 3
SIRT1	Sirtuin 1
SLC	Solute Carriers
SMAD3	Mothers Against Decapentaplegic Homolog 3
SPECT	Single-Photon Emission Computed Tomography
STAT1	Signal Transducer and Activator of Transcription 1
STAT3	Signal Transducer and Activator of Transcription 3
SWATH	Sequential Window Acquisition Of All Theoretical Fragment Ion Spectra
TBC1S10A	TBC1 Domain Family Member 10A
TEER	Transendothelial Electrical Resistance
TEM	Transmission Electron Microscopy
TGFB	Transforming Growth Factor Beta
TJ	Tight Junction
TLR4	Toll-Like Receptor 4
TMEM	Transmembrane Proteins
TNF-α	Tumor Necrosis Factor Alpha
TREM2	Triggering Receptor Expressed on Myeloid Cells 2
TRIF	TIR-Domain-Containing Adapter-Inducing Interferon-B
USA	United States of America
USPIO	Ultra Small Particles of Iron Oxide
VEGF	Vascular Endothelial Growth Factor
Zo-1	Zona Occludins-1

List of figures

List of tables

List of appendices

List of publications and abstracts

Allen SP, Seehra RS, Heath PR, Hall BPC, **Bates J**, Garwood CJ, Matuszyk MM, Wharton SB, Simpson JE. Transcriptomic Analysis of Human Astrocytes In Vitro Reveals Hypoxia-Induced Mitochondrial Dysfunction, Modulation of Metabolism, and Dysregulation of the Immune Response. *Int J Mol Sci.* 2020 Oct 28;21(21):8028. doi: 10.3390/ijms21218028. PMID: 33126586; PMCID: PMC7672558.

Al-Ahmady ZS, Dickie BR, Aldred I, Jasim DA, Barrington J, Haley M, Lemarchand E, Coutts G, Kaur S, **Bates J**, Curran S, Goddard R, Walker M, Parry-Jones A, Kostarelos K, Allan SM. Selective brain entry of lipid nanoparticles in haemorrhagic stroke is linked to biphasic blood-brain barrier disruption. *Theranostics*. 2022 May 26;12(10):4477-4497. doi: 10.7150/thno.72167. PMID: 35832077; PMCID: PMC9254235.

Abstract

Within physiological ageing, recent evidence has shown that alterations to blood-brain barrier (BBB) permeability are potentially caused by a shift towards non-selective entry of systemic molecules into the brain via transcytosis. The ability to exploit this to deliver therapeutic molecules to target age-related changes of the BBB via lipid nanoparticles is an area of particular interest.

In vivo C57BL/6 murine models were utlisied with ageing females ranging from 3-22 months in comparison to males at 3- and 18-months. Systemic inflammation was induced via lipopolysaccharide (LPS) in a separate cohort of 3- and 18-month females to investigate age-related neuroinflammatory responses. Mice were injected intravenously with fluorescently labelled lipid nanoparticles (DiI-lip) and other permeability markers such as albumin and dextran. Brain infiltration was then tracked post-injection using optical imaging and histological analysis, complemented with behavioural cognitive function tests. Neurovascular unit (NVU) components and pro-inflammatory cytokines were also assessed for changes during ageing to identify possible therapeutic targets. Anti-inflammatory interleukin-1 receptor antagonist (Il1-ra) was conjugated to liposomes to determine if inflammatory changes in physiological ageing were reduced.

Findings of the studies indicated that DiI-lip infiltration increased during ageing independent of sex but changes to NVU and transport mechanisms were regionally heterogenous. LPS-induced neuroinflammation did not cause significant changes to DiI-lip infiltration or NVU components but did increase adhesion molecule and cytokine expression in ageing mice. Proteomic results uncovered multiple protein expression changes when comparing aged mice to LPS mice. Reduction of adhesion molecules and microglial activation were found when aged mice were exposed to Il1-ra liposomes, but no changes were observed in BBB permeability or astrocytic activation.

Overall, this work highlights the potential of liposomes to deliver therapeutics through the aged BBB, but further work needs to be completed to understand the underlying transport mechanisms and translatability to the human environment.

1. Introduction

1.1. General Introduction

Increased understanding of disease and developments in medical treatments over the last century have extended the human lifespan, especially in developed countries with the average life expectancy in the USA increasing from 47 to 78 years between 1900-2010 (Crimmins, 2015; Partridge et al., 2018). Whilst increased lifespan has significant positive impacts upon society the increasing growth of the older population impacts on incidence of age-related diseases. Age is one of the main risk factors for dementia and other neurodegenerative disorders such as stroke and Parkinson's disease and further research has correlated age-related pathological phenotypes with disease states (Guerreiro & Bras, 2015). Case incidences of neurodegenerative disorders are rapidly increasing for example, meta-analysis data suggested that over 130 million people will have Alzheimer's disease (AD), the most common dementia, by 2050, up from 46.8 million in 2015 (Ford et al., 2018).

Historically, research into neurodegeneration and ageing was neuro-centric and tended to focus on pathological changes in neuronal cells, the fundamental cell type of the brain. However, the brain is a complex organ both structurally and functionally, consisting of a plethora of cell types forming complicated connections to undertake both simultaneous and complex tasks. Ageing is multifaceted but can be briefly described as cognitive decline accompanied by structural and physiological changes resulting from numerous contributors such as environment and genetics (Palmer & Ousman, 2018). However, research studies have identified several key structural, molecular, and morphological changes which may indicate brain ageing such as loss of brain volume, changes to vascular morphology and loss of myelin sheathing (Abdelkarim et al., 2019; Peters, 2006). One of the major macrostructures within the brain is the blood-brain barrier (BBB) which is multifunctional; controlling the movement of molecules to the parenchyma as well as playing key roles in homeostasis (Knox et al., 2022). Figure 1-1 summarises the potential changes to the BBB and associated cells during physiological ageing which will be discussed in depth throughout this body of work.

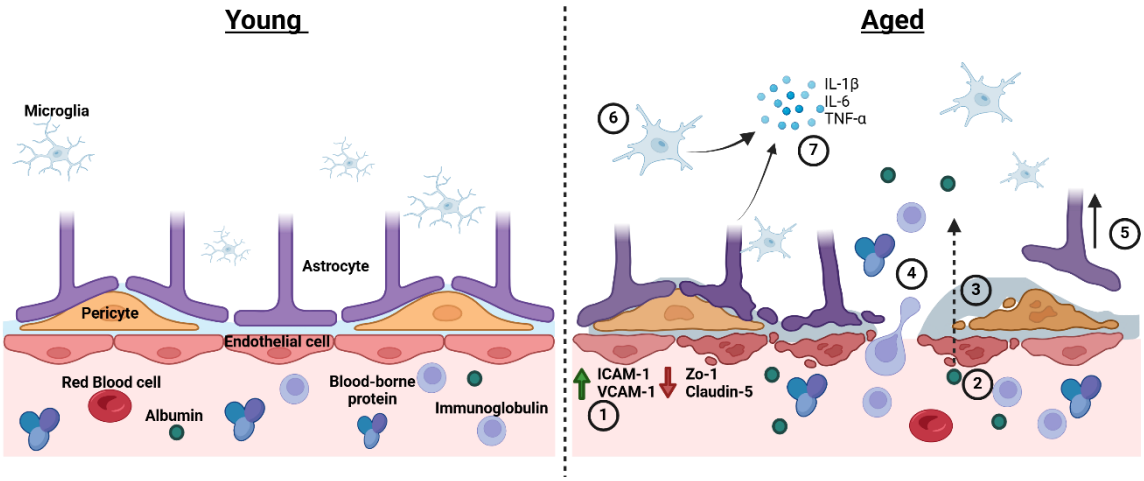

Figure 1-1: Comparison of young and aged showing potential blood-brain barrier and associated cells changes. (1) Increased vascular expression of adhesion molecules and decreased tight junction protein expression. (2) Increased caveolae-mediate transcytosis transporting molecules into the brain parenchyma. (3) Pericyte degermation and loss (4) Extravasation of blood-borne molecules such as leukocytes, immunoglobulins, and albumin. (5) Activation of astrocytes and detachment of end-feet from the vasculature. (6) Activation of microglial (7) Increased microglial and astrocytic production of pro-inflammatory cytokines. Adapted from (Knox et al., 2022), created via Biorender.com

1.2. BBB functionality

This dynamic, multicellular barrier separates the central nervous system (CNS) from the peripheral circulation and protects structures against potentially harmful substances via tight regulation and control of molecular transport. Functionality can be subdivided into groups such as maintaining homeostasis, regulating neurotransmitter levels, reducing the number of large molecules (>400 Da) entering the brain and protecting from toxins, culminating in maintenance of the relative immune privilege of the brain (Kadry et al., 2020; Muldoon et al., 2013). Previously it was believed this immune state to be absolute and that any change to BBB permeability would result in pathologies such as AD occurring. However, research has migrated towards a 'relative' immune state, based on the ability of the BBB to allow movement both in and out of the brain, dependant on molecule type under normal physiological functioning (Erickson & Banks, 2019). Multiple cellular components form and regulate the BBB, termed the neurovascular unit (NVU), and work in tandem to establish and maintain BBB integrity including endothelial cells, astrocytes and pericytes with support from microglia and neurons (Duncombe et al., 2017).

1.3. Transport and Cellular components of BBB.

1.3.1. Transport mechanisms

Paracellular transport through the BBB is restricted due to the presence of tight junctions (TJ) ensuring high selectivity over the movement of substances both into and from the brain parenchyma. However, multiple examples of transport mechanisms exist to allow the movement of vital molecules including simple diffusion, facilitated diffusion, efflux transporters and transcytosis which allow a range of molecules to pass the BBB varying from small lipids to larger molecules, visualised in figure 1-2.

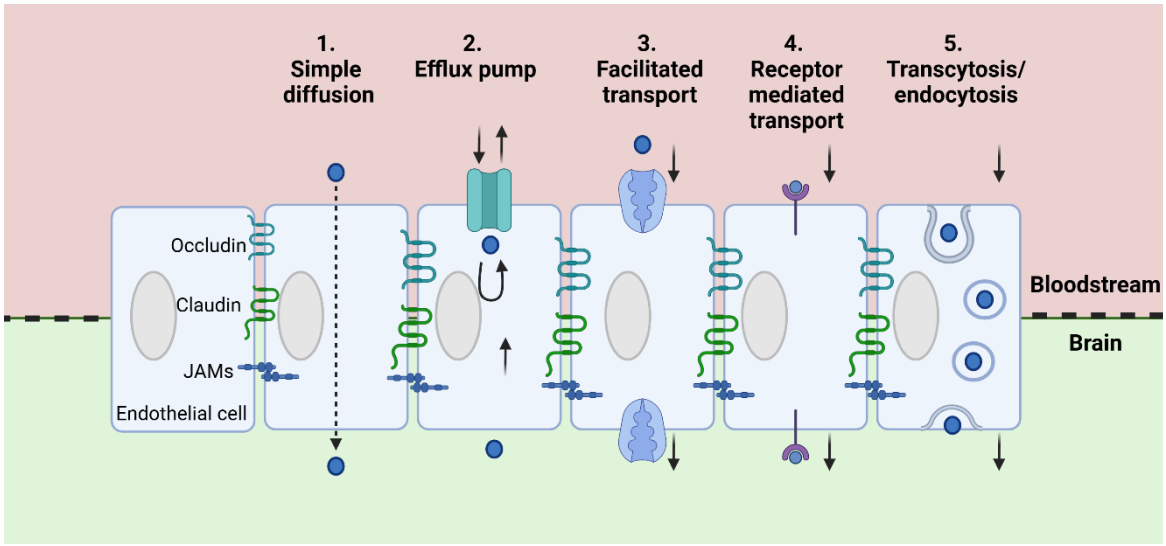

Figure 1-2: Diagrammatic representation of different blood-brain barrier transport mechanisms. (1) Simple diffusion of small lipid soluble molecules (2) Efflux pumps which uses ATP hydrolysis to move substances across the barrier (3) Facilitated transport (4) Receptor-mediated transport of molecules such as insulin (5) transcytosis and endocytosis which can transport plasma proteins such as albumin and positively charged molecules. JAM= junctional adhesion molecule. Adapted from (Al-Ahmady, 2018), created via Biorender.com.

1.3.2. Molecular transport through BBB

Glucose is essential for energy metabolism within cellular systems of the brain and maintenance of glucose transport is essential to prevent energy depletion and cell death. Glucose transport 1, a uniporter protein, (Glut-1) is the main transporter and is located within the BBB as well as neurons and astrocytes (Erickson & Banks, 2019). Some studies have identified a reduction in glucose transport and GLUT-1 expression during ageing, correlating

with BBB dysfunction (Bonte et al., 2017; Jiang et al., 2013; Mooradian et al., 1991). However, more research is required to isolate cell-specific loss of Glut-1 in ageing as some studies highlight that neuronal Glut-1 is lost at a higher rate than BBB Glut-1 (Ding et al., 2013).

The efflux protein, P-glycoprotein (P-gp) has been highlighted as a molecule affected by ageing in human and murine models with decreases in expression (Bors et al., 2018; Van Assema et al., 2012). This is important not just to ageing studies but also pathological research as the loss of P-gp has been linked to an inability to clear toxic amyloid beta (Aβ) from the brain, which contributes to further exacerbation of Alzheimer's disease (Storck et al., 2018). Human studies have further noted that there are different expression level patterns in males and females, with males more susceptible to changes during ageing, emphasising the need to be comprehensive in cohort selection with a mixed-gender cohort preferable (Van Assema et al., 2012).

Recently, research groups have expanded their techniques to study BBB leakage from the typical tracers, serum proteins and radioisotopes to the whole plasma proteome. Briefly, the plasma proteome can be defined as all the proteins which exist in blood samples and can be used to extract functional data regarding functional aspects of proteins through techniques such as mass spectrometry characterisation and protein microarray analysis (Anderson & Anderson, 2002). For example, Yang et al., 2020, demonstrated that ageing caused a shift in transport mechanism from specific ligand or receptor-mediated transport to non-specific caveolar transcytosis. The relevance of this is not yet fully understood but alludes to a more complicated transport change than previously anticipated during ageing which may explain how BBB leakage occurs on a molecular level. Further studies must be conducted to elucidate the impact of this on the ageing BBB and whether it is detrimental to normal functionality.

1.3.3. Endothelial cells

Brain endothelial cells (BEC) form the central cellular component of the BBB comprising approximately 85% of the BBB structure via a close-contact monolayer lining blood vessels (Montagne et al., 2017). Multiple studies have documented morphological changes in BEC's

during ageing including decreased cell coverage, thickening of the basement membrane and micro vessel thinning (Bhat, 2015; Brown & Thore, 2011; Hunter et al., 2012). Other studies have found that during physiological ageing, proliferation, and migration of BEC's is compromised, affecting their ability to produce a stable BBB (Murugesan et al., 2012).

BECs are held together tightly by TJ and adheren junction proteins. Numerous studies have shown changes to junctional proteins claudin-5 and Zona-Occuldins-1 (Zo-1) during both pathological and physiological ageing and demonstrate a direct impact on BBB permeability and TJ maintenance during (Lv et al., 2010; Mooradian et al., 2003; Park et al., 2014). For example, Elahy et al., 2015, investigated the effect of physiological ageing on the BBB via comparison of 3 month and 24-month-old mice by looking at links between BBB dysfunction and peripheral and neurological inflammation. This study correlated the impact of peripheral inflammation, a common co-morbidity in ageing, to BBB dysfunction through increases in pro-inflammatory tumour necrosis factor-alpha (TNF-α) which had been shown to affected TJ proteins such as occudin-1 and Zo-1 to suppress TJ activity, increasing BBB permeability. Human studies further confirmed age-dependant decreases in Zo-1 expression and hypothesised that this may be a driving factor in increased BBB leakage (Goodall et al., 2018). However, contradiction exists within the field (table 1-1) with both human and mouse studies also demonstrating no changes to TJ proteins in ageing, indicating that further research should be undertaken (Bell et al., 2010; Cummins et al., 2024; Tachibana et al., 2024).

1.3.4. Extracellular matrix and associated structures

The extracellular matrix (ECM) is a cellular scaffold which constitutes up to 40% of the overall brain volume, highlighting its importance in brain functionality (Soles et al., 2023).
Functionally, the ECM works as a physical part of the BBB, preventing the movement of soluble molecules as well as having roles in synapse growth and maintenance (Lam et al., 2019). Multiple different structures within the brain vasculature are associated with the ECM including the luminal glycocalyx and abluminal basement membrane (Reed et al, 2019).

Table 1-1: Human and mouse studies of tight junction protein changes in ageing.

Study	Tight junction protein	Species	Age	Effect
(Goodall et al., 2018)	Zo-1	Mouse	18-24 months	Decrease
(Elahy et al., 2015)	Occludin Zo-1	Mouse	24-months	Decrease
(Stamatovic et al., 2019)	Claudin 5 Zo-1	Mouse	22-months	Decrease
(Stamatovic et al., 2019)	Claudin 5 Zo-1	Human	75 years+	Decrease
(Mooradian et al., 2003)	Occludin	Rat	24-months	Decrease
(Tachibana et al., 2024)	Claudin-5	Human	70 years+	No change
(Bors et al., 2018)	TJ	Rat	14-16 months	Decrease
(Cummins et al., 2024)	Zo-1 Claudin-5 Occludin	Mouse	24-months	Decrease No change No change
(Bell et al., 2010)	Zo-1 Claudin-5 Occludin	Mouse	14-16 months	Decrease No change Decrease

1.3.4.1. Glycocalyx

The glycocalyx is a hairy layer of sugars located on the luminal side of the barrier and is thought to be the initial defence against movement through the BBB (Banks et al., 2021). Studies have shown that the glycocalyx prevents the infiltration of large molecules through the barrier whilst the EC's and extravascular components decrease permeability to smaller molecules (Kutuzov et al., 2018). The main functionality of the glycocalyx is to regulate blood flow and maintain homeostasis but has also been shown to have a role in the control of shear stress and as a protective mechanism against oxidative stress (Machin et al., 2018; Mason McClatchey et al., 2016). Shear stress is a tangenital force created via the flow of blood through the vessels and is vital for the functioning BBB, affecting multiple transport pathways and transport molecule properties, such as Zo-1, and therefore it crucial to control this force (Tarbell, 2010).

The glycocalyx is comprised of multiple proteoglycans, glycoproteins and plasma proteins as well as 5 types of glycosaminoglycans (GAG) (Reed et al., 2019). The most abundant of these are Heparan Sulfates but one GAG of particular relevance to ageing is Hyaluronan (HA) which is believed to be crucial in regulating the permeability of the glycocalyx and also aids in ECM

structure stabilisation and cell-adhesion interactions (Reed et al., 2019). However, this GAG, as well as the glycocalyx overall, have been overlooked historically within vascular research. This was due to loss during standard tissue processing techniques and inability to isolate the structure from the abluminal side with past data predominately being extrapolated from the overall parenchyma (Henry & Duling, 1999; Reed et al., 2019). Limited studies have investigated the glycocalyx in ageing, with one immunohistochemical study noting that HA accumulation in cortical regions occurred in the mouse brain but did not correlate this further with typical BBB dysfunction markers such as increased permability (Reed et al., 2018). Compromised BBB glycocalyx structure and function have been shown in lacunar stroke via dark field imaging (Martens et al., 2013). Electron microscopy to measure glycocalyx thickness and immunosorbent assays to determine GAG concentrations from rat plasma determined that BBB dysfucntion occurs due to glycocalyx degredation after cardiac arrest in rats (Zhu et al., 2018). Glycocalyx damage has also been correlated with subarachnoid haemorrhage induced ischaemia via immunosorbent assays of glycocalyx biomarkers (Bell et al., 2017). More studies need to be undertaken specifically looking at BBB damage and the glycocalyx to determine any significant effect that glycocalyx changes may possess.

HA has demonstrated an age-related increased expression, but this may be location-dependent as it seems to occur more in the grey matter than in other areas (Cargill et al., 2012; Lindwall et al., 2013). Interestingly, Howell & Gottschall, 2012, noted that following CNS injury increased expression of HA and other GAG correlated with glial scarring, indicating a role of glial cells with glycocalyx changes. This may be of relevance to physiological ageing which also can display glial reactivity and morphological changes which impact the integrity of BBB functions (Salas et al., 2020). Another avenue of interest is the effect of the glycocalyx on BBB transport mechanisms, as studies have shown links to both transcytosis and endocytosis, through specific GAG's acting as receptors (Joshi & Zuhorn, 2021; Leite et al., 2020). This area needs further investigation to elucidate relevance to ageing and also mechanisms of action that could be important when considering the shift to transcytosis in ageing (Yang et al., 2020).

The glycocalyx also has an anti-inflammatory functionality as it prevents the BEC signalling to pro-inflammatory adhesion molcules; intercellular adhesion molecule (ICAM-1) and vascular cell adhesion molecule (VCAM-1) (Schnoor et al., 2015). Conversley, increased thickness of the glycocalyx with ageing has been demonstrated in mice and humans and reported to correlate with the increased ability of red blood cells to penetrate the structure (Machin et al., 2018). However, to date, this has only been demosntrated in peripheral pulmonary and cardiac vasculature so relevance to the BBB needs determining. The glycocalyx coverage of brain EC's is significantly increased compared to peripheral structures and increased thickness would suggest lower adhesion molcule effects contradicting BBB specific findings (Ando et al., 2018).

1.3.4.2. Basement membrane

The basement membrane (BM) is also a crucial part of the BBB and is a filter meshwork surrounding the EC's and pericytes and is attached to the astrocytic end-feet via adhesion molecules (Morris et al., 2014). This structure, consisting of molecules such as collagen IV, fibronectin, laminin and some GAG's, is key for physically supporting the overall BBB structure and is also important for cell adhesion (Reed et al., 2019).

There are studies of the effect of ageing on the BM but in 30 month-old mice compared to 6 month-old mice, it has been found to increase in thickness which may be exacerbated by lipid droplets (Ceafalan et al., 2019). This study hypothesised that the inclusion of lipid droplets indicates an imbalance in lipid metabolism, which may be involved in neurodegeneration via impact on abnormal protein production. Multiple studies have investigated BM changes in human ageing and again identified increased thickness as well as increased stiffness which may be related to an accumulation of Collagen IV and laminins (Candiello et al., 2010; Uspenskaia et al., 2004)

1.3.6. Astrocytes

Astrocytes are the most abundant glial cell within the parenchyma and were considered as passive, functioning to support neuronal cells (Sadick & Liddelow, 2019). However, research

has discovered a plethora of functions such as maintenance of BBB homeostasis, the tripartite synapse and permeability of BBB (Garwood et al., 2017). Astrocytes are a heterogeneous cell type consisting of morphologically and functionally diverse sub-groups; including protoplasmic astrocytes in the grey matter, fibrous astrocytes in the white matter and interlaminar astrocytes which differ in function based on location (Garwood et al., 2017). Thus, when studying the cell type, consideration must be made that any expression changes in one region of the brain may not be consistent throughout the parenchyma (Rodríguez et al., 2014).

Astrocytic end-feet interact with BEC's contributing to the development, maintenance and regulation of the BBB (Palmer & Ousman, 2018). Under normal physiological conditions, astrocytes secrete the glycoprotein Sonic Hedgehog (Shh) which is then received by BEC's to aid BBB formation by upregulating TJ proteins from the development stage onwards (Xing et al., 2020). This is vital to maintaining BBB integrity as a lack of Shh has been shown to increase BBB permeability and compromise cell phenotypes, although no studies have currently found a link between this and physiological ageing (Alvarez et al., 2011). Ion and water homeostasis within the BBB are also controlled by perivascular astrocyte channels Kir4.1 and aquaporin-4 (Aqp4) (Abbott et al., 2006). Preliminary studies have noted that in an AD murine model, Aqp4 expression increased in ageing independent of pathology in the Cornu Ammonis (CA1) region which has been hypothesised to compensate for functional changes in astrocytes during the ageing process which agrees with findings from a human post-mortem cohort (Bronzuoli et al., 2019; Hoozemans et al., 2011). Furthermore, a study found a loss of Aqp4 perivascular localisation in an ageing human cohort, irrespective of pathology, which they hypothesised may result in brain vulnerability to neurodegeneration (Zeppenfeld et al., 2017).

Astrocytes play a role in regulating leukocyte infiltration into the brain, as astrocytic cytokines control key molecules such as VCAM-1 (Lécuyer et al., 2016). Secretory factors, such as glial-derived neurotrophic factor (GDNF) have been shown to modulate functionality of BBB via increased expression of claudin-5 and subsequently increasing the trans-endothelial electrical resistance (TEER) of the barrier (Igarashi et al., 1999). Astrocytes also have

significant vascular functions in neurovascular coupling (mediating communication between BEC's and neurons) and the regulation of blood flow, via changes in intracellular Ca^{2+} causing the release of vasoactive substances (Goodall et al., 2018).

Recently, more studies have been published specifically investigating physiological ageing and astrocytic function at the BBB. Evidence shows that expression of Glial Fibriallry Acidic Protein (GFAP) increases in ageing correlating with increased BBB permeability in both humans (Goodall et al., 2018; Verkerke et al., 2021) and rodents (Janota et al., 2015; Rodríguez et al., 2014; Verkerke et al., 2021). Changes to astrocytic signalling of transforming growth factor-Beta (TGFβ) may also occur during ageing which has been identified as a positive feedback pathway, increasing BBB permeability and infiltration of large molecules, such as albumin into the parenchyma (Verkerke et al., 2021). However, the highly heterogeneous population and different expression profiles of astrocytes make a comparison between studies difficult unless investigating the same brain architecture coupled with similar techniques/markers. Rodríguez et al., 2014, demonstrated this by investigating different astrocyte markers; GFAP, S100 calcium-binding protein B (S100β) and glutamate synthase in 3 brain regions, and found different patterns of expression in age with each combination. This has resulted in some investigations finding no significant alteration of the BBB due to astrocytes in the context of ageing (Janota et al., 2015; Mackic et al., 2002).

1.3.7. Pericytes

Pericytes are small mural cells intricately linked with the BBB and are the third component of the NVU, associated with all stages of BBB development, from embryogenesis and through ageing (Bennett & Kim, 2021). Historically, these cells were unrepresented within the literature and have only recently emerged as a key player in the NVU with implications in both healthy and diseased brains. Within the healthy brain vasculature, pericytes have multiple roles such as mediating the immune response through the release of cytokines such as TNF-α and controlling cerebral blood flow, through the expression of contractile proteins such as α-smooth muscle actin (Brown et al., 2019; Pieper et al., 2014). Interestingly, pericytes have also

been shown to have pluripotent ability and under the correct circumstances, can be transformed into neuronal and vascular cell types (Nakagomi et al., 2015; Nakata et al., 2017). This ability may have far-reaching consequences in NVU research, especially in *in vitro* BBB modelling where multicellular systems, including pericytes, are required to attempt to physiologically recreate the BBB environment.

Within the BBB system, pericytes possess multiple functions that aid in the maintenance of barrier integrity and functionality and form connections with BEC's via lock and socket junctions (Bennett & Kim, 2021). Shimizu et al., 2012 demonstrated pericytes ability to maintain the BBB integrity and increase TEER by releasing factors such as GDNF to increase the expression of existing TJ proteins and impact overall TJ number (Armulik et al., 2010). Further studies have shown the plethora of roles pericytes perform including toxin clearance, managing basal lamina protein levels, and also preventing unwanted leukocyte infiltration (Bennett & Kim, 2021; Daneman, Zhou, Kebede, et al., 2010; Winkler et al., 2011). Pericyte-astrocyte interactions are also key within the NVU in order to maintain functionality and this involves signalling which allows for polarisation of both the astrocytic end-feet and in more detail, AQP4, indicating a key role for pericytes in maintaining homeostasis of the BBB (Armulik et al., 2010; Gundersen et al., 2014).

Age-dependant changes are documented throughout the literature such as ultrastructural alterations, including the appearance of lipofuscin inclusions and increased mitochondria as well as pericyte loss from the BBB (Bennett & Kim, 2021; Hughes et al., 2006; Peters et al., 1991). The loss of pericytes has been shown in studies utilising genetic knockdown of platelet-derived growth factor receptor-β (PDGFRβ) signalling, which resulted in increased BBB permeability to serum proteins and a reduction in microcirculation (Bell et al., 2010; Nikolakopoulou et al., 2017). These findings preceded any inflammation or neurodegeneration, indicating that this is pericyte-specific as opposed to a consequence of other pathologies. This finding has been replicated in both rodent and human studies which have found an age-dependent loss of pericytes resulting in BBB dysfunction and also effecting

the transport mechanisms within the BBB (Daneman, Zhou, Kebede, et al., 2010; Erdö et al., 2017; Yang et al., 2020). Other studies have partially agreed with this result, such as Montagne et al., 2015, who observed that age-related pericyte loss in human subjects was seen in the hippocampus, hypothesising that this is the initial brain region to be affected by ageing. Other studies did not find pericyte loss but instead a detachment and migration of pericytes away from BEC's, again resulting in BBB dysfunction and permeability (Hughes et al., 2006). However, alternative studies have observed no change in pericyte number or coverage during ageing (Bors et al., 2018; Goodall et al., 2018; Ximerakis et al., 2019) and one study noted increased pericyte number through ageing (Peinado et al., 1998). Relevance of these historical findings may be diminished as it relied upon ultrastructural identification of pericytes instead of immunohistochemical or protein analysis, potentially leading to false positive or negative pericytic identification. Furthermore, the study focused exclusively on the parietal cortex which does not encapsulate age-vulnerable regions such as the hippocampus and frontal cortex.

Regional heterogeneity, in terms of brain and vasculature location may contribute to the variation in results, with some areas appearing to have increased vulnerability, such as the hippocampus, to age then others (Brown et al., 2019; Montagne et al., 2015; Peinado et al., 1998). Another consideration is sample size, as some studies have low participant numbers, especially in human studies, so expansion of groups may conclude with different results (Goodall et al., 2018).

Recently, another hypothesis has been postulated regarding age-related pericyte shifting to a hypertrophic PDGRFβ+ predominant phenotype change, correlating with reductions in claudin-5, TJ breakdown and increased BBB permeability (Bohannon et al., 2020). This is a similar theory to the astrocytic and microglial activation changes and may be more relevant to physiological ageing then complete pericyte loss.

1.4. BBB dysfunction and disruption

BBB dysfunction and disruption has been characterised by the infiltration of identifiable large molecules into the parenchyma, which ordinarily would not be able to pass (Erickson et al., 2020). These are markers such as immunoglobulin G (IgG), fibrinogen and albumin as well as tracers such as Evans blue dye (EBD), sodium fluorescein and dextran (Ahishali & Kaya, 2020). Increased infiltration of such molecules through the BBB into the brain have been shown not only to be valuable as markers of dysfunctional permeability but also directly contributing to an increase in molecules which can cause pathology hallmarking neurodegeneration (Petersen et al., 2018). For example, accumulations of fibrinogen have been known to form fibrin clots which have been linked to AD pathology (Paul et al., 2007). Studies have further suggested that BBB dysfunction could possibly be linked to cognitive decline in an age-dependant manner, further highlighting the importance of understanding BBB changes in physiological ageing.(Montagne et al., 2015; Verheggen et al, et al., 2020). Most studies have only utilised molecules as markers of BBB disruption, not progressing further into the mechanistic properties behind this shift to a dysfunctional state. Limited studies have identified possible causative mechanisms of infiltration such as the loss of Sirtuin 1 (Sirt1) which may contribute to tight junction disassembly or via a change in transport mechanisms towards caveolar transcytosis (Stamatovic et al., 2019; Yang et al., 2020). Transcytosis is one of numerous intracellular transport mechanisms in the BBB and can utilise 3 different endocytic vesicles to mediate transport; clathrin-coated pits, the type involved in most normal receptor-mediated transcytosis (RMT), macropinocytotic vesicles and caveolar (Mayor & Pagano, 2007; Pulgar, 2019).

Regarding physiological ageing, there is conflicting evidence which exists regarding the occurrence of BBB leakage and questioning the correlation between BBB disruption and dysfunction of the NVU. Numerous studies have noted a significant correlation between age and parenchymal infiltration in mice (Elahy et al., 2015; Stamatovic et al., 2019), rats (Bors et al., 2018; Salahuddin et al., 1988) and humans (Stamatovic et al., 2019). Alternatively, other

studies have found no age-dependant leakage in both murine and rat models (Banks et al., 2000; Stewart et al., 1987). Of note is a comparative study between mice and humans, which demonstrated in the murine model an age-dependant increase of infiltration, but the human cohort demonstrated no correlation (Goodall et al., 2018). Both technical and methodological differences found within studies investigating permeability and BBB dysfunction demonstrates the complexities in the field and that further research is required before any definite conclusions are drawn on the relevance of permeability changes to BBB. For example, studies have chosen to inject dyes *in vivo* or via immunohistochemical staining on post-mortem tissue which have resulted in varied findings (Goodall et al., 2018; Stamatovic et al., 2019). Furthermore, when comparing findings utilising similar methodologies, the analysis type has to be considered as this can change the interpretations of results, this is demonstrated when 2D and 3D analysis of transmission electron microscopy (TEM) images resulted in different findings for ultrastructural changes of the ageing BBB (Frías-Anaya et al., 2021).

Modern imaging techniques, such as dynamic contrast-enhanced magnetic resonance imaging (DCE-MRI) are also being utilised to examine BBB leakage, especially in humans, which allows investigations into living cohorts during the ageing process (Banks et al., 2021). But even using advanced technology conflicting data has been uncovered, for example, Montagne et al., 2015, observed a correlation between age and infiltration specifically in the hippocampus and postulated that may be the most susceptible region to BBB damage in ageing. Whilst Verheggen et al., 2020, disagreed and instead noted that there was an age-dependant leakage through the BBB into the grey and white matter in comparison to hippocampal regions.

1.5. Inflammation in the ageing brain

Historically, the healthy CNS had been described as ‘immune privileged’ due to the BBB and other structures preventing peripheral inflammatory molecules from entering (Louveau et al., 2015). This meant that it was assumed that during physiological ageing, there was not a specific immune and inflammatory response. However, as ageing is a major factor in most

neurodegenerative diseases, it was prudent to investigate possible low-grade systemic inflammation present prior to pathology. Franceschi et al., 2007, coined the phrase 'inflammageing' and described this as the changes to composition of anti- and pro-inflammatory networks during physiological ageing. Subsequently, many cellular types have been identified as brain associated inflammatory cells such as microglia, astrocytes, macrophages, dendritic cells, monocytes, neutrophils and natural T-killer cells (Costa et al., 2021). Most of these cells are not normally present in large quantities within the healthy young brain, with microglia the largest population, and instead are predominantly within the circulating vasculature (Yang et al., 2010). Another key aspect of inflammageing is the presence of cytokines; specific pleiotropic proteins which are secreted by CNS cells and can act as either pro- or anti-inflammatory substances (Sartori et al., 2012). These can be divided into different sub-families such as interleukins (IL), interferons and tumour necrosis factor (TNF) which are all functionally distinct but work in combination to produce inflammatory effects (Konsman, 2022).

1.5.1. Anti-inflammatory profile

Inflammation inherently is not a negative biological response and in non-pathological conditions many components of the inflammatory response are required for maintaining homeostasis, remodelling the ECM and synaptic plasticity (Finger et al., 2021; Sochocka et al., 2017).

1.5.1.1. Anti-inflammatory Microglia

Microglia are the resident macrophage in the brain and therefore act to phagocytose cell debris and remove toxic materials such as amyloid beta (Richter et al., 2020). It has also been demonstrated that the presence of microglia is crucial for maintaining synaptic plasticity across the lifespan as depletion of the cell type induced a reduction in synaptic proteins leading to a decrease in glutamatergic synapses (Parkhurst et al., 2013). This study further linked ageing to a decrease in memory and learning, showing an important link between the

immune cell and cognitive abilities and proposed that this may be linked to the microglial production of BDNF (brain-derived neurotrophic factor).

1.5.1.2. Neuroprotective Cytokines

Anti-inflammatory cytokines are also present within the brain such as IL-4, IL-10 and TFG-β which act to reduce any inflammation present in the CNS (Sochocka et al., 2017).

IL-10 is one of the more abundant anti-inflammatory cytokines due to its origin in multiple cell types such as leukocytes, microglia, dendritic cells among others, also pointing towards its importance (De Malefyt et al., 1991; Saraiva et al., 2009). This cytokine is multi-functional and affects the inflammatory profile by not only reducing expression of pro-inflammatory cytokines, such as IL-6, and inhibits the expression of major histocompatibility complex II (MHC-II) which reduced antigen presentation (De Malefyt et al., 1991; Porro et al., 2020). IL-10 also works bifunctionally to reduce TNF-α as it not only reduces expression of the cytokine but has been shown in the cardiovascular system to reduce reactive oxygen species (ROS) production leading to TNF- α antagonism (Dhingra et al., 2009; Zemse et al., 2010). Within both human and mouse ageing, it has been shown that IL-10 polymorphisms correlate with increased lifespan (Cederholm et al., 2007; Dagdeviren et al., 2017; Dhingra et al., 2009). However, there has been some contradictions within the clinical setting which suggest that IL-10 is not related to longevity, and this may be linked to differences in populations and sex (Khabour & Barnawi, 2010; Wang et al., 2001).

1.5.1.3. Neuroprotective Interleukin 1-beta (IL-1β)

Although primarily associated with pro-inflammatory responses, low, almost undetectable, levels of IL-1β have been essential to the normal functioning of multiple homeostatic systems such as sleep, synaptic plasticity and appetite (Bourgognon & Cavanagh, 2020; del Rey et al., 2013; Liu & Quan, 2018). The existence of low-level IL-1β is shown to also be of importance in hippocampal memory and learning as the knock-out of the cytokine in 3-month mice demonstrated a significant drop in abilities on behaviour tasks such as water maze test, fear

conditioning and olfactory discrimination tests (Avital et al., 2003; Cibelli et al., 2010; Takemiya et al., 2017). Further studies also note that IL-1β is required for long term potentiation (LTP), but again used young *in vivo* models so is not reflective of the aged phenotype (del Rey et al., 2013). Other tests contradict some of these findings, although still show some cognitive decline with reduced IL-1β, as there was no change in fear conditioned responses or visual memory suggesting a region-specific requirement of the cytokine in young physiological conditions (Avital et al., 2003; Gonzalez et al., 2009).

1.5.2. Pro-inflammatory profile in ageing

As the brain physiologically ages, the phenotype of many cells transform from an anti-inflammatory state to a pro-inflammatory state including morphological and functional changes which effect the overall system with the brain and BBB. Many immune cell types are affected by ageing such as macrophages, neutrophils and dendritic cells but the most associated cells with inflammaging are microglia and the effect of increase cytokine burden (Finger et al., 2021).

1.5.2.1. Pro-inflammatory Cytokines

Within both human and *in vivo* studies, it has been shown that age correlated with an increase in the major pro-inflammatory cytokines above young physiological levels; IL-1β, TNF-α and IL-6 (Álvarez-Rodríguez et al., 2012; Lindbergh et al., 2020; Porcher et al., 2021; Ye & Johnson, 1999). There is a gap within the research in physiological ageing, as many of the studies investigate the expression of the cytokine and not the effect of the molecule on the brain and BBB. This may be because of the highly characterised effects of cytokines in either systemic infection-based models or neurodegeneration.

1.5.2.1.1. Pro-inflammatory TNF-α

TNF-α has been shown in relation to the BBB to activate the NF-Kβ pathway, which is important in further downstream induction of pro-inflammatory molecules and has also been linked to a decrease in claudin-5 expression *in vivo* during stroke or over-expression of TNF-α (Aslam et

al., 2012; Chen et al., 2019; Cheng et al., 2018). The effects on *in vivo* stroke models were confirmed *in vitro* via culturing of BBB with as specific blocker of TNF-α (infliximab) which resulted in the reduction of BBB permeability via TEER measurements (Chen et al., 2019). Ageing has been shown to link the increase of TNF-α with decreases in TJ proteins, especially occludin, suggesting that the paracellular transport is targeted by this cytokine (Elahy et al., 2015b). Further *in vitro* studies have linked increased TNF-α production with an increase in matrix metalloproteinase-9 (MMP-9) which is again linked to the disruption of the BBB (Barr et al., 2010; wei Ding et al., 2019). This is also important translationally as it has been shown that the inhibition of MMP-9 can decrease cognitive impairment in 14-month mice and may hint that the inhibition of TNF-α would be an upstream director of this effect (Ji et al., 2023).

1.5.2.1.2. Pro-inflammatory IL-1β

IL-1β is also a major inflammatory cytokine which is upregulated during brain ageing, especially in the hippocampal region (Porcher et al., 2021). The increased expression of IL-1β affects the BBB through a variety of mechanisms which either increase BBB permeability or activate neuroinflammatory pathways, such as Nuclear factor kappa-light-chain-enhancer of activated B cells (NF-kb) (Yang et al., 2022). Firstly. ICAM-1, TNF-α and IL-6 levels were increased in age with higher IL-1β levels (Labus et al., 2014; Starr et al., 2015). *In vitro* this resulted in decreased TEER and Zo-1 indicating dysfunction in BBB and increased permeability to leukocytes within the brain. Increased ICAM-1 has been observed during ageing in the human cortex but is questioned within the *in vivo* setting as studies note no increase in either ICAM-1 or similar VCAM-1 (Elahy et al., 2015; Miguel-Hidalgo et al., 2007).

The other major mechanism for BBB disruption is the activation of NF-kb pathway in astrocytes via the upregulation of hypoxia inducible factor 1 (HIF-1) and vascular endothelial growth factor A (VEGF-A) (Argaw et al., 2006). Older studies suggest that the activation of this pathway causes an increase in ICAM-1 and VCAM-1 but again is contradicted in later literatures (Elahy et al., 2015; Moynagh et al., 1994). The production and maintenance of the BBB by astrocytes is also inhibited by the presence of IL-1β as it downregulates sonic hedgehog (SHH) (Wang et

al., 2021; Wang et al., 2014). This occurs as the downstream transcription factor, Zinc finger protein (Gli-1) is curial to the expression of TJ proteins such as zo-1 and occludin, therefore affecting the paracellular transport pathway (Xia et al., 2013). Further qualifying the importance of SHH in BBB functionality, in a stroke mice model the introduction of SHH reduced BBB leakage and increased expression of Zo-1 (Xia et al., 2013). However, contradictory to this, Wang et al., 2021, propose that the transcytosis pathway is preferentially affected as albumin infiltrated the murine brain whilst biocytin-tetramethyl rhodamine, evaluating paracellular transport, was unchanged. This may link to ageing as it is noted that transcytosis is a major upregulated transport pathway in older mice (Yang et al., 2020).

1.5.2.1.3. Pro-inflammatory IL-6

The upregulation of IL-6 is also noted within ageing and can lead to increased inflammatory profile like the actions of TNF-α and IL-1β (Porcher et al., 2021; Tyrrell et al., 2020). It has been documented that Il-6 decreases BBB permeability via reduction in TJ protein expression and that in the ovine foetus, introduction of IL-6 antagonist reversed these effects and restored BBB functionality (Zhang et al., 2015). IL-6 also acts upon astrocytes in a hypertriglyceridemia model noting a decrease in Aqp4 which was reversed with increased IL-10 (Barabási et al., 2023). It is suggested that IL-6 increases neuroinflammation through activation of signal transducer and activator of transcription 3 (STAT3) in both neurons and microglia (Hu et al., 2020).

1.5.2.2. Pro-inflammatory Microglia

Within the field, it has been proposed that microglia are particularly affected by physiological ageing (Tay et al., 2017). This has recently been demonstrated in INK-ATTAC mice, where drug-induced elimination of senescent cells resulted in a decrease in mainly the microglia population, leading to an increase in cognitive ability and reduction in cytokines (Ogrodnik, 2021). It was historically accepted that in the presence of inflammation, microglia switch from a resting ‘M1’ phenotype to an active ‘M2’ phenotype, but this has been challenged and seen

as an oversimplification of the complex changes to characteristic of the brain immune cell and its effects on the overall brain macrosystem.

Morphologically, it has been established that in ageing a shift to a dystrophic model occurs including an increased soma and decreased branch length to form an ameboid morphology (Latham et al., 2023). However, this may be a regional effect as Hart et al., 2012 established that white matter microglia had a more pronounced change then grey matter cells, shown with a significant increase in cluster of differentiation (CD) CD11 and CD68. This may be linked to the inherent heterogenous density of microglia populations as it is documented that the hippocampus has higher levels of the cell compared to the cerebellum (Lawson et al., 1990; Tan et al., 2019). Other studies have shown that in aged mice inflammation causes the distinct spatial populations to move closer together and be less dynamic and therefore slower in immune surveillance than in younger groups (Damani et al., 2011). This has the consequence of reduction in function when exposed to inflammatory stimuli and further damage accruing. Specific microglial sub-populations, such as lipid-droplet accumulating microglia (LDAM) are increased during ageing and present with differing transcriptomic profiles to other microglia; with a decrease in phagocytosis but increase in cytokine and ROS production leading to increasing inflammation (Marschallinger et al., 2020). This highlights the complex effects of age on microglia and the importance of investigating sub-populations and their variability for downstream therapeutic targeting.

Complicating the translatability of *in vivo* studies to the clinical setting is the variation between aged microglia morphology, with mouse and non-human primates displaying the discussed dystrophic model but in aged humans, this shift is not observed unless under neurogenerative conditions (Choi et al., 2022; Rodríguez-Callejas et al., 2019; Shahidehpour et al., 2021; Shobin et al., 2017). The changes in morphology also correlate with an increased production of pro-inflammatory cytokines, such as TNF-α, IL-1β and IL-6 during ageing is well documented within the murine model (Cyr & de Rivero Vaccari, 2023; Garner et al., 2018; Sierra et al., 2007).

Microglia activation also has deleterious effects on other cells within the parenchyma such as astrocytes and neurons, via acting on the important myelin sheath of neurons (Latham et al., 2023). These effects begin at differentiation of oligodendrocyte precursor cells (OPC's), which transform into oligodendrocytes that are the main producers of myelin for neurons (Kuhn et al., 2019). During ageing, it has been shown that microglia activation disrupts this process by inhibiting OPC differentiation leading to a decrease in myelin production (Baror et al., 2019; Luan et al., 2021). This has been shown to be damaging to neuronal function in disease states such as multiple sclerosis (Windener et al., 2024). The signal transducer and activator of transcription 1 (STAT1) pathway has been a proposed mechanisms behind these changes as this is upregulated in aged microglia and shown to contribute to the OPC differentiation inhibition in traumatic brain injury (Luan et al., 2021; Y. Zhao et al., 2022). An alternative theory links the production of transforming growth factor-beta (TGF-β) which is expressed by aged microglia and has been shown to inhibit OPC differentiation *in vitro* (Baror et al., 2019). Another consequence of myelin dysfunction is the increased accumulation of myelin debris during ageing, which is then phagocytosed by microglia (Xu et al., 2023). Safaiyan et al., 2016 demonstrated in the white matter of 24-month mice, an accumulation of the myelin-debris within the microglia producing lysosomal inclusions. Within neurodegeneration, it is known that these inclusions cause further microglial senescence exacerbating the cellular inflammatory phenotype and increasing the burden upon the wider parenchyma (Latham et al., 2023; Rim et al., 2024).

There are multiple signalling pathways affected by ageing that link to the increased inflammatory phenotype of microglia. One of these is the decreased expression of CX3C Motif Chemokine Receptor 1 (CX3CL1) chemokine which binds to the CX3CR1 exclusively in the microglia within the CNS (Mecca et al., 2018). When young mice are CX3CL1 deficient, the microglial transcriptome resembles that of the ageing phenotype, including increased production of IL-1β, suggesting that it is very important in the overall shift to inflammation (Gyoneva et al., 2019). This downregulation is also observed in a BALB/C mouse model of

inflammation comparing age with lipopolysaccharide (LPS) injection where they observed a downregulation in the aged controls as well as the LPS condition correlating with a decrease in anti-inflammatory TGFβ (Wynne et al., 2010). Another potential mechanism for the ageing microglial phenotype is the decrease in CD200 receptor which has been found to be an important regulator in maintaining the microglial resting state (Latham et al., 2023; Lyons et al., 2007). During stress and ageing in rats, it has been shown *in vivo* and *in vitro* that decreases in the receptor correlated to the activation of microglia and increased production of cytokines TNF-α and IL-1β and the decrease in neuroprotective IL-4 (Frank et al., 2018; Lyons et al., 2007; Oria et al., 2018). Further increases in IL-1β production by microglia may be caused by the age-related reduction of SIRT1, as in knockout mice, the removal of the protein activated the NF-kB pathway and exacerbated cognitive decline (Cho et al., 2015).

Dysregulation of iron homeostasis may also be a potential mechanism for the activation of microglia within ageing (Levi et al., 2024). It has been shown *in vitro* that both IL-6 and TNF-α cause the induction of divalent iron transporter 1 (DMT1), an iron influx transporter, causing the accumulation of iron within the microglia (Rathore et al., 2012; Urrutia et al., 2013; Zhou et al., 2017). Within AD human samples and *in vivo* models, increased microglial iron was linked to increased ionized calcium binding adapter molecule 1(Iba-1) and decreased transmembrane protein expression linked with Aβ plaque formation and increased neurodegeneration (Kenkhuis et al., 2021; McIntosh et al., 2019). Interestingly, the same group found in induced pluripotent stem cell (iPSC) derived microglia, that the iron accumulation did not affect the inflammatory status of the microglia but did induce oxidative stress, leading to further neuroinflammation in the surrounding brain tissue (Kenkhuis et al., 2022). Within ageing marmosets, it has been shown that the increase in iron accumulation may be due to the increase in ferratin within the microglia but interestingly, the amount of ferratin-positive microglia within the aged hippocampus and cortex decreased (Rodríguez-Callejas et al., 2019). Iron accumulation is linked to increased BBB permeability as increased iron deposits lead to senescence of BEC's preceding decreases in cognitive ability (Noh et al., 2023).

Interestingly, a sex-dependent effect of iron accumulation was observed in the study, with females more vulnerable to dysfunction then males, further indicating that sex differences contribute to BBB variation in ageing.

1.6. Methodological approaches to investigating age-related BBB changes

Multiple methodologies can be utilised to study the BBB in ageing dependent investigations based upon the aims and predicted outcomes of the work, for example, changes to protein localisation and morphology can be investigated via immunohistochemical staining but other techniques such as western blotting may be more suitable for expression change aims. Various approaches can be implemented including *in vitro*, and *in vivo* approaches with a range of techniques as detailed in table 1-2 along with postmortem, human tissue analysis and clinical imaging studies in humans are crucial to validate the translation potential for preclinical observations. Table 1-2 chronologically summarises current literature, demonstrating a historical preference for post-mortem studies, but as technology has advanced, molecular and imaging techniques have been applied.

Human approaches are considered the gold standard to investigate the BBB in ageing and many post-mortem and neuroimaging studies have implemented human modelling to enhance the field (Chiu et al., 2015; Montagne et al., 2015; Shao et al., 2020). However, accessibility to human cohorts is difficult due to the feasibility and availability of participants. Human samples are also limited regarding techniques that can be employed and more stringent ethical considerations (Goodall et al., 2018; Viggars et al., 2011; Waller et al., 2016). Alternatively, most studies implement models of other species, as demonstrated in 1-2 with 95% of the studies employing non-human models.

Table 1-2: Characteristics of studies investigating Blood-brain barrier and ageing highlighting species selected, sex of cohort and experimental models/techniques chosen

Study	Species	Sex	Outcome measure				
			Post-mortem	**Imaging**	**Behavioural**	**Molecular**	***In vitro***
(Rapoport et al., 1979)	Rat (senescent)	Not stated	•				
(Stewart et al., 1987)	Human	Mixed	•	•			
(Mooradian et al., 1991)	Rat	Male	•				
(Peters et al., 1991)	Mk	Not stated	•				
(Ueno et al., 1996)	Mouse (SAMP8)	Not stated	•				
(Peinado et al., 1998)	Rat	Male					
(Su et al., 1998)	Canine	Mixed	•	•	•		
(Mooradian et al., 2003)	Rat	Male	•				
(Hughes et al., 2006)	Rat	Not stated	•				•
(del Valle et al., 2009)	Mouse (SAMP8)	Male	•				
(Bell et al., 2010)	Mouse	Not stated	•	•	•		
(Wu et al., 2010)	Mouse (SAMP8)	Not stated	•				
(Viggars et al., 2011)	Human	Mixed	•				
(Van Assema et al., 2012)	Human	Mixed	•				
(Ding et al., 2013)	Mouse	Female	•				
(Rodríguez et al., 2014)	Mouse	Male	•				
(Chiu et al., 2015)	Human	Mixed	•				
(Elahy et al., 2015)	Mouse	Female	•				
(Janota et al., 2015)	Mouse	Male	•	•			
(Nation et al., 2019)	Human	Mixed		•			
(Sartorius et al., 2015)	Mouse	Male	•	•			

	Human	Mixed	•	•			
(Bonte et al., 2017)	Human	Mixed	•	•			
(Duncombe et al., 2017)	Mouse	Male	•		•		
(Osgood et al., 2017)	Rat	Male	•		•		
(Nahirney et al., 2016)	Mouse	Male		•			
(Yamazaki et al., 2016)	Mouse	Not stated					•
(Hoffman et al., 2017)	Mouse	Male	•		•	•	
(Nikolakopoulou et al., 2017)	Mouse	Mixed	•				
(Bors et al., 2018)	Rat	Male	•	•			
(E. F. Goodall et al., 2018)	Mouse	Not stated	•				
	Human	Not stated	•				
(Ceafalan et al., 2019)	Mouse	Not stated	•	•			
(Emily F. Goodall et al., 2019)	Mouse	Male	•			•	
	Human	Mixed					
(Nation et al., 2019)	Human	Mixed	•	•		•	
(Senatorov et al., 2019)	Mouse	Mixed	•	•	•		
	Human	Mixed					
(Stamatovic et al., 2019)	Mouse	Mixed	•				•
	Human	Mixed	•				•
(Ximerakis et al., 2019)	Mouse	Not stated				•	
(Bohannon et al., 2020)	Human	Mixed	•				
	Monkey	Mixed					
(Chen et al., 2020)	Mouse	Not stated	•				
(Hill et al., 2020)	Mouse	Female		•			
(Kiss et al., 2020)	Mouse	Male				•	

(Shao et al., 2020)	Human	Mixed		•			
(Verheggen, et al., 2020)	Human	Mixed		•			
(Verheggen, et al., 2020)	Human	Mixed		•			
(Yang et al., 2020a)	Mouse	Male	•				
(Almanzar et al., 2020)	Mouse	Mixed				•	
(Zhao et al., 2020)	Mouse	Male				•	
(Frías-Anaya et al., 2021)	Mouse	Female	•	•			
(Versele et al., 2022)	Human	N/A		•			•
(Choi et al., 2022)	Mouse	Male	•	•			
(Giacobbo et al., 2022)	Mouse	Male		•			
(Britton et al., 2022)	Mouse	Male	•	•	•	•	
(Halder & Milner, 2022)	Mouse	Female	•	•	•		
(Hendrickx et al., 2022)	Mouse	Male		•	•		
(Noh et al., 2023)	Primary mouse culture	Mixed		•	•	•	•
(Ji et al., 2023)	Mouse	Male	•	•	•	•	
(Yuan et al., 2023)	Mouse	Male	•		•		
(Bakhtiari et al., 2023)	Human	Male		•			
(Cyr & de Rivero Vaccari, 2023)	Mouse	Mixed	•				
(Windener et al., 2024)	Primary mouse culture	Mixed	•				•
(Cummins et al., 2024)	Mouse	Mixed	•	•			
(Shao et al., 2024)	Human	Mixed		•			
(Healy et al., 2024)	Mouse	Mixed	•		•	•	
(Hu et al., 2024)	Mouse	Female	•		•		

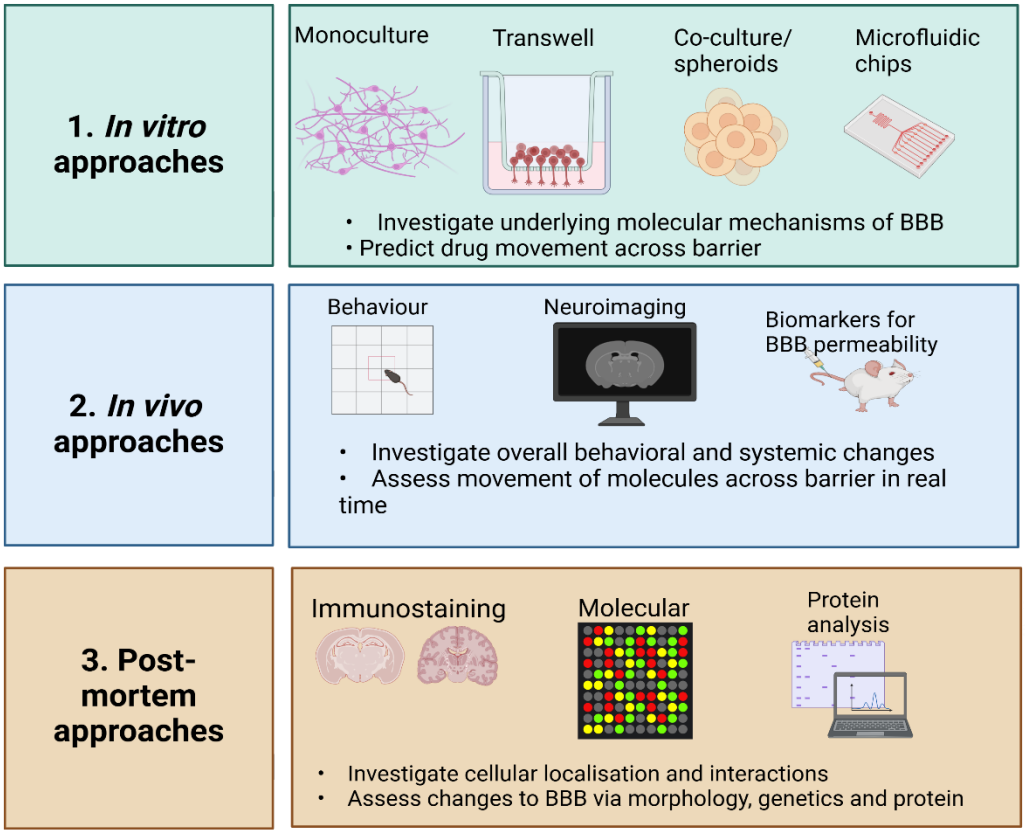

Figure 1-3: Overview of methodological approaches to BBB investigations. Highlighted are three streams (1) In vitro approaches including diverse types of culture systems used (2) In vivo approaches visualizing different experiments available (3) post-mortem approaches which can be conducted in human or animal specimens. Each section includes a brief description of the common aims for each approach. Produced in Biorender.com

1.6.1. Approaches to investigating brain ageing modelling.

1.6.1.1. In vitro models

In vivo studies can be useful for identifying the functional consequences of BBB dysfunction but may have more limited use for examining the underlying molecular mechanisms. However, *in vitro* models can be used to determine molecular changes and various models exist (Williams-Medina et al., 2021). Certain benchmarking criteria are commonly used to assess model suitability including shear wall stress, ultrastructure, expression of TJ markers, permeability, and TEER (Destefano et al., 2018). Currently, no *in vitro* model successfully encapsulates all of these factors or replicates the *in vivo* environment in its entirety (Bagchi et al., 2019). Changes to permeability and TJ markers during ageing makes it difficult to check the validity of *in vitro* models as the main criteria can be compromised (Verheggen, et al., 2020).

Multiple species and cell types can be used as BBB *in vitro* models and the advantages and limitations are summarised in table 1-3.

Monoculture models, although simplistic have been utlisied within ageing BBB studies to investigate changes to a singular cell type (Logsdon et al., 2021; Musafargani et al., 2020). Stamatovic et al., 2019 utilised a Transwell monoculture of primary mouse endothelial cells as a model of ageing. This investigated Sirt1 expression via quantitative polymerase chain reaction (qPCR) and depleting or overexpressing Sirt1 to compare the permeability of the cells via the addition of a fluorescently conjugated bovine serum albumin tracer. The study demonstrated that BBB permeability correlated with Sirt1 loss and that may be linked to decreases in claudin-5 expression. This research demonstrated that even with limitations, monocultures can be used to investigate age-related BBB changes in the field, especially when investigating molecular mechanisms of BBB dysfunction. The most promising cell type moving forward in BBB modelling is induced pluripotent stem cells (iPSC's), which can be obtained from ageing patients and reprogrammed to BBB cell types such as endothelial cells, astrocytes and pericytes, to quickly model the ageing phenotype and increase shear stress in the model (Linville et al., 2019).

Another important consideration when designing an *in vitro* model is whether to use a dynamic or static system, with subtypes of each shown in table 1-4. Static systems, the most common of which is the Transwell system, involve endothelial cells grown on a 2-dimensional filter within a compartment, representing the luminal side of the BBB with an electrical current running through the system (Weiss et al., 2009). Other cell types can be grown on the other side of the filter or on the base of the well, representing the abluminal BBB. Many of the BBB essential criteria needed to increase the suitability of a model such as high TEER, low permeability and expression of TJ and cell markers can be achieved within a dynamic model to a higher level than in static models. Importantly, dynamic models also allow the replication of cerebral blood flow and shear stress which are not achievable in static models (Williams-Medina et al., 2021; Yeon et al., 2012).

Table 1-3: Advantages and limitations of cell types utilised for in vitro studies into blood-brain barrier changes.

Cell type	Examples	Advantages	Limitations	References
Rodent primary cells	Mouse Rat	• Expression of tight junction proteins (Claudin-5, -3, occludin) • Expression of P-gp and Glut-1 transport proteins. • Tri-culture systems available	• Low TEER • Difficult to maintain cultures and require large amounts of cells. • Not representative of human cells	(Lukic-Panin et al., 2012 ; Stamatovic et al., 2019) (Zhang et al., 2016) (Molino et al., 2014)
Human primary cells		• Reflect translatable phenotype	• Not easy to obtain. • Inefficient cell numbers when obtained and lose phenotypic properties	(Wang et al., 2015) (Helms et al., 2015) (Stone et al., 2019) (Shawahna et al., 2013)
Immortalised human cell lines	hCMEDC/D3 hBMEC	• Readily available • Well characterised • Express transport proteins	• Low TEER • Do not reflect transport of BBB. • Low claudin-5 expression	(Helms et al., 2015) (Weksler et al., 2013) (Ahn et al., 2020) (Daniels et al., 2013)
Mouse immortalised cell lines	bEND.5 bEND.3 cEND cerebEND	• Readily available • Stable through passaging • High yields • Reduced variation between cells	• Reduced barrier tightness • Reduction in tight junction expression • Interspecies variation	(Idris et al., 2018) (Yang et al., 2007) (Shayan et al., 2011)
Human iPSC		• Model phenotype of donor • Mimic sheer stress • Low permeability • High TEER	• Need careful phenotyping of transformed cells. • More expertise required to produce cells	(Campisi et al., 2018) (Lippmann et al., 2014) (Roux et al., 2019)

Table 1-4: Advantages and limitations of in vitro systems for investigating the blood-brain barrier.

System type	Model type	Cell type(s)	Uses	Advantages	Limitations	References
Static	Transwell monoculture	Endothelial cells	• High-throughput basic studies • Signalling pathways • Transporter kinetics	• Simple • Easy to use.	• Does not replicate NVU. • No sheer stress • High permeability	(Williams-Medina et al., 2021) (Bagchi et al., 2019) (Stamatovic et al., 2019)
	Co-culture	Endothelial cells with other NVU components	• Permeability studies • Cell interaction	• Replicates NVU components • Increased expression of tight junctions • Higher TEER and low permeability	• No sheer stress • No direct cell-cell contact • Incomplete TJ production at edge of model	(Ahn et al., 2020) (Stone et al., 2019) (Kulczar et al., 2017)
Dynamic	Dynamic In Vitro-BBB	Endothelial cells with other NVU components	• Drug development and optimisation • Pathophysiology of disease	• Provides sheer stress. • Replicates NVU phenotype • Expression of transporters and TJ • High TEER • Low permeability	• Need large number of cells. • Increased time to achieve TEER	(Pas, 2018) (Prashanth et al., 2021)
	Microfluidic	Endothelial cells with other NVU components Can be patient derived pluripotent stem cells (iPSC's)	• Cell migration • Drug permeability • Pharmacokinetics	• Provides sheer stress. • iPSC can replicate phenotype of participant. • Expression of transporters and TJ	• Prohibitive cost • Hard to maintain. • Need specialist technology. • Vessel diameter not representative	(Bhalerao et al., 2020) (Lee & Leong, 2020) (Campisi et al., 2018) (Y. Shin et al., 2019)

Microfluidic models, including organ-on-a-chip technology which consist of microchannels on a chip through which fluids are injected to achieve specific cellular conditions whilst also mimicking vessel matrixes such as ECM, may be the most promising dynamic *in vitro* model (Williams-Medina et al., 2021). This could be accomplished by producing a co-culture of cells derived from iPSC's to produce the most accurate representation of phenotype and morphology, especially when utilising patient- derived iPSC's to mimic physiology although currently, no model has investigated physiological ageing (Campisi et al., 2018; Lee et al., 2020; Shin et al., 2019). Another aspect to consider is the ability of a model to replicate the ECM, which is key for maintaining BBB structure. Many microfluidic culture systems use a material to mimic this, such as fibrin, but this is comparably weak to the *in* vivo environment (Linville & Searson, 2021). Recent advances have favoured ECM hydrogels, such as collagen-based, which possess a higher similarity to the *in vivo* ECM than other materials whilst also being adjustable chemically and physically to tailor the model to characteristics of study interest (Chen et al., 2021).

There has been limited use of *in vitro* models pertaining to physiological ageing, which may be due to the field being recently relevant and so studies may be utilising this technology currently. This may also be conflated by challenges in recreating the ageing phenotype compounded by difficulties overcoming low proliferation due to lengthened cell cycle and high cell death of aged cells, making obtaining sufficient cell numbers for assays challenging (Nassrally et al., 2019; Ogrodnik, 2021).

Osipova et al., 2018 recently suggested a multitude of solutions to this. Firstly, they suggested acquiring cells from iPSC cultures of an aged cohort or cells isolated from senescent animal models (e.g., Senescence Accelerated Mice 8 (SAMP8) mice) to overcome the obstacle of ageing cells via the passage. The group also suggested inducing the senescent phenotype in young cells by delivery of several factors and manipulating age-related pathways. However,

these cells would require extensive phenotype validation to ensure that ageing had been replicated (González-Gualda et al., 2021).

1.6.1.2. In vivo approaches

The BBB is a highly conserved system across vertebrates, and some invertebrates such as zebrafish, thus implementing *in vivo* animal approaches are a useful tool (O'Brown et al., 2018). Utilizing *in vivo* models has the advantage of being able to produce high throughput, controlled experiments whilst still observing a dynamic and living environment (Banks, 2010). There are a plethora of investigations which utilise *in* vivo approaches such as injection of, for example, contrast agents used in BBB permeability assays, neuroimaging such as DCE-MRI, micro dialysis sampling and behavioural studies (Kuhnline Sloan et al., 2012).

1.6.1.2.1. Rodent models

Murine models of BBB are the most used model and offer the potential for genetic modification to examine a particular target (O'Brown et al., 2018; Yuan et al., 2011). For example, Bell et al., 2010, used a mouse model with knockdown for the pericyte marker PDGFRβ to demonstrate the effects of the loss of this receptor during ageing. However, when using *in vivo* models, it is important to consider whether cellular differences exist between the proposed model species and humans. In mice and rats, it has been shown that BEC's express many of the crucial molecules in TJ formation as well as transporters such as GLUT-1 and P-gp (Daneman, Zhou, Agalliu, et al., 2010). However, some differences have been identified, including a different mechanism for P-gp transport in mice and differential uptake of some receptor antagonists (Erdo & Krajcsi, 2019; Syvänen et al., 2009). Thus, extrapolation of results from rodents to humans may not always be relevant without further validation studies in human post-mortem tissue.

Many studies, 60% of the literature identified in table 1-2 exclusively used male mice, but this may not reflect age-related BBB damage. To ensure results from such models are valid for both sexes research studies should implement the use of a mixed-sex model as implemented in

20% of current murine studies within table 1-2. (Senatorov et al., 2019; Stamatovic et al., 2019).

Most murine *in vivo* ageing studies use the common C57BL/6J inbred mouse model for BBB investigations (Goodall et al., 2018; Hill et al., 2020; Nahirney et al., 2016). This strain is advantageous as genetic alterations to investigate changes in specific markers are easily achieved, such as with PDGFRβ (Nikolakopoulou et al., 2017). However, in order to research changes with ageing, this requires the use of aged animals which is time-consuming and costly (Kõks et al., 2016). To counteract this, studies have chosen specific accelerated ageing models such as the SAMP-8 (del Valle et al., 2009; Fernández et al., 2021). Pelegrí et al., 2007 demonstrated in the SAMP8 model that the hippocampus displayed age-related BBB disruption whilst Liu et al., 2020, noted that decreases in cognitive ability correlated with ageing. However, care must be taken when employing SAMP8 mice models for physiological ageing as studies have shown this model to also exhibit pathological phenotypes such as accumulation of Aβ (Kõks et al., 2016; Liu et al., 2020). Therefore, any correlation with physiological age must be tentative and may be used as a proof-of-concept study with follow up investigations in normal aged animals.

1.7. Technical approaches for age-related BBB study

1.7.1. Post-mortem tissue investigations

The use of human post-mortem tissue is restricted due to it being a fixed point in time at the end-stage life and cannot encapsulate dynamic changes unlike live neuroimaging studies (Sun et al., 2021). However, tissue obtained post-mortem can be investigated using a variety of methods to provide information on protein and genetic expression (Bors et al., 2018c; Hoffman et al., 2017; Ximerakis et al., 2019).

The increasing complexity of genetic and molecular approaches available to examine post-mortem tissue is impacted by tissue quality (Wimmer et al., 2018). Tissue is typically preserved via formalin-fixed paraffin embedded (FFPE) or frozen tissue. FFPE tissue is advantageous due

to ease of long-term storage whilst frozen specimens retain tissue and genetic architecture and are more suited to specific techniques, such as molecular microarray studies (Goodall et al., 2018; Wimmer et al., 2018).

Other factors to consider when using post-mortem tissue include the agonal state which is crucial for ribonucleic acid (RNA) quality, thus, affecting results of techniques reliant upon this such as microarrays and western blotting (Tomita et al., 2004). In addition, the time between death and storage of tissue, i.e. post-mortem interval (PMI), can affect protein and nucleic acid integrity as well as the activity of enzymes (Blair et al., 2016). Thus, it is important to correlate any results with PMI time especially within brain studies as neurodegenerative markers have been shown to be vulnerable to expression changes with increased PMI (Lundström et al., 2019; Pikkarainen et al., 2010).

1.7.1.1. Markers of BBB Alterations

1.7.1.1.1. Permeability markers

Increased permeability of the BBB is a hallmark of dysfunction; thus, many studies implement techniques enabling the investigation and visualisation of leakage into the parenchyma. Such techniques rely on the use of a BBB tracer and numerous factors which need to be considered include potential for toxicity, non-specific binding, whether the substance is metabolically active/inert (Saunders et al., 2015). It is possible to use endogenous markers to characterise BBB permeability such as EBD which has been commonly used in *in vivo* models due to noted reliability and sensitivity (del Valle et al., 2009; Nahirney et al., 2016). EBD is a non-toxic azo dye that can remain in circulation over time and allows for permeability to be assessed by colorimetric analysis (Saunders et al., 2015). However, researchers are questioning EBD suitability as non-specific binding of albumin may occur as well as some reports of toxicity in animals (Saunders et al., 2015; Sun et al., 2021). An improvement upon the use of EBD is dextran which is advantageous as it exists at multiple molecular weights, allowing studies to determine the extent of permeability and identify the most susceptible regions to the

breakdown of the BBB in response to particular treatment or disease, for example (Stamatovic et al., 2019; Sun et al., 2021).

Plasma proteins have also been heavily utilised to assess BBB permeability, including albumin and IgG. Ageing studies have applied both markers to examine their infiltration into the brain exclusively in post-mortem tissue (Elahy et al., 2015; Pelegrí et al., 2007; Senatorov et al., 2019). The inability for plasma proteins to be detected in live imaging studies limits their usability in comparison to other endogenous markers which can be measured/visualised via multiple methods. Furthermore, recent investigations have questioned the reliability of IgG as a marker of permeability as it may not originate exclusively in blood vessels (Sun et al., 2021). Albumin may be more appealing, especially when conjugated with a fluorescent dye, as it allows for both permeability quantification and determination of transcellular transport changes (Ahishali & Kaya, 2020; Park et al., 2018). However, Goodall et al., 2018, noted that albumin infiltration can be affected by PMI and so the correlation with this is required to ensure that results can be comparable across the research field as findings could differ if this is not considered.

1.7.1.1.2. NVU components

Cellular markers are employed in the detection and quantification of marker expression during ageing of cellular components of the NVU. There are two main challenges to this type of methodology: the heterogeneous nature of cell populations and the specificity of cellular markers. Astrocytic markers have been well characterised, with GFAP regarded as the 'gold standard' throughout many studies of ageing (Goodall et al., 2018; Janota et al., 2015). One of the main justifications of GFAP is that it can label a substantial proportion of the cell morphology (Jurga et al., 2021). However, GFAP possesses a preference to immunolabel reactive astrocytes, meaning that cells in the unreactive phenotype remain unstained (Garwood et al., 2017). During ageing, some cells may not express the reactive phenotype, resulting in inaccurate staining patterns only immunolabelling reactive cells. Zhang et al.,

2019, suggested the simultaneous use of astrocytic markers to produce a more detailed pattern of expression but considerations must be made that expression patterns of markers may be altered during ageing (Boisvert et al., 2018; Rodríguez et al., 2014). Studies should incorporate more than one astrocytic marker for accurate identification and can choose from a variety of classical markers with different expression patterns (table 1-5) or newly discovered markers such as Ras-related protein Rab-6A (Melzer et al., 2021).

Pericytes have a varied morphological population dependant on functionality and location but are not as thoroughly characterised as astrocytes, exacerbated by confusion over what differentiates a pericyte from other contractile mural cells such as vascular smooth muscle cells, but this can be overcome via transcriptomics (Brown et al., 2019; Vanlandewijck et al., 2018). The lack of a universal classification system has resulted in confusing and contradictory literature and future correlations of pericyte expression and ageing need to be tentative until an agreement can be made. Compounding the issues of pericyte identification is the lack of a specific marker, with many studies colocalising two common markers, neural-glial antigen 2 (NG2) and PDGFRβ to confirm morphology (Jung et al., 2018). The use of whole organ clearing, and subsequent 3D immunofluorescent imaging is a new technique shown in ageing studies to detect changes to widespread changes to pericyte (NG2/ PDGFRβ) expression and could be applied to post-mortem samples from humans as well as rodent models (Chen et al., 2021).

The identification of BEC's has been more reliable than that of astrocytes and pericytes, due to phenotypic markers, such as Platelet Endothelial Cell Adhesion Molecule (PECAM-1) being unique and specific to BEC's throughout the parenchyma, therefore allowing for more certainty that the staining present is for the target cell (Elahy et al., 2015; Fernández et al., 2021). However, Mbagwu & Filgueira, 2020, noted that there are regional differences in PECAM-1 expression meaning that further studies should be carried out to identify location-based variation in ageing or other pathologies.

Table 1-5: Protein markers utilised in astrocyte expression studies.

Marker	Expression pattern	Astrocyte Phenotype	Specificity	References
Glial fibrillary acidic protein	• Cell body cytoplasm • Proximal processes	• Reactive	• Astrocytes • Neural progenitor cells	(Sofroniew & Vinters, 2010) (Ito et al., 2016)
Glutamate synthetase	• Cell body cytoplasm • Fine processes	• -	• Astrocytes • Oligodendrocytes	(Zhang et al., 2019) (Anlauf & Derouiche, 2013)
NMYC downstream-regulated gene 2 (NDRG2)	• Cytosol	• Non-reactive mature	• Predominately astrocytes	(Flügge et al., 2014)
Vimentin	• Cytoplasm • Fine processes	• Reactive	• Astrocytes • Endothelial cells	(O'Leary et al., 2020)
S100B	• Intracellular membranes • Cytoskeleton • Processes	• -	• Astrocytes • Oligodendrocytes • Epithelial cells • Neurons	(Brozzi et al., 2009)
ALDH1L1	• Extensive processes • Cell body	• -	• Astrocytes	(Yang et al., 2011)

1.7.2. Neuroimaging techniques

The main limitation of post-mortem techniques is that it is static and cannot visualise dynamic changes which may be crucial in understanding how dysfunction in ageing occurs over time. However, neuroimaging techniques can be utilised to overcome this which can be used in both *in vivo* and clinical applications (Breuer et al., 2017). Imaging allows for three-dimensional mapping of BBB function and can be repeated multiple times in the same animal, enabling longitudinal assessment of ageing effects in the same animal (Giridharan et al., 2019). There are multiple techniques which can be applied to BBB leakage in ageing, each with advantages and limitations (summarised in table 1-6).

Bors et al., 2018, utilised single photon emission computed tomography (SPECT) to investigate efflux transporters in ageing and found that P-gp expression was reduced with age in rats and correlated this with increased BBB permeability. Positron emission tomography (PET) scanning has also been applied in ageing studies (Ding et al., 2013; Yang et al., 2020) and has the advantage of using fluorine-18 emitters which can be readily available for labelling a wide variety of molecules (Breuer et al., 2017). Two-photon and multi-photon imaging have also been used to great effect when investigating BBB in ageing, especially when combined with optical coherence tomography, which allows for repeated measurements in animals without the need for toxic tracers (Bell & Zlokovic, 2009; Nyúl-Tóth et al., 2021). The most promising technique for ageing studies is DCE-MRI which primarily investigates BBB permeability via the measurement of intravenously injected gadolinium-based contrast agents (GBCA) extravasation from the blood to the parenchyma. This has been widely implemented in neurological studies in *in vivo* rat and mouse studies, as well as human studies, and the results have been comparable to post-mortem studies (Hoffman et al., 2017; Montagne et al., 2015; Senatorov et al., 2019)

Table 1-6: Advantages and disadvantages of imaging techniques for blood-brain barrier changes.

Imaging type	Advantages	Disadvantages	References
Positron emission tomography (PET)	• Small volumes of tracer needed. • Non-invasive	• Dynamic protocols complicated	(Breuer et al., 2017 ; Simoncic et al., 2017)
Computed tomography (CT)	• Easily available • Can be used on patients eliminated from MRI studies. • Quick process	• Iodide contrast exposes participants to radiation • Participants may have adverse reactions to contrast. • Low sensitivity reduces detailed scans	(Veksler et al., 2014)
Dynamic contrast emission- magnetic resonance imaging (DCE-MRI)	• Increased sensitivity to BBB changes • Gadolinium tracers eliminated exposure to radiation. • Multiple contrast agents for different study aims	• No standardised post-image analysis • High cost and operational expertise • Increased time to acquire images • Large time delays in sequential imaging • Signal-noise ratio can be high	(Heye et al., 2014 ; Varatharaj et al., 2019 ; Veksler et al., 2014)
Single photon emission compute tomography (SPECT)	• High sensitivity to contrast agent	• Low spatial resolution means low sensitivity to small changes. • Exposes participant to radiation	(Veksler et al., 2014)
Optical coherence tomography (OCT)	• Can look at large tissue areas in more depth. • Does not need tracers	• Low spatial resolution • Complicated analysis required	(Nyúl-Tóth et al., 2021)
Multiphoton microscopy	• Provides subcellular visualisation at 500-600µm depth. • Reduced photobleaching	• Hard to image sub-cortical regions, e.g. hippocampus	(Cho et al., 2011 ; Lee et al., 2018)
Arterial spin labelling magnetic resonance imaging (ASL-MRI)	• No tracer required. • Picks up subtle BBB changes	• Difficult to investigate small brain regions. • May not reflect dysfunction. • Time-consuming	(Gold et al., 2021 ; Ohene et al., 2021 ; Shao et al., 2020)

Age-related permeability changes have been found to be subtle in comparison to severe pathologies such as stroke and brain tumours, and so the molecular weight (Mw) of the contrast agent is an important consideration. Gadolinium has a Mw of approximately 550Da which may be too large for small permeability changes to BBB and so the subtle changes may not be detected using this methodology, so recent literature has explored the use of other agents with smaller Mw such as water. Approaches that aim to probe water exchange across the BBB can be performed using arterial spin-labelling (ASL) MRI sequences, eliminating the need for GBCA's (Ohene et al., 2021; Stringer et al., 2021). Mouse studies using a multiple-echo-time (multi-TE) ASL MRI have found that there is a 32% increase in water exchange between adult (7 months) and aged (27 months) animals (Dickie et al., 2019; Ohene et al., 2021).

Further optimisation of these protocols is required as many have focused on large regions of the brain such as the cortex and reproducibility issues combined with the need for higher resolution MRI may need to focus on smaller important regions such as the key age-related areas; the hippocampus and amygdala (Ohene et al., 2021; Shao et al., 2020). Multiple mechanisms of water exchange are responsible for permeability and so any leakage measured may not be due to ageing (Dickie et al., 2020). However, Ktrans also has limitations as it is influenced by the surface area of capillaries, meaning normalisation of vessel size and density is necessary for comparisons (Heye et al., 2016).

1.7.3. Molecular studies

Another recent advancement is the use of molecular studies, including RNA and single cell sequencing to enhance the analysis of gene expression profiles, enhancing immunostaining and imaging studies to investigate genetic changes (Huntley et al., 2014). Fewer studies have utilised the techniques (summarised in table 1-7) but have been able to identify differential expression patterns within BBB-associated cells in ageing. Digital spatial profiling is a new technique which aims to further advance the field via the simultaneous analysis of cell marker

Table 1-7: Molecular studies investigating ageing within the brain.

Study	Species	Cell types	Isolation method	Investigation
(Goodall et al., 2019)	Human, mouse	Microvascular	LCM	Transcriptomic and miRNA profiling
(Kumar et al., 2013)	Human	Bulk tissue and neurons	Bulk tissue and LCM	Microarray
(Simpson et al., 2011)	Human	Astrocytes	LCM	Microarray analysis of astrocyte transcriptome
(Ximerakis et al., 2019)	Mouse	25,including endothelial cells, astrocytes and pericytes	FACS	Single-cell transcriptomics
(Ximerakis et al., 2018)	Mouse	25,including endothelial cells, astrocytes and pericytes	FACS	Single-cell transcriptomics
(Almanzar et al., 2020)	Mouse	Multiple including endothelial cells	FACS	Single-cell transcriptomics
(Chen et al., 2020)	Mouse	Endothelial cells	Flow cytometry	Single-cell RNA sequencing
(Zhao et al., 2020)	Mouse	Endothelial cells	FACS	Single-cell transcriptomics
(Boisvert et al., 2018)	Mouse	Astrocytes	Ribotag	Microarray analysis of astrocyte transcriptome
(Orre et al., 2014)	Mouse	Microglia and astrocytes	FACS	Transcriptomics
(Davie et al., 2018)	Drosophila	Glia and neuronal cells	FACS	Single-cell transcriptomics
(Galatro et al., 2017)	Human, Mouse	Microglia	FACS	Transcriptomics
(Kiss et al., 2020)	Mouse	Endothelial cells	Centrifugation	Single-cell RNA sequencing
(L. Zhao et al., 2020)	Mouse	Whole brain	FACS	Single-cell sequencing

expression profiles on FFPE tissue allowing for regional investigations with no studies exclusively studying physiological ageing to date (Fadul et al., 2020).

1.8. Therapeutic strategies targeting aged blood-brain barrier.

As demonstrated in the above sections, the impact of age on the BBB is complex and can lead to a decrease in cognitive ability and the potential to cascade into neurodegeneration. Current strategies to modify the effects of blood-brain barrier disruption in ageing including changes to exercise and diet (Gaspar-Silva et al., 2023). Increasing exercise has shown in aged humans to decrease production of pro-inflammatory cytokines, such as IL-6 and TNF-α, as well as increase expression of SIRT1 both leading to a decrease in BBB permeability (Cho & Roh, 2022; Chupel et al., 2018). Interestingly, both studies exclusively used female subjects, suggesting a sex related effect of exercise and BBB rejuvenation. Within *in vivo* studies, similar affects were observed in ageing but only in the presence of apolipoprotein E (APOE), a protein associated with AD, suggesting that neurodegeneration may drive these changes as opposed to physiological ageing (Raulin et al., 2022; Soto et al., 2015). Dietary changes have also been observed to positively impact aged BBB as 20%-40% reduction in calories in mouse and human studies has increased cerebral blood flow and cognitive abilities (Calingasan & Gibson, 2000; Hoffman et al., 2017; Witte et al., 2009). Another dietary impact has been metabolite increase as both resveratrol and nicotinamide adenine dinucleotide additions have enhanced cognitive function linked to increased SIRT1 expression in ageing (Cicero et al., 2019; Gocmez et al., 2016; Xie et al., 2019).However, one of the main challenges in implementation of these changes in the aged population is the decreased motor capabilities, limiting exercise and inability to change diets, limiting the impact these can have on the wider populace.

Pharmacologically, there has been some therapeutic strategies available targeting ageing, although these have been preferentially focused on models of AD (Bussian et al., 2018; Yao et al., 2024). Both studies used *in vivo* mouse models, with either genetic targeting in INK-ATTAC mice or administration of common senolytic combination, dasatinib and quercetin to target microglia and reduce BBB permeability. treatment of age-related diseases, such as AD (Chu et

al., 2022). Senolytics, designed to target senescence cells by inducing apoptosis, have demonstrated rescue of cognitive ability in Tau Senomorphics, anti-inflammatory drugs, have also been observed *in vivo* to rescue effects on the BBB during ageing related to AD. There are different mechanistic approaches to anti-inflammatories such as inhibition of NF-kB pathway or promotion of apoptosis via molecules such as metformin and curcumin (Liu et al., 2017; Lopes-Paciencia et al., 2019; Moiseeva et al., 2013; Sun et al., 2018). An alternative strategy for reducing inflammation is the targeting of specific inflammatory cytokines (Chu et al., 2022). Reduction in AD pathology was observed along with rescue of cognition in rats administered with Tocilizumab, an IL-6 receptor antagonist, or anakinra, an IL-1β receptor antagonist in macaques (Batista et al., 2021; Elcioğlu et al., 2016). The conservation of effects across species lends credence to the therapeutic possibilities of IL family antagonism.

1.8.1. Alternative administration routes avoiding BBB

Only <2% of drug molecules can pass through the healthy BBB with an average maximum size of 400 Da, meaning that many potentially viable therapies cannot access the target brain region (Pardridge, 2005; Teleanu et al., 2022). Other physiochemical properties also hinder the transport of molecules transcellularly such as lipophilicity, hydrogen bonds and polarity (Chikhale et al., 1994; Pardridge, 2012). Ideally, molecules need to have less than 6 hydrogen bonds, which could be achieved via chemical structure modification and be non-polar to cross through the BBB (Geldenhuys et al., 2015; Kadry et al., 2020b)

Different administration routes have been investigated as potential diversions around the BBB including intracerebral, intrathecal, and intranasal (Mittal et al., 2022). The main issue with both intracerebral and intrathecal routes is the highly invasive nature of the techniques, rendering it unusable unless for severe neuropathology. This means that discussed therapies above like Tocilizumab, are not relevant to physiological ageing studies (Elcioğlu et al., 2016). Furthermore, Furtado et al., 2018 states that only 1-2% of drugs administered this route pass through to the parenchyma, making it inefficient as well as invasive. Intranasal administration is less invasive than other methods and bypasses the BBB and has been shown in an *in vivo*

obesity model to admit large 6500 Da neuropeptide into the brain with high accumulation in many brain regions (Jeong et al., 2022; Nonaka et al., 2008). Solid nanoparticles containing Efavirenz, a Human Immunodeficiency Virus therapy, successfully crossed into the brain demonstrating proof-of-concept for this route (Gupta et al., 2017). However, the surface area of the nasal cavity limits the amount of therapy administered in one injection and so is a limitation of delivery system, as shown in chemotherapy trials (Sarin, 2009). Low water solubility of drugs also is a hinderance as it means that most of the drug volume does not reach the target brain region, but potential solubilises or encapsulation into nanoparticles may alleviate this problem (Pires et al., 2022).

Ultrasound has also been used to transiently open the BBB to allow for therapeutics to enter the brain without need for invasive techniques (Gandhi et al., 2022). Studies in glioblastoma mice models have shown that the use of ultrasound allows for the increased permeability of both paracellular and transcellular pathways without damaging the affected tissue areas to successfully administer drugs (Zhang et al., 2017). Human clinical trials have utilised this technique in for safety tests in AD, brain cancers and motor neuron disease as well as *in vivo* studies highlighting the wide-ranging use of this method (Abrahao et al., 2019; Carpentier et al., 2024; Lipsman et al., 2018; Tsai et al., 2018). However, potential side effects of neuroinflammation, cell apoptosis and haemorrhaging have been observed in *in vivo* studies, showing that further experimental work to confirm safety needs to be completed (McMahon & Hynynen, 2017; Shin et al., 2018). Another limitation of this method is the optimum size of potential drugs or carriers, such as nanoparticles, to cross through the openings. Ohta et al., 2020, demonstrated the differences between *in vitro* and *in vivo* size requirements, showing that smaller gold nanoparticles, 15 nm diameter, were the best at penetrating through the BBB whilst cell models showed a larger size permeability.

1.9. Nanoparticle drug delivery

The above techniques and drugs have all either included drugs that pass through the BBB or bypass the barrier, with major limitations on feasibility surrounding safety, dose amount and

invasiveness. One alternative that is currently gathering interest is the use of nanoparticles which can pass through the BBB (Chu et al., 2022; Juhairiyah & de Lange, 2021; Mittal et al., 2022). Nanoparticles can be categorised into diverse types; lipid based, inorganic and polymeric which all have promise in the passage through the BBB. Table 1-8 summarises previous nanoparticle studies in ageing or age-related neurodegeneration.

1.9.1. Lipid-based nanoparticles

Lipid-based nanoparticles, also called liposomes, are primarily composed of phospholipid bilayer with the ability to encapsulate both hydrophilic and hydrophobic drugs (Juhairiyah & de Lange, 2021). Within the CNS, clinically available liposomes have been used in meningitis, glioblastoma and other brain tumours, highlighting the liposomal ability to pass through the BBB in pathology (Domínguez et al., 2005; Lippens, 1999; Lu et al., 2024). Liposomes are not capable of passing through BBB via paracellular transport, but many *in vivo* studies have documented the transport of liposomes through RMT, especially caveolae-mediated transcytosis (Al-Ahmady et al., 2019; Liu et al., 2024; Reginald-Opara et al., 2022).

Size of liposomes is crucial for the transport through the BBB and classically are optimal at 100 nm (Bitounis et al., 2012; Morse et al., 2022). However, in models of traumatic brain injury and AD, it has been noted that liposomes up to 200 nm can cross the BBB, with the increasing size being advantageous to the amount of drug cargo loaded (Cruz et al., 2016; Rodrigues et al., 2020). Compositionally, ‘naked’ liposomes consist of phospholipids, but it has been shown that these struggle to cross the BBB, meaning functionalisation elements must be added to modify physical properties (Teixeira et al., 2023). There are several types of functionalisation strategies, one of the most common is the addition of polyethylene glycol (PEG) which reduces liposomal binding to plasma, increasing circulation time within the body (Raju et al., 2023). PEGylation of liposomes has been observed to increase liposome effectiveness *in vivo* within cancer, inflammation and viral settings (Diniz et al., 2020; Hattori & Hattori, 2016; Mondal & Ghosh, 2023). Cholesterol can also be added to increase the stability of liposomes and has also been demonstrated to increase liposome uniformity by decreasing polydispersal index

Table 1-8: Nanoparticle studies in physiological ageing.

Study	Species	Age/ weight (months/gram)	Target	Nanoparticle type	Size (nm)
Age					
(Bony et al., 2021)	Mouse	12	Claudin-1	Gold	3
(Tracy et al., 2023)	Mouse	13-18	CD44	PGLA	200
(Rehman et al., 2020)	Mouse *in vitro*	-	Transferrin	Gold	2
Alzheimer's disease					
(Meng et al., 2015)	Mouse	2-3	Aβ	Liposome	90-163
(Mourtas et al., 2014)	*In vitro*	-	Aβ	Liposome	116-159
(Kuo et al., 2020)	Rat	N/S	ApoE	Liposome	157
(Neves et al., 2016a)	*In vitro*	-	ApoE	SLN	<200
(Lazar et al., 2013)	Mouse	10-12	Aβ	Liposome	207
(Fidelis et al., 2019)	Mouse *In vitro*	3	Aβ	Liposome	291-312
(Zhang et al., 2020)	Rats	200-300g	Cognitive function	Gold	10-15
(dos Santos Tramontin et al., 2020)	Rat	250-300g	Inflammation	Gold	20
(Yang et al., 2021)	Mouse	25-30g	NF-kB	PGLA	200
(Mathew et al., 2012)	*In vitro*	-	Aβ	PGLA	150-200
Stroke					
(Amani et al., 2019)	Mouse *In vitro*	2/3	Inflammation	Selenium	12
(Al-Ahmady et al., 2019)	Mouse	3	Untargeted	liposome	100
(Al-Ahmady et al., 2019)	Mouse	3	Untargeted	Liposome	100
(Kim et al., 2009)	Rat	1/2	tPA	Liposome	150-170
(Chen et al., 2012)	*In vitro*	-	tPA	Silica-coated magnetic	100
(Lv et al., 2018)			ROS	Polymeric	163
(Santos et al., 2018)	Mouse	N/S	Untargeted	Dendrimer	N/S
Neuroinflammation					
(Mi et al., 2022)	*In vitro*	-	NF-kB	Selenium	30-80
(Gonzalez-Carter et al., 2017)	*In vitro*	-	H_2S-synthesizing enzymes	Silver	50
(Ralvenius et al., 2024)	Mouse *In vitro*	2	PU.1	Liposome	N/S

*N/S= not stated, PGLA=Poly (lactic-co-glycolic acid), ApoE= Apolipoprotein E, SLN= solid lipid nanoparticles, ROS= reactive oxygen species, NF-kB= Nuclear factor kappa-light-chain-enhancer of activated B.

and shifting the morphology to the desired spherical shape (Kaddah et al., 2018). However, caution must be observed in increasing cholesterol concentration as the increase causes an increase in size, which can reduce overall BBB permeability (Briuglia et al., 2015).

The transferrin family, which can target receptors exclusively expressed in brain endothelium, have been utilised to increase BBB permeability *in vitro* resulting in greater uptake of drug into the parenchyma (Johnsen et al., 2017). This has further been explored *in vivo* and AD and could have potential in the ageing setting (Diniz et al., 2020; Kong et al., 2020; Lee & Leong, 2020; Yang et al., 2021). Lactoferrin is a specific member of the transferrin family and has been shown *in vitro* in human endothelial cells and *in vivo* in an AD rat model to increase BBB permeability and targeting to the brain (Kuo & Wang, 2014; Meng et al., 2015). Within the rat model, curcumin encapsulated liposomes with lactoferrin displayed a 1.39-fold increased parenchymal infiltration in comparison to control liposomes without the glycoprotein. Other functional options are APOE4, but this is not as translatable to ageing with the lower APOE expression, or insulin (Neves et al., 2016; Ross et al., 2018). Further specificity can be achieved via the conjugation of antibodies to the surface of the liposomes, the use of antibody scFv46.1 has demonstrated a 10-fold increase in brain uptake *in vitro* and uses the RMT transcytosis route *in vivo* (Georgieva et al., 2020; Ye et al., 2022).

Although limited studies have been conducted on physiological ageing, the developments in the AD field show promise and could be adapted to target age-related effects in non-AD brains, particularly as transcytosis increases during ageing, providing a mechanistic transport route (Yang et al., 2020).

1.9.2. Polymeric nanoparticles

Polymeric liposomes are biodegradable and consist of a polymer matrix for stabilisation and come in many forms; micelles, dendrimers, polymers (Chu et al., 2022; Mittal et al., 2022).

Dendrimers are branched and possess multiple drug attachment sites which is advantageous for dual drug therapies, however, increased toxicity has been linked to branching, so this must be controlled (Al-Azzawi et al., 2018). There are multiple *in vivo* studies within the AD field demonstrating viability of dendrimers and can reduce inflammation by targeting microglia which could potentially be translated into reduction in imflammaging phenotypes (Liu et al., 2021; Zhang et al., 2016). One concern with dendrimers is the cytotoxicity of some components, as polyamidoamine (PAMAM) amine groups protonate and cause cell membrane disruption. This can be counteracted by low concentrations of PAMAM or by functionalisation like liposomes, for example PEGylation (Arbez-Gindre et al., 2023).

Other types of polymeric nanoparticle are composed of other polymers such as poly(alkyl cyanoacrylate) (PGLA) which does not have the same cytotoxicity as PAMAM (Chu et al., 2022). These can then be further functionalised to cross the BBB and have been shown to decrease ROS, TNF-α and IL-6 as well as increase cognition when conjugated with peptide cyclic CRTIGPSVC in AD (Huang et al., 2017). Tracy et al., 2023, used a PGLA nanoparticle conjugated to CD44 and demonstrated that the particles infiltrate the astrocytes and microglia in the hippocampus of both AD and age-control mice but not young littermates. This lends credence to utilising nanoparticles in ageing and were 200 nm in size, with further work incorporating therapies the next step.

1.9.3. Inorganic nanoparticles

Inorganic nanoparticles are made of varied materials, normally metallic in nature, such as gold (AuNP), silver and magnetic nanoparticles (Martano et al., 2022). One of the most promising inorganic nanoparticles are AuNP as these have shown low toxicity compared to polymer varieties and can range between 3-200 nm (Chu et al., 2022). However, some studies still note a toxic element in high concentrations, so this must be considered in all AuNP studies (Soenen et al., 2011). One advantage of AuNP's is that they can be smaller than other nanoparticles and reduce effect of Aβ in AD, therefore have a high chance of transport through BBB (Gao et al., 2015). In the context of physiological ageing, there is a small number of recent studies which

document that AuNP cross the BBB in age both *in vitro* and *in vivo* (Bony et al., 2021; Rehman et al., 2020). Bony et al., 2021, used 3 nm AuNP targeting claudin-1 in 2- and 12-month mice demonstrating a non-significant increase in AuNP infiltration but a decrease in BBB permeability. Increasing the age of the mice to represent older ages (18-24 months in C57BL/6) mice would be beneficial to see long-term physiological ageing effects.

1.10. Aims and objectives.

The overall aims of this research project were to investigate the changes to the BBB during physiological ageing and the potential to exploit age-related deviations using nanoparticles as drug delivery carriers of therapeutics. Multiple studies were conducted within the murine *in vivo* setting to explore changes to the BBB and associated cells in ageing and neuroinflammation. Particular attention was paid to the sex differences observed during ageing and relation to drug delivery. Further encapsulation of an anti-inflammatory therapy to nanoparticles investigated the efficacy of targeting age-related changes.

1.10.1. Objectives and Hypotheses

The aims of the thesis are as follows:

1. To enhance the understanding of age-related changes to the BBB and associated cells in female and male mouse brain (Chapter 3)
2. To determine if liposome nanoparticle infiltration was increased during physiological ageing and inflammation (Chapter 3 and 4)
3. To assess changes to BBB ageing when exposed to an LPS-induced inflammatory phenotype (Chapter 4)
4. To explore the potential of conjugating IL1-ra to liposomes in the context of reducing inflammation in ageing murine brain (Chapter 5)

Hypotheses

1. Physiological ageing will decrease BBB function through increased permeability and inflammatory profile combined with decreases in cell expression
2. Nanoparticle infiltration will increase in physiological ageing and neuroinflammation
3. IL1-ra-liposomes will decrease inflammatory profile of aged brain

2. Materials and Methods

2.1. Contribution statement

All research methodology, data collection, analysis and thesis writing were completed by the author of this thesis. The only methodological exceptions were as follows; Dr Zahraa Al-Ahmady completed intravenous injections of mouse tail vein and MATLAB analysis of MRI data, Dr Rob Morris and Jim Hall ran the MRI machine, Dr Dominic Craske and Dr Graham Hickman completed TEM imaging and Dr David Boocock and Clare Coveney completed mass spectrometry of protein samples.

2.2. Animal care and husbandry

2.2.1. Animal Care

All mice were housed according to the 'Code of Practice for the Housing and Care of Animals Used in Scientific Procedures' in conjunction with the United Kingdom Home Office requirements. The design of the study followed the scientific objectives of United Kingdom's Act 1986 by causing minimum distress or suffering to the animals. All mice were housed at the bioscience support facility (BSF) at Nottingham Trent University under PP2325961 project licence.

2.2.2. Animal Housing

C57BL/6 mice (Charles River, UK) were housed in Techniplast Sealsafe plus cages with up to 4 mice per cage containing corncob bedding and a range of environmental enrichment items (Datesand Ltd, Cheshire, UK). The animal unit was kept under controlled conditions of 12-hour light/dark cycle beginning at 7:00am; temperature of 20-24°C, humidity of 45-64% and ventilation of at least 15 air changes per hour. Prior to the onset of study, mice were acclimatised for a period of at least 5 days in the BSF. At the onset of the study, each animal per cage was randomly selected via members of the university BSF, and ear-notch completed for further identification. For the duration of each study, mice were fed *ad libitum* with standard chow (Rodent 2018, Envigo global certified diet, USA) and tap water.

2.2.3. Animal Research: Reporting of *In Vivo* Experiments (ARRIVE) guidelines

All studies within this body of research follow ARRIVE guidelines where possible including blinding and randomisation to reduce bias within analysis. Details of this can be found in Table 2-1 and throughout the body of work.

2.3. Study design and power calculations

Each study design, including mouse age, sex and group number is noted in individual results chapters. Power calculation to determine the optimal number of mice to observe DiI-liposome infiltration was based on estimated effect size (m1-m2) of 2.07 e-04 and standard deviation of 1.02 e-4 suggesting a sample size of 5 (Al-Ahmady et al., 2022).

2.4. Behaviour testing

To determine the effect of ageing on cognitive function *in vivo*, mice underwent novel object and novel location recognition testing. These tests allow for investigation into the inherent preference of mice to investigate novel objects over familiar objects and as mouse cognition declines, the ability to distinguish between novel and familiar objects also declines. This can then be represented as a ratio of investigation times and used to determine cognitive ability of the aged mice.

2.4.1. Behaviour validation

Before the main cohort was analysed for cognitive decline, optimisation tests were carried out on a separate cohort of male C57BL/6 mice (n=12) which were then randomly split into trial groups of 3. Eight objects (table 2-2) were selected for novel object validation based on being of similar height and ability of mice to climb. Mice were then handled for at least 5 days by the investigator to allow for familiarisation with handling and movement. Each group of 3 were randomly assigned an object combination of the eight objects over 3 days to test preferences or aversion to any object, to a total of 10 tests per mouse. Each mouse was exposed to a 30cm x30cm plastic box (Ikea, UK) with each of the two objects positioned at diagonally opposite

Table 2-1: ARRIVE guidelines. Information detailing study adherence to ARRIVE guidelines.

ARRIVE guidelines	Chapter 3	Chapter 4	Chapter 5
Study design	• 3,6,12,18 and 22 month females • 3 and 18 month males • Experimental unit: single animal	• 3 and 18 month female mice • 0, 0.25 or 1 mg/kg LPS • Experimental unit: single animal	• Vehicle, free drug formulation and liposomal drug formulation • Experimental unit: Cage of animals
Sample size	• Based on power calculations of liposome infiltration • See chapter 3 for group size	• Based on power calculations of liposome infiltration • See chapter 4 for group size	• Power uncalculated • See 5 chapter for group size
Inclusion and exclusion criteria	• All animals initially included • Exclusion based on: - Insufficient perfusion - Tissue loss during immunostaining - Death of animal prior to perfusion • Find exact n-numbers in chapter	• All animals initially included • Exclusion based on: - Insufficient perfusion - Tissue loss during immunostaining - Death of animal prior to perfusion • Find exact n-numbers in chapter	• All animals initially included • Exclusion based on: - Insufficient perfusion - Tissue loss during immunostaining - Death of animal prior to perfusion • Find exact n-numbers in chapter
Randomisation	• No randomisation possible	• Randomisation of brain tissue by secondary researcher after extraction from animal	• Each experimental unit (cage) included animal from each study group
Blinding	• No blinding possible	• Blinding of brain tissue from researcher 1 by researcher 2 after extraction from animal	• Blinding of study group from researcher 1 • Researcher 2 performed all injections
Outcome measures	• See chapter 3	• See chapter 4	• See chapter 5
Statistical methods	• See chapter 3.2	• See Chapter 4.2	• See chapter 5.2
Experimental animals	• C57BL/6 mice	• C57BL/6 mice	• C57BL/6 mice
Experimental procedures	• See chapter 3.2	• See chapter 4.2	• See chapter 5.2
Results	• See chapter 3.3	• See chapter 4.3	• See chapter 5.3

corners of the box, approximately 2.5cm away from the box edge. Each session was recorded using Any maze (version 7.1) using a digital USB camera (Stoelting, USA) for a total of 5 minutes.

Table 2-2 Objects for behavioural studies.

No	**object type**
1	Bottle
2	Tube
3	Pentagon stack
4	Cylinder stack
5	Toblerone
6	square pyramid
7	20ml tube
8	clear 50ml

Mouse videos were then watched by the researcher and time of investigation of each object noted and totalled. Each video investigation time was then calculated via the following formula:

$$Discrimination\ index = \frac{Investigation\ time\ of\ object\ A}{Investigation\ time\ of\ object\ A + object\ B}$$

After calculations, any object combination with a discrimination index above 0.2 was excluded from further study. The intention is to have a low discrimination index, indicating that the mice do not have an inherent attraction to one object. Once objects were identified with a low discrimination index, 3 combinations with one object (object 1) were chosen to move forward to behavioural testing.

2.4.2. Acclimatisation to arena

To determine the cognitive effect of ageing incorporating multiple brain regions, novel object recognition (NOR) tests were carried out. Mice were handled for 5 consecutive days prior to the beginning of any testing by the researcher in the behaviour suite to ensure acclimatisation to the environment and handling. During this time, mice were transported isingly housed and placed into empty arena. Before each experimental run and each individual mouse, the arena was cleaned with 70% ethanol to remove any scent which would influence mouse behaviour.

2.4.3. Novel object recognition

Initially, mice were trained to recognise the familiar object by being placed into an arena with two identical objects, object 1, for 10 minutes. These were secured in opposite corners approximately 2cm from the edge of the arena. Within each experimental group, mice were assigned one of top left or top right to set the starting positions of the objects to ensure no place bias in experiment. After 10 minutes, the mice were removed from the arena and returned to single housing whilst all objects and arena were cleaned with 70% ethanol. To investigate short-, medium- and long-term cognition, mice were tested with inter trial periods of 5 minutes, 1 hour and 24 hours after the initial training video was completed within the same mouse. Mice were returned to the arena with 1 familiar object remaining in the same position throughout all trials and a different novel object for each timepoint measured. This was randomised throughout the group to ensure all 4 corners were equally used as the familiar object position to remove bias. Immediately after mice entered the arena, video was recorded for 5 minutes.

2.4.4. Novel object location

To test changes to hippocampal based cognition, mice were also subjected to novel object location (NOL) experiments (Denninger et al., 2018). This followed a similar formula to that of NOR but instead of objects changing, the position of the objects was altered to test spatial learning. Briefly, the objects remained the same as the training objects and the same position was selected as familiar as the NOR test for consistency. The novel object was then tested with an inter-trial period of 1 hour and 24 hours respectively, moving the novel object to a different corner of the arena each time.

After both NOR and NOL testing, each video was manually scored by the researcher and overall investigation time of each object was determined. The discrimination index of each trial period was calculated using the equation for each age cohort. Normality was tested utilising the Shapiro-Wilk test and statistical significance determine via either one-way analysis of variance

(ANOVA) and Tukey's multiple comparison test or Kruskal-Wallis test followed by Dunn's multiple comparison test based on data normality.

2.5. Liposome preparation

2.5.1. DiI-liposome

To study the uptake of liposomes to the brain and peripheral organs, DiI-liposomes were prepared utilising the thin film hydration method followed by extrusion (Zhang, 2017). Lipids used in liposomes preparation were as follows: 1,2-distearoyl-sn-glycero-3-phosphoethanolamine-N-[methoxy (polyethylene glycol)-2000 (DSPE-PEG-2000), hydrogenated soy phosphatidylcholine (HSPC) (Lipoids, UK) and 1,2-distearoyl-sn-glycero-3-phosphoethanolamine-N-[methoxy (polyethylene glycol)-2000 (ammonium salt) (DSPE-PEG(2000)Maleimide) (Merck, Germany), DiI (Invitrogen, UK) and Cholesterol (Sigma-Aldrich, UK).

Before preparation of liposomes, individual lipid components were dissolved in 4:1 mixture of chloroform: methanol to concentrations and overall ratio HSPC: Chol: DSPE-PEG2000 (56.3:38.2:5.5 mol/mol%) to an overall concentration of 12.5mM. Once the DiI had been added to the mixture, all following procedures were protected from light. Lipids were made to a total of 4ml per batch in a round bottomed flask and solvents were evaporated using a rotary evaporator (IKA, RV 10, UK) for 1 hour at 130rpm with the water bath set at 40°C. Lipids were hydrated using 4-(2-Hydroxyethyl)-1-Piperazineethanesulfonic Acid (HEPES) buffer (20mM HEPES, 150mM sodium chloride (NaCl), pH 7.4) and sonicated for 1 minute in a bath sonicator (VSC300TH, VWR, UK). Liposome size was then reduced via the extrusion method utilising 800nm, 200nm and 100nm polycarbonate filter membranes (Whatman, VWR, UK) for 5:5:20 times respectively on a mini extruder (Avanti Polar Lipids, Alabaster, AL). Prior to delivery into *in vivo* models, liposomes were filtered using 0.2 µm filter (Merck Millipore, UK) in a sterile environment.

2.5.2. IL1-ra-liposome

To study the effect of Interleukin 1-recpetor antagonist conjugated to liposomes (IL1-ra-lip), liposomes without DiI were prepared utilising the same techniques as DiI-liposomes. Liposomes were produced to the final volume of 6 ml per batch and composed of: HSPC: Chol: DSPE-PEG2000: DSPE-PEG-Malemide (56.3:38.2:3.5:2 mol/mol%) to a final concentration of 25 mM. Under deoxygenated conditions, IL1-ra was thiolated via combination with Traut's reagent (Thermofisher, UK) at 1:20 ratio for 1-hour continuous stirring at room temperature to produce 4.472 mg IL1-ra: 1 ml buffer (pH 8, 25 mM HEPES, 140 mM NaCl, 3 mM ethylenediaminetetraacetic acid (EDTA)). To remove unreacted Traut reagent, the solution was run through Sephadex G50 (Sigma-Aldrich, UK) columns in triplicate, the columns were pre-equilibrated to deoxygenated HBS buffer to decrease oxygenation.

Thiolated IL1-ra (Kineret, Amgen, USA) and liposomes were combined at 1:10 molar ratio in pH 7.4 HBS buffer at left continuously stirring at room temperature overnight in deoxygenated conditions. To stop the reaction and block uncoupled liposomes, cysteine hydrochloric acid (Thermofisher, UK) was added to a final concentration of 1mM (Loomis et al., 2010). Conjugated IL1-ra-liposomes were then concentrated via centrifugation in Viva spin 20 columns (Sartorius, Fisher, USA) at 10000 revolutions per minute (rpm) for 10-minute sessions until each batch has a 2 ml volume. Unconjugated IL1-ra was removed via running through a Sepharose CL-4b column (Sigma-Aldrich, UK) hydrated with pH 7.4 HBS in triplicate. IL1-ra protein concentration was determined and further solutions further concentrated to 1 mg/ml via centrifugation and stored at 4°C for up to a week before use.

2.6. Liposome characterisation

2.6.1. Size and zeta potential

To characterise the DiI-lip, dynamic light scattering (DLS) was used to determine size and zeta potential (surface charge) of each liposome. Each batch was diluted 1:100 using purified and filtered with distilled water to a total of 3ml in a disposable cuvette. To measure zeta potential,

the samples were measured in a 1ml zeta cuvette in a 1:10 dilution to total of 1ml. Measurements were taken in triplicate on NanoPlus (Particulate Systems, USA) via the software NanoPlus version 5.22/3.00 (Particulate Systems, USA) with date displayed as average ± standard error or mean (SEM).

2.6.2. Fluorescence intensity

To check fluorescence intensity of DiI-lip before *in vivo* administration, the Carry UV-VIS compact spectrophotometer (Agilent, UK) was employed, with samples diluted in HEPES buffer to a concentration of 1:800 to a final volume of 4 ml. Measurements were taken at excitation 540nm and emission 567 wavelengths in triplicate and expressed as average ± SEM.

2.6.3. Protein concentration

To determine the amount of IL1-ra protein conjugated to the surface of liposomes, the enhanced pierce bicinchoninic acid (BCA) assay (Thermofisher, UK) was utilised according to manufacturer guidelines. This colorimetric assay worked via the reduction of Cu^{2+} to Cu^{1+} resulting in the formation of BCA/copper complexes forming a purple colour with increasing protein concentration (Cortés-Ríos et al., 2020). Each sample of IL1-ra-lip was diluted to a ration of 1:20 in BCA reagent (reagent A and reagent B, 1:50) to a total of 600 µl. IL1-ra was used as the protein standards and diluted to a range between 1-0.005 mg/ml in RIPA buffer, again to 600 µl. Samples were then heated at 60° for 30 minutes in darkness followed by reading on Tecan plate reader (Tecan, Switzerland) at 562 nm at 37°C. Protein concentration of liposomes was then calculated via extrapolation of the standard curve.

2.6.4. Lipid composition

To quantify the phospholipid concentration, present within a liposome sample, the Stewarts assay was implemented. IL1-ra-lip stocks were diluted to 2.5 mM in HEPES buffer and then added to chloroform and Stewart's reagent (Sigma-Aldrich, UK) (ratio 1:50:25) and vortexed to ensure sufficient reagent mixing. Standards were created from liposomes of each corresponding IL1-ra-lip batch prior to protein conjugation ranging from 25- 0.78 mM. All

samples were incubated for 1 hour at room temperature protected from light before being centrifuged at 13000 rpm for 1 minutes. Samples from the chloroform layer were measured at 280-800 nm using Cary UV-VIS spectrophotometer (Agilent, USA) and lipid concentration determined via standard curve extrapolation at 485 nm.

2.7. *In vivo* injections

2.7.1. Injection of permeability markers and DiI-liposomes

Albumin fluorescently conjugated to AF488, 5mg or 3000 Mw Dextran fluorescently conjugated to AF488 (Thermofisher, UK) were reconstituted to 10mg/ml in sterile phosphate buffered saline (PBS) prior to intravenous (I.V) injections. Individual mice were anaesthetised via inhalation using oxygen and nitrous oxide followed by isoflurane and tail heated to 37°C using heat pad to allow for tail vein to be injected. Mice were then I.V injected by either Dr Zahraa Al-Ahmady or principal researcher with the following combinations of fluorescent particle: DiI-lip, DiI-lip + albumin or DiI-lip + dextran to 10mg/ml. Animals were monitored after cessation of anaesthesia to ensure full recovery.

2.7.2. Injection of LPS

LPS (E.coli 0111:B4, Sigma-Aldrich, UK) was appropriately diluted in sterile PBS from stock to either 1 mg/kg or 0.25 mg/kg and kept on ice until administration. Individual mice were I.P injected with the designated dose or PBS vehicle control. Animals were monitored daily after injection for clinical observations.

2.7.3. Injection of IL1-ra-lip

Individual mice were anaesthetised via inhalation using oxygen and nitrous oxide followed by isoflurane and tail heated to 37°C using heat pad to allow for tail vein to be injected. Mice were then I.V injected by Dr Zahraa Al-Ahmady with either IL1-ra-lip, IL1-ra (Swedish Orphan Biovitrum, Sweden) or HBS vehicle control. Animals were monitored after cessation of anaesthesia to ensure full recovery.

2.7.4. Animal culling

2-hours post I.V injection, animals were intraperitoneally (I.P) injected with 200mg/ml dolethal (Vetoquinol Ltd, UK). Mice were then transcardially perfused with ice cold 0.9% saline for 2 minutes for DiI-lip studies followed by 4% paraformaldehyde (Sigma-Aldrich, UK) in 0.1M PBS for a further 2 minutes for albumin and dextran studies. Brain, spleen, liver, lung, heart and kidneys were then weighed and imaged using *In Vivo* Imaging system (IVIS) before disposal of all organs except brain and spleen. For DiI-lip only, LPS and IL1-ra-lip studies, brain hemispheres were separated, and one hemisphere and spleen were snap frozen in liquid nitrogen for protein or molecular studies. The other hemisphere, and brains from albumin and dextran studies, were submerged in 4% PFA and kept at 4°C for 48 hours. Brains were then transferred to 30% sucrose (Sigma-Aldrich, UK), acting as a cryoprotectant, for a further 48 hours and frozen in isopentane (Sigma-Aldrich, UK). All hemispheres and spleens were stored in ultra-low temperature freezers until further analysis was completed.

2.7.5. Paraformaldehyde (PFA) preparation

4% PFA was prepared by heating 1x PBS to 60°C prior to adding 40g/l PFA. Sodium hydroxide pellets (Sigma-Aldrich, UK) were added to the solution to allow for PFA dissolution prior to removing the solution from heat and keeping at room temperature for minimum 1 hour. PFA was then transferred to 4°C overnight and then filtered with 0.2µm bottle filter (ThermoFisher, UK) and pH was adjusted to 7.5 with 1M hydrochloric acid (Sigma-Aldrich, UK).

2.8. *In vivo* optical imaging and analysis of DiI-lip, Albumin and Dextran for brain and peripheral organs

To assess the infiltration of DiI-liposomes, albumin or dextran into the mice, optical imaging of brain and peripheral organs (spleen, lung, heart, liver, kidney) was undertaken immediately following cardiac perfusion. Organ images were acquired on the IVIS Lumina II Imaging System (Caliper Life Sciences Corp, USA) at specific settings dependant on fluorophore and target organ including exposure time and excitation and emission filters (table 2-3). Image analysis

was completed on Living Image software 4.5.2 (Caliper Life Sciences Corp, USA) on fluorescence efficiency settings whereby each emitted photon was equal to that of individual pixels. Infiltration of each target was quantified via equal regions of interest and displayed as the ratio of emitted light and incident light (total efficiency). For representative images, each organ was adjusted to minimum and maximum scales based on visualising the quantifiable results (table 2-2).

Table 2-3: Settings for organ optical imaging. Details for DiI-liposome, albumin, and dextran imaging of either brain or peripheral organs detailing exposure time, binning, field of view (FOV), excitation and emission filters and minimum and maximum scale for representative images.

Target	Organ	Exposure (ms)	Binning	FOV	Excitation (nm)	Emission (nm)	Min scale	Max scale
DiI-liposome	Brain	1	(M) 4	10	520	570	5.00e-5	1.00e-3
	Peripheral organs	1	HR (4/2)	12.5	520	570	2.00e-3	1.50e-2
Albumin	Brain	0.5	HR (4/2)	10	480	520	1.00e-4	3.55e-4
Dextran	Brain	0.5	M (4)	10	480	520	2.00e-4	1.00e-3

2.9. Mouse plasma extraction and storage

Prior to cardiac perfusion, a 21-gauge needle (BD Microlance, Switzerland) was inserted into the heart and blood extracted and placed into heparinised tubes (Sarstedt, Germany) and centrifuged at 2000g for 5 minutes. The serum was then removed and stored in ultra-low temperature freezer for downstream ELISA analysis.

2.10. Tissue sectioning

Immunofluorescence and immunohistochemical staining were utilised to investigate expression of different NVU components of the brains harvested from male and female ageing cohort. Each brain hemisphere was covered in optical cutting temperature (OCT; VWR, UK) before sectioning (30µm thickness) on the Leica CMV1860 cryostat.

2.11. Immunofluorescence staining

Tissue slides were then stored in ultra-low temperature freezers until use whereby they were defrosted for 20-minutes, and OCT removed via x1PBS wash for 10 minutes. For DiI-lip infiltration, the slides underwent no further processing and immediately coverslipped (see below). Slides were then rinsed in tap water and left vertically to dry at 37°C for 1 hour. Specifically optimised stains (table 2-4) required antigen retrieval; slides were incubated in 100°C 10mM EDTA Ph6 (Sigma-Aldrich, UK) for 10 minutes before washing with ultrapure water in triplicate. All immunofluorescence stains then underwent a blocking step with 5% species specific serum for a further 1 hour (Jackson Immunoresearch Laboratories Inc, USA) in a humidifying chamber. Primary antibodies specific to protein of interest were incubated at 4°C overnight at optimised concentrations (table 2-4). For each run, a negative control slide (without any primary antibody) was included with the same protocol except instead of primary antibody, was incubated in blocking solution.

After 24 hours, primary antibodies were removed from the slides via triplicate washes of 0.1% PBS-tween 20 (Sigma-Aldrich, UK) before being incubated at room temperature for an hour in secondary antibody corresponding to species of blocking and primary antibody steps (table 2-4), ensuring a humid and dark environment. Post-incubation, slides were again washed in 0.1% PBS-tween20 for 5 minutes in triplicate before being washed for 1 minute in distilled water and left to dry overnight. Coverslips (Sigma-Aldrich, UK) were mounted onto slides using ProLong™ Gold Antifade Mountant (Invitrogen, UK) and left to dry before being cleaned of excess mountant using 70% ethanol.

Images were obtained using the Leica Thunder imager microscope utilising the Leica application suite (LAS X) software. Each region of interest; Cornu Ammonis (CA3), CA1 and dentate gyrus hippocampal regions and two cortex and striatal region were imaged in triplicate per anatomical area at x40 magnification (coronal level -1.94mm from bregma). Each immunofluorescence stain was imaged using specific exposure times which remained consistent across the ageing cohort. Following image acquisition, deconvolution and

background subtraction was completed using Leica Thunder and lightning large volume computational clearing proprietary software.

Table 2-4: Antibodies for immunofluorescent studies. Primary and secondary antibodies used for immunofluorescence studies including the dilution factor and use of antigen retrieval.

Antibody	Antigen retrieval	Dilution factor	Supplier	Product code
Goat anti-mouse CD31	N	1:100	Bio-techne	AF3628
Rabbit anti-mouse Caveolin-1	N	1:150	Cell Signalling Technologies	3267T
Rabbit Anti-mouse NG2	N	1:50	Merck Millipore	Ab5320
Rabbit Anti-mouse iba-1	Y	1:300	Alpha Laboratories	019-19741
Chicken Anti-mouse GFAP	N	1:500	Thermofisher	PA110004
Mouse Anti-mouse ICAM-1	N	1:50	Biotechne	NBP2-22541
Donkey anti-goat 647nm	-	1:500	Invitrogen	A-21447
donkey anti-goat 488nm	-	1:500	Invitrogen	A-11055
donkey anti-rabbit 647nm	-	1:400	Invitrogen	A-31473
Donkey anti-chicken 488nm	-	1:800	Jackson Immunoresearch	703-545-155
Donkey anti-mouse 647 nm	-	1:500	Invitrogen	A-31571

To quantify the expression of each fluorescence channel as well as colocalisation between channels, Image J macros were employed. Initially, multiple-coloured background macro was applied to determine threshold levels of individual stains to eliminate background staining. Analysis continued by initiating the multiple colour analysis macro which produced histograms correlating to the number of pixels labelled with individual colour channels in each image. These channels included the classical red, green and blue corresponding with each

immunofluorescence stain in addition to cyan, yellow, magenta and white which reported colocalisation between 2 or all 3 colour channels respectively.

For analysis requiring the % area of endothelial cells, the individual channel for Cluster of Differentiation 31 (CD31-also PECAM-1) was extracted from the multichannel image. Within ImageJ, images were then transformed into the 8-bit format and threshold adjusted to minimum 50 and maximum 255 on the default setting. The % area was then measured of this detected area and used for individual corresponding images for analysis.

2.12. Immunohistochemical staining

To determine permeability of BBB during ageing, immunohistochemistry for immunoglobulin G (IgG) was completed. Slides were removed from ULT freezer and defrosted for 10 minutes prior to washing in 1xPBS in triplicate for 10 minutes to remove traces of OCT. Endogenous peroxidases were then blocked using 0.3% hydrogen peroxide ($H_2O_{2)}$ in distilled water (ddH_2O) for 10 minutes in a humidifying chamber followed by a further x3 10-minute washes in PBS. Further blocking was carried out via 10% horse serum (Vector laboratories, USA) in 0.3% triton-PBS solution for 1 hour at room temperature. Slides were then incubated overnight at 4°C in horse-anti-mouse IgG biotinylated antibody (Vector laboratories, USA) at 1:250 overnight. Blocking was removed via triplicate PBS washes for 10 minutes before incubation for 1 hour with avidin-biotin complex (ABC) (Vector laboratories, USA). PBS was then used to wash excess ABC from slides in triplicate before incubation with diaminobenzidine (DAB) for 4 minutes before further washing with PBS. Slides were allowed to dry thoroughly before cover slipping using Eukitt® Quick-hardening mounting medium (Sigma-Aldrich, UK).

Images were obtained on the Leica Thunder imaging system utilising brightfield settings and camera at x20 magnification. Image settings were as follows: exposure, 50ms, red green blue (RGB) colour channels: (8.4, 1.0, 18.4), Illumination settings were as listed; 121 intensities with 5 aperture and Tl-Fld. Exported images were uploaded to ImageJ whereby they were transformed to 8-bit images and positive regions of immunoreactivity were selected via

thresholding on default setting to 0 minimum and 100 maximum. Per region, 2 images were collected, and the average of the % area immunoreactivity was quantified per cohort group. The Shapiro-Wilks test was employed to test for normality and based on results either the one-way ANOVA and Tukey's multiple comparison test or Kruskal-Wallis test followed by Dunn's multiple comparison test were used to determine statistical significance.

2.12.1. Prussian blue iron staining

To further assess BBB permeability and cerebral microbleeds, Prussian blue histological staining quantified the amount of iron accumulation within the brain parenchyma. The key principle behind this technique is that ferrocyanide will react with any ferric ion present within the brain tissue producing ferric ferrocyanide which produces a quantifiable blue pigment (Liu et al., 2014). Briefly, frozen brain sections were allowed to thaw prior to rehydration in ddH_2O. 20% aqueous solution of hydrochloric acid and 10% aqueous solution of potassium ferrocyanide (Sigma-Aldrich, UK) were combined 50:50 and tissue immediately incubated for 20 minutes. Triplicate ddH_2O washes removed excess solution prior to incubation with nuclear fast red (Sigma-Aldrich, UK) for 5 minutes. Dehydration of tissue through a gradient of methanol and 2 changes of xylene (Sigma-Aldrich, UK) was performed prior to coverslipping using Eukitt® Quick-hardening mounting medium (Sigma-Aldrich, UK).

Images were obtained on the Leica Thunder imaging system utilising brightfield settings and camera at x20 magnification. Image settings were as follows: exposure, 50ms, RGB colour channels: (8.4, 1.0, 18.4), Illumination settings were as listed; 121 intensities with 5 aperture and Tl-Fld. Exported images were uploaded to ImageJ whereby they were transformed to 8-bit images and positive regions of immunoreactivity were selected via thresholding on default setting to 0 minimum and 75 maximum. Per region, 2 images were collected, and the average of the % area immunoreactivity was quantified per cohort group.

2.13. Tissue homogenisation

For downstream protein analysis assays, such as Enzyme-Linked Immunosorbent Assay (ELISA) and Mass Spectrometry, brain tissue from flash frozen hemispheres was obtained. On dry ice, the hemispheres were sliced to acquire the part of the hemisphere containing the hippocampal region and weighed, all brains were approximately 100 mg ± 20 mg. Using a small glass pestle and mortar, each tissue was individually homogenised in 400µl solution containing; 1% protease Max (Promega, USA), x1 RIPA buffer (Merck, Germany), 1% HALT protease inhibitor (Fisher, UK) and 0.1% 100 mM PMSF protease inhibitor (Fisher, UK) in dH_2O. Individual homogenate was transferred to 1 ml glass millitube (Covaris, USA) and incubated on ice for 10 minutes to allow lysis development. Homogenates were then sonicated using S220 focused ultrasonicator (Covaris, UK) using the following settings: x3 30 second 200 pulses split by 30 second rests at 4°C. Samples were then centrifuged using Frontier 5513R (Ohaus, Switzerland) at 4°C for 10 minutes on highest g setting before being transferred to clean 1.5 ml Eppendorf and either kept at 4°C for short-term use or -80°C for long-term storage.

2.13.1. BCA protein quantification

To determine protein concentration of tissue homogenates, the BCA protein assay for quantification was conducted. Albumin standards were diluted to a range of 0-2000 µg/ml and samples diluted 10-fold in RIPA buffer. Working reagent was created from BCA reagent A and B at 50:1 ratio and added to microplate at 1:8 (sample: working reagent) ratio. Microplate was then incubated at 37 °C for 30 minutes in darkness prior to reading of plate at 562 nm on Tecan plate reader. Protein concentration of liposomes was then calculated via extrapolation of the standard curve.

2.14. Mass Spectrometry

To investigate protein expression in brain lysate, proteomics via mass spectrometry was conducted to see effects of ageing and LPS induced inflammation. After protein quantification, 50 µg protein was extracted and sent to the Nottingham Trent University biological mass

spectrometry and clinical proteomic facility lead by David Boocock and Clare Coveney who completed all experimental aspects after samples were transferred.

Each lysate was passed through an S-trap micro column (Protifi, USA) and vacuum-concentrated to remove buffers and reconstituted in 300 µl before being injected by autosampler (Waters M-class) onto a SciexZenoTOF 7600. Analysis was conducted using the Optiflow source in positive sequential window acquisition of all theoretical fragment ion spectra (SWATH) mode to produce generation of protein library. DI-ANN 1.8.1 was used to process SWATH data utilising the FASTA digest for library-free and deep learning options. The Swissprot Mouse May 2022 database was used for the analysis and output data was further analysed on AMICA 3.0.1(Didusch et al., 2022).

The following settings were used on AMICA; filter on count values: 2, minimum valid values in group: 3, normalisation method: none, imputation: minimum (downshift 2.8, width 0.3). To produce values for differential expression of proteins in each condition as well normalisation and log 2-fold change set at 0.3 with unadjusted p-values (0.05) following recommendations from literature (Cox et al., 2014; Pascovici et al., 2016). Volcano plots of expression compared to 3-month vehicle, or 18-month vehicle groups were created using log (fold change) and -log (10) (p-value) data.

2.14.1 Functional pathway analysis

Ingenuity pathway analysis (IPA) (Qiagen, UK) was utlisied the elucidate upstream canonical and functional pathways to understand the effect of systemic inflammation on the aged brain samples. The top up/down regulated proteins were calculated based on an expression fold change (-0.3<, 0.3<) with a significance of $p \leq 0.05$ based on Fisher's exact test.

2.15. *In vivo m*agnetic resonance imaging (MRI)

2.15.1 Microparticle of iron oxide production

To visualise changes to BBB, microparticles of iron oxide (MPIO) were functionalised with VCAM-1 antibody (BD Biosciences, USA) according to previous literature work (Gauberti et al.,

2018). Briefly, 1µM dynabead myone tosylacivated MPIO (Thermo Fisher, UK) were resuspended and added to a falcon tube before being washed in triplicate with 0.1 M borate buffer (Thermo Fisher, UK) by magnetic separation. MPIO's were resuspended with 200 µg VCAM-1 antibody in 37% 3 M ammonium sulfate (Sigma-Aldrich, UK) and 63% 0.1 M borate buffer before being incubated at 37°C for 48 hours under constant agitation. Magnetic separation of MPIO from supernatant occurred before resuspension with blocking buffer (0.5% bovine serum albumin in 0.005% Tween20-PBS) prior to a further 24 hour agitated incubation at 37°C. To prevent MPIO aggregation, sonication was completed on Soniprep 150 plus (MSE, UK) at 5 amplitude for 60 seconds on ice prior to triplicate magnetic separation washing of MPIO is washing buffer (0.1% bovine serum albumin in 0.005% Tween20-PBS). Final MPIO-VCAM-1 conjugate suspended in wash buffer and stored at 4°C under constant agitation prior to use.

2.15.2. MRI imaging

To visualise MPIO-VCAM-1 binding within the brain of aged mice, MRI imaging was undertaken. Imaging was conducted at Nottingham Trent University by the Imaging and Display research facility staff, Dr Robert Morris and Jim Hall.

Mice were anaesthetised via subcutaneous injection of 75 mg/kg Ketamine and 1 mg/kg Medetomidine before being placed into a 37 °C heating box (Clinpath, UK). Intravenous tail insertion of 27-gauge cannula was completed and secured in place before placing mouse on a heated mat within human extremity coil in Avanto1.5T MRI (Siemens, Switzerland). Animal position was confirmed in the homogenous region of the scanner by a localiser sequence before an isometric gradient spin (settings in table 2-5) was applied to ensure multidirectional analysis. Using a spoiled gradient echo sequence, T1 weighted pre-contrast images were acquired prior to injection of MPIO-VCAM-1 via cannula. 5-minutes after injection, mice were imaged identically to pre-contrast.

Pre- and post- contrast images were uploaded into MATLAB to quantify amount on MPIO-VCAM-1 binding in the region of interest. Briefly, threshold of the background image crated a mask to reduce and remove noise before a second threshold was applied to remove the peripheral mouse body to retain only the mouse skull and brain. MATLAB code then subtracted the contrast post-injection and difference calculated in the code.

2.15.3. Transmission electron microscopy (TEM)

To confirm that MPIO-VCAM-1 was not aggregated, the estimate size, TEM of MPIO's was undertaken pre- and post-sonication step. Glow discharged TEM mesh copper grid (Agar Scientific, UK) was incubated for 1 minute on MPIO sample before being washed in triplicate

Table 2-5: Specifications of MRI imaging.

Sequence parameter	Parameter value
Sequence Name	SGE_60_ISO
Slice thickness	0.6mm
Repetition time (TR)	200 ms
Echo time (TE)	13.2 ms
Averages	1
Field of view Phase	100 %
Oversampling	100 %
Flip angle	22 °
Field of view	71 mm

on ddH_2O) droplets. Grids were then stained with 1% uranyl acetate for 1 minute for visualisation and air dried prior to imaging. Imaging conducted by Imaging team at Nottingham Trent University; Dr Graham Hickman and Dr Dominic Craske.

2.16. ELISA tests

To test for changes to inflammatory markers in the peripheral blood system, ELISA's were carried out for proteins utilising serum extracted from the terminal animal. All experiments followed the standardised protocols for DuoSet ELISA kits (R&D Systems, UK) with specific reagent working conditions noted in table 2-6. Briefly, 96-well plates were coated with 100 µl capture antibody and incubated overnight at room temperature (RT) prior to triplicate stringent washing in PBS containing 0.05% Tween-20. Wells were then blocked for non-specific binding via 1% BSA-PBS for 1 hour at RT. Plates were then washed as previously stated before serum

samples or protein normalised brain homogenates were incubated for a minimum of 2 hours at RT at optimised concentrations table 2-6. After further washing steps, biotinylated detection antibody was incubated for 2 hours prior to another wash and incubation with streptavidin-HRP for 20 minutes. Final washing took place before 20 minutes incubation with 100 µl substrate solution directly followed by 50 µl stop solution. Plates were read immediately at 450 nm and 570 nm on Tecan plate reader. For analysis, 570nm values were subtracted from 450nm to account for wavelength correction and values of the standards were inputted into sigmoidal, 4PL curve. Absorbance values for cohort samples then extrapolated from the curve using GraphPad Prism.

Table 2-6: ELISA working concentrations. Final concentrations for capture antibody, protein standards, detection antibody, streptavidin-HRP and dilution of serum and protein standards. ELISA; enzyme-linked immunosorbent assay, Ab; antibody, DF: dilution factor, HRP: horseradish peroxidase.

ELISA kit	Capture Ab (µg/ml)	Standard (pg/ml)	Serum sample DF	Protein sample DF	Detection Ab (ng/ml)	Streptavidin-HRP
ICAM-1	2	125-8000	1:1000	1:100	12.5	1:200
IL-1β	4	15.6-1000	N/A	1:5	250	1:40
IL-6	2	15.6-1000	1:20-1:1000	1:10	75	1:40
VCAM-1	1	125-8000	1:10000	1:1000	100	1:200

2.17. Statistical analysis

All data was collated and inputted into GraphPad Prism 10 for all statistical analysis (except Mass spectrometry data). For all comparisons, the Shapiro-Wilks normality test was applied to determine normality of each cohort before further statistical tests. For comparisons of 2 groups, parametric datasets used unpaired T-test whilst non-parametric groups utilised Mann-Whitney test. For groups of more than 2 comparisons, dependant on analysis either the one-way analysis of variance followed by Tukey multiple comparison Post-hoc test or two-way analysis of variance was applied followed by Dunn's multiple comparison test under normal conditions. For non-parametric datasets, the Kruskal-Wallis test was followed by Dunn's multiple comparison test. Graphical representations signified mean ± standard error of mean (SEM) and all significant results were graphically annotated using the following ranking: * $p<0.05$, ** $p<0.01$, *** $p<0.001$.

3. The investigation of lifespan and sex on the blood-brain barrier and associated neurovascular unit components in relation to cognitive function

3.1. Introduction

As previously discussed, the effect of physiological ageing on the BBB is disputed regarding both permeability and changes to NVU components. When looking at previous research, it becomes apparent that many studies prefer to utilise male mice to investigate physiological ageing which may have been to alleviate any variations which occur naturally due to fluctuations in female hormone cycles (Pan et al., 2021; Sartorius et al., 2015; Sumbria et al., 2018). It is crucial to investigate sex differences related to BBB ageing and focus on females as the unreported group in comparison to males. This is important within BBB context as it has been documented in humans that BBB decline was more pronounced in the male cohort than females via MRI measurements (Moon et al., 2021; Shao et al., 2024). The lack of investigations into sexual dimorphism within *in vivo* models in comparison to clinical work highlights the importance of studying the female and male BBB changes. Some studies have researched BBB in both sexes but do not report on any differences observed in the cohorts and instead have focused on the group as a whole and not two distinct populations (Stamatovic et al., 2019; Britton et al., 2022).

Commonly within ageing studies, only two age points, classified as young and aged adult are compared, typically 3 months and 18 months (Frías-Anaya et al., 2021; Halder & Milner, 2022; Yang et al., 2020). The mouse strain C57BL/6 has been widely used in ageing studies as it is a well-defined strain commonly used in neurogenerative and genetic models and ages more rapidly than humans with 1/30th overall lifespan (Kõks et al., 2016; Yanai and Endo, 2021). The comparative ages of C57BL/6 mice are as follows: 3-6 months (20-30 years), 10-15 months (38-47 years) and 18-24 months (56-69 years) (Jackson et al., 2017; Yanai and Endo, 2021).

In C57BL/6 mice, it has been estimated that adolescence stops between post-natal day 50-70 in both males and females and full reproductive maturity at 3 months (Groó et al., 2013; Finch, 2014; Arellano et al , 2024). Due to the unpredictability of individual mouse adolescence, the prevailing age for adult mice is 3-months (92 days), ensuring the end of puberty and maturation of reproduction (Yanai and Endo, 2021). It has also been shown that development of major

brain regions, such as the hippocampus, ceases at approximately 77 days, justifying the use of 3-month mice as young adult (Fu et al., 2013). For older age groups, the lifespan and survival rate of specific mouse strains must be considered, for C57BL/6 mice, the survivorship of mice is 75% in 18–24-month mice but drops to 50% at 28-months, indicating for *in vivo* studies should ideally not progress past 24-months due to high mortality rates (Graber et al., 2015; Jackson et al., 2017; Yanai and Endo, 2021). Few studies have looked at a range of ages in either males or females to determine the progression of BBB changes. Investigating this progression would possibly identify novel therapeutic windows to target age-related changes, like in stroke models, where a biphasic therapeutic window has been identified (Al-Ahmady et al., 2019, 2022).

Within the brain, different regions are more vulnerable to age-related changes than others, particularly the hippocampal region. Functionally, the hippocampus has a role in spatial learning and memory, but in ageing, impaired LTP has been shown in rodents correlating with decreases in cognitive ability, specifically the consolidation of long-term memory (Lister and Barnes, 2009; Bettio, Rajendran and Gil-Mohapel, 2017; Patrick et al., 2024). When focusing on the BBB, human MRI studies demonstrate increased permeability of the hippocampus, further broken into 3 main hippocampal regions, CA1, CA3 and dentate gyrus (Montagne et al., 2015). *In vivo* studies have also replicated this, demonstrating hippocampal related cognitive decline, and highlighting the conservation of ageing effects on this brain region. (Wimmer et al., 2012; Koh, Spiegel, and Gallagher, 2014).

Although the hippocampus historically has been linked the most to BBB dysfunction in ageing, it is important to compare this to other brain regions to examine spatial effects of age. The cortex is a major structure in the brain and can be broken down into 4 lobes; frontal, temporal, occipital and parietal lobes with further functional breakdowns such as the motor and auditory cortex (Hogstrom et al., 2013). Regarding ageing, the motor cortex exhibits changes to synaptic plasticity and neuronal activity leading to a decline in motor function (Inoue and Nishimune, 2023). The auditory cortex also shows age-related decline such as the decreased recognition

of the spoken word and inability to decipher speech-in-noise (Rogers et al., 2020). Studies have investigated this mechanistically and propose that the changes to the neurotransmitter gamma-aminobutyric acid (GABA) in ageing could be driving these changes (Dobri and Ross, 2021). The striatum is also an important structure within the brain which is responsible for many cognitive functions such as motor and action planning (Bamford and Bamford, 2019). Within these models, increased BBB permeability has been observed so it is an important point to compare this to physiological ageing to determine if effects can be detected before pathology.

The tight control of molecular movement by the BBB is one of the major obstacles for delivery of therapeutics into the brain parenchyma as it is impermeable to the majority drug molecules (Pardridge, 2005). Even in severe neuropathology, such as AD, where increased BBB permeability has been established, the ability of small molecules to pass through is still minimal, with only 2% of molecules infiltrating the brain (Janelidze et al., 2017). Lipid nanoparticles (liposomes) have been considered as an alternative to free drug molecules and have been shown to infiltrate across the BBB in different neuropathology, such as Stroke, Parkinson's and AD (Al-Ahmady et al., 2019; Chu et al., 2022; Monge-Fuentes et al., 2021). There are multiple potential mechanisms of transport that allow for lipid nanoparticles to move through the BBB including caveolae/ receptor/ absorptive mediate transcytosis (CMT/ RMT /AMT) (Juhairiyah and de Lange, 2021). Particular attention should be shown to caveolae-mediated transcytosis as this has been shown in cancer and stroke models to be a mechanism of liposome transport (Sorets et al., 2020; Tylawsky et al., 2023). This is relevant as *in vivo* studies have demonstrated a link between physiological ageing and a shift towards this type of transport, indicating a possible pathway for liposomes to cross the BBB (Yang et al., 2020).

Another key aspect of ageing is the cognitive decline present as age progresses which has been shown previously in humans and rodents (Wimmer et al., 2012; Murman, 2015; Healy et al., 2024). It is important to determine if changes observed to BBB permeability or NVU components occur prior to or after significant cognitive deficits and whether this is related to

age-related inflammatory response (Wang et al., 2014; Zhao et al., 2020; Hillmer et al., 2023). Therapeutically, it would be beneficial for changes to be observed pre-cognition changes as this would provide a therapeutic window to target changes which could potentially delay or reduce the cognitive changes predominantly seen.

3.2. Aims and Objectives

This chapter aims to assess age-related changes to the BBB and NVU by comparing a range of ages in female and male mice. This will determine if there is a systematic change to the brain microvasculature in young, middle-aged, and aged mice in females whilst comparing to the male mice which historically have been the preferred *in vivo* model. The chapter also aims to demonstrate age-related changes in BBB permeability and correlate with an increased infiltration of lipid nanoparticles. Changes to caveolae-mediated transport through the BBB will be assessed to determine female and male aged-related changes. The effect of ageing on other NVU components will also be observed to determine any potential therapeutic targets. All changes identified will be correlated with changes to cognitive function to identify if BBB changes happen post- or pre-cognition changes. Ultimately, the findings in the chapter will add to the growing understanding and improve clarity of how physiological ageing affects the BBB as well as demonstrating the ability of nanoparticles to exploit these changes for drug delivery.

3.3. Hypotheses:

1. Ageing causes increased BBB permeability to large molecules and nanoparticles
2. Age-related changes to neurovascular unit components will occur prior to the onset of cognitive change
3. Increased in inflammatory response will occur with increased age

3.4. Methodology

Detailed methodology for all techniques used in this chapter of work can be found in Chapter 2.

3.4.1. **Study design**

Mice were purchased at the desired age up to the point of 18 months, whereby mice were kept onsite up until the desired age range. Mice were observed and bodyweights monitored twice weekly following guidelines for aged animals (Wilkinson et al., 2020). Each age point, females (3, 6, 12, 18, 22 months)/ males (3 and 18 months) were initially n=8 housed up to 4 mice per cage. This number was determined based on power calculation of nanoparticle infiltration (n=5) calculated from previous work (chapter 2.2) (Al-Ahmady et al., 2019, 2022). All mice underwent behavioural tests and injected with DiI-lip but then split into two groups: DiI-lip only (n=5) and taken forward for further immunofluorescence analysis or DiI-lip and albumin (n=3). The 22-month group consisted of n=7 due to mouse mortality and so was split into groups of n=4 and n=3 respectively. The separate Dextran study composed on n=3 male mice at 3- or 18- month ages. All predicted n-numbers are depicted in fig. 3-1 along with a diagrammatic representation of the overall study design.

3.4.2. **Behavioural testing**

Novel object recognition and novel object location testing were conducted to determine changes in cognitive ability across ageing in both sexes (2.4).

3.4.3. **Optical imaging**

Female brains were imaged for infiltration of DiI-liposomes and albumin whilst male cohorts investigated the effects of DiI-liposomes, albumin and dextran on brains as well as investigated the biodistribution of DiI-liposomes on heart, lungs, spleen, liver and kidney (2.8).

3.4.4. **Immunofluorescence staining**

Immunofluorescence staining was utilised to examine neurovascular unit components; CD31 for endothelial cells, GFAP for astrocytes and NG2 for pericytes (2.11). Inflammatory responses during ageing were investigated via expression of iba-1, representing the microglial population. Further studies examined transcytosis transport routes evaluating the expression

A

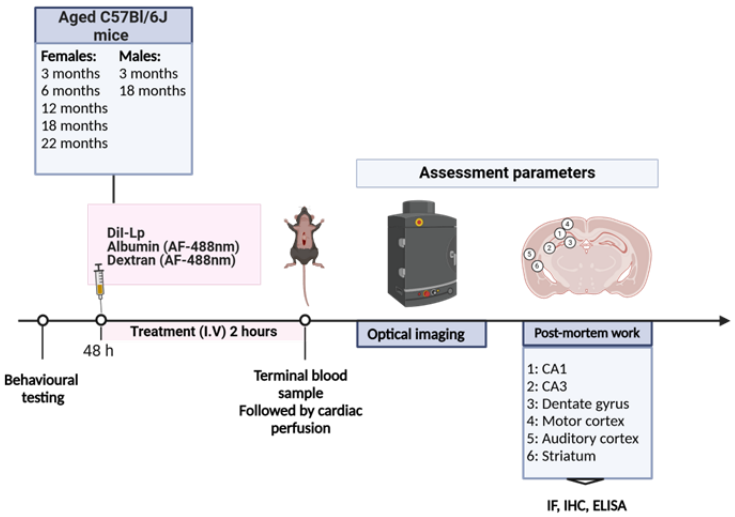

B

Sex	Age (months)	Behaviour	Dil-lip	Albumin + Dil-lip	Dextran	IF	IHC	ELISA
Female	3	8	5	3	-	5	8	5
	6	8	5	3	-	5	8	5
	12	8	5	3	-	5	8	5
	18	8	5	3	-	5	8	5
	22	7	4	3	-	4	7	4
Male	3	10	6	4	3	6	10	5
	18	16	8	3	3	10	16	5

*Dil-lip: Liposome, IF: Immunofluorescence, IHC: Immunohistochemistry, ELISA: enzyme-linked immunoassay.

Figure 3-1: Schematic representation of ageing mice study and study n-numbers. (A) Female and male mice at specific ages were injected intravenously with either Dil-lip, Dil-lip and albumin or Dil-lip and dextran and culled 2 hours post-injection. Prior to cardiac perfusion, terminal blood samples were obtained for downstream analysis. Optical imaging of brain and peripheral organs occurred immediately post-perfusion before brains treated for histological analysis. Diagrammatic representation of 6 regions of interest for post-mortem work. (B) Tabular representation of all mouse groups within the study specifying the sex and age of each cohort and the predicted n-number per assessment parameter.

of caveolin-1. Negative control images (without primary antibody) are found in appendix 3. Any tissue loss is recorded in appendix 4.

3.4.5. **Immunohistochemical staining.**

To determine permeability of BBB during ageing, immunohistochemistry for IgG was completed (2.12). Negative control images (without primary antibody) are found in appendix 3. Any tissue loss is recorded in appendix 4.

3.4.6. **ELISA tests**

For ageing studies, inflammatory markers ICAM-1 and VCAM-1 were examined using serum extracted terminally from each mouse group (2.16).

3.4.7. **Statistical analysis**

All statistical analysis was performed on GraphPad Prism for age-related effects on either male or female cohort (2.17). Normality was assessed in both cohorts via Shaprio-Wilkes test prior to downstream statistical tests. For comparison of the female cohort, either one-way analysis of variance applied followed by Tukey multiple comparison test under normal conditions or the Kruskal-Wallis test was followed by Dunn's multiple comparison test for non-parametric groups. For the male cohort, either an unpaired T-test or Mann-Whitney test were used based on normality. Graphical representations signified mean ± SEM and all significant results were graphically annotated using the following ranking: * $p<0.05$, ** $p<0.01$, *** $p<0.0001$.

3.5. Results

3.5.1. **Increased global infiltration of molecules into the ageing brain**

Increased permeability of the BBB to molecules during ageing has been demonstrated throughout the literature (Yang et al., 2020; Ohene et al., 2021; Pan et al., 2021). This project aims to ascertain if this permeability extends to nanoparticle infiltration. DiI-labelled

liposomes were manufactured in the laboratory setting and demonstrated to have similar size (nm), zeta-potential, fluorescence intensity and poly-dispersal index (fig. 3-2). This allows for comparisons in DiI-lip infiltration across the aged cohorts in both males and females. As liposomes have been shown to travel through the caveolae-mediated transcytosis transport route, albumin was assessed alongside the DiI-lip to correlate with proposed transport mechanisms as transcytosis is the main pathway of albumin infiltration.

To determine the global infiltration of DiI-lip and Albumin into the male and female brains, optical imaging was deployed (Fig. 3-3b-c). In females, DiI-lip significantly increased in the brain in a stepwise pattern from 3-22 months; with increases between 3- and 18-months ($H = 18.01_{(4,31)}$, $p=0.0486$), 6- and 18- months ($H = 18.01_{(4,31)}$, $p=0.0068$) and 6- and 22- months ($H=18.01_{(4,31)}$, $p=0.0345$) whilst albumin significantly increased to 18-months ($F=30.98_{(3.7)}$,$p=0.0009/0.0002/0.0016$) but not 22 months (fig.3-3c). In male brains, significant increases were shown in both DiI-lip ($T=6.4_{(17)}$) and Albumin ($T=1.563_{(7)}$), showing similar effects as the female groups (fig.3-3d-e). Dextran, a molecular smaller in size then both DiI-lip and albumin used to demonstrate tight junction permeability, did not show any significant changes in ageing (fig.3-3f). The increases in both albumin and DiI-lip but not dextran supports the hypothesis that ageing induces a semi-permeable BBB to specific molecule types based on transport pathways.

3.5.2. **Biodistribution of DiI-lip into peripheral organs**

To determine if the infiltration of DiI-lip into the brain during ageing was specific to the brain only, optical imaging of various peripheral organs was conducted in the male cohort. No significant increases were found in any tested organ which included the liver, heart, lung, spleen, or kidneys, indicating a brain organ specific effect when investigating physiological ageing (fig.3-4b).

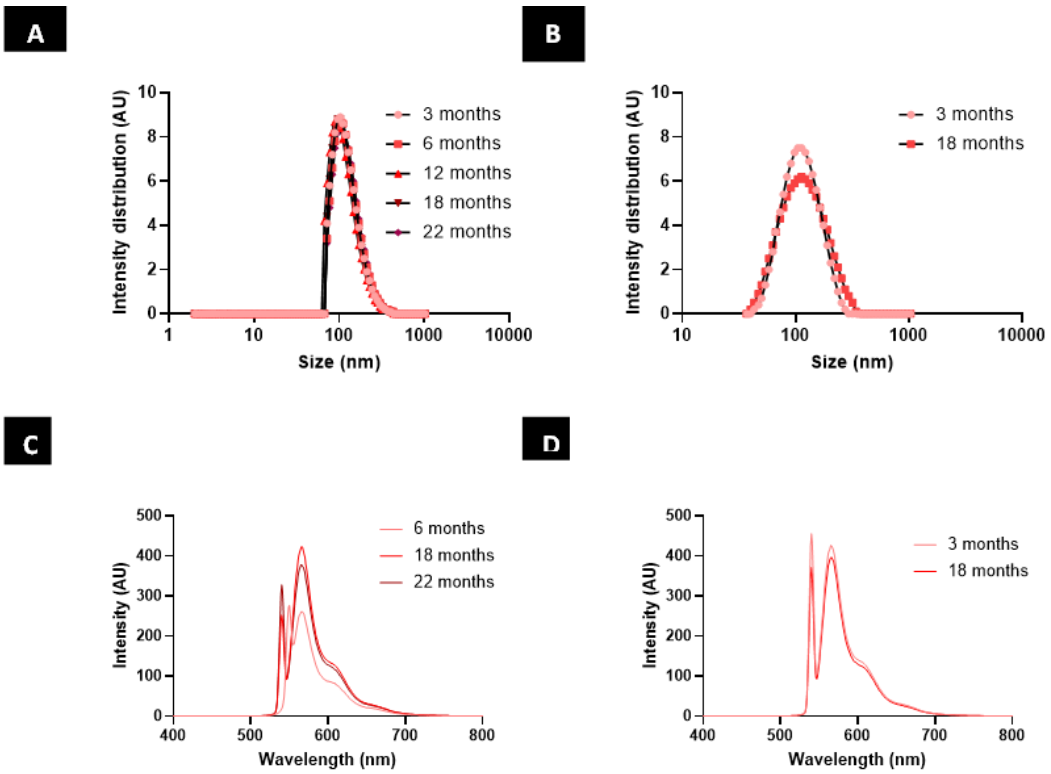

E

Sex	Aged (months)	Size ± SD (nm)	PDI ± SD	Zeta potential ± SD (mV)
Female	3	83.6 ± 2.042	0.130 ± 0.021	-19.0
	6	93.9	0.146	-14.1 ± 0.902
	12	85.6 ± 0.473	0.108 ± 0.012	-16.7
	18	85.2	0.148	-15.0 ± 0.500
	22	102.4	0.146	-15.3 ± 1.358
Male	3	114.1 ± 1.796	0.152 ± 0.014	-12.5 ± 0.643
	18	99.0 ± 0.629	0.173 ± 0.011	-10.5 ± 2.012
Lipid composition (12.5 mM)		HSPC:Chol:DSPE-PEG2000+DiI (56.3:38.2:5.5 mol/mol%)		

Figure 3-2: Liposome characterisation for ageing cohort. Liposomes were made with identical formulations using thin film hydration followed by extrusion. Size (in nm), zeta potential (ZP) and poly-dispersal index (PDI) were all completed in triplicate via dynamic light scattering. Fluorescence intensity was calculated using spectrophotometry set at 540nm (A) graphical representation of female cohort liposome size. (B) Graphical representation of male cohort liposome size. (C) Fluorescence intensity of average liposome batches in female cohort. (D) Fluorescence intensity of average liposome batches in female cohort. (E) Lipid compositions, size, Average PDI and ZP values for each liposomal cohort batch. All graphs created using GraphPad Prism

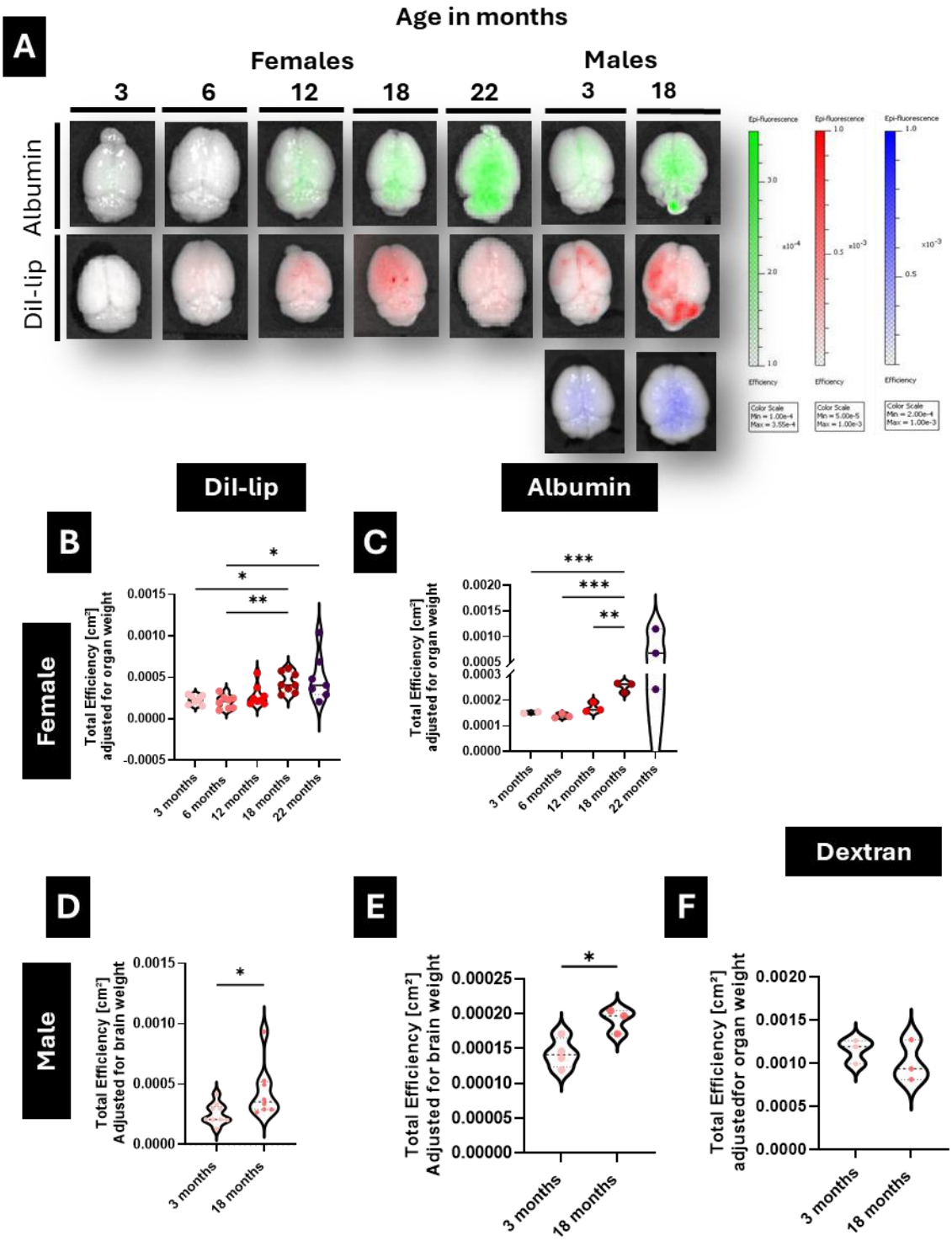

Figure 3-3: Optical imaging of global brain infiltration of Dil-liposome, Albumin and Dextran.C57BL/6 male mice groups at 3- and 18-months and female mice groups at 3-, 6-, 12-, 18-, 22-months received a single intravenous injection of Dil-lip and albumin 488nm or Dil-lip and Dextran 488nm. Cardiac perfusion was completed either 2-hours post-injection to remove circulating Dil-lip, albumin, and dextran. (A) Representative optical images of mouse brains indicating infiltration of albumin (green), Dil-liposomes (Red) and Dextran (blue). (B) Quantitative analysis of Dil-lip infiltration of female brains indicates significant increases across ageing (C) Quantitative analysis albumin infiltration showing significant increases in

female ageing. (D) Quantitative analysis of male DiI-lip infiltration showing significant infiltration increases. (E) Quantitative analysis of albumin infiltration showing significant increases in ageing. (F) Quantitative analysis of dextran infiltration showing no significant increases in ageing. Images obtained using *in vivo imaging system* (IVIS) and analysed using living systems software. Statistical analysis was completed using GraphPad Prism software using one-way analysis of variance followed by Tukey multiple comparison test or Kruskal-Wallis test followed by Dunn's multiple comparisons test or unpaired T-test based on Shaprio-Wilk test for normality. N=7-8 (liposome), 3-4 (albumin), 3 (dextran) ,average ± SEM, $p<0.05$ were considered significant.

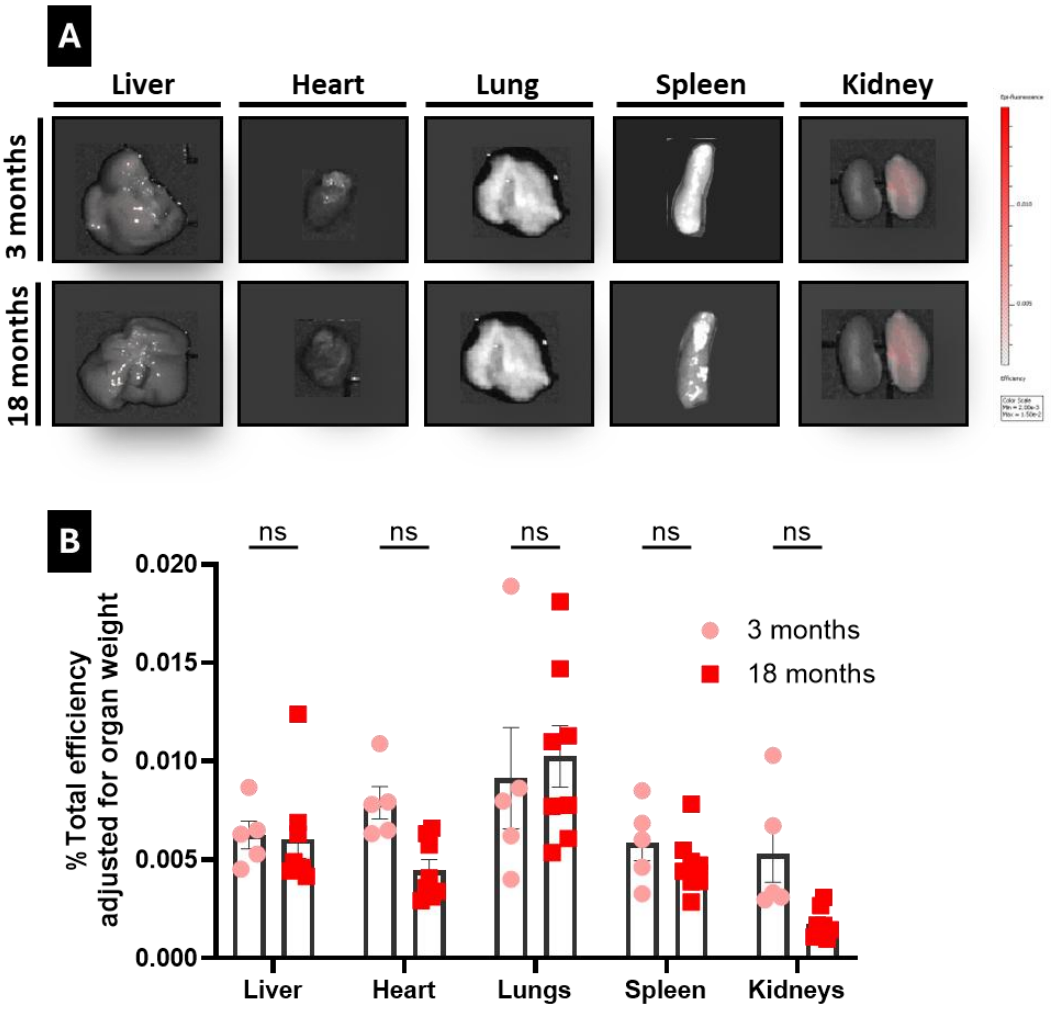

Figure 3-4: Optical imaging of biodistribution of DiI-liposomes in ageing male mice. C57BL/6 male mice groups at 3- and 18-months received a single intravenous injection of DiI-lip. Cardiac perfusion was completed 2 to remove circulating DiI-lip. (A) Representative optical images of male mouse brains indicating infiltration of DiI-liposomes (Red) (B) Quantification of all organs adjusted for organ weight demonstrated no significant changes in DiI-lip infiltration across ageing. Statistical analysis was completed using GraphPad Prism software using two-way analysis of variance followed by Sidak's multiple comparison test. N=5/8, average ± SEM, $p<0.05$ were considered significant.

3.5.3. **Regional differences of DiI-lip infiltration**

After looking into global infiltration of albumin and DiI-lip, it was important to further extract information relating to spatial infiltration into different age-vulnerable regions. In females, significant increases in DiI-lip infiltration have been observed in all measured hippocampal regions (fig.3-5b-d). DiI-lip infiltration increased in the CA1 ($F=6.591_{(4,19)}$,$p=0.0039$), CA3 ($F=20.48_{(4,19)}$, $p=<0.0001$) and dentate gyrus ($F=6.56_{(4,19)}$, $p=<0.0001$) between the 3- and 18-month group whilst only the CA1 region demonstrated the same significance at 22 months ($F=6.591_{(4,19)}$,$p=0.0114$). Similar increasing expression patterns were seen in the motor ($F(4,19)=6.56_{(4,19)}$, $p=0.032$) and auditory cortex ($F=8,319_{(4,19)}$, $p=0.0037$) as well as the striatum ($F(4, 19)=6.298_{(4,19)}$, $p=0.049$) but to less significant than observed in the hippocampal regions (fig.3-6b-d).

In the male cohort, the CA3 ($M=6.277_{(13)}$, $p=0.0109$), motor cortex ($M=6.302_{(13)}$, $p=0.0125$) and auditory cortex ($T=14.21_{(13)}$, $p=0.0101$) regions all displayed significant increases between 3- and 18-month but the CA1, dentate gyrus and striatal regions did not show significant changes (fig. 3-7b-g). Qualitatively, the expression of DiI-lip followed similar patterns in all regions (fig. 3-5,3-6, 3-7). Expression was observed in endothelial like structures as well as diffuse punctate staining throughout the rest of the tissue and was particularly strong in the cortical regions analysed. This means that 2-hours post-injection, there was still some co-localisation with endothelial cells, but that parenchymal infiltration of DiI-liposomes had begun to occur which did not qualitatively co-localise with the endothelial expression.

3.5.4. **Evaluation of transcytosis transport through BBB**

It has been documented that during ageing as well as in neurodegeneration such as Stroke, that there is a shift towards the transcytosis mechanism (Al-Ahmady et al., 2019; Yang et al., 2020). It has been noted that albumin is transported via transcytosis, this is comparable to DiI-lip infiltration may indicate possible similarities in the transport through the BBB (Hillmer et al., 2023).

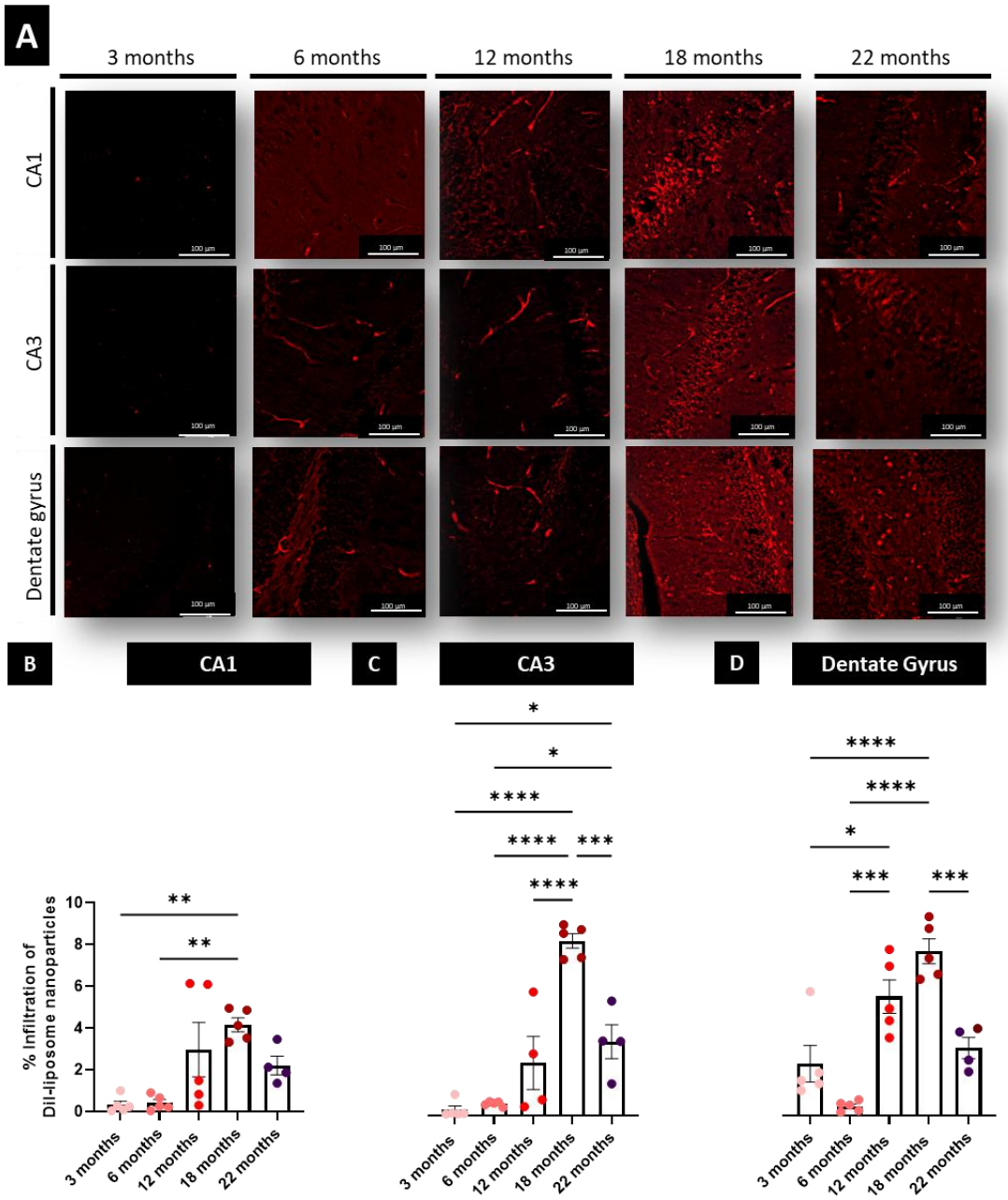

Figure 3-5: Dil-liposomes infiltration in ageing female hippocampal regions. C57BL/6 female mice groups at 3-, 6-, 12-, 18-, 22-months received a single intravenous injection of Dil-lip. Cardiac perfusion was completed 2 hours post-injection to remove circulating Dil-lip.(A) Representative immunofluorescence images of CA1, CA3 and dentate gyrus hippocampal regions -1.94mm from bregma indicating infiltration of Dil-liposomes (Red). (B) Quantitative analysis of CA1 region. (C) Quantitative analysis of CA3 region. (D). Quantitative analysis of dentate gyrus region. All regions indicate significant increase in infiltration across ageing. Images obtained at x40 magnification on Leica Thunder microscope and underwent large volume computational clearing (LVCC) prior to quantification in Image J. Statistical analysis was completed using GraphPad Prism software using one-way analysis of variance followed by Tukey multiple comparison test or Kruskal-Wallis test followed by Dunn's multiple comparisons test based on Shapiro-Wilk test for normality. N=4/5,average ± SEM, $p<0.05$ were considered significant. Scale bar represents 100µm.

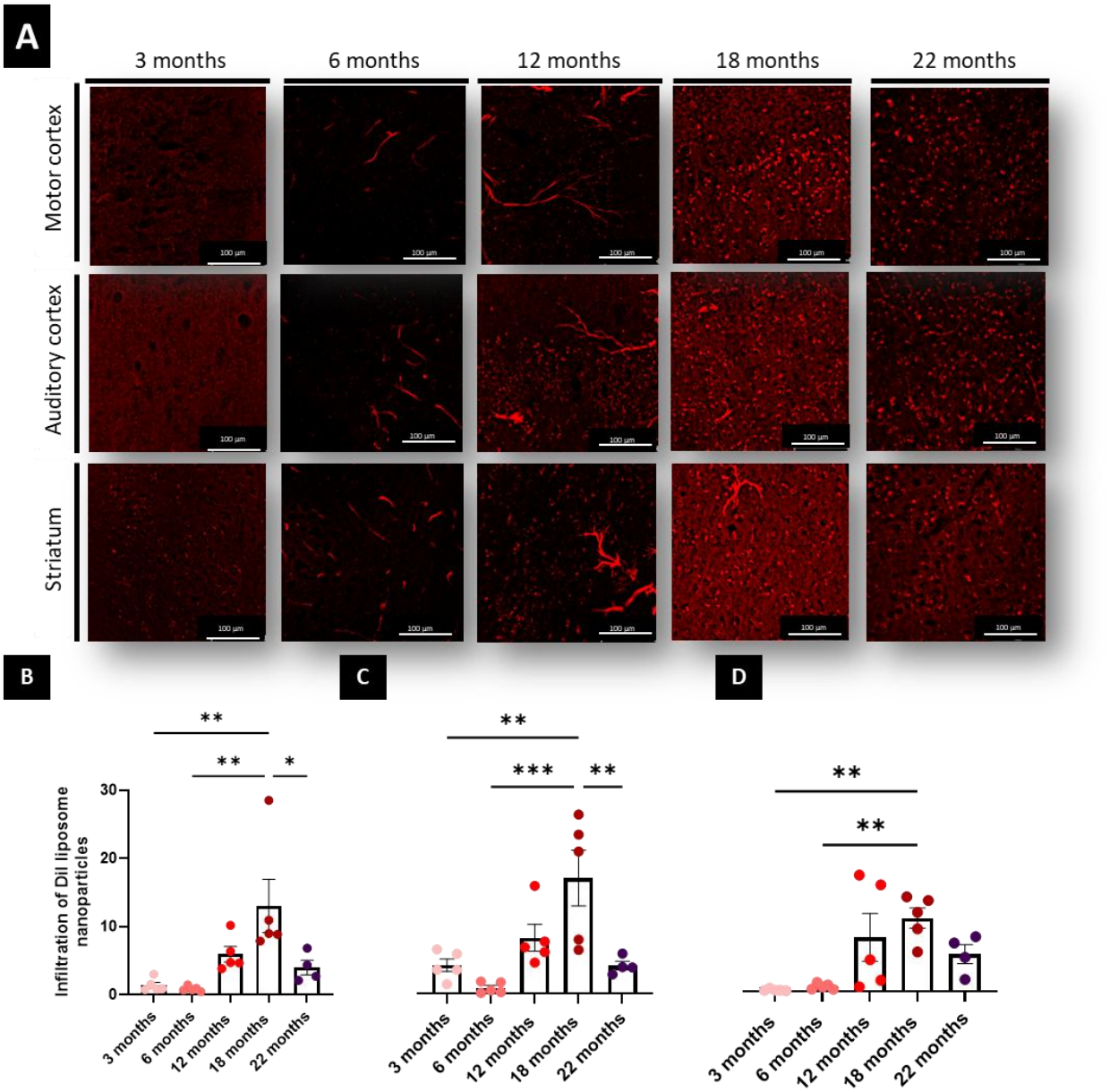

Figure 3-6: Dil-liposomes infiltration in ageing cortical and striatal regions. C57BL/6 female mice groups at 3-, 6-, 12-, 18-, 22-months received a single intravenous injection of Dil-lip. Cardiac perfusion was completed 2 hours post-injection to remove circulating Dil-lip.(A) Representative immunofluorescence images of motor cortex, auditory cortex, and striatum regions -1.94mm from bregma indicating infiltration of Dil-liposomes (Red). (B) Quantitative analysis of motor cortex region. (C) Quantitative analysis of auditory cortex region. (D). Quantitative analysis of striatal region. All regions indicate significant increase in infiltration across ageing. Images obtained at x40 magnification on Leica Thunder microscope and underwent large volume computational clearing (LVCC) prior to quantification in Image J. Statistical analysis was completed using GraphPad Prism software using one-way analysis of variance followed by Tukey multiple comparison test or Kruskal-Wallis test followed by Dunn's multiple comparisons test based on Shapiro-Wilk test for normality. N=4/5,average ± SEM, $p<0.05$ were considered significant. Scale bar represents 100µm.

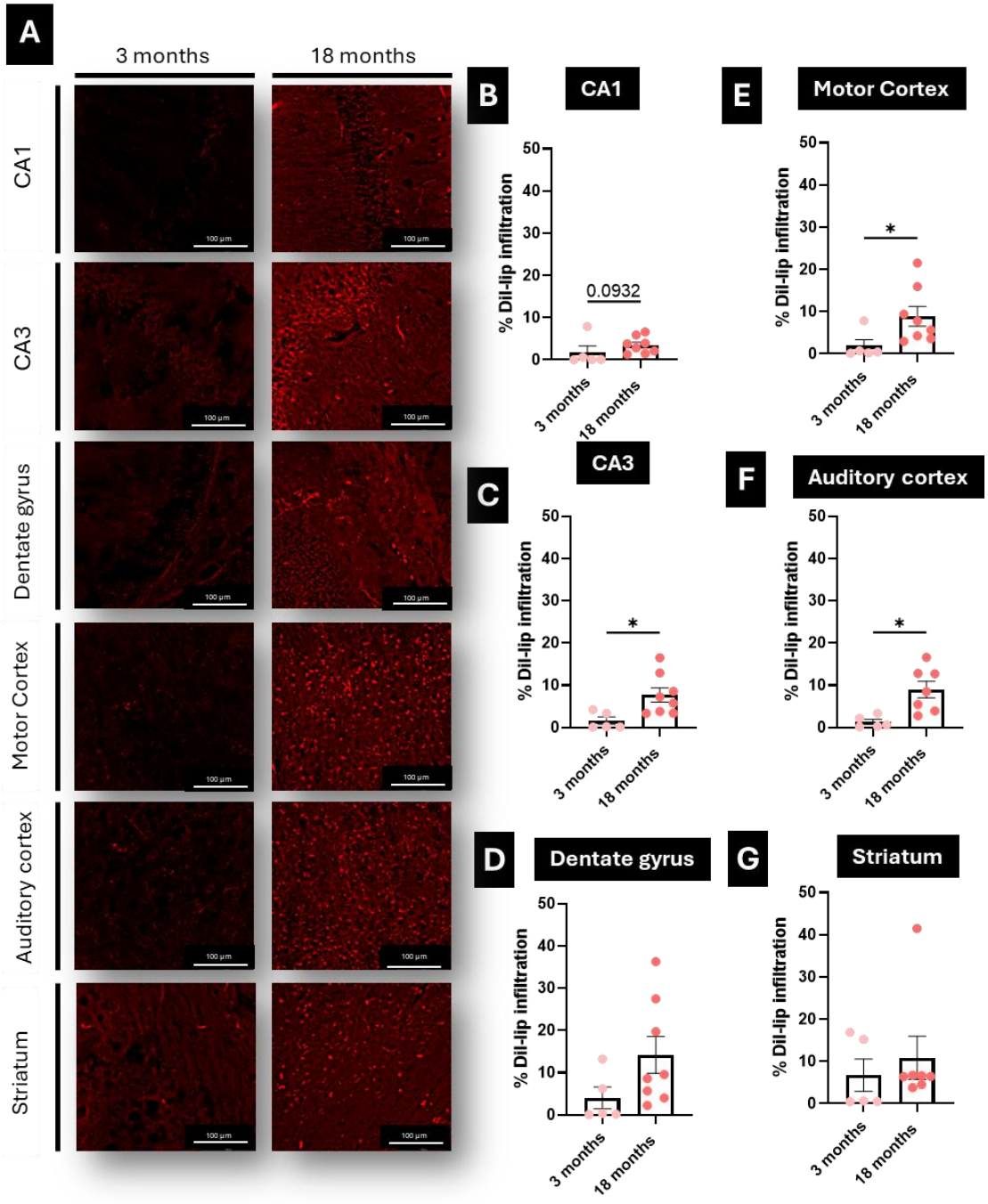

Figure 3-7: Dil-liposomes infiltration in ageing male brains regions. C57BL/6 male mice groups at 3- and 18-months received a single intravenous injection of Dil-lip. Cardiac perfusion was completed 2 hours post-injection to remove circulating Dil-lip.(A) Representative immunofluorescence images of CA1, CA3 and dentate gyrus hippocampal regions, motor and auditory cortical regions and striatal region -1.94mm from bregma indicating infiltration of Dil-liposomes (Red). (B) Quantitative analysis of CA1 region. (C) Quantitative analysis of CA3 region. (D). Quantitative analysis of dentate gyrus region. (E) Quantitative analysis of motor cortex region. (F) Quantitative analysis of auditory cortex region. (G) Quantitative analysis of striatum region. All regions indicate trends to increasing Dil-lip. Images obtained at x40 magnification on Leica Thunder microscope and underwent large volume computational clearing (LVCC) prior to quantification in Image J. Statistical analysis was completed using GraphPad Prism software using one-way analysis of variance followed by Tukey multiple comparison test or Kruskal-Wallis test followed by Dunn's multiple comparisons test based on Shaprio-Wilk test for normality. N=5-8,average ± SEM, $p<0.05$ were considered significant. Scale bar represents 100µm.

To further investigate infiltration, permeability to albumin was also explored (fig. 3-8-3-13). Increasing trends were observed in each female region, with low expression in 3–12-month groups with a significant expression increase in 18 months. This increase was significant in multiple regions including CA3 ($F=14.93_{(4,10)}$, p=0.0259) (fig.3-9f), CA1 ($F=14.93_{(4,10)}$, p=0.0007) (fig. 3-8f), striatum ($H=12.57_{(4,12)}$, p= <0.0001) (fig. 3-13f), auditory cortex ($H(4, 12) =12.23_{(4,12)}$, p=0.0259) (fig. 3-12f) and motor cortex ($H=10.70_{(4,12)}$, p=0.191) (fig.3-11f). All regions also display a non-significant decrease in albumin infiltration in the 22-month group in comparison to the 18-month group. Within the male cohort, significant albumin increases were observed in the three available regions: CA1 ($T=7.084_{(7)}$, p=0.0006) (fig. 3-14f) CA3 ($T=20.51_{(7)}$, p=<0.0001) (fig.3-15f) and dentate gyrus ($T=9.766_{(7)}$, p=0.0013) (fig.3-16f), demonstrating an increased permeability to albumin in the males in comparison to the females. The other regions were not quantifiable due to tissue damage in the low n-number cohort in the three available regions: CA1 ($T=7.084_{(7)}$, p=0.0006) (fig. 3-14f) CA3 ($T=20.51_{(7)}$, p=<0.0001) (fig.3-15f) and dentate gyrus ($T=9.766_{(7)}$, p=0.0013) (fig.3-16f), demonstrating an increased permeability to albumin in the males in comparison to the females. The other regions were not quantifiable due to tissue damage in the low n-number cohort.

To track if infiltration of DiI-lip and albumin colocalised, suggesting a similar transport route, the interaction between albumin and DiI-lip was quantified. In females and males, all 18-month groups in each region demonstrated significantly increased colocalisation from 3 months group (all p=<0.0489) (fig. 3-8-3-17g), except for the female motor cortex (fig. 3-11g) and dentate gyrus (fig. 3-10g), which displayed non-significant increasing trends. The pattern of colocalisation reflected that of albumin infiltration, suggesting that similar transport routes were being followed.

To further determine if caveolae-mediated transport is linked to the infiltration of DiI-lip, immunofluorescence staining of caveolin-1, one of the main markers for caveolin transport alongside DiI-lip and CD31 antibodies (Pandit et al., 2020). To ensure that cav-1 expression was linked to the vasculature, the expression levels were normalised to %area coverage of CD31

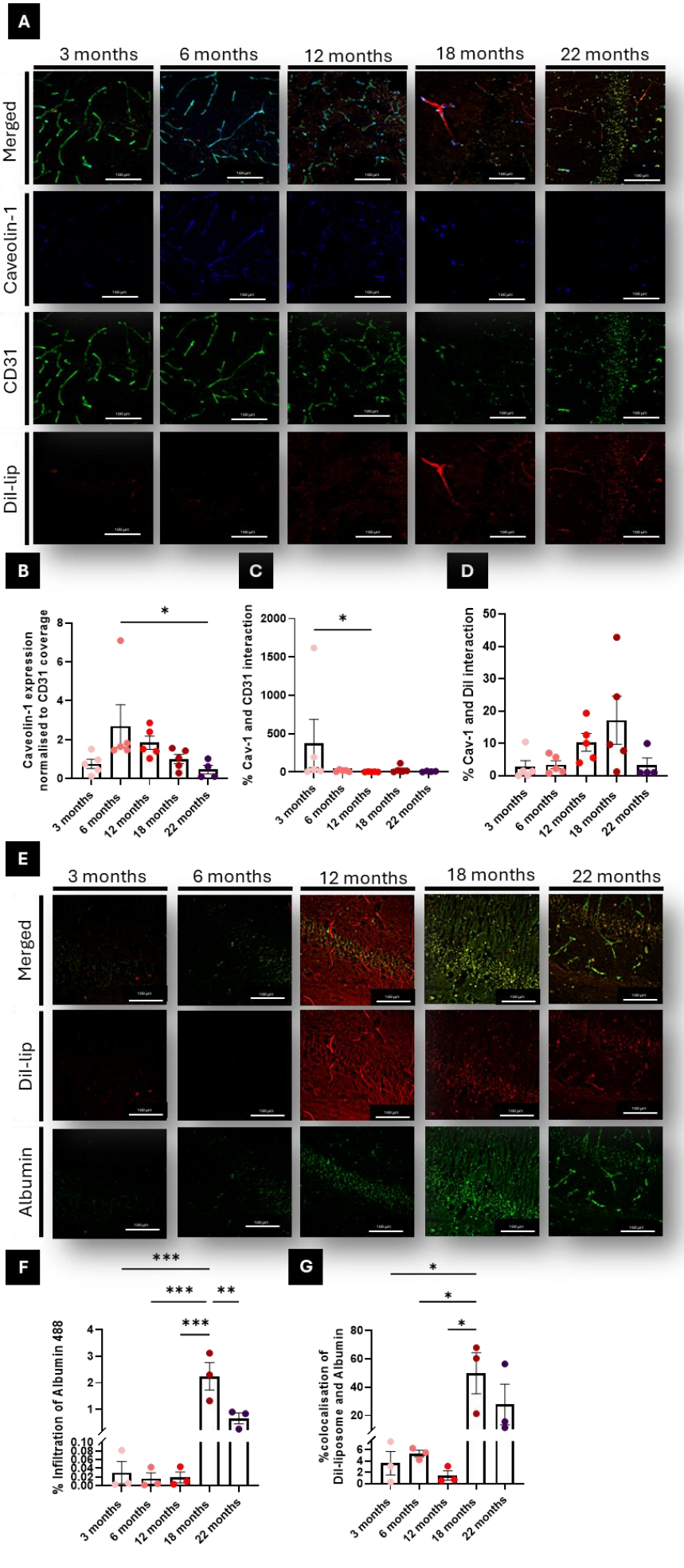
A
3 months
6 months
12 months
18 months
22 months
Merged
Caveolin-1
CD31
Dil-lip
B
Caveolin-1 expression normalised to CD31 coverage
C
% Cav-1 and CD31 interaction
D
% Cav-1 and Dil interaction
E
3 months
6 months
12 months
18 months
22 months
Merged
Dil-lip
Albumin
F
% Infiltration of Albumin 488
G
%colocalisation of Dil-liposome and Albumin

Figure 3-8: Evaluation of transcytosis transport in ageing female CA1 hippocampal region. C57BL/6 female mice groups at 3-, 6-, 12-, 18-, 22-months received a single intravenous injection of DiI-lip or DiI-lip and albumin. Cardiac perfusion was completed 2 hours post-injection to remove circulating DiI-lip and albumin.(A) Representative immunofluorescence images of CA1 hippocampal region -1.94mm from the bregma demonstrate expression of CD31 (green), Caveolin-1 (blue) and DiI-lip (Red). (B) Quantitative analysis of Caveolin-1 expression across ageing demonstrated decreasing expression between 6- and 22 months. (C) Quantitative interaction between CD31 and caveolin-1 expression normalised to CD31 expression demonstrated decreased expression from 3 months to older ages. (D) Quantitative interaction between caveolin-1 and DiI-lip expression normalised to caveolin-1 expression displayed trends to increases across ageing. (E) Representative immunofluorescence images of CA1 hippocampal region -1.94mm from bregma indicating infiltration of albumin (green) and DiI-liposomes (Red). (F) Quantitative analysis albumin infiltration demonstrating non-significant trends of increasing infiltration. (G) Quantitative analysis albumin and DiI-lip colocalisation showing increases in ageing. Images obtained at x40 magnification on Leica Thunder microscope and underwent large volume computational clearing (LVCC) prior to quantification in Image J. Statistical analysis was completed using GraphPad Prism software using one-way analysis of variance followed by Tukey multiple comparison test or Kruskal-Wallis test followed by Dunn's multiple comparisons test based on Shaprio-Wilk test for normality. N=4-5 (caveolin-1), 3 (albumin),average ± SEM, $p<0.05$ were considered significant. Scale bar represents 100µm.

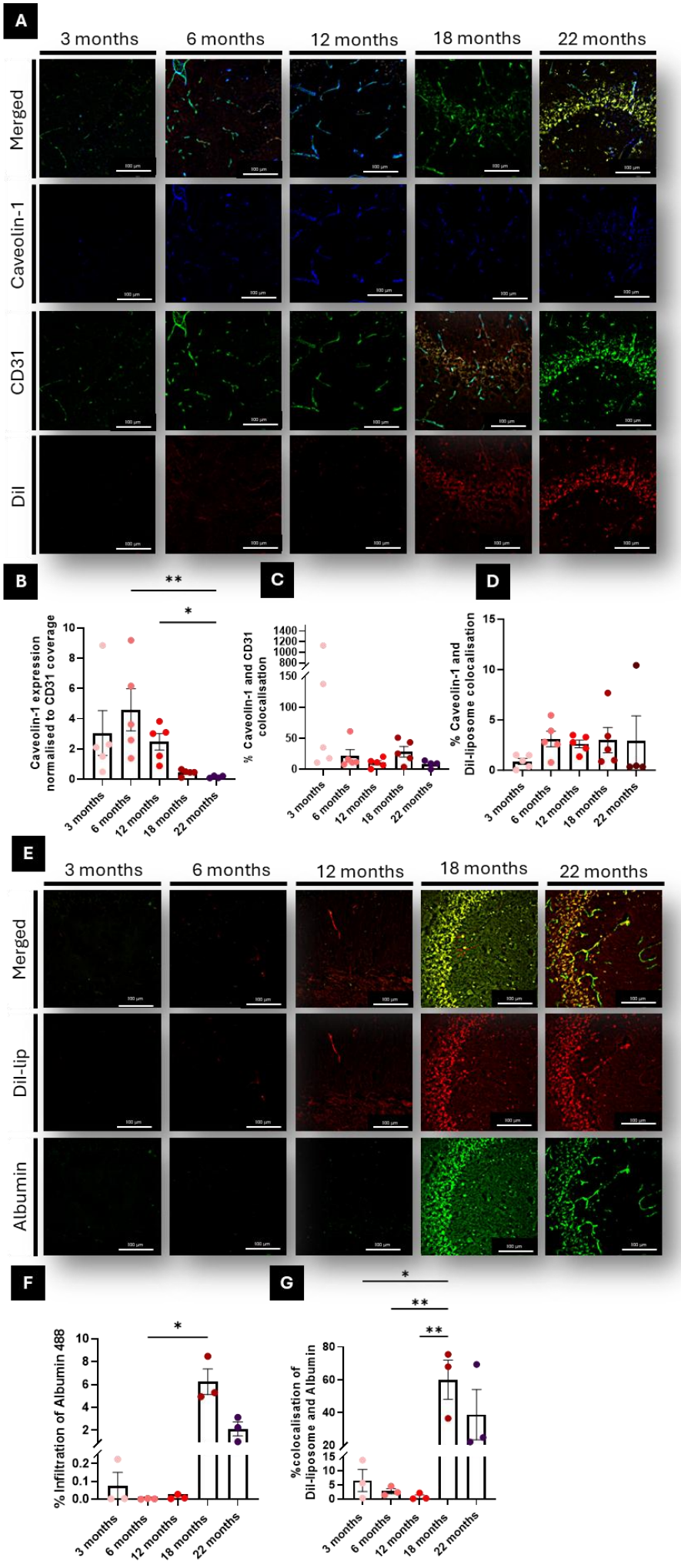
A
3 months
6 months
12 months
18 months
22 months
Merged
Caveolin-1
CD31
DiI
B
C
D
**
*
Caveolin-1 expression normalised to CD31 coverage
% Caveolin-1 and CD31 colocalisation
% Caveolin-1 and DiI-liposome colocalisation
E
Merged
DiI-lip
Albumin
F
G
% Infiltration of Albumin 488
%colocalisation of DiI-liposome and Albumin

Figure 3-9: Evaluation of transcytosis transport in ageing female CA3 hippocampal region.C57BL/6 female mice groups at 3-, 6-, 12-, 18-, 22-months received a single intravenous injection of DiI-lip or DiI-lip and albumin. Cardiac perfusion was completed 2 hours post-injection to remove circulating DiI-lip and albumin. (A) Representative immunofluorescence images of CA3 hippocampal region -1.94mm from the bregma demonstrate expression of CD31 (green), Caveolin-1 (blue) and DiI-lip (Red). (B) Quantitative analysis of Caveolin-1 expression across ageing demonstrated decreasing expression between in 6- and 12-months to 22 months (C) Quantitative interaction between CD31 and caveolin-1 expression normalised to CD31 expression demonstrated no changes to older ages. (D) Quantitative interaction between caveolin-1 and DiI-lip expression normalised to caveolin-1 expression displayed trends to increases across ageing from 3-month group. (E) Representative immunofluorescence images of CA3 hippocampal region -1.94mm from bregma indicating infiltration of albumin (green) and DiI-liposomes (Red). (F) Quantitative analysis albumin infiltration demonstrating significant trends of increasing infiltration. (G) Quantitative analysis albumin and DiI-lip colocalisation showing increases in ageing. Images obtained at x40 magnification on Leica Thunder microscope and underwent large volume computational clearing (LVCC) prior to quantification in Image J. Statistical analysis was completed using GraphPad Prism software using one-way analysis of variance followed by Tukey multiple comparison test or Kruskal-Wallis test followed by Dunn's multiple comparisons test based on Shaprio-Wilk test for normality. N=4-5 (caveolin-1), 3 (albumin),average ± SEM, $p<0.05$ were considered significant. Scale bar represents 100µm.

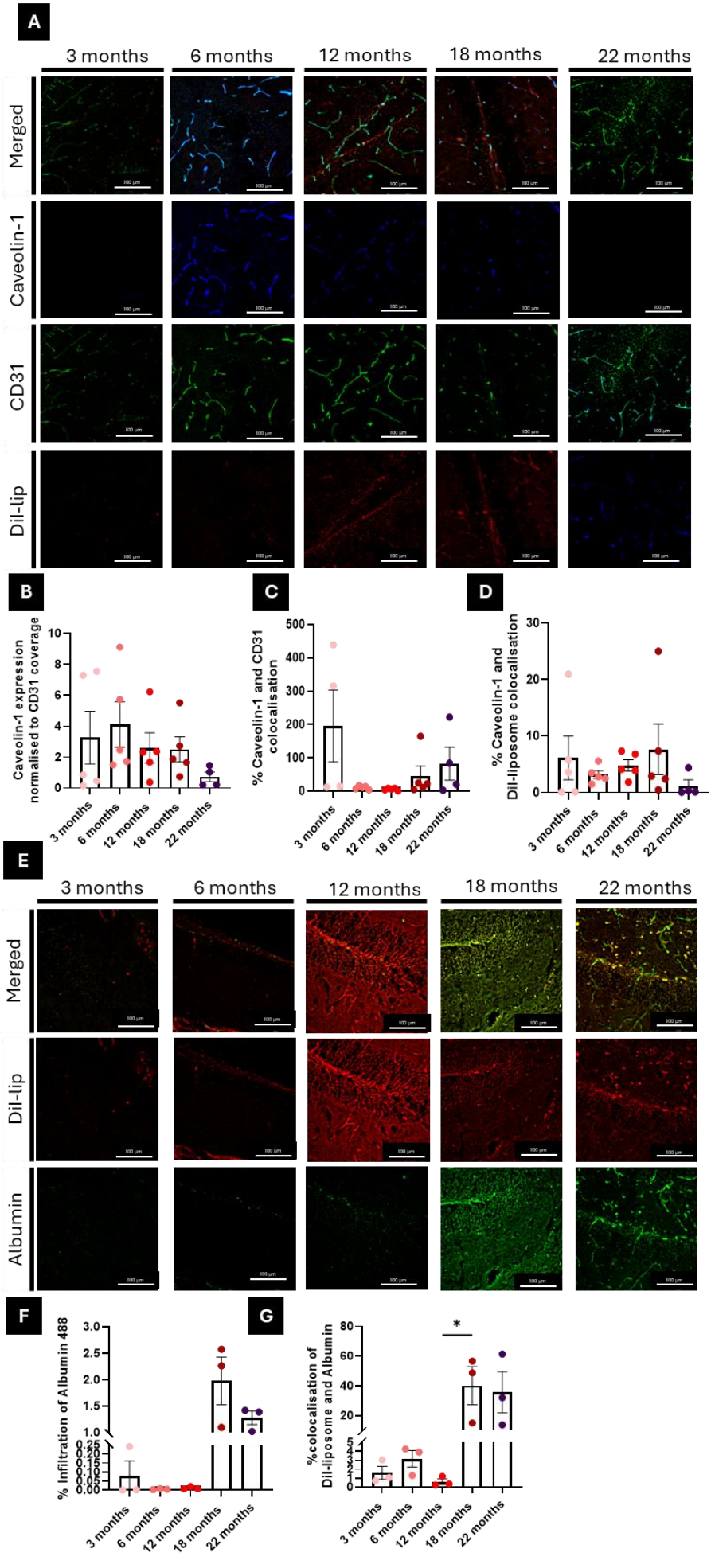
A
3 months
6 months
12 months
18 months
22 months
Merged
Caveolin-1
CD31
Dil-lip
B
Caveolin-1 expression normalised to CD31 coverage
C
% Caveolin-1 and CD31 colocalisation
D
% Caveolin-1 and Dil-liposome colocalisation
E
Albumin
F
% Infiltration of Albumin 488
G
%colocalisation of Dil-liposome and Albumin
*

Figure 3-10 : Evaluation of transcytosis transport in ageing female dentate gyrus hippocampal region. C57BL/6 female mice groups at 3-, 6-, 12-, 18-, 22-months received a single intravenous injection of DiI-lip and albumin. Cardiac perfusion was completed 2 hours post-injection to remove circulating DiI-li and albumin.(A) Representative immunofluorescence images of dentate gyrus hippocampal region -1.94mm from the bregma demonstrate expression of CD31 (green), Caveolin-1 (blue) and DiI-lip (Red). (B) Quantitative analysis of Caveolin-1 expression across ageing demonstrated no significant changes to caveolin-1 throughout ageing. (C) Quantitative interaction between CD31 and caveolin-1 expression normalised to CD31 expression demonstrated no significant changes to colocalization from 3 months to older ages. (D) Quantitative interaction between caveolin-1 and DiI-lip expression normalised to caveolin-1 expression displayed no trends across ageing. (E) Representative immunofluorescence images of dentate gyrus hippocampal regions -1.94mm from bregma indicating infiltration of albumin (green) and DiI-liposomes (Red). (F) Quantitative analysis albumin infiltration demonstrating non-significant trends of increasing infiltration. (G) Quantitative analysis albumin and DiI-lip colocalisation showing increases in ageing. Images obtained at x40 magnification on Leica Thunder microscope and underwent large volume computational clearing (LVCC) prior to quantification in Image J. Statistical analysis was completed using GraphPad Prism software using one-way analysis of variance followed by Tukey multiple comparison test or Kruskal-Wallis test followed by Dunn's multiple comparisons test based on Shaprio-Wilk test for normality. N=4-5 (caveolin-1), 3 (albumin),,average ± SEM, $p<0.05$ were considered significant. Scale bar represents 100µm

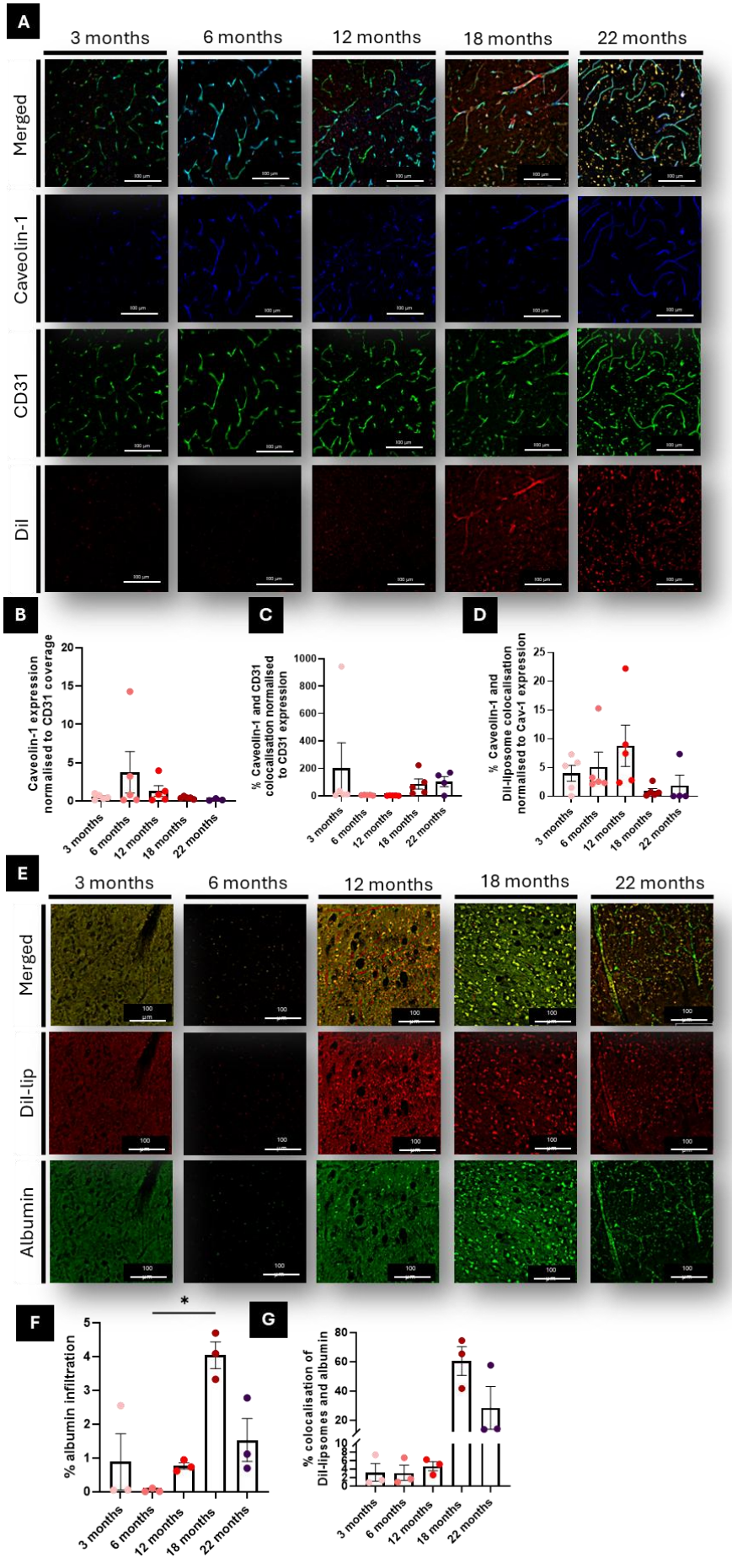
A
3 months
6 months
12 months
18 months
22 months
Merged
Caveolin-1
CD31
DiI
B
Caveolin-1 expression normalised to CD31 coverage
C
% Caveolin-1 and CD31 colocalisation normalised to CD31 expression
D
% Caveolin-1 and DiI-liposome colocalisation normalised to Cav-1 expression
E
Merged
DiI-lip
Albumin
F
% albumin infiltration
*
G
% colocalisation of DiI-liposomes and albumin

Figure 3-11: Evaluation of transcytosis transport in ageing female motor cortex region. C57BL/6 female mice groups at 3-, 6-, 12-, 18-, 22-months received a single intravenous injection of DiI-lip and albumin. Cardiac perfusion was completed 2 hours post-injection to remove circulating DiI-lip.(A) Representative immunofluorescence images of motor cortex region -1.94mm from the bregma demonstrate expression of CD31 (green), Caveolin-1 (blue) and DiI-lip (Red). (B) Quantitative analysis of Caveolin-1 expression across ageing demonstrated no significant changes to caveolin-1 throughout ageing. (C) Quantitative interaction between CD31 and caveolin-1 expression normalised to CD31 expression demonstrated no changes from 3 months to older ages. (D) Quantitative interaction between caveolin-1 and DiI-lip expression normalised to caveolin-1 expression displayed no changes. (E) Representative immunofluorescence images of motor cortex region -1.94mm from bregma indicating infiltration of albumin (green) and DiI-liposomes (Red). (F) Quantitative analysis albumin infiltration demonstrating non-significant trends of increasing infiltration. (G) Quantitative analysis albumin and DiI-lip colocalisation showing non-significant increases in ageing. Images obtained at x40 magnification on Leica Thunder microscope and underwent large volume computational clearing (LVCC) prior to quantification in Image J. Statistical analysis was completed using GraphPad Prism software using one-way analysis of variance followed by Tukey multiple comparison test or Kruskal-Wallis test followed by Dunn's multiple comparisons test based on Shaprio-Wilk test for normality. N=4-5 (caveolin-1), 3 (albumin),average ± SEM, $p<0.05$ were considered significant. Scale bar represents 100µm.

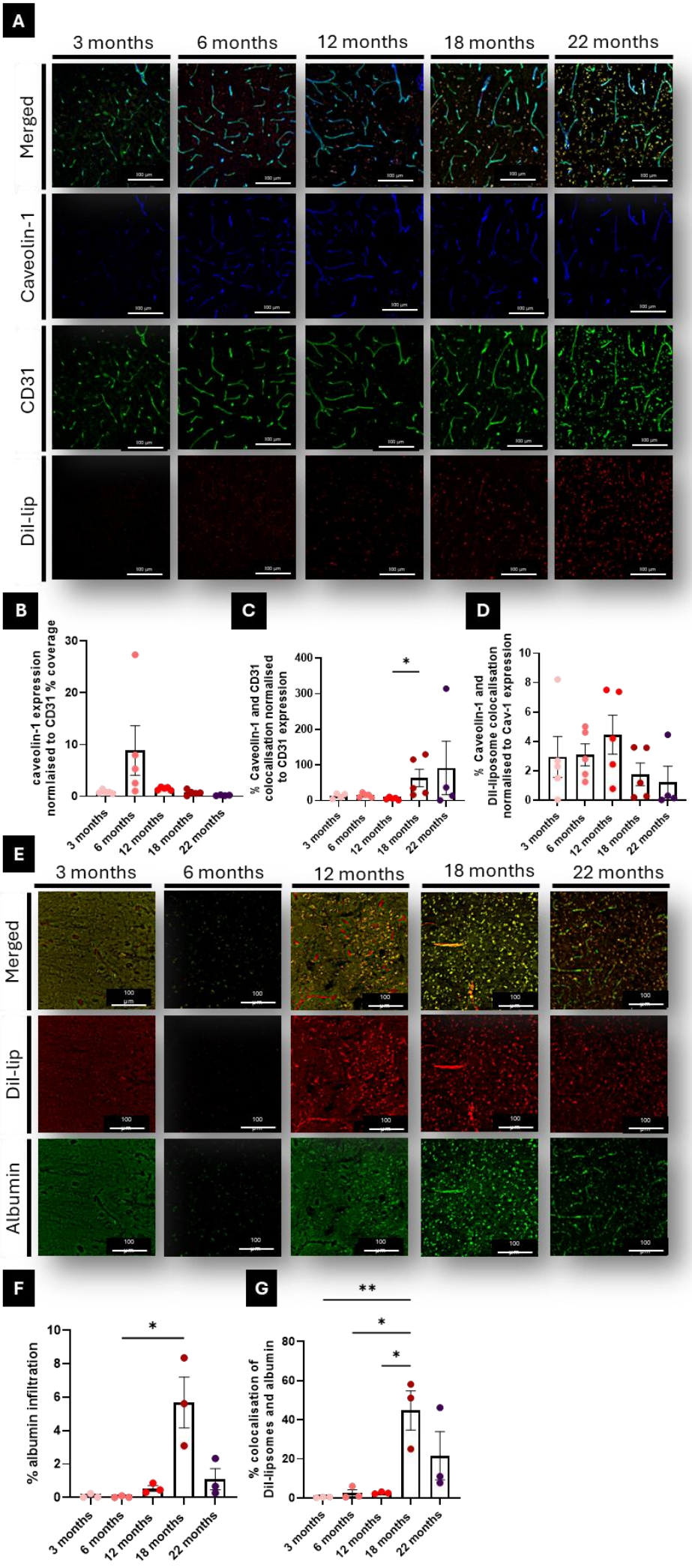
A
3 months
6 months
12 months
18 months
22 months
Merged
Caveolin-1
CD31
Dil-lip
B
caveolin-1 expression normlaised to CD31 % coverage
C
% Caveolin-1 and CD31 colocalisation normalised to CD31 expression
*
D
% Caveolin-1 and Dil-liposome colocalisation normalised to Cav-1 expression
E
Merged
Dil-lip
Albumin
F
% albumin infiltration
*
G
% colocalisation of Dil-lipsomes and albumin
**
*
*

Figure 3-12: Evaluation of transcytosis in ageing female auditory cortex region. C57BL/6 female mice groups at 3-, 6-, 12-, 18-, 22-months received a single intravenous injection of DiI-lip or DiI-lip and albumin. Cardiac perfusion was completed 2 hours post-injection to remove circulating DiI-lip and albumin.(A) Representative immunofluorescence images of auditory cortex region -1.94mm from the bregma demonstrate expression of CD31 (green), Caveolin-1 (blue) and DiI-lip (Red). (B) Quantitative analysis of Caveolin-1 expression across ageing demonstrated no significant changes to caveolin-1 throughout ageing. (C) Quantitative interaction between CD31 and caveolin-1 expression normalised to CD31 expression demonstrated increased expression from 12 months to 18-months. (D) Quantitative interaction between caveolin-1 and DiI-lip expression normalised to caveolin-1 expression displayed no trends across ageing. (E) Representative immunofluorescence images of auditory cortex region -1.94mm from bregma indicating infiltration of albumin (green) and DiI-liposomes (Red). (F) Quantitative analysis albumin infiltration demonstrating non-significant trends of increasing infiltration. (G) Quantitative analysis albumin and DiI-lip colocalisation showing increases in ageing. Images obtained at x40 magnification on Leica Thunder microscope and underwent large volume computational clearing (LVCC) prior to quantification in Image J. Statistical analysis was completed using GraphPad Prism software using one-way analysis of variance followed by Tukey multiple comparison test or Kruskal-Wallis test followed by Dunn's multiple comparisons test based on Shaprio-Wilk test for normality. N=4-5 (caveolin-1), 3 (albumin),average ± SEM, $p<0.05$ were considered significant. Scale bar represents 100µm.

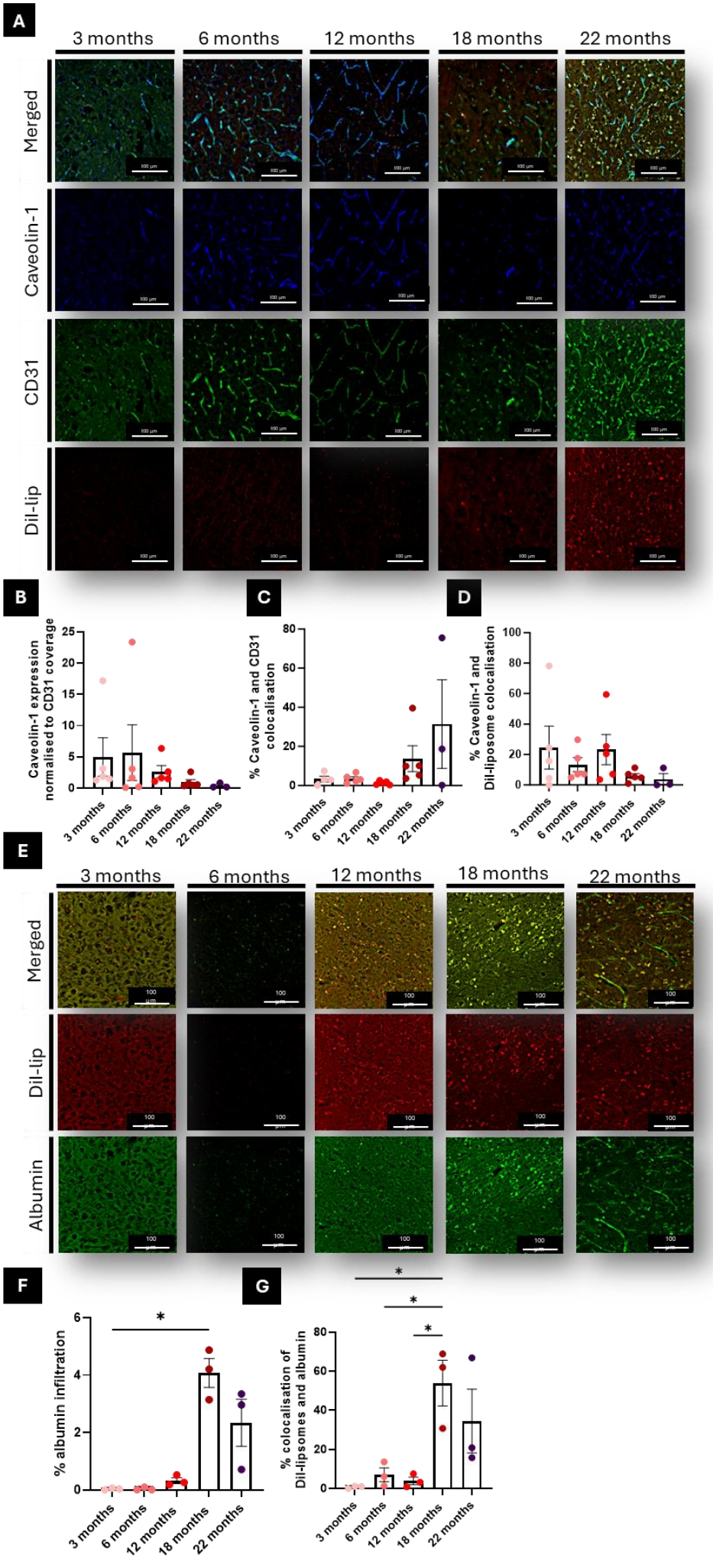
A
3 months
6 months
12 months
18 months
22 months
Merged
Caveolin-1
CD31
Dil-lip
B
Caveolin-1 expression normalised to CD31 coverage
C
% Caveolin-1 and CD31 colocalisation
D
% Caveolin-1 and Dil-liposome colocalisation
E
Merged
Dil-lip
Albumin
F
% albumin infiltration
G
% colocalisation of Dil-lipsomes and albumin

Figure 3-13: Caveolin-1 expression in ageing female striatum region. C57BL/6 female mice groups at 3-, 6-, 12-, 18-, 22-months received a single intravenous injection of DiI-lip or DiI-lip and albumin. Cardiac perfusion was completed 2 hours post-injection to remove circulating DiI-lip and albumin.(A) Representative immunofluorescence images of auditory cortex region -1.94mm from the bregma demonstrate expression of CD31 (green), Caveolin-1 (blue) and DiI-lip (Red). (B) Quantitative analysis of Caveolin-1 expression across ageing demonstrated no significant changes to caveolin-1 throughout ageing. (C) Quantitative interaction between CD31 and caveolin-1 expression normalised to CD31 expression demonstrated increased trends in colocalisation expression from 3 months to 22- months. (D) Quantitative interaction between caveolin-1 and DiI-lip expression normalised to caveolin-1 expression displayed no trends to across ageing. (E) Representative immunofluorescence images of striatum region -1.94mm from bregma indicating infiltration of albumin (green) and DiI-liposomes (Red). (F) Quantitative analysis albumin infiltration demonstrating non-significant trends of increasing infiltration. (G) Quantitative analysis albumin and DiI-lip colocalisation showing increases in ageing. Images obtained at x40 magnification on Leica Thunder microscope and underwent large volume computational clearing (LVCC) prior to quantification in Image J. Statistical analysis was completed using GraphPad Prism software using one-way analysis of variance followed by Tukey multiple comparison test or Kruskal-Wallis test followed by Dunn's multiple comparisons test based on Shaprio-Wilk test for normality. N=4-5 (caveolin-1), 3 (albumin),average ± SEM, $p<0.05$ were considered significant. Scale bar represents 100µm.

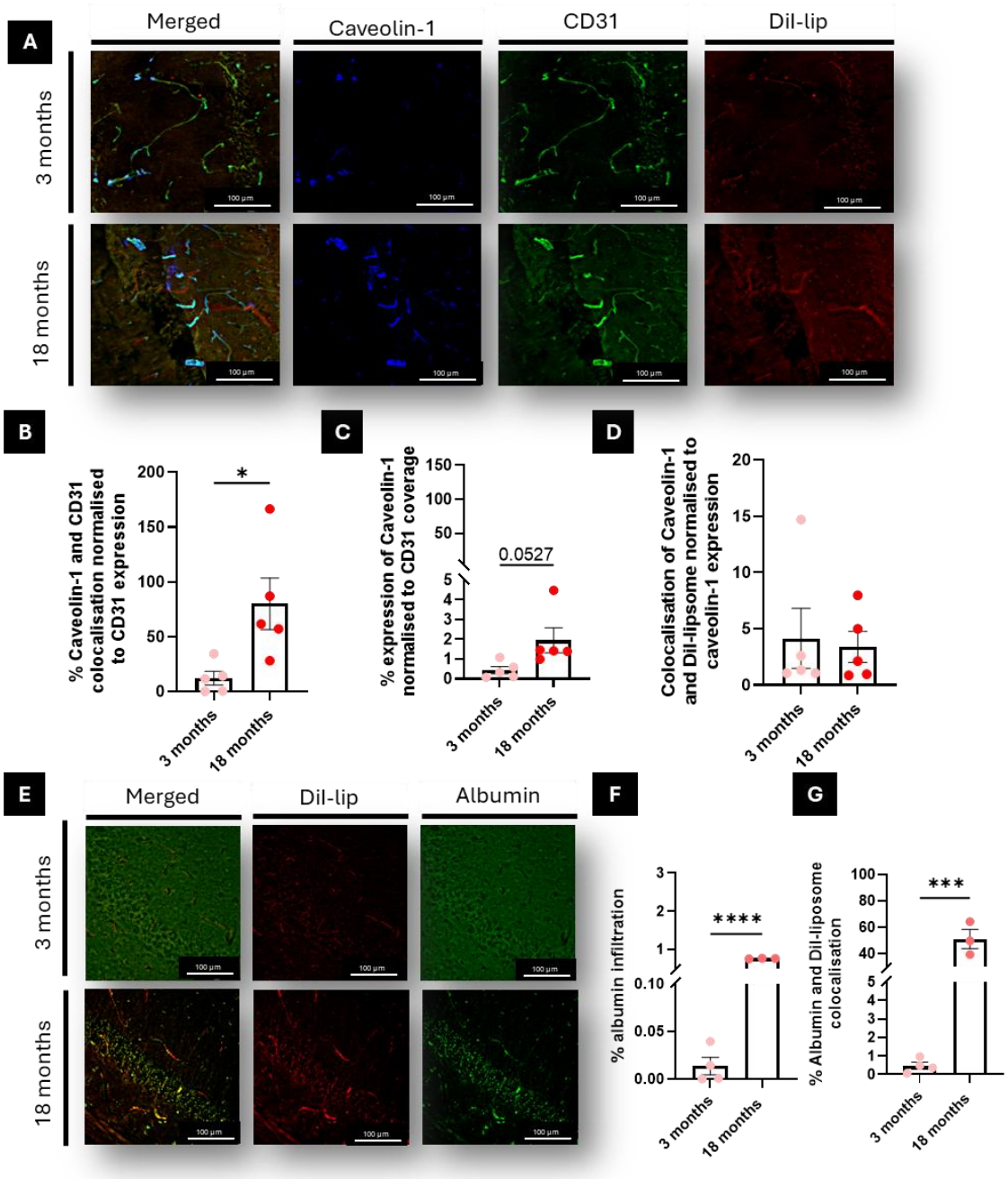

Figure 3-14: Evaluation of transcytosis pathway in ageing male CA1 hippocampal region. C57BL/6 male mice groups at 3 an 18-months old received a single intravenous injection of DiI-lip. Cardiac perfusion was completed 2 hours post-injection to remove circulating DiI-lip.(A) Representative immunofluorescence images of CA1 hippocampal region -1.94mm from the bregma demonstrate expression of CD31 (green), Caveolin-1 (blue) and DiI-lip (Red). (B) Quantitative analysis of Cav-1 expression across ageing demonstrated increasing expression in ageing. (C) Quantitative interaction between CD31 and Cav-1 expression normalised to CD31 coverage demonstrated increasing colocalization. (D) Quantitative interaction between Cav-1 and DiI-lip expression normalised to Cav-1 expression did not demonstrate any age-related changes. (E) Representative immunofluorescence images of dentate gyrus hippocampal regions -1.94mm from bregma indicating infiltration of albumin (green) and DiI-liposomes (Red). (F) Quantitative analysis albumin infiltration demonstrating significant trends of increasing infiltration. (G) Quantitative analysis albumin and DiI-lip colocalisation showing increases in ageing. Images obtained at x40 magnification on Leica Thunder microscope and underwent large volume computational clearing (LVCC) prior to quantification in Image J. Statistical analysis was completed using GraphPad Prism software using Shapiro Wilk test for normality followed by either a T-test or Mann-Whitney. N=5 (caveolin-1) N=3-4 (albumin), average ± SEM, $p<0.05$ were considered significant. Scale bar represents 100µm.

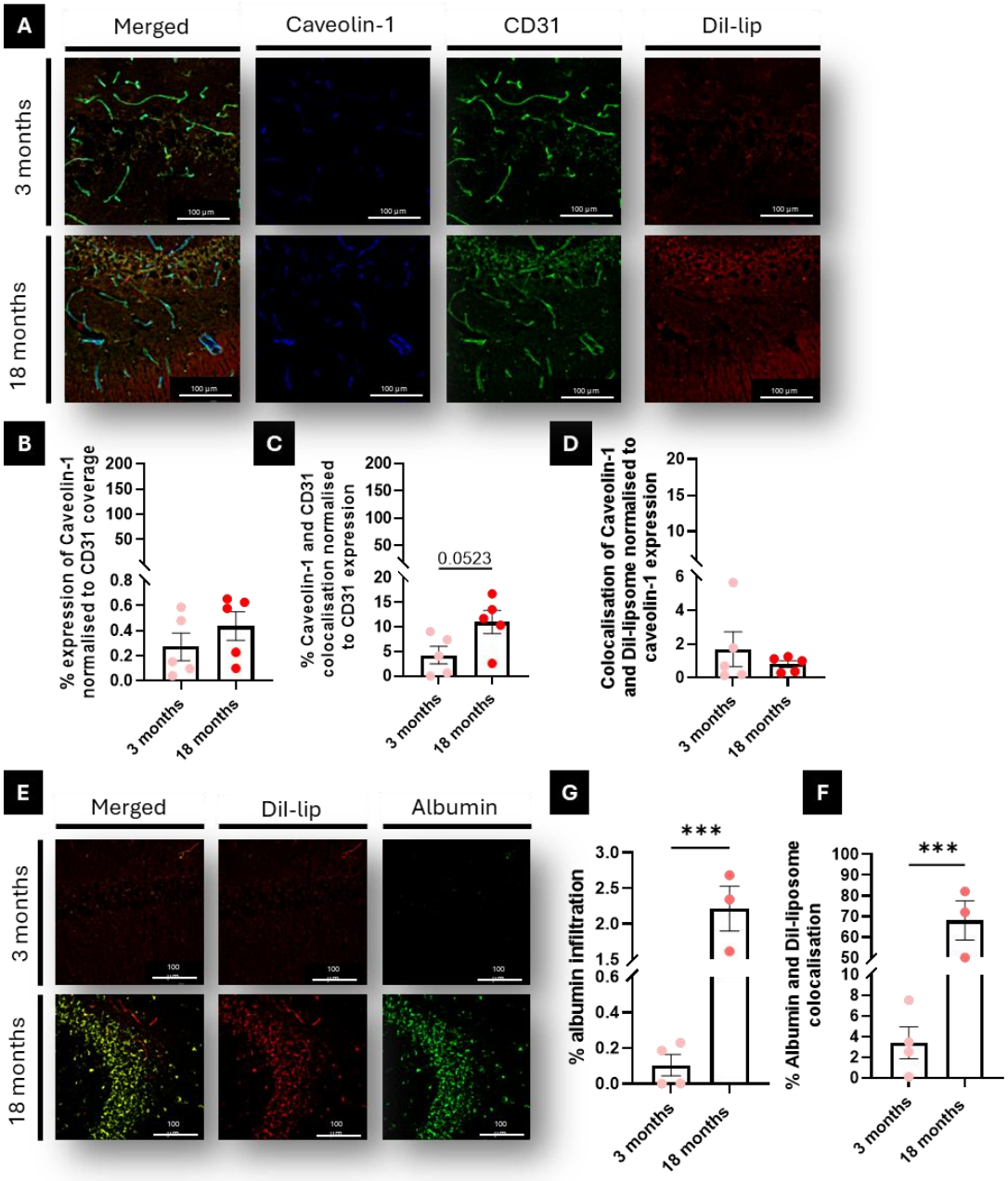

Figure 3-15: Evaluation of transcytosis pathway in ageing male CA3 hippocampal region. C57BL/6 male mice groups at 3 an 18-months old received a single intravenous injection of Dil-lip. Cardiac perfusion was completed 2 hours post-injection to remove circulating Dil-lip.(A) Representative immunofluorescence images of CA3 hippocampal region -1.94mm from the bregma demonstrate expression of CD31 (green), Caveolin-1 (blue) and Dil-lip (Red). (B) Quantitative analysis of Cav-1 expression across ageing demonstrated no significant expression changes in ageing. (C) Quantitative interaction between CD31 and Cav-1 expression normalised to CD31 coverage demonstrated non-significant increasing trends. (D) Quantitative interaction between Cav-1 and Dil-lip expression normalised to Cav-1 expression did not change across ageing. (E) Representative immunofluorescence images of dentate gyrus hippocampal regions -1.94mm from bregma indicating infiltration of albumin (green) and Dil-liposomes (Red). (F) Quantitative analysis albumin infiltration demonstrating significant trends of increasing infiltration. (G) Quantitative analysis albumin and Dil-lip colocalisation showing increases in ageing. Images obtained at x40 magnification on Leica Thunder microscope and underwent large volume computational clearing (LVCC) prior to quantification in Image J. Statistical analysis was completed using GraphPad Prism software using Shapiro Wilk test for normality followed by either a T-test or Mann-Whitney. N=5 *(*caveolin-1) N=3-4 (albumin),average ± SEM, $p<0.05$ were considered significant. Scale bar represents 100µm.

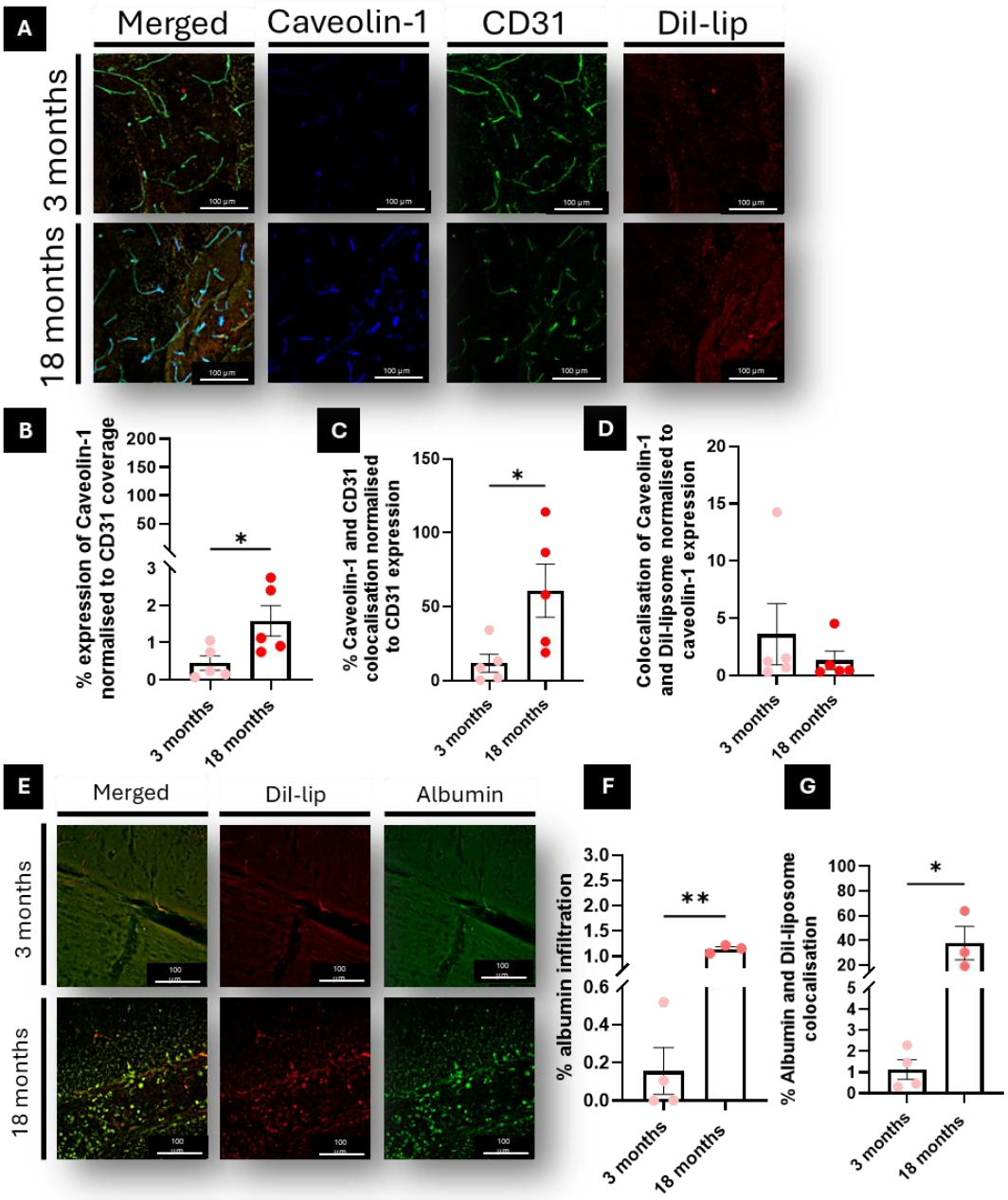

Figure 3-16: Evaluation of transcytosis pathway in ageing male dentate gyrus hippocampal region. C57BL/6 male mice groups at 3 an 18-months old received a single intravenous injection of DiI-lip. Cardiac perfusion was completed 2 hours post-injection to remove circulating DiI-lip.(A) Representative immunofluorescence images of dentate gyrus hippocampal region -1.94mm from the bregma demonstrate expression of CD31 (green), Caveolin-1 (blue) and DiI-lip (Red). (B) Quantitative analysis of cav-1 expression across ageing demonstrated increasing expression in ageing. (C) Quantitative interaction between CD31 and Cav-1 expression normalised to CD31 coverage demonstrated increasing colocalization in ageing. (D) Quantitative interaction between Cav-1 and DiI-lip expression normalised to Cav-1 expression did not significantly change across ageing. (E) Representative immunofluorescence images of dentate gyrus hippocampal regions -1.94mm from bregma indicating infiltration of albumin (green) and DiI-liposomes (Red). (F) Quantitative analysis albumin infiltration demonstrating significant trends of increasing infiltration. (G) Quantitative analysis albumin and DiI-lip colocalisation showing increases in ageing. Images obtained at x40 magnification on Leica Thunder microscope and underwent large volume computational clearing (LVCC) prior to quantification in Image J. Statistical analysis was completed using GraphPad Prism software using Shapiro Wilk test for normality followed by either a T-test or Mann-Whitney N=5 (caveolin-1) N=3-4 (albumin), average ± SEM, $p<0.05$ were considered significant. Scale bar represents 100µm.

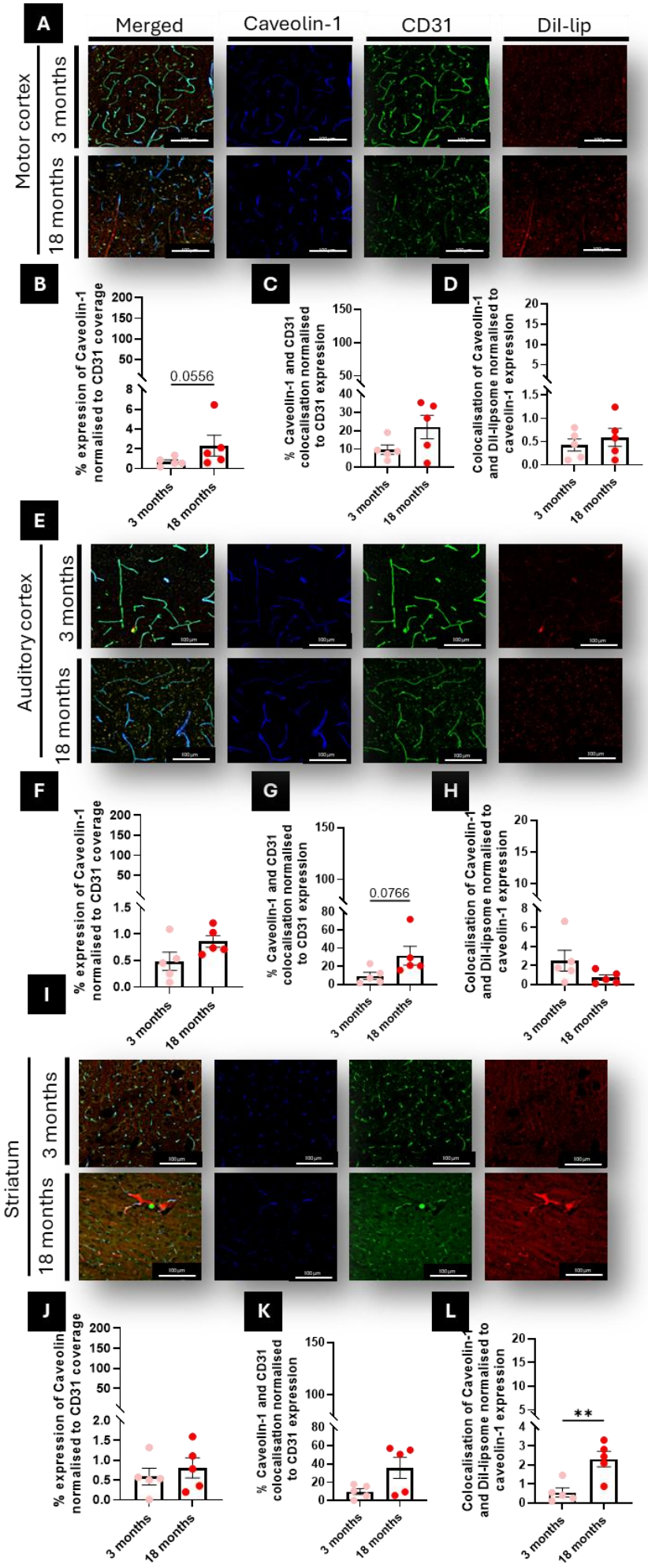
A
Merged
Caveolin-1
CD31
Dil-lip
Motor cortex
3 months
18 months
B
% expression of Caveolin-1 normalised to CD31 coverage
0.0556
3 months
18 months
C
% Caveolin-1 and CD31 colocalisation normalised to CD31 expression
D
Colocalisation of Caveolin-1 and Dil-lipsome normalised to caveolin-1 expression
E
Auditory cortex
F
G
0.0766
H
I
Striatum
J
K
L
**

Figure 3-17: Caveolin-1 expression in ageing male cortex and striatal regions. C57BL/6 male mice groups at 3 an 18-months old received a single intravenous injection of DiI-lip. Cardiac perfusion was completed 2 hours post-injection to remove circulating DiI-lip. (A) Motor cortex, (E) auditory cortex, (I) Striatum; representative immunofluorescence images of striatum region -1.94mm from the bregma demonstrate expression of CD31 (green), Caveolin-1 (blue) and DiI-lip (Red). Quantitative analysis of caveolin-1 expression normalised to CD31 endothelial coverage demonstrated no significant changes in (B) motor cortex, (F) auditory cortex and (J) striatum. No significant quantitative changes were seen across ageing regarding the interaction of Caveolin-1 and CD31 in (C) motor cortex, (G) auditory cortex or (K) striatum. Quantitative analysis of the interaction between caveolin-1 and DiI-lip, normalised to caveolin-1 expression, displayed no significant age changes in (D) motor cortex or (H) auditory cortex. The striatum region (L) showed significant increases in caveolin-1 and DiI-lip interaction in ageing. All images were obtained at x40 magnification on Leica Thunder microscope and underwent large volume computational clearing (LVCC) prior to quantification in Image J. Statistical analysis was completed using GraphPad Prism software using Shapiro Wilk test for normality followed by either a T-test or Mann-Whitney. N=5,average ± SEM, $p<0.05$ were considered significant. Scale bar represents 100µm.

within each image like methodology seen in previous literature (Yang et al., 2020). Interestingly, when investigating the expression patterns in the female cohort, there was a different overall expression pattern. Cav-1 in the CA1 ($H=13.19_{(4,19)}$, p=0.0104) (fig.3-14) and CA3 ($H=16.78_{(4,19)}$, p=0.0031) (fig.3-15b) demonstrated significant decreases in expression between the younger groups and 18- and 22-months from the 6-month group which is the inverse to the hypothesis expectations. Throughout all regions, the 6-month group produced the highest expression of cav-1 which then reduced stepwise through the rest of the age groups to 22-months, even if statistically non-significant the heterogenous pattens of this expression cannot be ignored (fig.3-8-3-17b). Within the male cohort, expected age-related significant increases of Cav-1 were seen within the dentate gyrus between 3- and 18-months ($T=4.620_{(10)}$, p=0.0369) (fig. 3-16b) whilst trends to increasing expression were observed in the CA1 ($T=14.09_{(10)}$, p=0.0627) (fig. 3-14b) and motor cortex regions ($U(10) =3_{(10)}$, p=0.0556) (fig. 3-17b). No significant trends were observed in the CA3, auditory cortex and striatum regions, demonstrating a region dependent expression of Cav-1 (fig. 3-15, 3-17f-j).

To confirm that the cav-1 expression was correlated to the vasculature, interactions between CD31 and cav-1 was examined from the same selected images. It would be expected that groups would display higher colocalisation of cav-1 and CD31 throughout ageing when cav-1 expression is increased. In the female cohort, regional variation persisted with no significant colocalisation changes in the CA3 (fig.3-9c), dentate gyrus (fig.3-10c), motor cortex (fig. 3-11c) and striatum (fig. 3-12c) across all aged groups. The CA1 region (fig.3-8c) showed increased colocalisation at 3 months in compassion to all other groups (significant with the 12-month group, $H=10.12_{(4, 19)}$, p=0.0365) whilst the auditory cortex has an inverse expression pattern, with the 18- and 22-months showing increased cav-1/CD31 interaction, with significance between the 12- and 18-month groups ($H=9.611_{(4, 19)}$, p=0.0244) (fig. 3-12c). In the male cohort, there was significant age-related increases as predicted in the colocalisation in the CA1 ($T=11.73_{(10)}$, p=0.0236) (fig.3-14c) and dentate gyrus ($T=8.655_{(10)}$, p=0.0320) (fig.3-16c) with non-significant trends in the CA3 ($T=1.745_{(10)}$, p=0.0523) (fig.3-15c) and auditory cortex ($T=7.067_{(10)}$,

p=0.0766) (fig.3-17g) when comparing the 3- to 18- month groups. The striatum region displayed limited trends towards increases in ageing groups (fig.3-17k).

Finally, colocalisation of Cav-1 and DiI-lip was investigated to determine if infiltration of nanoparticles follows the same pathways as cav-1. If they do interact, it would suggest a link between caveolin-mediated transcytosis and nanoparticle infiltration in age, comparable to that of stroke (Al-Ahmady et al., 2019). In the female cohort, there was no significant changes across ageing in any of the investigated regions (fig. 3-8- fig. 3-13d) indicating that Cav-1 did not interact with DiI-lip more in aged groups then in younger age groups. In the male cohort, only the striatum region (fig.3-17l) displayed predicted patterns with colocalisation increasing significantly from 3-month to 18-month groups ($T=2.996_{(4,10)}$, p=0.061). All other regions displayed no significant changes in interaction, although interestingly the auditory cortex did show a small trend to decreasing colocalisation, possibly indicating that cav-1 and DiI-lip are not interacting with age (fig. 3-14d.-fig. 3-17d,h).

3.5.5. **Extravasation of immunoglobulin G into brain parenchyma**

To determine if there is further BBB disruption leading to increased permeability, IgG extravasation was examined as previous literature has displayed significant increases in ageing in both murine and human models (Elahy et al., 2015; Goodall et al., 2018; Yang et al., 2020). Results of the current study show limited IgG infiltration into the brain across ageing. In the female cohort, there was no significant changes in the 3 hippocampal regions (fig.3-18e-g) and striatum but between 3- and 18- months there were significant increases in the auditory cortex ($H=10.74_{(32)}$, p= 0.022) and the motor cortex ($H=12.02_{(32)}$, p=0.043) (fig. 3-18b,c). Conversely, male mice display no significant changes comparing 3- to 18-month mice (fig. 3-19b-g). The results of this study are surprising and do not fully align with the literature or proposed actions of ageing on the BBB and so requires further discussion.

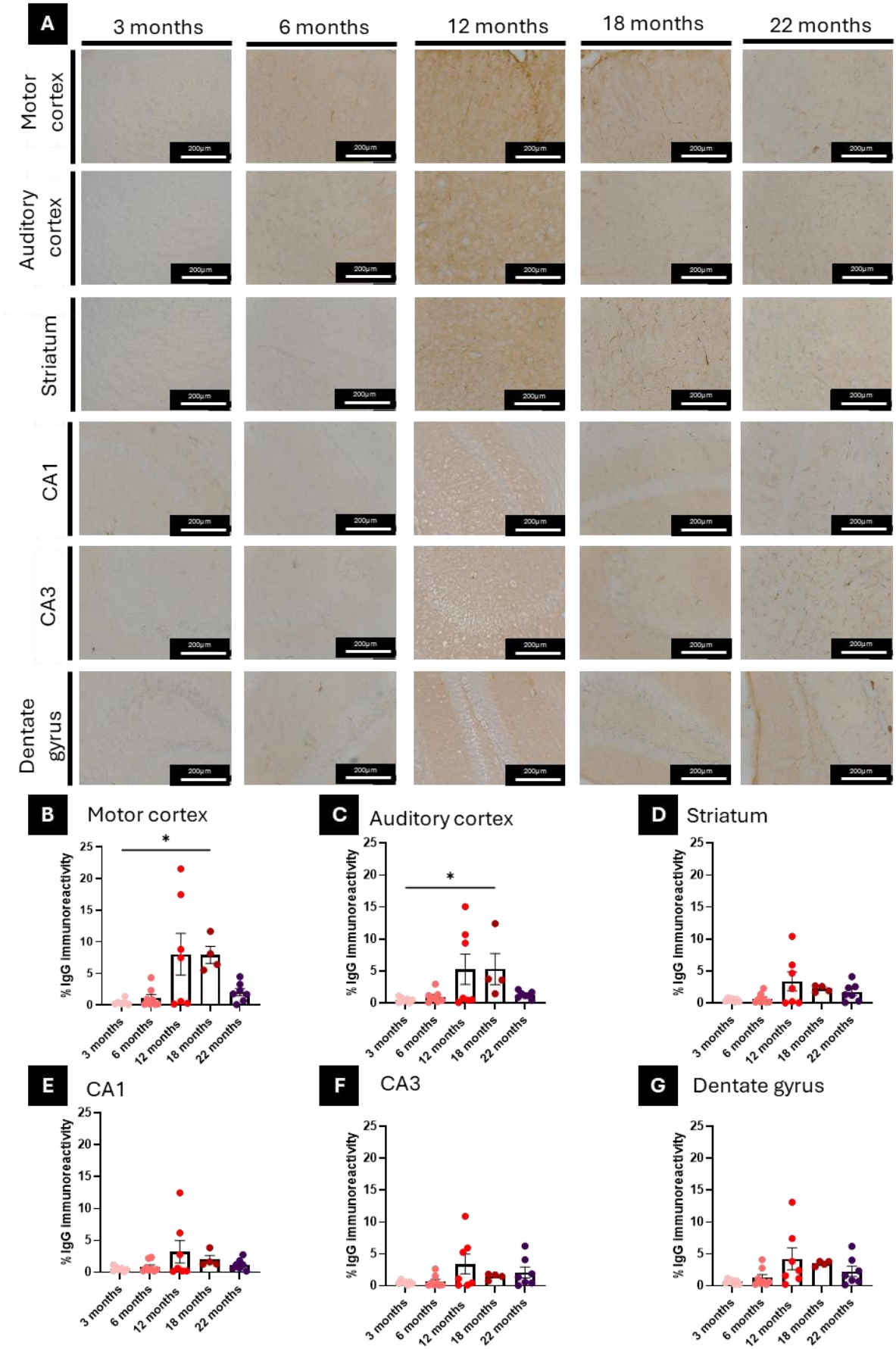

Figure 3-18: Immunoglobulin G infiltration in ageing female mouse brain. C57BL/6 female mice groups at 3-, 6-, 12-, 18-, 22-months. Cardiac perfusion was completed 2 hours post-injection to remove circulating DiI-lip. IgG immunohistochemistry conducted on 30µm cryosections approximately -1.94mm from bregma.(A) Representative immunofluorescence images of Motor and Auditory cortex,

striatum, CA1, CA3 and dentate gyrus regions indicating infiltration of Immunoglobulin G (Brown). (B) Quantitative analysis of motor cortex region showing significant increase in IgG with age. (C) Quantitative analysis of auditory cortex region, with significant increases in age. All other regions showed no changes through ageing; (D) striatum, (E) CA1, (F) CA3 and (G) dentate gyrus. Images obtained at x20 magnification on Leica Thunder microscope prior to quantification in Image J. Statistical analysis was completed using GraphPad Prism software using one-way analysis of variance followed by Tukey multiple comparison test or Kruskal-Wallis test followed by Dunn's multiple comparisons test based on Shapiro-Wilk test for normality. N=4-8,average ± SEM, $p<0.05$ were considered significant. Scale bar represents 200µm.

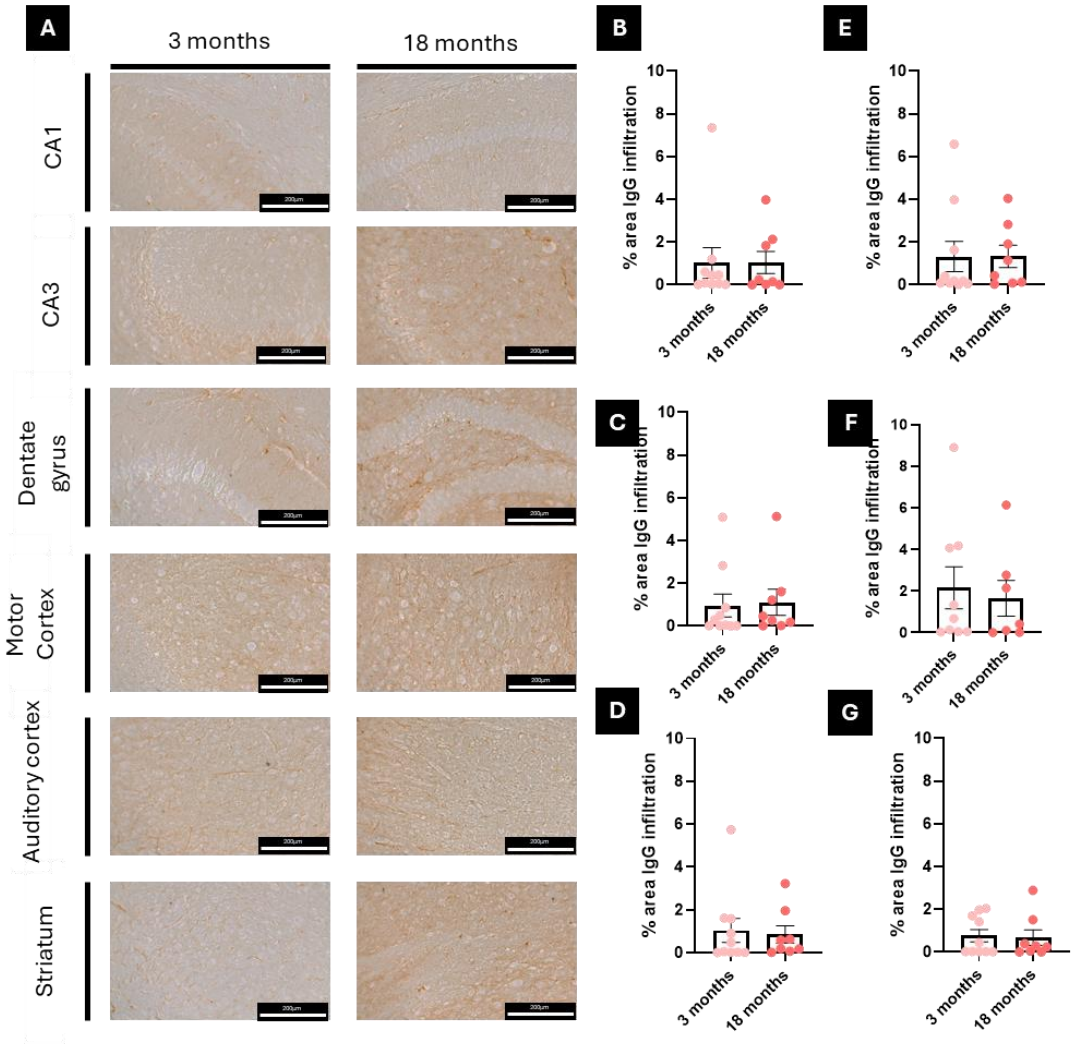

Figure 3-19: Immunoglobulin G infiltration in ageing male brains regions. C57BL/6 male mice groups at 3- and 18-months received a single intravenous injection of DiI-lip. Cardiac perfusion was completed 2 hours post-injection to remove circulating DiI-lip.(A) Representative immunohistochemical images of CA1, CA3 and dentate gyrus hippocampal regions, motor and auditory cortical regions and striatal region -1.94mm from bregma indicating infiltration of IgG (Brown). (B) Quantitative analysis of CA1 region. (C) Quantitative analysis of CA3 region. (D). Quantitative analysis of dentate gyrus region. (E) Quantitative analysis of motor cortex region. (F) Quantitative analysis of auditory cortex region. (G) Quantitative analysis of striatum region. All regions indicate no changes to IgG infiltration across ageing in all brain regions. Images obtained at x20 magnification on Leica Thunder microscope prior to quantification in Image J. Statistical analysis was completed using GraphPad Prism software using one-way analysis of variance followed by Tukey multiple comparison test or Kruskal-Wallis test followed by Dunn's multiple comparisons test based on Shapiro-Wilk test for normality. N=8-10,average ± SEM, $p<0.05$ were considered significant. Scale bar represents 200µm.

3.5.6. **Significant changes to astrocytic expression in cortical regions in ageing**

To determine age-related changes to astrocytic expression, one of the main components of the NVU, the protein marker GFAP was utilised along with CD31 for endothelial cells. In the female cohort, all three hippocampal regions displayed non-significant trends to increases in GFAP expression from 3-months to 22-months (fig.3-20- fig.3-25). There were significant increases in the CA3 region exclusively between the 12- and 18-month groups ($F=4.476_{(4,19)}$, p=0.0247) (fig. 3-21). Interestingly, both cortical regions examined (motor, $H=14.16_{(4,22)}$, p=0.0306 and auditory, $F=5.430_{(4,18)}$, p=0.0222) displayed significant increases in GFAP expression when comparing the 3-month groups to the 18- and 22-month groups (fig.3-23-fig. 3-24b). For the male cohort, more consistent increases in expression were observed in all regions expect for the auditory cortex, which demonstrated a non-significant trend, ($U=9_{(15)}$,p=0.053) (fig. 3- 27f). The remaining regions all demonstrated the higher GFAP expression in older age groups, indicating astrocyte activation including CA1, $U=5_{(15),}$ p=0.0127 (fig. 26b), CA3, $U=6_{(14)}$, p=0.029 (fig. 3-26f), dentate gyrus, $T=44.91_{(13)}$, p=0.039 (fig. 3-26j), motor cortex, T(13) =9, p=0.0046 (fig. 27b) and striatum, $U=3_{(15)}$, p=0.0047 (fig.3-27j).

It would be expected that during ageing, astrocytes would become detached from the BBB as end-feet retract (Bors et al., 2018). Therefore, it was purposeful to determine the interaction between GFAP and CD31 (representing the vasculature of the BBB) to see if this finding was replicated in these common markers. In the female cohort, all regions displayed no significant trends regarding CD31/GFAP colocalisation when normalised to CD31 expression, indicating that the interaction of these markers does not change during ageing (fig.3-20-3-25c). In the male cohort, similar expression patterns were observed whereby no significant changes to CD31 and GFAP interaction occurred (fig. 3-26-3-27c,g,k). However, in the motor cortex, there was a significant increase in GFAP and CD31 colocalisation, indicating a potential region-specific change to interactions (fig. 3-27c).

To determine further uptake of DiI-lip into astrocytic cells, the interaction between GFAP and DiI-lip was quantified for all regions. In the female cohort, the only region to show significant

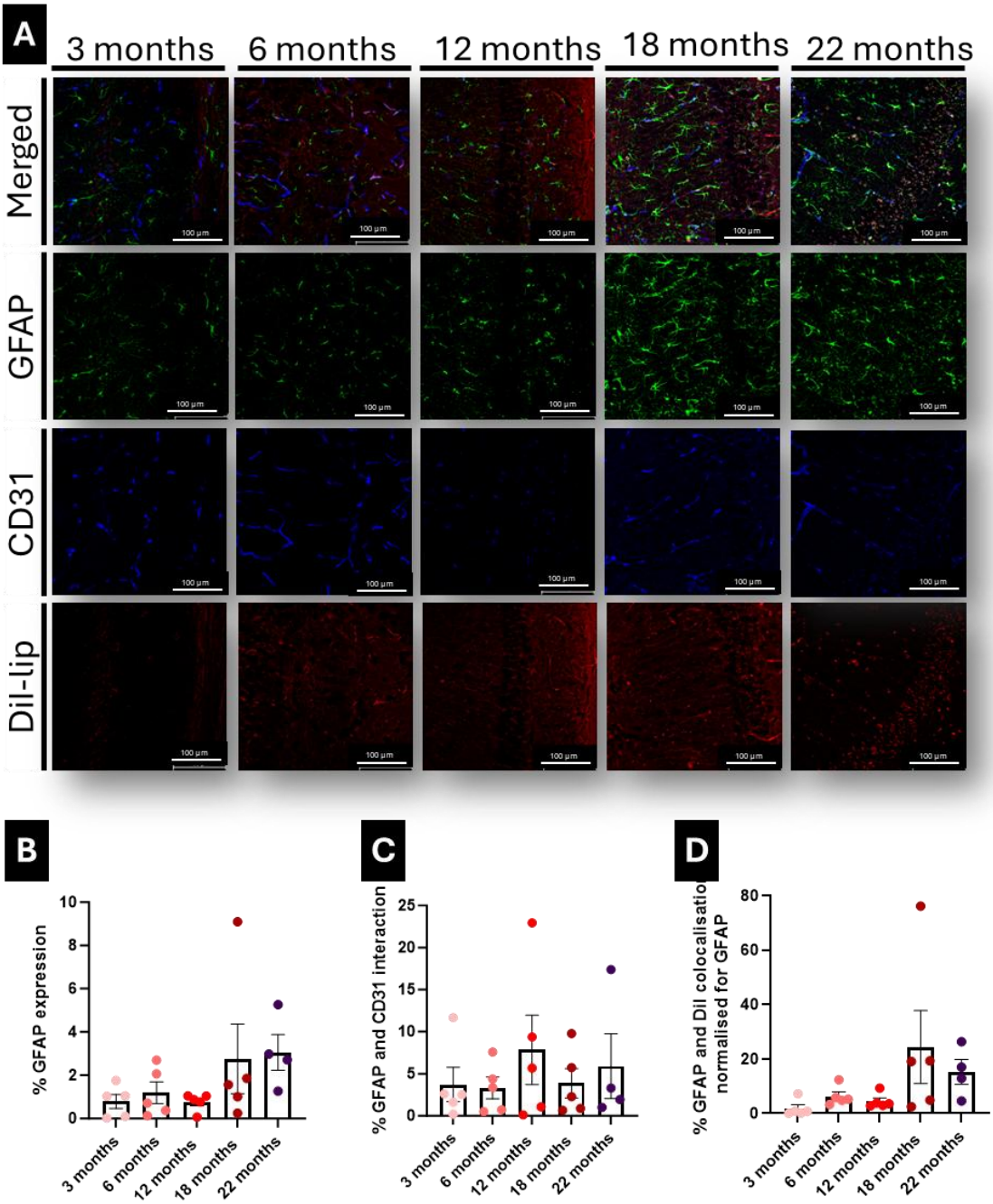

Figure 3-20: GFAP expression in ageing female CA1 hippocampal region. C57BL/6 female mice groups at 3-, 6-, 12-, 18-, 22-months received a single intravenous injection of DiI-lip. Cardiac perfusion was completed 2 hours post-injection to remove circulating DiI-lip.(A) Representative immunofluorescence images of CA1 hippocampal region -1.94mm from the bregma demonstrate expression of GFAP (green), CD31 (blue) and DiI-lip (Red). (B) Quantitative analysis of GFAP expression across ageing demonstrated increasing trends in ageing. (C) Quantitative interaction between CD31 and GFAP expression demonstrated no trends. (D) Quantitative interaction between GFAP and DiI-lip expression normalised to GFAP expression was not significantly increased across ageing. Images obtained at x40 magnification on Leica Thunder microscope and underwent large volume computational clearing (LVCC) prior to quantification in Image J. Statistical analysis was completed using GraphPad Prism software using one-way analysis of variance followed by Tukey multiple comparison test or Kruskal-Wallis test followed by Dunn's multiple comparisons test based on Shaprio-Wilk test for normality. N=4-5,average ± SEM, $p<0.05$ were considered significant. Scale bar represents 100µm.

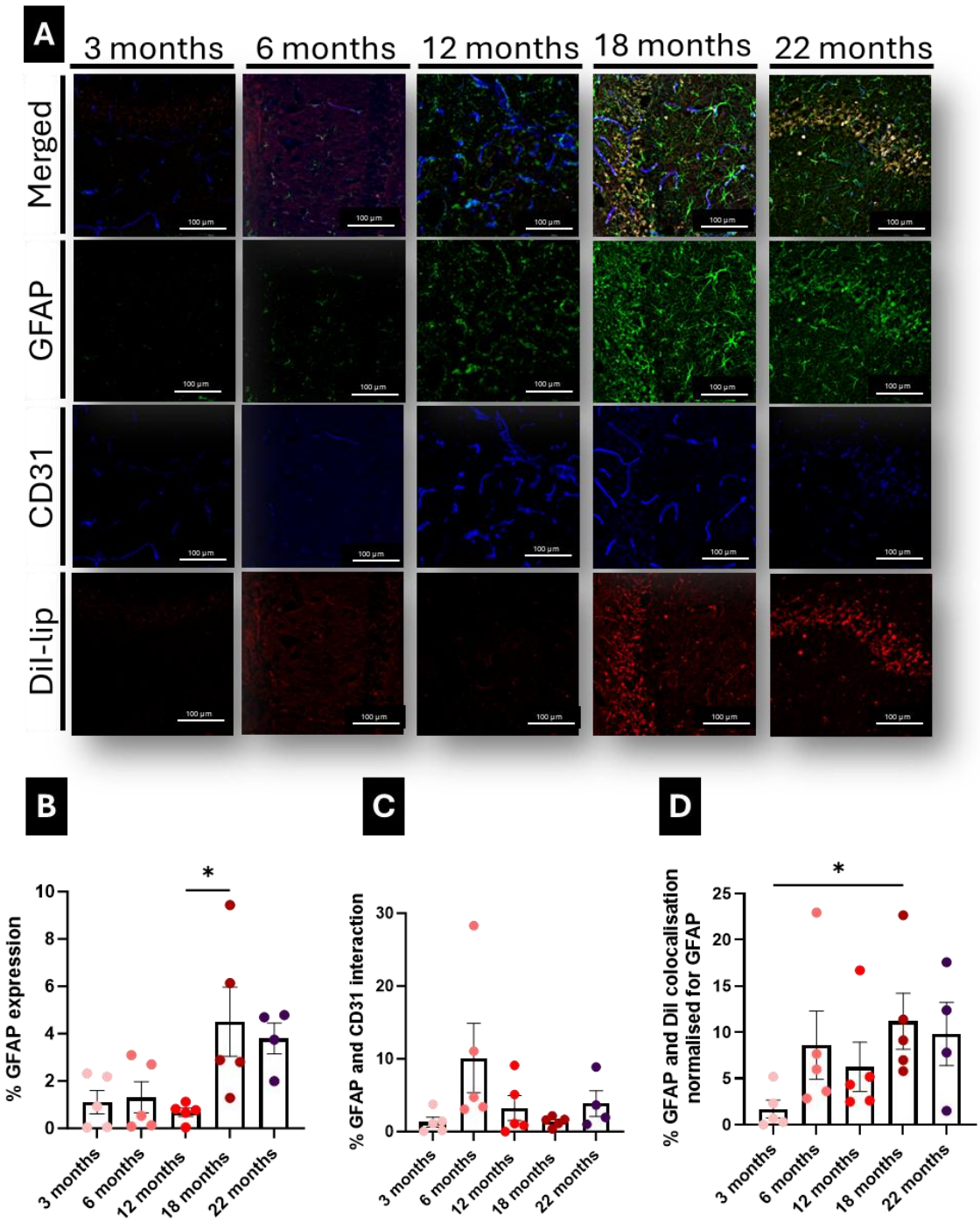

Figure 3-21: GFAP expression in ageing female CA3 hippocampal region. C57BL/6 female mice groups at 3-, 6-, 12-, 18-, 22-months received a single intravenous injection of DiI-lip. Cardiac perfusion was completed 2 hours post-injection to remove circulating DiI-lip.(A) Representative immunofluorescence images of CA3 hippocampal region -1.94mm from the bregma demonstrate expression of GFAP (green), CD31 (blue) and DiI-lip (Red). (B) Quantitative analysis of GFAP expression across ageing demonstrated increasing trends in ageing. (C) Quantitative interaction between CD31 and GFAP expression demonstrated no trends. (D) Quantitative interaction between GFAP and DiI-lip expression normalised to GFAP expression significantly increased across ageing. Images obtained at x40 magnification on Leica Thunder microscope and underwent large volume computational clearing (LVCC) prior to quantification in Image J. Statistical analysis was completed using GraphPad Prism software using one-way analysis of variance followed by Tukey multiple comparison test or Kruskal-Wallis test followed by Dunn's multiple comparisons test based on Shaprio-Wilk test for normality. N=4-5,average ± SEM, $p<0.05$ were considered significant. Scale bar represents 100µm.

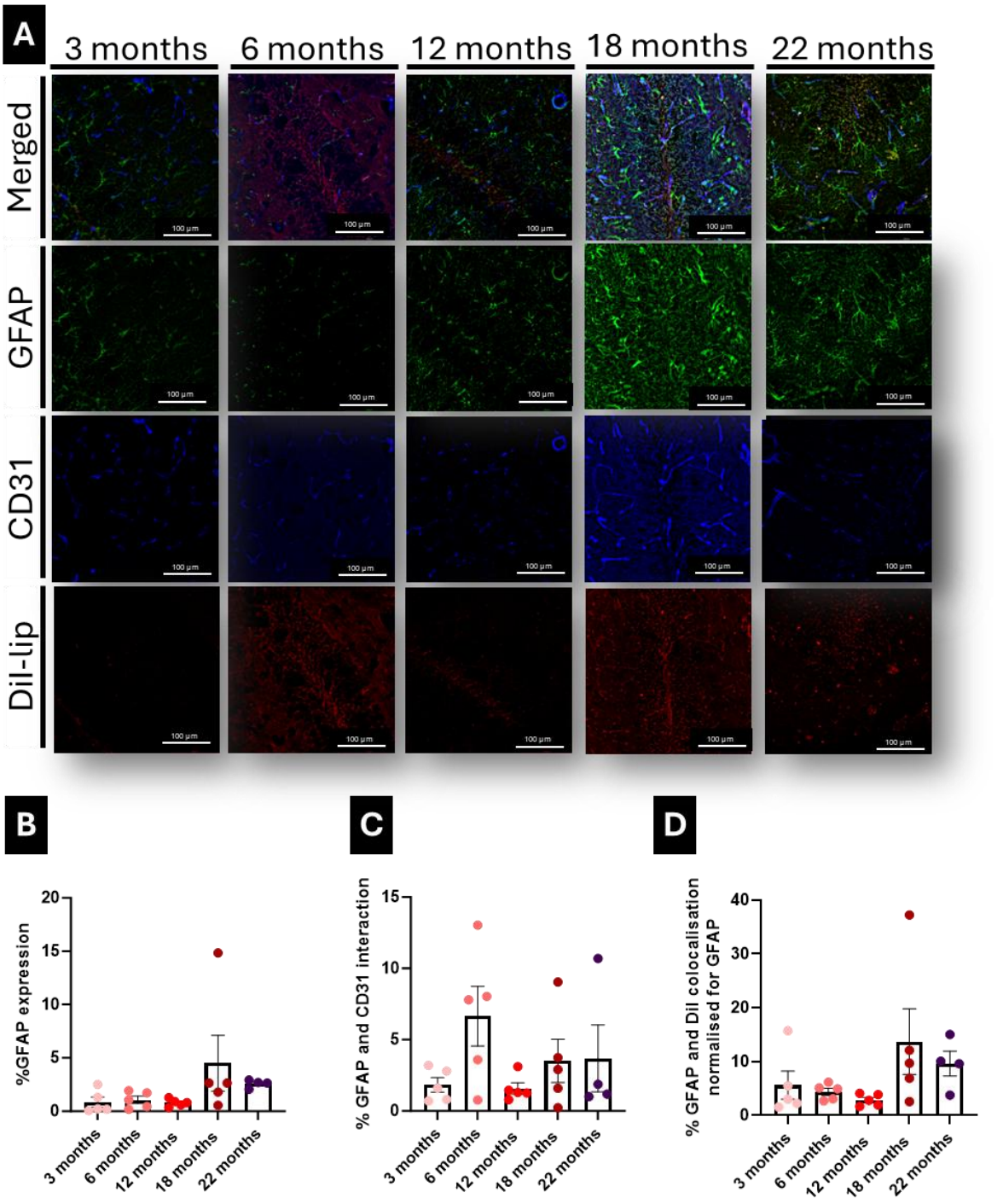

Figure 3-22: GFAP expression in ageing female dentate hippocampal region. C57BL/6 female mice groups at 3-, 6-, 12-, 18-, 22-months received a single intravenous injection of DiI-lip. Cardiac perfusion was completed 2 hours post-injection to remove circulating DiI-lip.(A) Representative immunofluorescence images of dentate gyrus hippocampal region -1.94mm from the bregma demonstrate expression of GFAP (green), CD31 (blue) and DiI-lip (Red). (B) Quantitative analysis of GFAP expression across ageing demonstrated no significant changes. (C) Quantitative interaction between CD31 and GFAP expression demonstrated increasing trend from 3-month group. (D) Quantitative interaction between GFAP and DiI-lip expression significantly increased across ageing. Images obtained at x40 magnification on Leica Thunder microscope and underwent large volume computational clearing (LVCC) prior to quantification in Image J. Statistical analysis was completed using GraphPad Prism software using one-way analysis of variance followed by Tukey multiple comparison test or Kruskal-Wallis test followed by Dunn's multiple comparisons test based on Shapiro-Wilk test for normality. N=4-5,average ± SEM, $p<0.05$ were considered significant. Scale bar represents 100µm.

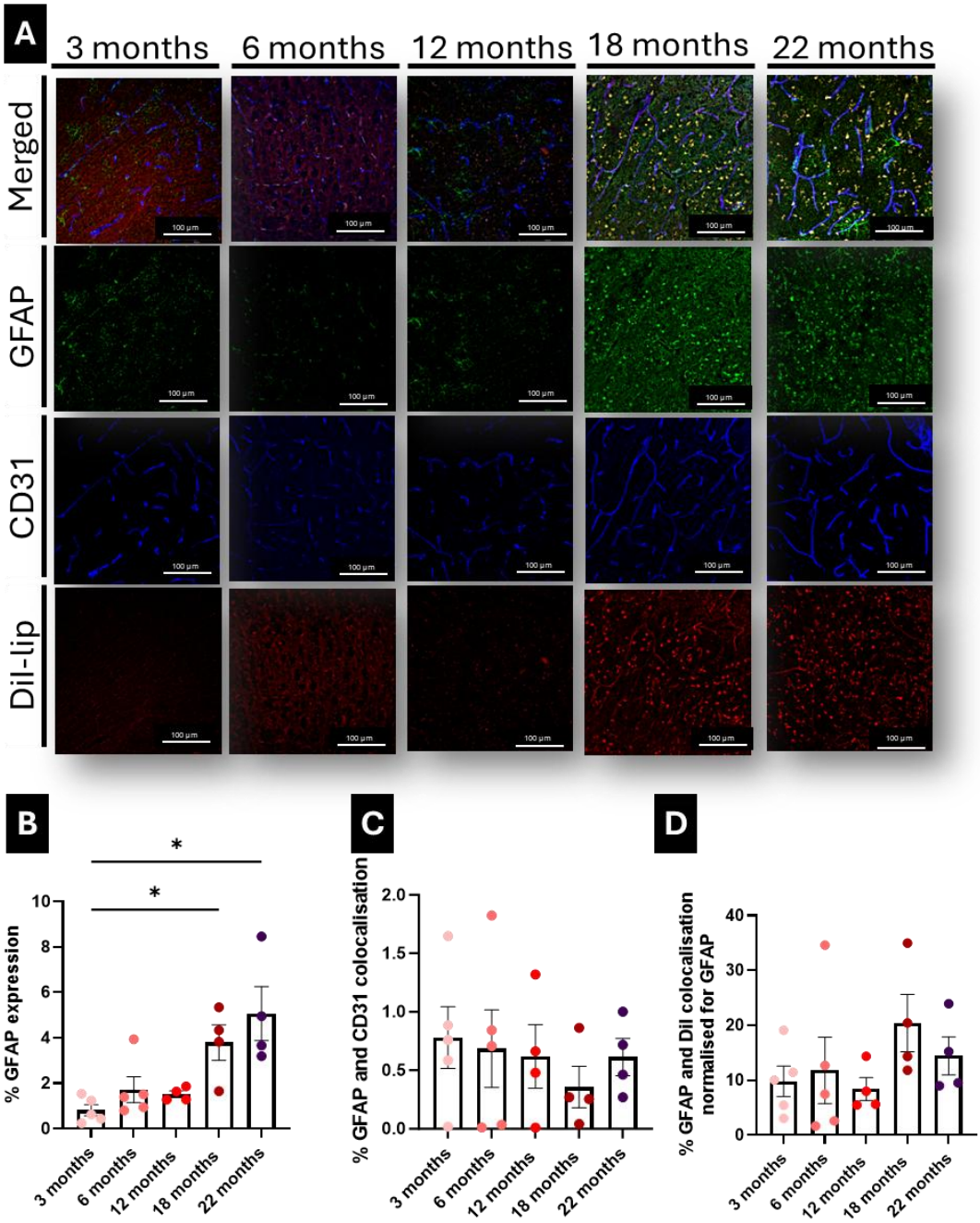

Figure 3-23: GFAP expression in ageing female motor cortex region. C57BL/6 female mice groups at 3-, 6-, 12-, 18-, 22-months received a single intravenous injection of DiI-lip. Cardiac perfusion was completed 2 hours post-injection to remove circulating DiI-lip.(A) Representative immunofluorescence images of motor cortex region -1.94mm from the bregma demonstrate expression of GFAP (green), CD31 (blue) and DiI-lip (Red). (B) Quantitative analysis of GFAP expression across ageing established increases in ageing. (C) Quantitative interaction between CD31 and GFAP expression demonstrated no changes in ageing. (D) Quantitative interaction between GFAP and DiI-lip expression normalised for GFAP expression showed no changes across ageing. Images obtained at x40 magnification on Leica Thunder microscope and underwent large volume computational clearing (LVCC) prior to quantification in Image J. Statistical analysis was completed using GraphPad Prism software using one-way analysis of variance followed by Tukey multiple comparison test or Kruskal-Wallis test followed by Dunn's multiple comparisons test based on Shapiro-Wilk test for normality. N=4-5,average ± SEM, $p<0.05$ were considered significant. Scale bar represents 100µm.

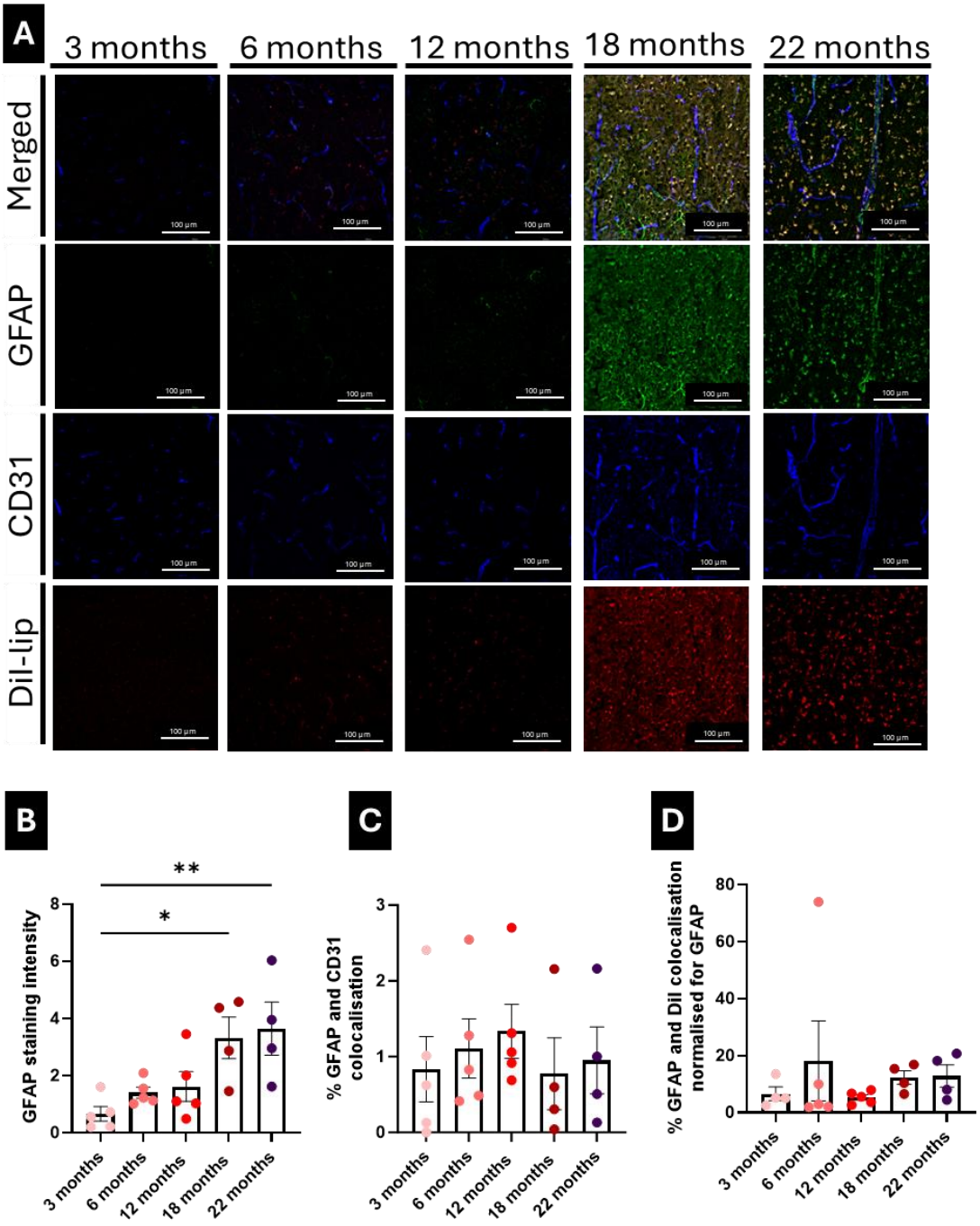

Figure 3-24 : GFAP expression in ageing auditory cortex region. C57BL/6 female mice groups at 3-, 6-, 12-, 18-, 22-months received a single intravenous injection of DiI-lip. Cardiac perfusion was completed 2 hours post-injection to remove circulating DiI-lip.(A) Representative immunofluorescence images of auditory cortex region -1.94mm from the bregma demonstrate expression of GFAP (green), CD31 (blue) and DiI-lip (Red). (B) Quantitative analysis of GFAP expression across ageing established increases in ageing. (C) Quantitative interaction between CD31 and GFAP expression demonstrated non-significant increases in ageing. (D) Quantitative interaction between GFAP and DiI-lip expression significantly increased across ageing. Images obtained at x40 magnification on Leica Thunder microscope and underwent large volume computational clearing (LVCC) prior to quantification in Image J. Statistical analysis was completed using GraphPad Prism software using one-way analysis of variance followed by Tukey multiple comparison test or Kruskal-Wallis test followed by Dunn's multiple comparisons test based on Shapiro-Wilk test for normality. N=4/5,average ± SEM, $p<0.05$ were considered significant. Scale bar represents 100µm.

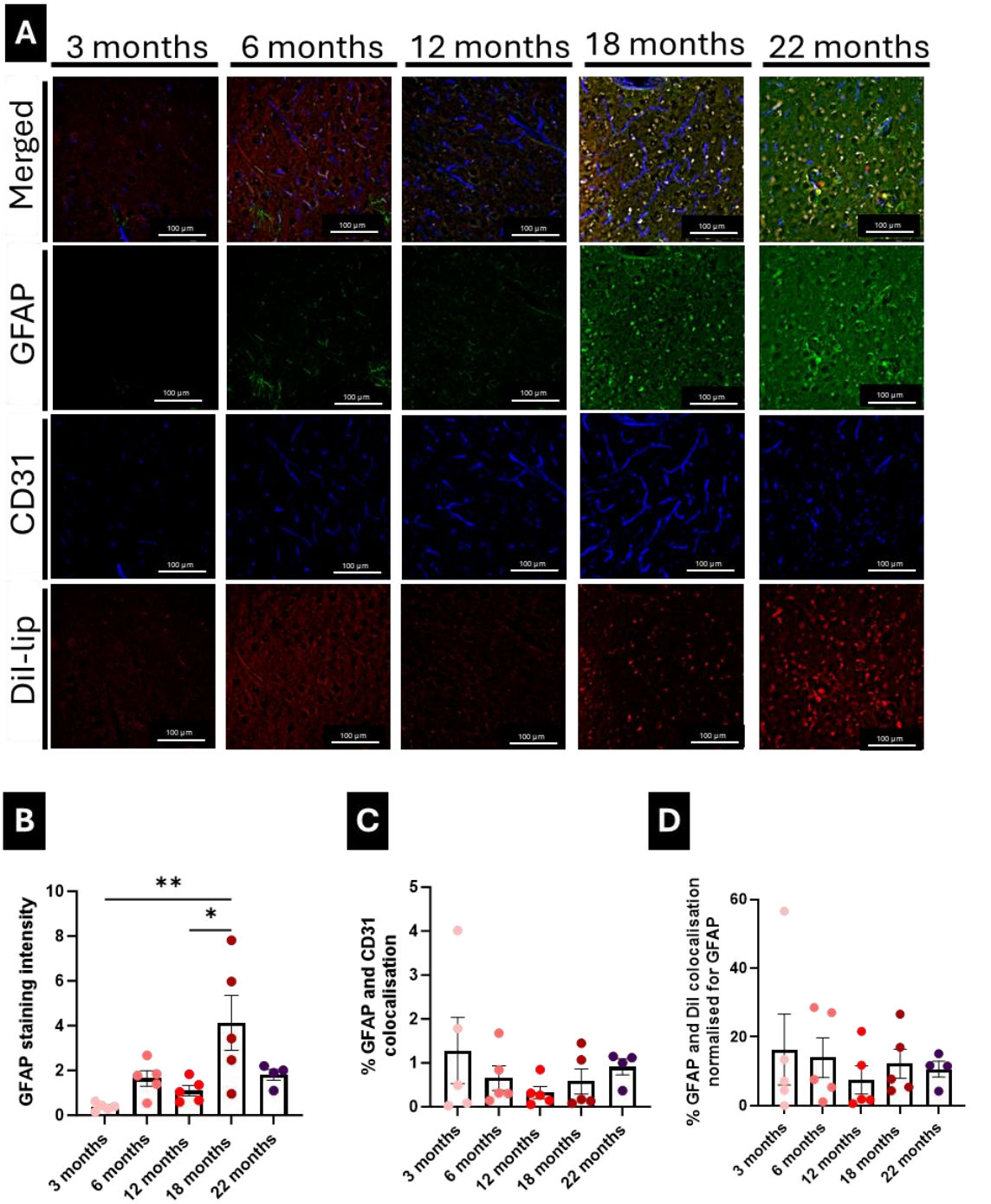

Figure 3-25: GFAP expression in female ageing striatal region. C57BL/6 female mice groups at 3-, 6-, 12-, 18-, 22-months received a single intravenous injection of DiI-lip. Cardiac perfusion was completed 2 hours post-injection to remove circulating DiI-lip.(A) Representative immunofluorescence images of striatal region -1.94mm from the bregma demonstrate expression of GFAP (green), CD31 (blue) and DiI-lip (Red). (B) Quantitative analysis of GFAP expression across ageing established increases in ageing. (C) Quantitative interaction between CD31 and GFAP expression demonstrated no changes. (D) Quantitative interaction between GFAP and DiI-lip expression normalised for GFAP did not change across ageing. Images obtained at x40 magnification on Leica Thunder microscope and underwent large volume computational clearing (LVCC) prior to quantification in Image J. Statistical analysis was completed using GraphPad Prism software using one-way analysis of variance followed by Tukey multiple comparison test or Kruskal-Wallis test followed by Dunn's multiple comparisons test based on Shapiro-Wilk test for normality. N=4-5,average ± SEM, $p<0.05$ were considered significant. Scale bar represents 100µm.

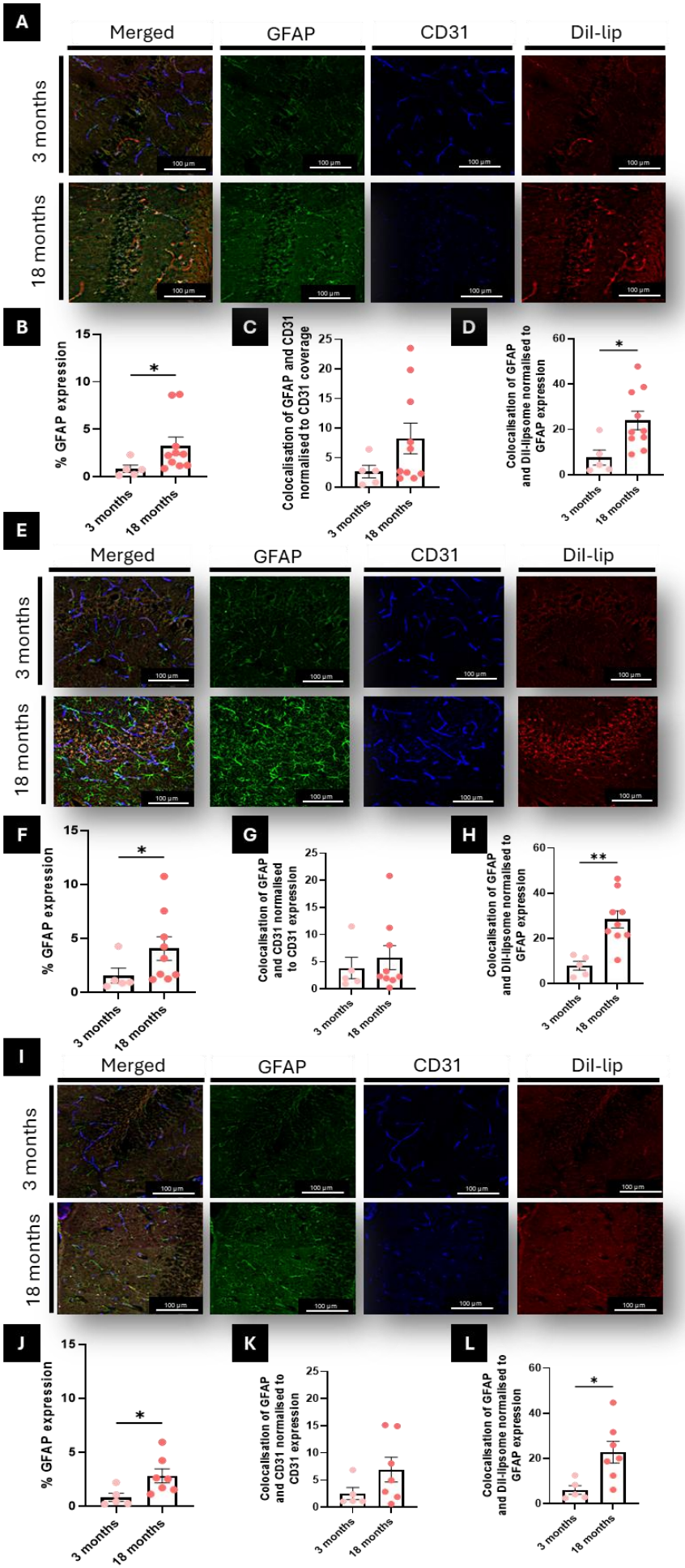
A
Merged
GFAP
CD31
DiI-lip
3 months
18 months
B
% GFAP expression
C
Colocalisation of GFAP and CD31 normalised to CD31 coverage
D
Colocalisation of GFAP and DiI-lipsome normalised to GFAP expression
E
F
G
Colocalisation of GFAP and CD31 normalised to CD31 expression
H
I
J
K
L

Figure 3-26: GFAP expression in ageing male hippocampus. C57BL/6 male mice groups at 3 an 18-months old received a single intravenous injection of DiI-lip. Cardiac perfusion was completed 2 hours post-injection to remove circulating DiI-lip.(A) Representative immunofluorescence images of CA1 hippocampal region -1.94mm from the bregma demonstrate expression of GFAP (green), CD31 (blue) and DiI-lip (Red). (B) Quantitative analysis of GFAP expression across ageing demonstrated increasing expression in ageing. (C) Quantitative interaction between CD31 and GFAP expression demonstrated increasing trends. (D) Quantitative interaction between GFAP and DiI-lip expression significantly increased across ageing. (E) CA3 region representative images. (F) Quantitative analysis of CA3 GFAP expression displayed significant increases. (G) Interaction between GFAP and CD31 in CA3 region demonstrated no significant changes in ageing. (H) Interaction between DiI-lip and GFAP significantly increased during ageing. (I) Dentate gyrus representative images. (J) Significant quantitative increases in GFAP expression in the dentate gyrus. (K) No significant changes to CD31 and GFAP interaction during ageing. (L) Interaction between DiI-lip and GFAP significantly increased during ageing. Images obtained at x40 magnification on Leica Thunder microscope and underwent large volume computational clearing (LVCC) prior to quantification in Image J. Statistical analysis was completed using GraphPad Prism software using Shapiro Wilk test for normality followed by either a T-test or Mann-Whitney. N=5/10,average ± SEM, $p<0.05$ were considered significant. Scale bar represents 100µm.

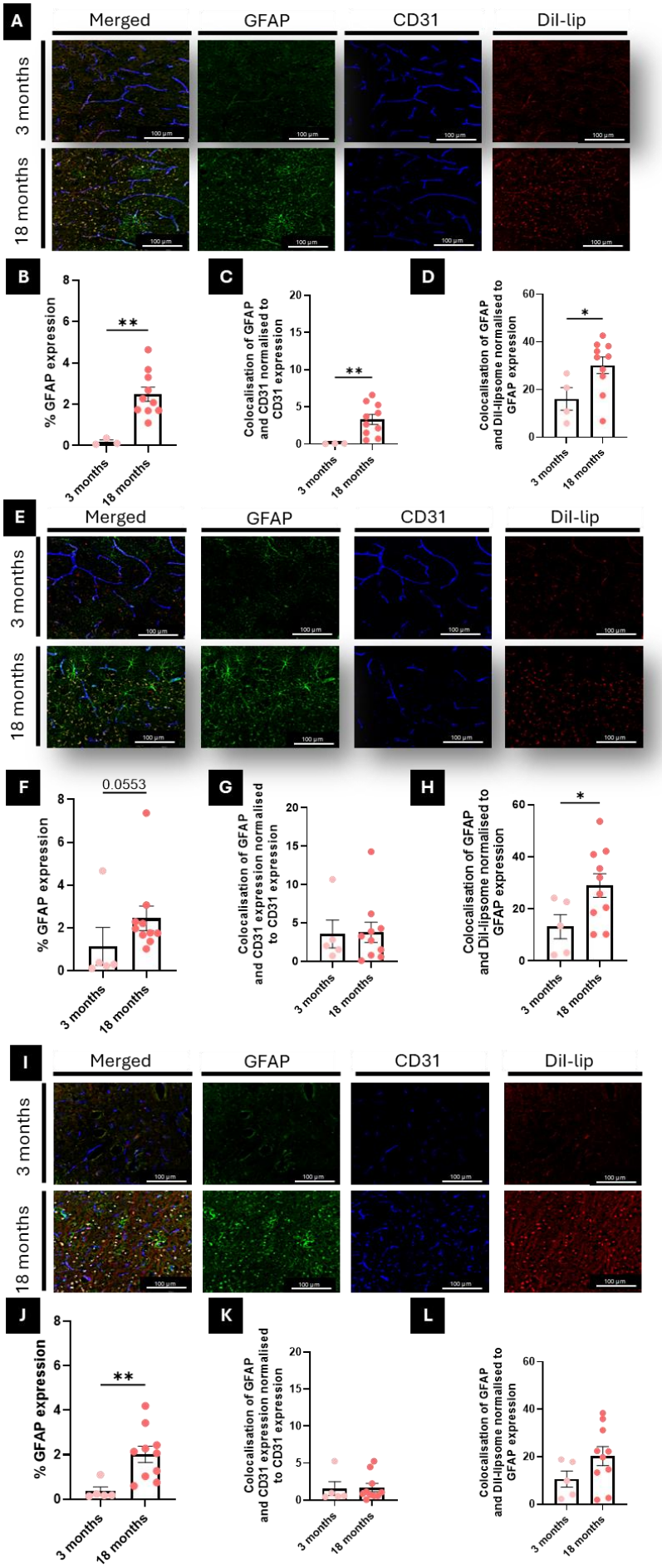
A
Merged
GFAP
CD31
DiI-lip
3 months
18 months
B
% GFAP expression
**
3 months
18 months
C
Colocalisation of GFAP and CD31 normalised to CD31 expression
**
3 months
18 months
D
Colocalisation of GFAP and DiI-lipsome normalised to GFAP expression
*
3 months
18 months
E
Merged
GFAP
CD31
DiI-lip
3 months
18 months
F
0.0553
% GFAP expression
3 months
18 months
G
Colocalisation of GFAP and CD31 expression normalised to CD31 expression
3 months
18 months
H
Colocalisation of GFAP and DiI-lipsome normalised to GFAP expression
*
3 months
18 months
I
Merged
GFAP
CD31
DiI-lip
3 months
18 months
J
% GFAP expression
**
3 months
18 months
K
Colocalisation of GFAP and CD31 expression normalised to CD31 expression
3 months
18 months
L
Colocalisation of GFAP and DiI-lipsome normalised to GFAP expression
3 months
18 months

Figure 3-27: GFAP expression in ageing male cortex and striatum. C57BL/6 male mice groups at 3 an 18-months old received a single intravenous injection of DiI-lip. Cardiac perfusion was completed 2 hours post-injection to remove circulating DiI-lip. Representative images of (A) motor cortex, (E) auditory cortex and (I) striatum regions -1.94mm from the bregma demonstrate expression of GFAP (green), CD31 (blue) and DiI-lip (Red). Quantitative analysis of GFAP expression demonstrated significant increases in ageing expression in motor cortex (B) and striatum (J) and non-significant increasing trends in auditory cortex (F). Significant increases in interaction of GFAP and CD31, normalised to CD31 expression, was observed in the motor cortex (C) but no trends in auditory cortex (G) or striatum (K). Quantitative analysis of the interaction of DiI-lip and GFAP, normalised to GFAP expression, saw significant age increases in the (D) motor cortex and (H) auditory cortex but no trends in the striatum (L). Images obtained at x40 magnification on Leica Thunder microscope and underwent large volume computational clearing (LVCC) prior to quantification in Image J. Statistical analysis was completed using GraphPad Prism software using Shapiro Wilk test for normality followed by either a T-test or Mann-Whitney. N=5/10,average ± SEM, $p<0.05$ were considered significant. Scale bar represents 100µm.

increases between 3- and 18- months ($H=10.20_{(4,24)}$, p=0.0372) in DiI-lip and GFAP interaction was the CA3 (fig. 3-21d) indicating possible uptake of DiI-lip in astrocytes in this region. In the male cohort, all hippocampal regions display significantly increased interactions between DiI-lip and GFAP (fig. 3-26d,h,l); CA1 ($T=3.065_{(15)=}$, p= 0.023), CA3 ($T=6.680_{(14)=}$, p= 0.0024) and dentate gyrus ($T=8.823_{(12)}$, p=0.0191). In the peripheral regions, the motor cortex (p=0.0499) and the auditory cortex (p=0.0493) (fig 3-27 d.h) displayed increasing interactions between DiI-lip and GFAP whilst the striatum exhibited non-significant increases in interaction (fig. 3-27l). The discrepancies between the male and female cohorts may suggest an increased astrocytic uptake of DiI-lip in the male brain but not female.

3.5.7. **Significant increases in endothelial cell coverage in ageing**

To investigate the effect of ageing on endothelial cell expression, the common marker CD31 was utilised. Despite the original hypothesis, CD31 expression increased in all regions analysed and was significantly increased in the CA3 (fig.3-28c), motor cortex (fig. 3-28e), auditory cortex (fig 3-28f) and striatum (fig. 3-28g) regions between 3- and 18-months. Non-significant trends were also observed in the CA1 (fig.3-28b) and dentate gyrus (fig. 3-28d) regions, especially in the dentate gyrus region.

3.5.8. **Pericyte changes in ageing female hippocampus**

To investigate changes to pericyte expression and interaction with the BBB through ageing, the pericyte marker NG2 was quantified. Within the female cohort, non-significant trend in the CA1 (fig. 3-29b) between the 3- and 18-month females. Significant decreases in NG2 expression were observed between 3- and 18-months in the CA3 ($H=11.18_{(4,23)}$, p=0.0259)(fig. 3-30b) and dentate gyrus ($H=12.82_{(4,23)}$, p=0.0216) (fig. 3-31b) signifying decreases in pericyte expression as well as a The motor cortex (fig. 3-32b) also demonstrates and non-significant decrease in NG2 expression through ageing whilst the auditory cortex (fig. 33b) and striatum (fig, 3-34b) do not present with a specific age-related expression pattern. This indicates hippocampal changes to pericyte expression which may spatial and not a global brain effect during ageing. In the male cohort, there was significant reductions in the expression of NG2 during ageing in

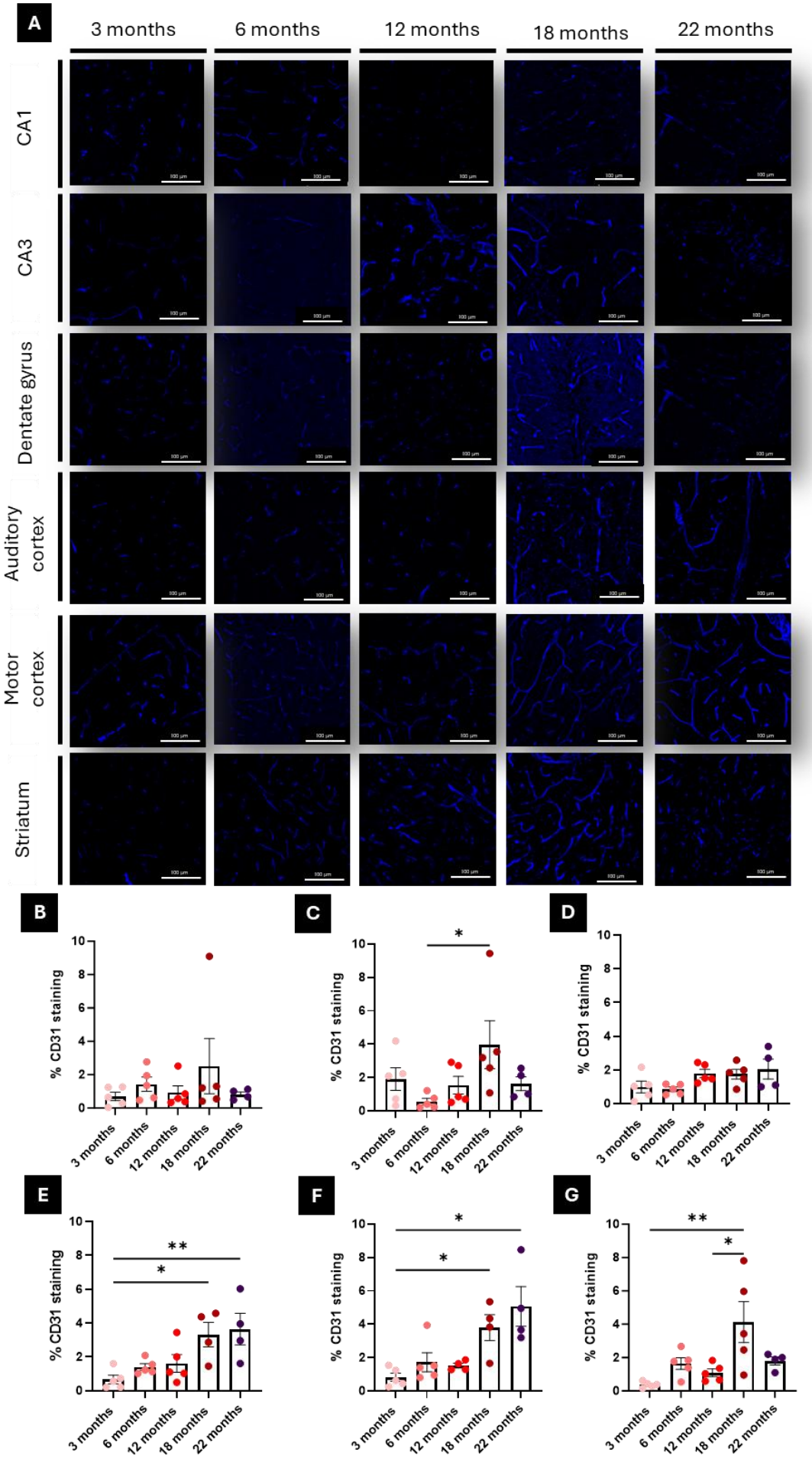
A
3 months
6 months
12 months
18 months
22 months
CA1
CA3
Dentate gyrus
Auditory cortex
Motor cortex
Striatum
B
C
D
E
F
G
% CD31 staining
3 months
6 months
12 months
18 months
22 months

Figure 3-28: CD31 expression in female ageing hippocampal region. C57BL/6 female mice groups at 3-, 6-, 12-, 18-, 22-months received a single intravenous injection of DiI-lip. Cardiac perfusion was completed 2 hours post-injection to remove circulating DiI-lip.(A) Representative immunofluorescence images of CA1, CA3 and dentate gyrus hippocampal region -1.94mm from the bregma demonstrate expression of CD31 (blue). (B) Quantitative analysis of CA1 CD31 expression across ageing demonstrated no trends in ageing. (C) Quantitative analysis of CA3 CD31 expression displayed significant increases in expression between 6- and 18- months. (D) Quantitative expression analysis of dentate gyrus CD31 demonstrating non-significant trends to increased expression in ageing. (E) Quantitative analysis of auditory cortex CD31 expression across ageing demonstrated significant trends in ageing. (F) Quantitative analysis of motor cortex CD31 expression displayed significant increases in expression between 3- and 18-/22-months. (G) Quantitative expression analysis of striatal CD31 demonstrating significant trends to increased expression in ageing. Images obtained at x40 magnification on Leica Thunder microscope and underwent large volume computational clearing (LVCC) prior to quantification in Image J. Statistical analysis was completed using GraphPad Prism software using one-way analysis of variance followed by Tukey multiple comparison test or Kruskal-Wallis test followed by Dunn's multiple comparisons test based on Shaprio-Wilk test for normality. N=4-5,average ± SEM, $p<0.05$ were considered significant. Scale bar represents 100µm.

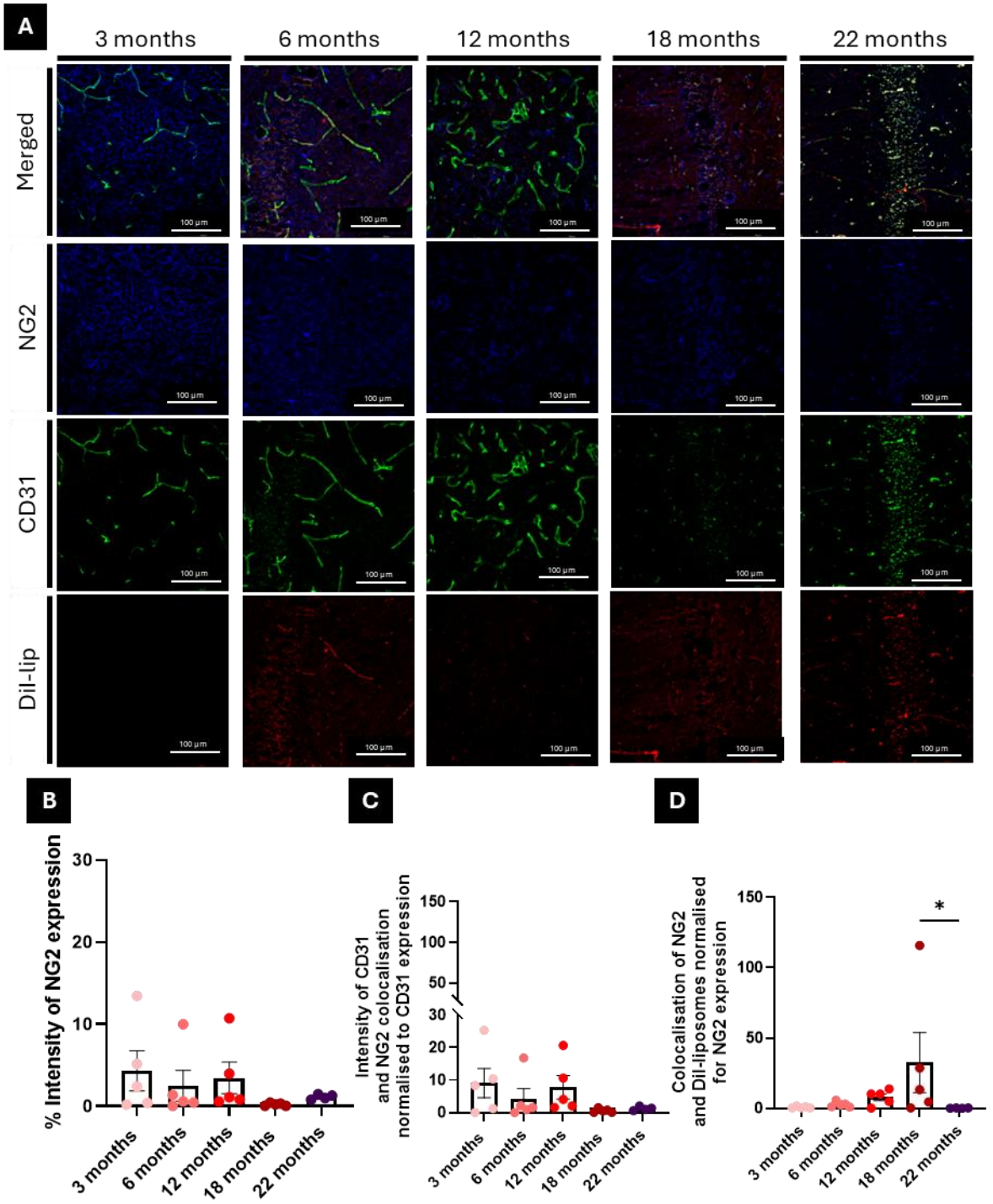

Figure 3-29: NG2 expression in ageing female CA1 hippocampal region. C57BL/6 female mice groups at 3-, 6-, 12-, 18-, 22-months received a single intravenous injection of DiI-lip. Cardiac perfusion was completed 2 hours post-injection to remove circulating DiI-lip.(A) Representative immunofluorescence images of CA1 hippocampal region -1.94mm from the bregma demonstrate expression of NG2 (blue), CD31 (green) and DiI-lip (red). (B) Quantitative analysis of NG2 expression across ageing demonstrated no significant trends in ageing. (C) Quantitative analysis of NG2 and CD31 interaction displayed non-significant decreases in expression. (D) Quantitative expression analysis of NG2 and DiI-lip trend to increased colocalisation up to 18 months and a significant decrease at 22-months. Statistical analysis was completed using one-way ANOVA followed by Tukey multiple comparison test or Kruskal-Wallis test followed by Dunn's multiple comparisons test based on Shaprio-Wilk test for normality. N=4/5,average ± SEM, $p<0.05$ were considered significant. Scale bar represents 100µm.

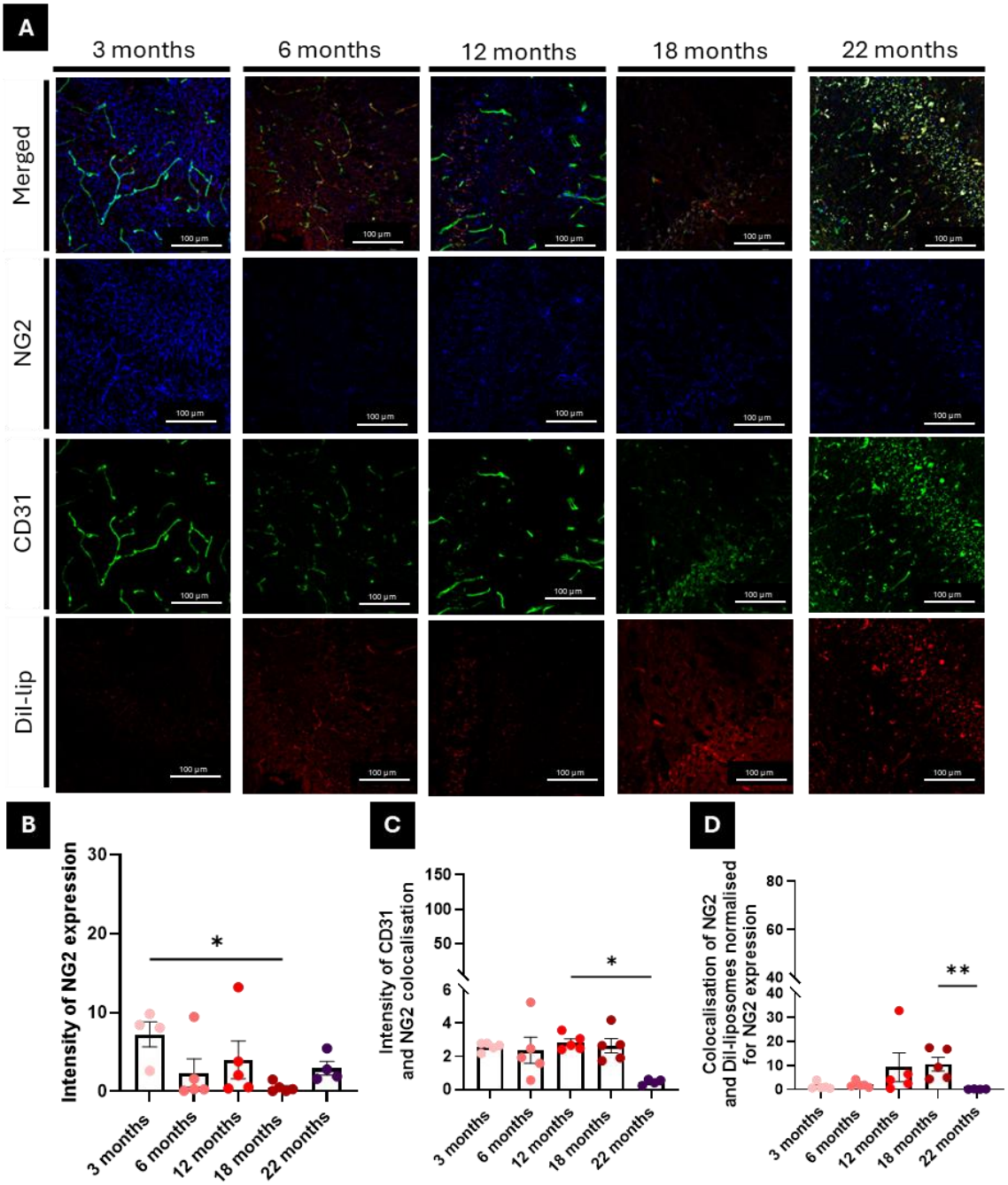

Figure 3-30: NG2 expression in ageing female CA3 hippocampal region. C57BL/6 female mice groups at 3-, 6-, 12-, 18-, 22-months received a single intravenous injection of DiI-lip. Cardiac perfusion was completed 2 hours post-injection to remove circulating DiI-lip.(A) Representative immunofluorescence images of CA3 hippocampal region -1.94mm from the bregma demonstrate expression of CD31 (blue). (B) Quantitative analysis of NG2 expression across ageing demonstrated decreasing trends in ageing. (C) Quantitative analysis of NG2 and CD31 colocalization normalised to CD31 expression, displaying significant decreases at 22 months. (D) Quantitative expression analysis of DiI-lip and NG2 colocalization, demonstrating a trend to increasing up to 18-months and then significant decrease at 22 months. Images obtained at x40 magnification on Leica Thunder microscope and underwent large volume computational clearing (LVCC) prior to quantification in Image J. Statistical analysis was completed using GraphPad Prism software using one-way analysis of variance followed by Tukey multiple comparison test or Kruskal-Wallis test followed by Dunn's multiple comparisons test based on Shaprio-Wilk test for normality. N=4/5,average ± SEM, $p<0.05$ were considered significant. Scale bar represents 100µm.

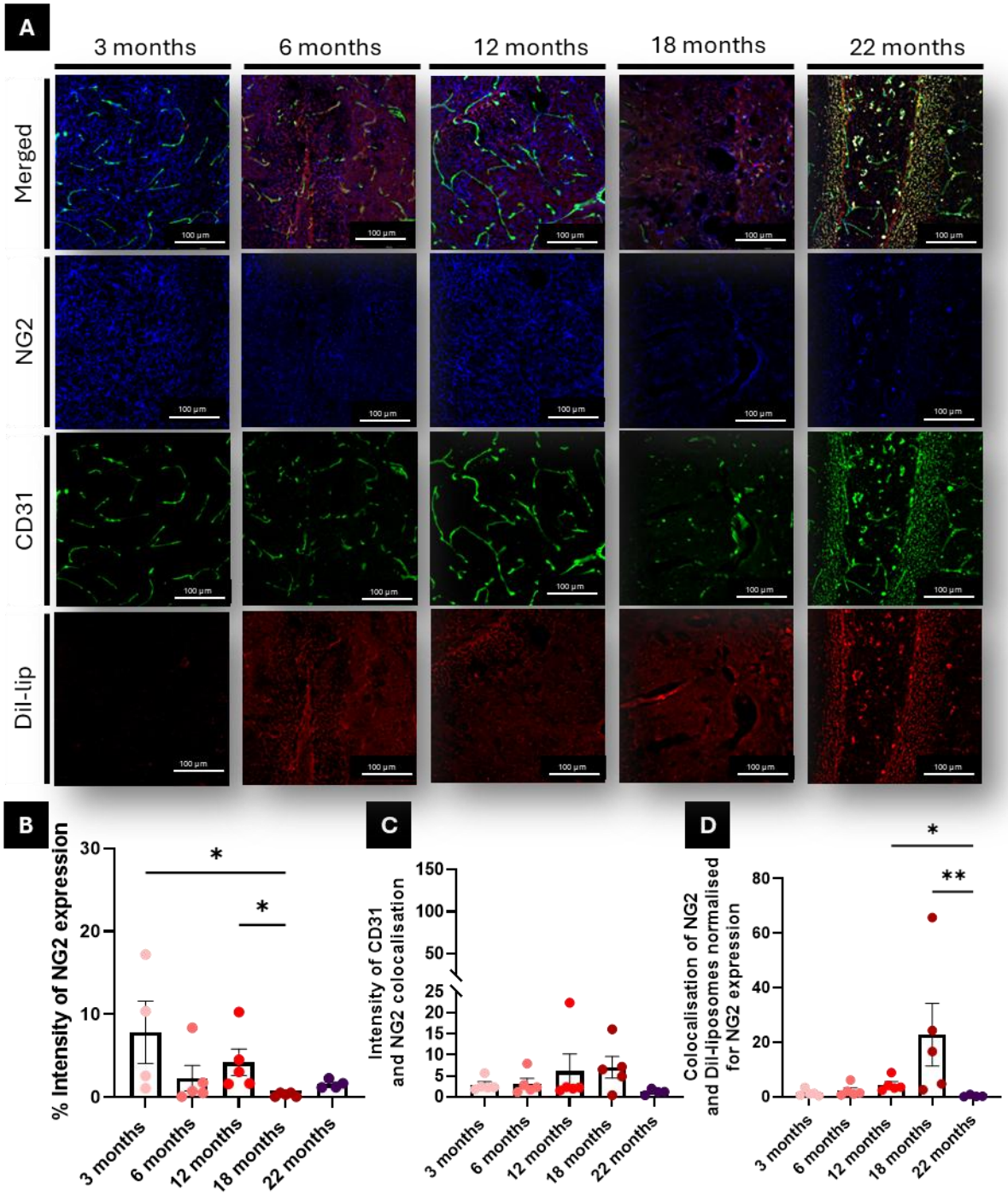

Figure 3-31: NG2 expression in ageing female dentate gyrus hippocampal region. C57BL/6 female mice groups at 3-, 6-, 12-, 18-, 22-months received a single intravenous injection of DiI-lip. Cardiac perfusion was completed 2 hours post-injection to remove circulating DiI-lip.(A) Representative immunofluorescence images of CA1 hippocampal region -1.94mm from the bregma demonstrate expression of NG2 (blue), CD31 (green) and DiI-lip (red). (B) Quantitative analysis of NG2 expression across ageing demonstrated no significant trends in ageing. (C) Quantitative analysis of NG2 and CD31 interaction displayed non-significant decreases in expression. (D) Quantitative expression analysis of NG2 and DiI-lip trend to increased colocalisation up to 18 months and a significant decrease at 22-months. Images obtained at x40 magnification on Leica Thunder microscope and underwent large volume computational clearing (LVCC) prior to quantification in Image J. Statistical analysis was completed using GraphPad Prism software using one-way analysis of variance followed by Tukey multiple comparison test or Kruskal-Wallis test followed by Dunn's multiple comparisons test based on Shaprio-Wilk test for normality. N=4/5,average ± SEM, $p<0.05$ were considered significant. Scale bar represents 100µm.

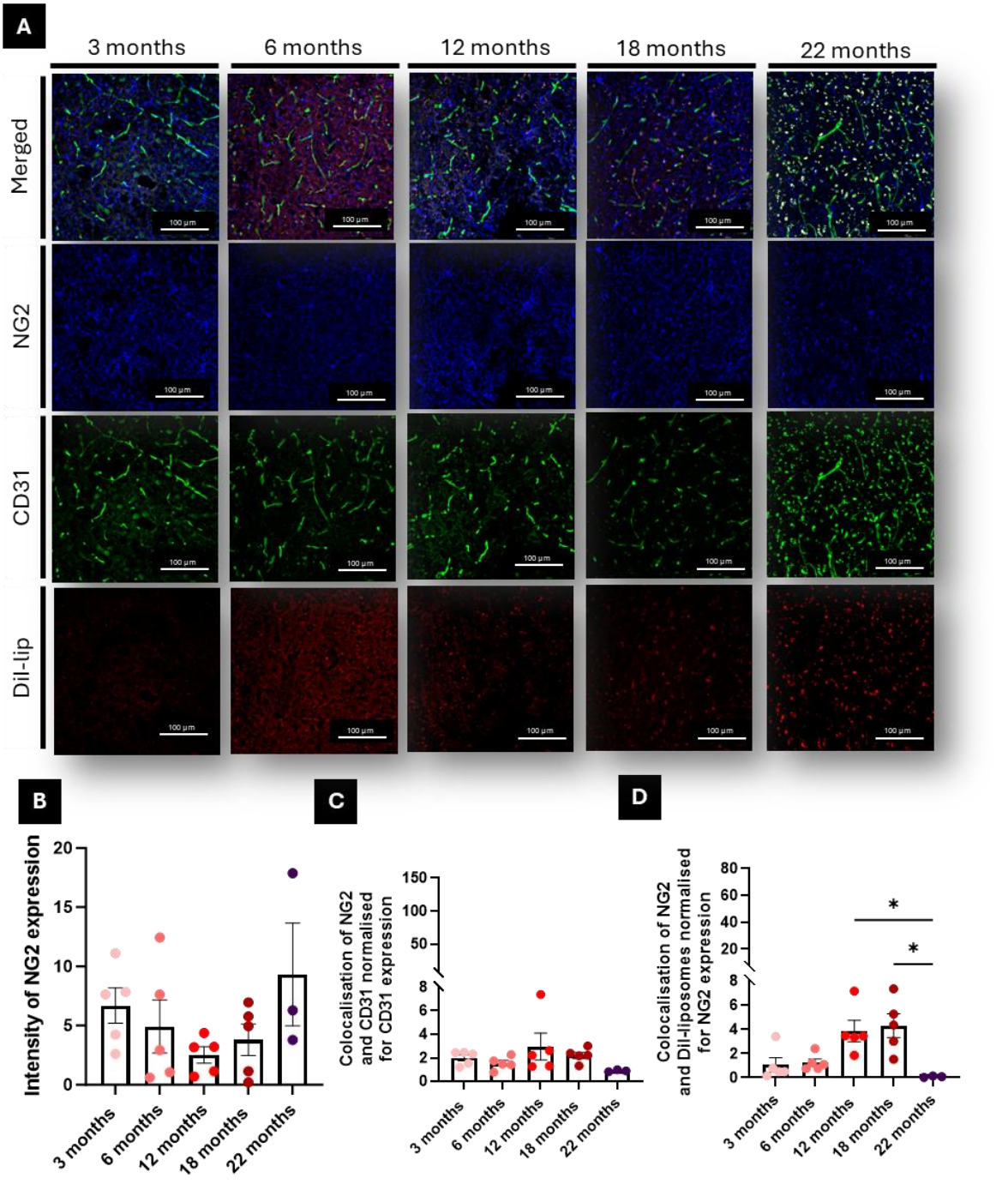

Figure 3-32: NG2 expression in ageing female motor cortex region. C57BL/6 female mice groups at 3-, 6-, 12-, 18-, 22-months received a single intravenous injection of DiI-lip. Cardiac perfusion was completed 2 hours post-injection to remove circulating DiI-lip. (A) Representative immunofluorescence images of motor cortex region -1.94mm from the bregma demonstrate expression of NG2 (blue), CD31 (green) and DiI-lip (red). (B) Quantitative analysis of NG2 expression across ageing demonstrated no significant trends in ageing. (C) Quantitative analysis of NG2 and CD31 interaction, normalised to CD31 expression, displayed non-significant decreases in expression. (D) Quantitative expression analysis of NG2 and DiI-lip trend to increased colocalisation up to 18 months and a significant decrease at 22-months. Images obtained at x40 magnification on Leica Thunder microscope and underwent large volume computational clearing (LVCC) prior to quantification in Image J. Statistical analysis was completed using GraphPad Prism software using one-way analysis of variance followed by Tukey multiple comparison test or Kruskal-Wallis test followed by Dunn's multiple comparisons test based on Shapiro-Wilk test for normality. N=4/5, average ± SEM, $p<0.05$ were considered significant. Scale bar represents 100µm.

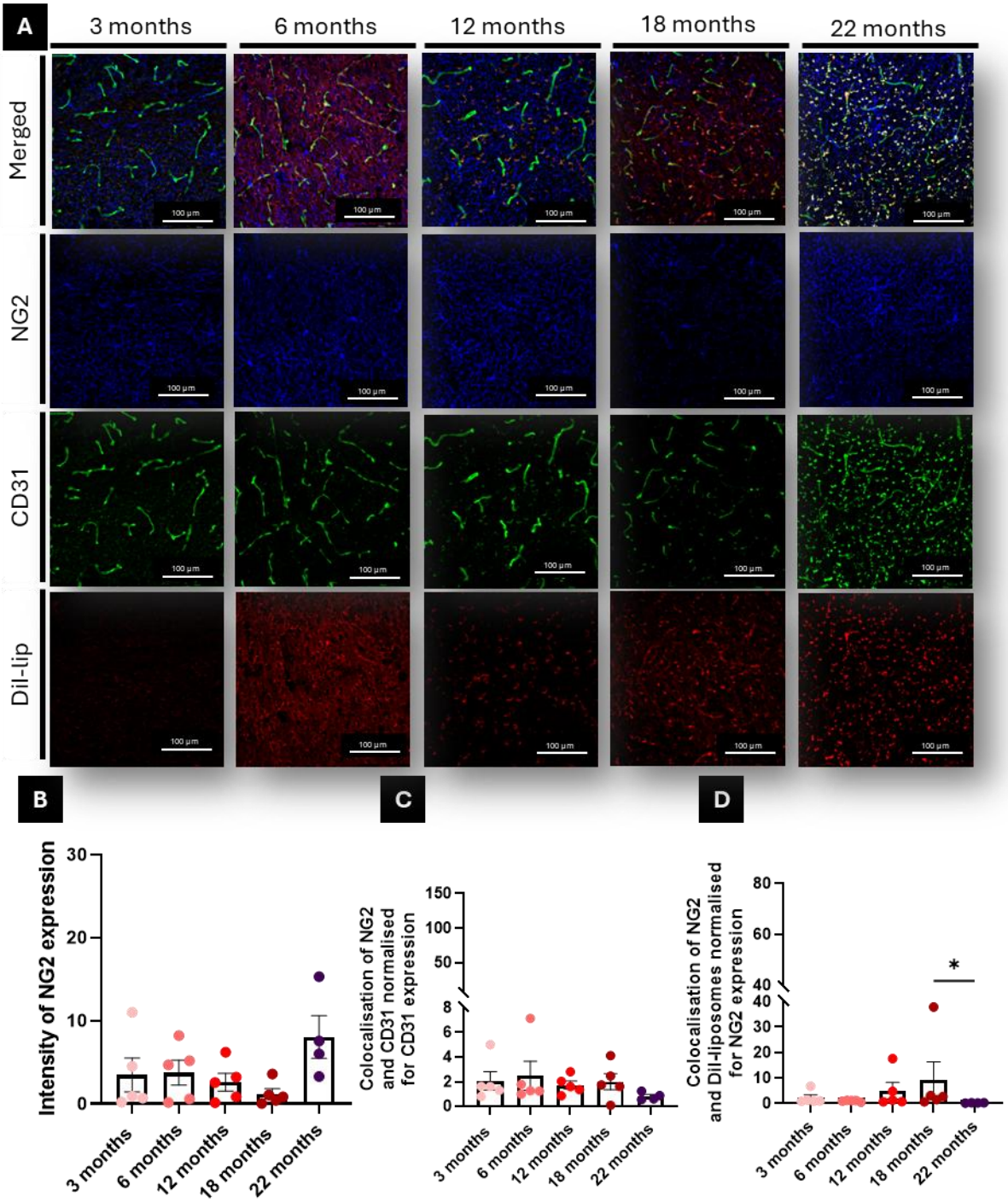

Figure 3-33: NG2 expression in ageing female auditory cortex region. C57BL/6 female mice groups at 3-, 6-, 12-, 18-, 22-months received a single intravenous injection of DiI-lip. Cardiac perfusion was completed 2 hours post-injection to remove circulating DiI-lip. (A) Representative immunofluorescence images of auditory cortex-1.94mm from the bregma demonstrate expression of NG2 (blue), CD31 (green) and DiI-lip (red). (B) Quantitative analysis of NG2 expression across ageing demonstrated no significant trends in ageing. (C) Quantitative analysis of NG2 and CD31 interaction displayed non-significant decreases in expression. (D) Quantitative expression analysis of NG2 and DiI-lip trend to increased colocalisation up to 18 months and a significant decrease at 22-months. Images obtained at x40 magnification on Leica Thunder microscope and underwent large volume computational clearing (LVCC) prior to quantification in Image J. Statistical analysis was completed using GraphPad Prism software using one-way analysis of variance followed by Tukey multiple comparison test or Kruskal-Wallis test followed by Dunn's multiple comparisons test based on Shapiro-Wilk test for normality. N=4/5, average ± SEM, $p<0.05$ were considered significant. Scale bar represents 100µm.

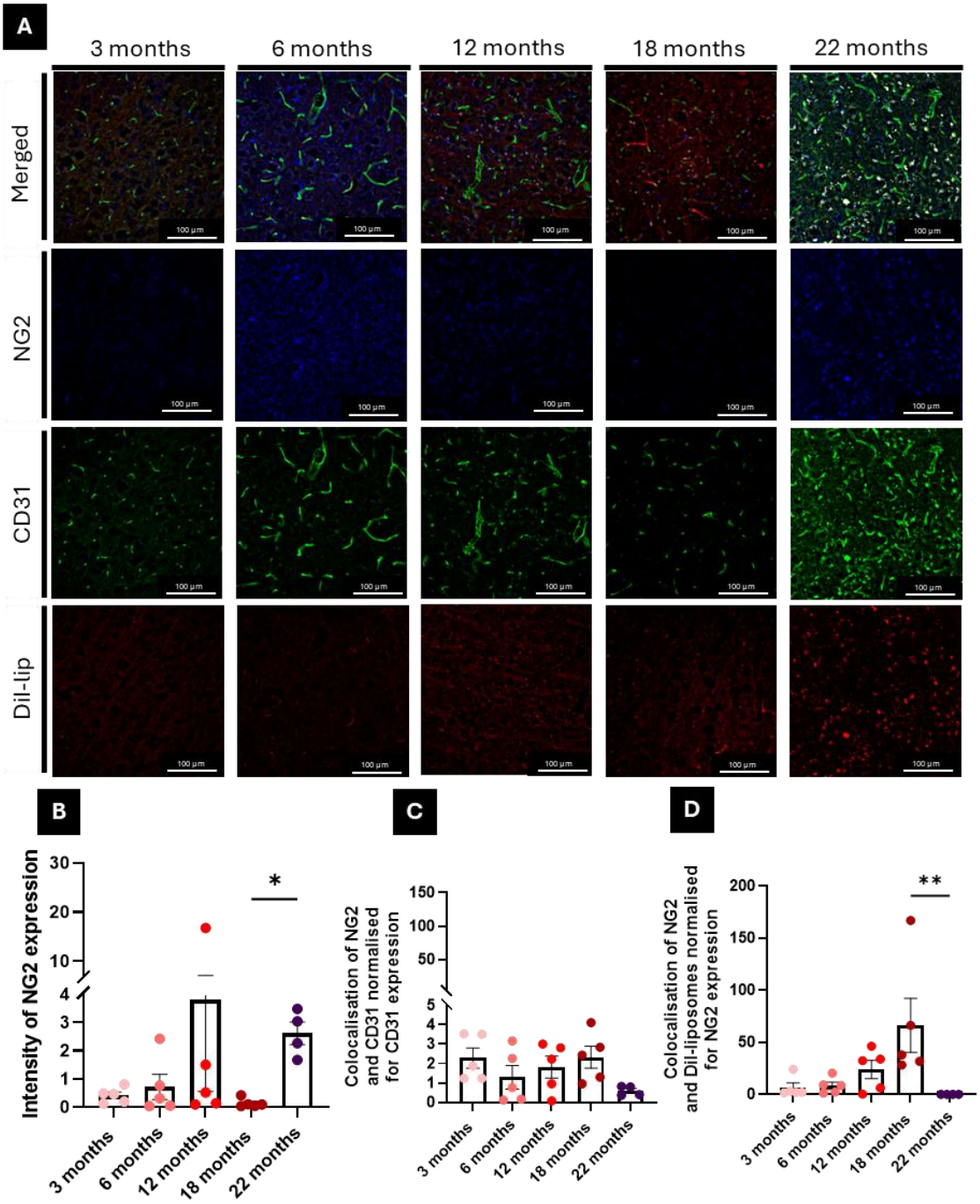

Figure 3-34: NG2 expression in ageing female striatum region. C57BL/6 female mice at 3-, 6-, 12-, 18- and 22- month mice intravenously injected with DiI-lip. Cardiac perfusion was completed 2 hours post-injection to remove circulating DiI-lip. (A) Representative immunofluorescence images of striatum 1.94mm from the bregma demonstrate expression of NG2 (blue), CD31 (green) and DiI-lip (red). (B) Quantitative analysis of NG2 expression across ageing demonstrated no significant trends in ageing, except an increase from 18- to 22-months. (C) Quantitative analysis of NG2 and CD31 interaction normalised to CD31 expression displayed no significant changes. (D) Quantitative expression analysis of NG2 and DiI-lip normalised to NG2 expression, trended to increased colocalisation up to 18 months and a significant decrease at 22-months. Images obtained at x40 magnification on Leica Thunder microscope and underwent large volume computational clearing (LVCC) prior to quantification in Image J. Statistical analysis was completed using GraphPad Prism software using one-way analysis of variance followed by Tukey multiple comparison test or Kruskal-Wallis test followed by Dunn's multiple comparisons test based on Shapiro-Wilk test for normality. N=4/5, average ± SEM, $p<0.05$ were considered significant. Scale bar represents 100µm.

the CA3 ($T=3.912_{(9)}$, p=0.0179) (fig. 3-35f) and motor cortex ($T=29_{(9)}$, p=0.0197) (fig. 3-36b) whilst all other areas displayed non-significant trends of lower expression in the 18-month group.

It has been hypothesised that during ageing, pericytes detach or are lost from the BBB leading to a loss of function, therefore it is imperative again to determine changes to interaction of the pericyte marker NG2 with the endothelial marker, CD31 (Yuan et al., 2023). Within the female cohort, there are no significant changes to NG2/CD31 interaction (fig. 3-29-fig. 3-34c) except for a significant decrease between the 12-month and 22-month group in the CA3 region ($H=11.06_{(4,23)}$, p=0.0306) (fig. 3-30c). Surprising results were identified in the hippocampal regions of the male brain, as the dentate gyrus region possessed a significantly increased interaction ($U=0_{(11)}$, p=0.0159) with the CA1 and CA3 showing no significant changes but a clear trend towards increased interaction (fig. 3-35c). Interestingly, the inverse was seen in the peripheral regions, with significant decreased interaction between the 3- and 18-month brains in the auditory cortex ($U=0_{(9)}$, p=0.0159) and striatal regions ($U=0_{(9)}$, p=0.0160) with the motor cortex displaying no changes (fig. 3-36c).

Examining the uptake of DiI-lip into pericyte revealed differences between the male and female cohorts once again. For the females, in all regions (fig. 3-29-fig.3-34d), there were no significant changes to DiI-lip interaction between the 3-month and 18-month groups. However, between the 18-month and 22-month groups, there was a significant decrease in interaction; CA1 (H=11.46(4, 24), p=0.0219), CA3 (H=16.74(4, 23), p=0.0014), dentate gyrus (H(4, 23) =16.43(4, 23), p=0.030), motor cortex (H=16.11(4, 23), p=0.0107), auditory cortex (H=16.13(4, 24), p=0.0014) and striatum (H=11.33(4, 24), p=0.0168). This differed from the male cohort which showed significant increases in DiI-lip and NG2 interaction in all regions except for the CA3 region (fig. 3-35h) and CA1 (U(10)=3, p=0.0556) (fig. 3-35d) which still indicated increasing trends between the age groups. The dentate gyrus (fig. 3-35l) demonstrated significant increases in DiI-lip and NG2 interaction ((T(10)=75.48, p=0.0041) along with the increasing interactions between NG2 and CD31 mentioned above. However, the motor cortex (U=0(10),

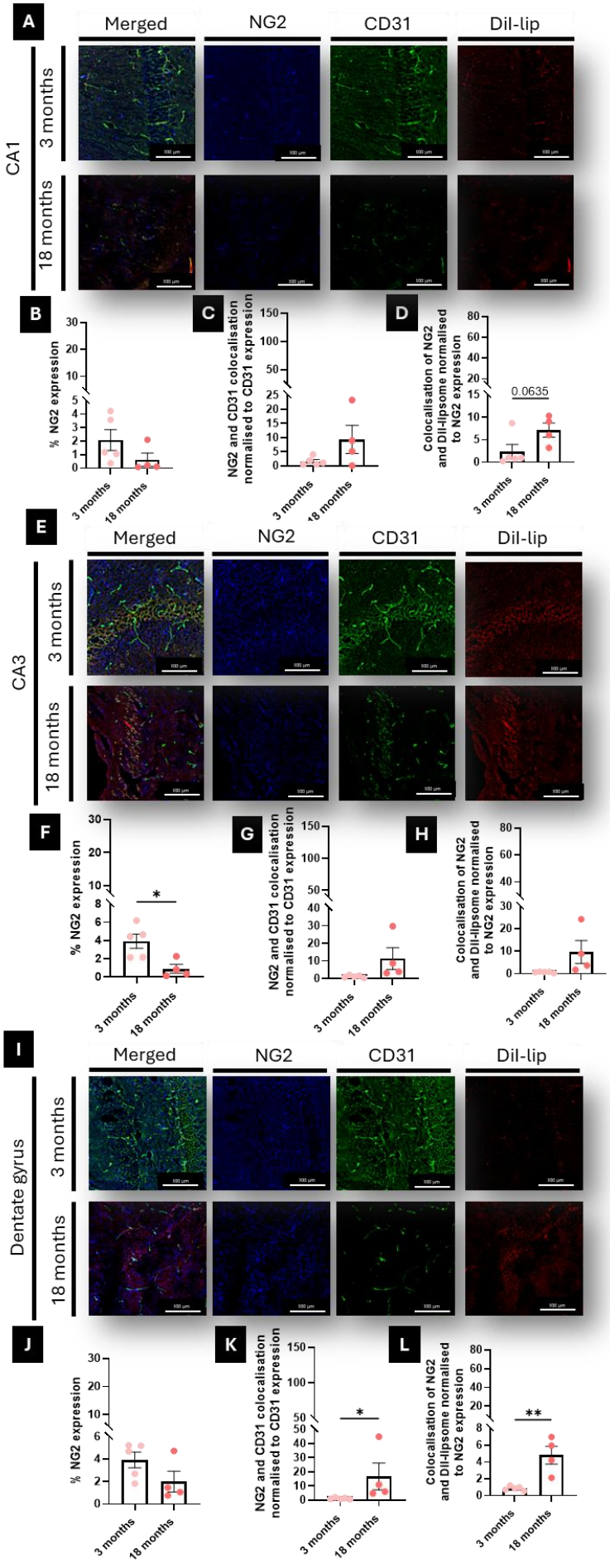
A
Merged
NG2
CD31
DiI-lip
CA1
3 months
18 months
B
% NG2 expression
C
NG2 and CD31 colocalisation normalised to CD31 expression
D
Colocalisation of NG2 and DiI-lipsome normalised to NG2 expression
0.0635
E
CA3
F
*
G
H
I
Dentate gyrus
J
K
*
L
**

Figure 3-35: NG2 expression in ageing male CA1 hippocampal regions. C57BL/6 male mice groups at 3 an 18-months old received a single intravenous injection of DiI-lip. Cardiac perfusion was completed 2 hours post-injection to remove circulating DiI-lip. Representative immunofluorescence images -1.94 mm from the bregma demonstrate expression of NG2 (blue), CD31 (green) and DiI-lip (red) for (A) CA1, (E) CA3 and (I) dentate gyrus. (B) Quantitative analysis of NG2 expression across ageing demonstrated no significant decreasing expression in ageing in CA1 region. (C) Quantitative interaction of CA1 region between CD31 and NG2 expression normalised to CD31 coverage demonstrated non-significant increasing trends. (D) Quantitative interaction between NG2 and DiI-lip expression normalised to NG2 expression did not significantly increase across ageing in CA1. (F) Quantitative analysis of NG2 expression in CA3 region across ageing demonstrated decreasing expression in ageing. (G) Quantitative interaction between CD31 and NG2 expression normalised to CD31 coverage demonstrated increasing trends in CA3 region. (H) CA3 region quantitative interaction between NG2 and DiI-lip expression normalised to NG2 expression non-significantly increased across ageing. (J) Dentate gyrus Quantitative analysis of NG2 expression across ageing demonstrated no significant expression changes. (K) Quantitative interaction between CD31 and NG2 expression normalised to CD31 coverage demonstrated increasing colocalisation of dentate gyrus. (L) Quantitative interaction between NG2 and DiI-lip expression normalised to NG2 expression significantly increased across ageing of dentate gyrus region. Images obtained at x40 magnification on Leica Thunder microscope and underwent large volume computational clearing (LVCC) prior to quantification in Image J. Statistical analysis was completed using GraphPad Prism software using Shapiro Wilk test for normality followed by either a T-test or Mann-Whitney. N=4-5, average ± SEM, $p<0.05$ were considered significant. Scale bar represents 100µm.

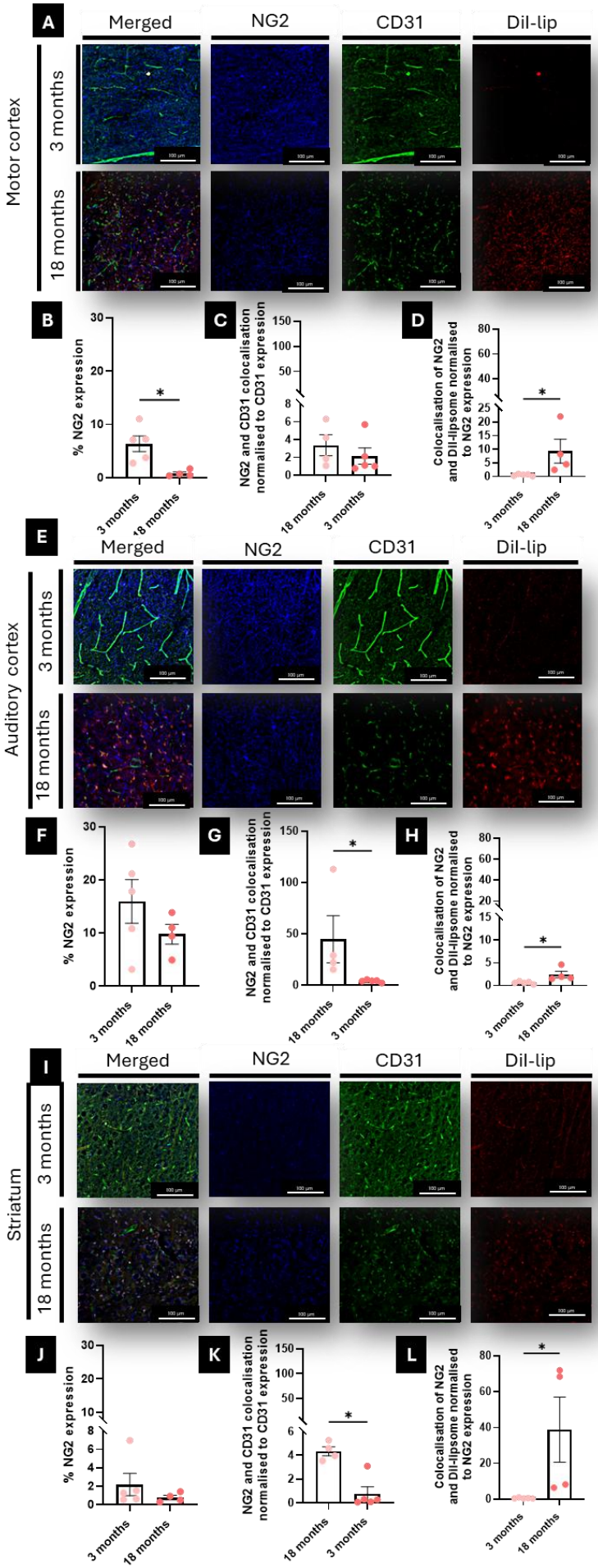
A
Merged
NG2
CD31
Dil-lip
Motor cortex
3 months
18 months
B
% NG2 expression
C
NG2 and CD31 colocalisation normalised to CD31 expression
D
Colocalisation of NG2 and Dil-lipsome normalised to NG2 expression
E
Auditory cortex
F
G
H
I
Striatum
J
K
L
3 months
18 months

Figure 3-36: NG2 expression in ageing male cortical and striatum regions. C57BL/6 male mice groups at 3 an 18-months old received a single intravenous injection of DiI-lip. Cardiac perfusion was completed 2 hours post-injection to remove circulating DiI-lip. Representative immunofluorescence images -1.94 mm from the bregma demonstrate expression of NG2 (blue), CD31 (green) and DiI-lip (red) for (A) motor cortex, (E) auditory cortex and (I) striatum. Motor cortex quantitative analysis: (B) Quantitative analysis of NG2 expression across ageing demonstrated decreasing expression in ageing. (C) Quantitative interaction between CD31 and NG2 expression normalised to CD31 coverage demonstrated no trends. (D) Quantitative interaction between NG2 and DiI-lip expression normalised to NG2 expression significantly increased across ageing. Auditory cortex quantitative analysis: (F) Quantitative analysis of NG2 expression across ageing demonstrated no significant changes. (G) Quantitative interaction between CD31 and NG2 expression normalised to CD31 coverage demonstrated decreasing colocalisation. (H) Quantitative interaction between NG2 and DiI-lip expression normalised to NG2 expression significantly increased across ageing. Striatum quantitative analysis: (J) Quantitative analysis of NG2 expression across ageing demonstrated no changes in ageing. (K) Quantitative interaction between CD31 and NG2 expression normalised to CD31 coverage demonstrated decreasing colocalisation. (L) Quantitative interaction between NG2 and DiI-lip expression normalised to NG2 expression significantly increased across ageing. Images obtained at x40 magnification on Leica Thunder microscope and underwent large volume computational clearing (LVCC) prior to quantification in Image J. Statistical analysis was completed using GraphPad Prism software using Shapiro Wilk test for normality followed by either a T-test or Mann-Whitney. N=4-5,average ± SEM, $p<0.05$ were considered significant. Scale bar represents 100µm.

p=0.0159) (fig. 3-36d), auditory cortex (U=1.337(9), p=0.0159) (fig. 3-36h) and the striatum (T=20501(9), p=0.0479) (fig.3-36l) all had the same increasing reaction but combined with the decreasing CD31/NG2 reaction, warranting further investigation.

3.5.9. **Inflammatory profile increase**

To examine the effects of inflammation on the aged brain, immunofluorescence for iba-1, the gold-standard marker for microglial cells, was conducted. Overall, in the female cohort there was limited significant increases in the iba-1 expression in the hippocampal regions but also a visual increase of most groups between the 3- month and 18- month groups (fig. 3-37b,d,f). The CA3 region did show significant increases between 3- and 18-months ($H=11.17_{(4,\ 29)}$, p=0.0248) (fig 3-37d) as well as non-significant increases between the 12- and 18- months in the CA1 region (H(4, 29)=8.553, p=0.0752) (fig 3-37b). The cortical and striatal regions demonstrated similar results, with visual trends to increasing iba-1 response during ageing that was not significant across all groups (fig. 3-38b,d,f). The auditory cortex (fig. 3-38d) did show significant increases in iba-1 expression to 18-month group from the 3- ($F=6.059_{(4,\ 25)}$, p=0.0109), 6- (p=0.0045) and 12-month groups (p=0.052). It was also observed in the motor cortex that iba-1 expression significantly increases between the 12- and 18-month groups ($H=10.40_{(4,\ 30)}$, p=0.0341 (fig. 3-38b). In the male hippocampal cohort, there was significant increase in iba-1 expression all regions; CA1 ($U=20_{(21)}$, p=0.0127), CA3 ($U= 22_{(21)}$, p=0.0197) and dentate gyrus ($T=1.083_{(20)}$, p=0.0037) (fig. 3-39b,d,f). Similar significant increasing iba-1 expression patterns were seen in the auditory cortex ($U=19_{(20)}$, p=0.0185) (fig. 3-40b) whilst in the motor cortex and striatum there were non-significant trends regarding iba-1 expression (fig. 3-40b,f).

To investigate the uptake of DiI-lip into the microglia cells, the interactions between DiI-lip and iba-1 were examined. In the female hippocampus (fig. 3-37c,e,g), there was no significant increases in interaction, therefore uptake, in any region. However, there are trends to increasing iba-1 uptake of DiI-lip in all regions with the 18- and 22- month groups possessing the highest interaction levels in each region. In the cortical and striatal region, this non-

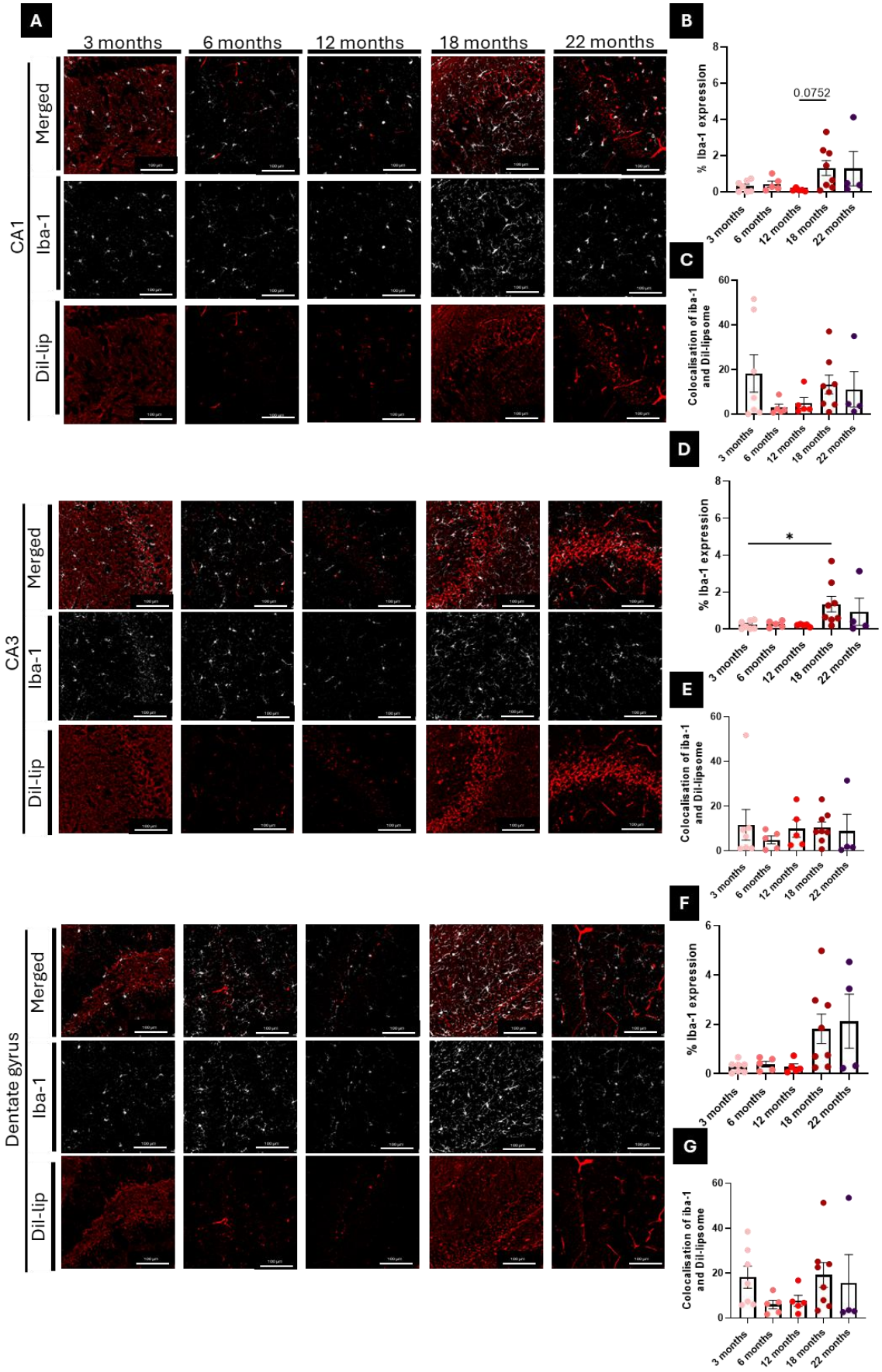

Figure 3-37: Iba-1 expression in ageing female hippocampal regions. C57BL/6 female mice groups at 3-, 6-, 12-, 18- and 22-months old received a single intravenous injection of DiI-lip. Cardiac perfusion was completed 2 hours post-injection to remove circulating DiI-lip. (A) Representative immunofluorescence images of CA1, CA3 and dentate gyrus regions -1.94mm from the bregma demonstrate expression of iba-1 (white) and DiI-lip (Red). (B) Quantitative analysis of iba-1 expression

in CA1 region demonstrated no significant changes ageing. (C) Quantitative interaction between iba-1 and DiI-lip expression in CA1 demonstrated no significant trends. (D) Quantitative iba-1 expression in the CA3 region showed significant increases in age. (E) Quantitative analysis of iba-1 and DiI-lip interaction in CA3 region demonstrated no trends. (F) Dentate gyrus Iba-1 expression quantification demonstrating non-significant trends to increase in age. (G) Quantitative analysis of interaction of DiI-lip and Iba-1 on the dentate gyrus showing no significant changes in interaction through age. Images obtained at x40 magnification on Leica Thunder microscope and underwent large volume computational clearing (LVCC) prior to quantification in Image J. Statistical analysis was completed using GraphPad Prism software using Shapiro Wilk test for normality followed by either a T-test or Mann-Whitney. N=4-8, average ± SEM, $p<0.05$ were considered significant. Scale bar represents 100μm.

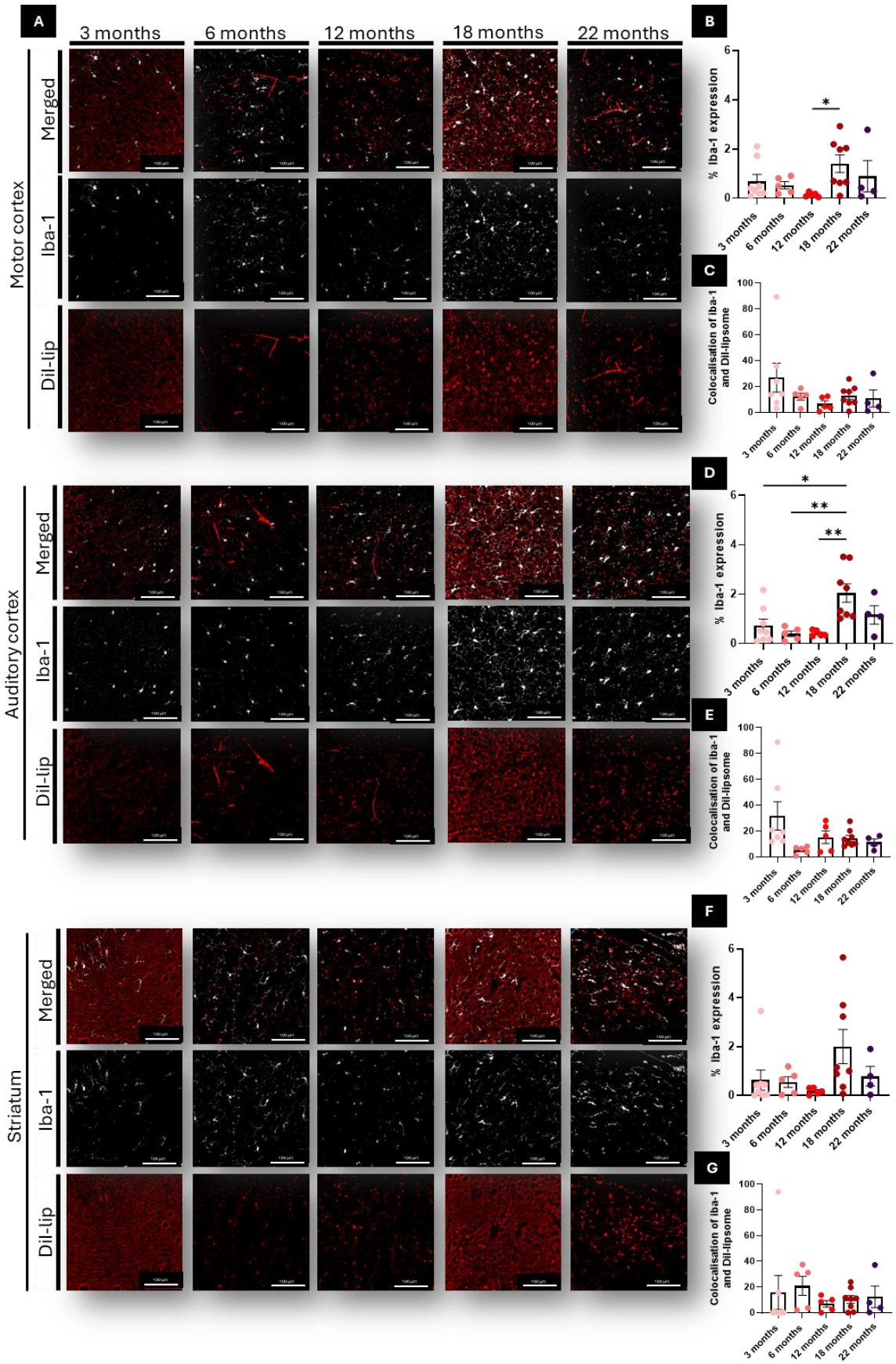

Figure 3-38: Iba-1 expression in ageing female cortical and striatal regions. C57BL/6 female mice groups at 3-, 6-, 12-, 18- and 22-months old received a single intravenous injection of Dil-lip. Cardiac perfusion was completed 2 hours post-injection to remove circulating Dil-lip. (A) Representative immunofluorescence images of motor cortex, auditory cortex and striatum regions -1.94mm from the bregma demonstrate expression of iba-1 (white) and Dil-lip (Red). Quantitative analysis of iba-1

expression in ageing showed significant ageing increases in the motor cortex (B) and auditory cortex (D) but significant changes in striatum (F). No significant changes were observed in ageing regarding the interaction of iba-1 and DiI-lip in the motor cortex (C), auditory cortex (E), or striatum (G). Images obtained at x40 magnification on Leica Thunder microscope and underwent large volume computational clearing (LVCC) prior to quantification in Image J. Statistical analysis was completed using GraphPad Prism software using Shapiro Wilk test for normality followed by either a T-test or Mann-Whitney. N=4-8,average ± SEM, $p<0.05$ were considered significant. Scale bar represents 100µm.

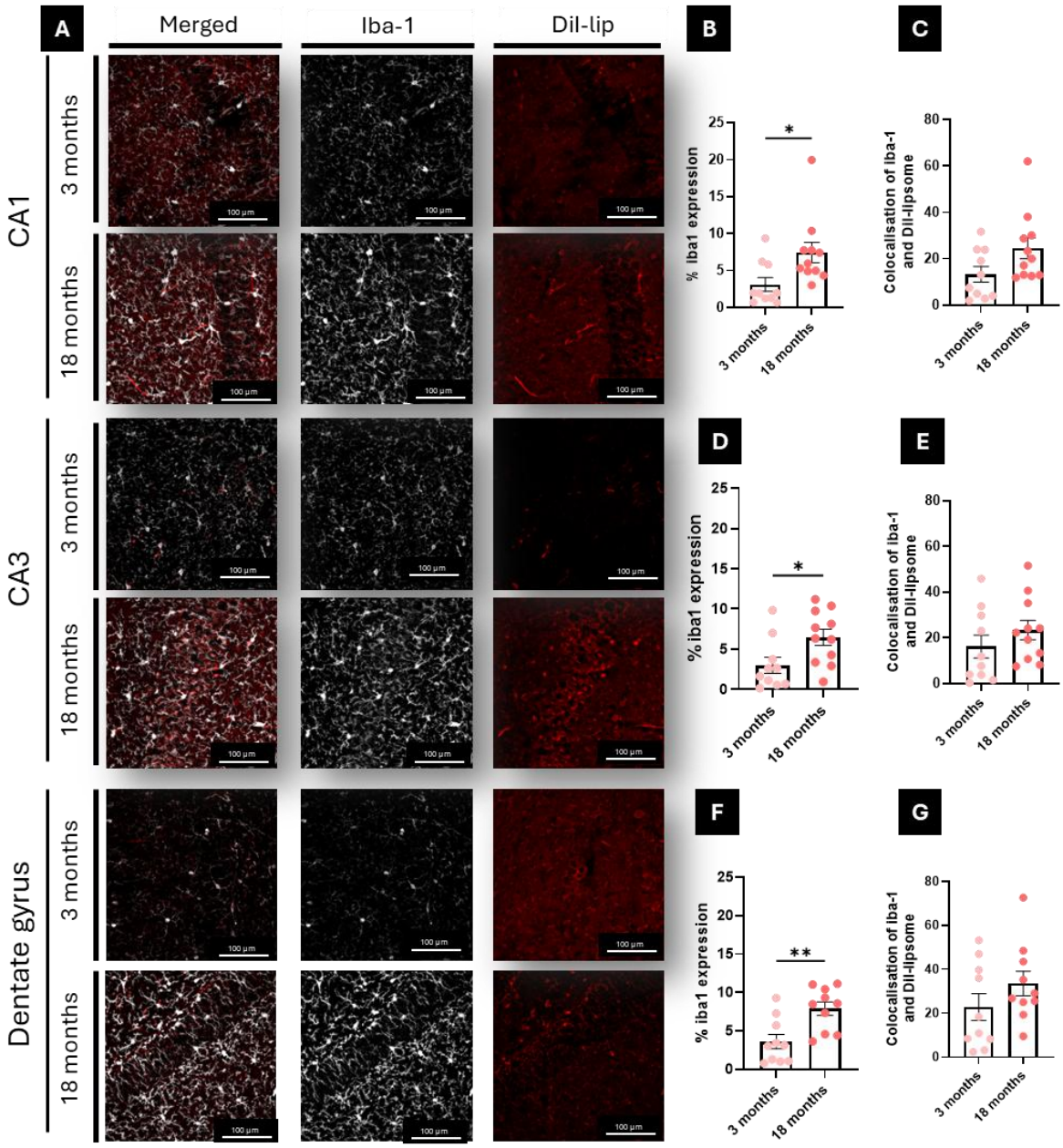

Figure 3-39: Iba-1 expression in ageing male hippocampal regions. C57BL/6 male mice groups at 3 an 18-months old received a single intravenous injection of DiI-lip. Cardiac perfusion was completed 2 hours post-injection to remove circulating DiI-lip. (A) Representative immunofluorescence images of CA1, CA3 and dentate gyrus hippocampal regions -1.94mm from the bregma demonstrate expression of iba-1 (white) and DiI-lip (Red). (B) Quantitative analysis of iba-1 expression in CA1 region demonstrated increasing expression in ageing. (C) Quantitative interaction between iba-1 and DiI-lip expression in CA1 demonstrated no significant trends. (D) Quantitative iba-1 expression in the CA3 region showed significant increases in age. (E) Quantitative analysis of iba-1 and DiI-lip interaction in CA3 demonstrated no trends. (F) Dentate gyrus Iba-1 expression quantification demonstrating significant trends to increase in age. (G) Dentate gyrus interaction of DiI-lip and Iba-1 showing no significant increases in interaction through age. Images obtained at x40 magnification on Leica Thunder microscope and underwent large volume computational clearing (LVCC) prior to quantification in Image J. Statistical analysis was completed using GraphPad Prism software using Shapiro Wilk test for normality followed by either a T-test or Mann-Whitney. N=10-11, average ± SEM, $p<0.05$ were considered significant. Scale bar represents 100µm.

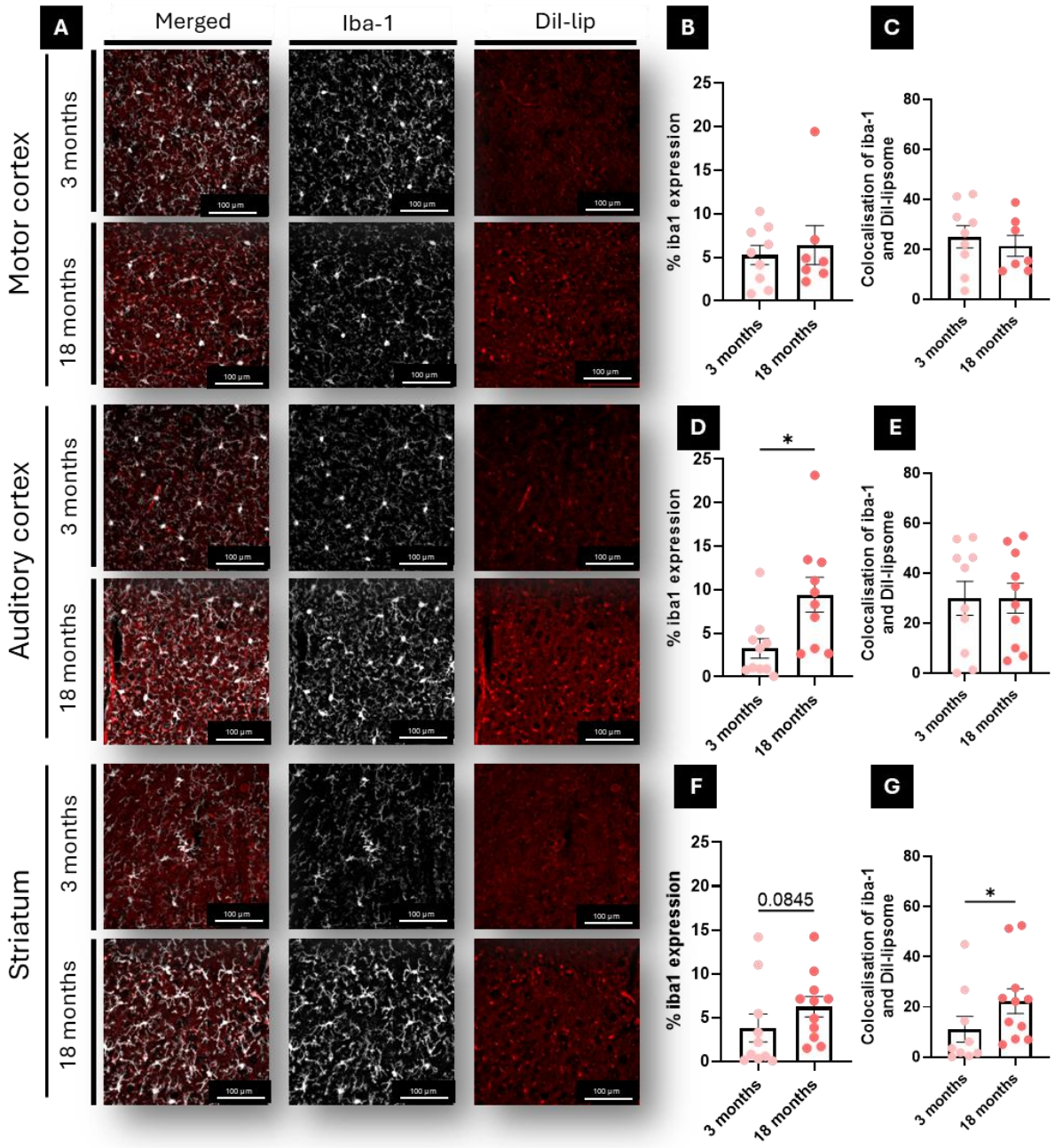

Figure 3-40: Iba-1 expression in ageing male cortical and striatal regions. C56BL/6 male mice groups at 3 an 18-months old received a single intravenous injection of DiI-lip. Cardiac perfusion was completed 2 hours post-injection to remove circulating DiI-lip. (A) Representative immunofluorescence images of motor cortex, auditory cortex, and striatum regions -1.94mm from the bregma demonstrate expression of iba-1 (white) and DiI-lip (Red). (B) Quantitative analysis of iba-1 expression in motor cortex region demonstrated no changes ageing. (C) Quantitative interaction between iba-1 and DiI-lip expression in motor cortex demonstrated no significant trends. (D) Quantitative iba-1 expression in the auditory cortex region showed significant increases in age. (E) Quantitative analysis of iba-1 and DiI-lip interaction in auditory cortex demonstrated no trends. (F) Striatal Iba-1 expression quantification demonstrating non-significant trends to increase in age. (G) Striatal interaction of DiI-lip and Iba-1 showing significant increases in interaction through age. Images obtained at x40 magnification on Leica Thunder microscope and underwent large volume computational clearing (LVCC) prior to quantification in Image J. Statistical analysis was completed using GraphPad Prism software using Shapiro Wilk test for normality followed by either a T-test or Mann-Whitney. N=7-11,average ± SEM, $p<0.05$ were considered significant. Scale bar represents 100µm.

significant increasing pattern is not present and there were no significant changes across age in any of region (fig. 3-38c,e,g). In the male cohort, significant increases in DiI-lip interaction with iba-1+ cells were present in the striatum ($U=23_{(20)}$, p=0.0465) (fig. 3-40g) but not in any of the other regions (fig. 3-39-3-40c,e,g). The results here signify that the hippocampus is more vulnerable to age-related iba-1 expression increase in comparison to the cortical and striatal regions.

To further investigate the inflammatory response of ageing, serum extracted from terminal blood samples underwent ELISA analysis for two inflammatory markers: ICAM-1 and VCAM-1. The results demonstrate that in females, ICAM-1 expression is not significantly altered (fig. 3-41a) but that VCAM-1 expression is significantly up-regulated in the 18 group in comparison to the 3 ($F=8.602_{(4,19)}$, p=0.0042), -6 (p=0.0123) and 12-month groups (p=0.0014) (fig. 3-41b). There was also a significant increase between the 12- and 22-month groups (p=0.0127) (fig. 3-41b). Within the male cohort, both ICAM-1 ($T=7.730_{(10)}$, p=0.0072) (fig. 3-41c) and VCAM-1 ($T=3.003_{(10)}$, p=0.0185) (fig.3-41d) expression significantly increased in the 18-month group. The data presented here signifies that the inflammatory profile of both females and males does indeed increase during ageing, especially to the 18-month group.

3.5.10. **Cognitive changes in mouse behaviour during ageing.**

To determine if the changes observed in NVU components and permeability occurred prior or during age-related cognitive decline, the NOR and NOL behavioural tests were implemented across the male and female cohorts. In females, no significant trends were observed at any timepoint in NOR (fig. 3-42b-d) or NOL (fig. 3-42i-j) showing no cognitive decline. In males, no significant differences were observed in NOR testing (fig. 3-43e-g) or the 24-hour NOL test (fig. 3-42l). However, at the 1-hour timepoint for males, there were significant decreased in novel object investigation time between the 3-month group and both 12- ($F=6.490_{(2,21)}$, p=0.0108) and 18- month group (p=0.0178) (fig. 3-42k).

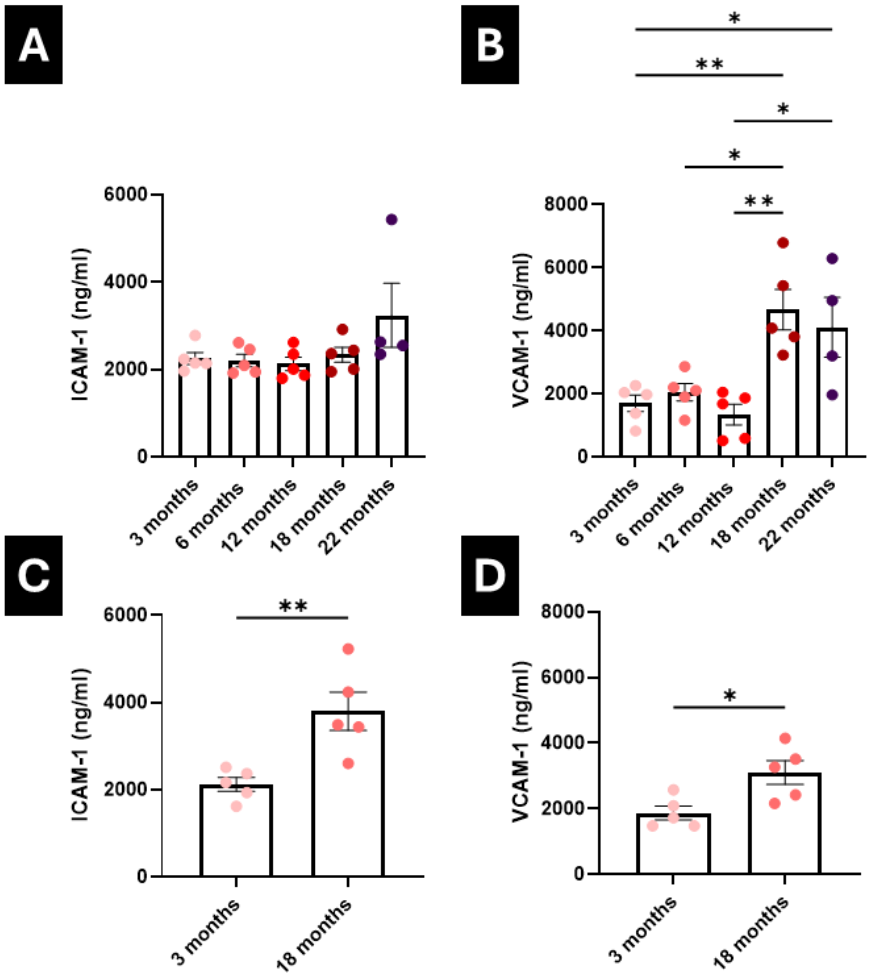

Figure 3-41: Inflammatory response in aged mouse serum. ICAM-1 and VCAM-1 enzyme-linked immunosorbent assay (ELISA) of ageing mouse serum. Male mice of 3- and 18-month or female mice at 3-. 6-.12-. 18- and 22-month mice serum was extracted from mouse heart during cardiac perfusion and serum removed via centrifugation. (A) Quantification of ICAM-1 of aged female serum demonstrated no significant increases. (B) Quantification of VCAM-1 aged female serum showed significant increases of protein at 18- and 22-month age groups. (C) Quantification of aged male ICAM-1 serum demonstrated significant increases in ageing. (D) Quantification of aged male VCAM-1 serum levels demonstrated significant increases in expression in ageing. Statistical analysis was completed using GraphPad Prism software using one-way analysis of variance followed by Tukey multiple comparison test or Kruskal-Wallis test followed by Dunn's multiple comparisons test based on Shapiro-Wilk test for normality. N=4/5,average ± SEM, $p<0.05$ were considered significant.

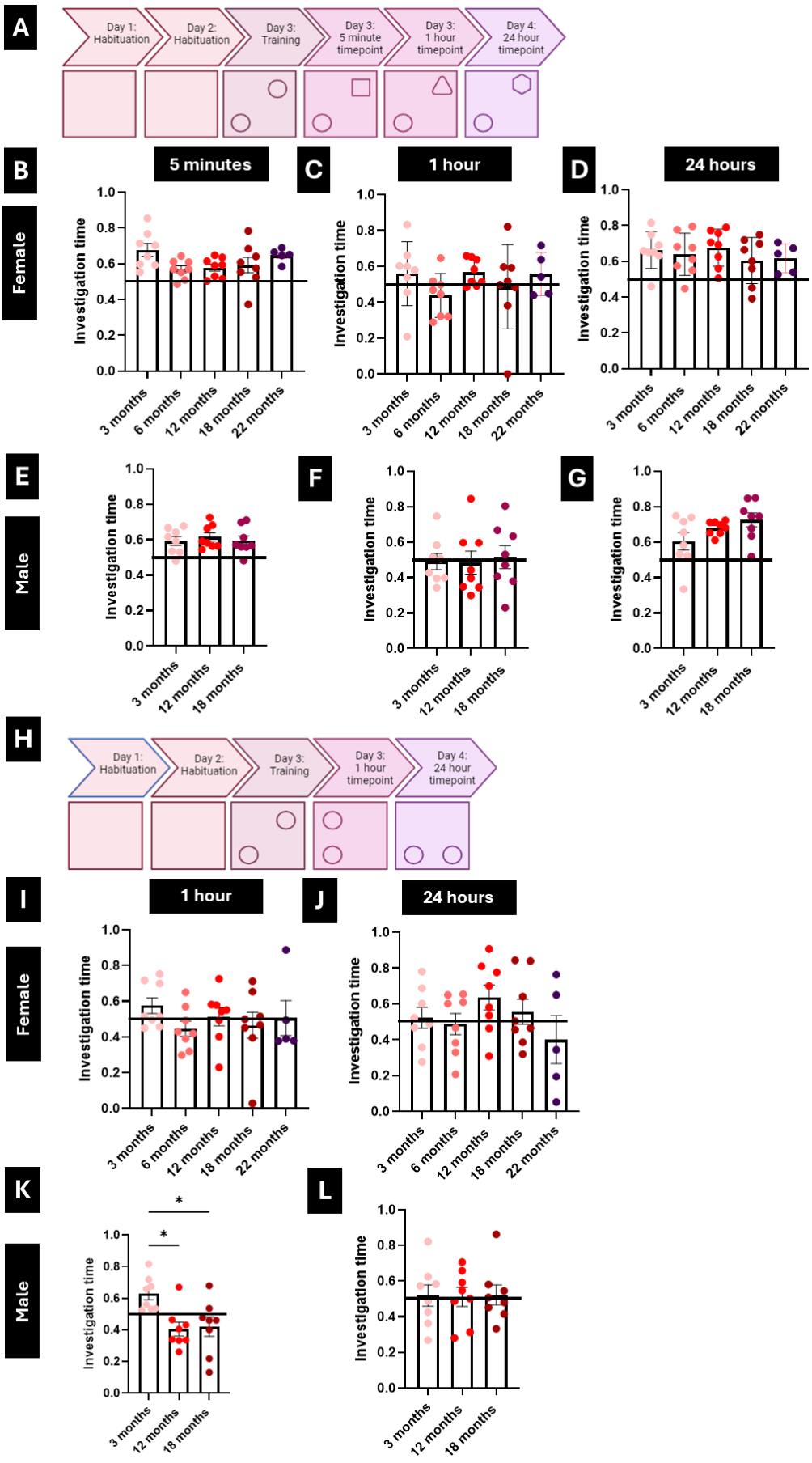

Figure 3-42: Novel object recognition tests in aged male and female mice. Female C57BL/6 3-,6-, 12- 18- and 22-months and male mice at 3-, 12- and 18-months underwent novel object and location

behavioural test. (A) Schematic representation of object recognition. (H) Schematic representation of location recognition. Mice were habituated in the arena for 5 minutes on day 1 and repeated on day 2. Mice were then trained for 10 minutes with two identical objects before intertrial periods of 5 minutes, 1 hour and 24 hours for object recognition (B-G) and 1- and 24-hours for location recognition (I-L). For each test, the mice were exposed to the arena for 5 minutes before being returned to the home cage. All training and test sessions were recorded and manually scored for investigation time of both the novel and training objects. Investigation time was calculated and plotted in graphical format. J. Statistical analysis was completed using GraphPad Prism software using one-way analysis of variance followed by Tukey multiple comparison test or Kruskal-Wallis test followed by Dunn's multiple comparisons test based on Shapiro-Wilk test for normality. N=5-8,average ± SEM, $p<0.05$ were considered significant.

3.6. Discussion

The results of this chapter aim to demonstrate the region-specific changes to the BBB architecture throughout ageing whilst comparing changes to BBB permeability. Permeability of the BBB increased during ageing and allowed for the infiltration of albumin and liposomes globally, but this is not reflected by dextran infiltration. Biodistribution of DiI-lip also showed no significant changes in peripheral organs, indicating a brain specific increase in nanoparticle infiltration. Complementing global changes, regional infiltration of albumin and liposomes also demonstrates significant increases in both males and females. This increase in permeability correlated with increases in caveolin-1 in the male brain but not the female brain. Permeability increases were not mirrored in IgG infiltration into the parenchyma. Evaluation of NVU components (astrocytes, endothelial cells and pericytes) presents a mixed picture whereby astrocytic activation and pericyte loss occurred in ageing to a greater extent in males than females. Endothelial cells increased expression during ageing in cortical, striatal regions whilst varied in hippocampal regions. The inflammatory profile of the mouse brain increased during ageing and changes were greater in the hippocampus more than peripheral regions. Further inflammatory studies also showed that there was a sex difference in the expression of ICAM-1 during ageing whereas VCAM-1 was increased in both males and females during ageing. Cognitive function was not changed during ageing in the female brain in either behavioural test but in males cognitive decline was observed in short-term memory.

3.6.1. **Increased global permeability of the BBB not linked to paracellular transport**

The initial premise for this chapter of work was that the increase in BBB permeability during ageing would facilitate infiltration of lipid nanoparticles into the brain. The findings demonstrated that in all regions tested, DiI-lip did indeed cross the BBB and stay in the parenchyma in an age-related effect, agreeing with the hypothesis. This is a novel finding in ageing that this nanoparticle formulation crosses the BBB and may be used as a potential delivery system for therapeutics. Recently, there have been similar studies which confirm nanoparticle infiltration into the ageing brain (Tracy et al., 2023). These nanoparticles

consisted of hyaluronic acid-poly(lactic-co-glycolic acid) (HA-PLGA) and had a size of 200nm, which is larger than our current study of approximately 100nm which shows that our nanoparticles should cross the ageing BBB as demonstrated. The conservation of infiltration between male and female mice, as shown by the IVIS data, demonstrates robust delivery of DiI-lip into the brain, allowing the field to consider possible therapeutic encapsulation.

Dextran was injected into a small sub-cohort of male mice to determine the effects of ageing on TJ permeability, which mechanistically is different to that of transcytosis. Figure 3-3 demonstrates that there is no increased dextran infiltration from 3 to 18-months indicating that the tight junction barrier was maintained. This agrees with some studies, such as Goodall et al., 2018 and Cummins et al., 2024, who saw no changes to Evans Blue or dextran 3 kDa infiltration into the brain through ageing. However, within the literature it has been shown that there is tight junction dysfunction leading to BBB permeability in ageing, which would suggest an increase in BBB permeability (Elahy et al., 2015; Stamatovic et al., 2019). To research this further, investigations into tight junction proteins, such as occludin, claudin-5 and zo-1 would be appropriate, whether in histological or protein-based assays. The increases observed also correlates with *in vivo* stroke studies, showing increasing DiI-lip infiltration in both ischaemic and haemorrhagic models (Al-Ahmady et al., 2019, 2022).

The increased infiltration of albumin at 18- and 22- months females and 18-month males (fig 3-3) also demonstrate that the BBB has increased permeability to larger molecules but also serves a dual purpose to suggest the possible transport mechanism of the nanoparticles. It has been shown in stroke cases as well as in other age-related studies, that albumin infiltration correlates with an increase in transcytosis at the BBB which further correlates with DiI-lip penetration (Al-Ahmady et al., 2019; Sorets et al., 2020; Hillmer et al., 2023).

3.6.2. **Increased albumin permeability tentatively linked to caveolin mediated transcytosis**

As it has been shown in ageing *in vivo* studies that there is a shift to caveolae-mediated transcytosis and therefore increase in caveolin-1 expression, it was prudent to correlate any infiltration of albumin to this marker (Yang et al., 2020). Previous studies have successfully correlated caveolin-1 expression with increased transcytosis and BBB permeability, but the current study is inconclusive. In the male group, in the CA1 and dentate gyrus hippocampal regions, there was a significant increase in caveolin-1 expression (fig. 3-8, 3-10) and trends towards increases in other regions. However, this is not as convincing for an effect in ageing compared to literature studies, this could potentially be explained by the techniques applied. Yang et al., 2020, isolated the micro vessels from the tissue and then labelled endothelial cells with lectin and caveolin-1 and imaged the staining at x63 magnification. This contrasted with the current study which did not isolate the micro vessels and imaged at x40 magnification, which may be why the results do not completely align. Another possible way to investigate the effect of caveolae-mediated transcytosis is to look at the protein marker Major Facilitator Super Family Domain Containing 2a (MSF2DA), which crucial in the formation and functioning of the BBB and is the inverse to caveolin-1 (Ben-Zvi et al., 2014). It has been shown in the literature that when caveolin-1 expression increases, MSF2DA decreases, and so the expected decrease in expression of this protein would also indicate a shift towards transcytosis (Yang et al., 2020).

In the female cohort, the expression pattern of caveolin-1 was different. The 6–12-month groups in each region presented with the highest expression of normalised caveolin-1 and then dropped again for the later age groups (fig. 3-8-3-13). This therefore does not correlate with the infiltration of albumin observed within the study, potentially indicating at an alternative transport route for both DiI-lip and albumin infiltration, such as receptor-mediated transcytosis. Transferrin is a possible receptor allowing for infiltration and has been shown to increase the uptake of liposomes through the BBB when specifically targeted (Johnsen et al.,

2017). However, studies *in vivo* have documented a decrease in transferrin expression during ageing so other potential targets should be explored (Yang et al., 2020).

Another aspect to consider for this study is the *in vivo* model utilised, up to yet, there has not been a study investigating the effect of caveolin-1 in middle aged (6-15 months) female mice, with historical data focusing on two timepoints (e.g. 3 months and 24 months) and/or male mice (Park *et al.*, 2018; Yang *et al.*, 2020). Therefore, it may be that the female transport mechanism differs from that of the males, which has been linked more conclusively with caveolae-mediated transcytosis and further studies would have to be conducted investigating correlation with different transport mechanisms. Other transport methods have been shown to have sex differences, linked to the amount of oestrogen present, such as P-gp efflux transporters and ABC transporters (BCRP and MRP)(Dalla *et al.*, 2022; Dion-Albert *et al.*, 2022). Research groups have investigated the effects of hormones further by performing ovariectomies on female rats, producing increased BBB permeability to EBD and function rescued via oestrogen treatment (Wilson *et al.*, 2008; Cipolla, Godfrey and Wiegman, 2009). It has also been demonstrated in human studies using diffusion prepared pseudo-continuous arterial spin labelling (DP-pCASL) MRI imaging, that age-related decline in BBB function was sex dependent, with males showing higher rates of decline (Shao et al., 2024). Furthermore, when investigating aged myocardial tissue in mice, caveolin-1 expression was different between males and females, with the female expression remaining more consistent and not leading to contractile dysfunction (Kiessling, 2024). It would be prudent to complete investigations of a similar avenue within the male and female mouse brain to determine if there is a comparable response, which may explain the sex differences observed in this study.

Further examination of caveolin-1 investigated the interactions between the protein and either CD31 for BBB or DiI-lip for cellular infiltration. In the female cohort, there was no significance in either interaction across ageing (fig. 3-8-fig. 3-13) further enforcing the theory that female brains are not influenced by caveolin-1 as much as males and that they do not correlate specifically with liposomes, when normalised for caveolin-1 expression. In the male cohort,

the 3 hippocampal regions all demonstrated trends, of which the dentate gyrus was significant, to increased interaction between CD31 and caveolin-1 in ageing, suggesting age-related effect on caveolin-1 which correlates with the literature studies (Park et al., 2018; Yang et al., 2020).

Further studies into BBB permeability investigated the extravasation of IgG into the parenchyma in females and males (fig. 3-18, 3-19). Within the literature, it is not conclusive regarding the infiltration of IgG during ageing as some show increased infiltration (Pelegrí et al., 2007; Yang et al., 2020; Khan et al., 2023) whilst other demonstrate no changes (Goodall et al., 2018; Cummins et al., 2024). This study did not show significant increases in any male region and only in the motor and auditory cortex of the female mice. Therefore, no conclusion can be made in this study showing that IgG infiltration occurs globally in the brain, but further work should be carried out using other techniques, such as MRI to determine permeability.

3.6.3. **Regional and sex differences of NVU component expression in ageing**

The findings presented in this chapter add to the growing field in physiological ageing that there are some changes to the NVU components. Firstly, astrocytic changes, were observed via the expression patterns of GFAP with male hippocampal and male/female cortical regions which correlates with findings in both humans (Goodall et al., 2018; Verkerke et al., 2021) and rodents (Rodríguez et al., 2014; Janota et al., 2015; Verkerke, Hol and Middeldorp, 2021) and with BBB permeability. This also aligns with the concept that astrocytes in ageing are not affected in number but instead transforming into the 'A1' activated phenotype which correlates with an increase in GFAP expression (Cohen and Torres, 2019; Britton *et al.*, 2022). No significant changes to GFAP expression was seen in the hippocampal region, which was unexpected due to this being an age vulnerable region but this has also been found in other studies, exemplfying the complexity of investigating age related changes to the NVU (Mackic *et al.*, 2002; Janota *et al.*, 2015). Rodríguez et al., 2014, demonstrated this by investigating different astrocyte markers; GFAP, S100β and glutamate synthase in 3 brain regions, and found different patterns of expression in age with each combination. For example, they reported that in the CA1

hippocampal region that there was a significant increase in surface area and volume in ageing but no differences were found in other markers such as S100β or glutamate sythase.

The next point of interest was the effect of ageing on astrocyte-endothelial interactions by colocalisation of GFAP and CD31. The data presented here showed no changes in any of the regions in both females and males which was suprising as it has been documented that astrocytes detach from the BBB during ageing (Heithoff *et al.*, 2021; Popov *et al.*, 2021). However, this may not be the best choice of morphological marker to investigate this aspect of astrocyte modification as the detachment is mainly in the astrocytic end-feet, where makers such as AQP4 would be more suitable as this expresses at the end-feet. Studies have shown that in ageing, there is a reduction in APQ4 expression and that this moves away from the endothelial cells (Duncombe et al., 2017).

DiI-liposome uptake by the astrocyte cell was investigated to see if they could be potential therapeutic targets of the nanoparticles. In the female brain, no significant changes were observed across the cortical regions in ageing but there was a significant increase in the dentate gyrus region and trends towards the same effect in CA1 and CA3. In the male cohort, all regions displayed a significant increase in aged mice. This demonstrates that there may be a regional effect of ageing on liposomal uptake via astrocytes and the hippocampus appears to be the most vulnerable to this. Correlation can be made to the literature studies stating that the hippocampus is age vulnerable and one of the first regions to display age effects and so this may be why the lipsome uptake is more in this region (Montagne et al., 2015). In this study, the quantfication was normlaised to GFAP levels to remove bias of increased expression so the findings should reflect more realistically the interaction between GFAP+ astrocytes and liposomes.

To investigate the effect of ageing on the main structure of the BBB, endothelial cell marker CD31 was explored. The results show that there was a non-significant increase in CD31 expression in the hippocampal regions and significant increase in the cortical and striatal regions. This was unexpected initially as the hypothesis is that ageing would lead to endothelial

cell damage and therefore a decrease in CD31 expression. However, studies have shown that endothelial cells markers are either overexpressed in ageing or remain at similar levels to that of young mice (Chen et al., 2020; Zhao et al., 2020; Dobner, Tóth and de Rooij, 2024). Alternatively, what should be investigated in the future is not the endothelial cell itself, but instead the tight junctions which are known to become dysfunctional and therefore result in increased BBB permeability (Cao, Xu and Liu, 2024). This would involve looking into expression changes of common tight junction markers affected by ageing, such as Zo-1, claudin-5 and occludin (Stamatovic et al., 2019; Yang et al., 2020; Jang, Choi and Kim, 2022).

We also investigate the effect of ageing on the pericyte population where in hippocampal regions, a significant decrease was observed. This agrees with previous studies showing losses in pericytes linked to increased BBB permeability (Bell *et al.*, 2010; Nikolakopoulou *et al.*, 2017). This finding was replicated in both rodent and human studies showing an age-dependant loss of pericytes resulting in dysfunction of BBB and associated transport mechanisms (Daneman et al., 2010; Erdö et al, 2017; Yang et al., 2020). However, no changes to the expression patterns in cortical or striatal regions highlight the heterogeneity of the ageing pericyte population (Abdelazim *et al.*, 2022). Regional heterogeneity, in terms of brain and vasculature location may contribute to variability in the literature, with some areas more age-vulnerable, such as the hippocampus (Peinado *et al.*, 1998; Montagne *et al.*, 2015; Brown *et al.*, 2019). Other studies have partially agreed with this result, such as Montagne et al., 2015, who observed that age-related pericyte loss in human subjects was seen in the hippocampus, hypothesising that this is the initial brain region to be affected by ageing. Another explanation of NG2 expression not decreasing is the production of the protein by other cell types, microglia have been shown in a mouse model to produce NG2 in aged mice but not young (Baror *et al.*, 2019). Further immunolabelling with other cellular makers, such as iba-1, CD11b or CD68 should be used to confirmed colocalisation of NG2 with microglial cells.

Other studies did not find pericyte loss but instead a detachment and migration of pericytes away from BEC's, again resulting in BBB dysfunction and permeability (Hughes et al., 2006;

Scheibel and Fried., 1983). However, alternative studies have observed no change in pericyte number or coverage during ageing (Bors et al., 2018; Goodall et al., 2018; Ximerakis et al., 2019) and one study noted an increase in pericyte number through ageing (Peinado *et al.*, 1998). Therefore, it was prudent to investigate interactions between CD31 and NG2 and in both sexes with regional variability. Only the male auditory cortex and striatum significantly reduced in colocalisation (fig. 3-37). Decreasing trends were observed in females at 22-months, suggesting that future studies should try to look at the 22–24-month range in C57BL/6 mice.

Opposite interactions between pericytes and DiI-lip are reported in this study between males and females. In the male cohort, the amount of uptake of DiI-lip into the pericyte increased significantly whilst in the females this decreased at the 22-month point. This suggests that the actions of the liposomes are different in each sex, which may relate back to the potential differing transport mechanisms of the nanoparticles discussed earlier in this chapter.

Further work should incorporate multiple pericyte morphological markers: CD13, PDGFR-β and desmin to gain clarity of pericytic changes. Immunolabelling with more than one marker will reduce the conflation of pericyte and smooth muscle cell expression. Another morphology marker which could be implemented is ATP binding cassette subfamily C member 9 (ABCC9) as this has no expression in arteriole smooth muscle cells and limited expression in the venule subtype (Vanlandewijck et al., 2018).

3.6.4. **Increasing inflammatory profile of the ageing mouse brain**

The next outcome analysed was the effect of inflammation on the ageing brain via Iba-1 immunofluorescence complemented by peripheral vasculature expression of ICAM-1 and VCAM-1. Within the female cohort, the expression of Iba-1 increased in the CA3 and auditory cortex region whilst was globally increased in the six quantified regions in the male cohort. This partially confirms the hypothesis that increased neuroinflammatory response would occur during ageing.

Previous literature showcases an increase in Iba-1, observed in human and mouse brain ageing (Hayakawa, Kato and Araki, 2007; Mangold *et al.*, 2017; Waller *et al.*, 2019; Garrido *et al.*, 2021). Correlating with the increased expression in the hippocampal regions, many studies have shown that this region is particularly vulnerable, with microglial morphology becoming amoeboid signalling a pro-inflammatory phenotype (Hayakawa, Kato and Araki, 2007; VanGuilder *et al.*, 2011). It is unexpected that the iba-1 response to ageing would be higher in the male group as female mice present with more microglia than males in the CA1 and dentate gyrus regions (Mouton *et al.*, 2002; Mangold *et al.*, 2017). Mangold et al., 2017, also looked at other pro-inflammatory microglial markers such as TREM2 showing similar age-related increases exacerbated by the female mice.

Conversely to the overall trend that microglial activation in ageing causes dysfunction, some studies have shown the inverse, suggesting a neuroprotective role. Pan et al., 2021, used 3- and 12-month mice to show that microglia regulated tyrosine/serine phosphatase and the mitogen-activate protein kinase (MAPK) pathway which resulted in less monocyte infiltration and signalled astrocytes to an unreactive phenotype, resulting in BBB integrity increases. Yegla et al., 2021, further found that the reduction in microglial number via intervention lead to an increased cognitive ability in aged and young rats, further indicating a neuroprotective role of microglia. However, the same study noted that when microglial population increased in ageing, the cognitive decline was still present, indicating that in aged mice microglial presence is not the driving mechanism of dysfunction. This is the inverse of the typical theory, which is that microglial activation in ageing results in increased inflammatory response but is only in 12-month mice and a different microglial response may occur at older age groups. (Waller *et al.*, 2019).

Changes in adhesion molecules, such as ICAM-1 and VCAM-1 have been shown to promote leukocyte adhesion as well BBB disruption and can be induced by increases in pro-inflammatory cytokines, such as TNF-α (Ohara *et al.*, 2000; Kallmann *et al.*, 2004). Within this study, peripheral ICAM-1 levels did not change during ageing, which correlates with past

literature in mouse and human studies (Miguel-Hidalgo *et al.*, 2007; Elahy *et al.*, 2015). This indicates that increases in ICAM-1 expression are correlated with neuropathology or systemic inflammation as opposed to physiological ageing (Drake *et al.*, 2021; Galea, 2021). Within the male cohort, significant ICAM-1 increases were observed during ageing, contrasting with the female cohort. Within a cell culture model of human brain microvascular endothelial cells, it was observed that in the presence of TNF-α, there was a significant fold-increase in males compared to females (Hunter, Jayachandran and Miller, 2019). *In vivo* studies focusing on lupus mice also showed an increase in ICAM-1, as well as VCAM-1, in environments high in TNF-α (McHale *et al.*, 1999). As it has been shown in ageing that TNF-α increases in the human and mouse brain, potentially, this could be a reason for the discrepancies in sex (Álvarez-Rodríguez *et al.*, 2012).

Within our cohort, VCAM-1 was significantly increased during ageing of both males and females, demonstrating a more robust age effect then found with ICAM-1. Within the literature, VCAM-1 increases have been shown in the plasma of both aged human and mouse cohorts and in a model of cerebral hypoperfusion, was linked to increased BBB permeability (Yousef *et al.*, 2019; Zhang *et al.*, 2024). Yousef et al., 2019 expands further to show that if blood from aged mice is transfused into young mice, then VCAM-1 expression increases and correlates with increased microglial activity. Like ICAM-1, VCAM-1 expression increases due to TNF-α increases, so both adhesion molecules may be affected by the same mechanisms (Ohara et al., 2000). However, contrasting results have been shown within *in vivo* models, demonstrating no significant increases in VCAM-1 during ageing females shown via the lack of leukocyte infiltration that would classically be associated with increase adhesion molecules (Elahy et al., 2015).

3.6.5. **Changes to BBB in ageing occurs prior to significant cognitive decline**

The final area of interest within this chapter was the effect of ageing on the cognitive ability of mice. The NOR and NOL tests were selected for this study due to the lack of specialised equipment required as well as being less stress inducing then other behavioural tests such as

the Morris water maze and rotarod (Traschütz et al., 2018). Multiple time points were also chosen to incorporate both short- and long-term memory to elucidate any differences in cognition in these two aspects. Within NOR testing, the use of multiple timepoints also allows correlation with different regions of the brain being recruited for the task; it has been shown that short-term NOR is linked to cortical regions but not the hippocampus, whilst longer term (over 10 minutes) has been shown to recruit the non-spatial hippocampal (Cohen and Stackman, 2015).

The results of the current work demonstrate no changes in memory throughout ageing at any of the three selected timepoints for either males or females. Short-term timepoints correlate with previous studies showing limited cognitive effects in mice up to 28-months age (Fahlström, Yu and Ulfhake, 2011). With the long-term memory studies (1 hour and 24 hours) the existing literature is contradictory with some studies indicating that in ageing there is a significant drop in cognitive function (Frick and Gresack, 2003; Yang, Zhou and Ma, 2019) whilst others note no changes to NOR function up to 15 months of age (Benice *et al.*, 2006; Fahlström, Yu and Ulfhake, 2011).

When looking into the effect of ageing on the novel location experiments, again there is no difference in the female mice at either 1 hour or 24-hour timepoints. NOL tests are expected to incorporate hippocampus dependant spatial memory and so is relevant to this study which has highlighted the hippocampal area as a region of age-related interest (Denninger, Smith and Kirby, 2018). It has been shown historically (Ammassari-Teule and Passino, 1997) and recently (Oliveira *et al.*, 2010) that modification to decrease hippocampal function results in increased cognitive decline. Studies have shown in ageing that long-term memory is affected but not short-term memory (Wimmer *et al.*, 2012) which partially agrees with our findings. Interestingly, for the male mice, significant reductions in cognitive ability have been shown at the 1 hour timepoint and also at the 24 hour timepoint all ages tested resulted in approximately 50% investigation time. This points to it being a timepoint assay related effect as opposed to an ageing effect.

One explanation for the variation in findings for NOR and NOL tests is that there is no standardised procedure for behavioural studies. For example, there are variations in the frequency of habituation, times of habituation, amount of time training the mice with the familiar object and also the shape and size of the arena (Şik *et al.*, 2003; Hammond, Tull and Stackman, 2004; Benice *et al.*, 2006; Oliveira *et al.*, 2010; Wimmer *et al.*, 2012b; Kudara *et al.*, 2023). This means that all comparisons between different studies have to be tentatively correlated as the mice behaviour is sensitive to changes such as the amount of handling occurring. Environmental discrepancies, such as smell or sound, could also impact mouse stress levels, altering their behaviour (Lueptow, 2017). Another aspect to consider when using behaviour testing which incorporates movement is the age-dependant reduction in locomotor activity which should be evaluated to ensure for movement correction (INGRAM, 1988).

In relation to the other aims and findings in this chapter, the lack of cognitive changes displayed suggests that the changes to the NVU components and permeability occur before cognitive decline can be assessed. This means that there is a potential therapeutic window prior to severe cognitive defects.

3.7. Limitations

This study is not without its limitations; with translatability being the major oversight within the workflow. This study is exclusively within the C57BL/6 mouse model and no work on human tissue was undertaken. Future work should focus on correlating changes observed in BBB permeability and NVU component changes to the clinical setting via histopathological staining and molecule studies on post-mortem tissue. This could utilise long-term research such as the cognitive function and ageing study, which has already demonstrated the prevalence on dementia in the population (Matthews *et al.*, 2013). Furthermore, the progression of ageing from young adult mice to aged mice was seen in females but only 2 timepoints were chosen for the males. In the future, the same experimental design should be adhered to for the male cohort, to examine progression of ageing and if there are any sex differences in the 6–12-month groups.

Although this study investigated the same parameters in both male and female mice, the analysis was kept separate between sexes. This allowed for investigation into the systematic timepoints in females that did not exist in the male cohort (6, 12 and 22 months). However, this limited the ability to compare expression levels between males and females, leading to overall trends observed instead of quantitative analysis. This means that sex comparisons made within this study should be taken tentatively and with caution when considering further work. Future studies should aim instead to compare sex directly, statistically utilising a 2-way ANOVA in order to fully elucidate any sex-related changes.

Another limitation of the study relates to the practicalities of conducting long-term ageing immunofluorescence studies. As this study took place over a 2 year time period, different age groups were stained immunofluorescently at different timepoints but then analysed on the same graph. The use of batches may have led to variation between staining patterns and therefore expression analysis, so this should be considered when planning potential work. In the future all groups in an immunofluorescence comparison should be stained on the same day to ensure no variation and reduce batch effect (Stopsack et al, 2021). Using an inter run control, which would be a slide consistently from the same animal, would help to mitigate any variation as this should result in the same pattern of expression regardless of run. If staining patterns changed within the inter run control, work would have to be analysed separately to ensure accurate conclusions.

Further investigations into the transport mechanism of DiI-liposomes needs to be undertaken as the findings of this study were inconclusive; with caveolin-1 expression not correlating with DiI-lip infiltration. For example, this could be using transport inhibitors such as sodium azide which *in vitro* blocks energy-dependant transport correlating with a decrease in liposomal uptake suggesting a mechanistic route (Montizaan *et al.*, 2020). Other inhibitors of transport could target micropinocytosis, endocytosis and transcytosis specifically to further pinpoint how DiI-lip infiltrated the brain in ageing (Francia *et al.*, 2019). If the nanoparticle infiltration is unaltered by inhibition of specific transport mechanisms, then they can be eliminated as the

transport route. For permeability studies, the use of complementary markers such as Evans Blue dye, sodium fluorescein or MRI would be useful to compare to the current study and add to the literature regarding BBB permeability in ageing (Dickie *et al.*, 2021).

Regarding inflammation, only adhesion molecules ICAM-1 and VCAM-1 in the peripheral blood supply were investigated. It is accepted within the literature that these are not the only age-related inflammatory markers and cytokines such as IL-1β, IL-6 and TNF-α are affected by ageing and may be direct mediators for downstream inflammatory phenotypes of cells such as astrocytes and microglia (Costa *et al.*, 2021). Testing of brain homogenates for these inflammatory molecules would also be beneficial to determine not only peripheral effects but localised effects down to specific brain regions.

Finally, although the study was powered to investigate BBB infiltration of liposomes, it was not possible to power this to every outcome variable (e.g. iba-1 and GFAP expression during ageing). This means that some of the results display non-significant trends with tentative conclusions, these would be more robust in an accurately powered study. For the male cohort, some comparisons (e.g. Iba-1 and GFAP analysis) were fully powered due to groups having to be repeated, allowing for extra tissue and experimental units. This was not conducted in female mice due to time and economic constraints, but the study should be repeated using power calculations derived from results in this study for specific parameters, for example different targets of immunofluorescence staining.

3.8. Conclusions

Within this chapter, multiple hypotheses have been addressed, firstly, ageing does increase the permeability of BBB to nanoparticles, allowing them to infiltrate into the brain parenchyma. Secondly, there are changes to the NVU components, such as increase astrocyte activation and decrease pericyte expression. However, this can be dependent on spatial factors and sex as male and female cohorts responded differently with age. Cognitive decline was not observed at these timepoints, indicating the potential to use of nanoparticles as a drug delivery

system before the onset of cognitive decline. Inflammatory markers also changed during ageing demonstrating an increase in microglial activation and VCAM-1 response. Overall, this chapter proves that nanoparticles could be used to target age-related changes to the NVU and associated cells before pathology. Further investigations need to be undertaken to further elucidate the potential of nanoparticles as age-related therapeutics.

4. Pilot study evaluating the effects of systemic inflammation on aged blood-brain barrier and associated cells

4.1. Introduction

As highlighted in chapter 3, the inflammatory profile of the female mouse brain changes during physiological ageing, with higher expression of microglial marker Iba-1 and increased peripheral VCAM-1 observed compared to males. Inflammation is categorised based upon the duration of its effect; acute within 2 weeks post-injury, sub-acute up to 6-weeks and chronic which lasts months or years (Germolec et al., 2018; Rafiyan et al., 2023; Zotova et al., 2023). Low-grade chronic inflammation (systemic) has been noted as a major hallmark of age progression within humans (Li et al., 2023; Meier et al., 2023).

Systemic inflammation has a widespread impact upon the brain and specifically the BBB and has been demonstrated to increase BBB permeability to albumin in humans (Elwood et al., 2017) as well as degradation of tight junction proteins and activation of astrocytes and microglia *in vivo* (Varatharaj & Galea, 2017). This is also noted to be an age-related event as studies in young mice have shown limited BBB degrading effects with systemic inflammation and only increased septic levels have displayed pro-inflammatory effects (Banks et al., 2015; Jaeger et al., 2009).

This may be due to the increased burden of pro-inflammatory metabolic conditions within ageing, as a consequence of age-related conditions including obesity, diabetes, and hypertension. Diabetes is increasing within the ageing population with both type I and type II and causes increases in pro-inflammatory IL-6 and the increase in NOD-, LRR- and pyrin domain-containing protein 3 (NLRP3) inflammasome within human and mouse models (Lee et al., 2013; Lukic et al., 2014; Yan et al., 2023; Yang et al., 2024). Hypertension, which affects up to 70% of the population over 65, has been shown *in vivo* to increase TNF-α and IL-6 levels as well as cause inflammation within the brain (Bautista et al., 2005; S. Li et al., 2006) as well as in human studies where it also stimulates NADPH oxidase to increase reactive oxygen species (ROS) production (Heitzer et al., 2001). Obesity is prevalent within 33% of female population over 60 years (Malenfant & Batsis, 2019) and causes an increase in pro-inflammatory adipokines within humans (Guarner & Rubio-Ruiz, 2014) and *in vivo* models (Bae et al., 2023;

Rohm et al., 2022). Furthermore, obesity has been linked to decreasing hippocampal plasticity and the activation of microglia leading to decreases in cognitive ability (Duffy et al., 2019; Hao et al., 2016).

The systemic inflammatory effects of the co-morbidities listed above could be investigated within ageing in separate or combination animal models (Guo et al., 2019; Oike et al., 2020). However, this involves long-term studies to confirm phenotypes of models and require an increased number of animals to sufficiently compare co-morbidity effects. This would also not specifically investigate the role of systemic inflammation on the ageing brain. Therefore, using an *in vivo* model specifically inducing the inflammatory response will provide a more focused study design. There are multiple methods to induce systemic inflammation within *in vivo* models including cytokine induction, polyinosinic: polycytidylic acid (poly I:C) caecal ligation and puncture (CLP), peritoneal contamination and infection (PCI), knockdown studies and LPS (Rafiyan et al., 2023). All models have been shown to act upon the CNS in a neuroinflammatory context and so could potentially be used to assess the effect of inflammation on the BBB. However, some models are more advantageous than others regarding ease of use, reproducibility, and suitability for systemic inflammation (table 4-1).

4.1.1. **LPS as a model of neuroinflammation**

LPS, known clinically as endotoxin, is a glycolipid component of gram-negative bacteria which has been shown *in vivo* to produce a neuroinflammatory response (Skrzypczak-Wiercioch & Sałat, 2022). The molecule acts upon the CNS via activation or toll-like receptor-4 (TLR4) which dimerises to activate myeloid differentiation factor 88 (MyD88) and TIR domain-containing adaptor inducing interferon-β (TRIF) (Hines et al., 2013). Activation of these binding molecules then causes activation of the MAPK pathway and consequently the NF-kB pathway (Liu et al., 2017; Skrzypczak-Wiercioch & Sałat, 2022) (fig. 4-1).

Table 4-1: Types of *in vivo* models of neuroinflammation. Known inflammatory effects, advantages of the model and concerns are stated.

Model	Effects	Benefits	Concerns	References
LPS	• ↑ BBB disruption • ↑Glial activation • ↑Cytokine levels • TLR4 acting	• Ease of use • Quick response • Low variability • Affects the BBB	• Dosage variances dilute LPS effect • Inflammatory changes disappear quickly • Not translatable to humans	(Lewis et al., 2016; Seemann et al., 2017; Skrzypczak-Wiercioch & Sałat, 2022)
Cytokine induction	• ↑ levels of introduced cytokine	• Confidence that results will be related to cytokine increases	• Not reflective of complex pathways of systemic inflammation	(Biesmans et al., 2015)
Poly I:C	• ↑ cytokine levels • ↑BBB permeability • Activate TLR3 acting	• Ease of administration • Affects the BBB	• Not as characterised as LPS	(Bao et al., 2022 ; Field et al., 2010 ; He et al., 2021)
PCI	• ↑microglia activation •	• Translatable to human studies • Quick response	• Characterisation of each sample needed • Increased study time	(Chung et al., 2023 ; Seemann et al., 2017 ; mei Wu et al., 2023)
CLP	• ↑ cytokines • ↑ myeloid infiltration	• Good model of human sepsis • Increased study duration	• More acute than chronic inflammation model • Intensive surgery required • Limited microglia activation • Variation between study designs • ↑ mortality rate in aged mice	(Deng et al., 2017 ; Hyde et al., 1990 ; Lewis et al., 2016 ; Seemann et al., 2017; Singer et al., 2016)

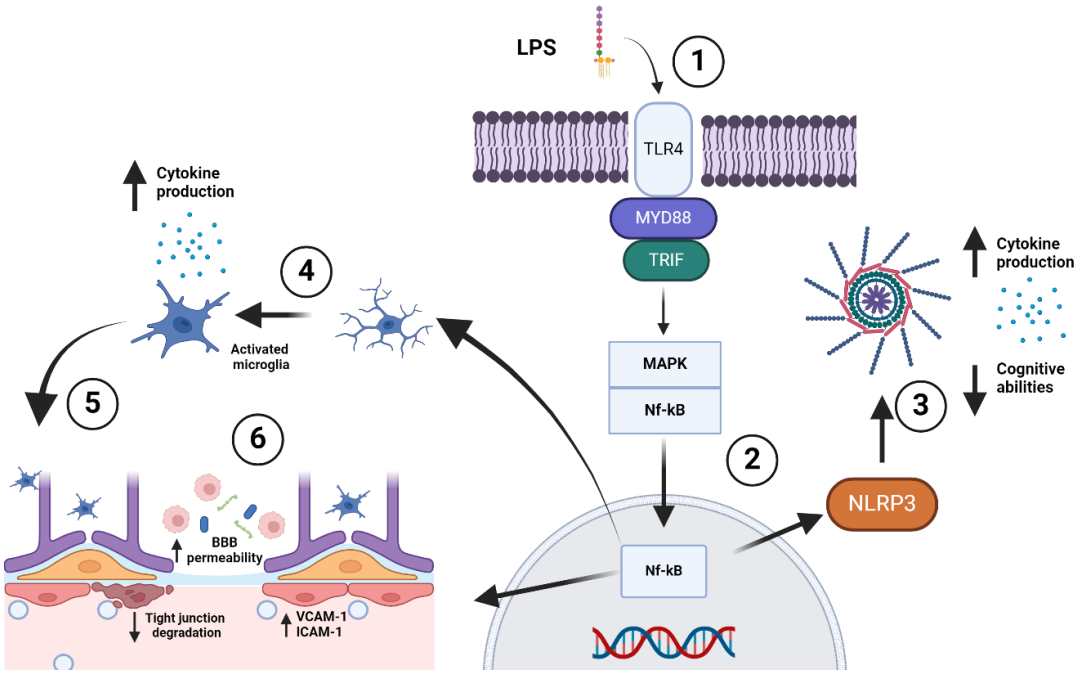

Figure 4-1: Mechanism of neurovascular response to LPS and downstream inflammatory effects. (1) LPS binds to toll-like receptor 4((TLR4) activating binding molecules myeloid differentiation factor 88 (MyD88) and TIR domain-containing adaptor inducing interferon-β (TRIF) to activate the Nuclear factor-κB pathway (2). (3) NF-Kb activates signalling pathway NLR family pyrin domain containing 3 (NLRP3) to activate the inflammasome and increase cytokine production and cognitive decline. LPS causes microglia to become activate (4) and migrate to the BBB (5). Tight junction degradation and increases in adhesion molecules ICAM-1 and VCAM-1 causes BBB permeability to blood-borne molecules. Adapted from Skrzypczak-Wiercioch & Salat, 2022 and Zhang et al, 2017 using biorender.com.

The activation of NF-kB has multiple downstream effects including the activation of the inflammasome via NLRP3 signalling leading to an increase in pro-inflammatory cytokine release and increase cognitive decline (Chen et al., 2023; Zhu et al., 2017). LPS further acts to increase neuroinflammation by activating microglia and astrocytes, leading increases in markers Iba-1 and GFAP and migration to the BBB (Haruwaka et al., 2019; Li et al., 2024; Vutukuri et al., 2018). Tight junction protein and SIRT1 expression have also been shown to decrease during LPS-induced inflammation, leading to BBB permeability to blood-borne albumin (Cheng et al., 2018; Li et al., 2024; Veszelka et al., 2007). Studies have demonstrated permeability to dextran as well as albumin after LPS mediated inflammatory response (Banks et al., 2015; Wang et al., 2017). Further changes to the BBB include expression of adhesion molecules ICAM-1 and VCAM-1, causing leukocyte infiltration into the brain parenchyma (Brezzo et al., 2020; Wong & Dorovini-Zis, 1992; Xiang et al., 2021). Iron accumulation is also

observed within the brain response to LPS, observed in the cortex and hippocampus (Li et al., 2024; Sumbria et al., 2018). This has been linked to two mechanisms of LPS induction of NF-kB; the expression of ROS and inhibition of SIRT1 (Xu et al., 2024).

4.1.2. **Nanoparticles in LPS models**

As inflammation is a hallmark of physiological ageing, it may be an appropriate target for nanoparticle therapeutics. Within LPS *in vitro* human cell line models, silver, selenium and polystyrene nanoparticles have been shown to reduce NF-kB pathway activation allowing for reduction in inflammation, with high concentrations of silver modulating the signalling of TLR4 and silymarin containing selenium particles inhibiting the nuclear translocation of NF-kB (Gliga et al., 2020; Mi et al., 2022). Complementary *in vivo* studies have demonstrated reductions in oxidative stress in both the zebrafish and mouse brains when injected with gold or liposome nanoparticles at supraphysiological levels of LPS (Hussein et al., 2024; Ralvenius et al., 2024). There are limited studies within the literature looking directly at the effect of LPS on nanoparticle administration within an ageing *in vivo* model. Barton et al., 2019, demonstrated within an ageing 5XFAD AD pathology model that superparamagnetic iron oxide (SPIO's) only cross into the BBB during both ageing and LPS conditions. Overall, there is a literature gap exploring the effect of LPS-induced systemic inflammation of aged mouse permeability to nanoparticles which requires further investigation.

4.2. Aims and objectives

This chapter aims to assess the impact of systemic inflammation on the aged BBB via a single-dose injection of LPS. The LPS model will aim to investigate the effect of LPS on ageing and also the effect of different LPS dosages with a low-grade inflammatory model (0.25 mg/kg) and high-grade (1 mg/kg) in the aged mice. The effect of LPS on BBB disruption will be assessed via iron accumulation and serum protein extraversion. The impact of systemic inflammation on BBB associated cells within ageing will be investigated via expression changes of microglia (Iba-1), astrocytes (GFAP), adhesion molecules (ICAM-1) and transport mechanism (Caveolin-1). Further analysis of brain tissue and peripheral serum samples will assess changes to cytokine

and adhesion molecule expression via ELISA and mass spectrometry to elucidate responses to LPS. Finally, the study will assess the infiltration of DiI-liposomes to see if infiltration into the brain is altered from physiological ageing.

4.2.1 Hypotheses

1. To assess if inflammation increases BBB permeability to DiI-liposomes, cerebral micro bleeding and circulating serum proteins in the context of ageing
2. To investigate if LPS-induced inflammation has a greater impact on microglial, astrocytic and adhesion molecule expression during ageing
3. To elucidate inflammatory profile of the brain microenvironment during LPS-induced aged mice

4.3. Methodology

4.3.1. Study design

Female C57BL/6 mice were purchased at either 3- or 18-months and were initially grouped into 5 categories based upon age and treatment with LPS (*E. Coli* O111:B4, Sigma-Aldrich, UK) as the following: 3-month vehicle control, 3-month 1 mg/kg LPS, 18-month vehicle control, 18-month 0.25 mg/kg and 18-month 1 mg/kg. All mice were observed for clinical indications based upon guidelines for aged animal use ((Wilkinson et al., 2020). Mice were randomly allocated within age groups into cages of n=4-5 and bodyweights monitored twice weekly prior to onset of study. Each mouse was injected intraperitoneally once with either the desired LPS dose or PBS as the vehicle control and monitored twice daily post-injection for 48 hours (2.7). 3-hours post-LPS injection, a single tail vein blood sample was recovered. Under anaesthesia, mice were injected with DiI-lip and 2-hours post-injection culled via cardiac perfusion with a terminal blood sample extracted. Brains and peripheral organs were weighed and optically imaged using IVIS before being either flash frozen in liquid nitrogen or submerged in 4% PFA for 48-hours before further processing. Final n-numbers are reported in (Figure 4-2), 2 18-month 1 mg/kg LPS mice had to be terminated early from the study due to pre-agreed humane

A

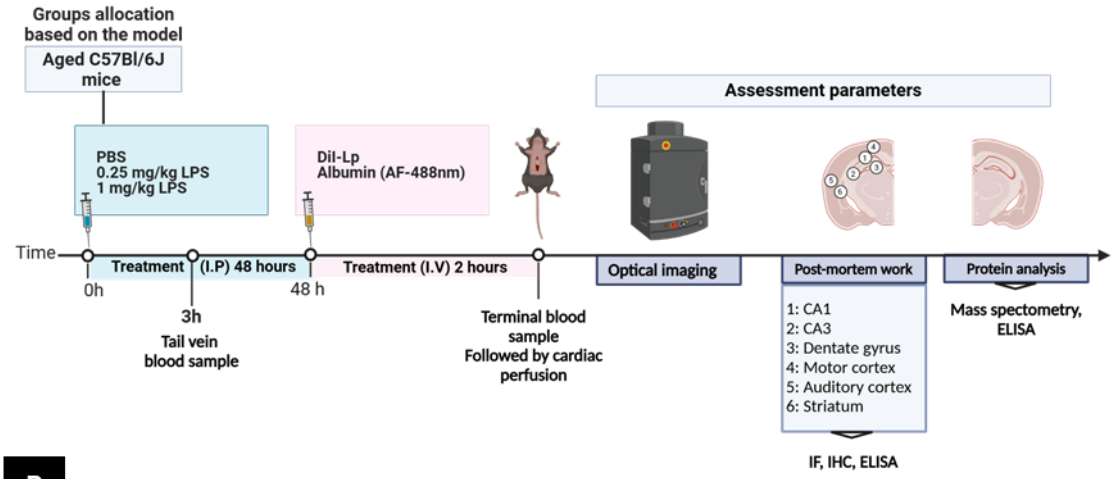

B

Age (months)	LPS dose (mg/kg)	DiI-lip	IF	IHC	ELISA	MS
3	0	4	4	4	4	4
	1	4	4	4	4	4
18	0	4	4	4	4	4
	0.25	4	4	4	4	4
	1	3	3	3	3	3

Figure 4-2: Schematic representation of LPS ageing mice study and study n-numbers. (A) 3-month and 18-month female mice were injected intraperitonially with either 0.25 mg/kg LPS, 1 mg/kg LPS or 0 mg/kg LPS vehicle control. 3-hours post-injection blood was extracted from the tail vein before being injected intravenously with DiI-lip 48-hours post LPS injection. 2-hours post DiI-lip administration, mice were culled via cardiac perfusion and terminal blood sample acquired. Optical imaging of brain and peripheral organs occurred immediately post-perfusion before brains treated for histological analysis. Diagrammatic representation of 6 regions of interest for post-mortem work and downstream analysis. (B) Tabular representation of all mouse groups within the study specifying the sex and age of each cohort and the predicted n-number per assessment parameter.

endpoints being reached. Another mouse from the 3-month vehicle group had to be removed from the study due to technical problems during the cardiac perfusion protocol. Final group numbers are as follows; n=3: 3-month vehicle, 18-month 1 mg/kg LPS, n=4: 3-month 1 mg/kg LPS, 18-month vehicle and 18-month 0.25 mg/kg LPS.

4.3.2. Liposome characterisation

DiI-lip were made via conjugation of DiI 555 nm with HSPC: Chol: DSPE-PEG2000 (56.3: 38.2: 5.5 mol/mol%) via thin-film hydration in a single batch for all mouse groups (2.5). The suitability of the liposomes was assessed via dynamic light scattering determining size (nm), PDI, zeta potential (mV) and fluorescence spectroscopy for DiI intensity (2.6).

4.3.3. Optical imaging

The brain and peripheral organs (heart, lungs, spleen, kidneys, and liver) were extracted from the mouse and optically imaged on IVIS for DiI-lip infiltration and values were normalised for organ weight across the cohort (2.8).

4.3.4. Immunohistochemical staining

To investigate the extravasation of serum proteins into the brain parenchyma, IgG was used immunohistochemically on brain cryosections (2.12). Negative control images (without primary antibody) are found in appendix 3. Any tissue loss is recorded in appendix 4.

4.3.5. Histological staining

To see if there was an increase in cerebral micro bleeding within an LPS-induced model of inflammation, Prussian blue iron staining was implemented (2.12). Any tissue loss is recorded in appendix 4.

4.3.6. Immunofluorescence

To assess DiI-lip infiltration, cryosections were submerged in PBS for 20 minutes before coverslipping with no further immunostaining. Immunofluorescence was utilised to investigate changes in expression of proteins involved in caveolae-mediated transcytosis (Caveolin-1), astrocyte activation (GFAP), microglial activation (Iba-1) and adhesion molecule (ICAM-1). For investigating the interaction of each cellular marker with the BBB, CD31 was used as an endothelial cell marker (2.11). Negative control images (without primary antibody) are found in appendix 3. Any tissue loss is recorded in appendix 4.

4.3.7. ELISA tests

To investigate the effect of LPS and ageing on pro-inflammatory cytokines and adhesion molecules, mouse serum or brain homogenate was prepared (2.9, 2.13). ELISA tests were carried out in both serum and homogenate for IL-6 and just homogenate in IL-1β to assess cytokine expression. Adhesion molecules were assessed via ELISA for ICAM-1 and VCAM-1 in both serum and brain homogenate samples (2.16).

4.3.8. Mass Spectrometry

To identify widespread protein expression changes, mass spectrometry of 50 µg brain homogenate was run through SciexZenoTOF 7600 mass spectrometer (2.14).

4.3.9. Protein expression analysis

After mass spectrometry was completed, datasets were analysed via Optiflow source and processed using DI-ANN software. Significant logP fold changes were identified via the AMICA 3.0.1 software (2.14).

5.3.9.1. Ingenuity pathway analysis

To identify functional pathways changed by ageing or systemic inflammation, ingenuity pathway analysis was performed on Log2 fold changes values of mass spectrometry dataset (2.14).

4.3.10. Statistical analysis

All statistical analysis and graphical representation were conducted on GraphPad Prism. For assessment of age and LPS effects on cellular markers and bodyweight changes after I.P LPS injection, a 2-way ANOVA followed by Dunn's multiple comparison test were employed. To investigate the effects of LPS dose on 18-month mice, either one-way analysis of variance followed by Tukey's multiple comparison test or Kruskal-Wallis test was followed by Dunn's multiple comparison test based upon Shapiro-Wilkes normality test. Graphical representations signified mean ± standard error of mean (SEM) and all significant results were graphically annotated using the following ranking: * $p<0.05$, ** $p<0.01$, *** $p<0.001$.

4.4. Results

4.4.1. Induction of inflammatory phenotype

One of the major characteristics of LPS induced systemic inflammation is the decrease in bodyweight (Piirsalu et al., 2020). Mice were weighed 48-hours post-injection and display bodyweight decreases in young and aged LPS treated mice between 10-19% whilst vehicle mice did not decrease in bodyweight (fig. 4-3a). Significant decreases in bodyweight were found between vehicle and 1 mg/kg LPS mice in young ($F=54.73_{(4,14)}$, $p=<0.0001$) and aged ($F=54.73_{(4,14)}$, $p=<0.0001$). Within the aged group, significant decreases in bodyweight were also observed in the 0.25 mg/kg LPS group compared to vehicle ($F=54.73_{(4,14)}$,$p=<0.0001$) and between 0.25 mg/kg and 1 mg/kg groups ($F=54.73_{(4,14)}$, $p=0.0213$). This demonstrates that not only LPS injection, but dosage levels are key for induction of the inflammatory phenotype.

Terminal weights of organs were compared to evaluate LPS-induced changes (fig. 4-3b). No significant changes were observed in the heart, lung, spleen, kidney or brain in either age of LPS dosage. Comparison of liver weight showed significant increases in weight from 3-month vehicle mice to and 18-month vehicle (age $F=382.9_{(5, 84)}$, LPS $F(=10.85_{(5, 84)}$, $p= 0.0431$) and 18-month 0.25 mg/kg (age $F=382.9_{(5, 84)}$, LPS $F=10.85_{(5, 84)}$, $p= 0.002$) but not 1 mg/kg dose of either age group.

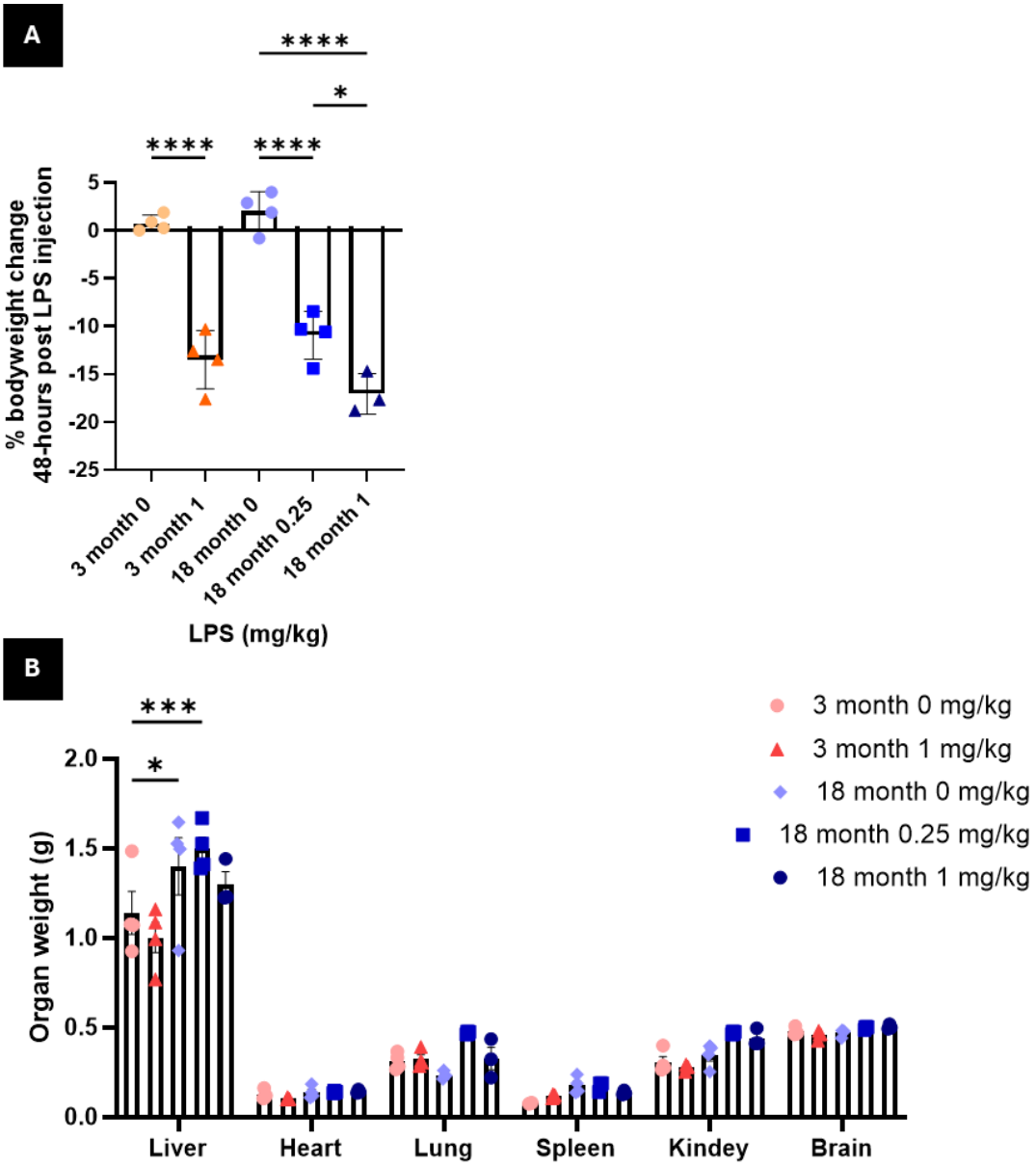

Figure 4-3: Effect of lipopolysaccharide (LPS) dose on young and aged mice. C57BL/6 female mice groups were injected with intraperitonially a single dose of lipopolysaccharide. 3-month mice received either 1 mg/kg or PBS vehicle control whilst 18-month mice were given, 1 mg/kg, 0.25 mg/kg or PBS vehicle control. (A) Changes to mouse bodyweight 48-hours post LPS injection demonstrating significant bodyweight losses in all LPS dosed groups compared to age-matched vehicle. (B) Weight of organs at 48-hours post LPS injection showing no significant changes in weight of the heart, lung, spleen or kidney. Significant liver weight increases were observed when comparing the 3-month vehicle to 18-month 0.25 mg/kg group. Statistical analysis was completed using GraphPad Prism software. For bodyweight analysis, one-way analysis of variance followed by Tukey multiple comparison test was utilised. For analysis of organ weight, two-way analysis of variance followed by Tukey's multiple comparison test evaluated changes in each organ. N=3-4,average ± SEM, $p<0.05$ were considered significant.

4.4.2. Infiltration of DiI-liposomes

Optical imaging of nanoparticle infiltration into brain and peripheral organs DiI-lip characteristics were evaluated via dynamic light scattering and showed appropriate size (110.6 nm) and charge (-11.6 mV) (fig.4-4a, c). Fluorescence spectroscopy also demonstrated expected fluorescence signal intensity at 549 nm for DiI conjugation to liposomes (fig.4-4b). Biodistribution of liposomes is important to evaluate potential off-target accumulation of the nanoparticles during a therapy intervention. Evaluation of infiltration of DiI-lip into the brain showed a significant increase between the 3-month vehicle and LPS groups (age $F=0.4617_{(1,10)}$, LPS $F=13.69_{(1,10)}$, $p= 0.0333$) but no significant infiltration changes between the 3 and 18-month groups (fig.4-5b). No significant changes were observed in the 18-month groups comparing vehicle to 1 or 0.25 mg/kg LPS (fig4-5b-e). Within the peripheral organs, no significant changes were observed in the heart, lungs or spleen throughout ageing or LPS injection (fig. 4-5e). Significant increase in infiltration of DiI-lip in the liver were observed in the 18-month 0.25 mg/kg group compared to 3-month vehicle ($F=8.684_{(4,14)}$, $p= 0.0047$), 3-month 1 mg/kg ($F=8.684_{(4,14)}$, $p= 0.0079$), 18-month vehicle ($F=8.684_{(4,14)}$, $p= 0.0047$) and 18-month 1 mg/kg ($F=8.684_{(4,14)}$, $p= 0.0012$). Similar infiltration patterns were observed in the kidneys, with increased DiI-lip within the 0.25 mg/kg 18-month groups compared to 3-month vehicle ($F=6.504_{(4,14)}$, $p= 0.0081$) and 18-month vehicle ($F=6.504_{(4,14)}$, $p= 0.0081$) but no other LPS injected groups. Results show that distribution changes are localised to the brain, liver and kidneys.

4.4.3. Region-specific infiltration of nanoparticles into the brain

To elucidate changes in specific brain regions and determine spatial homogeneity, DiI-lip infiltration was quantified in hippocampal (fig. 4-6) cortical and striatal regions (fig. 4-7). Within the hippocampus, no significant changes in DiI-lip infiltration were present in the CA1 or CA3 regions comparing age and 1 mg/kg LPS or doses of LPS in the 18-month age group (fig. 4-6b-e). Within the dentate gyrus, a significant increase of DiI-lip infiltration only occurred between the 3-month vehicle and 1 mg/kg LPS group (age F=5.369(1,10), LPS F=7.842(1,10), p= 0.0298),

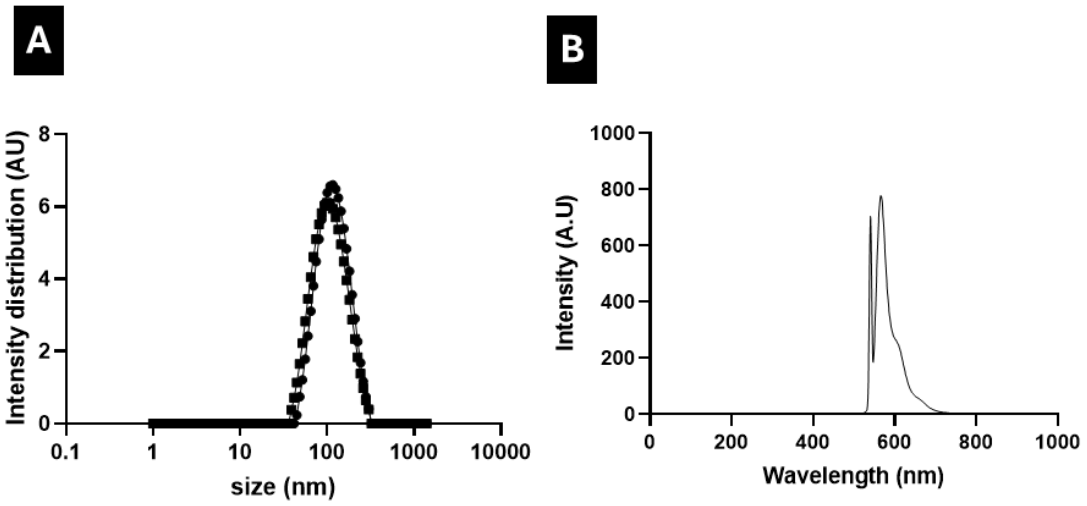

C

Lipid composition (12.5 mM)	Size ± SD (nm)	PDI ± SD	Zeta potential ± SD (mV)
HSPC:Chol:DSPE-PEG2000+DiI (56.3:38.2:5.5 mol/mol%)	110.6 ± 0.985	0.116 ± 0.014	-11.6 ± 0.529

Figure 4-4: Liposome characterisation for LPS cohort. Liposomes were made with identical formulations using thin film hydration followed by extrusion. Size (in nm), zeta potential (ZP) and poly-dispersal index (PDI) were all completed in triplicate via dynamic light scattering. Fluorescence intensity was calculated using spectrophotometry set at 540nm (A) Graphical representation of LPS cohort liposome size. (B) Fluorescence intensity of average liposome batches in LPS cohort. (E) Lipid compositions, size, Average PDI and ZP values for each liposomal cohort batch. All graphs created using GraphPad Prism

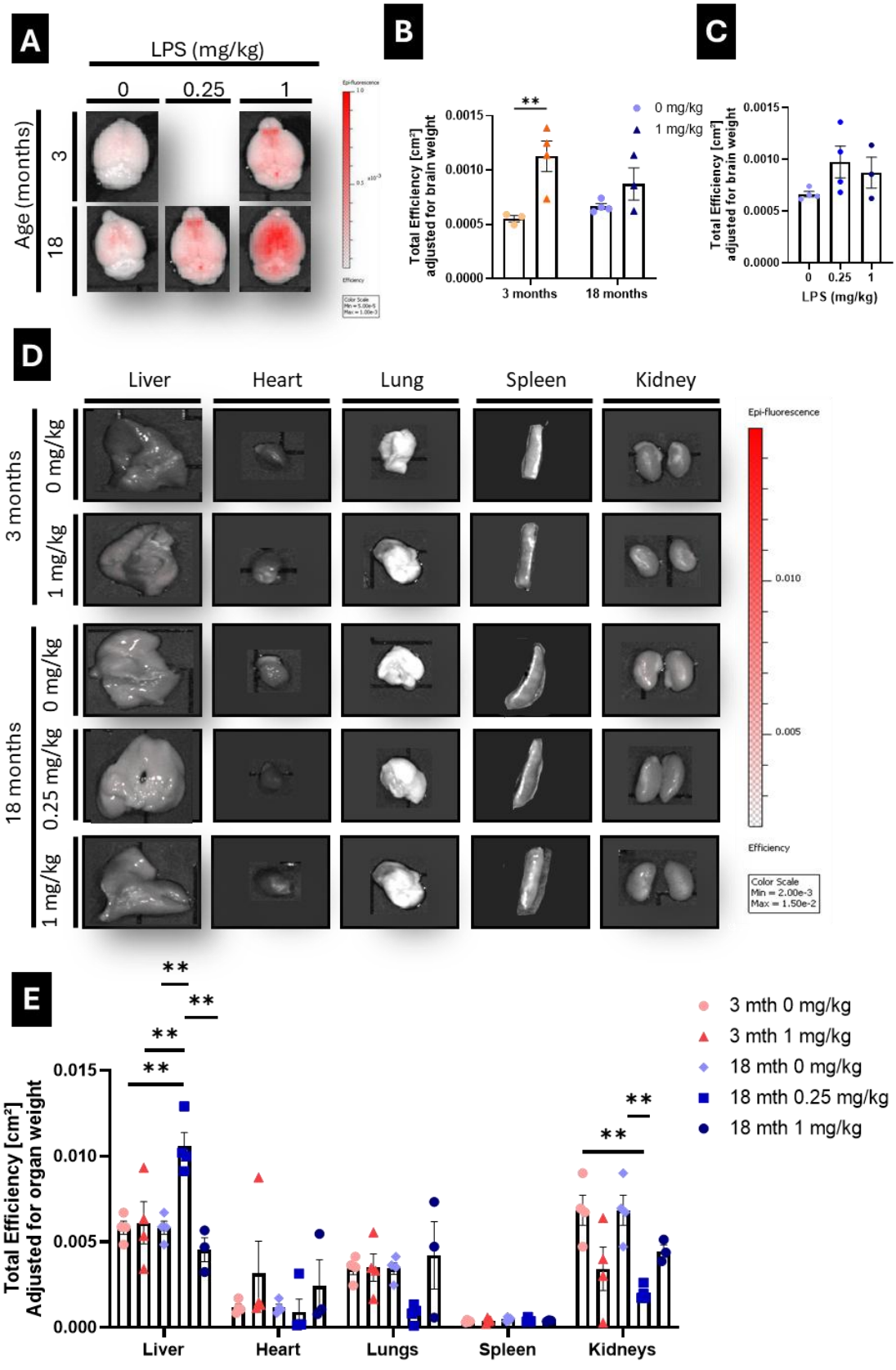

Figure 4-5: Optical imaging of global organ infiltration of DiI-liposome in LPS cohort. C57BL/6 female mice groups were injected intraperitonially with a single dose of lipopolysaccharide. 3-month mice received either 1 mg/kg or PBS vehicle control whilst 18-month mice were given, 1 mg/kg, 0.25 mg/kg or PBS vehicle control. 48-hours post injection, all mice were intravenously injected with DiI-lip and cardiac perfusion was completed 2 hours post-injection to remove circulating DiI-lip. (A) Representative optical images of mouse brains indicating infiltration of DiI-liposomes. (B)

Quantitative analysis of brain infiltration comparing aged and young demonstrated significant increases in DiI-lip between the 3-month vehicle and LPS groups. (C) Quantitative analysis of LPS doses in 18-month mice demonstrated no significant changes. (D) Representative optical images of peripheral organs in 3- and 18-month mice. (E) Quantitative analysis of all organs DiI-lip infiltration with the 0.25 mg/kg 18-month liver possessing significant increased infiltration to all other groups. In the kidneys, the 0.25 mg/kg 18-month group was significantly decreased to other groups. All other comparisons were not significantly changed. Images obtained using in vivo imaging system (IVIS) and analysed using living systems software. Statistical analysis was completed using GraphPad Prism software. For brain analysis, using one-way analysis of variance followed by Tukey multiple comparison test or Kruskal-Wallis test followed by Dunn's multiple comparisons test based on Shaprio-Wilk test for normality. For peripheral organ analysis, one-way analysis of variance followed by Tukey's multiple comparison test evaluated changes in each organ. N=3-4, average ± SEM, $p<0.05$ were considered significant.

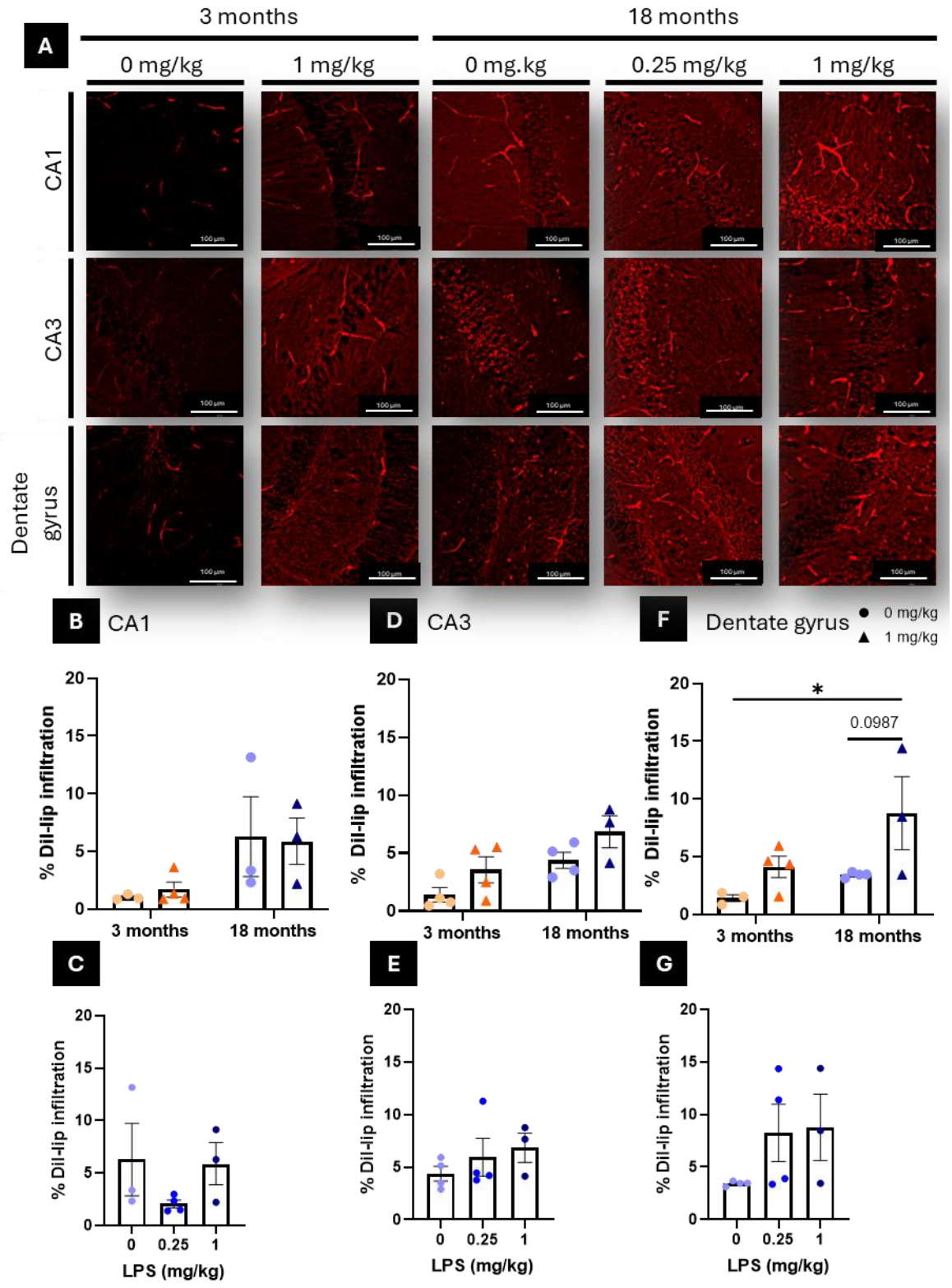

Figure 4-6: Dil-liposomes infiltration in inflammation and ageing hippocampal regions. C57BL/6 female mice groups were injected intraperitonially with a single dose of lipopolysaccharide. 3-month mice received either 1 mg/kg or PBS vehicle control whilst 18-month mice were given, 1 mg/kg, 0.25 mg/kg or PBS vehicle control. 48-hours post injection, all mice were intravenously injected with Dil-lip and cardiac perfusion was completed 2 hours post-injection to remove circulating Dil-lip. (A) Representative immunofluorescence images of CA1, CA3 and dentate gyrus hippocampal regions -1.94mm from bregma indicating infiltration of Dil-liposomes (Red). Quantitative analysis of young and aged infiltration in the CA1 (B), CA3 (D) and dentate gyrus (F) regions. Quantitative analysis of LPS dose in 18-month mice in CA1 (C), CA3 (E) and dentate gyrus (G) regions. All regions did not indicate significant changes in infiltration across ageing except for the dentate gyrus between 3-month vehicle

and 18-month 1 mg/kg where a significant increase of infiltration was observed. Images obtained at x40 magnification on Leica Thunder microscope and underwent large volume computational clearing (LVCC) prior to quantification in Image J. Statistical analysis was completed using GraphPad Prism software using one-way analysis of variance followed by Tukey multiple comparison test or Kruskal-Wallis test followed by Dunn's multiple comparisons test based on Shapiro-Wilk test for normality for comparison of 18-month dosages. For comparison of ageing, a two-way analysis of variance followed by Tukey's multiple comparison test was implemented. N=4/5,average ± SEM, $p<0.05$ were considered significant. Scale bar represents 100µm.

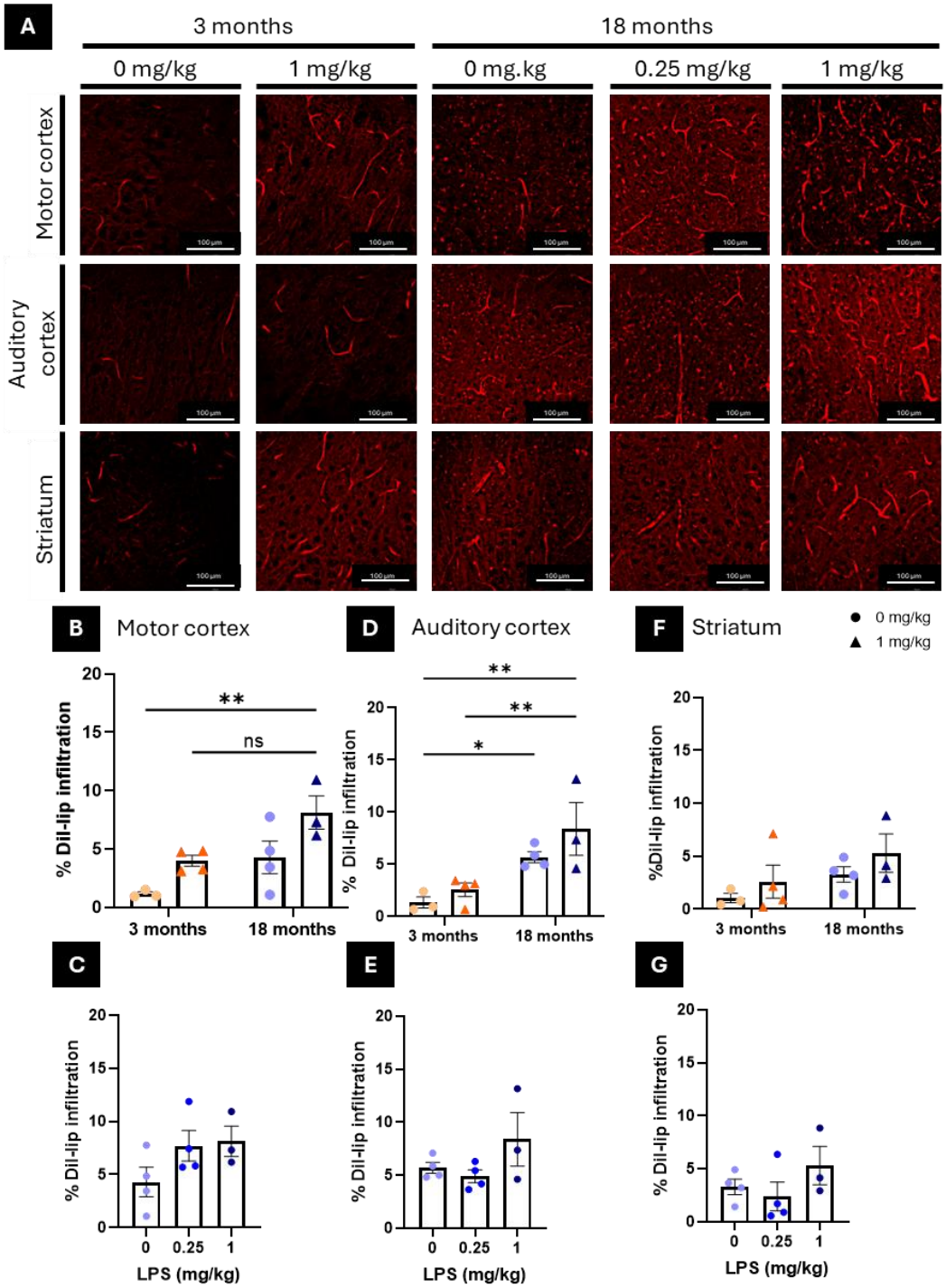

Figure 4-7: DiI-liposomes infiltration in inflammation and ageing cortical and striatal regions. C57BL/6 female mice groups were injected intraperitonially with a single dose of lipopolysaccharide. 3-month mice received either 1 mg/kg or PBS vehicle control whilst 18-month mice were given, 1 mg/kg, 0.25 mg/kg or PBS vehicle control. 48-hours post injection, all mice were intravenously injected with DiI-lip and cardiac perfusion was completed 2 hours post-injection to remove circulating DiI-lip. (A) Representative immunofluorescence images of motor cortex, auditory cortex and striatum regions -1.94mm from bregma indicating infiltration of DiI-liposomes (Red). Quantitative analysis of young and aged infiltration in the motor cortex (B), auditory cortex (D) and striatum (F) regions. Quantitative analysis of LPS dose in 18-month mice in motor cortex (C), auditory cortex (E) and striatum (G) regions. The motor cortex and auditory cortex displayed significant increases between 3-month vehicle and 18-month 1 mg/kg LPS. Auditory cortex also showed significant increase from the 3-month vehicle to the 18-month vehicle and the 3-month 1 mg/kg to 18-month 1 mg/kg LPS. All other analysis did not indicate significant changes in infiltration across ageing or LPS dose. Images obtained at x40 magnification on Leica Thunder microscope and

underwent large volume computational clearing (LVCC) prior to quantification in Image J. Statistical analysis was completed using GraphPad Prism software using one-way analysis of variance followed by Tukey multiple comparison test or Kruskal-Wallis test followed by Dunn's multiple comparisons test based on Shapiro-Wilk test for normality for comparison of 18-month dosages. For comparison of ageing, a two-way analysis of variance followed by Tukey's multiple comparison test was implemented. N=4/5,average ± SEM, $p<0.05$ were considered significant. Scale bar represents 100µm.

indicating that a combination of both age and LPS only increased DiI-lip infiltration (fig. 4-6f-g). Within the motor cortex, significant increases in infiltration occurred between the 3-month vehicle and 18-month 1 mg/kg LPS (age $F=11.77_{(1,10)}$, LPS $F=9.989_{(1,10)}$, $p=0.0065$), but no changes were observed between LPS dose in 18-month mice (fig 4-7b-c). The auditory cortex displayed similar significant increases between 3-month vehicle and 18-month 1 mg/kg LPS (age $F=18.33_{(1,10)}$, LPS $F=2.740_{(1,10)}$, $p= 0.0028$) along with increases between 1 mg/kg between age groups($p=0.0060$ (fig 4-7d). Qualitatively, DiI-lip infiltration in all regions was confined to endothelial cells resembling morphology but within the aged vehicle cohort, this appeared to become more punctate within the parenchyma which progressed further into the 1 mg/kg groups (figure 4-6, 4-7).

4.4.4. No changes to iron accumulation or IgG extravasation

To monitor increased BBB disruption within the aged systemic inflammation cohort, IgG accumulation was assessed. Within the hippocampal regions (CA1, CA3 and dentate gyrus), motor cortex and striatum there were no significant changes in the comparisons of young and aged groups with 1 mg/kg LPS or within the 18-month group of vehicle, 0.25 mg/kg and 1 mg/kg LPS (fig. 4-8b-k, j, m). Within the auditory cortex, significant IgG accumulation was found in the 18-month vehicle compared to the 3-month vehicle (age $F=9.414_{(1,9)}$, LPS $F=14.20_{(1,9)}$, $p= 0.0052$) or 3-month LPS (age $F=9.414_{(1,9)}$, LPS $F=14.20_{(1,9)}$, $p= 0.0188$) whilst no changes were seen in the comparison of LPS dose in 18-month mice (fig. 4-8l).

To complement IgG extravasation, iron accumulation was assessed to determine if increased cerebral micro bleeding occurred within inflammation. No significant increase in iron accumulation was observed in any region quantified in relation to age effect, LPS effect or LPS dosage effect fig.4-9b-m). Within the CA3 region, there was a non-significant trend towards increased iron between the 3-month vehicle and LPS groups (age $F=0.730_{(1,11)}$, LPS $F=6.117_{(1,11)}$, $p= 0.0828$) (fig.4-9c). Overall, no significant changes to BBB disruption were seen within this study.

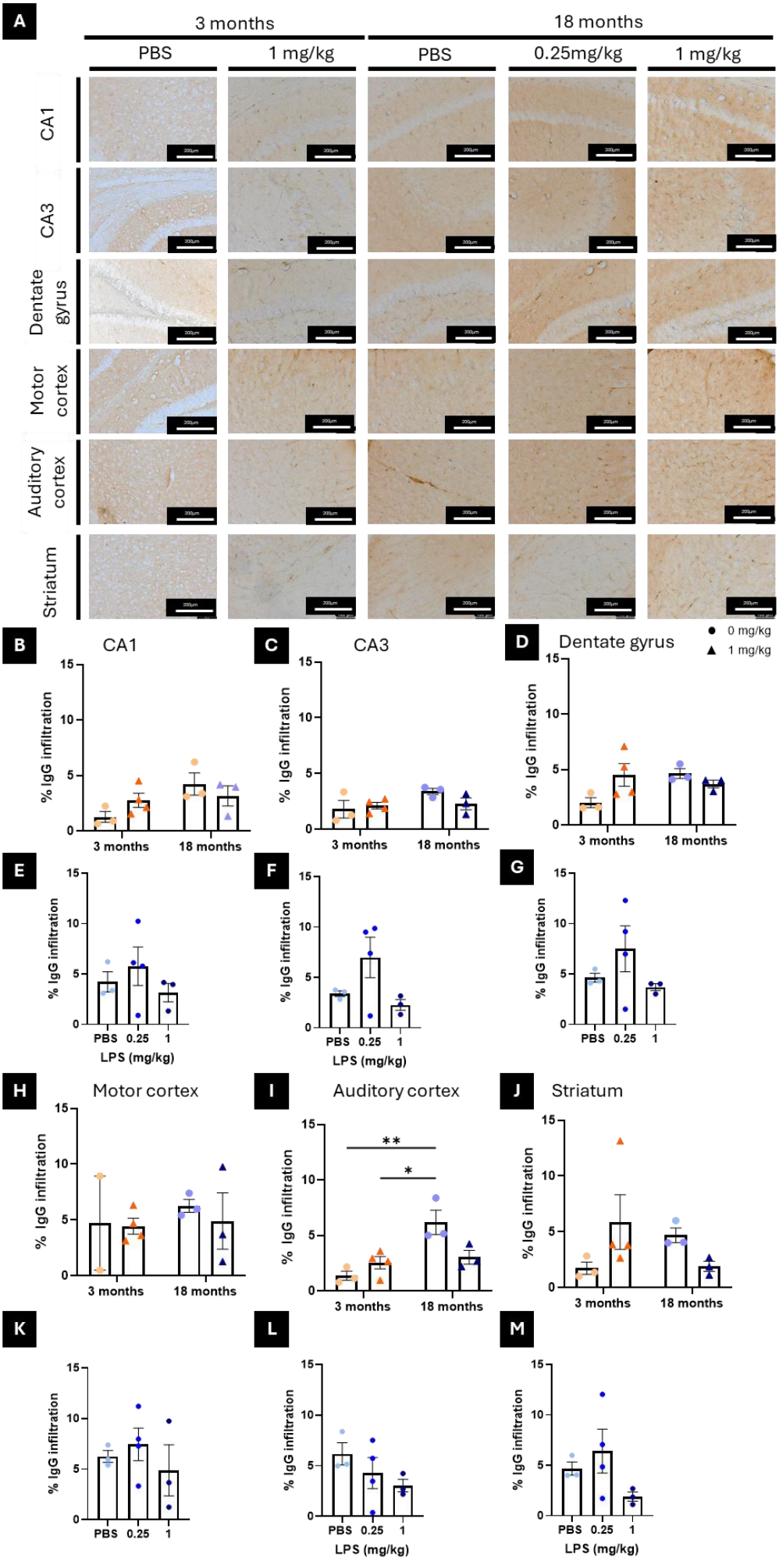
A
3 months
18 months
PBS
1 mg/kg
PBS
0.25mg/kg
1 mg/kg
CA1
CA3
Dentate gyrus
Motor cortex
Auditory cortex
Striatum
B
CA1
C
CA3
D
Dentate gyrus
0 mg/kg
1 mg/kg
% IgG infiltration
3 months
18 months
E
F
G
PBS
0.25
1
LPS (mg/kg)
H
Motor cortex
I
Auditory cortex
J
Striatum
**
*
K
L
M

Figure 4-8: Infiltration of IgG into LPS cohort mouse brain. C57BL/6 female mice groups were injected intraperitonially with a single dose of lipopolysaccharide. 3-month mice received either 1 mg/kg or PBS vehicle control whilst 18-month mice were given, 1 mg/kg, 0.25 mg/kg or PBS vehicle control. 48-hours post injection, all mice were intravenously injected with DiI-lip and cardiac perfusion was completed 2 hours post-injection to remove circulating DiI-lip. (A) Representative immunofluorescence images of Motor and Auditory cortex, striatum, CA1, CA3 and dentate gyrus regions indicating infiltration of Immunoglobulin G (Brown). Quantitative analysis comparing 3- and 18-month mice with either LPS or vehicle treatment in (B) CA1, (C) CA3, (D) Dentate gyrus, (H) Motor cortex, (I) Auditory cortex and (J) striatum demonstrated no significant changes except for the auditory cortex whereby 18-month vehicle was significantly increased to both 3-month conditions. Quantitative analysis of IgG infiltration in 18-month LPS doses demonstrated no significant changes in (E) CA1, (F) CA3, (G) dentate gyrus, (K) motor cortex, (L) auditory cortex and (M) striatum. Images obtained at x20 magnification on Leica Thunder microscope prior to quantification in Image J. Statistical analysis was completed using GraphPad Prism software. For analysis of comparison of 0 and 1 mg/kg LPS dose in ageing, two-way analysis of variance was utilised followed by Tukey multiple comparison test. For 18-month LPS dose studies, one-way analysis of variance followed by Tukey's multiple comparison test after conducting Shapiro-Wilks normality test. N=3-4,average ± SEM, $p<0.05$ were considered significant.

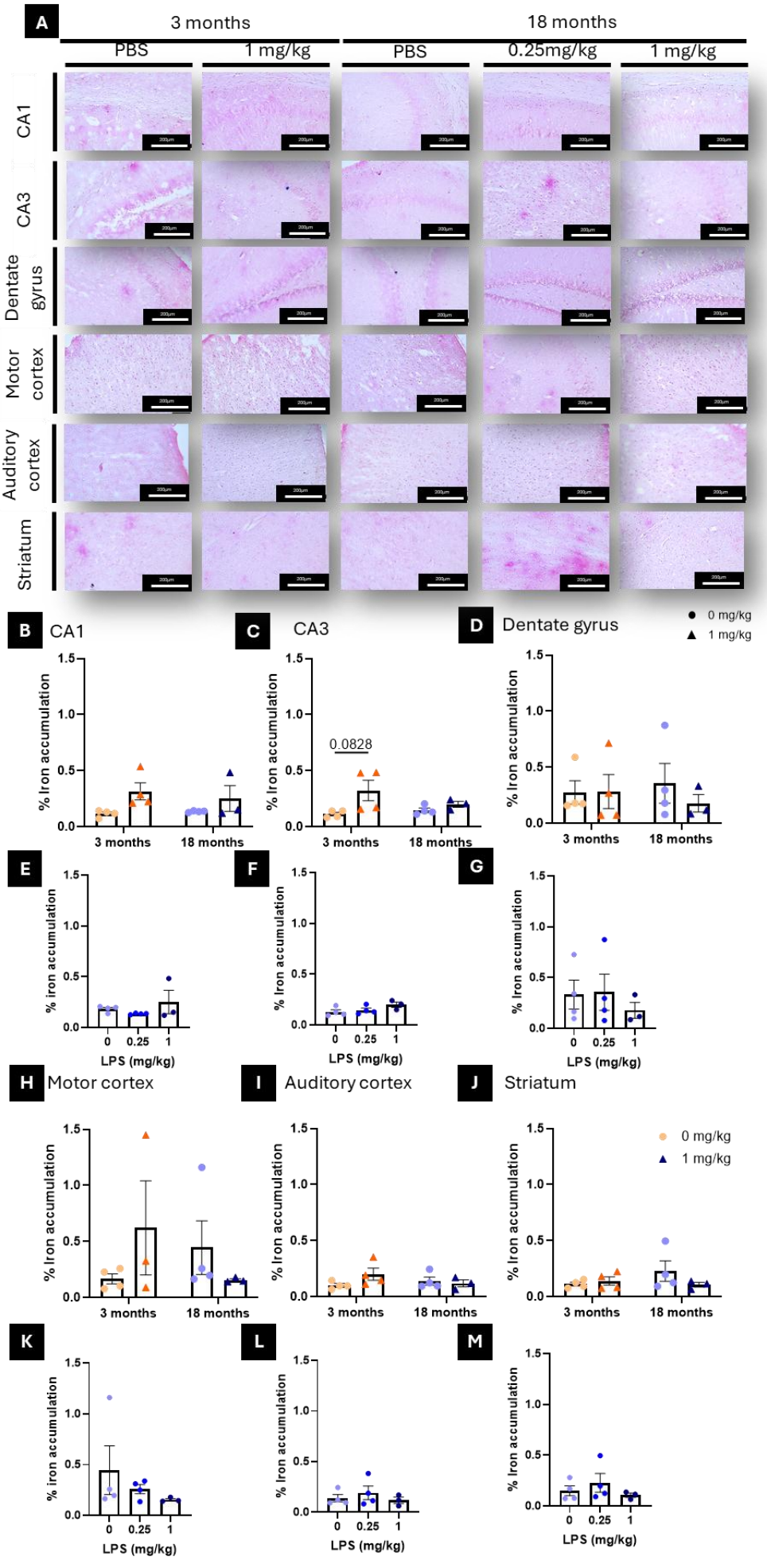
A
3 months
18 months
PBS
1 mg/kg
PBS
0.25mg/kg
1 mg/kg
CA1
CA3
Dentate gyrus
Motor cortex
Auditory cortex
Striatum
B CA1
C CA3
D Dentate gyrus
0 mg/kg
1 mg/kg
% Iron accumulation
0.0828
3 months
18 months
E
F
G
% iron accumulation
LPS (mg/kg)
H Motor cortex
I Auditory cortex
J Striatum
K
L
M

Figure 4-9: Infiltration of iron into LPS cohort mouse brain. C57BL/6 female mice groups were injected intraperitonially with a single dose of lipopolysaccharide. 3-month mice received either 1 mg/kg or PBS vehicle control whilst 18-month mice were given, 1 mg/kg, 0.25 mg/kg or PBS vehicle control. 48-hours post injection, all mice were intravenously injected with DiI-lip and cardiac perfusion was completed 2 hours post-injection to remove circulating DiI-lip. (A) Representative images of Prussian blue immunostaining of Motor and Auditory cortex, striatum, CA1, CA3 and dentate gyrus regions indicating infiltration of iron (blue). Quantitative analysis comparing 3- and 18-month mice with either LPS or vehicle treatment in (B) CA1, (C) CA3, (D) Dentate gyrus, (H) Motor cortex, (I) Auditory cortex and (J) striatum demonstrated no significant changes. Quantitative analysis of iron infiltration in 18-month LPS doses demonstrated no significant changes in (E) CA1, (F) CA3, (G) dentate gyrus, (K) motor cortex, (L) auditory cortex and (M) striatum. Images obtained at x20 magnification on Leica Thunder microscope prior to quantification in Image J. Statistical analysis was completed using GraphPad Prism software. For analysis of comparison of 0 and 1 mg/kg LPS dose in ageing, two-way analysis of variance was utilised followed by Tukey multiple comparison test. For 18-month LPS dose studies, one-way analysis of variance followed by Tukey's multiple comparison test after conducting Shapiro-Wilks normality test. N=3-4, average ± SEM, $p<0.05$ were considered significant.

4.4.5. Evaluating changes to caveolae-mediated transcytosis

As transcytosis is increased in ageing, and linked to nanoparticle infiltration, the expression of the transcytosis marker, caveolin-1 was assessed in relation to DiI-lip and the BBB through CD31 immunofluorescence staining. Firstly, the expression of caveolin-1, normalised to CD31 vascular coverage, was assessed and demonstrated no significant changes within the CA1 (fig. 4-10b-c), CA3 (fig.4-11b-c) dentate gyrus (fig.4-12b-c), auditory cortex (fig.4-14b-c) and striatum (fig. 4-15b-c) when comparing the 3-month group to the 18-month group or LPS dose in the aged group. The CA3 does show non-significant decreases with 1 mg/kg LPS group compared to the vehicle ($F=3.399_{(2,8)}$, p=0.0801) (fig.4-11c). Within the motor cortex, there were non-significant decreases in cav-1 expression between the 3-month LPS group and 18-month vehicle (age $F=7.104_{(1,10)}$, LPS $=0.7638_{(1,10)}$, p= 0.0878) and 18-month 1 mg/kg LPS (p= 0.0796) (fig. 4-13 b). Decreasing caveolin-1 expression was also observed between 0.25 mg/kg and 1 mg/kg in the 18-month age group ($F=3.882_{(2,8)}$, p= 0.0618) of the same region (fig. 4-13c).

When investigating the interaction of cav-1 and CD31 to correlate transcytosis with the BBB, no changes were observed comparing the effect of LPS throughout age or the dose of LPS at 18-months (Fig.4-10- 4-15 d-e). To determine if liposomes were transported through the transcytosis route during LPS or ageing, the interaction of DiI-lip and cav-1 was quantified. Results of this show no significant changes based on LPS dose or ageing in CA1 (fig. 4-10 f- g), (fig.4-13f-g), motor cortex (fig. 4-14f-g), auditory cortex (fig 4-14f-g) or striatum (fig. 4-15f-g). In the CA3 region, there was a non-significant decrease in interaction between cav-1 and DiI-lip between the 3-month LPS group and 18-month vehicle ($F=3.399_{(2,8)}$, p= 0.0944) but no changes in LPS dose at older age (fig. 4-11f-g). Inversely, in the dentate gyrus, there was no significant changes comparing the effect of age and LPS but there was a significant increase in interaction comparing the 18-month vehicle to 0.25 mg/kg LPS ($F=5.442_{(2,8)}$, p= 0.0302) (fig. 4-12f-g). Overall, neither age nor LPS had a had a significant impact on global caveolin-1 levels or their interactions with DiI-lip and BBB, indicating that this is not the transport route affiliated with DiI-lip infiltration.

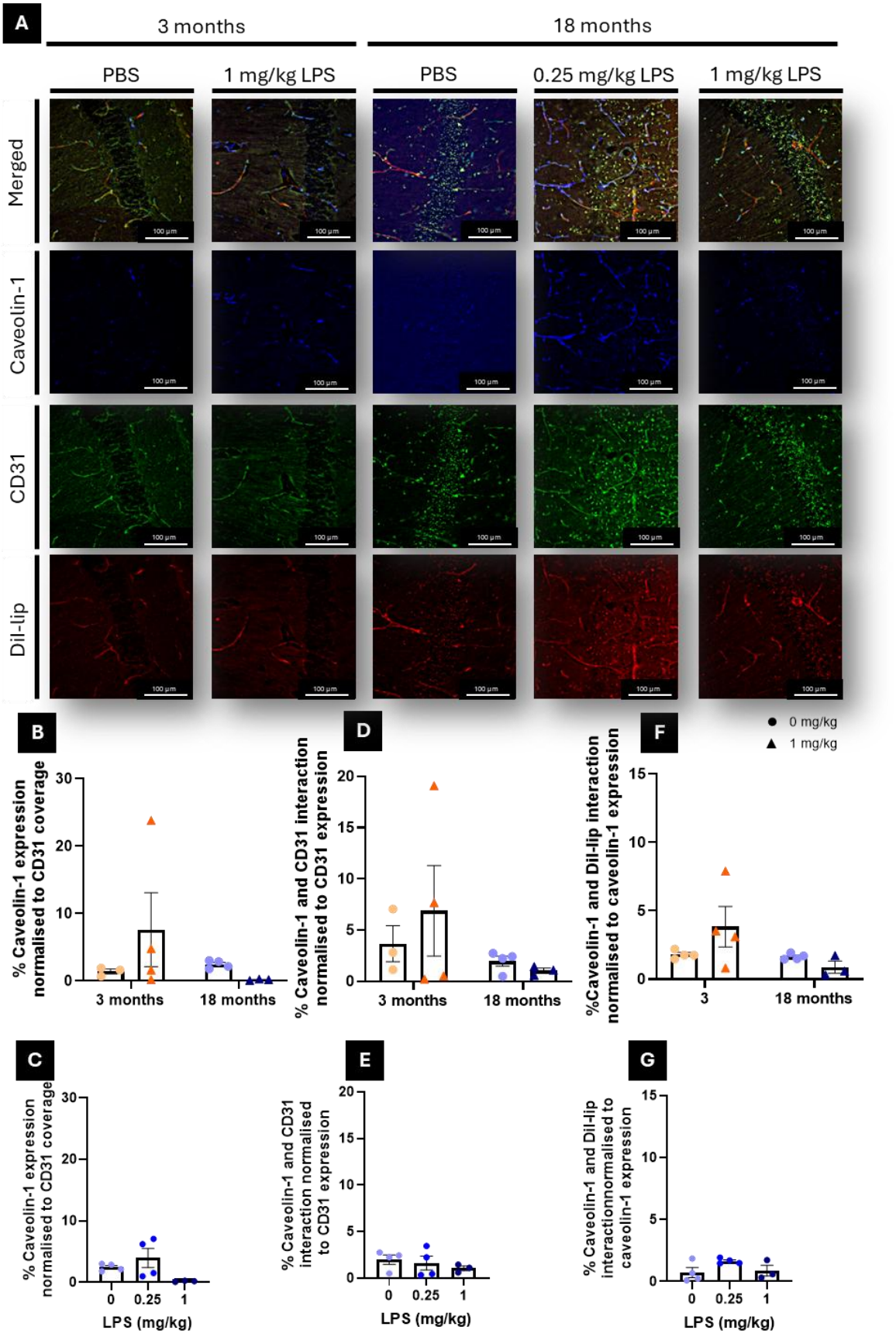

Figure 4-10: Evaluation of transcytosis transport in ageing and inflammation in CA1 hippocampal region. C57BL/6 female mice groups were injected intraperitonially with a single dose of lipopolysaccharide. 3-month mice received either 1 mg/kg or PBS vehicle control whilst 18-month mice were given, 1 mg/kg, 0.25 mg/kg or PBS vehicle control. 48-hours post injection, all mice were intravenously injected with DiI-lip and cardiac perfusion was completed 2 hours post-injection to remove circulating DiI-lip. (A) Representative immunofluorescence images of CA1 hippocampal

region -1.94mm from the bregma demonstrate expression of CD31 (green), Caveolin-1 (blue) and DiI-lip (Red). Quantitative analysis of caveolin-1 expression, normalised to endothelial cell coverage, when comparing LPS effect on aged groups (A) or dose of LPS in aged mice (C) demonstrated no significant changes. Quantitative analysis of the interaction between caveolin-1 and CD31 showed no significant effects in either the comparison of LPS on two age groups (D) or LPS dose on 18-month mice (E). The interaction of caveolin-1 and DiI-lip showed no significant changes in either the LPS and age comparison (F) or effect of different LPS doses on 18-month group (G). Images obtained at x40 magnification on Leica Thunder microscope and underwent large volume computational clearing prior to quantification in Image J. Statistical analysis was completed using GraphPad Prism software. For analysis of comparison of 1mgkg LPS dose in ageing, two-way analysis of variance was utilised followed by Tukey multiple comparison test. For 18-month LPS dose studies, one-way analysis of variance followed by Tukey's multiple comparison test after conducting Shapiro-Wilks normality test. N=3-4, average ± SEM, $p<0.05$ were considered significant.

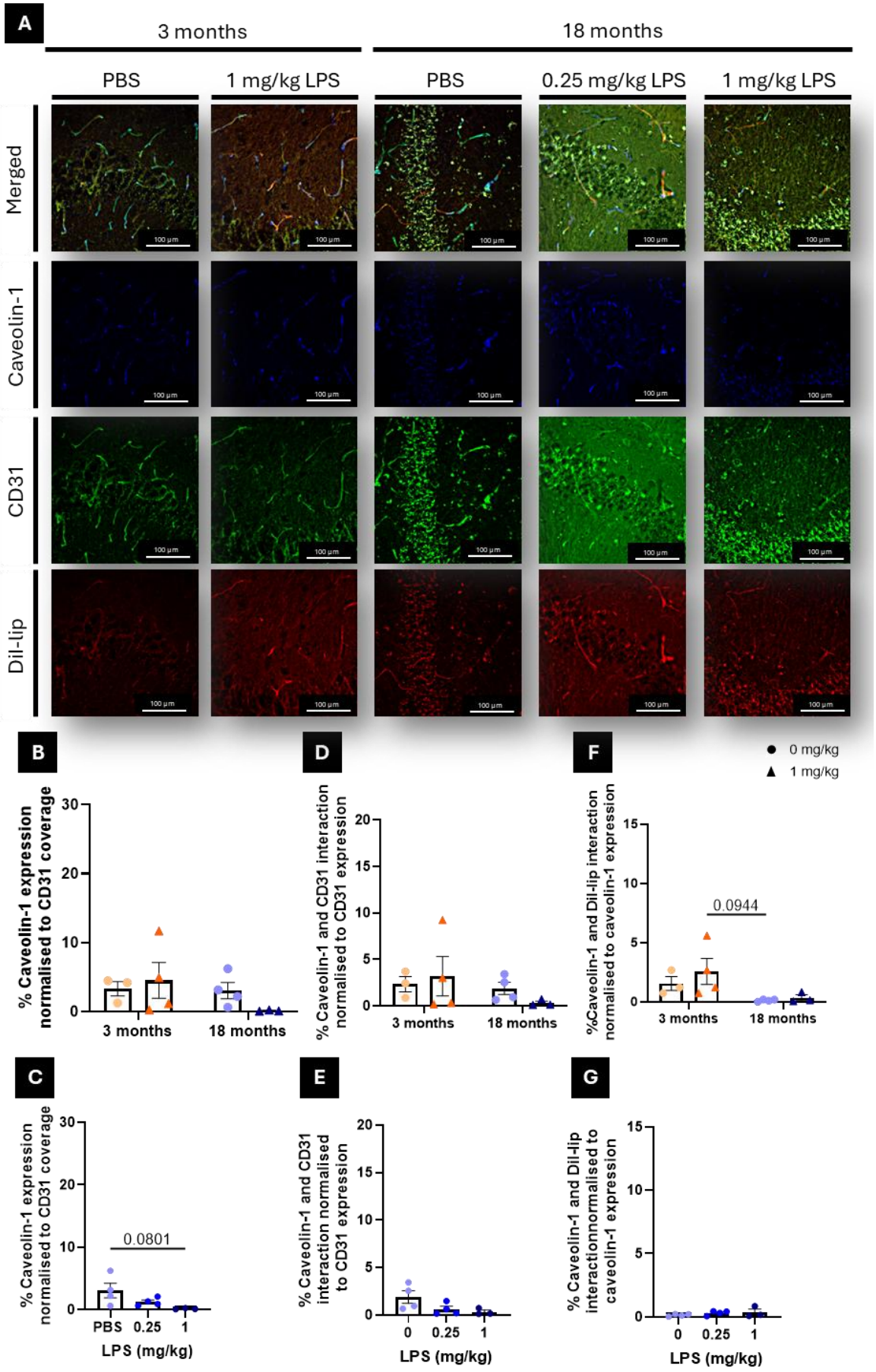

Figure 4-11: Evaluation of transcytosis transport in ageing and inflammation in CA3 hippocampal region. C57BL/6 female mice groups were injected intraperitonially with a single dose of lipopolysaccharide. 3-month mice received either 1 mg/kg or PBS vehicle control whilst 18-month

mice were given, 1 mg/kg, 0.25 mg/kg or PBS vehicle control. 48-hours post injection, all mice were intravenously injected with DiI-lip and cardiac perfusion was completed 2 hours post-injection to remove circulating DiI-lip. (A) Representative immunofluorescence images of CA3 hippocampal region -1.94mm from the bregma demonstrate expression of CD31 (green), Caveolin-1 (blue) and DiI-lip (Red). Quantitative analysis of caveolin-1 expression, normalised to endothelial cell coverage, when comparing LPS effect on aged groups (A) or dose of LPS in aged mice (C) demonstrated no significant changes. Quantitative analysis of the interaction between caveolin-1 and CD31 showed no significant effects in either the comparison of LPS on two age groups (D) or LPS dose on 18-month mice (E). The interaction of caveolin-1 and DiI-lip showed no significant changes in either the LPS and age comparison (F) or effect of different LPS doses on 18-month group (G). Images obtained at x40 magnification on Leica Thunder microscope and underwent large volume computational clearing prior to quantification in Image J. Statistical analysis was completed using GraphPad Prism software. For analysis of comparison of 1mgkg LPS dose in ageing, two-way analysis of variance was utilised followed by Tukey multiple comparison test. For 18-month LPS dose studies, one-way analysis of variance followed by Tukey's multiple comparison test after conducting Shapiro-Wilks normality test. N=3-4, average ± SEM, $p<0.05$ were considered significant.

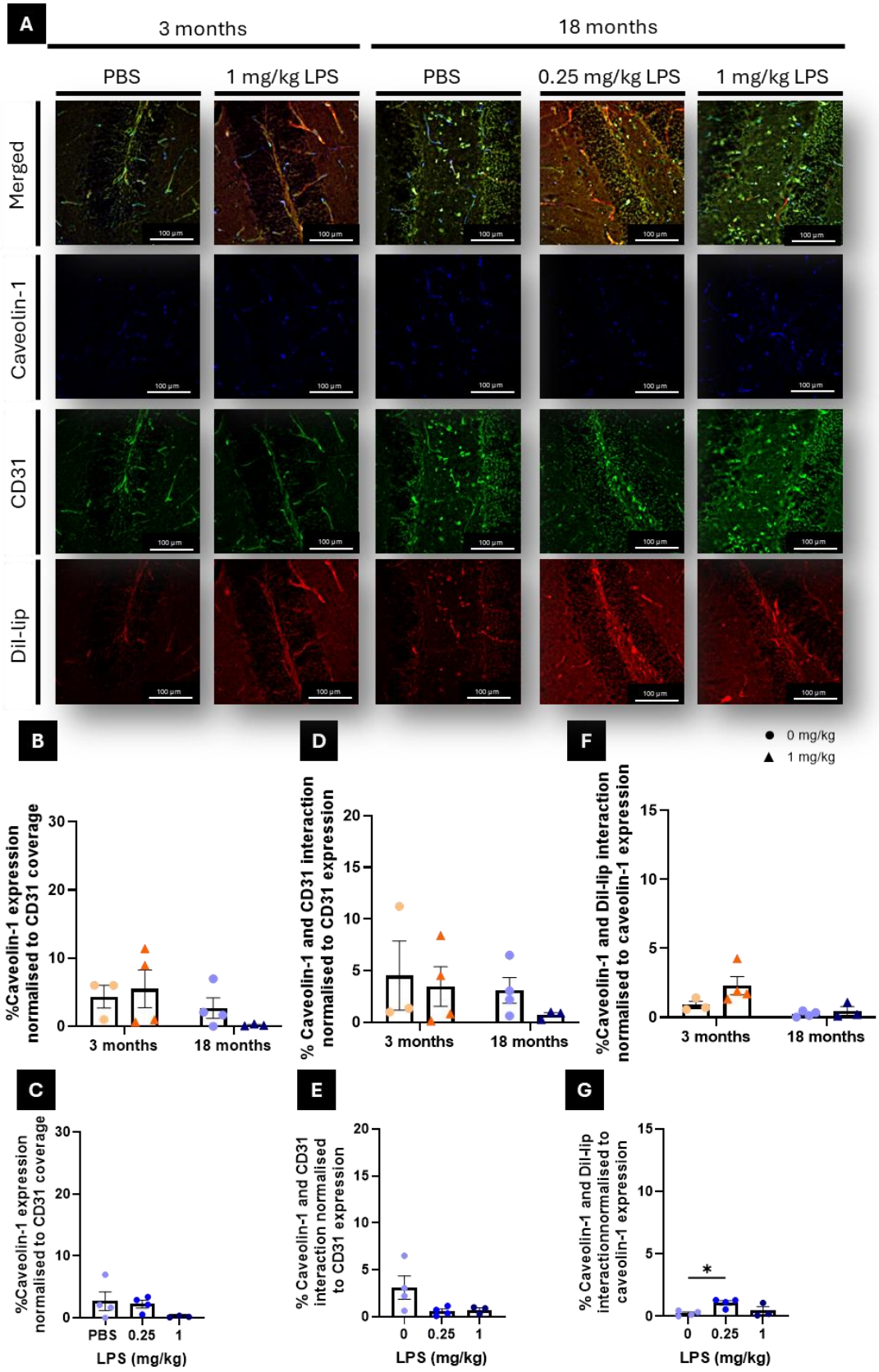

Figure 4-12: Evaluation of transcytosis transport in ageing and inflammation in dentate gyrus hippocampal region. C57BL/6 female mice groups were injected with intraperitonially a single dose of lipopolysaccharide. 3-month mice received either 1 mg/kg or PBS vehicle control whilst 18-month mice were given, 1 mg/kg, 0.25 mg/kg or PBS vehicle control. 48-hours post injection, all mice were intravenously injected with DiI-lip and cardiac perfusion was completed 2 hours post-injection to remove circulating DiI-lip. (A) Representative immunofluorescence images of dentate gyrus hippocampal region -1.94mm from the bregma demonstrate expression of CD31 (green), Caveolin-1

(blue) and DiI-lip (Red). Quantitative analysis of caveolin-1 expression, normalised to endothelial cell coverage, when comparing LPS effect on aged groups (A) or dose of LPS in aged mice (C) demonstrated no significant changes. Quantitative analysis of the interaction between caveolin-1 and CD31 showed no significant effects in either the comparison of LPS on two age groups (D) or LPS dose on 18-month mice (E). Quantification of the interaction of caveolin-1 and DiI-lip showed no significant changes in the LPS and age comparison (F) but there was a significant increase in the 0.25 mg/kg LPS group compared to vehicle in the 18-month group (G). Images obtained at x40 magnification on Leica Thunder microscope and underwent large volume computational clearing prior to quantification in Image J. Statistical analysis was completed using GraphPad Prism software. For analysis of comparison of 1mgkg LPS dose in ageing, two-way analysis of variance was utilised followed by Tukey multiple comparison test. For 18-month LPS dose studies, one-way analysis of variance followed by Tukey's multiple comparison test after conducting Shapiro-Wilks normality test. N=3-4,average ± SEM, $p<0.05$ were considered significant.

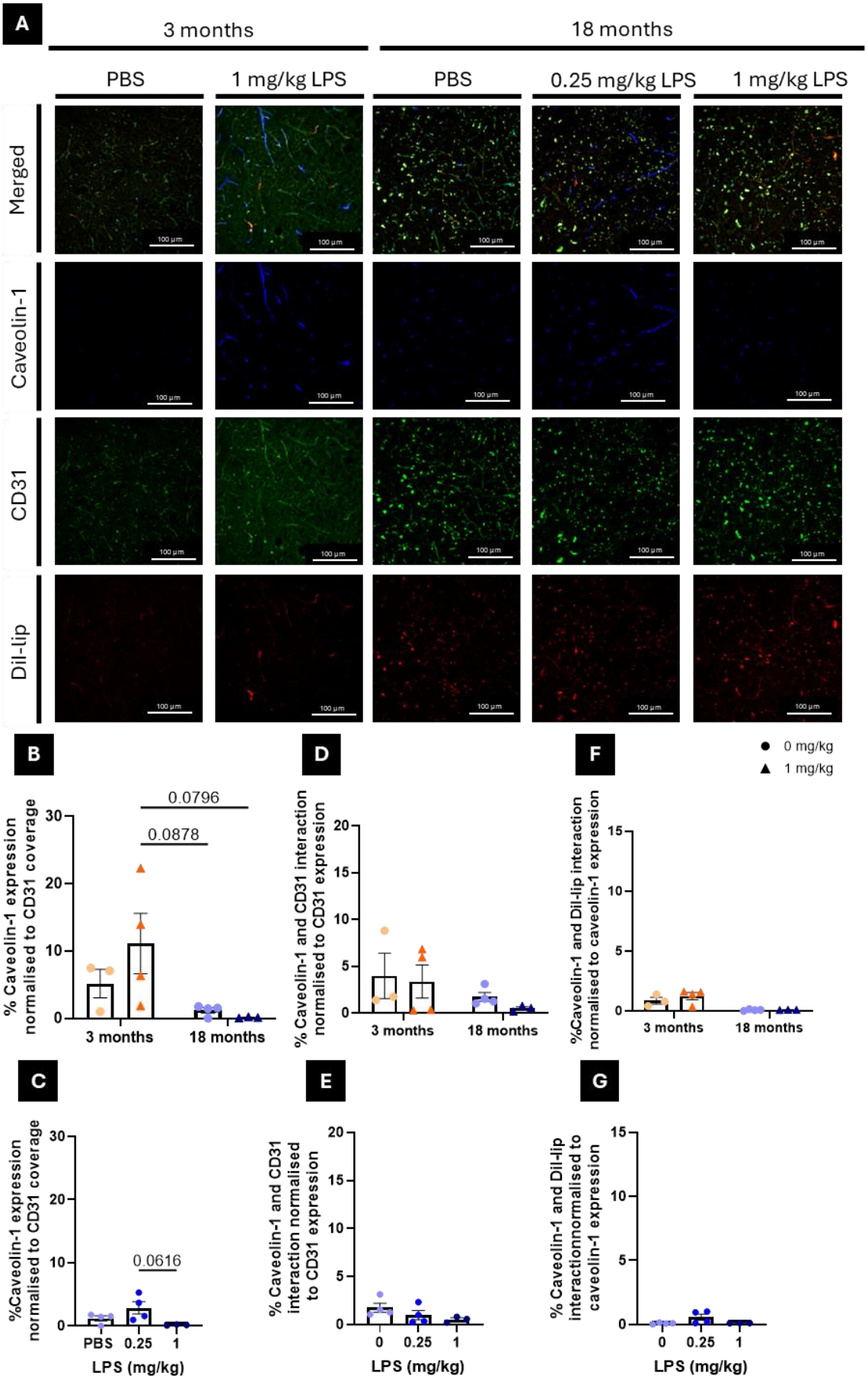

Figure 4-13: Evaluation of transcytosis transport in ageing and inflammation in motor cortex region. C57BL/6 female mice groups were injected with intraperitonially a single dose of lipopolysaccharide. 3-month mice received either 1 mg/kg or PBS vehicle control whilst 18-month

mice were given, 1 mg/kg, 0.25 mg/kg or PBS vehicle control. 48-hours post injection, all mice were intravenously injected with DiI-lip and cardiac perfusion was completed 2 hours post-injection to remove circulating DiI-lip. (A) Representative immunofluorescence images of motor cortex -1.94mm from the bregma demonstrate expression of CD31 (green), Caveolin-1 (blue) and DiI-lip (Red). Quantitative analysis of caveolin-1 expression, normalised to endothelial cell coverage, when comparing LPS effect on aged groups demonstrated non-significant decreasing trends between the 3-month 1 mg/kg LPS groups and both the vehicle and LPS 18-month groups (A). Quantification of LPS dose in aged mice showed non-significant decreases between the 0.25 mg/kg groups and 1 mg/kg group (C). No significant changes were observed after quantification of caveolin-1 interaction with CD31 in age (D) or dose (E) comparisons. Quantitative analysis of caveolin-1 and DiI-lip interaction in the age comparison (F) or 18-month LPS dose comparison (G) showed no significant changes. Images obtained at x40 magnification on Leica Thunder microscope and underwent large volume computational clearing prior to quantification in Image J. Statistical analysis was completed using GraphPad Prism software. For analysis of comparison of 1mgkg LPS dose in ageing, two-way analysis of variance was utilised followed by Tukey multiple comparison test. For 18-month LPS dose studies, one-way analysis of variance followed by Tukey's multiple comparison test after conducting Shapiro-Wilks normality test. N=3-4, average ± SEM, $p<0.05$ were considered significant.

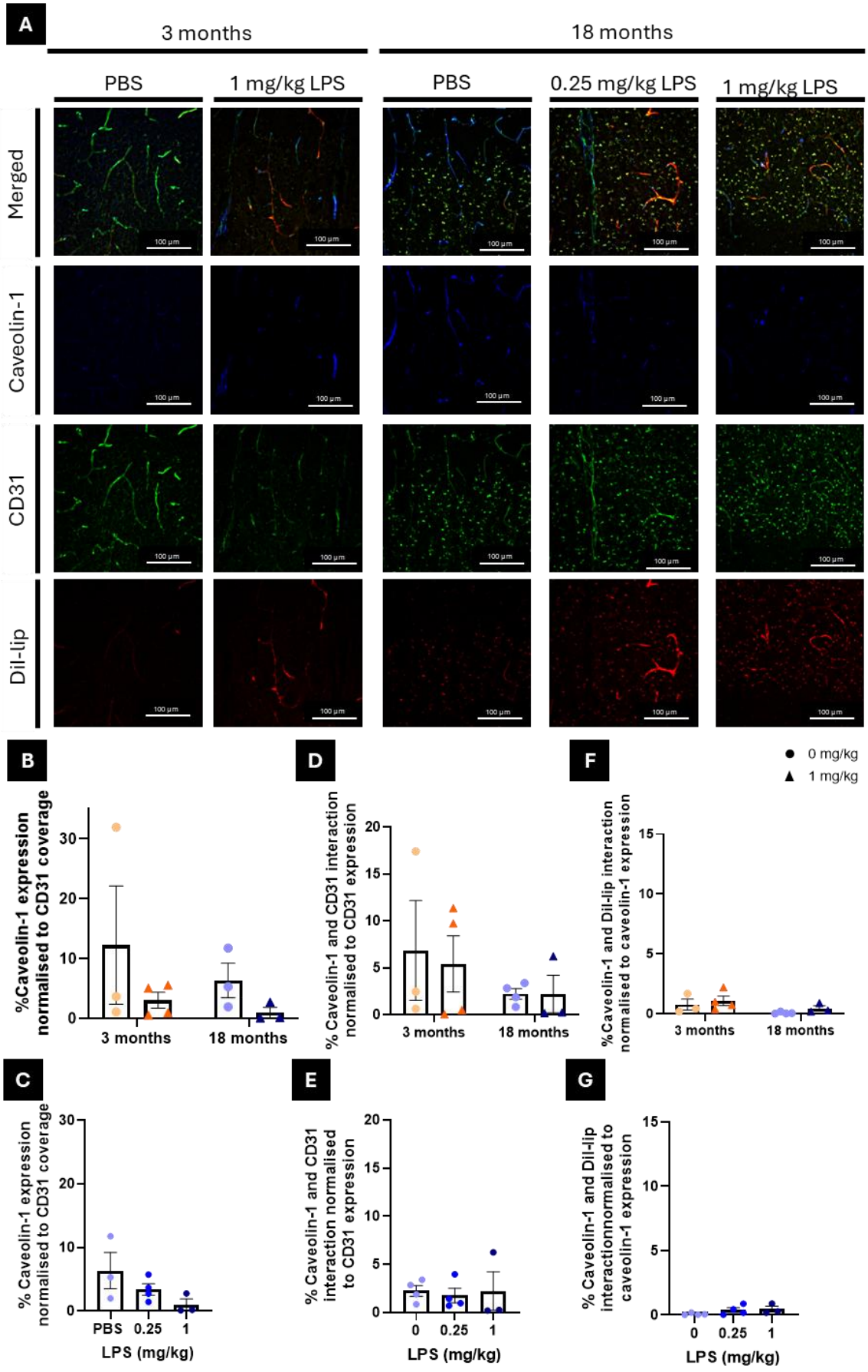

Figure 4-14: Evaluation of transcytosis transport in ageing and inflammation in auditory cortex region. C57BL/6 female mice groups were injected intraperitonially with a single dose of lipopolysaccharide. 3-month mice received either 1 mg/kg or PBS vehicle control whilst 18-month mice were given, 1 mg/kg, 0.25 mg/kg or PBS vehicle control. 48-hours post injection, all mice were

intravenously injected with DiI-lip and cardiac perfusion was completed 2 hours post-injection to remove circulating DiI-lip. (A) Representative immunofluorescence images of auditory cortex region -1.94mm from the bregma demonstrate expression of CD31 (green), Caveolin-1 (blue) and DiI-lip (Red). Quantitative analysis of caveolin-1 expression, normalised to endothelial cell coverage, with comparisons between ages (B) or 18-month LPS dose (C). Quantification of caveolin-1 and CD31 interaction between age groups (D) or 18-month LPS dose (E). Quantification of caveolin-1 and DiI-lip interaction in comparison of age groups (F) or 18-month LPS dose (G). All analysis was produced no significant changes in expression or interaction. Images obtained at x40 magnification on Leica Thunder microscope and underwent large volume computational clearing prior to quantification in Image J. Statistical analysis was completed using GraphPad Prism software. For analysis of comparison of 1mgkg LPS dose in ageing, two-way analysis of variance was utilised followed by Tukey multiple comparison test. For 18-month LPS dose studies, one-way analysis of variance followed by Tukey's multiple comparison test after conducting Shapiro-Wilks normality test. N=3-4,average ± SEM, $p<0.05$ were considered significant.

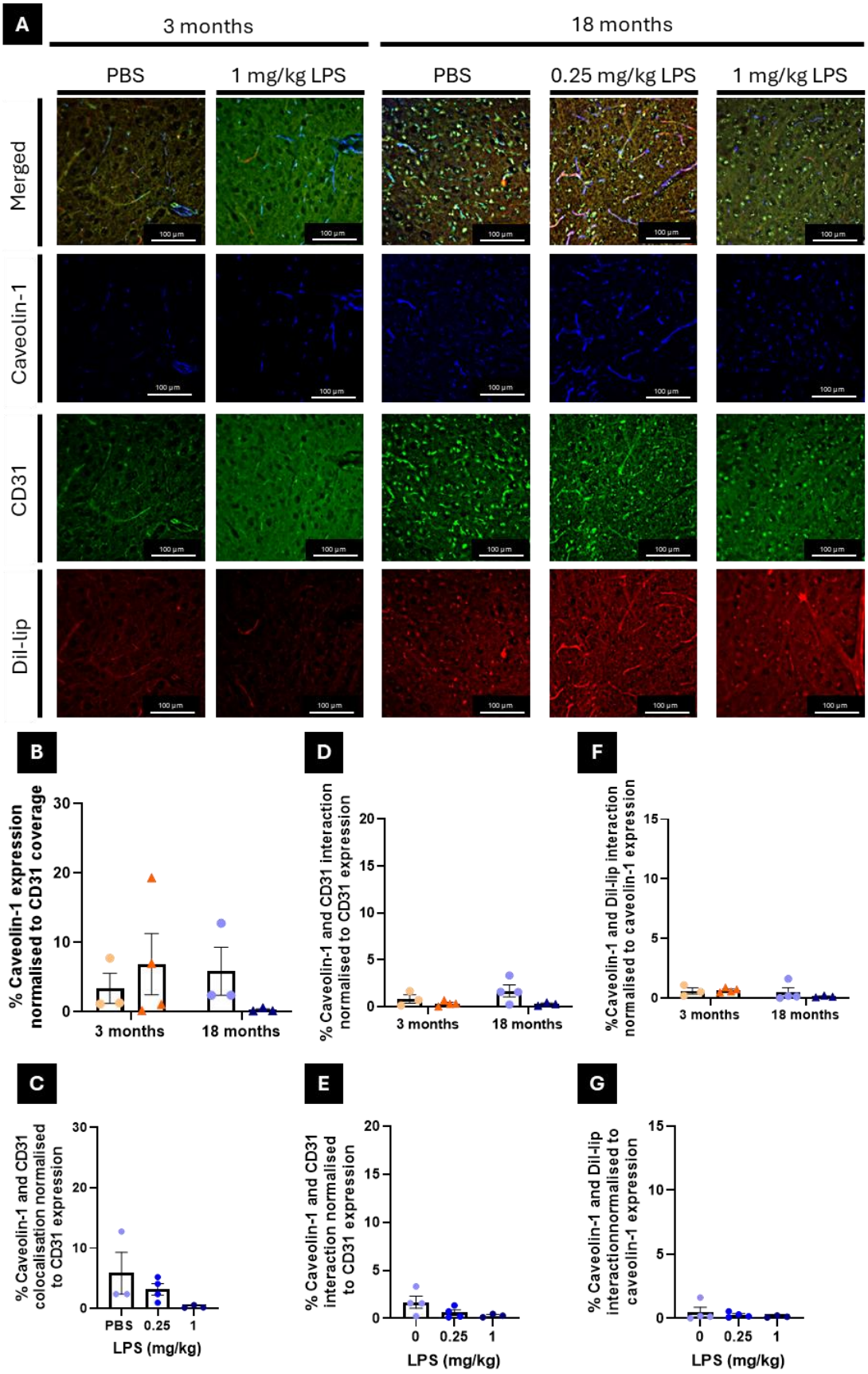

Figure 4-15: Evaluation of transcytosis transport in ageing and inflammation in striatum region. C57BL/6 female mice groups were injected intraperitonially with a single dose of lipopolysaccharide. 3-month mice received either 1 mg/kg or PBS vehicle control whilst 18-month mice were given, 1 mg/kg, 0.25 mg/kg or PBS vehicle control. 48-hours post injection, all mice were intravenously injected with DiI-lip and cardiac perfusion was completed 2 hours post-injection to remove circulating DiI-lip. (A) Representative immunofluorescence images of striatum region -1.94mm from

the bregma demonstrate expression of CD31 (green), Caveolin-1 (blue) and DiI-lip (Red). Quantitative analysis of caveolin-1 expression, normalised to endothelial cell coverage, with comparisons between ages (B) or 18-month LPS dose (C). Quantification of caveolin-1 and CD31 interaction between age groups (D) or 18-month LPS dose (E). Quantification of caveolin-1 and DiI-lip interaction in comparison of age groups (F) or 18-month LPS dose (G). All analysis was produced no significant changes in expression or interaction. Images obtained at x40 magnification on Leica Thunder microscope and underwent large volume computational clearing prior to quantification in Image J. Statistical analysis was completed using GraphPad Prism software. For analysis of comparison of 1mgkg LPS dose in ageing, two-way analysis of variance was utilised followed by Tukey multiple comparison test. For 18-month LPS dose studies, one-way analysis of variance followed by Tukey's multiple comparison test after conducting Shapiro-Wilks normality test. N=3-4, average ± SEM, $p<0.05$ were considered significant.

4.4.6. Changes to neurovascular unit associated inflammatory cells

5.4.6.1. Astrocytic changes in age and LPS conditions

Astrocyte activation has been linked to both ageing and inflammation within the brain therefore the expression of astrocyte activation marker, GFAP, was analysed. However, when comparing either the effect of age and LPS injection, or the effect of LPS dose on 18-month mice, there were no significant changes in GFAP expression in the CA1 (fig. 4-16b-c), CA3 (fig. 4-17b-c), dentate gyrus (fig. 4-18b-c) and auditory cortex (fig. 4-20b-c). Within the motor cortex, there was no effect of LPS dose on the aged brain (fig. 4-19c), but significant GFAP increases were observed between the 3-month vehicle and 18-month 1 mg/kg (age $F=0.478_{(1,10)}$, LPS $F=15.77_{(1,10)}$, $p=0.048$) (fig. 4-19b). Further non-significant GFAP expression increases were observed between vehicle and LPS treatment in 3-months ($F=0.478_{(1,10)}$, LPS $F=15.77_{(1,10)}$, $p=0.0602$) and 18-months ($F(1,10) =0.478_{(1,10)}$, LPS $F15.77_{(1,10)}$, $p=0.0918$). Within the striatum region, there again was no changes with LPS dose in 18-month mice but non-significant GFAP increases were seen in the 18-month vehicle (age $F=15.12_{(1,10)}$, LPS $F=0.479_{(1,10)}$, $p= 0.0645$) and 18-month LPS ($F=15.12_{(1,10)}$, LPS $F=0.479_{(1,10)}$, $p= 0.0527$) compared to the vehicle (fig. 4-21b-c). The expression of GFAP was not changed in multiple regions based on age or LPS but some regions indicated increased GFAP expression in LPS groups compared to the vehicle.

Correlation between astrocytes and the endothelial BBB cells has been indicated in age and inflammation to decrease as astrocytic end-feet retract from the BBB so CD31 and GFAP interactions were investigated. However, no significant changes were observed in any group comparing the effects of age and 1 mg/kg LPS injection (Fig. 4-16-4-21, d) or comparison of 0.25 and 1 mg/kg LPS in the 18-month group (Fig. 4-16-4-21 e). To determine if DiI-lip accumulate within the astrocyte, suggesting a potential targeted response, the interaction between DiI-lip and GFAP was investigated. Similarly to the interaction with CD31, no significant changes were observed in any region comparing age and LPS (Fig. 4-16-4-21 f) or LPS dose on 18-month mice (Fig. 4-16-4-21 g). Overall, the results suggest that age and

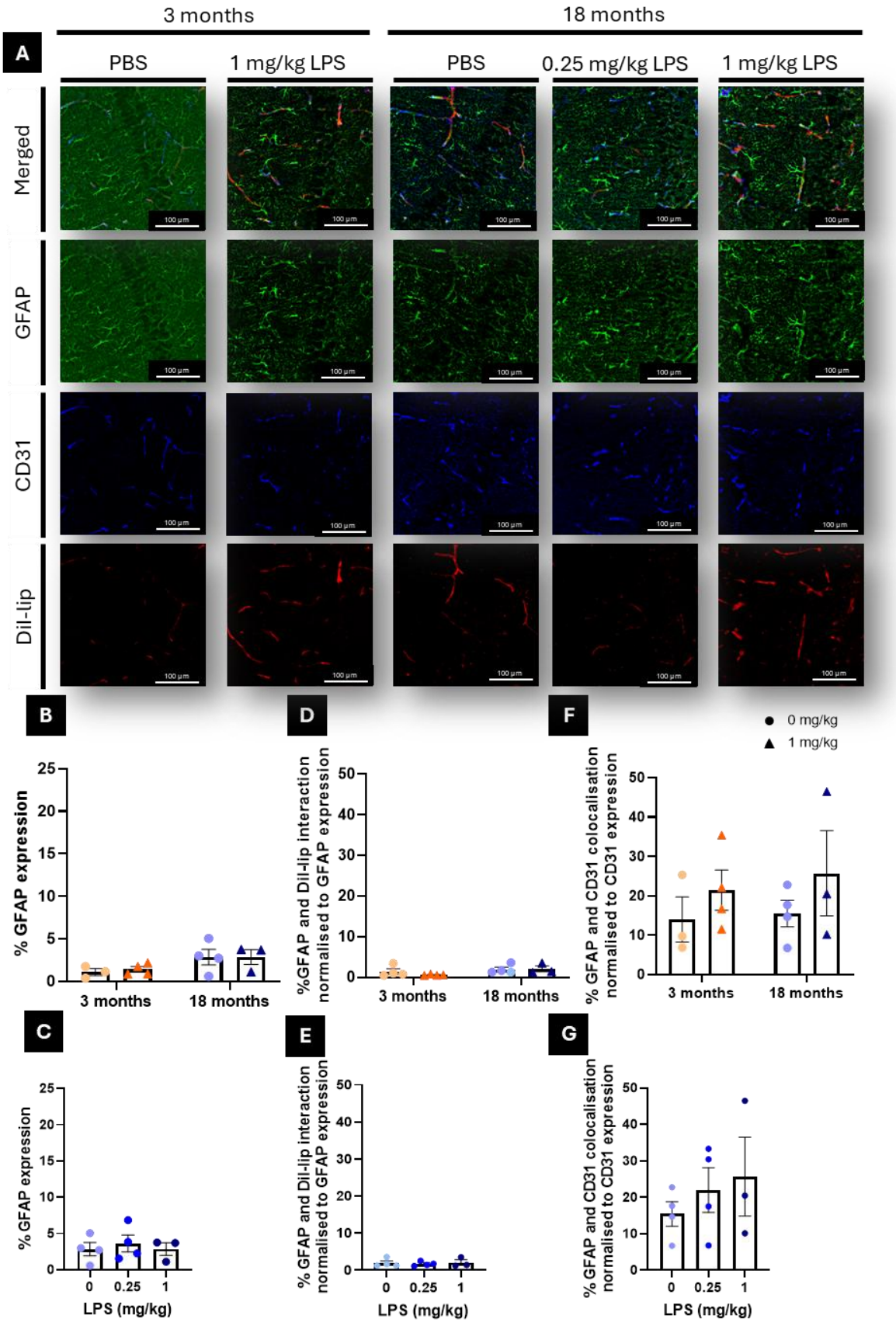

Figure 4-16: Evaluation of GFAP+ astrocyte expression transport in ageing and inflammation in CA1 hippocampal region. C57BL/6 female mice groups were injected intraperitonially with a single dose of lipopolysaccharide. 3-month mice received either 1 mg/kg or PBS vehicle control whilst 18-month mice were given, 1 mg/kg, 0.25 mg/kg or PBS vehicle control. 48-hours post injection, all mice were intravenously injected with DiI-lip and cardiac perfusion was completed 2 hours post-injection

to remove circulating DiI-lip. (A) Representative immunofluorescence images of CA1 region -1.94mm from the bregma demonstrate expression of CD31 (blue), GFAP (green) and DiI-lip (Red). Quantitative analysis of GFAP expression with comparisons between ages (B) or 18-month LPS dose (C). Quantification of GFAP and CD31 interaction between age groups (D) or 18-month LPS dose (E). Quantification of GFAP and DiI-lip interaction in comparison of age groups (F) or 18-month LPS dose (G). All analysis was produced no significant changes in expression or interaction. Images obtained at x40 magnification on Leica Thunder microscope and underwent large volume computational clearing prior to quantification in Image J. Statistical analysis was completed using GraphPad Prism software. For analysis of comparison of 1mgkg LPS dose in ageing, two-way analysis of variance was utilised followed by Tukey multiple comparison test. For 18-month LPS dose studies, one-way analysis of variance followed by Tukey's multiple comparison test after conducting Shapiro-Wilks normality test. N=3-4, average ± SEM, $p<0.05$ were considered significant.

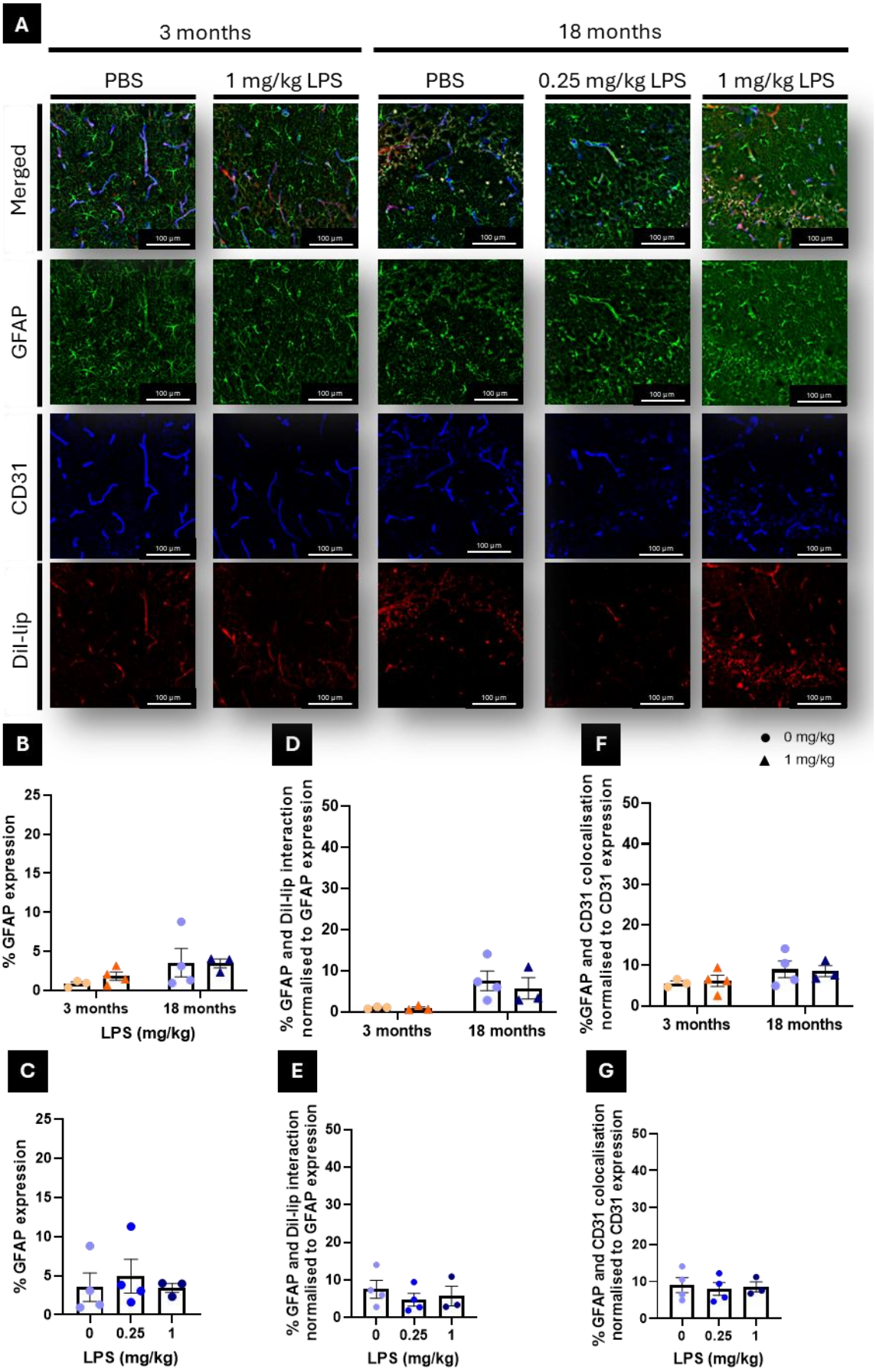

Figure 4-17: Evaluation of GFAP+ astrocyte expression transport in ageing and inflammation in CA3 region. C57BL/6 female mice groups were injected intraperitonially with a single dose of lipopolysaccharide. 3-month mice received either 1 mg/kg or PBS vehicle control whilst 18-month mice were given, 1 mg/kg, 0.25 mg/kg or PBS vehicle control. 48-hours post injection, all mice were

intravenously injected with DiI-lip and cardiac perfusion was completed 2 hours post-injection to remove circulating DiI-lip. (A) Representative immunofluorescence images of CA3 region -1.94mm from the bregma demonstrate expression of CD31 (blue), GFAP (green) and DiI-lip (Red). Quantitative analysis of GFAP expression, normalised to endothelial cell coverage, with comparisons between ages (B) or 18-month LPS dose (C). Quantification of GFAP and CD31 interaction between age groups (D) or 18-month LPS dose (E). Quantification of GFAP and DiI-lip interaction in comparison of age groups (F) or 18-month LPS dose (G). All analysis was produced no significant changes in expression or interaction. Images obtained at x40 magnification on Leica Thunder microscope and underwent large volume computational clearing prior to quantification in Image J. Statistical analysis was completed using GraphPad Prism software. For analysis of comparison of 1mgkg LPS dose in ageing, two-way analysis of variance was utilised followed by Tukey multiple comparison test. For 18-month LPS dose studies, one-way analysis of variance followed by Tukey's multiple comparison test after conducting Shapiro-Wilks normality test. N=3-4,average ± SEM, $p<0.05$ were considered significant.

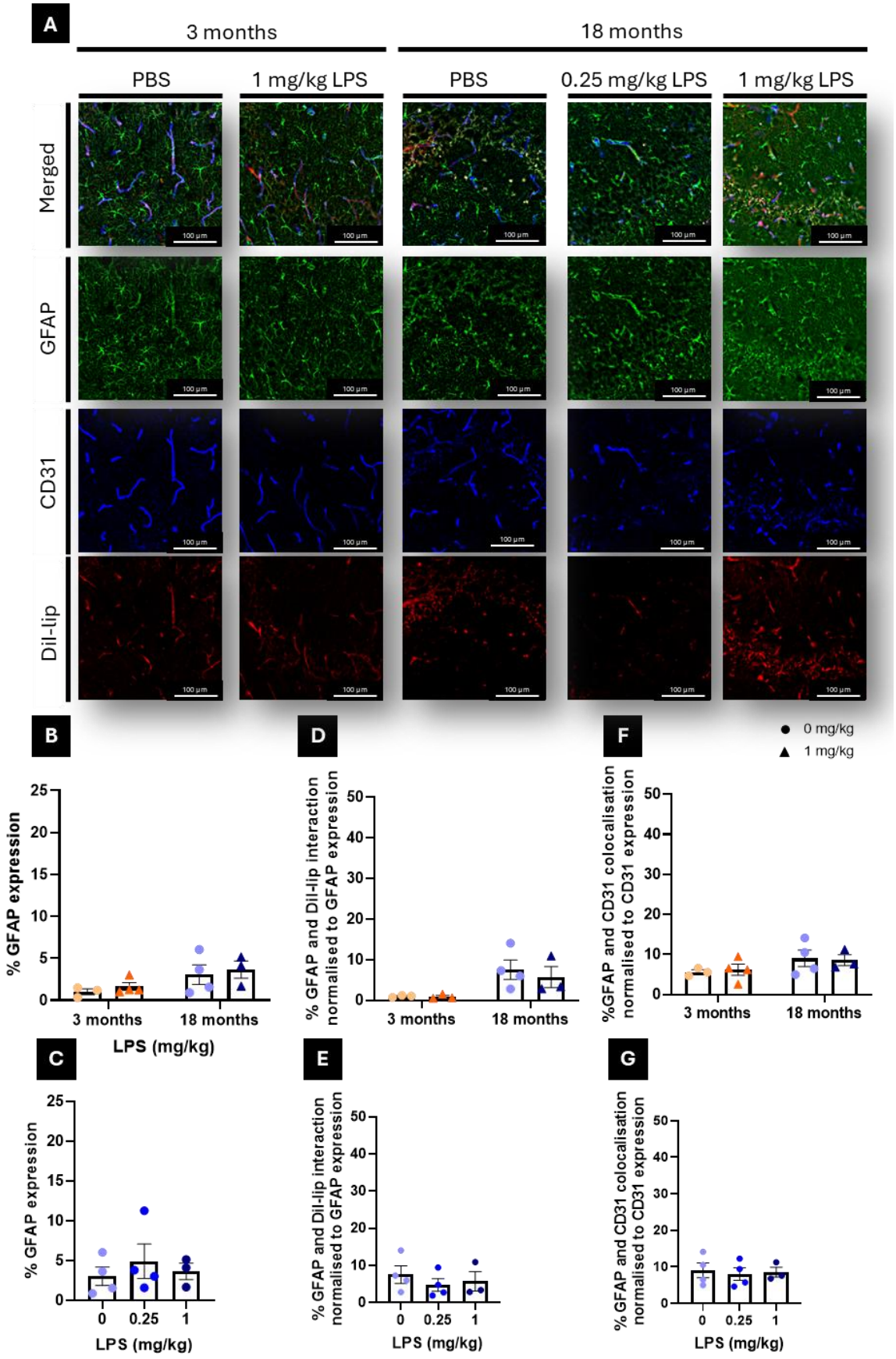

Figure 4-18: Evaluation of GFAP+ astrocyte expression transport in ageing and inflammation in dentate gyrus region. C57BL/6 female mice groups were injected intraperitonially with a single dose of lipopolysaccharide. 3-month mice received either 1 mg/kg or PBS vehicle control whilst 18-month mice were given, 1 mg/kg, 0.25 mg/kg or PBS vehicle control. 48-hours post injection, all mice were intravenously injected with DiI-lip and cardiac perfusion was completed 2 hours post-injection to

remove circulating DiI-lip. (A) Representative immunofluorescence images of dentate gyrus region -1.94mm from the bregma demonstrate expression CD31 (blue), GFAP (green) and DiI-lip (Red). Quantitative analysis of GFAP expression with comparisons between ages (B) or 18-month LPS dose (C). Quantification of GFAP and CD31 interaction between age groups (D) or 18-month LPS dose (E). Quantification of GFAP and DiI-lip interaction in comparison of age groups (F) or 18-month LPS dose (G). All analysis was produced no significant changes in expression or interaction. Images obtained at x40 magnification on Leica Thunder microscope and underwent large volume computational clearing prior to quantification in Image J. Statistical analysis was completed using GraphPad Prism software. For analysis of comparison of 1mgkg LPS dose in ageing, two-way analysis of variance was utilised followed by Tukey multiple comparison test. For 18-month LPS dose studies, one-way analysis of variance followed by Tukey's multiple comparison test after conducting Shapiro-Wilks normality test. N=3-4, average ± SEM, $p<0.05$ were considered significant.

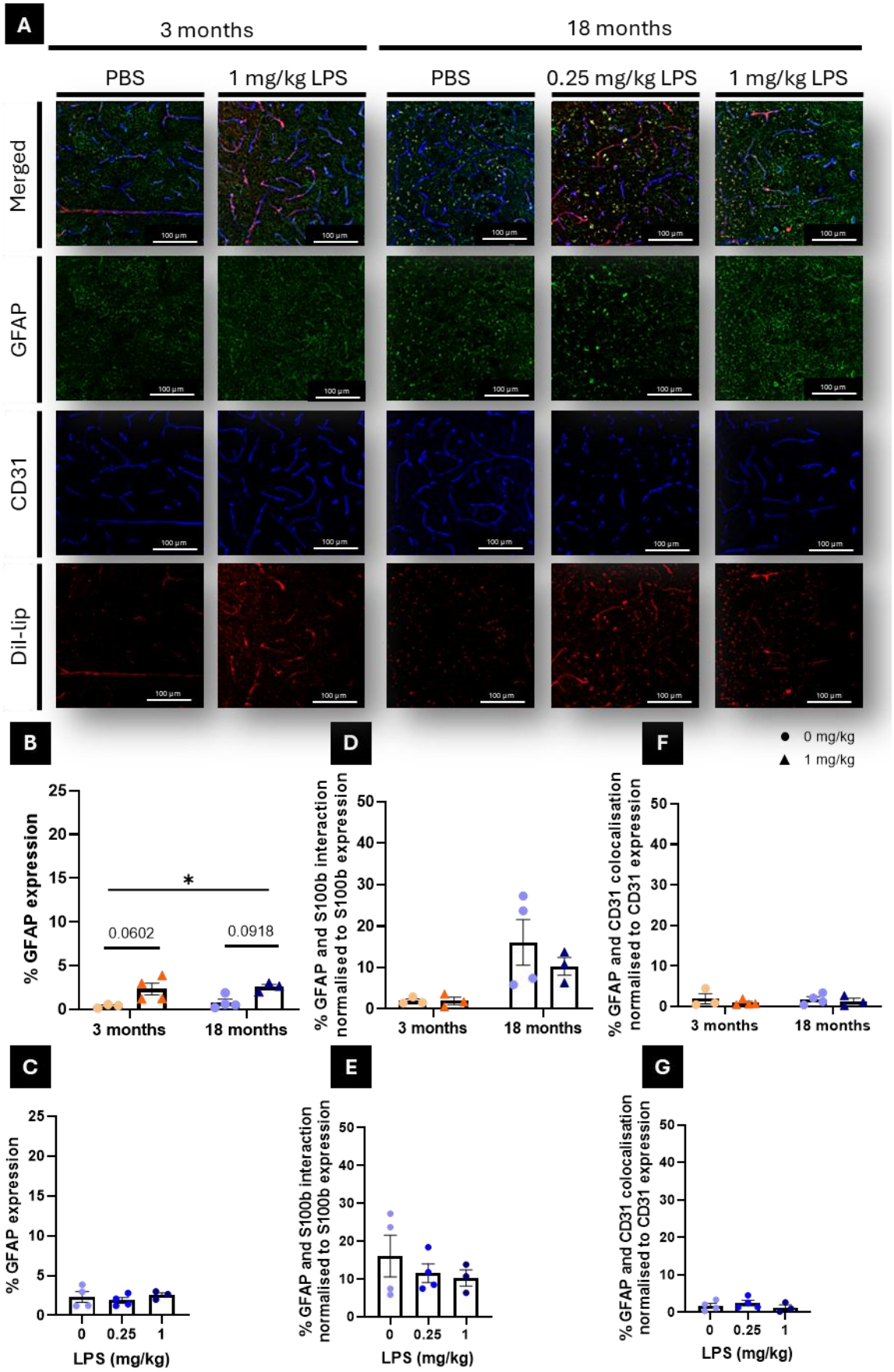

Figure 4-19: Evaluation of GFAP+ astrocyte expression transport in ageing and inflammation in motor cortex region. C57BL/6 female mice groups were injected intraperitonially with a single dose of lipopolysaccharide. 3-month mice received either 1 mg/kg or PBS vehicle control whilst 18-month mice were given, 1 mg/kg, 0.25 mg/kg or PBS vehicle control. 48-hours post injection, all mice were intravenously injected with DiI-lip and cardiac perfusion was completed 2 hours post-injection to

remove circulating DiI-lip. (A) Representative immunofluorescence images of motor cortex region -1.94mm from the bregma demonstrate expression of CD31 (blue), GFAP (green) and DiI-lip (Red). Quantitative analysis of GFAP expression with comparisons between ages (B) showing a significant increase in GFAP expression between 3-month vehicle and 18-month 1 mg/kg LPS. (C) Quantitative analysis of GFAP expression in 18-month LPS dose showed no significant changes. Quantification of GFAP and CD31 interaction between age groups (D) or 18-month LPS dose (E). Quantification of GFAP and DiI-lip interaction in comparison of age groups (F) or 18-month LPS dose (G). All interaction analysis was produced no significant changes in expression or interaction. Images obtained at x40 magnification on Leica Thunder microscope and underwent large volume computational clearing prior to quantification in Image J. Statistical analysis was completed using GraphPad Prism software. For analysis of comparison of 1mgkg LPS dose in ageing, two-way analysis of variance was utilised followed by Tukey multiple comparison test. For 18-month LPS dose studies, one-way analysis of variance followed by Tukey's multiple comparison test after conducting Shapiro-Wilks normality test. N=3-4, average ± SEM, $p<0.05$ were considered significant.

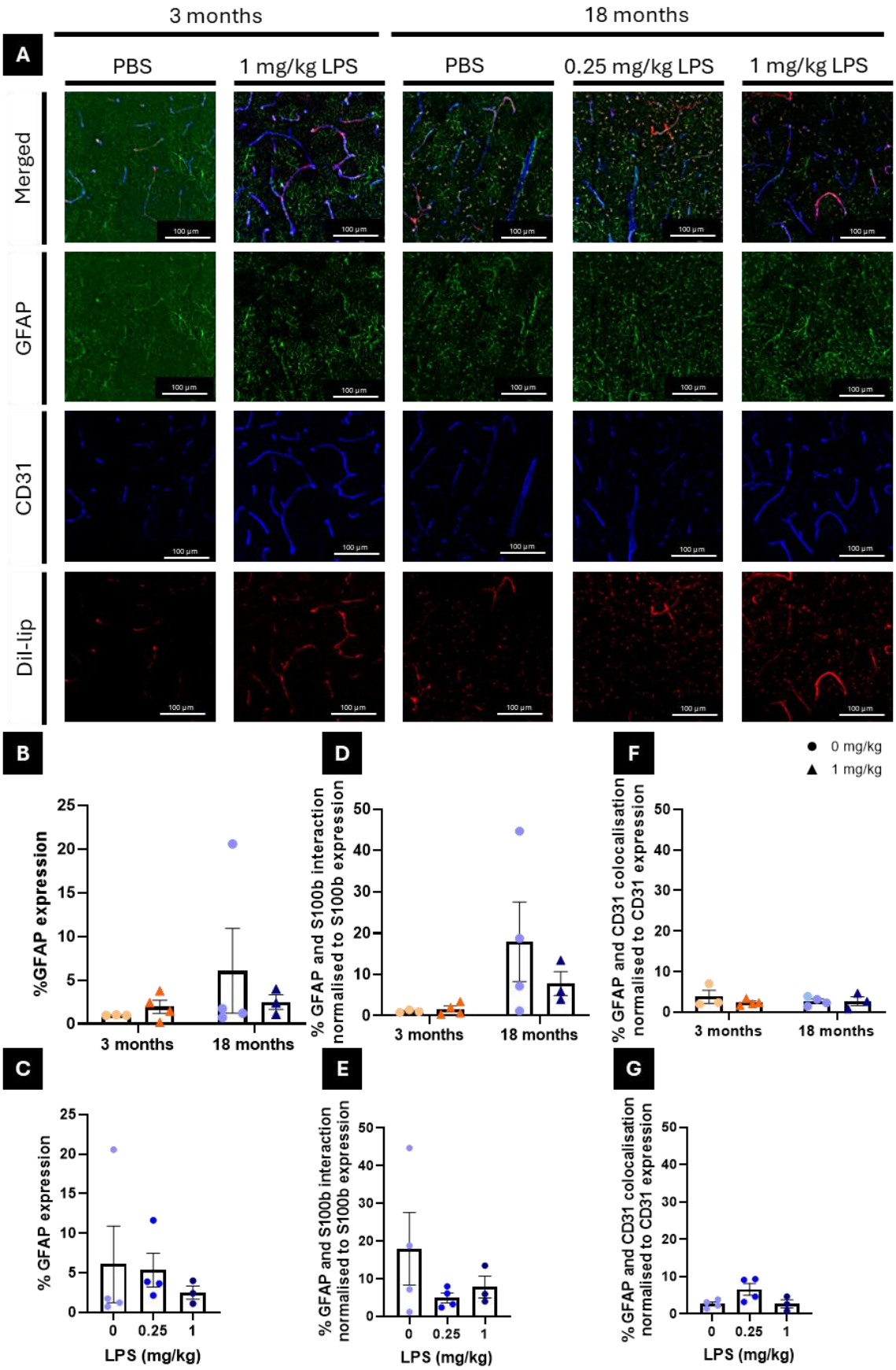

Figure 4-20: Evaluation of GFAP+ astrocyte expression transport in ageing and inflammation in auditory cortex region. C57BL/6 female mice groups were injected intraperitonially with a single dose of lipopolysaccharide. 3-month mice received either 1 mg/kg or PBS vehicle control whilst 18-month mice were given, 1 mg/kg, 0.25 mg/kg or PBS vehicle control. 48-hours post injection, all mice were intravenously injected with DiI-lip and cardiac perfusion was completed 2 hours post-injection

to remove circulating DiI-lip. (A) Representative immunofluorescence images of auditory cortex region -1.94mm from the bregma demonstrate expression of CD31 (blue), GFAP (green) and DiI-lip (Red). Quantitative analysis of GFAP expression with comparisons between ages (B) and analysis of 18-month LPS dose (C) Quantitative analysis of GFAP expression in 18-month LPS dose showed no significant changes. Quantification of GFAP and CD31 interaction between age groups (D) or 18-month LPS dose (E). Quantification of GFAP and DiI-lip interaction in comparison of age groups (F) or 18-month LPS dose (G). All analysis was produced no significant changes in expression or interaction. Images obtained at x40 magnification on Leica Thunder microscope and underwent large volume computational clearing prior to quantification in Image J. Statistical analysis was completed using GraphPad Prism software. For analysis of comparison of 1mgkg LPS dose in ageing, two-way analysis of variance was utilised followed by Tukey multiple comparison test. For 18-month LPS dose studies, one-way analysis of variance followed by Tukey's multiple comparison test after conducting Shapiro-Wilks normality test. N=3-4, average ± SEM, $p<0.05$ were considered significant.

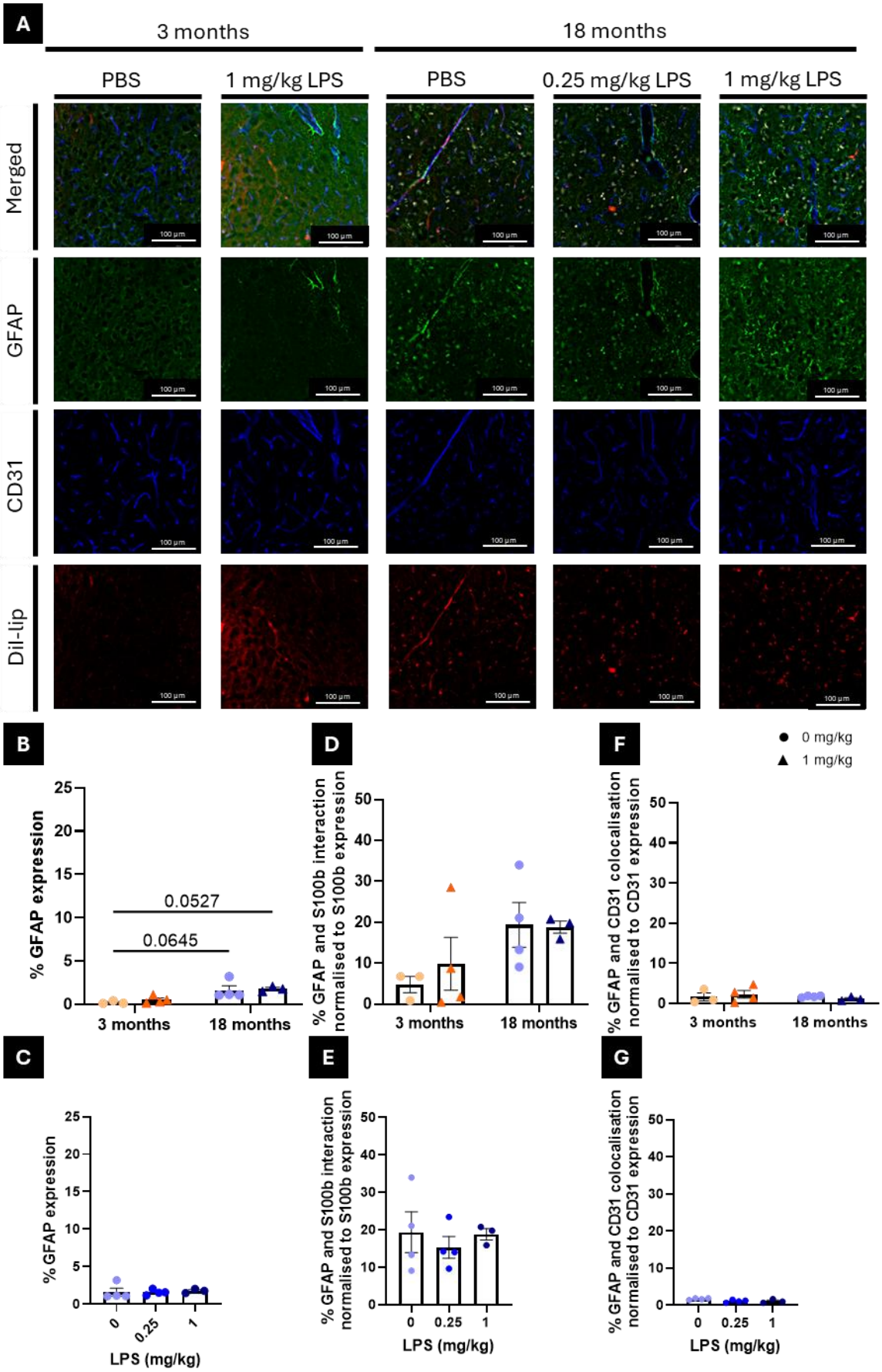

Figure 4-21: Evaluation of GFAP+ astrocyte expression transport in ageing and inflammation in striatum region. C57BL/6 female mice groups were injected intraperitonially with a single dose of lipopolysaccharide. 3-month mice received either 1 mg/kg or PBS vehicle control whilst 18-month mice were given, 1 mg/kg, 0.25 mg/kg or PBS vehicle control. 48-hours post injection, all mice were

intravenously injected with DiI-lip and cardiac perfusion was completed 2 hours post-injection to remove circulating DiI-lip. (A) Representative immunofluorescence images of striatum region -1.94mm from the bregma demonstrate expression CD31 (blue), GFAP (green) and DiI-lip (Red). Quantitative analysis of GFAP expression with comparisons between ages showed non-significant increases in GFAP expression in both 18-month groups in comparison to the 3-month vehicle control (B) and analysis of 18-month LPS dose which showed no significant changes (C) Quantitative analysis of GFAP expression in 18-month LPS dose showed no significant changes. Quantification of GFAP and CD31 interaction between age groups (D) or 18-month LPS dose (E). Quantification of GFAP and DiI-lip interaction in comparison of age groups (F) or 18-month LPS dose (G). All interaction analysis was produced no significant changes in expression or interaction. Images obtained at x40 magnification on Leica Thunder microscope and underwent large volume computational clearing prior to quantification in Image J. Statistical analysis was completed using GraphPad Prism software. For analysis of comparison of 1mgkg LPS dose in ageing, two-way analysis of variance was utilised followed by Tukey multiple comparison test. For 18-month LPS dose studies, one-way analysis of variance followed by Tukey's multiple comparison test after conducting Shapiro-Wilks normality test. N=3-4, average ± SEM, $p<0.05$ were considered significant.

systemic inflammation may play a role in astrocyte activation but not migration from the BBB or interaction with nanoparticles.

5.4.6.2. Microglial changes in age and LPS conditions

Microglial activation is a hallmark of neuroinflammation and so the expression of microglia marker, Iba-1 was examined in relation to expression and interaction with BBB (CD31) and nanoparticles (DiI-lip) (fig. 4-22-4-27). Within the CA1 region, significant increases in Iba-1 expression were observed between the 3-month vehicle and LPS group (age $F=0.455_{(1,11)}$, LPS $F=6.316_{(1,11)}$, p= 0.0312) but not within the age group or between different doses of LPS in 18-month cohort (fig. 4-22b-c). Expression of Iba-1 was not changed either when examining the effects of LPS and age or dose of LPS in the 18-month group in CA3 (fig. 4-23, b-c), motor cortex (fig. 4-25b-c), dentate gyrus (fig, 4-24b-c), auditory cortex (fig. 4-26b-c) or striatum (fig. 4-27b-c). Qualitative assessment shows that in all regions there were changes in microglial morphology, with an increased ameboid morphology (Fig. 4-22-4-27 a).

No significant changes to Iba-1 and CD31 interaction were observed in all analysed regions demonstrating no age or LPS dose effects on microglial migration (fig. 4-22-4-27d-e). The auditory cortex showed a significant increase in DiI-lip and Iba-1 interaction between the 3-month vehicle and LPS groups (age $F=0.456_{(1,9)}$, LPS $F=12.39_{(1,9)}$, p= 0.0280) with no significant increases to the 18-month LPS group (p= 0.0728) (fig. 26f). No other region demonstrated changes to the DiI-lip and Iba-1 interaction either when comparing age or LPS dose (fig. 4-22-,4-25, 4-27 f-g).

5.4.6.3. Adhesion molecule changes in age and LPS conditions

Adhesion molecules are also expressed during neuroinflammatory responses, so ICAM-1 was investigated via immunofluorescence. Quantification of the CA1 region (age $F=8.156_{(1,11)}$, LPS $F=5.805_{(1,11)}$) demonstrated significant increases of ICAM-1 expression in the 18-month 1 mg/kg group compared to the 3-month vehicle (p= 0.0043), 3-month LPS (p= 0.0032) and 18-month vehicle (p= 0.0054) (fig. 4-28a). The effect of LPS dose on 18-month mice demonstrated similar

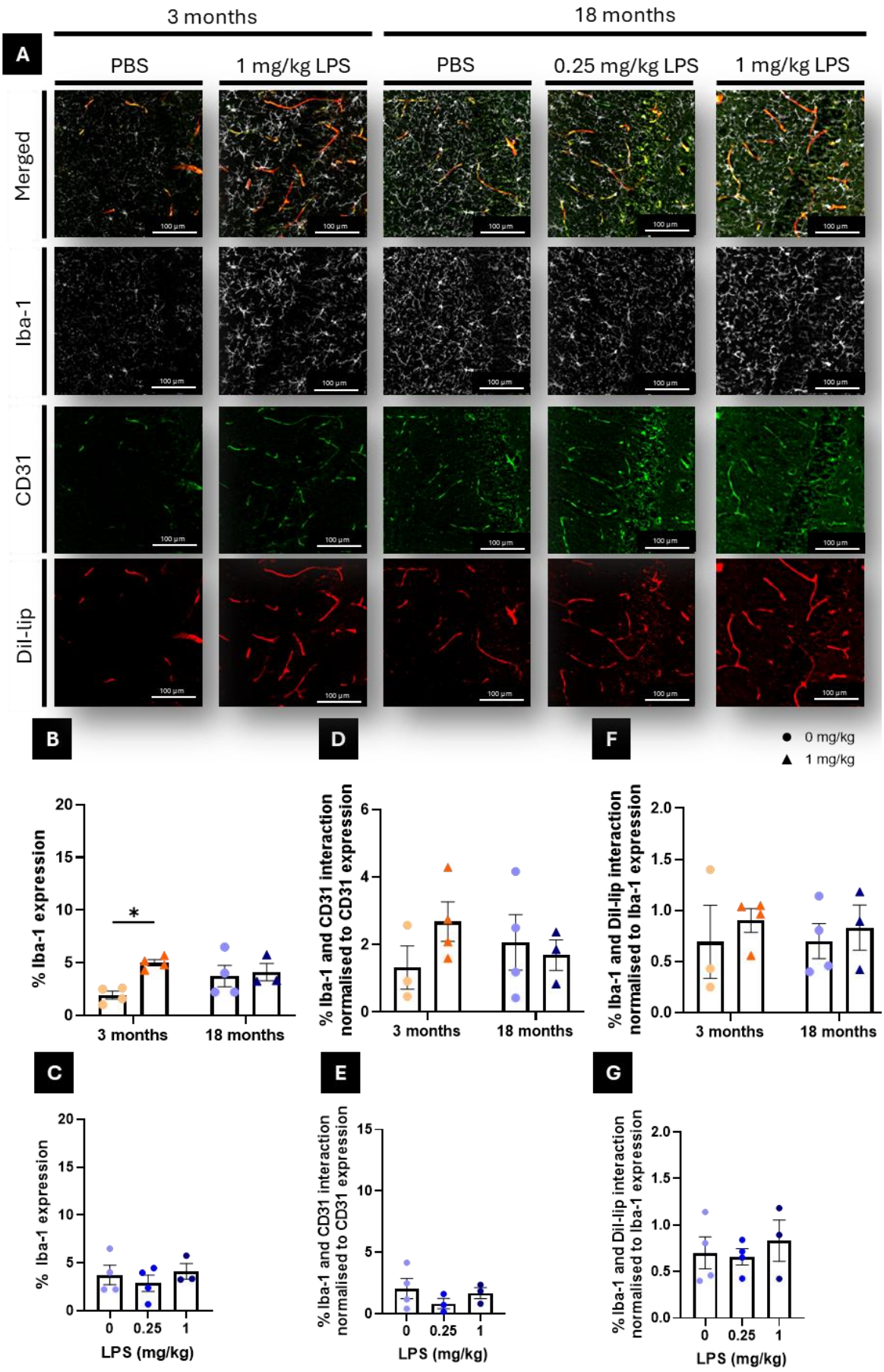

Figure 4-22: Evaluation of Iba-1+ microglial expression transport in ageing and inflammation in CA1 region. C57BL/6 female mice groups were injected intraperitonially with a single dose of lipopolysaccharide. 3-month mice received either 1 mg/kg or PBS vehicle control whilst 18-month

mice were given, 1 mg/kg, 0.25 mg/kg or PBS vehicle control. 48-hours post injection, all mice were intravenously injected with DiI-lip and cardiac perfusion was completed 2 hours post-injection to remove circulating DiI-lip. (A) Representative immunofluorescence images of CA1 region -1.94mm from the bregma demonstrate expression of CD31 (green), Iba-1 (white) and DiI-lip (Red). (B) Quantitative analysis of Iba-1 expression with comparisons between ages showing significant increased between 3-month vehicle and 1 mg/kg LPS dose. (C) Quantitative analysis shows no significant changes of 18-month LPS dose which showed no significant changes (C) Quantitative analysis of Iba-1 expression in 18-month LPS dose showed no significant changes. Quantification of Iba-1 and CD31 interaction between age groups (D) or 18-month LPS dose (E). Quantification of Iba-1 and DiI-lip interaction in comparison of age groups (F) or 18-month LPS dose (G). All interaction analysis was produced no significant changes in expression or interaction. Images obtained at x40 magnification on Leica Thunder microscope and underwent large volume computational clearing prior to quantification in Image J. Statistical analysis was completed using GraphPad Prism software. For analysis of comparison of 1mgkg LPS dose in ageing, two-way analysis of variance was utilised followed by Tukey multiple comparison test. For 18-month LPS dose studies, one-way analysis of variance followed by Tukey's multiple comparison test after conducting Shapiro-Wilks normality test. N=3-4, average ± SEM, $p<0.05$ were considered significant.

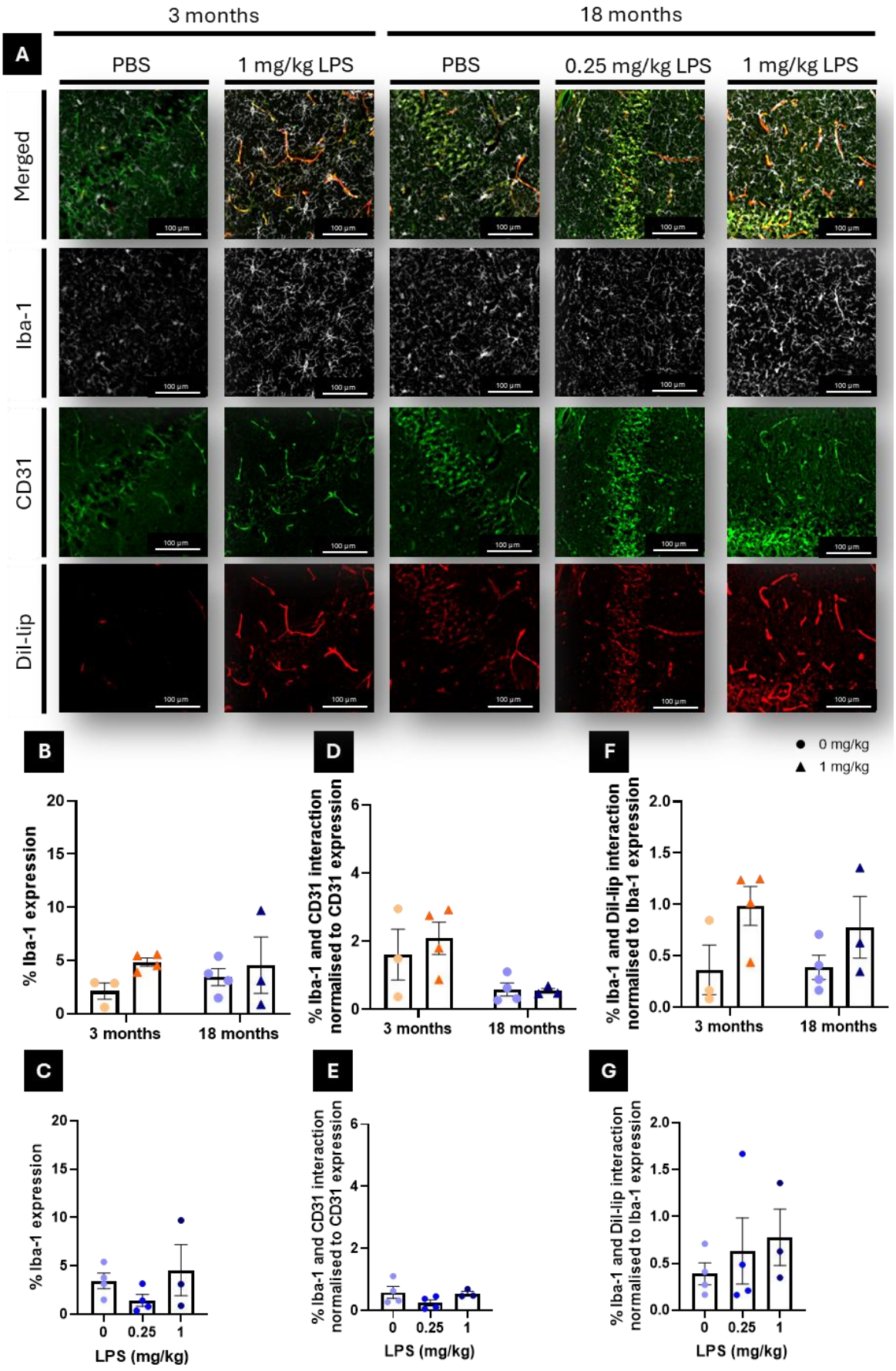

Figure 4-23: Evaluation of Iba-1+ microglial expression transport in ageing and inflammation in CA3 region. C57BL/6 female mice groups were injected intraperitonially with a single dose of lipopolysaccharide. 3-month mice received either 1 mg/kg or PBS vehicle control whilst 18-month mice were given, 1 mg/kg, 0.25 mg/kg or PBS vehicle control. 48-hours post injection, all mice were

intravenously injected with DiI-lip and cardiac perfusion was completed 2 hours post-injection to remove circulating DiI-lip. (A) Representative immunofluorescence images of CA3 region -1.94mm from the bregma demonstrate expression of CD31 (green), Iba-1 (white) and DiI-lip (Red). (B) Quantitative analysis of Iba-1 expression with comparisons between ages showed no significant changes. (C) Quantitative analysis shows no significant changes of 18-month LPS dose which showed no significant changes (C) Quantitative analysis of Iba-1 expression in 18-month LPS dose showed no significant changes. Quantification of Iba-1 and CD31 interaction between age groups (D) or 18-month LPS dose (E). Quantification of Iba-1 and DiI-lip interaction in comparison of age groups (F) or 18-month LPS dose (G). All interaction analysis was produced no significant changes in expression or interaction. Images obtained at x40 magnification on Leica Thunder microscope and underwent large volume computational clearing prior to quantification in Image J. Statistical analysis was completed using GraphPad Prism software. For analysis of comparison of 1mgkg LPS dose in ageing, two-way analysis of variance was utilised followed by Tukey multiple comparison test. For 18-month LPS dose studies, one-way analysis of variance followed by Tukey's multiple comparison test after conducting Shapiro-Wilks normality test. N=3-4, average ± SEM, $p<0.05$ were considered significant.

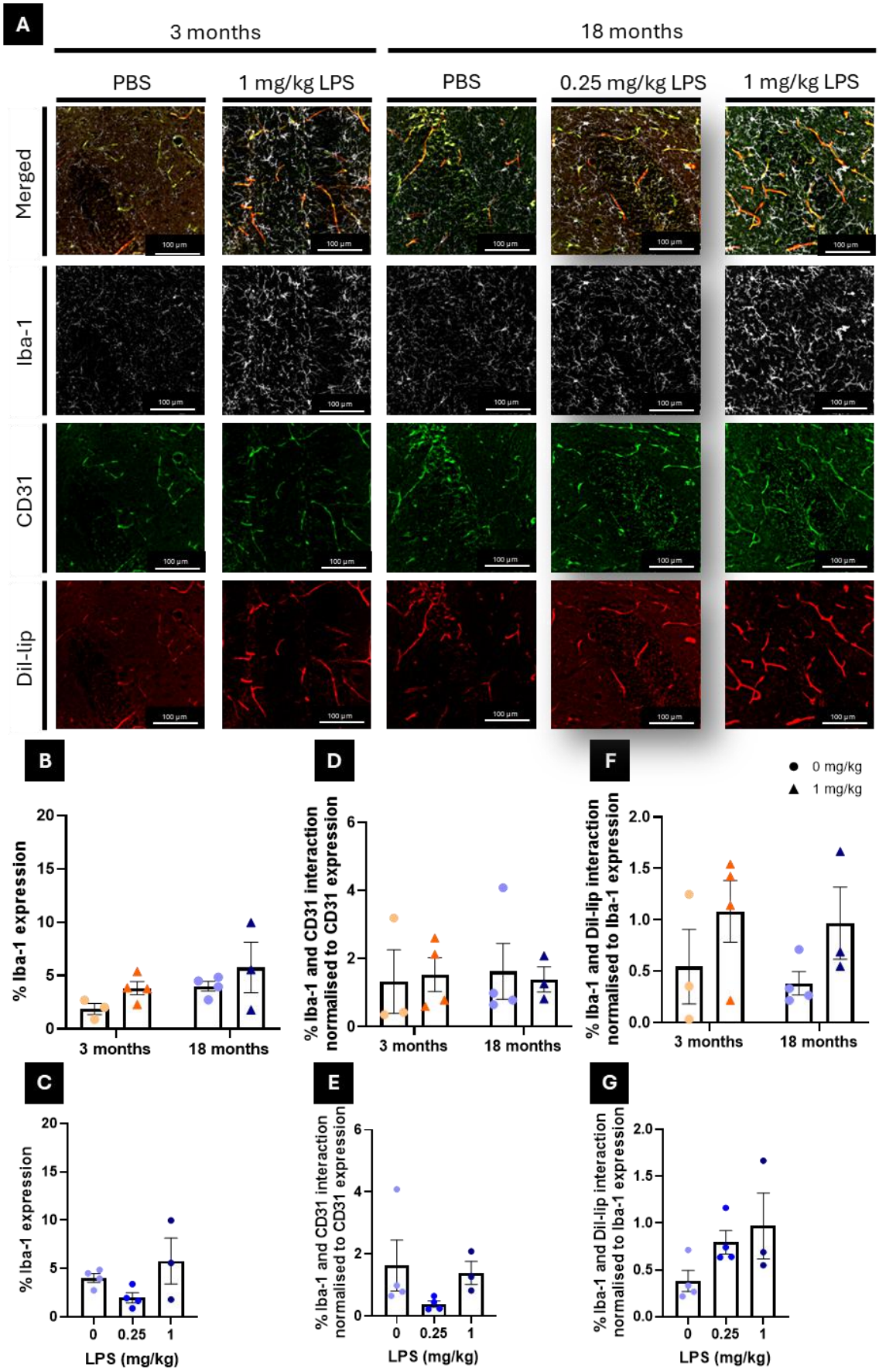

Figure 4-24: Evaluation of Iba-1+ microglial expression transport in ageing and inflammation in dentate gyrus region. C57BL/6 female mice groups were injected intraperitonially a single dose of lipopolysaccharide. 3-month mice received either 1 mg/kg or PBS vehicle control whilst 18-month mice were given, 1 mg/kg, 0.25 mg/kg or PBS vehicle control. 48-hours post injection, all mice were

intravenously injected with DiI-lip and cardiac perfusion was completed 2 hours post-injection to remove circulating DiI-lip. (A) Representative immunofluorescence images of dentate gyrus region -1.94mm from the bregma demonstrate expression of CD31 (green), Iba-1 (white) and DiI-lip (Red). (B) Quantitative analysis of Iba-1 expression with comparisons between ages showed no significant changes. (C) Quantitative analysis shows no significant changes of 18-month LPS dose which showed no significant changes (C) Quantitative analysis of Iba-1 expression in 18-month LPS dose showed no significant changes. Quantification of Iba-1 and CD31 interaction between age groups (D) or 18-month LPS dose (E). Quantification of Iba-1 and DiI-lip interaction in comparison of age groups (F) or 18-month LPS dose (G). All interaction analysis was produced no significant changes in expression or interaction. Images obtained at x40 magnification on Leica Thunder microscope and underwent large volume computational clearing prior to quantification in Image J. Statistical analysis was completed using GraphPad Prism software. For analysis of comparison of 1mgkg LPS dose in ageing, two-way analysis of variance was utilised followed by Tukey multiple comparison test. For 18-month LPS dose studies, one-way analysis of variance followed by Tukey's multiple comparison test after conducting Shapiro-Wilks normality test. N=3-4, average ± SEM, $p<0.05$ were considered significant.

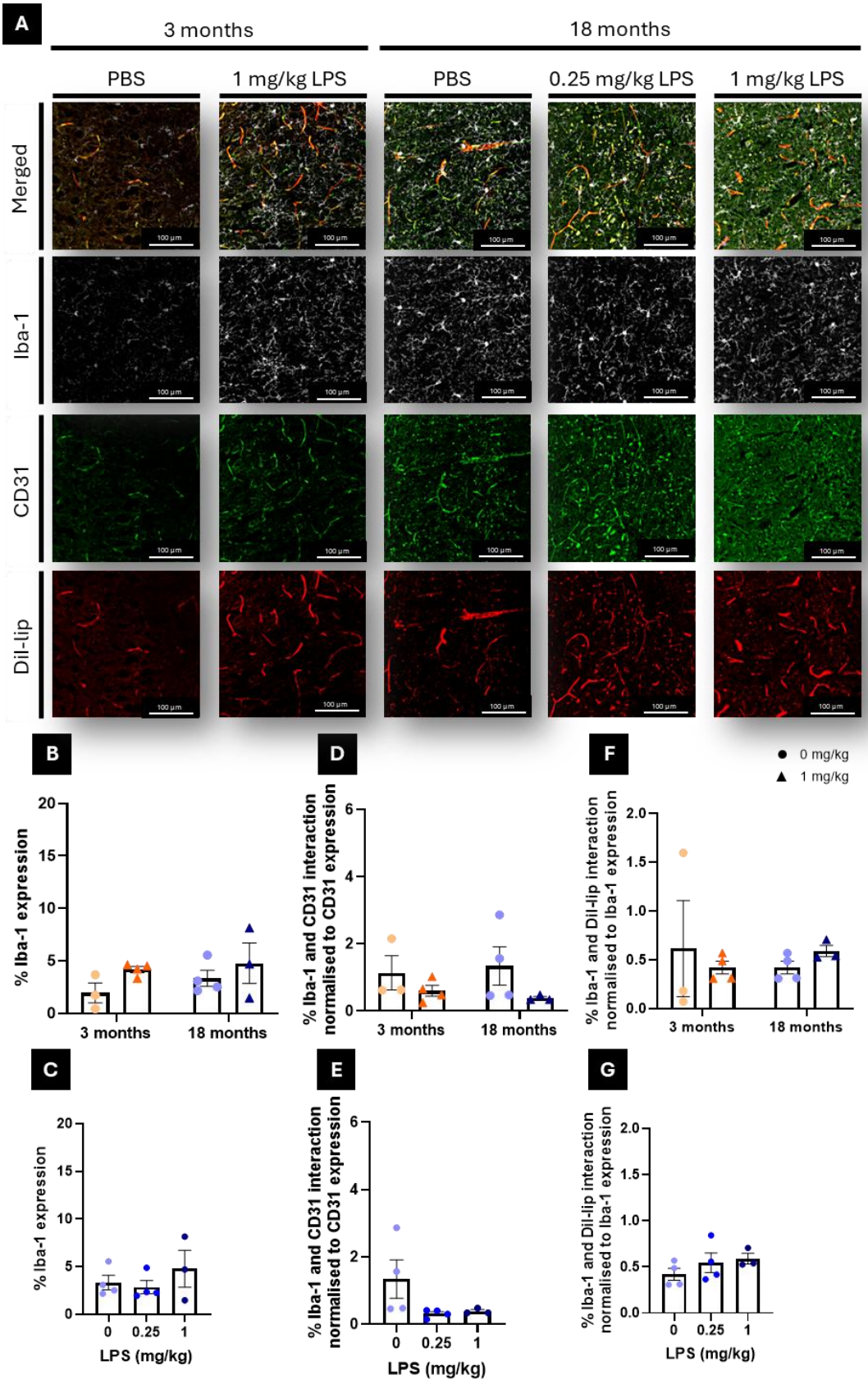

Figure 4-25: Evaluation of Iba-1+ microglial expression transport in ageing and inflammation in motor cortex region. C57BL/6 female mice groups were injected intraperitonially with a single dose of lipopolysaccharide. 3-month mice received either 1 mg/kg or PBS vehicle control whilst 18-month mice were given, 1 mg/kg, 0.25 mg/kg or PBS vehicle control. 48-hours post injection, all mice were intravenously injected with DiI-lip and cardiac perfusion was completed 2 hours post-injection to remove circulating DiI-lip. (A) Representative immunofluorescence images of motor cortex region -1.94mm from the bregma demonstrate expression of CD31 (green), Iba-1 (white) and DiI-lip (Red). (B)

Quantitative analysis of Iba-1 expression with comparisons between ages showed no significant changes. (C) Quantitative analysis shows no significant changes of 18-month LPS dose which showed no significant changes (C) Quantitative analysis of Iba-1 expression in 18-month LPS dose showed no significant changes. Quantification of Iba-1 and CD31 interaction between age groups (D) or 18-month LPS dose (E). Quantification of Iba-1 and DiI-lip interaction in comparison of age groups (F) or 18-month LPS dose (G). All interaction analysis was produced no significant changes in expression or interaction. Images obtained at x40 magnification on Leica Thunder microscope and underwent large volume computational clearing prior to quantification in Image J. Statistical analysis was completed using GraphPad Prism software. For analysis of comparison of 1mgkg LPS dose in ageing, two-way analysis of variance was utilised followed by Tukey multiple comparison test. For 18-month LPS dose studies, one-way analysis of variance followed by Tukey's multiple comparison test after conducting Shapiro-Wilks normality test. N=3-4, average ± SEM, $p<0.05$ were considered significant.

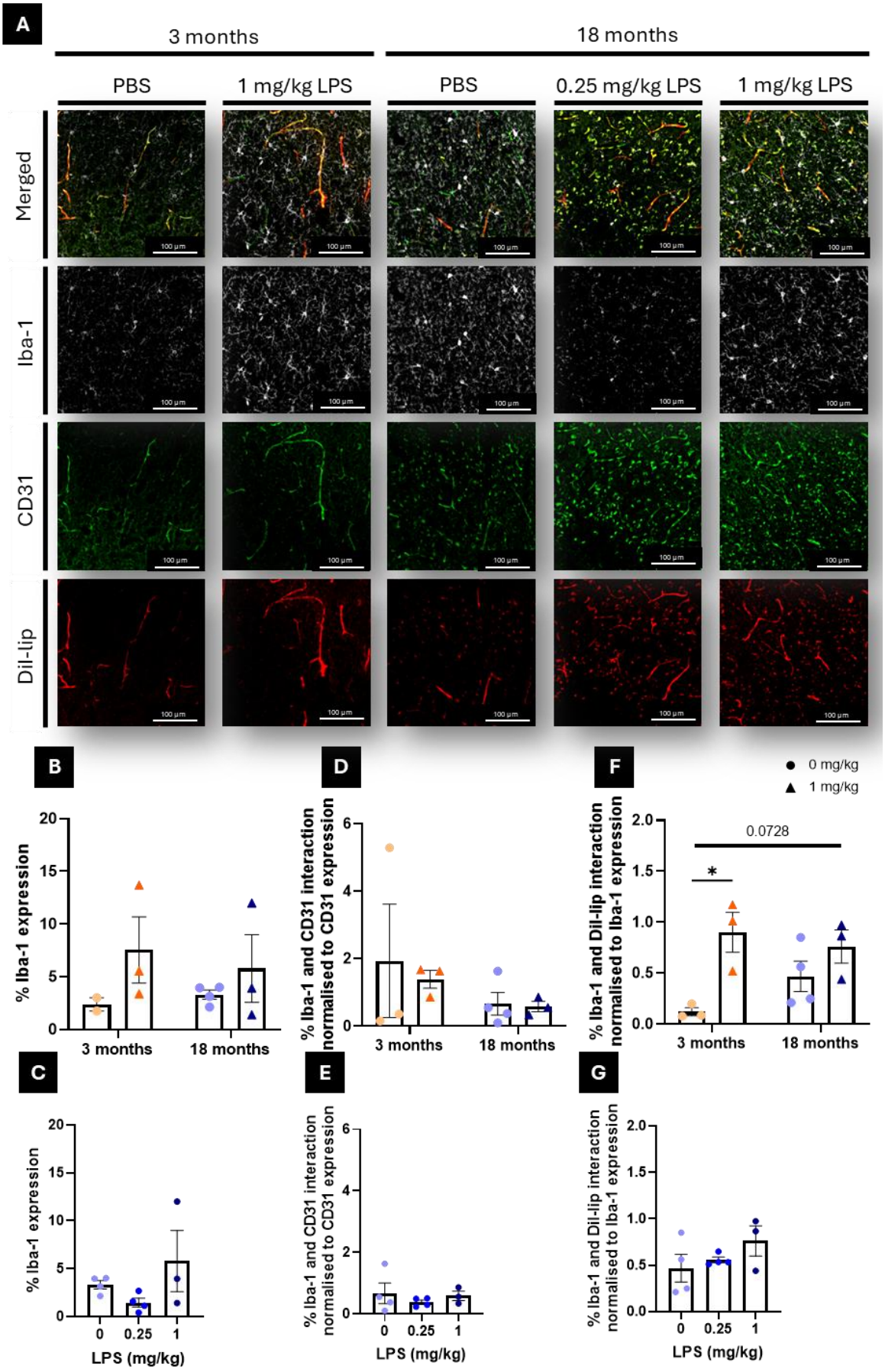

Figure 4-26: Evaluation of Iba-1+ microglial expression transport in ageing and inflammation in auditory cortex region. C57BL/6 female mice groups were injected intraperitonially a with single dose of lipopolysaccharide. 3-month mice received either 1 mg/kg or PBS vehicle control whilst 18-month mice were given, 1 mg/kg, 0.25 mg/kg or PBS vehicle control. 48-hours post injection, all mice

were intravenously injected with DiI-lip and cardiac perfusion was completed 2 hours post-injection to remove circulating DiI-lip. (A) Representative immunofluorescence images of auditory cortex region -1.94mm from the bregma demonstrate expression of CD31 (green), Iba-1 (white) and DiI-lip (Red). (B) Quantitative analysis of Iba-1 expression with comparisons between ages showed no significant changes. (C) Quantitative analysis shows no significant changes of 18-month LPS dose which showed no significant changes (C) Quantitative analysis of Iba-1 expression in 18-month LPS dose showed no significant changes. Quantification of Iba-1 and CD31 interaction between age groups (D) or 18-month LPS dose (E). All CD31 and Iba-1 interaction analysis was produced no significant changes. Quantification of Iba-1 and DiI-lip interaction in comparison of age groups displayed significant increases in interaction between 3-month vehicle and LPS group (F) or 18-month LPS dose, which showed no significant changes (G). All interaction analysis was produced no significant changes in expression or interaction. Images obtained at x40 magnification on Leica Thunder microscope and underwent large volume computational clearing prior to quantification in Image J. Statistical analysis was completed using GraphPad Prism software. For analysis of comparison of 1mgkg LPS dose in ageing, two-way analysis of variance was utilised followed by Tukey multiple comparison test. For 18-month LPS dose studies, one-way analysis of variance followed by Tukey's multiple comparison test after conducting Shapiro-Wilks normality test. N=3-4, average ± SEM, $p<0.05$ were considered significant.

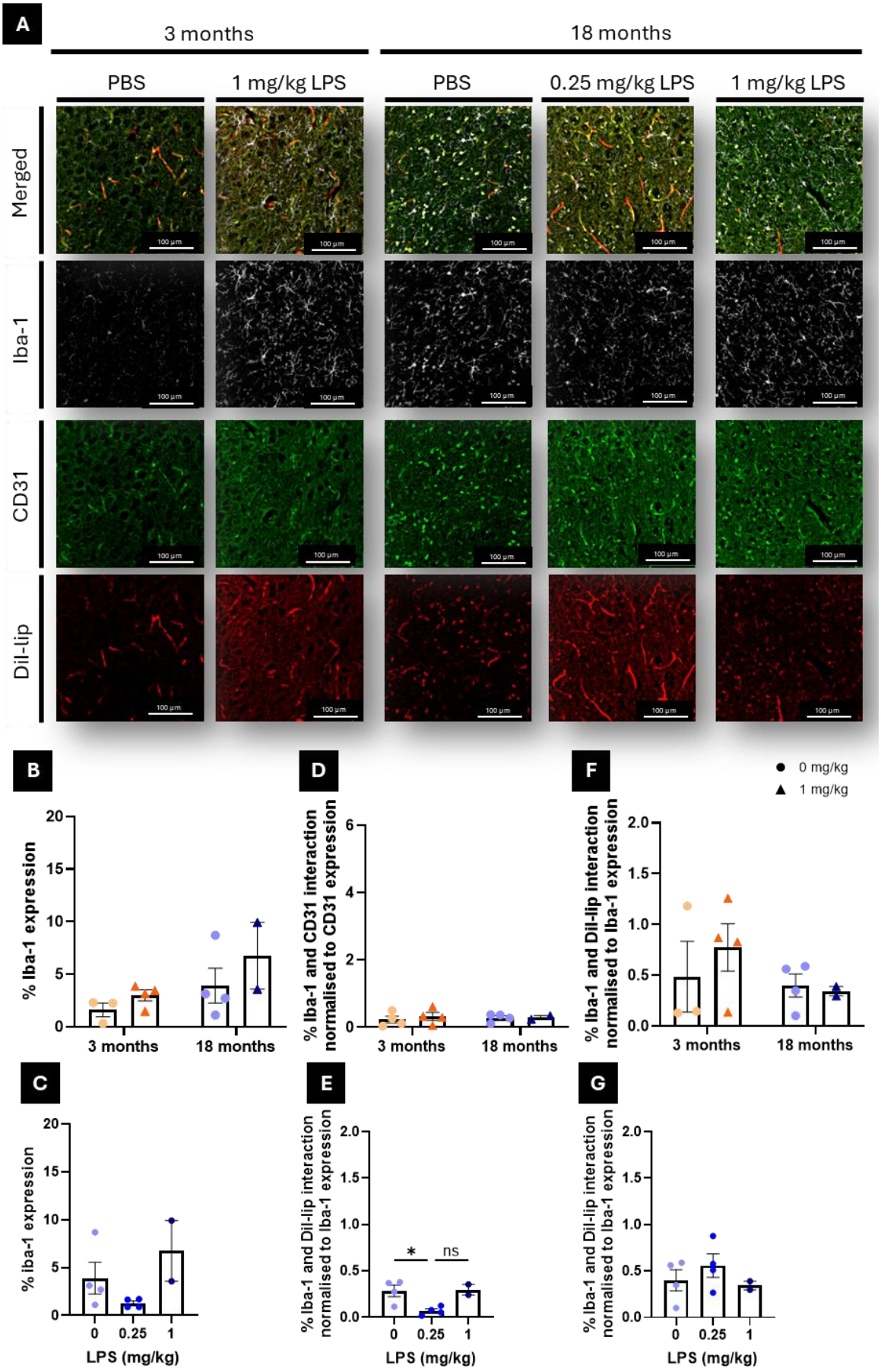

Figure 4-27: Evaluation of Iba-1+ microglial expression transport in ageing and inflammation in striatum region. C57BL/6 female mice groups were injected intraperitonially with a single dose of lipopolysaccharide. 3-month mice received either 1 mg/kg or PBS vehicle control whilst 18-month

mice were given, 1 mg/kg, 0.25 mg/kg or PBS vehicle control. 48-hours post injection, all mice were intravenously injected with DiI-lip and cardiac perfusion was completed 2 hours post-injection to remove circulating DiI-lip. (A) Representative immunofluorescence images of striatum region -1.94 mm from the bregma demonstrate expression of CD31 (green), Iba-1 (white) and DiI-lip (Red). (B) Quantitative analysis of Iba-1 expression with comparisons between ages showed no significant changes. (C) Quantitative analysis shows no significant changes of 18-month LPS dose which showed no significant changes (C) Quantitative analysis of Iba-1 expression in 18-month LPS dose showed no significant changes. Quantification of Iba-1 and CD31 interaction between age groups (D) or 18-month LPS dose (E). All CD31 and Iba-1 interaction analysis was produced no significant changes. Quantification of Iba-1 and DiI-lip interaction in comparison of age groups displayed significant increases in interaction between 3-month vehicle and LPS group (F) or 18-month LPS dose, which showed no significant changes (G). All interaction analysis was produced no significant changes in expression or interaction. Images obtained at x40 magnification on Leica Thunder microscope and underwent large volume computational clearing prior to quantification in Image J. Statistical analysis was completed using GraphPad Prism software. For analysis of comparison of 1mgkg LPS dose in ageing, two-way analysis of variance was utilised followed by Tukey multiple comparison test. For 18-month LPS dose studies, one-way analysis of variance followed by Tukey's multiple comparison test after conducting Shapiro-Wilks normality test. N=3-4, average ± SEM, $p<0.05$ were considered significant.

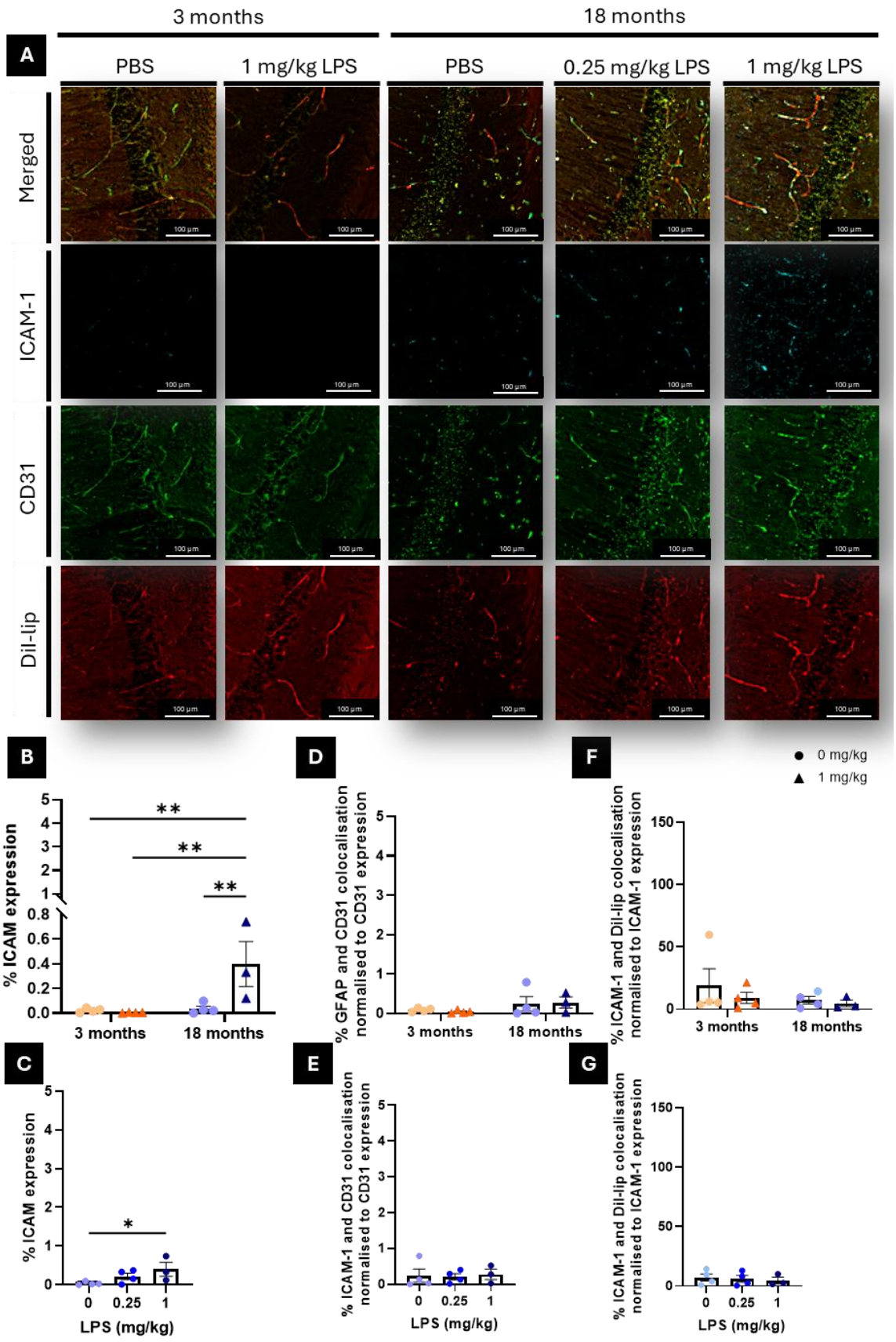

Figure 4-28: Effect of ageing and inflammation on ICAM-1 expression in CA1 region. Female C57BL/6 mice at either 3- or 18- months were intraperitoneally injected with either 0.25 mg/kg, 1 mg/kg or 0 mg/kg vehicle control 48 hours prior to intravenous injection with DiI-lip. 2-hours post I.V injection mice were culled with cardiac perfusion to removed excess DiI-lip. (A) Representative images of CA1 region -1.94mm from the bregma demonstrate expression of ICAM-1 (cyan), CD31 (green) and DiI-lip (Red). ICAM-1 expression quantification significantly increased from young to aged

mice (A) and between no LPS and high LPS doses in 18-month mice (C). Quantification of CD31 and ICAM-1 interaction demonstrated no significant changes in ageing or LPS dosage (D-E). Quantitative analysis of DiI-lip and ICAM-1 interaction displaying no changes in either ageing or LPS doses (F-G). Images obtained at x40 magnification on Leica Thunder microscope and underwent large volume computational clearing (LVCC) prior to quantification in Image J. Statistical analysis was completed using GraphPad Prism software using Shapiro Wilk test for normality. This proceeded either a using one-way analysis of variance followed by Tukey multiple comparison test or Kruskal-Wallis test followed by Dunn's multiple comparisons for comparisons of LPS dose in aged mice. To compare young and aged mice for LPS; two-way analysis of variance followed by Tukey's multiple comparison test. N=3-4, average ± SEM, $p<0.05$ were considered significant. Scale bar represents 100µm.

increasing ICAM-1 trends from vehicle to 1 mg/kg LPS ($F=4.698_{(4,14)}$, p= 0.0130) but no significant changes between the 0.25 mg/kg and 1 mg/kg group (fig.4-28c). Similar expression patterns were observed throughout the regions analysed with ICAM-1 expression significantly upregulated in 1 mg/kg LPS from 3-month vehicle in dentate gyrus (age $F(1,11) =8.091_{(1,11)}$, LPS $F=5.692_{(1,11)}$ p= 0.0062), motor cortex (age $F(1,11) =12.02_{(1,11)}$, LPS $F(1,11) =10.22_{(1,11)}$, p= 0.040), auditory cortex (age $F(1,11) =19.28_{(1,11)}$, LPS $F=7.78_{(1,11)}$, p=0.0043) and striatum (age $F(1,11) =11.02_{(1,11)}$, LPS $F(1,11) =3.812_{(1,11)}$, p=0.0189) (Fig. 4-29-4-33b). Significant ICAM-1 increases were also observed from the 3-month 1 mg/kg LPS and 18-month vehicle to the 18-month 1 mg/kg LPS (p=<0.0463) in all above regions. In the CA3 region (fig. 4-29b), a non-significant increasing trend was observed between the 3-month and 18-month LPS groups (age $F=7.375_{(1,11)}$, LPS $F=0.300_{(1,11)}$, p= 0.0884). This indicated that ICAM-1 within the brain required both age and systemic inflammation to be highly expressed.

Interaction between Iba-1 and CD31 or DiI-lip was investigated to observe in ICAM-1 was associated with the BBB or liposomal infiltration. Throughout all regions, no changes were observed when comparing interactions of 3- and 18-month mice either with or without LPS stimulation (fig. 4-28-4-33 d, f) or looking at the effects of a lower (0.25 mg/kg) dose of LPS (fig. 4-28-4-33 e, g).

4.4.7. Inflammatory profile changes

To further characterise the inflammatory response within the aged systemic inflammation mouse model, ELISA for adhesion molecules ICAM-1 and VCAM-1 and cytokines IL-6 and IL-1β were performed in brain tissue homogenate and peripheral serum samples. ICAM-1 expression was shown in terminal brain samples to be significantly increased in both LPS and not ageing (fig. 4-34 a). Significant increases were shown between vehicle and 1 mg/kg LPS in 3-months (age $F=5.674_{(1,11)}$, LPS $F=154.2_{(1,11)}$, p=<0.0001) and 18-months (age $F=5.674_{(1,11)}$, LPS $F=154.2_{(1,11)}$,p=<0.0001) as well as between age; 3-month vehicle was significantly lower than 18-month LPS (age $F=5.674_{(1,11)}$, LPS $=154.2_{(1,11)}$,p=<0.0001) and vice versa (age $F=5.674_{(1,11)}$, LPS $=154.2_{(1,11)}$,p=<0.0001). This was also reflected in the comparison between aged LPS

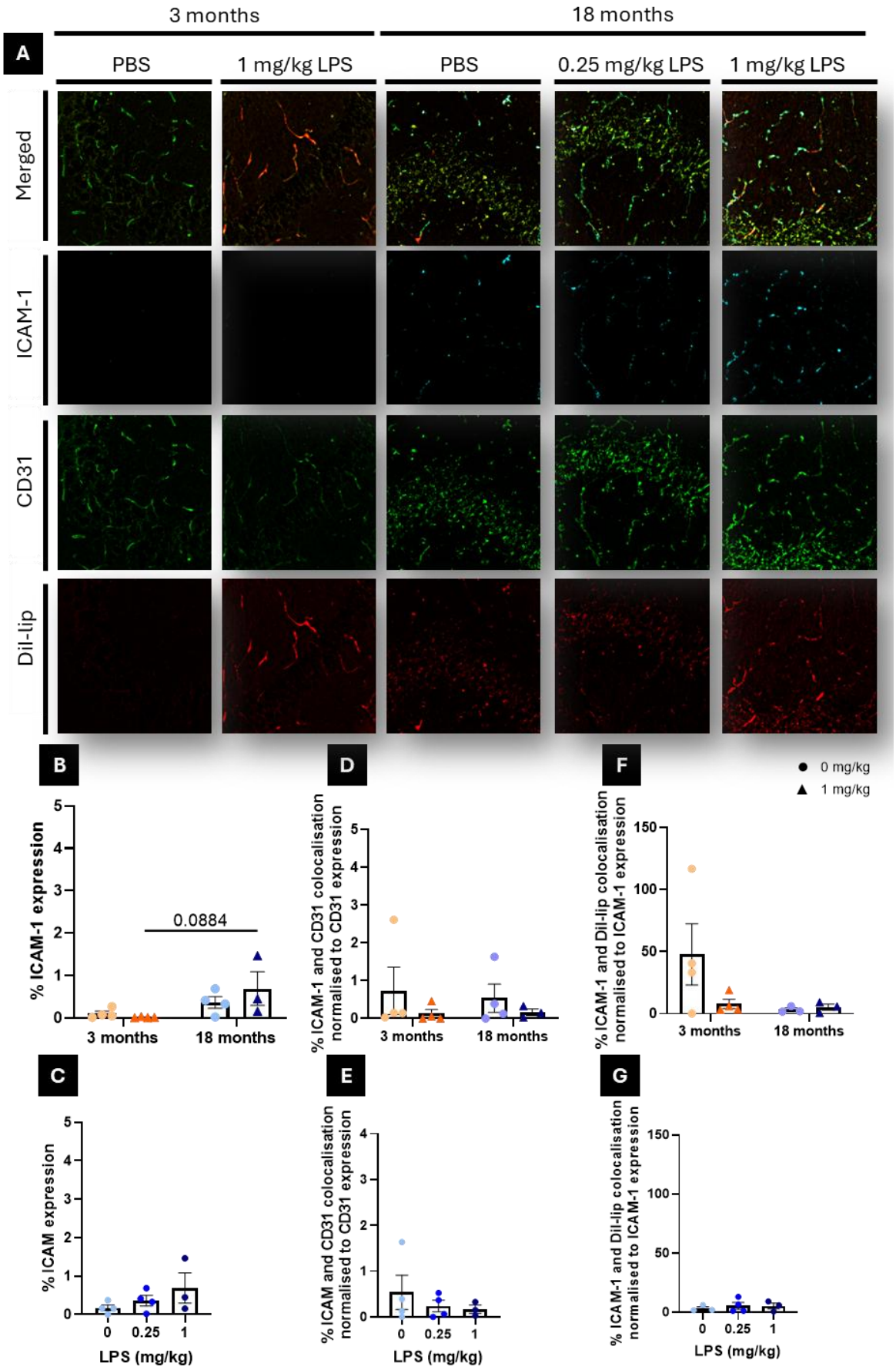

Figure 4-29: Effect of ageing and inflammation on ICAM-1 expression in CA3 region. Female C57BL/6 mice at either 3- or 18- months were intraperitoneally injected with either 0.25 mg/kg, 1 mg/kg or 0 mg/kg vehicle control 48 hours prior to intravenous injection with DiI-lip. 2-hours post I.V

injection mice were culled with cardiac perfusion to removed excess DiI-lip. (A) Representative images of CA3 region -1.94mm from the bregma demonstrate expression of ICAM-1 (cyan), CD31 (green) and DiI-lip (Red). (B) Quantitative analysis of ICAM-1 expression between 3- and 18- month groups displayed a non-significant increase in expression between 3-month and 18-months at 1 mg/kg LPS. (C) No significant changes in the ICAM-1 expression from quantitative analysis of 18-month LPS doses. Quantification of CD31 and ICAM-1 interaction demonstrated no significant changes in ageing or LPS dosage (D-E). Quantitative analysis of DiI-lip and ICAM-1 interaction displaying no changes in either ageing or LPS doses (F-G). Images obtained at x40 magnification on Leica Thunder microscope and underwent large volume computational clearing (LVCC) prior to quantification in Image J. Statistical analysis was completed using GraphPad Prism software using Shapiro Wilk test for normality. This proceeded either a using one-way analysis of variance followed by Tukey multiple comparison test or Kruskal-Wallis test followed by Dunn's multiple comparisons for comparisons of LPS dose in aged mice. To compare young and aged mice for LPS; 2-way analysis of variance followed by Tukey's multiple comparison test. N=3-4, average ± SEM, $p<0.05$ were considered significant. Scale bar represents 100µm.

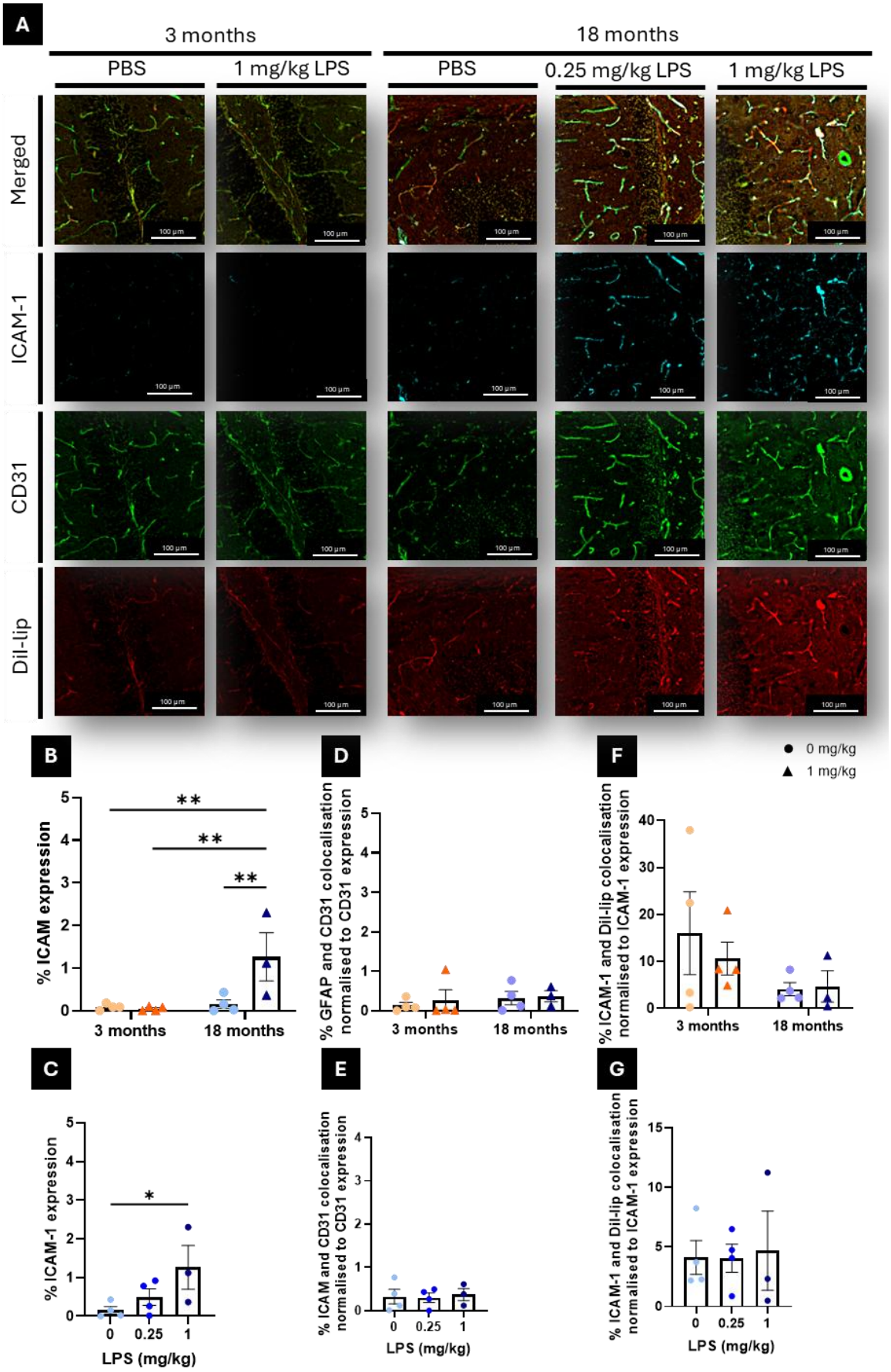

Figure 4-30: Effect of ageing and inflammation on ICAM-1 expression in dentate gyrus region. Female C57BL/6 mice at either 3- or 18- months were intraperitoneally injected with either 0.25 mg/kg, 1 mg/kg or 0 mg/kg vehicle control 48 hours prior to intravenous injection with DiI-lip. 2-hours post I.V injection mice were culled with cardiac perfusion to removed excess DiI-lip. (A)

Representative images of dentate gyrus region -1.94mm from the bregma demonstrate expression of ICAM-1 (cyan), CD31 (green) and DiI-lip (Red). (B) Quantitative analysis of ICAM-1 expression between 3- and 18- month groups displayed a significant increased from 3-month vehicle, 1 mg/kg LPS and 18-month vehicle to 18-month 1 mg/kg LPS. (C) Significant increase in ICAM-1 observed between 18-month vehicle and 18-month 1 mg/kg LPS Quantification of CD31 and ICAM-1 interaction demonstrated no significant changes in ageing or LPS dosage (D-E). Quantitative analysis of DiI-lip and ICAM-1 interaction displaying no changes in either ageing or LPS doses (F-G). Images obtained at x40 magnification on Leica Thunder microscope and underwent large volume computational clearing (LVCC) prior to quantification in Image J. Statistical analysis was completed using GraphPad Prism software using Shapiro Wilk test for normality. This proceeded either a using one-way analysis of variance followed by Tukey multiple comparison test or Kruskal-Wallis test followed by Dunn's multiple comparisons for comparisons of LPS dose in aged mice. To compare young and aged mice for LPS effects; two-way analysis of variance followed by Tukey's multiple comparison test. N=3-4, average ± SEM, $p<0.05$ were considered significant. Scale bar represents 100µm.

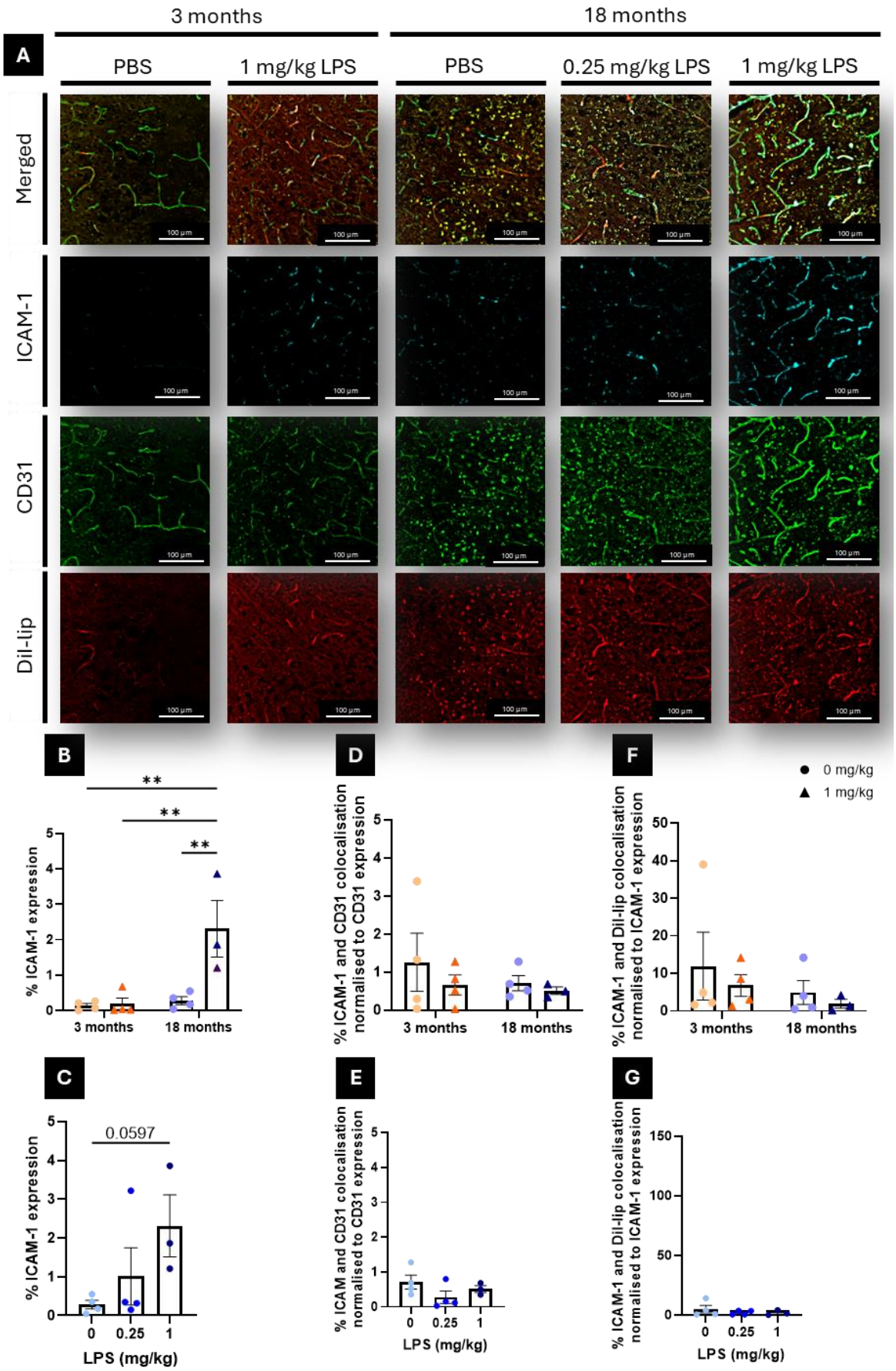

Figure 4-31: Effect of ageing and inflammation on ICAM-1 expression in motor cortex region. Female C57BL/6 mice at either 3- or 18- months were intraperitoneally injected with either 0.25 mg/kg, 1 mg/kg or 0 mg/kg vehicle control 48 hours prior to intravenous injection with DiI-lip. 2-hours post I.V injection mice were culled with cardiac perfusion to removed excess DiI-lip. (A)

Representative images of motor cortex region -1.94mm from the bregma demonstrate expression of ICAM-1 (cyan), CD31 (green) and DiI-lip (Red). (B) Quantitative analysis of ICAM-1 expression between 3- and 18- month groups displayed a significant increased from 3-month vehicle, 1 mg/kg LPS and 18-month vehicle to 18-month 1 mg/kg LPS. (C) Non-significant increase in ICAM-1 observed between 18-month vehicle and 18-month 1 mg/kg LPS Quantification of CD31 and ICAM-1 interaction demonstrated no significant changes in ageing or LPS dosage (D-E). Quantitative analysis of DiI-lip and ICAM-1 interaction displaying no changes in either ageing or LPS doses (F-G). Images obtained at x40 magnification on Leica Thunder microscope and underwent large volume computational clearing (LVCC) prior to quantification in Image J. Statistical analysis was completed using GraphPad Prism software using Shapiro Wilk test for normality. This proceeded either a using one-way analysis of variance followed by Tukey multiple comparison test or Kruskal-Wallis test followed by Dunn's multiple comparisons for comparisons of LPS dose in aged mice. To compare young and aged mice for LPS effects; two-way analysis of variance followed by Tukey's multiple comparison test. N=3-4, average ± SEM, $p<0.05$ were considered significant. Scale bar represents 100µm.

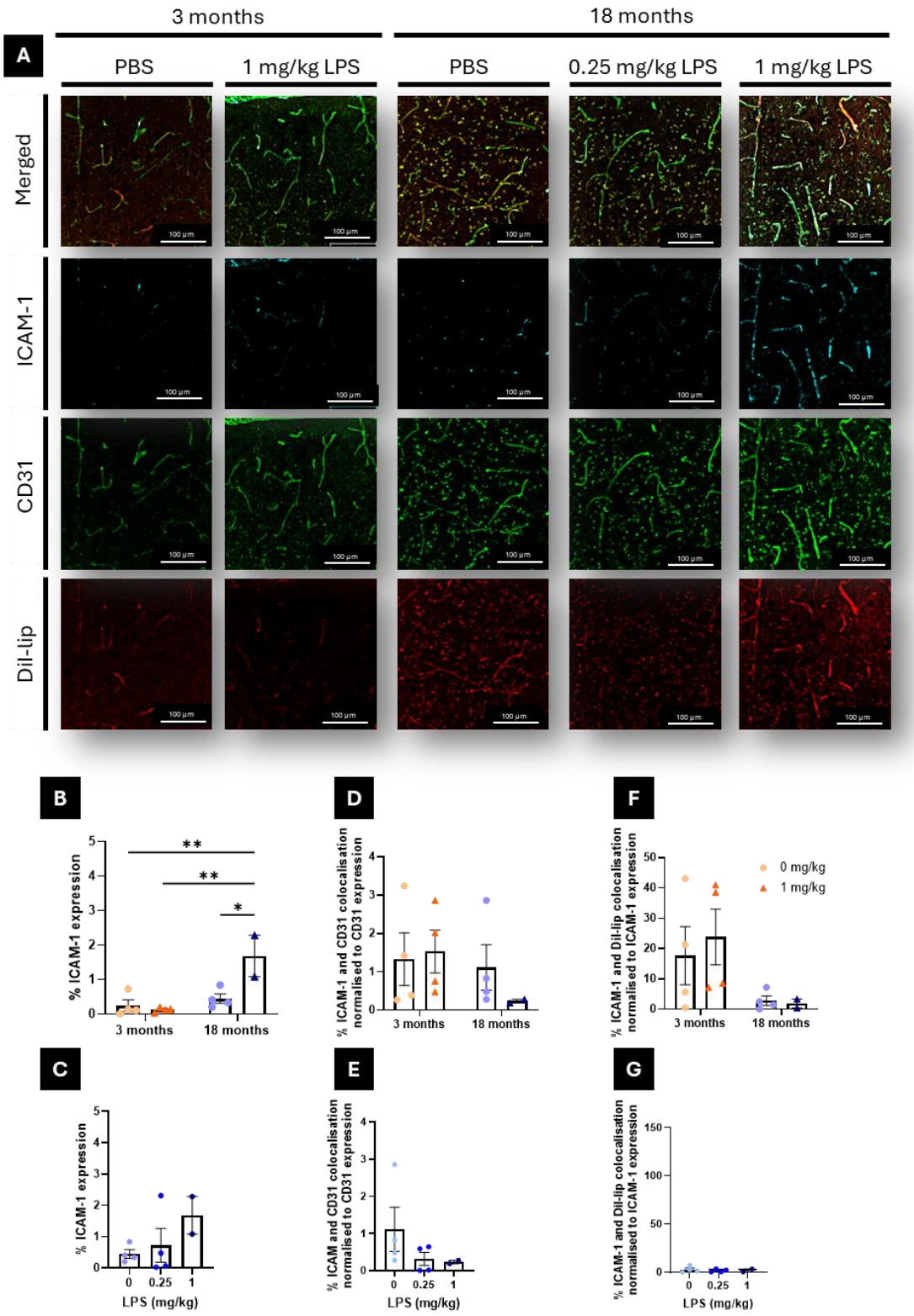

Figure 4-32: Effect of ageing and inflammation on ICAM-1 expression in auditory cortex region. Female C57BL/6 mice at either 3- or 18- months were intraperitoneally injected with either 0.25 mg/kg, 1 mg/kg or 0 mg/kg vehicle control 48 hours prior to intravenous injection with DiI-lip. 2-hours post I.V injection mice were culled with cardiac perfusion to removed excess DiI-lip. (A) Representative images of auditory cortex region -1.94mm from the bregma demonstrate expression of ICAM-1 (cyan), CD31 (green) and DiI-lip (Red). (B) Quantitative analysis of ICAM-1 expression between 3- and 18- month groups displayed a significant increased from 3-month vehicle, 1 mg/kg LPS and 18-month vehicle to 18-month 1 mg/kg LPS. (C) No significant changes in ICAM-1 observed between 18-month vehicle and 18-month 1 mg/kg LPS Quantification of CD31 and ICAM-1 interaction demonstrated no significant changes in ageing or LPS dosage (D-E). Quantitative analysis of DiI-lip

and ICAM-1 interaction displaying no changes in either ageing or LPS doses (F-G). Images obtained at x40 magnification on Leica Thunder microscope and underwent large volume computational clearing (LVCC) prior to quantification in Image J. Statistical analysis was completed using GraphPad Prism software using Shapiro Wilk test for normality. This proceeded either a using one-way analysis of variance followed by Tukey multiple comparison test or Kruskal-Wallis test followed by Dunn's multiple comparisons for comparisons of LPS dose in aged mice. To compare young and aged mice for LPS effects; two-way analysis of variance followed by Tukey's multiple comparison test. N=2-4, average ± SEM, $p<0.05$ were considered significant. Scale bar represents 100µm.

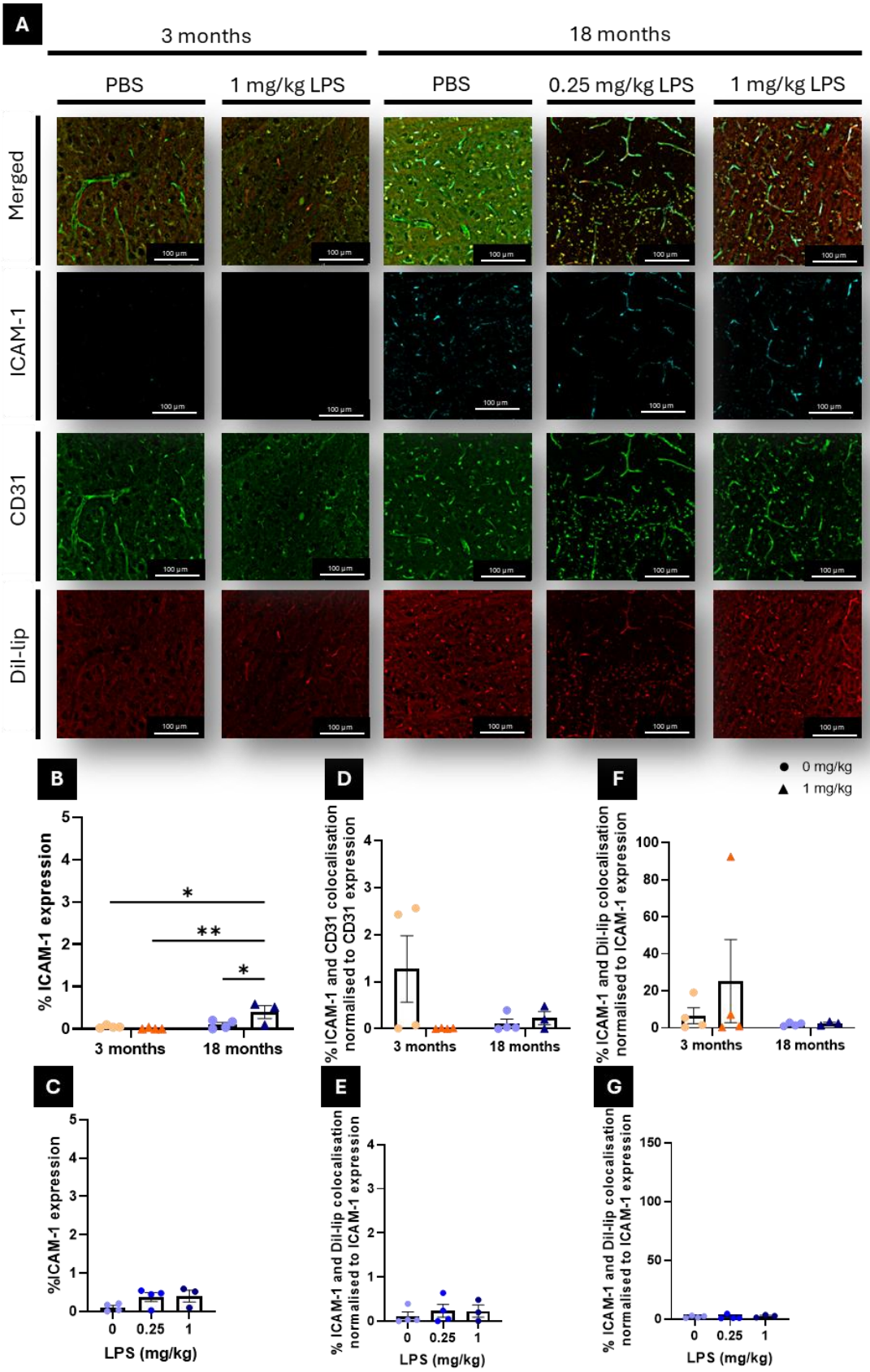

Figure 4-33: Effect of ageing and inflammation on ICAM-1 expression in striatum region. Female C57BL/6 mice at either 3- or 18- months were intraperitoneally injected with either 0.25 mg/kg, 1 mg/kg or 0 mg/kg vehicle control 48 hours prior to intravenous injection with DiI-lip. 2-hours post I.V injection mice were culled with cardiac perfusion to removed excess DiI-lip. (A) Representative images of striatum region -1.94mm from the bregma demonstrate expression of ICAM-1 (cyan), CD31 (green) and DiI-lip (Red). (B) Quantitative analysis of ICAM-1 expression between 3- and 18- month groups displayed a significant increased from 3-month vehicle, 1 mg/kg LPS and 18-month vehicle to

18-month 1 mg/kg LPS. (C) No significant changes in ICAM-1 observed between 18-month vehicle and 18-month 1 mg/kg LPS Quantification of CD31 and ICAM-1 interaction demonstrated no significant changes in ageing or LPS dosage (D-E). Quantitative analysis of DiI-lip and ICAM-1 interaction displaying no changes in either ageing or LPS doses (F-G). Images obtained at x40 magnification on Leica Thunder microscope and underwent large volume computational clearing (LVCC) prior to quantification in Image J. Statistical analysis was completed using GraphPad Prism software using Shapiro Wilk test for normality. This proceeded either a using one-way analysis of variance followed by Tukey multiple comparison test or Kruskal-Wallis test followed by Dunn's multiple comparisons for comparisons of LPS dose in aged mice. To compare young and aged mice for LPS effects; two-way analysis of variance followed by Tukey's multiple comparison test. N=2-4, average ± SEM, $p<0.05$ were considered significant. Scale bar represents 100μm.

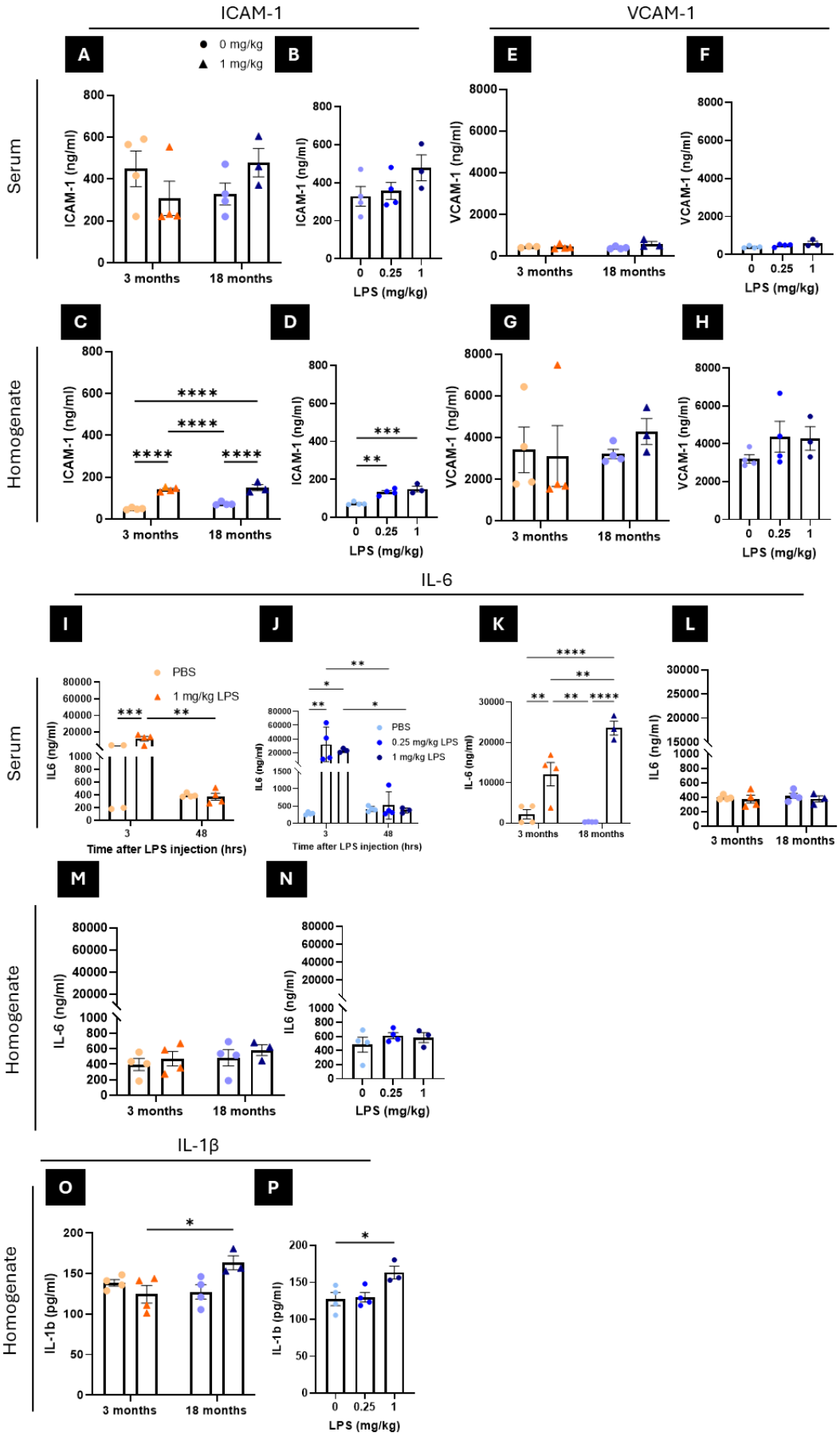

Figure 4-34: Inflammatory cytokine and adhesion molecule expression in LPS and ageing conditions. Female C57BL/6 mice at either 3- or 18- months were intraperitoneally injected with either 0.25 mg/kg, 1 mg/kg or 0 mg/kg vehicle control 48 hours prior to intravenous injection with DiI-

lip. 2-hours post I.V injection mice were culled with cardiac perfusion to removed excess DiI-lip. ELISA's were conducted on serum was extracted from blood 3- and 48-hours post-LPS injection and brain homogenate from terminal samples. Comparison of ICAM-1 levels in serum showed significant increases in ageing (A) and LPS dose at 18-months (B). No significant changes were seen in brain ICAM-1 (C-D). VCAM-1 expression levels had no significant changes in either serum or brain samples (E-H). IL-6 expression was significantly increased in 3-hour serum samples when treated with LPS in both young (I) and aged (J) samples. Significant IL-6 increases in serum from aged LPS mice was observed in serum samples at 3-hours (K) but not 48-hours (L). No changes were observed in the IL-6 levels of brain (M-N). Significant increases in IL-1β brain homogenate expression between 3-month and 18-month 1 mg/kg group (O) and between 0 and 1 mg/kg in 18-month mice (P). Statistical analysis was completed using GraphPad Prism software using Shapiro Wilk test for normality. This proceeded either a using one-way analysis of variance followed by Tukey multiple comparison test or Kruskal-Wallis test followed by Dunn's multiple comparisons for comparisons of LPS dose in aged mice. To compare young and aged mice for LPS effects; two-way analysis of variance followed by Tukey's multiple comparison test. N=3-4, average ± SEM, $p<0.05$ were considered significant. Scale bar represents 100µm.

doses as both the 0.25 mg/kg ($F=20.25_{(2,8)}$, p=0.0030) and 1 mg/kg ($F=20.25_{(2,8)}$, p=0.0010) had higher ICAM-1 expression then the vehicle (fig. 4-34 b). However, this increased expression is not reflected in the serum as no significant changes were observed in either age related LPS effects or effects of LPS dose in 18-month mice (fig. 4-34 c-d). VCAM-1 expression resulted in no significant changes in either the brain homogenate (fig. 4-34 c) or serum samples (fig. 4-34 d). These results show that adhesion molecules were increased during LPS dosage in both 3- and 18-month mice, but age did not influence the expression.

The cytokine IL-6 was also significantly increased in the short-term (3-hours) post-LPS injection. LPS treated groups compared to vehicle in the 3-month groups (age $F=6.913_{(1,11)}$, LPS $F=84.25_{(1,11)}$, p= 0.0007) and the 18-month group for 0.25 mg/kg (age $F=6.913_{(1,11)}$, LPS $F=84.25_{(1,11)}$, p= 0.0021) and 1 mg/kg (age $F=6.913_{(1,11)}$, LPS $F=84.25_{(1,11)}$, p=0.0334) groups (fig. 4-34 l). This increase in IL-6 expression was not conserved throughout the study and terminal serum samples (48-hours) there was no significant difference between vehicle and LPS treatment in both age groups (fig. 4-34 i). Similar expression patterns were observed in the 18-month group as IL-6 expression was significantly higher in the 0.25 and 1 mg/kg groups at 3-hours post injection compared to the 3 hour 18-month vehicle (time $F=15.48_{(1,6)}$, LPS $F=4.445_{(1,6)}$, p= 0.0021/0.0034) (fig. 4-34 j). Decreases in serum levels at48-hours were significant between 0.25 mg/kg (time $F=15.48_{(1,6)}$, LPS $F=4.445_{(1,6)}$, p= 0.0031) and 1 mg/kg (time $F=15.48_{(1,6)}$, LPS $F=4.445_{(1,6)}$, p= 0.0302). LPS groups but not the vehicle control. Further comparison of 3-hour IL-6 levels show a significant increase between the 1 mg/kg 18-month group compared to the 3-month group (p=0.0059) (fig. 4-34 k).

At 48-hours, all IL-6 serum levels were consistent and showed no significant changes in LPS dose or age (fig. 4-34 l). This reflected data shown in the brain tissue homogenate, as no significant changes were observed either when comparing the effect of LPS and ageing (figure m) or the dose of LPS at 18-months (fig. 4-34 n). Overall, both LPS and ageing increase the expression of IL-6 within the peripheral system but only in the short-term following LPS injection. Another cytokine linked to systemic inflammation is IL-1β and within

this study was analysed via ELISA on only brain homogenate. IL-1β levels significantly increased between the 3-month and 18-month 1 mg/kg LPS groups (age $F=2.602_{(1,11)}$, LPS $F=1.627_{(1,11)}$, p= 0.0440) but not between vehicle age (fig. 4-34 o). Cytokine levels were also increased between 18-month vehicle and 1 mg/kg LPS ($F=5.590_{(2,8)}$, p=0.0371) but not the lower 0.25 mg/kg dose (fig. 4-34 p). This data suggests that LPS has the dominant effect on IL-1β expression but that it can be intensified by ageing.

4.4.8. Global protein changes with systemic inflammation

The results of the chapter so far focus on specific target molecules, but it is important to understand these changes in the context of global proteomic changes during ageing and LPS-induced inflammation. Four comparisons were chosen to investigate from the mass spectrometry dataset: 3-month vehicle vs 18-month vehicle, 3-month vehicle vs 3-month 1 mg/kg LPS, 18-month vehicle vs 0.25 mg/kg LPS and 18-month vehicle vs 1 mg/kg LPS. Significant data for all comparisons was set at p-value ≤0.05 and fold change ≥0.3 or ≤-0.3.

The effect of LPS dose on 18-month mouse brain was visualised in volcano plots showing protein expression changes in 18-month vehicle vs 0.25 mg/kg (fig. 4-35a) and 1 mg/kg (fig. 4-35b) with significant changes marked in red. There were 101 significantly up-regulated proteins and 102 down-regulated proteins in the 0.25 mg/kg comparison whilst in 1 mg/kg, 125 up-regulated proteins and 90 down-regulated proteins were quantified. Analysis of both showed no significant changes in GFAP, ICAM-1, VCAM-1 and caveolin-1 protein expression. Using IPA, the top 5 canonical and disease function pathways were determined for both conditions fig. 4-35c) with neutrophil degranulation being a common canonical pathway (fold change 3.8/4.4) whilst organismal injury, neurological disease, psychological disorders and hereditary disorder all were common comparisons in disease function pathways. Fig. 4-35d shows the pathway network for 18-month 1 mg/kg, showing the common connections between changed protein expression including IL-1β, IL-6, NF-kB, STAT1 and TNF. No pathway network was obtained for 0.25 mg/kg LPS group due to a lack of connections in IPA software.

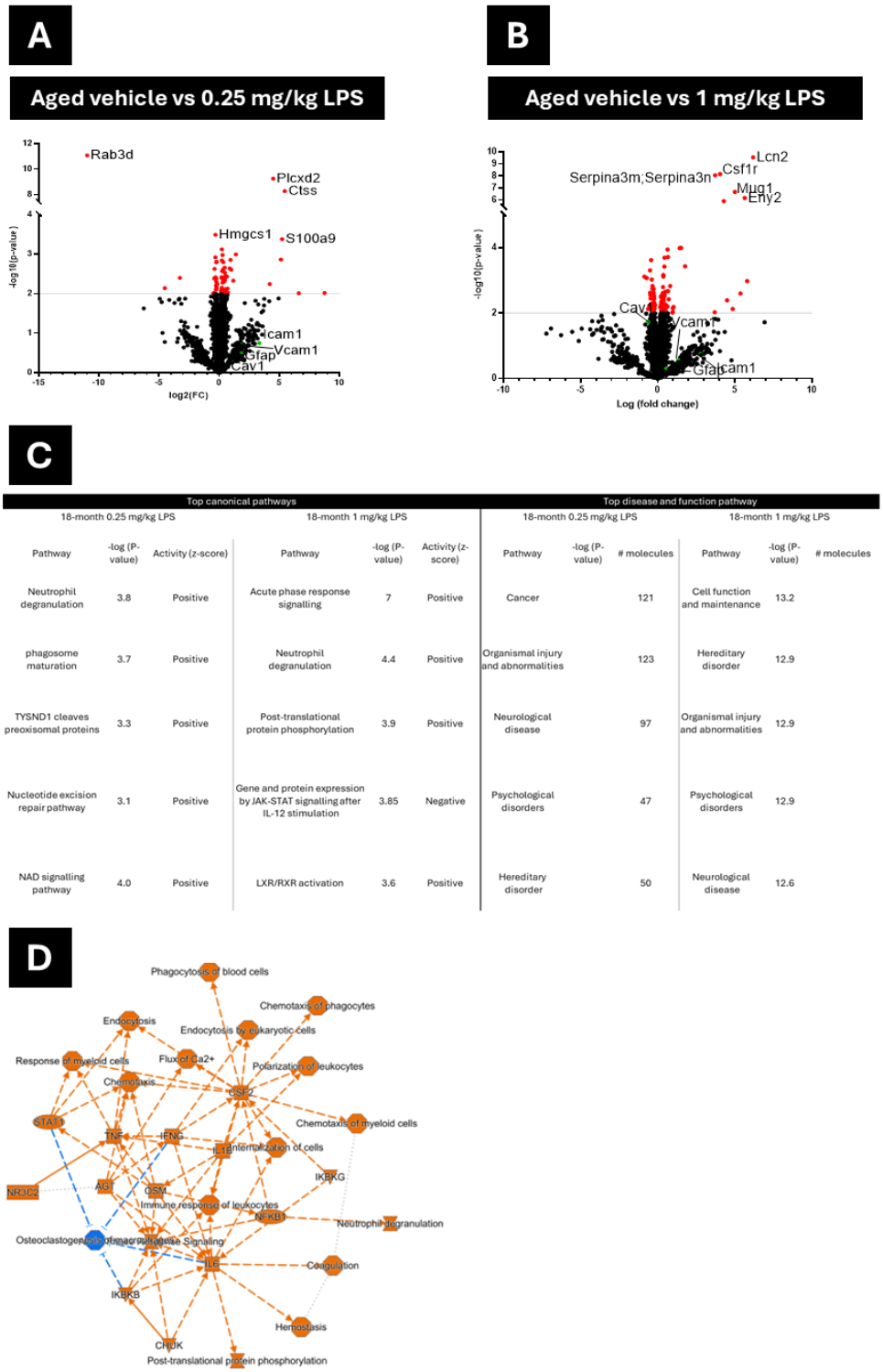

Figure 4-35: Proteomic changes to mouse brain during inflammation of aged mice. C57BL/6 female mice groups were injected intraperitonially a single dose of lipopolysaccharide. 18-month mice were given, 1 mg/kg, 0.25 mg/kg or PBS vehicle control. 48-hours post injection before cardiac perfusion. Brains were flash frozen and homogenised before running on SciexZenoTOF 7600 Mass spectrometer. (A) Volcano plot showing differential proteins comparing vehicle to 0.25 mg/kg LPS. (B) Volcano plot showing differential proteins comparing vehicle to 1 mg/kg LPS. Significantly changed proteins labelled in red and top 5 changed proteins identified plus proteins of interest. (C) Ingenuity pathway analysis (IPA) showing the most changed canonical pathways and disease and function pathways for comparison of vehicle to either 0.25 or 1 mg/kg LPS. (D) Pathway network of 1 mg/kg LPS group visualised using IPA software. Data expressed as mean ± SEM with significance determined by log fold change 0.3 and p-value ≥ 0.05.

The 3-month vehicle group was compared to both 18-month vehicle (fig. 4-36a) and 3-month 1 mg/kg LPS (fig. 4-36b) to determine changes in either ageing or LPS-inflammation. Volcano plot of 18-month vehicle demonstrates significant fold-change in 134 up-regulated proteins and 67 down-regulated proteins including GFAP (FC 0.77, p= 0.007) and caveolin-1 (FC 0.62, p=0.003). 3-month 1 mg/kg LPS group demonstrated 162 up-regulated and 39 down-regulated proteins with ICAM-1 up-regulated (FC 3.91, p= 0.000008) with no significant changes to other proteins of interest. Top canonical pathway analysis showed common increases including neutrophil degranulation and response to elevated platelet cytosolic Ca^{2+} with neurological disease, organismal injury and abnormalities and cancer being among shared disease function pathways changed compared to 3-month vehicle (fig. 4-36c). Network pathways emphasised organismal death in 18-month vehicle group (fig. 4-36d) whilst 3-month 1 mg/kg LPS highlighted TLR-4, TGFB1 and IRF3 as key areas affected (fig. 4-36e).

Generation of a hierarchical heatmap demonstrates individual clustering of 3-month vehicle mice and 1 18-month vehicle mouse with similarities some similarities between the other groups (fig. 4-37a). The 18-month LPS-treated groups showed the largest similarity clustered together and then further grouped with the 3-month LPS group. Analysis to determine similarities between comparisons showed 36 similar up-regulated and 14 down-regulated proteins comparing 18-month vehicle to both LPS-treated groups (fig. 4-37b-d). Comparisons of 18-month vehicle and 3-month 1 mg/kg LPS to the 3-month vehicle group resulted in 30 similar up-regulated proteins and 4 down-regulated proteins (fig. 4-37e-g).

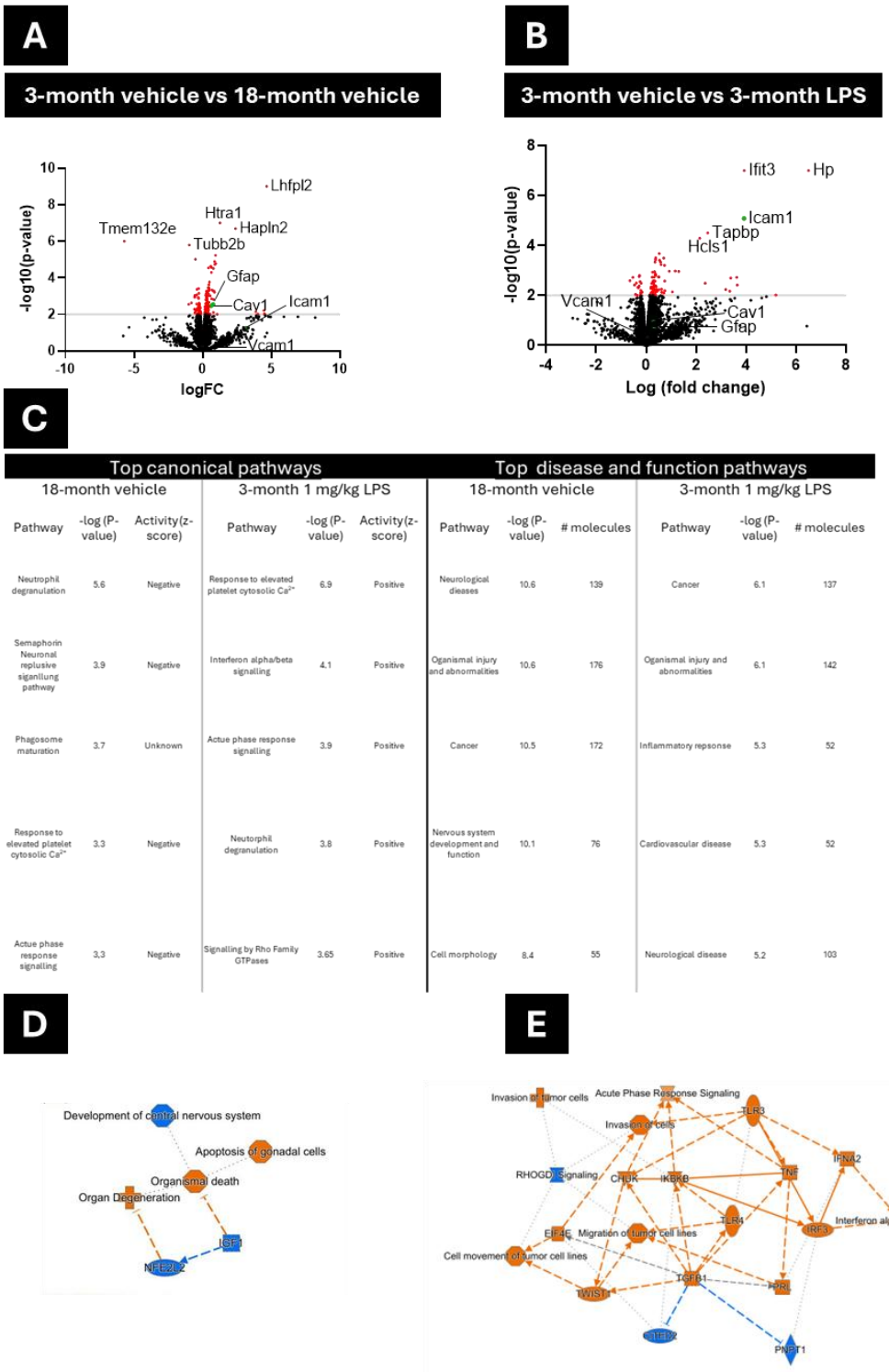

Figure 4-36: Proteomic changes to mouse brain comparing ageing and LPS .C57BL/6 female mice groups were injected intraperitonially a single dose of lipopolysaccharide or PBS vehicle up to the age of 18-months. 48-hours post injection before cardiac perfusion. Brains were flash frozen and homogenised before running on SciexZenoTOF 7600 Mass spectrometer. (A) Volcano plot showing differential proteins comparing 3-month vehicle to 18-month vehicle. (B) Volcano plot showing differential proteins comparing 3-month vehicle to 1 mg/kg LPS. Significantly changed proteins labelled in red and top 5 changed proteins identified plus proteins of interest. (C) Ingenuity pathway analysis (IPA) showing the most changed canonical pathways and disease and function pathways for comparison of vehicle to either 0.25 or 1 mg/kg LPS. (D) Pathway network of 18-month vehicle group visualised using IPA software. (E) Pathway network of 3-month 1 mg/kg group visualised using IPA software Data expressed as mean ± SEM with significance determined by log fold change 0.3 and p-value ≥ 0.05.

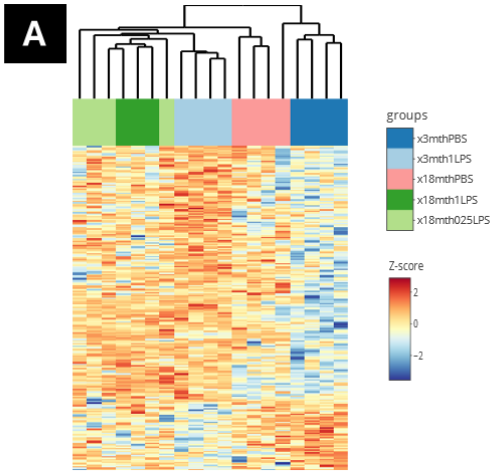

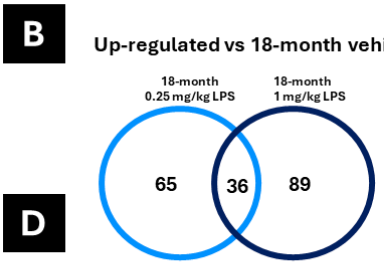

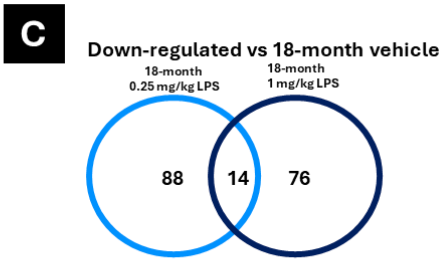

D

Common up-regulated genes			
↑ Anxa2	↑ Fgg	↑ **Stat1**	↑ Smad1;Smad5
↑ Apod	↑ Fkbp5	↑ Tsc22d4	↑ Polr2b
↑ B2m	↑ Gstt2;Gstt3	↑ Uevld	↑ Ptgds
↑ **Cd38**	↑ Hp	↑ Uprt	↑ Pcbd1
↑ Cox6a1	↑ Hpx	↑ Vps25	↑ Plcxd2
↑ Cp	↑ Hspb1	↑ Rps6ka1	↑ Plin4
↑ Crot	↑ Lcp1	↑ **S100a9**	↑ Dag1
↑ Ctss	↑ Msn;Rdx	↑ Dynlt1	↑ **Serpina3m; Serpina3n**
↑ Cyp2s1	↑ Parva	↑ Etnppl	↑ **Serpina3k**

Common down-regulated genes	
↓ Atp11b	↓ Hmgcs1
↓ Crtc1	↓ Mvd
↓ Diras1;Diras2	↓ Pip4p1;Pip4p2
↓ Dph5	↓ Pmch
↓ Epha5;Epha7	↓ Rab3d
↓ Fhl2	↓ Sbf1;Sbf2
↓ Fmr1	↓ Tyro3

E

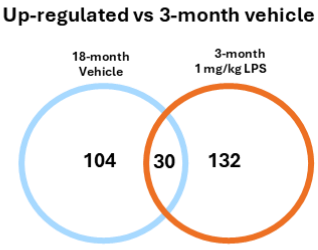

F

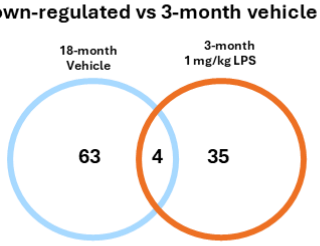

G

Common up-regulated genes				Common down-regulated genes
↑ Plxnc1	↑ Capg	↑ C1qb	↑ Galt	↓ Esp8
↑ Cnnm1	↑ Nelfb	↑ Ahsa2	↑ **Serpina3n**	↓ Dgkd;Dgkh
↑ Lamp2	↑ Ctsz	↑ C1qa	↑ Lhfpl2	↓ Tbc1d10a
↑ Dcun1d1;Dcun1d2	↑ Ctps1;Ctps2	↑ Htra1	↑ Ube2b	↓ Ubxn7
↑ Arhgap25	↑ Lpcat2	↑ Ifit3	↑ Thsd1	
↑ Pelo	↑ Epha5;Epha7	↑ Grid1;Grid2	↑ Pikfyve	
↑ Gng5	↑ C1qc	↑ Snx19		
↑ Tecpr1	↑ Vcan	↑ Pbp2;Pebp1		

Figure 4-37: Comparative changes to protein expression during ageing and LPS-induced inflammation. C57BL/6 female mice groups were injected intraperitonially a single dose of

lipopolysaccharide. 3-month mice received either 1 mg/kg or PBS vehicle control whilst 18-month mice were given, 1 mg/kg, 0.25 mg/kg or PBS vehicle control. 48-hours post injection, all mice were cardiac perfused before brains were flash frozen and homogenised before running on SciexZenoTOF 7600 Mass spectrometer. (A) Heatmap of proteins expressed within the brain samples displaying hierarchical clustering of sample groups. Venn diagrams showing the common up-regulated (B) and down-regulated (C) proteins comparing 18-month vehicle to either 0.25 or 1 mg/kg LPS. (D) Table listing common protein genes up- or down-regulated in 18-month mice with 0.25 or 1 mg/kg LPS. Venn diagrams showing the common up-regulated (E) and down-regulated (F) proteins comparing 3-month vehicle to either 18-month vehicle or 3-month 1 mg/kg LPS. (G). Table listing common protein genes up- or down-regulated from 3-month mice in either 18-month vehicle or 3-month 1 mg/kg LPS. Heatmap generated using AMICA v3.0.1 and venn diagrams generated in Microsoft office software. Data expressed as mean ± SEM with significance determined by log fold change 0.3 and p-value ≥ 0.05.

4.5. Discussion

This chapter aimed to demonstrate LPS-induced inflammatory changes to the BBB and whether age exacerbated observed effects whilst assessing changes to permeability. Global brain infiltration of nanoparticles was increased with LPS challenge but not during ageing. Biodistribution of liposomes within peripheral organs demonstrated no significant changes in age or inflammation expect for in the 0.25 mg/kg aged LPS group, found to have increased liver levels but decreased kidney infiltration. Region-specific analysis uncovered variation in liposome expression throughout the brain, with the dentate gyrus and cortex being vulnerable to increased infiltration in the aged LPS group. Further investigations into BBB permeability found no changes to IgG or iron levels within the brain during inflammation or ageing, complemented by no changes in cavolin-1 expression, correlating to changes to BBB transcytosis. Activation of astrocytes (via GFAP) or microglia (Iba-1) were not significantly affected by either age or LPS-induced inflammation whilst the adhesion molecule ICAM-1 was only increased in the aged, high LPS-dose group. ELISA assays complemented histological results and showed an increase in ICAM-1 during LPS response in brain tissue whilst showing no changes in VCAM-1 levels in either the brain or serum samples. Pro-inflammatory cytokine expression was investigated finding increases in IL-1β when LPS induction coincided with ageing in the brain whilst no changes in IL-6 were observed at this terminal timepoint in either brain or serum samples. 3-hours post-LPS there was an induction in IL-6 serum levels, affected by both ageing and LPS treatment. Analysis of proteomic comparisons between ageing and inflammatory groups showed widespread up-regulated and down-regulated proteins in both ageing and LPS-dosage.

4.5.1. Infiltration of liposomes affected by age and LPS

This study was the first known to investigate the effect of the infiltration of liposomes during LPS-induced inflammation in the context of physiological ageing. Investigations globally into the brain demonstrate a significant increase in infiltration in young brains with LPS but not with the aged mice at any LPS dose. As DiI-lip have been shown in fig. 3-5, 3-6 to significantly

increase infiltration in the aged female brain, it may be that LPS does not increase this and that it has reached a plateau of infiltration. It has been shown *in vivo* that LPS causes an increase in albumin and dextran infiltration into the brain so it would be an interesting comparison to complete a study investigating transcellular and paracellular pathway changes after LPS administration (Banks et al., 2015; Wang et al., 2017).

It is important to assess biodistribution of nanoparticles through the body to determine if accumulation of DiI-lip was changed by LPS, with results showing no change in LPS or age in the heart, lungs or spleen. However, in the liver, there was an increase in uptake in the 18-month 0.25 mg/kg LPS group compared to all others. This may be explained as LPS has been shown to induce liver injury in mice and that liver injury may cause accumulation of liposomes (Hamesch et al., 2015; Liu et al., 2024). However, if this was the case then similar uptake increases would be expected in the 3- and 18-month 1 mg/kg groups which is absent here. Complementing the increase in liver uptake was a decrease in kidney uptake in the same group, indicating that this is where the liposomes have been redirected from, but the mechanistic reason behind this in exclusively the 0.25 mg/kg LPS group requires further work. The absence of uptake changes in peripheral organs in the 1 mg/kg LPS groups in both ages demonstrates the effective targeting of the brain by DiI-lip, showing the potential to target brain inflammation specifically with this formulation.

Contrasting to the global optical imaging results, significant DiI-lip uptake was found in the dentate gyrus, motor cortex and auditory cortex when comparing 3-month vehicle to 18-month 1 mg/kg LPS groups. This shows that LPS-induced neuroinflammation does influence infiltration, showing promise for delivery of therapeutics in inflammaging. There is limited previous work looking at liposomes to treat LPS-induced inflammation in mouse models, but two studies have shown promising results (Ralvenius et al., 2024; Yadav et al., 2016). Both studies targeted neuroinflammation with small interfering ribonucleic acid molecules encapsulated in liposomes showing decreases in Iba1/GFAP+ cells and reduction in TNF-α. However, both studies utilised young mice, which would not encapsulate changes during

physiological ageing. Yadav et al., 2016 used intranasal administration which bypassed the BBB so did not reflect if peripheral administration routes would cross BBB. Ralvenius et al., 2024, compared the use of I.P and intracerebroventricular administration and found that although a lower potency, I.P liposomes crossed the BBB and had therapeutic effects localised to the cortex, correlating with the current study.

4.5.2. No LPS-induced changes to BBB permeability or transport

Within this study, there was no observed change in IgG accumulation within any brain region irrespective of group age or LPS dose. Stolp et al., 2005, noted in young adult rats that a single dose of LPS between 0.2-10 mg/kg did not result in increased permeability after 48-hours correlating with the data found here. Further studies in young mice agreed that 1 mg/kg would not produce increased permeability, demonstrated in either single or combination dose of LPS under 3 mg/kg 24-hours (Banks et al., 2015),5 minutes (Banks & Robinson, 2010) or 28-hours (Erickson & Banks, 2018) post LPS injection. Ageing studies also demonstrated that low dose LPS does not cause BBB disruption at 0.33 (Banks et al., 2015; Knopp, Baumann, et al., 2022), 0.25 or 0.5 mg/kg (Wang et al., 2017).

However, the same study showed that 1 mg/kg LPS increased IgG infiltration in 28-month mice, so it was expected that similar trends would occur in the 18-month 1 mg/kg group which was not observed (Wang et al., 2017). This study was conducted on rats so may not translate directly to this murine model and analysed the permeability at 24-hours post injection. As LPS-driven inflammation is known to occur in short timeframes, it may be that 48-hours is too far after injection to see effects (Seemann et al., 2017). The single dose of LPS may also be insufficient to observe significant BBB disruption as studies in young mice at 4 mg/kg (Vutukuri et al., 2018), 3 mg/kg (Banks et al., 2015) and 10 mg/kg (Bien-Ly et al., 2015) showing increased BBB permeability to albumin, dextran and sodium fluorescein as well as multiple doses (Erickson et al., 2018; Haruwaka et al., 2019). . These studies were all in young mice and so it would be expected to be observed during ageing (Britton et al., 2022). However, mortality of 18-

month mice was comprised during the current study at 1 mg/kg so these higher dose amounts would not be ethical or feasible.

No iron accumulation was observed in either age or LPS inflammation during this study which directly contradicts previous literature which demonstrated that aged mice had increased iron deposits (Sumbria et al., 2018; Zeng et al., 2018). However, both studies used a 3-dose regime to produce the effect, highlighting that a single dose of LPS may not be able to show full long-term systemic inflammation effects. The use of Prussian blue staining, regularly utilised with stroke models due to being straightforward and cost-effective, may not be the most suitable target for iron accumulation in a model without significant brain bleeding (Castellani et al., 2016).

Other studies have investigated iron accumulation through hepcidin (iron regulating hormone), or ferritin (extracellular iron storage) showing changes during LPS-induced inflammation in young mice (Li et al., 2024; Tong Ong et al., 2005; Wang et al., 2008; You et al., 2017). These increases have been accompanied by increases in IL-6, microglial activation and cognitive impairment, showcasing the importance of iron dysregulation in inflammation. Li et al., 2024, dosed mice with Deferoxamine, an iron chelator reducing ferroptosis, post-LPS and noted recovery in all above parameters. However, as with IgG accumulation, time after LPS injection may be critical, as hepcidin increases were noted 12 hours-post LPS but levels had returned to baseline at 24-30 hours indicating that the current study would not observe the effects (Wang et al., 2008).

Regional heterogeneity was also observed within the literature, with the cortex being particularly vulnerable to iron dysregulation (Li et al., 2024; Wang et al., 2008; You et al., 2017). The hippocampus shows contradictory data with some studies showing increased hepcidin (Li et al., 2024; You et al., 2017) but other showing no change (Wang et al., 2008). This may be due to the direct ICV administration route as opposed to traditional peripheral I.P or I.V injections. Iron dysregulation and ferroptosis have been linked to decreases in SIRT1, which correlates to increased BBB permeability in ageing studies (Stamatovic et al., 2019; Xu et al., 2024).

Therefore, it would be prudent to further explore this avenue within the age and LPS context with the markers mentioned here.

As increased BBB permeability had been found in LPS-induced models, it was important to decipher the transport mechanism changes behind this. As mentioned above, albumin/cerebrospinal fluid ratios changed with LPS administration, indicating transcellular transport routes (Tincu et al., 2023). However, no changes to caveolin-1 expression were observed in ageing or LPS conditions with non-significant decreases in expression seen in ageing in the motor cortex. This correlates with findings in chapter 3, which improves the robustness of result that in female mice, caveolin-1 decreases in age. However, Wang et al., 2019, also noted no change in caveolin-1 expression after 7.5 mg/kg LPS injection but post-treatment with a sepsis drug showed a decrease in caveolin-1 that correlated with decreased BBB permeability. This indicates that although expression of caveolin-1 is not affected by LPS, the mechanistic effect is. Other transcellular transport mechanisms should be explored as human immunodeficiency viruses in a LPS model was identified as transcellularly transported but was not caveolae-mediated 2008 (Dohgu & Banks, 2008). Efflux transporters, such as P-gp, have also been investigated, showing decreases in function when exposed to LPS allowing for accumulation of neurotoxins in the brain such as amyloid-beta (Hartz et al., 2006; Salkeni et al., 2009).

4.5.3. Age and inflammation driven effects astrocyte activation

Activation of astrocytes has been heavily linked to neuroinflammation, being activated via NF-kB and STAT3 pathways and producing pro-inflammatory molecules such as IL-1β, IL-6 and reactive oxygen species (Giovannoni & Quintana, 2020; Rothhammer & Quintana, 2015; Sheng et al., 2013). The common astrocyte marker, GFAP, has been widely used to characterise activation and has been studied extensively in inflammation studies (Jurga et al., 2021). Within the current study, limited GFAP changes were observed either comparing LPS in young and aged mice or in different LPS doses in aged mice. The motor cortex was the only region to identify significant GFAP increases between 3-month vehicle and 18-month 1 mg/kg LPS whilst

the striatal region showed similar but non-significant trends. This finding is consistent with studies which have also shown in young and aged mice no changes to GFAP expression with LPS (Knopp, Baumann, et al., 2022). Vizuete et al., 2022, used a young rat model to show that at 1 mg/kg (like our current high dose LPS), that GFAP expression was increased in the brain 6-hours post-LPS but had decreased to baseline at 24-hours. This indicates that LPS-induced GFAP expression was dependent on time after inflammatory insult. Furthering this, a study using x2 doses of 0.5 mg/kg demonstrated no GFAP increases at 3-, 4-, 6- or 8-days post injection (Jung et al., 2023). However, a study in 20-month rats displayed an increase in GFAP at 1, 3 and 7 days but used a higher dose point of 2 mg/kg LPS.

Multiple studies in both adults (2-3 months) and aged (over 16-months) have shown that LPS does induce an increase in GFAP expression, but all these studies have either had higher LPS doses or reduced study timeframes than our current study (table 4-2). Within a 3- month versus 18-month ageing model, a regimen of 3 doses over 24-hours at 1 mg/kg resulted in increased expression after 7-days only in the 18-month mice (Sumbria et al., 2018). Similarly, comparisons of 1, 6 and 21-month mice of a single 0.5 mg/kg LPS after 24-hours displayed increased GFAP levels in the 21-month LPS group but not the younger groups (Allen et al., 2023). These studies highlight the exacerbation of neuroinflammation in ageing, which was reflected in the motor cortex region within this study.

Further GFAP interactions were investigated here, specifically looking at CD31 and GFAP to observe if astrocytes migrate from the BBB during age and inflammation. *In* vivo studies in mice and sheep have shown that LPS inflammation caused activated astrocytic end-feet to detach from the BBB, possibly via phagocytosis of the end-feet by microglia, leading to BBB damage (Disdier et al., 2020; Haruwaka et al., 2019; Xingi et al., 2023). Xingi *et al,* 2023 used a transgenic GFAP+ mouse strain with Rhodamine B dextran as a marker of the vasculature in 2-photon imaging to show that interactions between astrocytes and BBB were reduced at both 4 and 8 days. Further analysis used AQP4 staining to enforce the finding, also showing decreased correlation with CD31. This suggests that future work should instead either use 3D

Table 4-2: Correlation of rodent LPS study design and GFAP expression. Tabular representation stating age of subjects, serotype of LPS, dose of LPS (mg/kg), number of doses, LPS incubation time and effect on GFAP expression. Studies ordered by LPS dose. N. S= not stated.

Study	Age (months)	Serotype	Dose (mg/kg)	# doses	Dose interval	GFAP changes
(Hu et al., 2017)	10-12 day	N. S	0.05	1	1 week	↑
(Mota et al, 2020)	6	N.S	0.1	1	4-hours	↑
(Kang et al., 2019)	2	N. S	0.25	2	24-hours	↑
(Knopp, Banks, et al., 2022)	16-18	O55:B5	0.33	1	28-hours	=
(Jung et al., 2023)	2	O111: B4	0.5	2	3, 4, 6, 8 days	=
(Allen et al., 2023)	1, 6, 21	O111: B4	0.5	1	24-hours	↑
(Murtaj et al., 2019)	2, 17-18	O55:B5	0.63	1	6-hours	Trends to ↑
(Wang et al., 2019)	2	O111: B4	0.83	1	24-hours	↑
(Haruwaka et al., 2019)	2	N. S	1	1/ x7 over 7 days	1 week +	↑
(Banks et al., 2015)	> 2	N. S	1	X7 over 7 days	24-hours	↑
(Sumbria et al., 2018)	3, 18	N. S	1	3	1 week	↑ (18-month)
(Vizuete et al., 2022)	1	O55:B5	1	1	6, 24-hours	↑/=
(Fu et al., 2014)	20		2	1	0.5, 2, 6-hours 1, 3, 7, 30-days	= ↑
(Vutukuri et al., 2018)	> 2	O55:B5	4	1	4-hours	↑
(Xingi et al., 2023)	2	O55:B5	5	2	4, 8 days	↑
(Diaz-Castro et al., 2021)	2	O55:B5	5	1	1, 2, 14 day	↑
(Liddelow et al., 2017)	<1	O55:B5	5	1	N. S	=
(Ralvenius et al., 2024)	2	O55:B5	10	1	N. S	↑

imaging software such as IMARIS to look at interactions opposed to the current 2D image analysis or use AQP4 as a more suitable marker.

No correlations were made during the study with DiI-lip, indicating that astrocytic uptake of DiI-lip does not occur during either ageing or neuroinflammation. Therefore, astrocytes would be an unsuitable target moving forward for anti-inflammatory liposomal based therapies. Overall, the effect of LPS on GFAP expression in young and aged brain is dose and incubation dependent. With single doses at longer timepoints have a reduced effect on GFAP expression compared to higher doses at shorter timepoints (table 4-2). This indicates that although LPS increases astrocyte activation, it does so beyond the parameters of the current study, highlighting that low-grade systemic inflammation may not cause significant changes and that a more severe phenotype would cause this.

4.5.4. No changes to microglial activation in ageing LPS mice

Microglial expression has been shown clinically to be up regulated during increased inflammatory response through ageing, Parkinson's disease, and AD. (Kim & Joh, 2006; Pelvig et al., 2008; Schuitemaker et al., 2012). However, clinical literature investigating the impact of systemic inflammation specifically in physiological ageing is lacking, so the investigation of this with i*n vivo* models is crucial for further insight.

Here, the common microglial marker Iba-1, has been assessed in an LPS model of ageing using 3- and 18-month mice, displaying limited significant changes either when comparing response of LPS in ageing or LPS dose within the aged 18-month cohort. The only significant change observed was within the CA1 region, Iba-1 was increased in 3-month mice when exposed to 1 mg/kg LPS for 48-hours. This may suggest that the CA1 and hippocampus is more vulnerable to microglial changes and would correlate with human studies noting that the hippocampus is vulnerable to age-related BBB permeability (Montagne et al., 2015). Haruwaka et al, 2019 demonstrated the link between increased microglial Iba-1 activity and BBB infiltration of dextran, showing minocycline induced inhibition of microglia decreased BBB permeability. Hu

et al 2017, also showed a decrease in Iba-1 expression in LPS exposed neonatal rats with melatonin, which inhibits the TLR4 and NF-kB pathway insinuating that microglial activation is linked to LPS pathway induction.

However, it was expected from previous literature that Iba-1 would be homogenously increased by LPS irrespective of age, throughout the hippocampal and cortical regions (Banks et al., 2015; Chen et al., 2012; Marschallinger et al., 2020; Qin et al., 2007). However, not dissimilar to astrocytic activation, the effect of LPS appears to be short-term with higher doses of LPS (>1 mg/kg), multiple doses or shortened experimental timeline (<48-hours) displaying the broadest effects on Iba-1 expression. Chen et al, 2012, showed that a single 1 mg/kg LPS dose displayed no Iba-1 changes whilst 2 or more doses increased the microglial activity marker significantly. Qin et al, 2007 remarked that there can be long term microglial activation observed up to 10-months post-injection, but this was with 5 mg/kg, a 5-fold increase from the current study.

When investigating the effect of age on LPS impact, it was hypothesized that this would increase activation when compared to young adult LPS mice, but this was not shown in this study. Some previous literature agrees with this, as a single low-dose LPS (0.1-0.63 mg/kg) injection compared in 2 month versus 18–21-month mice displayed significant changes in aged mice but not LPS mice at the same ages (Hart et al., 2012; Murtaj et al., 2019). This suggests that Iba-1 expression may be driven by ageing instead of low-grade systemic inflammation and that higher inflammatory stimuli are required to produce a significant effect.

Other methodology should be explored in the future to further characterise microglia population as Iba-1 is not the only marker of increased activity. Toll-like receptor 2, triggering receptor expressed on myeloid cells 2 (TREM2), CD163, FC/80 and CD11b have all shown increased expression in aged LPS studies, increasing the confidence that microglial activation is occurring, even if Iba-1 is not showing significant changes (Chen et al., 2012; Hart et al., 2012; Murtaj et al., 2019; Nikodemova et al., 2016). Of note is TREM2, which has decreased when animals treated with nanoparticle anti-inflammatory therapeutics (Ralvenius et al.,

2024; Sharma et al., 2023). This suggests that further work with the current liposomal formulation should look at anti-inflammatory therapeutics and assess a wide array of markers to gather an overview of microglial effects. Although the current study did not show significant increases in LPS-induced liposome infiltration, the concept that ageing alone allows for passage is further shown in these two studies lending future potential to the current formulation.

Age-related increases of microglia, linked to Iba-1 expression, in systemic inflammatory conditions has also been shown to effect cytokine production such as IL-1β, TNF-α and IL-6 (Garner et al., 2018; Nikodemova et al., 2016; Qin et al., 2007; Wynne et al., 2010). Microglia were isolated via flow cytometry and the amount cytokine expression assessed, confirming microglial activity as opposed to general brain expression. It would be worthwhile to repeat similar experiments with a repeat of the current study plan to elucidate if this occurs in the 0.25 mg/kg or 1 mg/kg 18-month groups. Wynne et al., 2010,noted that the increase of microglial IL-1β exclusively in the aged LPS groups correlated with decreases in CX3C motif chemokine receptor 1(CX_3CX1). This led to a possible therapeutic target which could be attenuated with TGFβ which simultaneously increased CX_3CX1 and decreased IL-1β which may act through the mothers against decapentaplegic homolog 3 (SMAD3) pathway (Tichauer et al., 2014).

Morphological changes to microglia, although not assessed in this body of work, may provide further information on how LPS and ageing affect the immune cell. General microglial changes observed within the literature include increased soma size, decreased process length and overall switch to an ameboid hypertrophic morphology (Jung et al., 2023; Qin et al., 2007; Sierra et al., 2007). These morphological changes have been correlated with Iba-1 increases as well as genes identified in a microarray study such as CD163, IL4a and Mannose receptor C-type 1 (Chen et al., 2012).

Studies have also noted behavioural changes to aged mice dosed with LPS such as decreasing burrowing and spatial memory (linked to hippocampal decline) as well as classical sickness behaviours (Chen et al., 2008; Hart et al., 2012; Huang et al., 2008).

4.5.5. Age and inflammation drive adhesion molecule activation

The study also aimed to investigate the effect of ageing and inflammation on adhesion molecules, specifically ICAM-1 and VCAM-1. Both molecules have been widely investigated in neuropathology, linking to an increased inflammatory profiles as in stroke (Jing et al., 2014; Lindsberg et al., 1996; Rakhimbaeva & Abdurakhmonova, 2023) schizophrenia (Cai et al., 2018, 2020) and AD (Chen et al., 2023; Drake et al., 2018, 2021; Hochstrasser et al., 2010; Otgongerel et al., 2023). However, there is limited data on the effect of adhesion molecules on neuroinflammation in physiologically aged mice models.

Within this body of work, immunofluorescence throughout each region show significantly higher expression of ICAM-1 in the 18-month 1 mg/kg LPS dose compared to 3-month LPS dose or vehicle at either age. This indicates that ICAM-1 requires both ageing and inflammatory stimuli to increase expression. ELISA data also shows that ICAM-1 is increased in brain tissue but that 1 mg/kg LPS at both ages produces the higher ICAM-1 expression, conversely indicating that inflammation is the driver of the response. No ICAM-1 expression changes were observed in the serum of either aged or LPS groups, signifying a brain-specific response.

Miguel-Hidalgo et al., 2007, demonstrated within an aged human cohort that ICAM-1 expression was increased within the orbitofrontal cortex dependant on age and that this correlates with astrocytic activation. Further murine studies in exclusively young cohorts show significant cortical and hippocampal ICAM-1 increases at 2-4 mg/kg doses after 24-hours (Brezzo et al., 2020; Swartzlander et al., 2018). *In vitro* LPS studies have linked the NF-kB pathway to the increases in ICAM-1 through gene and protein studies, with an NF-kB inhibitor reducing the levels of ICAM-1 in endothelial cells (Lee et al., 2015; Wong & Dorovini-Zis, 1992).

Pro-inflammatory cytokine expression may be linked to increased ICAM-1 as a study in mouse using an intracerebroventricular (ICV) dose of TNF-α in 4–16-month mice displayed up-regulated ICAM-1 in the hippocampus (Xu et al., 2010). Within this study it was shown that ageing on its own does not induce ICAM-1, agreeing with our current findings and that

augmentation by a secondary inflammatory stimuli was required. Separate studies have shown that both LPS and age independently and together increase TNF-α expression, (Huang et al., 2008; Porcher et al., 2021; Zhao et al., 2019).

Although not tested during this workflow, increased ICAM-1 has been shown to impact behaviour of mice including reducing cognitive function and decreasing sensorimotor function (Bhowmick et al., 2021; Cai et al., 2020; Zhao et al., 2019). These were all in models other than ageing so it would be critical to examine the effect of age and LPS on these parameters in correlation to ICAM-1. Furthermore, ICAM-1 has been revealed in an aged brain injury model to increase leukocyte infiltration, ROS and cytokines within the brain (Adamson et al., 1999; Knox et al., 2022). However, Elahy et al, 2015 remarked that in an aged model there was no increased leukocyte infiltration suggesting that physiological age exclusively would not have these effects and increased inflammation is required.

VCAM-1 expression was tested here using ELISA techniques only as there was not an optimised antibody for immunofluorescence with no significant changes were observed in either brain or serum samples. This may be timepoint related as an *in vitro* study using b.END.3 endothelial cells noted that VCAM-1 increased with LPS incubation between 12-24 hours but decreased back to baseline at 48-hours (Wong et al, 1999). As the samples were terminal, after 48-hours this would corelate with previous findings. Other studies *in vitro* utilised the same cell line showing correlation between LPS and increased VCAM-1 expression (Hortelano et al., 2010; Lee et al., 2017). Limited mouse models have also shown increases in VCAM-1 expression, with Swartzlander et al, 2018 demonstrating gene expression increases in 4 mg/kg LPS model. Yousef et al, 2019 further explored the impact of LPS induction on VCAM-1 in 18-month mice hippocampus, showing that not only is this increased but the injection of plasma from the old mice into young adult mice resulted in similar pathologies including activated microglia. This was shown to be VCAM-1 dependant as the inhibition of the adhesion molecule reverted the young mouse hippocampi to physiological levels.

Overall, the current work has found a novel increase in ICAM-1 in aging at a relatively low LPS dose compared to literature values. This suggests that ICAM-1 may be a target in the future for reduction inflammaging, but first further work must elucidate the impact of ICAM-1 on overall cognitive abilities. Knockdown or knockout ICAM-1 mouse studies should also be employed to determine if deleterious effects are reduced.

4.5.6. LPS-induced cytokine production

Increases of pro-inflammatory cytokines, such as IL-6 and IL-1β have been used to characterise and confirm inflammatory responses within the brain (Noori et al., 2020). Single LPS doses have noted these increases and so it was essential that they were examined during this study (Mota & Kelly, 2020; O'Neil et al., 2018; Vizuete et al., 2022; Vutukuri et al., 2018).

In the current study, it was found that IL-6 expression was not altered in either serum or brain samples at termination (48-hours) but was induced by LPS and further exacerbated by ageing at 3-hours post-injection. This indicates a time-dependant cytokine response which was reflected by an ageing study, observing increased IL-6 at 3-hours which then returned to baseline at 24-hours in 10-month mice (Nikodemova et al., 2016). Knopp et al, 2022 also displayed that in 16–18-month mice, a single 0.33 mg/kg injection did not elevate cytokine levels after 28-hours. Dose of LPS may therefore be crucial for cytokine levels as Erickson et al. 2018 demonstrated that after 28-hours 0.33 mg/kg showed no responses, but 3 mg/kg did. Rezaei et al., 2024, further investigated this in both the hippocampal and cortical regions of young mice brains, showing that a range 0f 0.125-2 mg/kg did not induce IL-6 expression 18-hours post-injection.

The increase in IL-6 may contribute to changes in LPS-induced sickness behaviour as the inhibition of Il-6 resulted in decreased sickness effects correlating with decreases in STAT3 activation and downstream reduction of NF-kB activation (Beurel & Jope, 2009; Burton et al., 2011). Furthermore, IL-6 has been linked to cognitive decline and administration with inhibitor Allopregnanolone, reducing working memory deficits of radial arm water maze in 24-month

mice (Parks et al., 2020). Relating Il-6 to BBB dysfunction in systemic inflammation, administering a cyclooxygenase enzyme inhibitor, indomethacin, reduced cytokine expression correlating with decreased BBB permeability to albumin, indicating effects on transcellular pathways (Banks et al., 2015). This overall effect was conserved in a mice model of periodontal inflammation, which increased BBB permeability (Furutama et al., 2020).

IL-1β was also assessed in brain homogenate samples 48-hours post-LPS and demonstrated a significant increase in age but only in the 1 mg/kg LPS groups, with further increases between 18-month vehicle and 1 mg/kg. Unfortunately, measurement of IL-1β in the 3-hour serum samples was not possible due to failure of optimisation but future work should investigate this. This demonstrates a differing expression profile to IL-6 which showed no increases at this timepoint. One theory may be that IL-6 attenuates IL-1β expression and therefore, when IL-6 levels decrease over time after LPS injection, IL-1β increases (Minogue et al., 2012). Another concept is that both cytokines are independent to each other, as IL-1β expression was increased in an IL-6 -/- aged (22-24 month) LPS model compared to 3–5-month mice with or without LPS (Garner et al., 2018).

Previous work predominantly focused on shorter timeframes for assessment of IL-1β levels so the up regulation at 48-hours points to LPS affecting levels for a long period of time (Henry et al., 2009; Vizuete et al., 2022). This suggests that IL-1β may be a potential anti-inflammatory therapeutic target in the future as time constraints are not as critical. IL-1β administration without LPS has been shown *in vivo* to increase neuronal activation and leucocyte infiltration combined with decreased motor skills, highlighting the wide-ranging effects of IL-1. This may be through activation of MyD88, which would instigate the same inflammatory pathways as LPS injection causing BBB dysfunction (Gosselin & Rivest, 2008; Zhu et al., 2012).

Another cytokine which should be explored in the future is TNF-α which has also been shown in LPS ageing studies to be increased (Murtaj et al., 2019; Sierra et al., 2007). Direct administration of TNF-α has been linked to increases of adhesion molecules such as ICAM-1,

which is of particular interest in this study as ICAM-1 levels were shown to increase (Xu et al., 2010).

4.5.7. Widespread proteomic changes to LPS-induced aged brain

The current study has been focused on specific proteins which were expected to be affected by either age or LPS inflammation, but this is limited to the targets instead of the overall changes to the brain under aged LPS conditions. Proteomics allows for a widespread investigation into changes that occur and allows for in-depth pathway analysis not only to see what is canonically changed but also potential diseases.

Correlation between immunofluorescence and ELISA study could take place via proteomics of caveolin-1, ICAM-1, VCAM-1 and GFAP. When comparing the effect of LPS dose on 18-month mice, it was shown that in 0.25 mg/kg none of the above proteins were changed which agree with the data generated in this study, suggesting that 0.25 mg/kg does not affect the aged brain in a significant manner. When comparing 1 mg/kg, only ICAM-1 differs in significance as immunofluorescence demonstrated significant increases whilst proteomics did not. Overall, the changes observed highlight the importance of multiple techniques investigating similar parameters.

When comparing increases in physiological age, there are some discrepancies as both GFAP and caveolin-1 were up-regulated which is more translatable to previous literature (Yang et al., 2020). No increase in VCAM-1 expression was observed unlike in the ELISA data, which correlates with previous work and may suggest that the brain does not increase VCAM-1 but serum does during ageing (Elahy et al., 2015). When investigating the effect of LPS on young mice, GFAP, caveolin-1 and VCAM-1 all reflect the same outcomes from the current study, pointing towards this being a consolidated effect. However, ICAM-1 was significantly increased in the proteomics study which may suggest that LPS independently of age also increases the adhesion molecule expression.

Using ingenuity pathway analysis, the changes to the proteome in each condition were be collated and a network pathway created to visually display connections. 18-month LPS mice have an increased network which recruited IL-1β, IL-6, STAT1 and NF-kB1 highlighting the increased inflammatory response of aged mice, correlating with findings within this study. Interestingly, the polarisation of leukocytes was up regulated which may highlight increases in adhesion molecules resulting in infiltration of leukocytes through BBB (Peng et al., 2021).

Conversely, within the 3 and 18-month vehicle comparison, this included up regulation of organismal death and degeneration with down regulation of CNS development. These all correlate with physiological ageing but when compared to the LPS pathways, is very limited showing no links with inflammatory signally pathways. Alternatively, when looking at the effect of 1 mg/kg on 3-month mice, TLR4 and TNF are up-regulated along with acute phase response signalling (Ciesielska et al., 2021; Nikodemova et al., 2016).

Pathway analysis also showed the most affected canonically with neutrophil degranulation being significantly changed in all compared datasets but within LPS groups this was up regulated and in ageing, down regulated. Neutrophil degranulation refers to the release of proinflammatory substances into the surrounding tissue with stimuli such as sepsis, arthritis and asthma (Lacy, 2006). It would be expected that this pathway was not up-regulated during physiological ageing as the BBB may prevent the crossing of neutrophils into the brain (Kanashiro et al., 2020; Manda-Handzlik & Demkow, 2019). *In vivo* studies using LPS have shown that CD11b neutrophils increase in the brain 4 hours post-injection and that this is specific to cortical regions (Aries et al., 2024; Mol et al., 2021). The current study used whole hemisphere brain homogenate as opposed to Aries et al, 2024 and therefore could not specify which regions were affected. Wu et al., 2020 demonstrated that neutrophil entry and degranulation within the brain was induced by C-X-C Motif Chemokine Receptor 2 and an antagonist of this reduced the migration of cells. This pathway suggests that neutrophil activation is present regardless of age or LPS dose, meaning that it could be a potential target in the future to reduce neuroinflammatory responses.

When comparing disease function pathways, both neurological disease and organismal abnormalities are common through all analysed datasets showing the importance of both in ageing and neuroinflammation. In both conditions, morphological changes to cells such as microglia and astrocytes have been reported, confirming the vast array of changes within the model (Goodall et al., 2018; Jung et al., 2023; Qin et al., 2007). Hierarchical clustering of the overall proteome shows specific grouping of the 3-month vehicle group independently of LPS conditions whilst 18-month LPS conditions were grouped together separately to 3-month LPS. This further highlights the differences observed in an aged inflammatory environment and shows the importance of investigating these changes more thoroughly.

For future targeting, identification of important proteins must be elucidated from the wider dataset, therefore, common up/down regulated proteins were found either comparing 3-month vehicle to age or 1 mg/kg LPS or 18-month vehicle to 0.25/1 mg/kg LPS.

From this, several key proteins were up-regulated within the 18-month LPS cohort including S100 calcium binding protein A9 (S100a9), CD38 and Stat1 whilst important down-regulated proteins were ATPase phospholipid transporting 11B (Atp11b), CREB-regulated transcription coactivator 1 (Crtc1) and Fragile X Messenger Ribonucleoprotein 1 (Fmr1). CD38 expression has been linked to reduction in nicotinamide adenine dinucleotide (NAD) during murine ageing leading to mitochondrial dysfunction through the SIRT3 pathway (Camacho-Pereira et al., 2016). Further work expanded this into LPS-induced neuroinflammation, displaying increased cortical and hippocampal CD38 leading to activation of astrocytes and microglia acting through the NF-kB pathway (Roboon et al., 2021). The same study showed that inhibition of CD38 reduced glial activation in LPS proving it is a suitable anti-inflammatory target. S100a9 has been shown to increase in both ageing and inflammation within humans and murine models (Denstaedt et al., 2018; Swindell et al., 2013; Wang et al., 2018). Denstaedt et al, 2018 displayed links between S100a9 in a CLP model to neutrophil migration in the brain, linking back to the neutrophil degranulation pathway shown in this study. The same study also noted that decreased S100a9 caused reductions in microglial TNF-α and ROS production,

highlighting the importance of the protein in the inflammatory cascade. STAT1 has been shown both *in vitro* and *in vivo* to induce macrophage activation and iNOS production, leading to an inflammatory environment (Ohmori & Hamilton, 2001). Further work in inflammatory models shows decreased astrocytic GFAP expression and cytokine expression in STAT1 -/- mice (Imitola et al., 2023). Cognitive decline has also been noted with increased STAT1 expression, showing decreased memory and spatial learning in STAT1+ mice compared to -/- (Hsu et al., 2013).

Lysosome-associated membrane protein-2 (LAMP-2) was also increased in ageing which has been linked to the dysfunction of microglia and hippocampus during inflammation (Quick et al., 2023; Rothaug et al., 2015). Increased LAMP-2 has interestingly been linked to increased uptake of nanoparticles through the BBB, suggesting a possible mechanism for transport instead of caveolae-mediated transcytosis (Lamson et al., 2024; Muscetti et al., 2023). Further investigations would be warranted to explore this within the context of liposomes featured in this body of work.

Common down-regulated proteins ATP11b and CrtC1 are involved in normal hippocampal functioning such as plasticity and memory learning and reduction of either protein induces cognitive impairment and senescence of the hippocampus correlated with decreases in MAPK pathway and correlates with age-related hippocampal decline (Liu et al., 2022; Wang et al., 2019; Wang et al., 2023; Yan et al., 2021). CrtC1 was seen in a rat model of LPS inflammation to be reduced and was linked to decreases in BDNF (Shu et al., 2020). Fmr1 was also down-regulated in both LPS models and fmr -/- mice have shown increased microglial activation with LPS treatment correlated with increased cytokines, mitochondrial dysfunction and phagocytosis (Hodges et al., 2020; Parrott et al., 2021).

When comparing the 3-month vehicle to 18-month vehicle and 3-month LPS to determine commonality, there were only 4 common down-regulated proteins including Epidermal growth factor receptor kinase substrate 8 (Esp8) and TBC1 domain family member 10A (Tbc1d10a). Reduction of Esp8 has been shown in LPS studies to decrease cognitive function in mice by

decreasing the LTP action potential, believed to be through actin capping (Menna et al., 2013; Stamatakou et al., 2013). Tbc1d10a has been shown to functionally regulate the secretion of exosomes from neuroglia, especially oligodendrocytes, via Rab GTPase but the inhibition of these through reduction in Tbc1d10a intracellular accumulation of exosomes leading to damage (Hsu et al., 2010). However, limited work has been conducted on ageing or inflammation regarding this protein so this may be a novel finding within the field warranting further investigation.

Key up-regulated proteins include Rho GTPase activating protein 25 (Arhgap25) which has been shown within inflammation to increase the granulocytes of neutrophils (Csépányi-Kömi et al., 2012; Pinosanu et al., 2023; Subhash et al., 2019). This links to the neutrophil degranulation pathway identified in this study, further highlighting the importance of this in neuroinflammation. Interferon-induced protein with tetratricopeptide repeats 3 (Ifit3) which is normally absent in healthy tissue but is expressed in reaction to stimuli such as LPS (Fensterl & Sen, 2011; Garces et al., 2023). Both ageing (in the context of AD) and low-grade LPS inflammation have been linked to Ifit3 expression in the brain agreeing with the findings shown in the current study (Harmon et al., 2022; Naler et al., 2022). Naler *et al,* 2022 noted that the increase in Ifit3 was present in low-grade LPS (100pg/ml) and not high-grade (1 ug/ml) which may explain why this was up-regulated during 3-month inflammation and not the exacerbated 18-month companion.

Interestingly, serine protease inhibitor clade A member 3n (Serpin3n) was the only protein commonly up regulated throughout both ageing and inflammation, suggesting that this is very important in the mechanisms for each. Serpin3n is mainly expressed within astrocytes has been shown to increase in human ageing with correlations to cognitive dysfunction (Cluett et al., 2010; H. Kim et al., 2022). Age-induced expression has also been observed *in vivo* with 24-month mice possessing a 4-fold increase compared to 4-month mice (Boisvert et al., 2018; Clarke et al., 2018). Clarke *et al* further demonstrated in 14-month mice that Serpin3n was independent to cytokine production with IL-1β and TNF-α -/- models but the inverse is not

independent and reduction in Serpina3n reduces TNF-α (Kim et al., 2022). The same study also administered Serpin3n in culture, resulting in BBB dysfunction *in vivo* with reductions in claudin-5 and increases in VCAM-1. However, this did not result in increased BBB permeability to dextran but was conducted in young adult mice so further ageing may be required for this effect.

Clarke et al, 2018 also investigated the impact of age and LPS, showing that 24-month LPS treated mice had significantly more Serpina3n expression then either aged-matched controls or young LPS mice. The mechanism of action has been investigated showing activation of key inflammatory pathway molecule STAT3 leading to NF-kB activation (Kim et al., 2022). This activity was dependent on both factor as STAT3 -/- mice resulted in no BBB or cognitive dysfunction with increased Serpin3n.

This highlights Serpin3n as a key protein in inflammatory effects both in age and LPS induction, potentially opening an avenue for targeted nanoparticle treatment. So far, there have been limited studies aimed specifically at targeting Serpin3n in ageing but a study in hippocampal stab injury used an MMP2 inhibitor to target the protein resulting in decreased memory and learning deficits (Wang et al., 2020). Further encouragement for treatment is that in young adult mice, inhibition or administration of Serpina3n did not have any deleterious effects mentioned above and performed normal functions in myelination and cell development (Zhu et al., 2024). This suggests that any inhibition would selectively target age-related effects of increased Serpin3n.

4.6. Limitations and future work

The aim of this chapter was to provide pilot data as proof-of-concept that LPS-induced inflammation was affected by age leading to changes in nanoparticle infiltration. Therefore, this study was not powered sufficiently, and group numbers were determined by availability of 18-month mice when the work was scheduled. Future work would need to be correctly powered and could utilise the nanoparticle infiltration data provided in this body of work for

power calculations. This study also did not include a 3-month group with 0.25 mg/kg LPS injection so if the experiment was repeated this would need to be included to directly compare the effect of ageing on the inflammatory response but also to see if there is a dose-dependent response in young mice, like that identified in the 18-month group here.

Furthermore, due to the lack of a 3-month 0.25 mg/kg group, comparisons between groups were not included in a single analysis. Instead, these were split into a 2-way ANOVA comparing 1 mg/kg LPS and vehicle in ageing and a 1-way ANOVA comparing LPS doses in 18-month mice. This meant that the 0.25 mg/kg groups was not included in any age comparison, limiting its impact in this study as it was not compared to the expression levels of any parameter in the 3-month group (vehicle or LPS). In the future, any repeat of the study should include a young 0.25 mg/kg group so that full analysis can be conducted using a 2-way ANOVA statistical method.

The exclusion of male mice is another limitation of this study as the comparison between sex is crucial to translatability of findings to a clinical setting. Investigations into LPS-induced sex differences in the BBB context are limited so this would add to an important gap within the literature. It has been shown *in vivo* that there are differences between the response of males and females to LPS injection with females showing increased cytokine production and anxiety behaviour and males an increase in GFAP+ astrocyte response (Dockman et al., 2022; Murtaj et al., 2019). However, other studies have shown that estrogen produced in females may be neuroprotective, reducing lymphocyte migration and BBB disruption (Maggioli et al., 2016). Experiments would have to determine levels of estrogen within each subject or have a female group with lower estrogen levels, via gonadectomy or ovariectomy to accurately assess the sex differences (Itoh et al., 2023).

Another limitation of this study was the investigation of only a single marker for astrocytes, microglia and adhesion molecules limiting the analysis of each cell type. No significant changes were observed in Iba-1+ cells but the marker TREM2 may be more suitable and has been shown in ageing studies to decrease with LPS inflammation in the hippocampus, cortex and cerebellum (Murtaj et al., 2019). The current study also focused on the expression and

colocalisation of cellular markers with DiI-lip and CD31 but not morphological changes. Quantitative analysis utilising available ImageJ plugins such as Sholl analysis, providing information on branch length, number of branches and volume of soma for both glial cell types, which could reflect more functional changes in ageing inflammation then classical expression (Murtaj et al., 2019). Furthermore, for ELISA protein investigations, the use of a multiplex system instead of the above selected molecules would provide more information regarding the changing inflammatoru profile in age and neuroinflammation (Manglani et al., 2019).

The current study, due to restrictions in the animal licence, could use a single dose point of LPS injection but this limits comparison to previous literature with many utilising a multi-dose strategy. Future work should focus on administering multiple does over a longer timeframe with lower LPS concentration to compare to previous work and more accurately mimic long-term systemic inflammation caused by age-related co-morbidities.

Comparability to previous literature is also a limitation within this study as many studies have used higher doses of LPS to assess BBB disruption (table 4-3). However, care must be taken as LPS dose above 5 mg/kg induces septic shock and 10 mg/kg is almost at lethality of young adult mice, meaning that these are not relevant models for low-grade systemic inflammation (Qin et al., 2007; Tateda et al., 1996). Also of consideration is the mortality of aged mice vs young adult mice as studies have shown the survival rate of mice injected with 2.5 mg/kg LPS is 100% after 48-hours in 4-month mice but this drops to only 30% in 24-month mice (Starr et al., 2010; Tateda et al., 1996). This correlates with our own study whereby 2 18-month mice experienced death within 48-hours of a single 1 mg/kg LPS dose. This may explain the lack of age-related LPS studies as the dose required for observed effects in young adult mice would cause mortality in aged counterparts.

Overall, the variability of LPS literature leads to a conflicting picture of how systemic inflammation affects the aged BBB and further work must be implemented to further characterise the changes. Table 4-3 lists the main studies investigating BBB with LPS showcasing this variability within a relatively small cohort of papers.

4.7. Concluding remarks

Overall, this study did not show convincing evidence that systemic inflammation within ageing caused significant increases in infiltration of nanoparticles, iron or blood-borne proteins. Changes to astrocytic and microglial activation were not significant during this study but did show non-significant trends which could be expanded with higher n-numbers. However, the combination of age and LPS did affect adhesion molecules (specifically ICAM-1) and pro-inflammatory cytokines (Il-1β and IL-6) but the time of examining each component is critical to the inflammatory outcomes. Wide-spread changes were observed in proteomics, pointing to common changes in age and LPS linked to the STA3 and NF-kb pathways, particularly the upregulation of astrocytic Serpina3n. Targeting the identified inflammatory pathways and related adhesion molecules could have the potential to reduce systemic inflammatory effects on the brain microenvironment.

Table 4-3: Differing study design investigation LPS-induced inflammation on the BBB studies. Details of murine-based studies specifying sex, age, LPS serotype, route of administration, LPS dose, dose regime and time duration between dosing and termination of the study. Order determined by maximal LPS dose.

Study	Sex	Age (months)	LPS serotype	Admin route	Dose amount (mg/kg)	# doses	Post-dose interval
(Hu et al., 2017)	Mixed	10-12 day	N. S	I.P	0.05	1	1 week
(Knopp, Banks, et al., 2022)	Female	16-18	O55:B5	I.P	0.33	1	28-hours
(Murtaj et al., 2019)	Mixed	2, 17-18	O55:B5	I.P	0.63	1	6-hours
(Banks et al., 2015)	Male	> 2	N. S	I.P	1	X7 over 7 days	24-hours
(X. Wang et al., 2017)	Male	24-28	N. S	I.P	1	1	24 hours
(Sumbria et al., 2018b)	Mixed	3, 18	N. S	I.P	1	3	1 week
(Chen et al., 2012)	Male	2	O55:B5	I.P	1	1, 2, 4 days	24-hours post-final injection
(Y. Liu et al., 2021)	Mixed	2	O111:B4	I.P	1	1	7- days
(Zheng et al., 2022)	N. S	N. S	N. S	I.P	1	1	24-hours
(Ralvenius et al., 2024)	Male	2	O55:B5	I.C/I.P	1	1	N. S
(Haruwaka et al., 2019)	Male	2	N. S	I.P	1	1/ x7 over 7 days	1 week +
(Erickson et al., 2018)	Mixed	2	N. S	I.P	0.3, 3 3	1 3	28-hours
(Logsdon et al., 2020)	Mixed	2	N. S	I.P	3	3	28-hours
(Barton et al., 2019)	Mixed	3-5, 13-15	O111:B4	I.V	3	1	30-hours
(Jangula & Murphy, 2013)	Male	2	O55:B5	I.P	3	3 1	2-hours 2- hours
(Maggioli et al., 2016)	Mixed	2, 15	N. S	I.P	3	1	4, 24-hours, 7-days
(Vutukuri et al., 2018)	Male	> 2	O55:B5	I.P	4	1	4-hours
(Xingi et al., 2023)	Mixed	2	O55:B5	I.P	5	2	1, 4, 8 days
(Long et al., 2020)	Male	N. S	O55:B5	I.T	8	1	12-hours

(Banks & Robinson, 2010)	Male	2	ATCC 7823.	J. V	9.4	1	>20-minutes
(Britton et al., 2022)	Male	2, 24	O55:B5	I.P	10	1	6-hours

* I. P= intraperitoneal, I. T= intrathecal, J. V= jugular vein, I. V= intravenous, I.C= intracisternal, N. S= not stated

5. Assessing the impact of liposomal delivery of an anti-inflammatory therapeutic on the aged cerebrovascular system

5.1. Introduction

Within the previous two chapters, it has been demonstrated that in the aged mouse brain, an increased inflammatory response occurs. Therefore, the targeting of age-related inflammation is an avenue of increased interest within the field. Environmental methods of reducing inflammation include changes to diet and increasing exercise, both of which have been demonstrated in human trials to reduce neuroinflammation (Kip & Parr-Brownlie, 2023). However, compliance to these environmental changes can be low within the aged population, especially increasing exercise due to decreased motor capabilities (Clark & Taylor, 2011).

Anti-inflammatory therapeutics, such as glucocorticoids (GC) or non-steroidal anti-inflammatory drugs (NSAIDS) have been prescribed to either treat or prevent inflammatory responses. However, the use of GCs in the context of reducing age-related neuroinflammation should be avoided due to severe side-effects (Hill & Spencer-Segal, 2021). Cushing's disease is a well-known effect of long-term GC administration and has been linked to hippocampal atrophy as well as a reduction of cognitive abilities (Dekkers et al., 2022; Patil et al., 2007). *In vitro* and *in vivo* studies have also shown that within the brain, GC's can cause a pro-inflammatory response, increasing cytokines IL-6 and IL-1β prior to onset of another inflammatory event and may be linked to administration prior to significant inflammatory event (Frank et al., 2010; Horowitz et al., 2020). Compounding these effects is the need to administer high doses of GC's, such as dexamethasone, to pass the BBB (de Kloet et al., 1975). Altogether, GC's are not suitable as a choice for anti-inflammatories in the brain.

NSAID's, such as ibuprofen, are safer and have been shown to reduce neuroinflammation in AD and Parkinson's disease (Auriel et al., 2014; Gao et al., 2011). Studies have shown in aged humans that NSAID's can reduce neuroinflammation (Le et al., 2018; Walther et al., 2011). Le et al., 2018, demonstrated in a clinical trial that a high dose (600mg) of ibuprofen decreased

overall brain hallmarks of neuroinflammation in age, passing the BBB. Administering ibuprofen *in* vivo to an ageing mouse model with enhanced NF-kB reduced neuroinflammation via reduction in pro-inflammatory cytokines and activated microglia, as well as increasing cognitive abilities in y-maze tasks (Fielder et al., 2020). However, high and consistent treatment with NSAID's clinically has shown increased risk of renal and cardiovascular failure as well as stroke within the older population (Choi et al., 2010; Marcum & Hanlon, 2010).

Alternatively, to the above discussed treatments which target global inflammatory processes, it may be more valuable to investigate the antagonism of specific pro-inflammatory molecules. IL-1β is a pro-inflammatory cytokine which has been shown in ageing to significantly increase within the brain (Porcher et al., 2021). This increase is associated with BBB disruption, being linked via downregulation of SHH in astrocytes and WnT in endothelial cells, increasing BBB permeability (Fetsko et al., 2023; Wang et al., 2014).

Currently, there not any studies *in vivo* or clinically that have investigated antagonism of IL-1 within physiologically aged subjects. However, there are multiple Il1 targeting drugs which have been utilised in other inflammatory related conditions such as rheumatoid arthritis, cryopyrin-associated periodic syndromes (CAPS), peritonitis, COVID-19 and AD (Calabrese et al., 2002; Church & McDermott, 2010; Khani et al., 2022; Kitazawa et al., 2011; Lin et al., 2021). Therapies targeting IL-1 can be categorised into three main subgroups; neutralisers of IL-1, sequesters of IL-1 and receptor antagonists (Dinarello et al., 2012).

Neutralisers of IL-1β are typically specific antibodies that mechanistically act by binding to IL-1β and blocking the ability to bind to the IL-1 receptor meaning it is non-functional (Chakraborty et al., 2012). This is advantageous as no interactions with IL-1α occur, allowing for the perseveration of IL-1α as this can act locally as an anti-inflammatory promoting production of IL-8 (Dinarello, 2018). The main clinically approved neutralisers are

Canakinumab and Gevokizumab and are used as treatments in conditions such as CAPS, atherosclerosis and diabetes (Cavelti-Weder et al., 2012; Church & McDermott, 2010; Lin et al., 2021; Ridker et al., 2017). Cavelti-Weder et al., 2012, demonstrated in humans, that low levels of antibody are required to target the pg/ml expression of IL-1β, meaning that a single dose is adequate for treatment.

The second type of IL-1 blocking is by sequestering the cytokine molecule with Rilonacept being the main drug within this category (Dinarello et al., 2012). This drug was initially approved for clinical use in the CAPS setting and is composed of two chain of IL-1 receptor which then bind to the molecule and prevent it binding to the actual receptor (Van Tassell et al., 2013). Further phase III clinical trials have also shown positive anti-inflammatory results within the pericarditis setting (Klein et al., 2021).

The final type of molecule targeting IL-1 is the IL-1-receptor antagonists (IL1-ra), which binds to the receptor on the cell membrane and block binding of IL-1, rendering it inert (Murray et al., 2015). The main molecule of interest in this category is Anakinra, which was the first anti-IL1 drug clinically approved in 2002 for rheumatoid arthritis (Calabrese et al., 2002). Since this point, there has been interest in applications to other inflammatory conditions with clinical trials being conducted in diseases related to diabetes, heart, cancer, COVID-19 and the brain (fig 5-1).

In relation to the brain, multiple *in vivo* studies have investigated the potential of IL1-ra to reduce stroke related inflammation (Pradillo et al., 2012, 2017; Xia et al., 2014). The key findings of these studies relate to reduction in overall infarct volume but also decreases in ICAM-1, TNF-α and IL-1β levels. This all lead to a reduction in ROS and leukocyte infiltration which may cause less damage to the BBB. Pradillo et al, 2017, linked this to ageing via comparison of aged and young rats and demonstrated a higher effect in the elderly cohort.

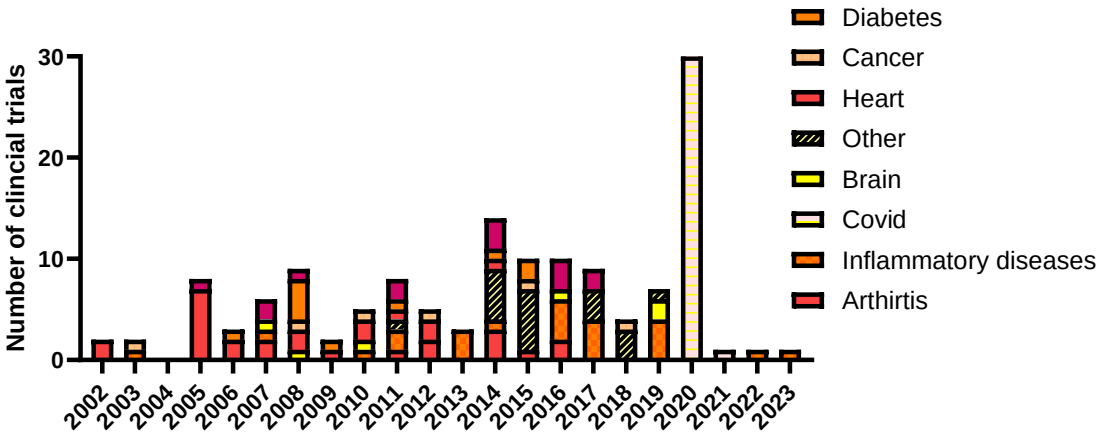

Figure 5-1: Clinical trials of Anakinra. Graphical representation of clinical trials using IL1-ra, Anakinra, from 2002 to 2023 categorising each study based on target organ or disease. Data based off https://trialsearch.who.int/.

Human clinical trials have been conducted within the stroke setting with promising results for reduction in inflammation (Cliteur et al., 2024; Emsley et al., 2005; Parry-Jones et al., 2023). Within epilepsy, IL1-ra has also reduced microglial activation further demonstrating anti-inflammatory affects within the brain (Zakharova et al., 2024).

In the setting of physiological ageing, the ability of IL1-ra to cross the BBB is debated as *in vivo* this has not been the case, due to 17.3 KDa molecule being larger than the 400 Da limit for normal penetration (Murray et al., 2015; Powers et al., 2020). However, *in vitro* and clinical studies have noted that IL1-ra can pass through the BBB so further work is required to elucidate this (Galea et al., 2011; Sjöström et al., 2021). IL1-ra also has a short half-life of 4-6 hours, leading to increased dosages or ineffectiveness of the drug (Akash et al., 2013). Both the short circulation time and potential inability to cross the BBB points towards encapsulation into nanoparticles to penetrate the BBB and increase effectiveness. An *in vivo* rat study of periodontitis utilising PLGA nanoparticles loaded with IL1-ra showed an increased half-life of IL1-ra and was non-toxic (Ren et al., 2021).

5.2. Aims and objectives

This chapter aims to, for the first time, use IL1-ra to reduce inflammation in the physiologically ageing brain. Evaluation of liposomal IL1-ra effectiveness on the aged female mouse brain will be compared to the free drug and vehicle control. Changes to key cells within brain inflammation, astrocytes, and microglia, will be quantified as well as key inflammatory cytokines and adhesion molecules. The infiltration of blood-borne molecules through the BBB will be assessed to determine the rescuing effect of IL1-ra-lip. Overall, this chapter will determine if Il1-ra is a potential therapeutic for age-related inflammation and if the liposome formulation enhances the effects.

5.2.1. Hypotheses

1. That IL1ra-lip will reduce inflammatory response of aged brain
2. That IL1ra-lip will have a greater anti-inflammatory effect then IL1ra free drug
3. That IL1ra-lip will reduce permeability of BBB in aged mouse

5.3. Methodology

Detailed methodology can be found within chapter 2 of this body of work. The overall study design is visualised within fig. 5-2.

5.3.1. Study design

Female mice were purchased from Charles River at 18 months of age and measured twice weekly for changes to bodyweight adhering to guidelines set out by (Wilkinson et al., 2020). Mice were housed in n=3 for a total of 21 mice for the study, with each cage containing a mouse per condition, equalling n=7 experimental units. Within each cage, mice were assigned to a group; vehicle control, IL1-ra-lip or free IL1-ra, based on ear notching carried out randomly by a member of Nottingham Trent University barrier support facility. Over a 2-week period, each

A

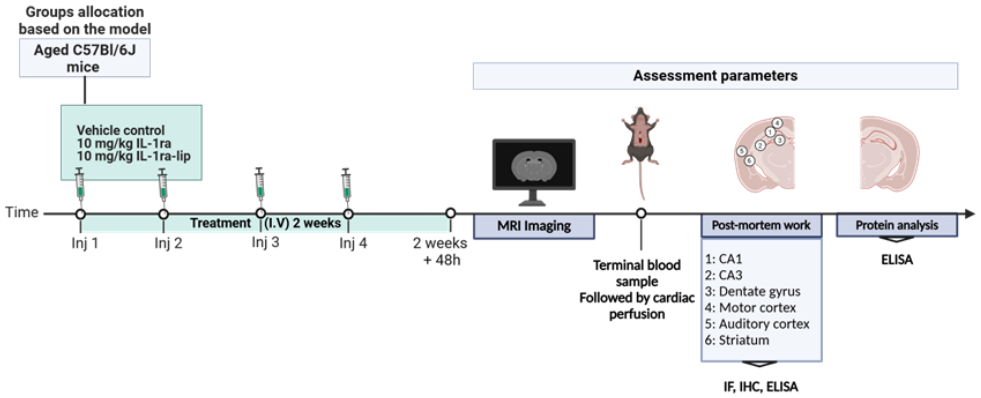

B

Therapy condition	MRI	IF	IHC	ELISA	MS
Vehicle control	7	7	7	7	7
IL1-ra	7	7	7	7	7
IL1-ra-lip	6	6	6	6	6

*MRI: Magnetic resonance imaging, IF: Immunofluorescence, IHC: Immunohistochemistry, ELISA: enzyme-linked immunoassay, MCAo: Middle cerebral artery occlusion.

Figure 5-2: Schematic representation of ageing IL1-ra-lip therapy study and study n-numbers. (A) Diagrammatic representation of study plan. 18-month female mice were injected intravenously with either IL1-ra-lip, IL1-ra or vehicle control on 4 occasions over a 2-week period. 48-hours post final injection mice underwent MRI imaging with VCAM-1-MPIO contrast agent prior to terminal blood sample collection and cardiac perfusion. Brain hemispheres were split and used for listed downstream analysis techniques. (B) Tabular representation of all mouse groups within the study specifying the sex and age of each cohort and the predicted n-number per assessment parameter.

mouse was injected intravenously via tail vein, under anaesthesia, with the assigned treatment to a total of 4 injections (2.7). Blinding of the study to the researcher occurred, with Zahraa Al-Ahmady performing the I.V injections and the groups not divulged to the principal investigator until after all quantification analysis was completed. One mouse in the IL1-ra-lip group was excluded from the study as it died during initial experiments due to previously unknown clinical co-morbidities.

5.3.2. Liposome production and characterisation

Liposomes were produced with the following composition HSPC: Chol: DSPE-PEG2000: DSPE-PEG-Maleimide (56.3:38.2:3.5:2 mol/mol%) and IL1-ra (Kineret; Amgen, USA) attached to the phospholipid bilayer via coupling reaction (2.5.2). Further characterisation of liposomes included size, zeta potential, IL1-ra protein concentration and lipid composition to determine homogeneity between batches and suitability for the study (2.6).

5.3.3. MRI

To determine the presence of endothelial VCAM-1, mice underwent MRI imaging with MPIO-VCAM-1 contrast agent. Pre- and post-contrast binding was quantified using a MATLAB script (2. 15).

5.3.4. Immunohistochemistry

Tissue cryosections were stained immunohistochemically for IgG to determine BBB permeability and extravasation into brain parenchyma (2.12). Negative control images (without primary antibody) are found in appendix 3. Any tissue loss is recorded in appendix 4.

5.3.5. Immunofluorescence

To determine changes to astrocytic and microglial expression within the three groups, GFAP, S100β and iba-1 respectively were quantified via immunofluorescence. Potential changes to

interaction with the BBB were assessed with colocalisation studies between the cellular marker and CD31 (2. 11). Negative control images (without primary antibody) are found in appendix 3. Any tissue loss is recorded in appendix 4.

5.3.6. ELISA

To assess changes to brain levels of adhesion molecules (ICAM-1 and VCAM-1) and pro-inflammatory cytokines (IL-1β), tissue was homogenised prior to target-specific ELISA's (2. 13, 2. 16). Comparison of brain expression levels and peripheral levels of ICAM-1 and VCAM-1, as well as pro-inflammatory IL-6, were conducted via extraction of plasma from blood samples and ran through appropriate ELISA methods (2. 9, 2.16).

5.3.7. Statistical analysis

Comparison of all 3 groups was undertaken for experimental outcomes using GraphPad Prism software. The Shapiro-Wilks test for normality determined whether datasets were parametric or non-parametric and either the 1-way ANOVA or Kruskal-Wallis statistical tests completed. To evaluate changes in each group, either the Tukey or Dunn's multiple comparison test followed either test. For analysis of ICAM-1 and VCAM-1 expression, 2-way analysis of variance compared brain and serum sample differences. Graphical representations signified mean ± standard error of mean (SEM) and all significant results were graphically annotated using the following ranking: * $p<0.05$, ** $p<0.01$, *** $p<0.001$ (2.17).

5.4. Results

5.4.1. Characterisation of Il1-ra-lip

To ensure that each batch of Il1-ra-lip were homogeneous measurements of the size, PDI and zeta potential were taken (fig. 5-3). All PDI were below 0.2, demonstrating a monodisperse nanoparticle formulation. The size ranged from 134-168 nm, but all were below the 200 nm limit for BBB permeability. Zeta-potential all showed strongly negative liposomes between -23.9 and -32.1.

5.4.2. Decreased VCAM-1 binding with Il1-ra-lip

To assess the expression of VCAM-1 of 18-month female mice when treated with Il1-ra-lip, mice underwent functional MRI utilising VCAM-1-MPIO as the contrast *agent* (fig. 5-4e). Binding of VCAM-1-MPIO was significantly reduced by treatment with Il1-ra-lip ($F=6.461_{(2,15)}$, $p=0.0056$) but was not significantly reduced by unconjugated Il1-ra ($F=6.461_{(2,15)}$, $p=0.5224$). This demonstrates that the expression of VCAM-1 was only reduced by the liposomal formulation and not the free drug.

5.4.3. No effect of Il1-ra-lip in BBB permeability

To determine the effect of Il1-ra-lip on BBB permeability, infiltration of IgG was assessed and resulted in no significant changes to the vehicle control in any hippocampal (CA1, CA3, dentate gyrus, cortical (motor and auditory) or striatal regions (fig. 5-5b-g). No changes were observed in the same experiment between the vehicle control and free Il1-ra or between free-Il1-ra and Il1-ra-lip.

5.4.4. No changes in astrocytic expression

One hypothesis of this study was that Il1-ra-lip would decrease the neuroinflammatory activation of astrocytes. To assess this, tissue was immunofluorescently labelled with GFAP,

and treatment group compared to vehicle control and free Il1-ra. Within the hippocampal regions, no significant changes to GFAP expression were observed (fig. 5-6b, g, l). To assess

A

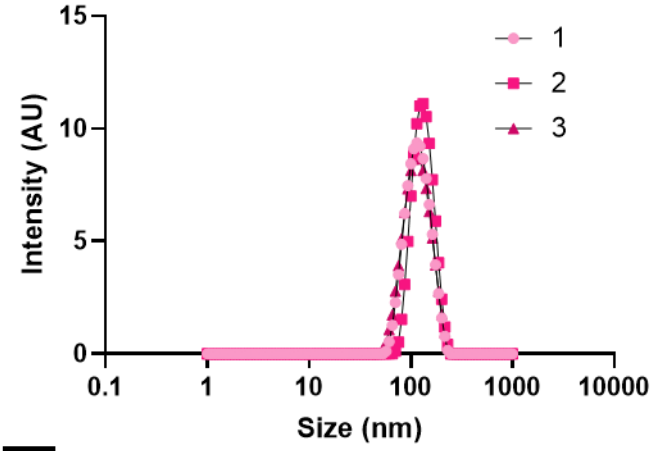

B

Batch	Size ± SD (nm)	PDI ± SD	Zeta potential ± SD (mV)
1	148 ± 3.46	0.097 ± 0.02	-27.7 ± 1.61
2	168 ± 1.24	0.170 ± 0.02	-32.1 ± 1.00
3	134 ± 1.91	0.097 ± 0.02	-23.9 ± 0.321
Lipid composition (25 mM)	HSPC:Chol:DSPE-PEG2000:DSPE-PEG-Malemide (56.3:38.2:3.5:2 mol/mol%)		
IL1-ra : Lipid (ng/µM/ml)	15.62		

Figure 5-3: Liposome characterisation for IL1-ra-lip therapy cohort. Liposomes were made with identical formulations using thin film hydration followed by extrusion. IL1-ra was conjugated to the liposome and size (in nm), zeta potential (ZP) and poly-dispersal index (PDI) were all completed in triplicate via dynamic light scattering. Amount of IL1-ra protein conjugation and lipid composition were also measured across batches and presented as a ratio of protein: lipid composition. (A) Graphical representation of LPS cohort liposome size. (B) Fluorescence intensity of average liposome batches in LPS cohort. (E) Lipid compositions, size, Average PDI, ZP, protein concentration and lipid amount values for each liposomal cohort batch. All graphs created using GraphPad Prism

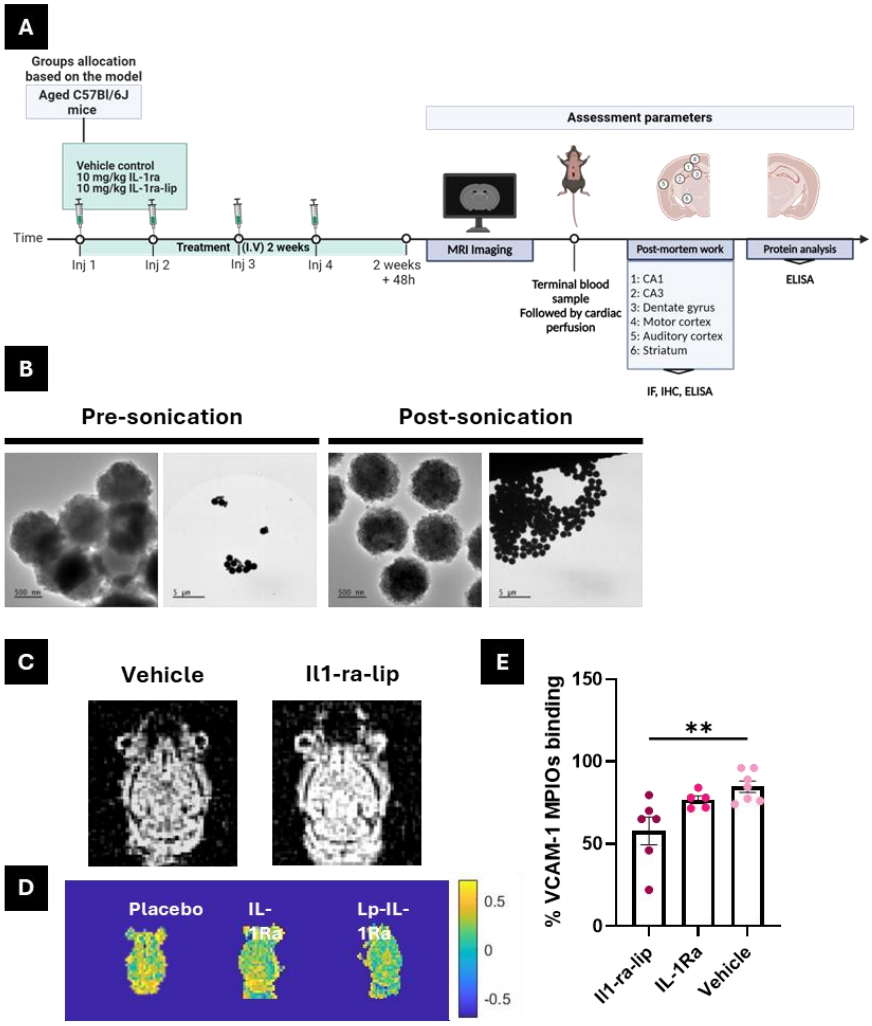

Figure 5-4: Evaluation of VCAM-1 binding in IL1-ra-lip therapy study. C57BL/6 18-month female mice groups were injected intravenously with either IL1-ra-lip, IL1-ra or vehicle control 4 times over 2 weeks. Pre-contrast MRI imagine acquired background levels per mouse and then were injected intravenously with VCAM-1-MPIO. 5-minutes post-injection, further MRI images were acquired and then underwent MRI imaging prior to cardiac perfusion. (A) Diagrammatic representation of study design. (B) Representative transmission electron microscopy images showing aggregation of VCAM-1-MPIO pre-sonication but not post-sonication. (C) Representative MRI images of Vehicle and IL1-ra-lip. (D) Representative images of MATLAB analysis of comparison between pre- and post- contrast images. (E) Quantification of VCAM-1 binding demonstrating significant decreases in binding in IL1-ra-lip compared to vehicle control. Statistical analysis was completed using GraphPad Prism software using a one-way analysis of variance followed by Tukey's multiple comparison test dependent on Shapiro-Wilkes normality test. N=5-7, average ± SEM, $p<0.05$ were considered significant

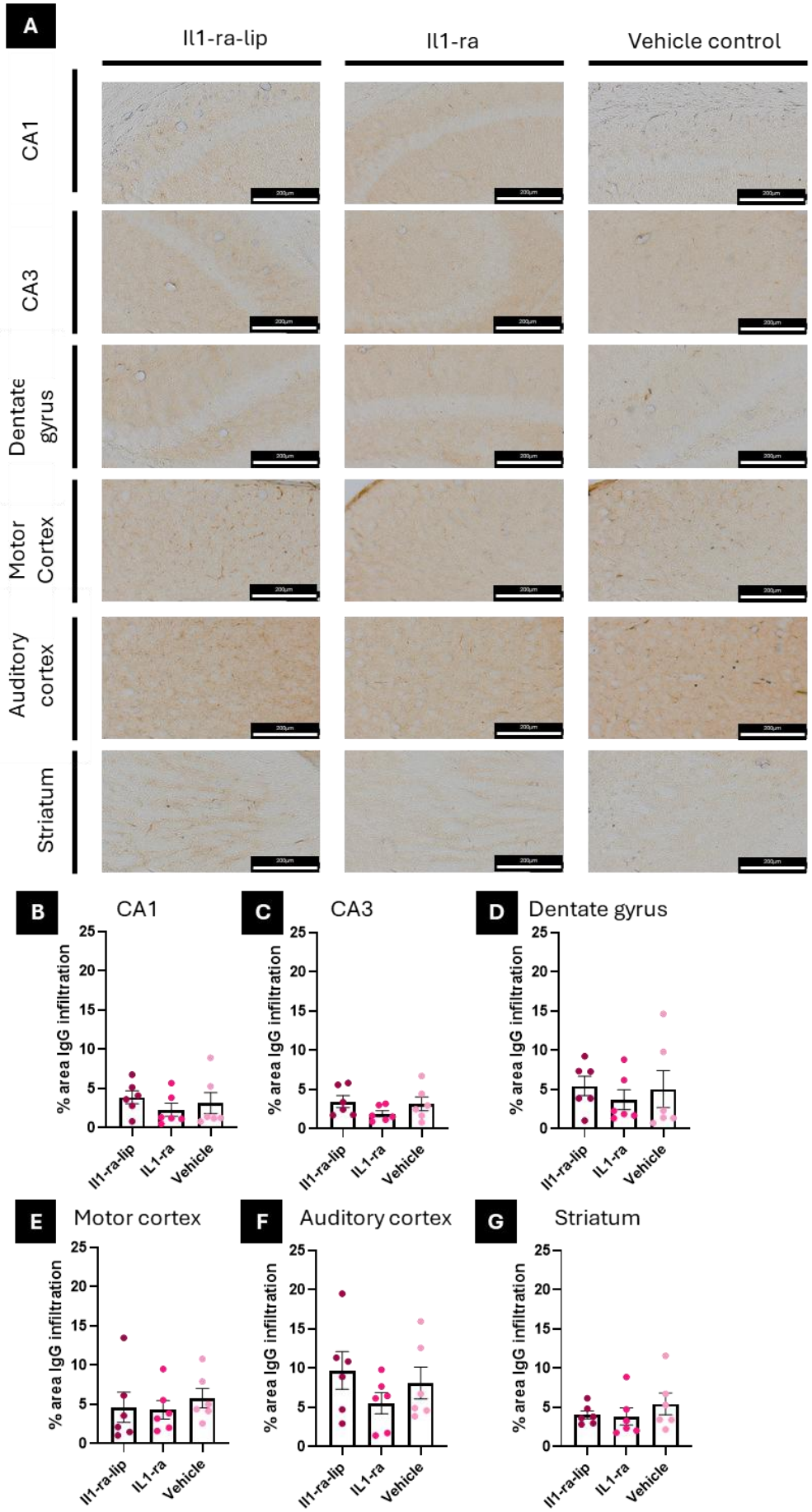
A
Il1-ra-lip
Il1-ra
Vehicle control
CA1
CA3
Dentate gyrus
Motor Cortex
Auditory cortex
Striatum
B
CA1
C
CA3
D
Dentate gyrus
% area IgG infiltration
Il1-ra-lip
IL1-ra
Vehicle
E
Motor cortex
F
Auditory cortex
G
Striatum

Figure 5-5: Immunoglobulin G infiltration in IL1-ra-lip therapy study brain. C57BL/6 18-month female mice groups were injected intravenously with either IL1-ra-lip, IL1-ra or vehicle control 4 times over 2 weeks. Mice then underwent MRI imaging prior to cardiac perfusion. (A) Representative immunohistochemical images of CA1, CA3 and dentate gyrus hippocampal regions, motor and auditory cortical regions and striatal region -1.94mm from bregma indicating infiltration of IgG (Brown). Quantitative analysis of all regions demonstrated no significant changes in; (B) CA1 region, (C) CA3 region, (D) dentate gyrus region, (E) motor cortex, (F) auditory cortex, (G) striatum. obtained at x20 magnification on Leica Thunder microscope prior to quantification in Image J. Statistical analysis was completed using GraphPad Prism software using one-way analysis of variance followed by Tukey multiple comparison test or Kruskal-Wallis test followed by Dunn's multiple comparisons test based on Shapiro-Wilk test for normality. N=6, average ± SEM, $p<0.05$ were considered significant. Scale bar represents 200µm.

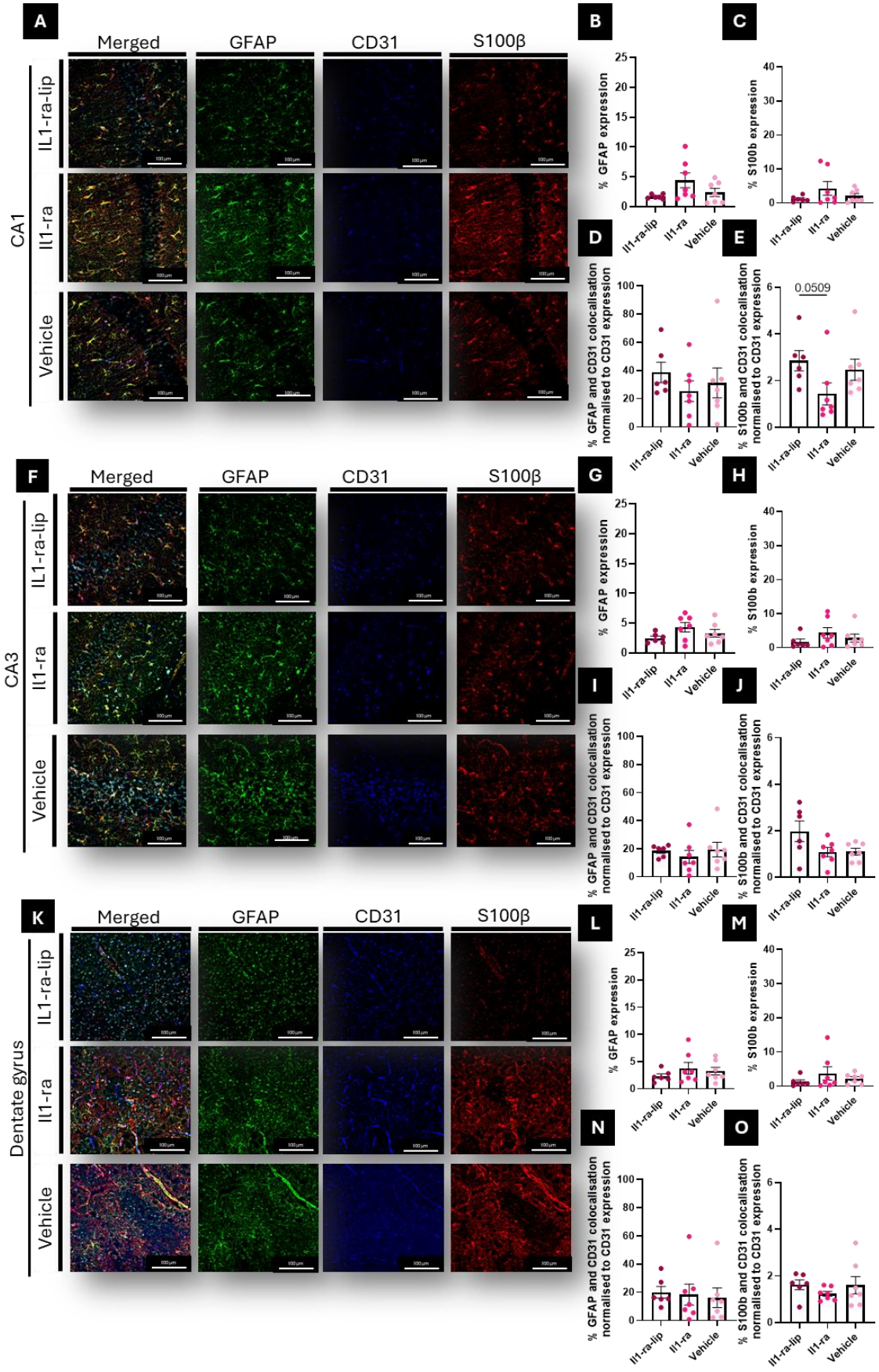
A
Merged
GFAP
CD31
S100β
CA1
IL1-ra-lip
Il1-ra
Vehicle
B
% GFAP expression
C
% S100b expression
Il1-ra-lip
Il1-ra
Vehicle
D
% GFAP and CD31 colocalisation normalised to CD31 expression
E
% S100b and CD31 colocalisation normalised to CD31 expression
0.0509
F
CA3
G
H
I
J
K
Dentate gyrus
L
M
N
O

Figure 5-6: Evaluation of GFAP+ astrocyte expression in IL1-ra-lip therapy study in hippocampal regions. C57BL/6 18-month female mice groups were injected intravenously with either IL1-ra-lip, IL1-ra or vehicle control 4 times over 2 weeks. Mice then underwent MRI imaging prior to cardiac perfusion. Representative immunofluorescence images of CA1 (A), CA3 (F) and dentate gyrus (K) region -1.94mm from the bregma demonstrate expression of CD31 (blue), GFAP (green) and s100β (Red). Quantitative analysis of the CA1 region demonstrated no significant changes in expression in (B) GFAP expression, (C) s100β expression, (D) GFAP and CD31 interaction and (E) s100β and CD31 interaction. Quantitative analysis of the CA3 region demonstrated no significant changes in expression in (G) GFAP expression, (H) s100β expression, (I) GFAP and CD31 interaction and (J) s100β and CD31 interaction. Quantitative analysis of the dentate gyrus region demonstrated no significant changes in expression in (L) GFAP expression, (M) s100β expression, (N) GFAP and CD31 interaction and ()) s100β and CD31 interaction. Images obtained at x40 magnification on Leica Thunder microscope and underwent large volume computational clearing prior to quantification in Image J. Statistical analysis was completed using GraphPad Prism software using either a one-way analysis of variance followed by Tukey's multiple comparison test or Kruskal-Wallis test followed by Dunn's multiple comparison test dependent on Shapiro-Wilkes normality test. N=6-7, average ± SEM, $p<0.05$ were considered significant.

close interactions of astrocytes with the BBB, the correlation of GFAP+ and CD31+ cells were quantified, resulting in no significant changes in any condition (fig. 5-6 d, i, n). Within the motor cortex, auditory cortex and striatum, similar patterns of GFAP expression (fog. 5-7b, g, l) and GFAP/CD31 (fig. 5-7d, i, n) interaction occurred with no significant changes between any group. The auditory cortex did display a non-significant decrease between the Il1-ra-lip and Il1-ra group interaction of GFAP and CD31 ($F=2.812_{(2,16)}$, p=0.0816) (figure 5-7n).

Further analysis of astrocyte inflammatory state was conducted via staining of S100β, involved in the activation of GFAP and NF-kB pathway induction (Langeh & Singh, 2021). Within the hippocampus, no significant changes were observed when comparing Il1-ra-lip to either the vehicle control or free Il1-ra (fig. 5-6c, h, m). Further analysis of interactions of S100β and CD31 resulted in no significant changes in any hippocampal region (fig. 5-6e, j, o). Quantification of S100β expression indicated no significant changes within the cortical or striatal regions (fig. 5-7c, h, m) and no changes to S100β/CD31 interaction within auditory cortex and striatum (fog. 5-7 j,o). In the CA1, there was a non-significant trend of decreasing interaction of S100β/CD31 from the Il1-ra-lip group to Il1-ra free drug ($H=6.265_{(2, 20)}$, p=0.0509) (fig. 5-7e).

5.4.5. Changes in microglial activation

To assess changes to microglial activation when aged mice were treated with Il1-ra-lip, Iba-1 immunolabelling of hippocampal, cortical, and striatal regions was undertaken. Within the CA1 region, there was a significant decrease in Iba-1 expression between Il1-ra and vehicle (F=4.983(2,18), p=0.0227) and a non-significant decrease between Il1-ra-lip and vehicle (F =4.983 (2,18),p=0.0593) (fig. 5-8 b). Similar expression patterns were observed in the CA3 (fig. 5-8 e), with Il1-ra demonstrating a reducing trend compared to vehicle (F=2.978(2,18), p=0.0891) and dentate gyrus (fig. 5-8 h) with non-significant trends to decreased Iba-1 expression than vehicle in Il1-ra (F=2.978(2,18), p=0.0531) and Il1-ra-lip (F=2.978(2,18),

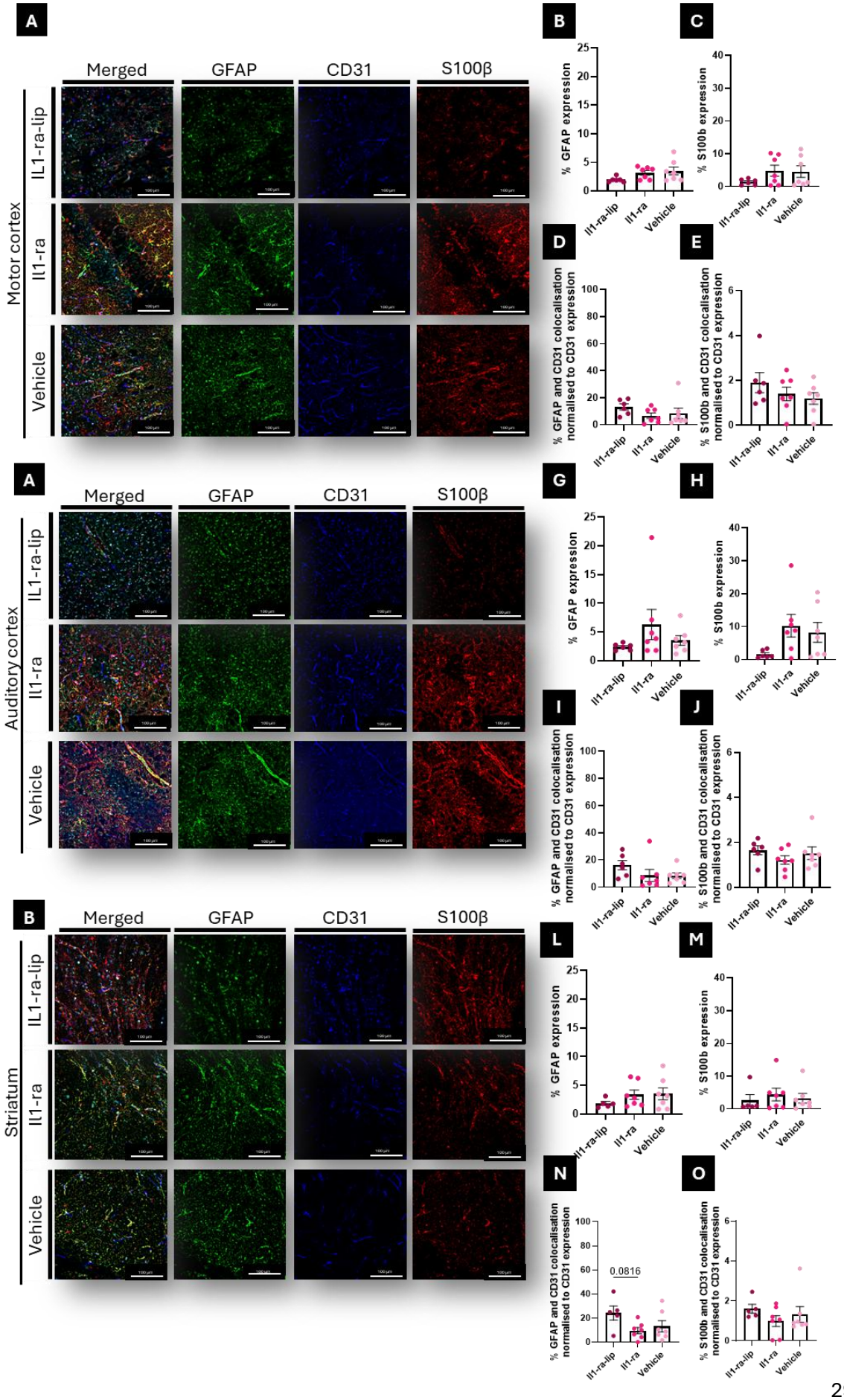
A
Merged
GFAP
CD31
S100β
Motor cortex
IL1-ra-lip
Il1-ra
Vehicle
B
% GFAP expression
C
% S100b expression
D
% GFAP and CD31 colocalisation normalised to CD31 expression
E
% S100b and CD31 colocalisation normalised to CD31 expression
Il1-ra-lip
Il1-ra
Vehicle
A
Auditory cortex
G
H
I
J
B
Striatum
L
M
N
O
0.0816

Figure 5-7: Evaluation of GFAP+ astrocyte expression in IL1-ra-lip therapy study in cortical and striatum regions. C57BL/6 18-month female mice groups were injected intravenously with either IL1-ra-lip, IL1-ra or vehicle control 4 times over 2 weeks. Mice then underwent MRI imaging prior to cardiac perfusion. Representative immunofluorescence images of motor cortex (A), auditory cortex (F) and striatum (K) region -1.94mm from the bregma demonstrate expression of CD31 (blue), GFAP (green) and s100β (Red). Quantitative analysis of the motor cortex region demonstrated no significant changes in expression in (B) GFAP expression, (C) s100β expression, (D) GFAP and CD31 interaction and (E) s100β and CD31 interaction, with a non-significant decrease in interaction between the IL1-ra-lip and IL1-ra groups. Quantitative analysis of the auditory cortex region demonstrated no significant changes in expression in (G) GFAP expression, (H) s100β expression, (I) GFAP and CD31 interaction and (J) s100β and CD31 interaction. Quantitative analysis of the striatum region demonstrated no significant changes in expression in (L) GFAP expression, (M) s100β expression, (N) GFAP and CD31 interaction and ()) s100β and CD31 interaction. Images obtained at x40 magnification on Leica Thunder microscope and underwent large volume computational clearing prior to quantification in Image J. Statistical analysis was completed using GraphPad Prism software using either a one-way analysis of variance followed by Tukey's multiple comparison test or Kruskal-Wallis test followed by Dunn's multiple comparison test dependent on Shapiro-Wilkes normality test. N=6-7, average ± SEM, $p<0.05$ were considered significant.

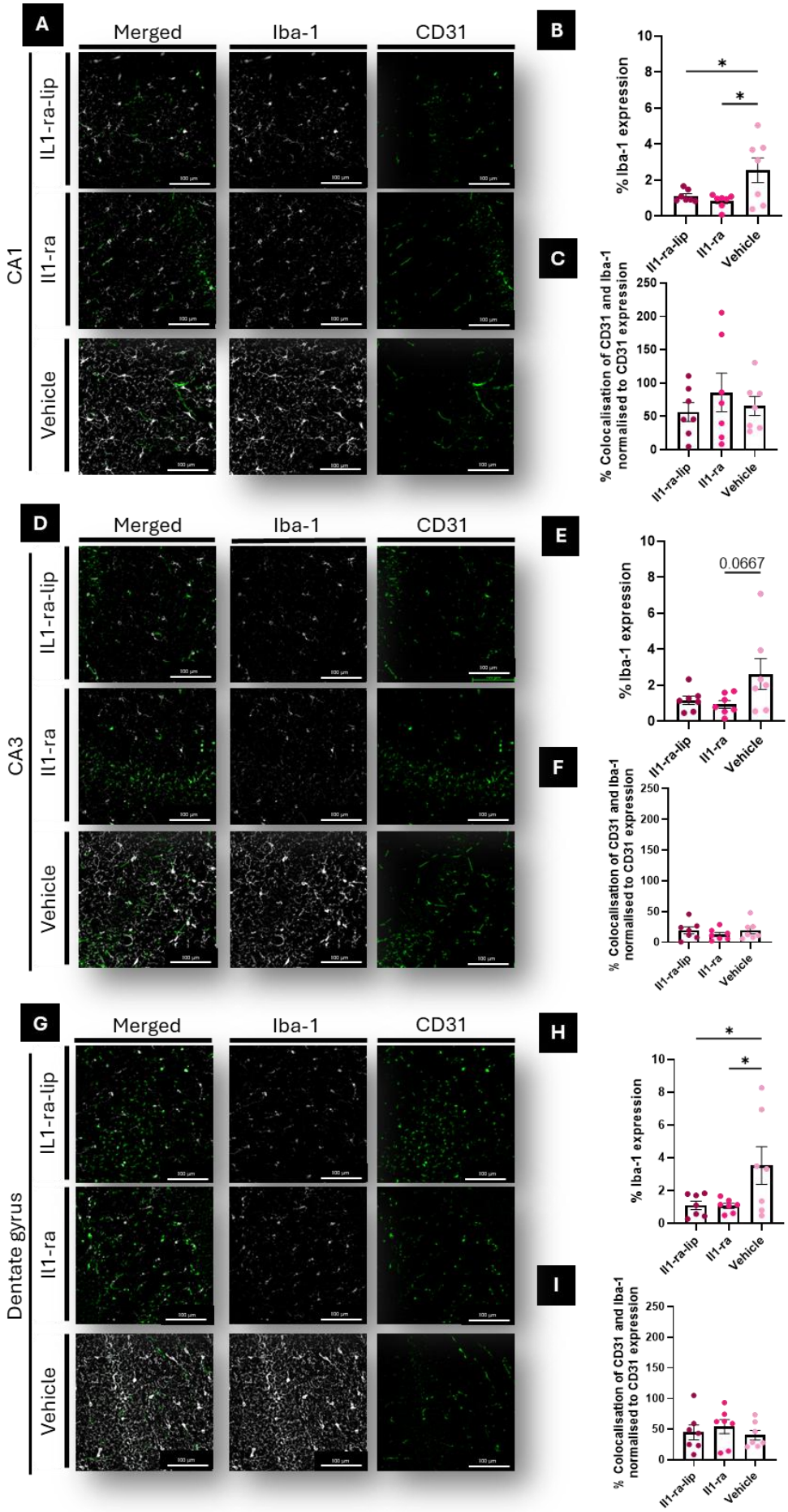
A
Merged
Iba-1
CD31
CA1
IL1-ra-lip
Il1-ra
Vehicle
B
% Iba-1 expression
*
*
Il1-ra-lip
Il1-ra
Vehicle
C
% Colocalisation of CD31 and Iba-1 normalised to CD31 expression
D
CA3
E
0.0667
F
G
Dentate gyrus
H
I

Figure 5-8: Evaluation of Iba-1+ microglial expression in IL1-ra-lip therapy study in hippocampal regions. C57BL/6 18-month female mice groups were injected intravenously with either IL1-ra-lip, IL1-ra or vehicle control 4 times over 2 weeks. Mice then underwent MRI imaging prior to cardiac perfusion. Representative immunofluorescence images of CA1 (A), CA3 (D) and dentate gyrus (G) region -1.94mm from the bregma demonstrate expression of CD31 (green) and Iba-1 (white). Quantitative analysis of CA1 region demonstrated significant decreased in IL1-ra Iba-1 expression compared to vehicle (B) and no significant changes to Iba-1 and CD31 interaction (C). Quantitative analysis of CA3 region showed non-significant decreases in Iba-1 expression between Il1-ra and vehicle groups (E) and no change to the CD31 and Iba-1 interaction (F). Dentate gyrus quantification demonstrated non-significant decreases in Iba-1 expression in both IL1-ra-lip and Il1-ra compared to vehicle control (H) and no changes to CD31 and Iba-1 interaction (I). Images obtained at x40 magnification on Leica Thunder microscope and underwent large volume computational clearing prior to quantification in Image J. Statistical analysis was completed using GraphPad Prism software using either a one-way analysis of variance followed by Tukey's multiple comparison test or Kruskal-Wallis test followed by Dunn's multiple comparison test dependent on Shapiro-Wilkes normality test. N=6-7, average ± SEM, $p<0.05$ were considered significant.

p=0.0560). No significant differences were observed between the Il1-ra-lip and Il1-ra free drug in any region (fig. 5-8 b, e,h). Interactions between the microglial and BBB were assessed via correlation of hippocampal Iba-1 and CD31 but showed no significant differences between Il1-ra-lip, Il1-ra or vehicle control (fig. 5-8, c, f, i).

Cortical regions (motor and auditory) and striatal region were assessed to determine if the hippocampus was more affected by Il1-ra-lip treatment or if it is a homogenous brain response. Within the motor cortex, there was a non-significant decrease in Iba-1 expression in the Il1-ra-lip group compared to the vehicle ($F= 2.849_{(2,18)}$, p=0.0878) (fig. 5-9 b) and a non-significant decrease in Iba-1/CD31 interaction ($F=2.849_{(2,18)}$, p=0.0912) (fig. 5-9 c). In the auditory cortex, there was no significant changes between any group regarding both Iba-1 expression and the interaction of Iba-1 and CD31 (fig. 5-9 e-f). Within the striatum, there was a non-significant decrease of Iba-1 expression between Il1-ra and vehicle ($F=3.378_{(2,18)}$, p=0.0699) but not between either the vehicle and Il1-ra-lip or free drug and liposome (fig. 5-9 h). No significance was found between the interaction of Iba-1 and CD31 in the striatal region (fig. 5-9 i).

5.4.6. Inflammatory profile not changed by Il1-ra-lip

Evaluation of changes to adhesion molecule expression and pro-inflammatory cytokines when 18-month mice were treated with IL1-ra-lip or free IL1-ra was carried out via ELISA on either brain homogenate or mouse serum (fig. 5-10). This allowed the comparison of the peripheral system and brain to evaluate any changes. Within ICAM-1 expression, there were no significant changes between Il1-ra-lip, Il1-ra and vehicle groups in either brain homogenate or serum samples (fig. 5-10a). ICAM-1 brain homogenate levels were significantly higher than those from the serum samples ($F=1.060_{(2,25)}$, p=<0.0001). VCAM-1 expression displayed similar patterns to that of ICAM-1, with no significant changes to expression in individual regions but significantly higher ICAM-1 expression in the brain compared to serum ($F=1.130_{(2, 35)}$, p=≤0.0019) (fig. 5-10b).

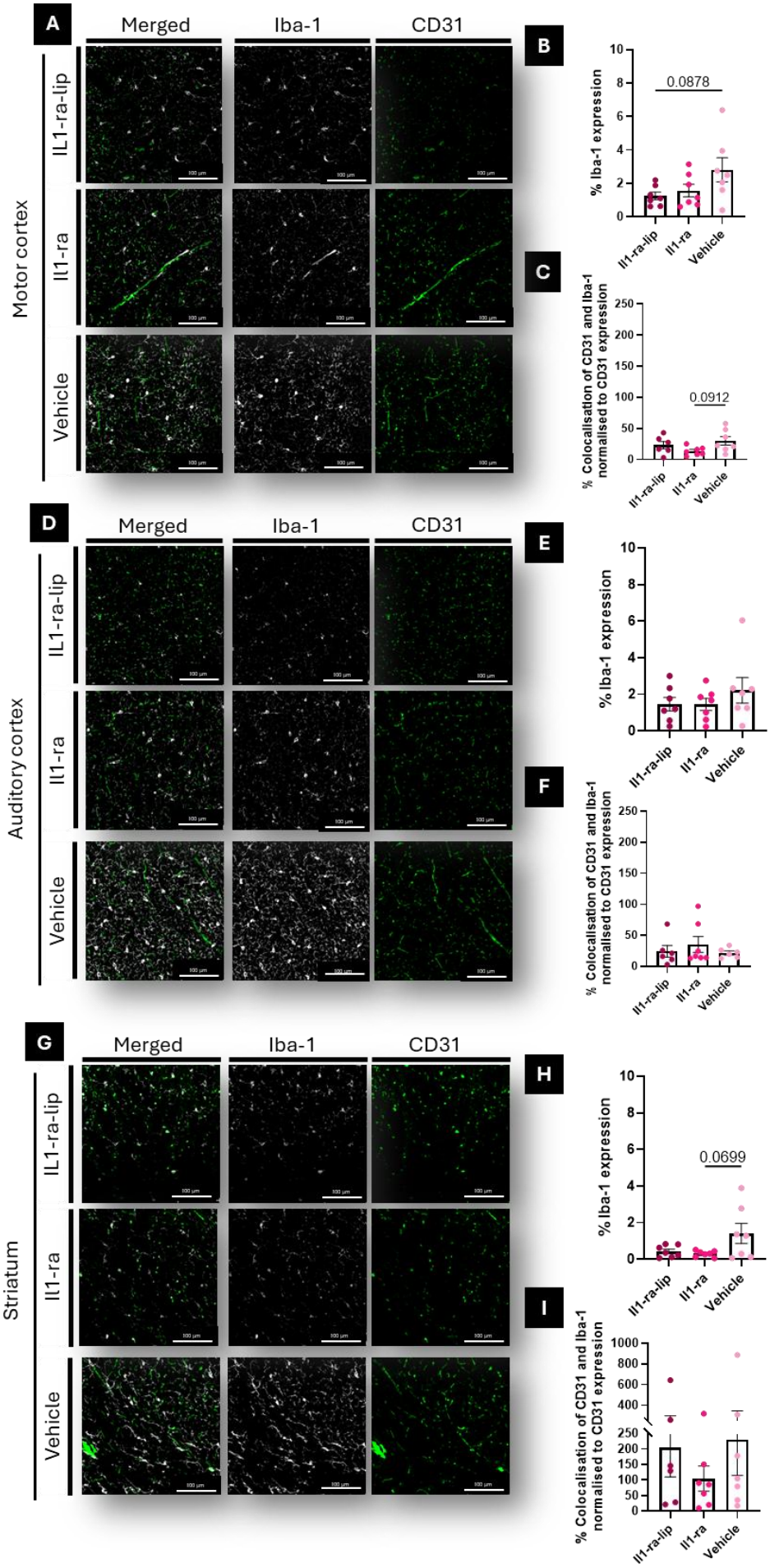
A
Merged
Iba-1
CD31
Motor cortex
IL1-ra-lip
Il1-ra
Vehicle
B
% Iba-1 expression
0.0878
Il1-ra-lip
Il1-ra
Vehicle
C
% Colocalisation of CD31 and Iba-1 normalised to CD31 expression
0.0912
D
Auditory cortex
E
F
G
Striatum
H
0.0699
I

Figure 5-9: Evaluation of Iba-1+ microglial expression in IL1-ra-lip therapy study in cortical and striatum regions. C57BL/6 18-month female mice groups were injected intravenously with either IL1-ra-lip, IL1-ra or vehicle control 4 times over 2 weeks. Mice then underwent MRI imaging prior to cardiac perfusion. Representative immunofluorescence images of motor cortex (A), auditory cortex (D) and striatum (G) region -1.94mm from the bregma demonstrate expression of CD31 (green) and Iba-1 (white). Quantitative analysis of motor cortex region demonstrated non-significant decreased in IL1-ra-lip Iba-1 expression compared to vehicle (B) and non-significant decreases in the Il1-ra to vehicle group in Iba-1 and CD31 interaction (C). Quantitative analysis of auditory cortex region showed no significant changes in Iba-1 expression between Il1-ra and vehicle groups (E) and no change to the CD31 and Iba-1 interaction (F). Striatum quantification demonstrated non-significant decreases in Iba-1 expression in both Il1-ra compared to vehicle control (H) and no changes to CD31 and Iba-1 interaction (I). Images obtained at x40 magnification on Leica Thunder microscope and underwent large volume computational clearing prior to quantification in Image J. Statistical analysis was completed using GraphPad Prism software using either a one-way analysis of variance followed by Tukey's multiple comparison test or Kruskal-Wallis test followed by Dunn's multiple comparison test dependent on Shapiro-Wilkes normality test. N=6-7, average ± SEM, $p<0.05$ were considered significant.

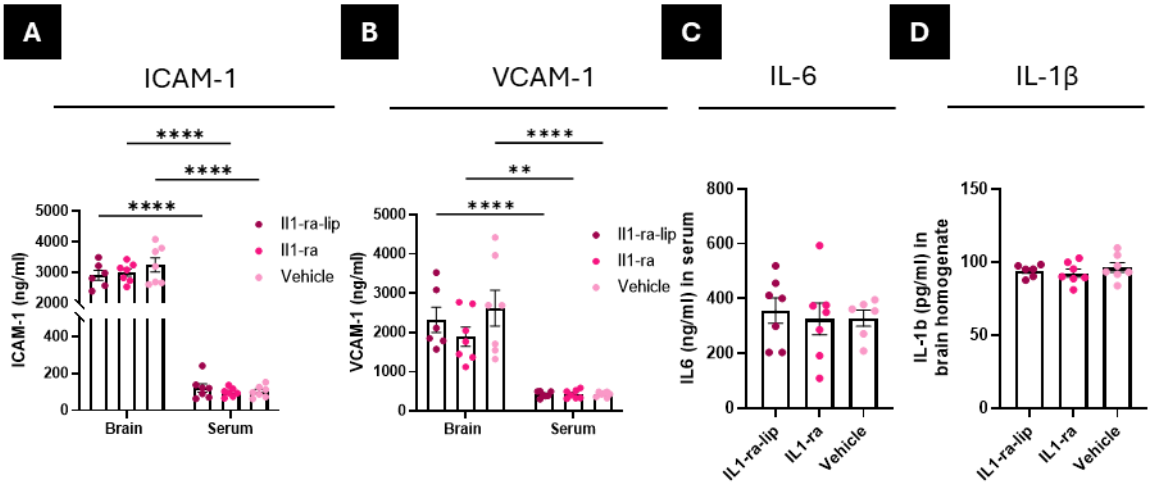

Figure 5-10: Inflammatory response in IL1-ra-lip therapy study serum and brain. ICAM-1, VCAM-1, IL-6 and IL-1β enzyme-linked immunosorbent assay (ELISA) of ageing mouse serum and brain homogenate. C57BL/6 18-month female mice groups were injected intravenously with either IL1-ra-lip, IL1-ra or vehicle control 4 times over 2 weeks. Mice then underwent MRI imaging prior to cardiac perfusion. (A) Quantification of ICAM-1 expression serum or homogenate levels. (B) VCAM-1 expression quantification in both serum and brain homogenate. (C) IL-6 level quantification in serum samples. (D) IL-1β expression quantification in brain homogenate. All samples demonstrated no significant changes in all markers investigated. Statistical analysis was completed using GraphPad Prism software using one-way analysis of variance for individual sample types or two-way analysis of variance for comparing different sample types followed by Tukey multiple comparison test or Kruskal-Wallis test followed by Dunn's multiple comparisons test based on Shapiro-Wilk test for normality. N=6-7, average ± SEM, $p<0.05$ were considered significant. Scale bar represents 100µm.

No significant changes were observed between any groups in the serum expression of IL-6 or brain expression of IL1-β (fig. 5-10 c-d).

5.5. Discussion

The results of this chapter aim to elucidate the potential anti-inflammatory effect of liposomes conjugated with Il1-ra in the context of physiological ageing. The expression and binding of adhesion molecule VCAM-1 was reduced significantly by Il1-ra-lip but not the free drug compared to the vehicle control when using MRI. No effect on BBB permeability was observed as IgG extravasation did not change. Evaluation of astrocytic activity via both GFAP and S100β demonstrated no significant changes throughout the groups and similarly. Microglial Iba-1 expression was also reduced from the vehicle, but similar effects were observed between the Il1-ra and free drug groups. The inflammatory profile of the brain and serum was not changed from vehicle conditions when Il1-ra-lip or Il1-ra were administered for either pro-inflammatory cytokines or adhesion molecules.

5.5.1. Adhesion molecules decrease when exposed to Il1-ra-lip

Within chapter 3, it was shown that in females peripheral VCAM-1 expression was increased during ageing. To see the impact of VCAM-1 expression in ageing, conjugation of VCAM-1 antibody to a contrastaphore, MPIO's, allowed for highly specific investigation of the adhesion molecule using MRI (Gauberti et al., 2018). MPIO's were preferential to their previous counterpart, ultra-small particles of iron oxide (USPIO's) as they are at least 1μm in size and cannot pass through the BBB(Gauberti et al., 2013). As VCAM-1 is expressed on the luminal side of the vasculature, USPIO's passing through the BBB reduced binding to luminal proteins (Gauberti, Fournier, et al., 2018).

Functional MRI using VCAM-1 MPIO's as contrast agents have been highly characterised within different *in vivo* models of AD, stroke, multiple sclerosis and systemic inflammation (Gauberti et al., 2013; Gauberti, Fournier, et al., 2018; McAteer et al., 2007; Montagne et al., 2012). Montagne et al, 2012 utilised this in an aged model of Swiss mice (3 and 24-months) and

observed increased VCAM-1 expression in the older groups, agreeing with the outcomes of our serum study in mice among others (Halder & Milner, 2022). This contrasts with Elahy *et al*, 2015, who saw no increased expression in VCAM-1 during ageing, but only used 12-month-old mice indicating that the increase in VCAM-1 is exclusive to older aged groups. IL-1β has been shown in *in vivo* and *in* vitro models to regulate levels of VCAM-1 in the brain as there was a direct correlation between IL-1β treatment and increasing VCAM-1 (O'Carroll et al., 2015; Versele et al., 2022). This knowledge justified the results shown here, observing that IL1-ra-lip significantly reduced VCAM-1 expression. Interestingly, the same effect was not seen in the free drug and this thesis hypothesises that it may be due to the increased half-life and circulation times of liposomal drugs, allowing for more Il1-ra to act upon the brain.

As this study was novel and no previous research had investigated the effect of Il1-ra-lip on VCAM-1 expression, more studies should follow to confirm the results as well as look at the effect of other adhesion molecules such as ICAM-1. The literature also notes that TNF-α administration has a greater effect on VCAM-1 expression then Il-1β (O'Carroll et al., 2015; Versele et al., 2022). Complementary studies using clinically approved TNF-α inhibitors, such as Infliximab and Certolizumab, could uncover increased effectiveness from this study (Kaushik & Moots, 2005; Mitoma et al., 2005).

5.5.2. No changes to BBB permeability

No changes to IgG extravasation when Il1-ra-lip was administered, into the brain parenchyma was observed in this study in any of the 6 regions analysed. This does correlate with findings in the previous chapters which show limited changes to IgG infiltration across both ageing and LPS-induced systemic inflammation (Chapters 3 and 4). However, in previous literature, injections of IL-1β resulted in BBB permeability increases, possibly by downregulating Shh or Wnt pathways (Fetsko et al., 2024; Ho & Kelly, 2020; Skaria et al., 2017; Wang et al., 2014b).

Within human encephalitis and traumatic brain injury studies, increased Il1-ra resulted in decreased BBB permeability when analysis the cerebral spinal fluid/albumin ratio (Michael et al., 2016; To et al., 2023). Decreases in IgG were observed in young, aged (16-months) and corpulent (high-fat diet) mice models of stroke when Il1-ra was administered, suggesting that the effect was dependent on the stroke pathology and not age (Greenhalgh et al., 2010; Pradillo et al., 2017; Zhang et al., 2018). However, the dose of Il1-ra varied from our study, with one study using 50 mg/kg Il1-ra compared to 10 mg/kg in the current study (Zhang et al., 2018). This suggests that to observe a larger effect on the BBB, a higher dose of Il1-ra-lip may be required in the future. Another alternative is that the time after therapeutic administration was not accurate to show changes in BBB permeability, within zebrafish, injection of IL-1β increased BBB permeability 6-hours post dose but by 27-hours this had returned to baseline levels (Blamire et al., 2000) This suggests a shorter time before animal sacrifice may allow for increased visualisation of BBB permeability changes.

Alternate techniques for investigating BBB should also be considered to fully confirm if BBB permeability in ageing is unaffected by Il1-ra-lip. Multiple studies have used EBD or dextran's to observe permeability effects, showing a reduction in permeability in a stroke mouse model and zebrafish adult model (Fetsko et al., 2024; Zhang et al., 2018). Further in-depth analysis could follow looking into changes in paracellular and transcellular transport pathways. Versele et al., 2022, showed in an *in vitro* human BBB Transwell system that paracellular transport of 400 Da lucifer yellow was increased when IL-1β was injected into the system. This study then went on to show decreases in Zo-1 and Claudin-5 expression at mRNA and protein level, correlating with il1-ra stroke therapy where the two tight junction proteins increased expression (Zhang et al., 2018). This correlates with ageing as Zo-1 has been shown in humans to decrease with age so it would be prudent to see the effect of Il1-ra-lip on tight junction activity (Goodall et al., 2018).

5.5.3. No changes to astrocyte activation

Within this study, results show no effect on astrocyte activation, via GFAP and S100β, or migration of astrocytes when exposed to IL1-ra either in liposomal form or free drug. This was unexpected as within previous research there is a strong correlation between IL1 expression and activation of astrocytes through GFAP which has been linked to activation of the NF-kB pathway of inflammation (Cotto et al., 2019; Sticozzi et al., 2013). Furthermore, Sama et al., 2008, demonstrated that reduction in physiological levels of IL1ra in young mice results in a decreased astrocyte activation of nuclear factor of activated T cells which are linked to cytokine expression. Knockout of IL1 or administration of IL1-ra caused decreased activation of astrocytes with reductions in both S100β and GFAP *in vivo* but both studies implemented an LPS ageing inflammatory or AD model (Hsieh et al., 2020; Kitazawa et al., 2011; Liddelow et al., 2017). This suggests that systemic inflammation would play a role in the effectiveness of IL1-ra-lip.

However, in a multiple sclerosis mouse model, it was shown that IL1 expression affected the BBB related endothelial cells in an increased capacity to astrocytes (Hauptmann et al., 2020). This may suggest that astrocytes would not be the cell type to express significant changes when provided with a low dose of IL1-ra. Also, Clarke et al., 2018, noted that although astrocyte activation occurs during ageing, that IL1 effects on the cell are dependent on production from microglia. This may explain why an effect in microglial activation was observed in this study before any astrocytic changes.

Other markers of astrocyte activation, such as chemokine (C-X-C motif) ligand 1 (CXCL1) would be suitable for investigation as Il1-ra inhibited expression in stroke mice (Huang et al., 2023). The knockdown of Il1 in a stroke model further provided evidence for this protein to be investigated as it was reduced correlating with decrease in VCAM-1 and ICAM-1 expression at BBB (Schädlich et al., 2022). Within ageing, CXCL1 was increased between 3-month and 16-

month mice and correlated with IL-1β expression (Wolfe et al., 2018). Furthermore, within chapter 3, it was shown that in ageing, male mice exhibited more significant changes in astrocyte expression then the female cohort, so a neuroprotective mechanism may be occurring naturally before administration of therapeutic (Ferreira, 2023).

5.5.4. Decreased microglial activity with Il1-ra-lip

Within the current study, the microglial activation marker Iba-1 was significantly decreased in some hippocampal areas or presented with a non-significant decreasing trend. This correlates with past literature noting that reductions in IL-1β signalling reduce the activation of microglia, visualised by morphology reverting to a homeostatic phenotype (Monif et al., 2016). IL-1β is expressed by microglia in inflammatory states and the presence of this further potentiates inflammatory responses not only by microglia but also other cell such as astrocytes (Finger et al., 2021; Garner et al., 2018; Porcher et al., 2021; Zhu et al., 2019). This means that the presence of Il1-ra should reduce not only the microglial inflammation but also the overall inflammatory profile of the subject. Within a mouse study, knockout of Il1-ra led to microglial activation in AD, demonstrating that Il1-ra levels are linked to changes to microglial phenotype (Craft et al., 2005). Monif *et al,* 2016 postulates that the decreases in Il-1β are linked to the decrease in the purinergic receptor P_2X_7R activation, which has been shown in spinal cord injury mouse models to release excess cytokines into the parenchyma with Il-1β (Fan et al., 2020).

In the current study, there was a similar decrease in Il1-ra-lip and Il1-ra free drug in the hippocampal regions which indicates that this effect was not due to conjugation with liposomes. This shows that Il1-ra does indeed affect the expression of Iba-1+ microglial, indicating an anti-inflammatory effect. This may lend credence to the principle that Il1-ra can pass the BBB as it is certainly affecting the microglia but also that the liposomes do not ameliorate this effect (Sjöstedt et al., 2014). Regional heterogeneity was displayed when

comparing hippocampal microglia and cortical, with lower degrees of significant decreases of both free drug and liposomal formulations to vehicle. Grabert et al., 2016, isolated microglial populations from 4-, 12- and 22-month mice and investigated transcriptional variability. Key findings were that in middle age, there were distinct populations of microglia between the cortical, striatal and hippocampal regions but that at 22-months these sub-populations merged. This indicates that further studies using Il1-ra-lip should extend the lifespan of mice to at least 22-months to determine regional homogeneity of microglia populations for a global effect of the therapy.

It would be a worthwhile to repeat the same study with an increased incubation between the last therapy injection and post-mortem studies as the circulation of the liposomal drug should increase compared to the free drug, meaning effects should last longer. Comparison of microglial activation over 1-week post-injection should be investigated to see if Il1-ra-lip prolongs anti-inflammatory affects more than that of the free drug.

It has been shown in systemic inflammation that microglia migrate towards the vasculature, especially in the hippocampus, and that in up to 12-month mice at least 30% of the microglial population is associated with the BBB (Bowyer et al., 2020; Grossmann et al., 2002; Knopp et al., 2022). This has not been extrapolated to physiological ageing, but the inflammatory age-related response may cause similar affects. It has been hypothesised that this may not be a pro-inflammatory effect, and that the proximity of microglia may prevent the entry of bacteria into the brain and another study showed that microglia migration occurred before BBB permeability, possibly to prevent such occurrences (Bowyer et al., 2020; Haruwaka et al., 2019). Within this study, there was limited change in the interaction of Iba-1 and CD31, representing the microglia and endothelial cells, with only a non-significant decrease from vehicle in the motor cortex region. This may indicate that migration of microglia to the

vasculature only occurs in more severe inflammatory conditions and so introduction of Il1-ra-lip would not have any effect on this.

Overall decreased expression of Iba-1 in microglia suggests that there is an anti-inflammatory effect of Il1-ra in ageing which up to now has not been shown but further work must be undertaken to see if this has a functional anti-inflammatory effect.

5.5.5. No changes to inflammatory profile

This study also investigated the effect of Il1-ra-lip on the expression of pro-inflammatory cytokines (IL-6 and IL-1β) and adhesion molecules (VCAM-1 and ICAM-1) in both serum and brain samples. There were no changes to any molecule when comparing each therapeutic condition. This was unexpected as the injection of IL-1β into either stroke mice, wild-type mice or *in vitro studies,* resulted in the increased expression of ICAM-1, VCAM-1 and IL-6 (Labus et al., 2014; Tsakiri et al., 2008; Versele et al., 2022). Protein knockout mice (Il1 -/-) also demonstrated no IL-6 expression, solidifying the regulatory function of Il1 on other pro-inflammatory cytokines (Tsakiri et al., 2008; Venugopal et al., 2021). However, tentative comparisons can be made to knockout studies as the current study intended to reduce Il-1 effects as opposed to eliminating them in entirety.

Other studies have also shown within stroke models, the administration of IL1-ra reduced the expression levels of IL-6 and ICAM-1 after a single dose (Pradillo et al., 2017; Venugopal et al., 2021). However, both studies examined brain IL-6 levels and Pradillo *et al,* 2017 also noted no IL-6 changes in serum samples, like the findings in the current study. This indicates that the comparison of brain and serum samples is critical to understanding the full effect of Il1-ra.

Interestingly, when comparing the ICAM-1 and VCAM-1 levels, significantly higher protein expression was found in the brain of all groups compared to their serum counterparts. This may indicate that in ageing both adhesion molecules migrated towards the brain and BBB, like the

inflammatory phenotype in cerebral hypoperfusion (Zhang et al., 2024). However, no changes in discrete sample types were observed with Il1-ra/ Il1-ra-lip introduction which contrasts with a study in chikungunya virus which correlated increases in Il1-ra to decreases in VCAM-1 (Chirathaworn et al., 2022). This indicates that the current study parameters do not have an effect on adhesion molecule expression regardless of liposome conjugation and further studies with varied timelines or dosages may prove more effective.

The absence of Il-1β changes when exposed to Il1-ra were surprising but may reflect that IL-1β was still present within the brain homogenate. This was rendered functionally inactive as it was unable to bind to the receptor. Il-1β is predominantly expressed via microglial signalling and so it would be expected that the reduction in activated microglia observed would correlate with decreased cytokine expression (Zhu et al., 2019). However, other cell such as astrocytes, are involved in the secretion and signalling of Il-1β, with no effect of Il1-ra/-lip seen on this cell type so may explain why there was not a microglia-dependant decrease (Sama et al., 2008).

Overall, the hypothesis that Il1-ra-lip would reduce the levels of adhesion molecules and cytokines in the brain was not shown in this study and further work would need to be completed to build confidence in this finding.

5.6. Limitations and future work

The absence of a young (3-month) mouse group to compare to the age group is the major limitation of this study to confirm that it is an age-related effect. The current study can compare between liposome, free drug and vehicle but it cannot elucidate if similar effects would be observed in younger mouse models. Another limitation is not investigating the amount of IL1 present within the aged cohort before onset of therapy, this could have been achieved by taking tail vein blood samples and extracting serum. As this study aims to reduce IL1 binding, it would be helpful to know what the normal physiological level of IL1 within the mouse model is prior

therapy administration to see if in individual mice this was changed. Conducting experiments, such as ELISA's, investigating the amount of IL1-ra within the brain in all conditions would show if the liposomal formulation allowed for greater BBB penetration. Further histological experiments post-mortem should also look at the distribution of the Il1-ra-lip within the brain to determine regional distribution, possibly though incorporating DiI into the liposome formulation. Unfortunately, due to time and financial restrictions this experiment could not be performed for this thesis.

Microglial effects were observed within this study using both the Il1-ra and Il1-ra-lip to similar levels. As the half-life of Il1-ra is relatively short and that the PEGylation of liposomes increases circulation duration, it would be advantageous to extend the time between therapy administration and post-mortem studies beyond 48-hours. In theory, the IL1-ra-lip therapy should have a longer duration of effect then the free drug, which would be preferable for translational studies as fewer doses would be required.

No changes to BBB permeability or disruption were observed with no changed IgG extravasation in any compared group. However, this was also the case in chapter 4, suggesting that IgG may not be the most appropriate model to investigate BBB permeability. Future studies should consider the use of dextran's, Evans Blue or MRI studies to gain more insight into potential changes to BBB and transport within when treated with Il1-ra-lip.

5.7. Conclusions

In conclusion, this chapter assessed the potential use of liposomes to deliver anti-inflammatory IL1-ra into the brain of aged mice. The main findings show a reduction in adhesion molecule VCAM-1 and microglial marker Iba-1 without having any significant changes of astrocytic activation, cytokine expression or BBB permeability. The results of the study point towards a potential, for the first time, use of Il1-ra as an anti-inflammatory within

physiological ageing, but more work needs to be undertaken to decipher mechanistic properties as well as the advantages of conjugating to liposomes.

6. Final discussion

Despite a growing body of work investigating the effect of ageing on the BBB, there are gaps within the field such as the effect of sex and if further neuroinflammation exacerbates the ageing effect. Nanoparticles have been a recent advancement in drug delivery through the BBB but have not been widely applied to the ageing setting, focusing primarily on neuropathological disease states. The current work aimed to investigate the following themes: a) enhance the understanding of sex differences to ageing BBB, b) determine if liposome nanoparticles infiltrated the brain parenchyma during ageing, c) to assess changes to the BBB and nanoparticle infiltration in an induced neuroinflammatory state, and d) explore the potential of anti-inflammatory liposomes within the ageing brain.

6.1. Key Study findings

In this work, we used an *in vivo* murine model to examine age related effects on the BBB associated cells and if dysfunction of the BBB allowed liposome nanoparticles to enter. Specifically, the effect of ageing on endothelial cells, astrocytes, pericytes and microglia were quantified alongside cognitive behavioural tests to determine correlation between cellular changes and behavioural deficits. We found that nanoparticles and albumin infiltration did increase during ageing homogenously across hippocampal, cortical, and striatal regions of both males and females insinuating that caveolin-mediated transcytosis was a possible transport mechanism (Al-Ahmady et al., 2019; Sorets et al., 2020). Further investigation into caveolin-1 expression revealed sex differences contradicting previous literature knowledge, with middle aged female mice expressing the protein more than their aged counterparts. BBB permeability was also assessed via IgG extravasation but unexpectedly demonstrated no changes in ageing. Changes to NVU components across ageing were inconsistent between sex but certain regions displayed increased GFAP+ and Iba-1+ expression whilst NG2 was reduced. These changes occurred before the onset of significant cognitive decline within both sexes.

Increased neuroinflammation was induced by LPS administration in female mice, highlighting changes to adhesion molecules throughout the brain whilst exacerbation of liposomal infiltration occurred regionally in the dentate gyrus and cortical regions. No changes to GFAP+ or Iba-1+ were observed demonstrating limited effects of the LPS-model. Pro-inflammatory cytokine increase did correlate with age and LPS induced neuroinflammation along with wide-ranging protein expression changes. Serpin3n was highlighted as a particular protein of interest, up regulated in ageing and LPS models.

Finally, the potential of liposomes conjugated with an anti-inflammatory drug (Il1-ra) demonstrated reductions in adhesion molecule binding but did not change BBB permeability or GFAP+ astrocytic expression. The binding of adhesion molecules VCAM-1 was reduced from vehicle only in the liposomal formulation, suggesting that nanoparticles enhance the effects of Il1-ra at the vasculature. Changes to microglial Iba-1+ activation were present but within both the liposomal drug and free-drug cohorts, suggesting a limited effect of liposomes on drug potential. This thesis contributes to the existing knowledge surrounding ageing of the BBB with positive liposomal results for targeting increased neuroinflammation over time.

6.2. Limitations

Each study within this thesis was underpowered for certain research parameters meaning that limited significant changes were observed. Multiple trends such as increases in GFAP+ cells in ageing may have been proven significant with appropriately powered study as observed widely in previous literature. Mice numbers of all studies were limited due to the financial burden of ageing *in vivo* studies as well as the time required to age mice to appropriate age-points. This showcases that although ageing studies are possible during a time-restricted academia-based project, more time and funding are required to obtain appropriate study numbers. This is especially apparent in the 22-month aged female group as this group number was reduced due to mouse mortality, an increased number of mice would be required specifically for this group

to achieve power and increase the age to the target 24-28 months which would be more representative of human ageing at 70 years+ (Jackson et al., 2017; Kang et al., 2022).

Furthermore, the study did not quantify the amount of estrogen present within the female cohort and whether this changed during ageing. Mice oestrous cycles decrease during ageing, but this was shown not to correlate with a significant decrease in estrogen production, unlike hormonal changes of human females during menopause (Blenck et al., 2016; Nelson et al., 1981). However, between sexes the difference in estrogen production could be a potential explanation behind observed sex-dependent effects on BBB components in this study as estrogen is noted to be neuroprotective against BBB breakdown and lymphocyte trafficking (Kuruca et al., 2017; Maggioli et al., 2016). Therefore, in the future it would be interesting to confirm estrogen concentration in ageing cohorts and to compare female without estrogen (via ovariectomy) (Cipolla et al., 2009; McNamara et al., 2010).

This thesis was carried out exclusively in inbred C57BL/6 mice which limits the translatability to human studies. The advantage of using mice is that they have reduced genetic and physiological variability leading to increased robustness of data, but this also does not capture the complexity of human subjects (Sittig et al., 2016). C57BL/6 mice have also been compared to other inbred mouse strains and found to have the least number of single nucleotide polymorphisms, further showing their homogeneity (Keane et al., 2011). Schaffenrath et al., 2021, investigated inbred and wild-type derived strains in the context of BBB permeability in ageing, showing consistent increased BBB permeability to sodium fluorescein in inbred mice but high variability in the wild-type mice. This also applied within a mouse and human comparative study, with permeability to serum proteins more diverse in the human post-mortem samples (Goodall et al., 2018).

Within the context of the BBB, transcriptomic analysis of human and mouse vasculature demonstrated that there is a significant similarity between the two species with levels of claudin-5, MSF2DA and PDGRβ being conserved (Song et al., 2020). However, there were differences observed in other pericyte markers such as CD13, also known as aminopeptidase N, which had decreased human expression or vitronectin which was completely absent from the human population and is a specific murine pericyte marker. Astrocytic changes are also observed with an increased astrocyte: neuron ratio in humans (1:1.4) compared to mice (1:3) which may possibly reflect a greater effect of the glial cell on human brains (Degl'Innocenti & Dell'Anno, 2023). This links directly to the BBB as the increase in human astrocytes correlates with increased AQA4 end-feet expression at the vasculature (Ramos-Zaldívar et al., 2022). Recent investigations into human astrocytes have also found an age-related human/ hominoid specific population, varicose, which are not present in murine models, however the functionality of this astrocyte sub-type is yet to be elucidated so impact may be restricted (Degl'Innocenti & Dell'Anno, 2023; Falcone et al., 2019; Rasmussen & Smith, 2022).

Transport mechanisms of the BBB are widely conserved but some specific differences may be impactful in translation of liposome infiltration into the brain. Some solute carriers (SLC) transporters have been found to have lower expression in humans then mice such as SLC3A2 and SLC2A1 which are utilised in receptor meditated transcytosis (Chew et al., 2023; Song et al., 2020; Zhang et al., 2020). Furthermore, low-density lipoprotein receptor–related protein 1 has been shown to be reduced in humans, this transporter in mice functions to maintain BBB integrity suggesting that different proteins are involved in the human brain (Storck et al., 2021; Zhang et al., 2020). Modelling both mouse and human BBB highlighted the decreased expression of P-gP in humans by decreased amounts of digitoxin and paclitaxel infiltration into the parenchyma (Verscheijden et al., 2021). As our results did not confirm that caveolin-1 mediated transcytosis was the mechanism of liposomal infiltration, therefore, attention must

be paid to identifying entry routes of the nanoparticles before attempting to translate to humans. If one of the identified transporters above is the mechanism behind liposomes, then they may not have the same effect in a human model.

6.3. Future work

Future directions of each study have been noted within their corresponding chapters and the impact of key findings are displayed in table 6-1. The current study is one of the first to investigate the effect of ageing on the female BBB across a range of ages in the lifespan instead of choosing a single young and aged timepoint. However, the companion male group , consisted of 3- and 18-month mice. The next steps of the study would be to complete the male cohort similar to previous literature to compare middle aged male mice to females (Britton et al., 2022).Within both the LPS (chapter 4) and Il1-ra-lip (chapter 5) studies, the effect of sex would need to be determined by repeating the experiments within male mice cohorts. This is especially important as sex changes were seen within the physiological ageing cohort.

Assessment of pro-inflammatory co-morbidities which also occur during ageing (chapter 4), such as obesity and hypertension, should also be used to determine changes to the BBB microenvironment in conjugation and independently to LPS. Modelling obesity *in vivo* can be achieved through feeding mice a high-fat diet, being successfully implemented in stroke, AD and ageing models previously (Elhaik Goldman et al., 2018; Oike et al., 2020; Pradillo et al., 2017). Hypertension could be modelled by administration of angiotensin II and have been shown in young mice to increase BBB permeability to dextran's (Biancardi et al., 2014; Buttler et al., 2017). The application of these models within ageing will progress findings shown in this study regarding effects on NVU components and more crucially, whether infiltration of liposomes is increased or conserved with these co-morbidities. This thesis identified Serpin3n as a particular protein of interest, up-regulated in both ageing and LPS-induce

Table 6-1: Impact of research findings.

Key Findings	Chapter	Impact	Future work
Liposome nanoparticles increased infiltration during ageing	3	The first study to show that liposomes could be used as novel drug delivery systems during ageing without neurodegeneration for molecules previously unable to cross the BBB	To utilise liposomal based delivery systems to target brain deterioration before the onset of neurodegeneration
Sex differences in aged caveolin-1 expression	3	Identification of differences in age-related transcytosis induction indicating different nanoparticle uptake routes	To investigate alternative paracellular and transcellular transport changes during ageing of female mice and determine if sex differences translate to human samples.
Ageing and inflammation increased adhesion molecule expression	4	ICAM-1 could be a potential therapeutic target to reduce brain inflammation during ageing	To encapsulate ICAM-1 inhibitors into liposomes during
Serpin3n identified as up-regulated protein during ageing and neuroinflammation	4	Adds to the pre-existing literature that Serpin3n is intrinsically linked to ageing and inflammation Low-levels of LPS induce up-regulation as well as high-dose sepsis models	To target Serpin3n expression as an anti-inflammatory therapeutic

Liposome conjugate Il1-ra reduced VCAM-1 binding at BBB	5	This is the first ageing study to show that Il1-ra can reduce inflammatory effects. Liposomes increase the impact of Il1-ra in ageing	To investigate other markers of BBB dysfunction (ICAM-1, p-selectin, claudin-5) in functional MRI studies To use alternative methods to quantify VCAM-1 changes at BBB level
Il1-ra reduces Iba-1 expression in ageing microglia	5	Il1-ra, regardless of liposome delivery, had anti-inflammatory effects within the ageing mouse brain	Utilise alternative microglial markers (TREM2, F4/80, CD163) to capture full effect of Il1-ra To increase interval between therapeutic delivery and assessment to determine long-term liposomal effects

neuroinflammation. Further studies should attempt to elucidate functionality of this within the BBB and potentially target this *in vitro*, *in vivo* and clinically.

Whilst promising results were observed in the Il1-ra-lip therapy study, the results were not conclusive and showed some overlap between free drug and liposomal drug effects. The next phase of this research would be to distinguish effects of Il1-ra in its free and nanoparticle form, possibly through increasing the timeframe of the study. It is hypothesised here that the PEGylation of liposomes would increase drug circulation time, elevating the effect of the drug longer term compared to free drug. Increases to either Il1-ra-lip concentration or frequency of dosage may also be impactful as there were no observed effects on BBB permeability or astrocyte expression. Finally, a study comparing the effects of Il1-ra in young and aged male and female mice would be required for increased efficacy confidence to move forward with clinical translation studies.

Although this thesis investigated proteomic changes to the brain during ageing, the brain samples were from whole brain homogenate, not allowing for spatial investigations similar to the immunofluorescence work. The use of digital spatial profiling, which allows for precise transcriptomic analysis from tissue regions, would advance this area. Recent work has investigated this in ageing male mice, demonstrating widespread inflammatory changes in the hippocampus and white matter regions (Kiss et al., 2022). All immunofluorescence in this thesis was completed in 2-dimensions but utilising 3-dimension imaging software would enable increased precision especially when investigating the interaction of liposomes and potential transport mechanisms in the BBB (Abcouwer et al., 2021; Villaseñor & Collin, 2017).

In hindsight, the reliance of *in vivo* optical imaging and immunofluorescence to investigate the infiltration of DiI-lip may be limited in specificity based upon the equipment available. Promise has been shown using radiolabelled nanobodies and PET scans to produce highly sensitive

spatial data, however, this involves the use of radioisotopes so further complicates studies (Li & Wang, 2023). For further BBB permeability increases, the use of IgG was limited, and, in the future, other techniques should be implemented to provide more data on this parameter. The use of EBD in a separate cohort would allow for comparison of BBB breakdown to the DiI-lip infiltration and may show differences to the IgG techniques (Bake & Sohrabji, 2004; Conq et al., 2023; Goodall et al., 2018). Progressing further but limited in this study by availability and economic burden, the use of MRI would be invaluable for investigating small changes to BBB permeability as discussed in fig 1-6. Specifically, the quantification of trans-BBB exchange of water, instead of classical contrast based MRI, may allow for the detection of slight permeability changes as shown in Dickie et al., 2019, in AD rats.

The study was unable to quantify changes to TJ proteins, such as Zo-1 and Claudin-5 due to failure of antibody optimisation. Immunofluorescence may not have been the most appropriate technique to investigate hard to image proteins and an ultrastructural approach utilising TEM may have allowed for in-depth imaging of the BBB protein changes (Ceafalan et al., 2019; Frías-Anaya et al., 2021). Zhu et al., 2022, also showed this technique is useful for the detection of key glycocalyx proteins to allow for investigations into this key structure within the BBB in ageing which up to now has not be thoroughly studied.

6.4. Concluding remarks

To summarise, this thesis has fulfilled its aims to investigate the impact of ageing and neuroinflammation on the BBB and determine the potential of nanoparticles as a drug delivery system. Identification of changes to the NVU components adds to the growing literature showing regional and sex specific differences in age-related expression. Adding to the limited previous research, it has been shown that liposome nanoparticles infiltrate the brain during physiological ageing and when conjugated to a pro-inflammatory cytokine receptor antagonist, reduce neuroinflammatory cell expression. This thesis highlights the need for

further work investigating the mechanistic properties of liposomes crossing the BBB to deliver therapeutics.

7. Appendix

7.1. Appendix 1: PIPS Reflective Statement

Note to examiners:

This statement is included as an appendix to the thesis in order that the thesis accurately captures the PhD training experienced by the candidate as a BBSRC Doctoral Training Partnership student.

The Professional Internship for PhD Students is a compulsory 3-month placement which must be undertaken by DTP students. It is usually centred on a specific project and must not be related to the PhD project. This reflective statement is designed to capture the skills development which has taken place during the student's placement and the impact on their career plans it has had.

PIPS Reflective Statement:

The PIP placement was based a Sygnature discovery, a world-leading pharmaceutical research company based in Nottingham. My project was entitled 'molecular glue degrader screening' and had the overall aim to develop biophysical capabilities to screen compound libraries for molecular glues. To validate and characterise hits from previous work at the company, using mainly two techniques: surface plasmon resonance (SPR) and Homogeneous time-resolved fluorescence (HTRF). The theory and techniques applied during this project were not familiar before the onset, requiring effort for training on specific equipment pieces as well as improving my knowledge base through learning seminars provided by the company.

Seminars included drug binding, CNS drug discovery and the use of PROteolysis TArgeting Chimeras in drug discovery. Through this I gained experience with equipment to enhance reagent movement as it was required to work in nl volumes. This involved using an ECHO

instrument which had to be programmed with specific dose-response concentrations to dispense the proteins of interest using sound wave. The HTRF assay investigated protein ratio stoichiometry and resulted in validation of previous findings within the company, allowing for the project to proceed. Unfortunately, the SPR machine was heavily utlisied and so was unavailable for my project. To move forward with the work, microscale thermophoresis (MST) was employed as the alternative to investigate protein binding, but this experiment did not result in usable findings. It is believed that the fluorescence conjugation required for this assay obscured the protein binding site and so future work would require the initial planned use of SPR.

At the onset of the project, I set SMART targets to allow the placement to be the most beneficial to my portfolio growth. The first target was to work on communication with different types of project stakeholders. I achieved this through meetings with my direct supervisor and associated group, whereby I gave updates on the project progress, to the wider bioscience department through a presentation in the monthly departmental meeting and to a client by virtual meetings providing updates on feasibility of techniques. This translated directly back to my PhD as I was more confident presenting my data not only to the lab group but in national and international conferences.

The next SMART target was to gain a broader knowledge base, and this was achieved through the learning seminars but also the application of techniques including ECHO, HTRF and MST. This work assisted with my PhD project as work consisted of fluorescently conjugating fluorophores to proteins which was a similar technique to conjugating therapy to liposomes during the results chapter of this thesis. Finally, an aim of the presentation was to improve my professionalism in preparation for the end of the PhD. I achieved this goal through communication within the bioscience department and industrial clients as well as the use of an electronic laboratory book system (Dotmatics). After the placement had concluded I work

on collaborations both within the university and externally with an industrial partner, and the communication and professionalism skills used in the placement allowed me to be effective in these projects.

Whilst I was on this placement, I gained invaluable insight into the scientific industrial sector, including the responsibilities of the individual scientist, how to communicate with professional clients and the pace of the sector in contrast to academia. This has made me consider whether I would in the future apply for a career in industry or academia; industry provides increased financial security but with this a loss of authority and independence over projects.

7.2. Appendix 2: Mass spectrometry Up and down regulated proteins

8. 3-month vehicle vs 18-month vehicle: Down-regulated proteins

Protein	Abbreviation	Log (fold change)	p-value
Cholesterol transporter ABCA5	Abca5	-0.946	0.012
Aldehyde dehydrogenase X, mitochondrial	Aldh1b1	-0.321	0.005
Beta-arrestin-2	Arrb2	-0.506	0.027
Ankyrin repeat and SOCS box protein 6	Asb6	-0.360	0.032
Set1/Ash2 histone methyltransferase complex subunit ASH2	Ash2l	-3.127	0.046
Carbonic anhydrase 4	Ca4	-0.378	0.016
Neural cell adhesion molecule L1-like protein	Chl1	-0.327	0.001
Dihydropyrimidinase-related protein 1	Crmp1;Dpysl3	-0.304	0.009
Cystathionine gamma-lyase	Cth	-0.510	0.019
Diacylglycerol kinase eta	Dgkd;Dgkh	-0.508	0.007
7-dehydrocholesterol reductase	Dhcr7	-0.366	0.018
DnaJ homolog subfamily B member 12	Dnajb12	-0.370	0.015
Dihydropyrimidinase-related protein 3	Dpysl3	-0.444	0.001
Dihydropyrimidinase-related protein 5	Dpysl5	-0.451	0.003
Dynein light chain Tctex-type 1	Dynlt1	-2.703	0.015
ER membrane protein complex subunit 10	Emc10	-0.449	0.045
Glycerophosphocholine cholinephosphodiesterase ENPP6	Enpp6	-0.425	0.000
Epidermal growth factor receptor kinase substrate 8	Eps8	-0.449	0.012
Ethanolamine-phosphate phospho-lyase	Etnppl	-0.427	0.010
rRNA 2'-O-methyltransferase fibrillarin	Fbl	-0.514	0.006
GDNF family receptor alpha-1	Gfra1	-0.460	0.006
Golgin subfamily A member 7	Golga7	-0.346	0.039
Hippocalcin-like protein 1	Hpcal1	-0.398	0.016
Protein-S-isoprenylcysteine O-methyltransferase	Icmt	-3.372	0.019
IgLON family member 5	Iglon5	-0.395	0.005
Protein Red	Ik	-0.501	0.041
	K22E_HUMAN	-1.150	0.033
Calsenilin	Kcnip3	-0.504	0.041
Kinesin heavy chain isoform 5A	Kif5a	-0.321	0.027
Keratin, type II cytoskeletal 79	Krt79	-1.075	0.040
Volume-regulated anion channel subunit LRRC8A	Lrrc8a;Lrrc8c	-0.469	0.023
Myristoylated alanine-rich C-kinase substrate	Marcks	-0.560	0.001
MARCKS-related protein	Marcksl1	-1.022	0.013

Megakaryocyte-associated tyrosine-protein kinase	Matk	-0.409	0.030
InaD-like protein	Mpdz;Patj	-0.345	0.036
Large ribosomal subunit protein bL28m	Mrpl28	-0.425	0.025
Neuronal calcium sensor 1	Ncs1	-0.311	0.001
NAD-capped RNA hydrolase NUDT12	Nudt12	-0.883	0.033
Uridine diphosphate glucose pyrophosphatase NUDT14	Nudt14	-4.257	0.015
Plasminogen receptor (KT)	Plgrkt	-0.328	0.046
Phospholipid phosphatase-related protein type 3	Plppr3	-0.362	0.011
cAMP-dependent protein kinase catalytic subunit beta	Prkacb	-0.366	0.040
Tyrosine-protein phosphatase non-receptor type 4	Ptpn4	-0.724	0.015
Protein Njmu-R1	Q9CYI0	-0.333	0.048
Reticulocalbin-1	Rcn1	-0.334	0.047
Protein RER1	Rer1	-0.589	0.006
Reactive oxygen species modulator 1	Romo1	-0.320	0.028
Ras-related protein R-Ras	Rras;Rras2	-0.578	0.001
Ras-related protein R-Ras2	Rras2	-0.833	0.002
Serine protease inhibitor A3M	Serpina3m	-3.658	0.019
Solute carrier family 25 member 33	Slc25a33	-0.539	0.023
Zinc transporter ZIP12	Slc39a12	-0.377	0.034
Synaptotagmin-7	Syt7	-0.307	0.003
Serine/threonine-protein kinase TAO2	Taok2	-0.607	0.001
TBC1 domain family member 10A	Tbc1d10a	-0.588	0.008
Transducin beta-like protein 2	Tbl2	-0.459	0.014
Transmembrane protein 132E	Tmem132e	-5.718	0.000
Tenascin	Tnc	-0.536	0.000
Mitochondrial import receptor subunit TOM20 homolog	Tomm20	-0.359	0.038
DNA topoisomerase 2-beta	Top2b	-0.438	0.010
TSC22 domain family protein 4	Tsc22d4	-1.032	0.003
Tetraspanin-7	Tspan7	-0.347	0.027
Tubulin beta-2A chain	Tubb2a;Tubb2b;Tubb6	-0.316	0.032
Tubulin beta-2B chain	Tubb2b	-0.979	0.000
UBX domain-containing protein 7	Ubxn7	-0.310	0.000
Tyrosine-protein kinase Yes	Yes1	-0.611	0.005
Zinc finger protein 42	Yy1;Yy2;Zfp42	-2.846	0.037
3-month vehicle vs 18-month vehicle: Up-regulated proteins			
Ras-related protein Rab-3D	Rab3d	8.185	0.015
Mitogen-activated protein kinase 13	Mapk13	6.925	0.013
Thrombospondin type-1 domain-containing protein 1	Thsd1	5.905	0.013
Diphthine methyl ester synthase	Dph5	4.934	0.014

AMSH-like protease	Stambpl1	4.919	0.013
Ubiquitin-conjugating enzyme E2 B	Ube2b	4.788	0.014
LHFPL tetraspan subfamily member 2 protein	Lhfpl2	4.654	0.000
Tetraspanin-15	Tspan15	4.552	0.012
Sodium/myo-inositol cotransporter	Slc5a3	4.507	0.009
Transmembrane protein 87A	Tmem87a	4.488	0.010
Serine protease inhibitor A3N	Serpina3n	4.455	0.006
Putative Dol-P-Glc:Glc(2)Man(9)GlcNAc(2)-PP-Dol alpha-1,2-glucosyltransferase	Alg10b	4.306	0.021
Galactose-1-phosphate uridylyltransferase	Galt	4.095	0.013
Phosphatidylethanolamine-binding protein 1	Pbp2;Pebp1	4.054	0.014
tRNA-dihydrouridine(47) synthase [NAD(P)(+)]-like	Dus3l	4.037	0.017
Parafibromin	Cdc73	4.017	0.010
Sorting nexin-19	Snx19	3.931	0.014
Small VCP/p97-interacting protein	Svip	3.903	0.014
E3 ubiquitin-protein ligase RNF181	Rnf181	3.891	0.011
Galactose mutarotase	Galm	3.866	0.007
Protein phosphatase 1 regulatory subunit 37	Ppp1r37	3.864	0.014
Ig gamma-2A chain C region, A allele	Igh-1a;Ighg	3.714	0.020
Periodic tryptophan protein 1 homolog	Pwp1	3.688	0.016
Glutamate receptor ionotropic, delta-2	Grid1;Grid2	3.526	0.024
Serine/threonine-protein kinase LMTK1	Aatk	3.510	0.013
Interferon-induced protein with tetratricopeptide repeats 3	Ifit3	3.360	0.016
ATP-binding cassette sub-family C member 4	Abcc4	3.191	0.016
Sulfiredoxin-1	Srxn1	2.595	0.039
Hyaluronan and proteoglycan link protein 2	Hapln2	2.387	0.000
Serine protease HTRA1	Htra1	1.248	0.000
Aggrecan core protein	Acan	1.039	0.010
Complement C1q subcomponent subunit A	C1qa	0.941	0.000
Palmitoyl-protein thioesterase 1	Ppt1	0.925	0.000
Activator of 90 kDa heat shock protein ATPase homolog 2	Ahsa2	0.884	0.019
Complement C1q subcomponent subunit B	C1qb	0.880	0.000
Ferritin light chain 1	Ftl1	0.861	0.000
Hyaluronan and proteoglycan link protein 1	Hapln1	0.854	0.001
Synaptophysin-like protein 1	Sypl1	0.827	0.047

Sphingomyelin phosphodiesterase	Smpd1	0.817	0.019
1-phosphatidylinositol 3-phosphate 5-kinase	Pikfyve	0.802	0.012
Ferritin heavy chain	Fth1	0.797	0.001
Versican core protein	Vcan	0.794	0.001
Complement C1q subcomponent subunit C	C1qc	0.777	0.000
Ephrin type-A receptor 5	Epha5;Epha7	0.770	0.008
Lysophosphatidylcholine acyltransferase 2	Lpcat2	0.757	0.002
Glial fibrillary acidic protein	Gfap	0.751	0.003
Cytosolic carboxypeptidase 1	Agtpbp1	0.700	0.020
CTP synthase 2	Ctps1;Ctps2	0.694	0.013
Prosaposin	Psap	0.688	0.043
Guanine nucleotide-binding protein G(I)/G(S)/G(O) subunit gamma-3	Gng3	0.679	0.023
Cathepsin Z	Ctsz	0.677	0.000
Negative elongation factor B	Nelfb	0.674	0.047
Macrophage-capping protein	Capg	0.639	0.022
Tripeptidyl-peptidase 1	Tpp1	0.637	0.000
CD9 antigen	Cd9	0.634	0.001
Insulin-degrading enzyme	Ide	0.629	0.000
Caveolin-1	Cav1	0.622	0.003
Tectonin beta-propeller repeat-containing protein 1	Tecpr1	0.599	0.029
Dynein light chain Tctex-type 3	Dynlt3	0.598	0.045
Tensin-1	Tns1;Tns3	0.590	0.035
Acid ceramidase	Asah1	0.584	0.000
Vezatin	Vezt	0.572	0.043
NADH dehydrogenase [ubiquinone] flavoprotein 3, mitochondrial	Ndufv3	0.557	0.038
Vimentin	Vim	0.550	0.037
Rhotekin	Rtkn	0.545	0.044
Guanine nucleotide-binding protein G(I)/G(S)/G(O) subunit gamma-5	Gng5	0.537	0.019
Basal cell adhesion molecule	Bcam	0.536	0.010
Myosin-11	Myh11;Myh9	0.534	0.001
Shootin-1	Shtn1	0.529	0.023
WASH complex subunit 3	Washc3	0.507	0.028
Protein pelota homolog	Pelo	0.507	0.023
Protein S100-B	S100b	0.503	0.029
Myelin proteolipid protein	Plp1	0.499	0.047
Vimentin	Des;Vim	0.499	0.010
Plastin-1	Pls1	0.482	0.000
Myelin-oligodendrocyte glycoprotein	Mog	0.482	0.000
Rho GTPase-activating protein 25	Arhgap25	0.479	0.013
DCN1-like protein 2	Dcun1d1;Dcun1d2	0.479	0.042

Ribose-phosphate pyrophosphokinase 2	Prps2	0.468	0.000
Isochorismatase domain-containing protein 2A	Isoc2a	0.457	0.004
Probable aminopeptidase NPEPL1	Npepl1	0.451	0.022
Choline transporter-like protein 1	Slc44a1	0.446	0.002
Fumarylacetoacetase	Fah	0.443	0.000
Aspartoacylase	Aspa	0.436	0.000
Carbonic anhydrase 2	Ca2	0.433	0.000
NmrA-like family domain-containing protein 1	Nmral1	0.432	0.004
Glutamate carboxypeptidase 2	Folh1	0.425	0.001
Myosin light polypeptide 6	Myl6;Myl6b	0.423	0.011
Annexin A11	Anxa11	0.419	0.013
Myeloid leukemia factor 2	Mlf2	0.415	0.001
Cathepsin D	Ctsd	0.414	0.000
Choline transporter-like protein 2	Slc44a2	0.408	0.006
Prosaposin receptor GPR37	Gpr37	0.404	0.008
Peptidyl-prolyl cis-trans isomerase F, mitochondrial	Ppie;Ppif	0.404	0.021
CREB-regulated transcription coactivator 1	Crtc1	0.401	0.017
UPF0598 protein C8orf82 homolog	Q8VE95	0.400	0.013
Astrocytic phosphoprotein PEA-15	Pea15	0.395	0.015
Lysosome-associated membrane glycoprotein 2	Lamp2	0.394	0.005
Trafficking protein particle complex subunit 13	Trappc13	0.394	0.001
Beta-2-syntrophin	Sntb2	0.392	0.004
Myosin light polypeptide 6	Myl6	0.390	0.021
Alanine aminotransferase 1	Gpt	0.387	0.002
Glutathione S-transferase Mu 2	Gstm2;Gstm7	0.387	0.006
Neurocan core protein	Ncan	0.386	0.006
Kynurenine--oxoglutarate transaminase 3	Kyat3	0.385	0.000
Ubiquinone biosynthesis monooxygenase COQ6, mitochondrial	Coq6	0.383	0.004
Serine/threonine-protein phosphatase 2A catalytic subunit alpha isoform	Ppp2ca	0.381	0.025
F-box only protein 7	Fbxo7	0.378	0.013
Mitochondrial dynamics protein MID51	Mief1	0.375	0.017
Glycolipid transfer protein	Gltp	0.373	0.012
Dynactin subunit 3	Dctn3	0.368	0.004
RNA-binding protein Musashi homolog 2	Msi2	0.368	0.028
Leucine-rich repeat LGI family member 3	Lgi3	0.362	0.003
Thioredoxin, mitochondrial	Txn2	0.359	0.005
DnaJ homolog subfamily B member 4	Dnajb1;Dnajb4	0.359	0.045

Ephrin-B3	Efnb3	0.358	0.003
Disintegrin and metalloproteinase domain-containing protein 10	Adam10	0.348	0.002
Myelin basic protein	Mbp	0.342	0.006
Large ribosomal subunit protein uL29m	Mrpl47	0.341	0.032
Galectin-related protein	Lgalsl	0.338	0.004
Cilia- and flagella-associated protein 20	Cfap20	0.334	0.045
Oligoribonuclease, mitochondrial	Rexo2	0.334	0.044
Dolichyl-phosphate beta-glucosyltransferase	Alg5	0.330	0.034
Engulfment and cell motility protein 1	Elmo1	0.328	0.010
Metal transporter CNNM1	Cnnm1	0.323	0.015
Ermin	Ermn	0.323	0.001
Anillin	Anln	0.319	0.022
Plexin-C1	Plxnc1	0.318	0.015
Small ribosomal subunit protein bS1m	Mrps28	0.314	0.003
Leucine-rich repeat LGI family member 2	Lgi2	0.313	0.002
Ubiquinol-cytochrome c reductase complex assembly factor 2	Uqcc2	0.313	0.031
Transcription activator BRG1	Smarca2;Smarca4	0.305	0.035
Tropomyosin alpha-4 chain	Tpm4	0.303	0.044
Delta-aminolevulinic acid dehydratase	Alad	0.301	0.002

18-month vehicle vs 18-month 1 mg/kg LPS: Down-regulated genes

Protein	Abbreviation	Log (fold change)	p-value
Ras-related protein Rab-3D	Rab3d	-7.222	0.043
Mitogen-activated protein kinase 13	Mapk13	-6.925	0.030
Phospholipid-transporting ATPase IF	Atp11b	-6.275	0.048
Bardet-Biedl syndrome 7 protein homolog	Bbs7	-5.549	0.038
Diphthine methyl ester synthase	Dph5	-4.934	0.030
Cadherin-11	Cdh11;Cdh8	-4.371	0.032
Cytohesin-3	Cyth3	-4.255	0.047
Arf-GAP with dual PH domain-containing protein 2	Adap2	-4.252	0.018
Tyrosine-protein kinase Mer	Mertk	-4.163	0.042
Transmembrane protein 87A	Tmem87a	-3.964	0.033
Uncharacterized protein C6orf47 homolog	D17h6s53e	-3.840	0.018
Periodic tryptophan protein 1 homolog	Pwp1	-3.688	0.035
Keratin, type I cytoskeletal 15	Krt15;Krt16;Krt222;Krt42	-3.682	0.030
Type 1 phosphatidylinositol 4,5-bisphosphate 4-phosphatase	Pip4p1;Pip4p2	-3.656	0.012
H/ACA ribonucleoprotein complex subunit 1	Gar1	-3.617	0.027
Galactose mutarotase	Galm	-3.576	0.017
Tetratricopeptide repeat protein 27	Ttc27	-3.479	0.039
Synaptic vesicle glycoprotein 2B	Sv2a;Sv2b	-3.262	0.030
Centrosomal protein of 41 kDa	Cep41	-3.076	0.031
7-methylguanosine phosphate-specific 5'-nucleotidase	Nt5c3b	-3.070	0.030
Inosine-5'-monophosphate dehydrogenase 1	Impdh1	-2.968	0.037
Serine/threonine-protein kinase 4	Stk4	-2.826	0.011
E3 ubiquitin-protein ligase MIB1	Mib1;Rnf34	-2.743	0.049
Activator of 90 kDa heat shock protein ATPase homolog 2	Ahsa2	-2.700	0.024
Kinesin-like protein KIF3C	Kif3c	-2.467	0.034
FERM domain-containing protein 4A	Frmd4a	-2.323	0.034
THO complex subunit 2	Thoc2	-2.196	0.047
DGAT1/2-independent enzyme synthesizing storage lipids	Tmem68	-0.871	0.001
Regulating synaptic membrane exocytosis protein 3	Rims1;Rims3	-0.811	0.023
Pro-MCH	Pmch	-0.746	0.011
Myelin-associated oligodendrocyte basic protein	Mobp	-0.714	0.001
Vimentin	Vim	-0.644	0.039

Myosin phosphatase Rho-interacting protein	Mprip	-0.623	0.019
Neuroserpin	Serpini1	-0.623	0.008
Claudin-11	Cldn11	-0.584	0.027
E3 ubiquitin-protein ligase RNF31	Rnf31	-0.541	0.044
Membrane-associated guanylate kinase, WW and PDZ domain-containing protein 3	Magi3	-0.534	0.033
Diphosphomevalonate decarboxylase	Mvd	-0.526	0.018
Tyrosine-protein kinase receptor TYRO3	Tyro3	-0.524	0.006
Myotubularin-related protein 13	Sbf1;Sbf2	-0.524	0.045
Protein shisa-4	Shisa4	-0.504	0.001
Inositol hexakisphosphate kinase 1	Ip6k1	-0.496	0.039
Four and a half LIM domains protein 2	Fhl2	-0.491	0.002
Cyclin-dependent kinase 17	Cdk17	-0.483	0.015
Unconventional myosin-Id	Myo1d	-0.481	0.006
Serine/arginine-rich splicing factor 10	Srsf10	-0.472	0.003
2-hydroxyacylsphingosine 1-beta-galactosyltransferase	Ugt8	-0.467	0.004
Ephrin type-A receptor 5	Epha5;Epha7	-0.464	0.036
Glucocorticoid receptor	Nr3c1	-0.462	0.024
Heterogeneous nuclear ribonucleoproteins C1/C2	Hnrnpc	-0.462	0.005
Tropomodulin-1	Tmod1	-0.452	0.007
Transmembrane protein 9B	Tmem9b	-0.449	0.012
RalBP1-associated Eps domain-containing protein 1	Reps1;Reps2	-0.446	0.048
RNA polymerase-associated protein RTF1 homolog	Rtf1	-0.441	0.018
Ubiquitin carboxyl-terminal hydrolase 39	Usp39	-0.433	0.012
Hydroxymethylglutaryl-CoA synthase, cytoplasmic	Hmgcs1	-0.427	0.000
Tripartite motif-containing protein 46	Trim46	-0.426	0.006
Synaptic vesicular amine transporter	Slc18a2	-0.425	0.039
Glycine amidinotransferase, mitochondrial	Gatm	-0.410	0.006
Formin-2	Fmn2	-0.403	0.025
Bromodomain-containing protein 4	Brd4	-0.393	0.040
Acidic leucine-rich nuclear phosphoprotein 32 family member E	Anp32e	-0.391	0.001
RNA-binding protein Raly	Raly	-0.388	0.016
RNA binding motif protein, X-linked-like-1	Rbmx;Rbmxl1	-0.383	0.012
Caveolin-1	Cav1	-0.379	0.020
GTP-binding protein Di-Ras2	Diras1;Diras2	-0.363	0.019
Synaptopodin	Synpo	-0.359	0.043
Rootletin	Crocc	-0.354	0.011

Fragile X messenger ribonucleoprotein 1	Fmr1	-0.349	0.002
Spermatid perinuclear RNA-binding protein	Ilf3;Strbp	-0.341	0.001
Ubiquinol-cytochrome c reductase complex assembly factor 2	Uqcc2	-0.338	0.006
Scaffold attachment factor B1	Safb	-0.337	0.027
Calcium/calmodulin-dependent protein kinase 2	Camkk2	-0.334	0.006
CREB-regulated transcription coactivator 1	Crtc1	-0.331	0.036
ATP-dependent RNA helicase A	Dhx9	-0.330	0.018
Neurofilament light polypeptide	Ina;Nefl;Nefm	-0.329	0.042
Coiled-coil domain-containing protein 177	Ccdc177	-0.325	0.005
Spermatid perinuclear RNA-binding protein	Strbp	-0.323	0.047
Matrin-3	Matr3	-0.321	0.042
Girdin	Ccdc88a	-0.321	0.021
Rho guanine nucleotide exchange factor 17	Arhgef17	-0.320	0.025
Calmin	Clmn	-0.315	0.027
U1 small nuclear ribonucleoprotein 70 kDa	Snrnp70	-0.312	0.013
TBC1 domain family member 24	Tbc1d24	-0.311	0.022
Golgi-associated PDZ and coiled-coil motif-containing protein	Gopc	-0.308	0.017
Serine/threonine-protein phosphatase 6 regulatory subunit 1	Ppp6r1	-0.306	0.009
18-month vehicle vs 18-month 1 mg/kg LPS: Down-regulated genes			
Protein	Abbreviation	Log (fold change)	p-value
Thymidine kinase 2, mitochondrial	Tk2	0.301	0.004
Moesin	Msn	0.302	0.005
Serotransferrin	Tf	0.305	0.024
PI-PLC X domain-containing protein 3	Plcxd3	0.305	0.005
Potassium-transporting ATPase alpha chain 1	Atp4a	0.306	0.044
Ras-related protein Rab-22A	Rab22a	0.306	0.030
Extracellular superoxide dismutase [Cu-Zn]	Sod3	0.312	0.045
Sodium- and chloride-dependent GABA transporter 3	Slc6a11	0.313	0.004
Peroxisomal carnitine O-octanoyltransferase	Crot	0.317	0.016
Delta(3,5)-Delta(2,4)-dienoyl-CoA isomerase, mitochondrial	Ech1	0.321	0.006
Solute carrier family 7 member 14	Slc7a14	0.324	0.017

Signal transducer and activator of transcription 1	Stat1	0.325	0.011
MYG1 exonuclease	Myg1	0.328	0.004
Succinate dehydrogenase [ubiquinone] cytochrome b small subunit, mitochondrial	Sdhd	0.330	0.040
Tubulin beta-2B chain	Tubb2b	0.330	0.003
ADP-ribosylation factor-like protein 6	Arl6	0.337	0.003
E3 UFM1-protein ligase 1	Ufl1	0.338	0.008
Glutathione S-transferase theta-2	Gstt2;Gstt3	0.339	0.003
Leucine-rich repeat and immunoglobulin-like domain-containing nogo receptor-interacting protein 2	Lingo2	0.341	0.002
Dystroglycan 1	Dag1	0.342	0.010
Annexin A2	Anxa2	0.349	0.007
Transport and Golgi organization 2 homolog	Tango2	0.350	0.029
Protein YIF1B	Yif1b	0.351	0.025
Heterochromatin protein 1-binding protein 3	Hp1bp3	0.352	0.049
Dual specificity phosphatase 28	Dusp28	0.357	0.001
Coatomer subunit gamma-1	Copg1	0.358	0.026
Plastin-2	Lcp1	0.362	0.001
Neuroligin 4-like	Nlgn1;Nlgn2;Nlgn3;Nlgn4l	0.368	0.039
C-terminal-binding protein 2	Ctbp2	0.374	0.017
Golgin subfamily A member 7	Golga7	0.374	0.018
Probable proline--tRNA ligase, mitochondrial	Pars2	0.376	0.004
Eukaryotic translation initiation factor 1	Eif1	0.377	0.004
Thiopurine S-methyltransferase	Tpmt	0.385	0.029
Inhibitor of nuclear factor kappa-B kinase subunit beta	Ikbkb	0.388	0.025
Protein PALS2	Mpp2;Pals2	0.395	0.036
Alpha-parvin	Parva	0.410	0.030
Large ribosomal subunit protein bL20m	Mrpl20	0.412	0.010
MARCKS-related protein	Marcksl1	0.414	0.048
Protein archease	Zbtb8os	0.414	0.048
ADP-ribosyl cyclase/cyclic ADP-ribose hydrolase 1	Cd38	0.417	0.021
Gap junction beta-6 protein	Gjb6	0.422	0.027
RNA-binding protein 3	Rbm3	0.424	0.018
Uracil phosphoribosyltransferase homolog	Uprt	0.427	0.011
Peptidyl-prolyl cis-trans isomerase FKBP5	Fkbp5	0.429	0.015
Moesin	Msn;Rdx	0.432	0.000

Cytosolic 5'-nucleotidase 1A	Nt5c1a	0.435	0.012
Heat shock protein beta-1	Hspb1	0.440	0.019
Vacuolar protein-sorting-associated protein 25	Vps25	0.442	0.000
Bcl-2-like protein 2	Bcl2l2	0.444	0.003
Aquaporin-4	Aqp4	0.446	0.039
Protein-glutamine gamma-glutamyltransferase 2	Tgm2	0.451	0.003
Ubiquitin-conjugating enzyme E2 variant 3	Uevld	0.458	0.008
BLOC-1-related complex subunit 5	Borcs5	0.459	0.026
Tryptophan--tRNA ligase, mitochondrial	Wars2	0.467	0.025
Ubiquitin carboxyl-terminal hydrolase MINDY-1	Mindy1	0.467	0.018
Voltage-gated potassium channel subunit beta-1	Kcnab1	0.477	0.006
DNA-directed RNA polymerase II subunit RPB2	Polr2b	0.486	0.008
Thymocyte nuclear protein 1	Thyn1	0.489	0.039
TSC22 domain family protein 4	Tsc22d4	0.490	0.002
Ribosomal protein S6 kinase alpha-1	Rps6ka1	0.499	0.023
Cytochrome P450 2S1	Cyp2s1	0.503	0.014
Transmembrane and coiled-coil domains protein 1	Tmcc1	0.520	0.019
Metal transporter CNNM2	Cnnm2	0.524	0.024
ER membrane protein complex subunit 5	Mmgt1	0.526	0.009
Chromobox protein homolog 5	Cbx5	0.532	0.043
Sister chromatid cohesion protein PDS5 homolog B	Pds5b	0.536	0.021
Glutamate decarboxylase 1	Gad1;Gad2	0.537	0.006
Lysophospholipid acyltransferase 2	Mboat2	0.537	0.011
Pterin-4-alpha-carbinolamine dehydratase	Pcbd1	0.552	0.023
Tudor-interacting repair regulator protein	Nudt16l1	0.562	0.034
Histone H1.4	H1-4	0.596	0.048
Pregnancy zone protein	Pzp	0.623	0.011
Beta-2-microglobulin	B2m	0.626	0.006
Integrin beta-2	Itgb2	0.632	0.038
Prostaglandin-H2 D-isomerase	Ptgds	0.633	0.000
Coiled-coil domain-containing protein 91	Ccdc91	0.633	0.041
Metallothionein-3	Mt3	0.654	0.010
Beta-arrestin-2	Arrb2	0.667	0.000
Ethanolamine-phosphate phospho-lyase	Etnppl	0.670	0.002

ADP-ribosylation factor-like protein 6-interacting protein 1	Arl6ip1	0.679	0.026
Methyl-CpG-binding protein 2	Mecp2	0.687	0.050
High affinity immunoglobulin epsilon receptor subunit gamma	Fcer1g	0.694	0.014
Receptor-type tyrosine-protein phosphatase mu	Ptprm;Ptprt	0.705	0.046
Protein S100-A11	S100a11	0.719	0.004
Hemoglobin subunit beta-1	Hbb-b1	0.741	0.017
Hemoglobin subunit alpha	Hba	0.769	0.015
Proteasome activator complex subunit 1	Psme1;Psme2	0.777	0.016
Perilipin-4	Plin4	0.808	0.002
Complement C3	C3	0.810	0.049
Sodium- and chloride-dependent glycine transporter 2	Slc6a5	0.839	0.035
L-xylulose reductase	Dcxr	0.855	0.024
Ceruloplasmin	Cp	0.950	0.010
Apolipoprotein A-I	Apoa1	0.957	0.030
Mothers against decapentaplegic homolog 1	Smad1;Smad5	0.977	0.009
Cytochrome c oxidase subunit 6A1, mitochondrial	Cox6a1	0.982	0.007
Carbonic anhydrase 1	Ca1	1.019	0.007
Sulfotransferase 1A1	Sult1a1	1.026	0.027
Apolipoprotein D	Apod	1.420	0.000
Fibrinogen gamma chain	Fgg	1.515	0.000
Hemopexin	Hpx	1.771	0.000
Annexin A1	Anxa1	2.318	0.047
Dynein light chain Tctex-type 1	Dynlt1	2.561	0.038
Acyl-coenzyme A thioesterase 8	Acot8	3.002	0.049
Nucleoporin Nup37	Nup37	3.216	0.020
Allograft inflammatory factor 1	Aif1	3.253	0.022
Cathepsin S	Ctss	3.627	0.037
Heat shock protein beta-8	Hspb8	3.693	0.010
Serine protease inhibitor A3M	Serpina3m;Serpina3n	3.716	0.000
Uridine phosphorylase 1	Upp1	3.737	0.015
Complement C4-B	C4b	3.924	0.016
Metallothionein-2	Mt2	3.930	0.041
Macrophage colony-stimulating factor 1 receptor	Csf1r	4.040	0.000
PI-PLC X domain-containing protein 2	Plcxd2	4.283	0.000
Replication protein A 32 kDa subunit	Rpa2	4.346	0.038

18-month vehicle vs 18-month 0.25 mg/kg LPS: Up-regulated genes

Protein	Abbreviation	Log (fold change)	p-value
Ras-related protein Rab-3D	Rab3d	-10.976	0.000
Phospholipid-transporting ATPase IF	Atp11b	-6.275	0.024
Diphthine methyl ester synthase	Dph5	-4.934	0.013
Coiled-coil domain-containing protein 115	Ccdc115	-4.786	0.016
Leucine-rich repeat-containing protein 4	Lrrc4	-4.526	0.007
Prominin-1	Prom1	-4.150	0.015
Type 1 phosphatidylinositol 4,5-bisphosphate 4-phosphatase	Pip4p1;Pip4p2	-3.713	0.017
Sulfiredoxin-1	Srxn1	-3.358	0.014
ER membrane protein complex subunit 4	Emc4	-3.309	0.013
Vacuolar protein sorting-associated protein 37B	Vps37b	-3.272	0.004
Alkyldihydroxyacetonephosphate synthase, peroxisomal	Agps	-3.165	0.050
1-acylglycerol-3-phosphate O-acyltransferase ABHD5	Abhd5	-3.148	0.018
Nuclear inhibitor of protein phosphatase 1	Ppp1r8	-2.825	0.013
Ras-related protein Rab-3D	Rab3d;Rap1a;Rap1b	-0.763	0.036
GTP-binding protein Di-Ras2	Diras1;Diras2	-0.712	0.016
Coronin-6	Coro1c;Coro6	-0.676	0.012
Pleiotrophin	Ptn	-0.673	0.031
Tumor necrosis factor receptor superfamily member 21	Tnfrsf21	-0.616	0.049
Costars family protein ABRACL	Abracl	-0.607	0.047
Myotubularin-related protein 13	Sbf1;Sbf2	-0.566	0.038
CD99 antigen-like protein 2	Cd99l2	-0.564	0.035
1-phosphatidylinositol 3-phosphate 5-kinase	Pikfyve	-0.559	0.018
Cytosolic carboxypeptidase 1	Agtpbp1	-0.520	0.024
Ras-related C3 botulinum toxin substrate 3	Cdc42;Rac1;Rac3;Rhog	-0.482	0.032
Fragile X messenger ribonucleoprotein 1	Fmr1	-0.459	0.010
Pro-MCH	Pmch	-0.455	0.010
Nucleotidyltransferase MB21D2	Mb21d2	-0.455	0.033
Translocon-associated protein subunit gamma	Ssr3	-0.447	0.026
CKLF-like MARVEL transmembrane domain-containing protein 4	Cmtm4	-0.430	0.035
THO complex subunit 3	Thoc3	-0.426	0.038

VPS10 domain-containing receptor SorCS3	Sorcs3	-0.423	0.022
Diphosphomevalonate decarboxylase	Mvd	-0.422	0.027
CREB-regulated transcription coactivator 1	Crtc1	-0.418	0.012
PX domain-containing protein kinase-like protein	Pxk	-0.413	0.004
COMM domain-containing protein 10	Commd10	-0.389	0.011
Mitochondrial import inner membrane translocase subunit Tim8 B	Timm8b	-0.387	0.030
Syntaxin-6	Stx6	-0.386	0.002
Ubiquitin-conjugating enzyme E2 E3	Ube2e2;Ube2e3	-0.385	0.036
Tyrosine-protein kinase receptor TYRO3	Tyro3	-0.383	0.041
Four and a half LIM domains protein 2	Fhl2	-0.381	0.024
Ephrin type-A receptor 5	Epha5;Epha7	-0.380	0.048
Myosin-10	Myh10;Myh14	-0.350	0.047
Transforming acidic coiled-coil-containing protein 1	Tacc1	-0.345	0.013
Potassium voltage-gated channel subfamily B member 1	Kcnb1	-0.342	0.012
Putative RNA-binding protein Luc7-like 1	Luc7l	-0.337	0.018
RNA cytosine C(5)-methyltransferase NSUN2	Nsun2	-0.328	0.041
Hepatoma-derived growth factor-related protein 2	Hdgfl2	-0.318	0.045
Leucine-rich repeat-containing protein 4B	Lrrc4b	-0.317	0.001
LETM1 domain-containing protein 1	Letmd1	-0.315	0.025
Activated RNA polymerase II transcriptional coactivator p15	Sub1	-0.314	0.032
Hydroxymethylglutaryl-CoA synthase, cytoplasmic	Hmgcs1	-0.313	0.000
Small ribosomal subunit protein bS1m	Mrps28	-0.309	0.004
18-month vehicle vs 18-month 0.25 mg/kg LPS: Down-regulated genes			
Protein	Abbreviation	Log (fold change)	p-value
Vacuolar protein-sorting-associated protein 25	Vps25	0.301	0.004
Lysosome-associated membrane glycoprotein 1	Lamp1	0.301	0.034
Plastin-2	Lcp1	0.303	0.012

Annexin A2	Anxa2	0.304	0.002
Aromatic-L-amino-acid decarboxylase	Ddc	0.311	0.034
Centromere/kinetochore protein zw10 homolog	Zw10	0.328	0.037
Transgelin-2	Tagln2	0.338	0.002
Ubiquitin-conjugating enzyme E2 variant 3	Uevld	0.339	0.031
Anaphase-promoting complex subunit 1	Anapc1	0.341	0.024
Fatty acid CoA ligase Acsl3	Acsl3;Acsl4	0.344	0.027
Microtubule-associated proteins 1A/1B light chain 3B	Map1lc3b	0.348	0.048
Alpha-parvin	Parva	0.348	0.033
E3 ubiquitin-protein ligase MARCHF5	Marchf5	0.349	0.015
bMERB domain-containing protein 1	Bmerb1	0.349	0.008
Moesin	Msn;Rdx	0.358	0.008
DNA-directed RNA polymerases I, II, and III subunit RPABC1	Polr2e	0.360	0.035
Guanine nucleotide exchange factor C9orf72 homolog	C9orf72	0.362	0.025
Scrapie-responsive protein 1	Scrg1	0.364	0.036
Signal transducer and activator of transcription 1	Stat1	0.366	0.010
Peroxisomal acyl-coenzyme A oxidase 1	Acox1	0.370	0.039
Protein SON	Son	0.376	0.015
FUN14 domain-containing protein 1	Fundc1	0.378	0.021
Uracil phosphoribosyltransferase homolog	Uprt	0.382	0.041
Pleckstrin homology domain-containing family B member 1	Plekhb1	0.388	0.011
InaD-like protein	Mpdz;Patj	0.395	0.004
Tyrosine-protein kinase Yes	Yes1	0.397	0.029
Dystroglycan 1	Dag1	0.400	0.005
Peptidyl-prolyl cis-trans isomerase FKBP5	Fkbp5	0.403	0.015
Voltage-dependent N-type calcium channel subunit alpha-1B	Cacna1b	0.408	0.018
TATA box-binding protein-like 1	Tbpl1	0.409	0.042
DnaJ homolog subfamily C member 10	Dnajc10	0.411	0.032
Sec1 family domain-containing protein 2	Scfd2	0.414	0.019

Ubiquinol-cytochrome c reductase complex assembly factor 1	Uqcc1	0.419	0.020
TNF receptor-associated factor 3	Traf3	0.421	0.026
Ethanolamine-phosphate phospho-lyase	Etnppl	0.424	0.038
Protein phosphatase 1 regulatory subunit 12C	Ppp1r12c	0.427	0.005
Heat shock protein beta-1	Hspb1	0.429	0.027
Nicotinate phosphoribosyltransferase	Naprt	0.439	0.018
Jouberin	Ahi1	0.443	0.036
Threonine synthase-like 2	Thnsl2	0.445	0.029
Prostaglandin-H2 D-isomerase	Ptgds	0.448	0.020
Volume-regulated anion channel subunit LRRC8A	Lrrc8a;Lrrc8c	0.450	0.019
Nuclear receptor-interacting protein 2	Nrip2	0.450	0.016
Ectonucleoside triphosphate diphosphohydrolase 3	Entpd3	0.454	0.021
Ubiquitin-associated and SH3 domain-containing protein B	Ubash3b	0.455	0.002
ADP-ribosyl cyclase/cyclic ADP-ribose hydrolase 1	Cd38	0.457	0.012
Peripherin	Prph	0.464	0.031
Glutathione S-transferase theta-2	Gstt2;Gstt3	0.464	0.004
Synaptotagmin-6	Syt6	0.467	0.027
Peroxisomal carnitine O-octanoyltransferase	Crot	0.472	0.003
Ribosomal protein S6 kinase alpha-1	Rps6ka1	0.476	0.012
Solute carrier family 22 member 4	Slc22a4	0.482	0.026
Microsomal glutathione S-transferase 1	Mgst1	0.483	0.017
Glutamate receptor ionotropic, delta-2	Grid2	0.514	0.004
KN motif and ankyrin repeat domain-containing protein 4	Kank4	0.520	0.033
Asc-type amino acid transporter 1	Slc7a10	0.527	0.034
Cerebellin-1	Cbln1	0.536	0.008
Ras-related protein Rab-27B	Rab27a;Rab27b	0.536	0.011
Cystathionine gamma-lyase	Cth	0.540	0.024
Cytochrome c oxidase subunit 6A1, mitochondrial	Cox6a1	0.564	0.009
Protein RER1	Rer1	0.596	0.015

Pterin-4-alpha-carbinolamine dehydratase	Pcbd1	0.599	0.039
Cytochrome P450 2S1	Cyp2s1	0.627	0.013
Mothers against decapentaplegic homolog 1	Smad1;Smad5	0.646	0.043
Polypeptide N-acetylgalactosaminyltransferase 16	Galnt16	0.651	0.033
Perilipin-4	Plin4	0.653	0.004
Sentrin-specific protease 3	Senp3	0.675	0.011
Beta-2-microglobulin	B2m	0.692	0.007
BAI1-associated protein 3	Baiap3	0.695	0.030
Protein Red	Ik	0.722	0.009
	REF_HEVBR	0.723	0.034
Potassium-transporting ATPase alpha chain 1	Atp1a4;Atp4a	0.743	0.032
Phytanoyl-CoA dioxygenase domain-containing protein 1	Phyhd1	0.804	0.045
NAD-capped RNA hydrolase NUDT12	Nudt12	0.870	0.036
DNA-directed RNA polymerase II subunit RPB2	Polr2b	0.876	0.002
Probable global transcription activator SNF2L2	Smarca2	0.923	0.040
TSC22 domain family protein 4	Tsc22d4	0.937	0.036
Ceruloplasmin	Cp	0.938	0.001
Fibrinogen gamma chain	Fgg	1.000	0.002
Apolipoprotein D	Apod	1.173	0.005
Hemopexin	Hpx	1.389	0.001
TBC1 domain family member 1	Tbc1d1	2.129	0.017
Interferon-induced protein with tetratricopeptide repeats 3	Ifit3	2.669	0.046
Dynein light chain Tctex-type 1	Dynlt1	3.018	0.015
Replication protein A 70 kDa DNA-binding subunit	Rpa1	3.246	0.019
Galectin-3-binding protein	Lgals3bp	3.517	0.030
Vasodilator-stimulated phosphoprotein	Vasp	3.660	0.027
Ceramide synthase	Tlcd3b	3.733	0.020
Protein-S-isoprenylcysteine O-methyltransferase	Icmt	3.749	0.014
Chromatin complexes subunit BAP18	Bap18	4.166	0.016
Serine protease inhibitor A3K	Serpina3k	4.209	0.006
PI-PLC X domain-containing protein 2	Plcxd2	4.495	0.000
Protein FAM167A	Fam167a	4.934	0.013
Serine protease inhibitor A3K	Serpina3k;Serpina3m;Serpina3n	5.132	0.001

Protein S100-A9	S100a9	5.230	0.000
Cathepsin S	Ctss	5.456	0.000
Haptoglobin	Hp	6.613	0.010
Ras-related protein Rab-3C	Rab3b;Rab3c	8.758	0.010
Chromobox protein homolog 5	Cbx5	0.532	0.043
Sister chromatid cohesion protein PDS5 homolog B	Pds5b	0.536	0.021
Glutamate decarboxylase 1	Gad1;Gad2	0.537	0.006
Lysophospholipid acyltransferase 2	Mboat2	0.537	0.011
Pterin-4-alpha-carbinolamine dehydratase	Pcbd1	0.552	0.023
Tudor-interacting repair regulator protein	Nudt16l1	0.562	0.034
Histone H1.4	H1-4	0.596	0.048
Pregnancy zone protein	Pzp	0.623	0.011
Beta-2-microglobulin	B2m	0.626	0.006
Integrin beta-2	Itgb2	0.632	0.038
Prostaglandin-H2 D-isomerase	Ptgds	0.633	0.000
Coiled-coil domain-containing protein 91	Ccdc91	0.633	0.041
Metallothionein-3	Mt3	0.654	0.010
Beta-arrestin-2	Arrb2	0.667	0.000
Ethanolamine-phosphate phospho-lyase	Etnppl	0.670	0.002
ADP-ribosylation factor-like protein 6-interacting protein 1	Arl6ip1	0.679	0.026
Methyl-CpG-binding protein 2	Mecp2	0.687	0.050
High affinity immunoglobulin epsilon receptor subunit gamma	Fcer1g	0.694	0.014
Receptor-type tyrosine-protein phosphatase mu	Ptprm;Ptprt	0.705	0.046
Protein S100-A11	S100a11	0.719	0.004
Hemoglobin subunit beta-1	Hbb-b1	0.741	0.017
Hemoglobin subunit alpha	Hba	0.769	0.015
Proteasome activator complex subunit 1	Psme1;Psme2	0.777	0.016
Perilipin-4	Plin4	0.808	0.002
Complement C3	C3	0.810	0.049
Sodium- and chloride-dependent glycine transporter 2	Slc6a5	0.839	0.035
L-xylulose reductase	Dcxr	0.855	0.024
Ceruloplasmin	Cp	0.950	0.010
Apolipoprotein A-I	Apoa1	0.957	0.030
Mothers against decapentaplegic homolog 1	Smad1;Smad5	0.977	0.009
Cytochrome c oxidase subunit 6A1, mitochondrial	Cox6a1	0.982	0.007

Carbonic anhydrase 1	Ca1	1.019	0.007
Sulfotransferase 1A1	Sult1a1	1.026	0.027
Apolipoprotein D	Apod	1.420	0.000
Fibrinogen gamma chain	Fgg	1.515	0.000
Hemopexin	Hpx	1.771	0.000
Annexin A1	Anxa1	2.318	0.047
Dynein light chain Tctex-type 1	Dynlt1	2.561	0.038
Acyl-coenzyme A thioesterase 8	Acot8	3.002	0.049
Nucleoporin Nup37	Nup37	3.216	0.020
Allograft inflammatory factor 1	Aif1	3.253	0.022
Cathepsin S	Ctss	3.627	0.037
Heat shock protein beta-8	Hspb8	3.693	0.010
Serine protease inhibitor A3M	Serpina3m;Serpina3n	3.716	0.000
Uridine phosphorylase 1	Upp1	3.737	0.015
Complement C4-B	C4b	3.924	0.016
Metallothionein-2	Mt2	3.930	0.041
Macrophage colony-stimulating factor 1 receptor	Csf1r	4.040	0.000
PI-PLC X domain-containing protein 2	Plcxd2	4.283	0.000
Replication protein A 32 kDa subunit	Rpa2	4.346	0.038

3-month vehicle vs 3-month 1 mg/kg LPS: Down-regulated genes

Protein name	Abbreviation	Log (fold change)	p-value
Stomatin	Stom	-1.959	0.018
Nuclear inhibitor of protein phosphatase 1	Ppp1r8	-1.830	0.021
Cell cycle exit and neuronal differentiation protein 1	Cend1	-1.014	0.031
Ras-related protein Rab-3D	Rab3d;Rap1a;Rap1b	-0.745	0.031
Cytoplasmic dynein 2 intermediate chain 2	Dync2i2	-0.675	0.028
Leucine-rich repeat-containing protein 4	Lrrc4	-0.666	0.017
SWI/SNF-related matrix-associated actin-dependent regulator of chromatin subfamily A-like protein 1	Smarcal1	-0.652	0.003
NADH dehydrogenase [ubiquinone] 1 alpha subcomplex subunit 3	Ndufa3	-0.619	0.015
G-protein-signaling modulator 1	Gpsm1;Gpsm2	-0.589	0.020
Mitogen-activated protein kinase 14	Mapk14	-0.562	0.048
cAMP-regulated phosphoprotein 19	Arpp19	-0.534	0.015
Excitatory amino acid transporter 3	Slc1a1	-0.531	0.002
GTP-binding protein Di-Ras2	Diras1;Diras2	-0.505	0.015
Ephrin type-B receptor 3	Ephb3	-0.465	0.004
Glutamate receptor 2	Gria2;Gria3;Gria4	-0.447	0.034
Epidermal growth factor receptor kinase substrate 8	Eps8	-0.433	0.020
Phosphatidylethanolamine-binding protein 2	Pbp2	-0.422	0.009
Fibroblast growth factor receptor 3	Fgfr3	-0.398	0.024
Myosin-10	Myh10;Myh14	-0.392	0.003
ER membrane protein complex subunit 6	Emc6	-0.385	0.018
Noelin-2	Olfm2	-0.381	0.013
Diacylglycerol kinase eta	Dgkd;Dgkh	-0.368	0.036
Synaptopodin	Synpo	-0.364	0.021
Proteasome subunit beta type-8	Psmb8	-0.361	0.019

Polypeptide N-acetylgalactosaminyltransferase 2	Galnt2	-0.361	0.038
Dihydropyrimidinase-related protein 2	Crmp1;Dpysl2;Dpysl3	-0.361	0.010
LysM and putative peptidoglycan-binding domain-containing protein 2	Lysmd2	-0.347	0.022
TBC1 domain family member 10A	Tbc1d10a	-0.346	0.013
Neurabin-2	Ppp1r9b	-0.345	0.043
Probable mitochondrial glutathione transporter SLC25A40	Slc25a40	-0.335	0.038
Reticulon-4 receptor-like 2	Rtn4rl2	-0.331	0.020
Adhesion G protein-coupled receptor L1	Adgrl1;Adgrl2	-0.331	0.022
Large ribosomal subunit protein eL29	Rpl29	-0.330	0.005
UBX domain-containing protein 7	Ubxn7	-0.320	0.020
Alpha-endosulfine	Ensa	-0.318	0.048
Plexin-A1	Plxna1;Plxna4	-0.316	0.035
Nucleosome assembly protein 1-like 1	Nap1l1;Nap1l4	-0.309	0.020
Beta-synuclein	Sncb;Sncg	-0.309	0.005
Methyltransferase-like 26	Mettl26	-0.304	0.019
18-month vehicle vs 18-month 1 mg/kg LPS: Up-regulated genes			
Protein name	Abbreviation	Log (fold change)	p-value
Trafficking protein particle complex subunit 1	Trappc1	0.313	0.009
Liprin-alpha-3	Ppfia2;Ppfia3	0.313	0.004
Aromatic-L-amino-acid decarboxylase	Ddc	0.318	0.039
Hsp90 co-chaperone Cdc37-like 1	Cdc37l1	0.318	0.032
E3 ubiquitin-protein ligase MARCHF5	Marchf5	0.318	0.024
Volume-regulated anion channel subunit LRRC8A	Lrrc8a	0.319	0.002
Plexin-C1	Plxnc1	0.321	0.023
Tubulin beta-4B chain	Tubb2a;Tubb2b;Tubb3;Tubb4a;Tubb4b;Tubb5	0.324	0.004
Serine/threonine-protein phosphatase 2A 55 kDa	Ppp2r2d	0.325	0.003

regulatory subunit B delta isoform			
Retinol dehydrogenase 13	Rdh13	0.326	0.049
Protein FAM3C	Fam3c	0.327	0.036
Serine protease HTRA1	Htra1	0.329	0.019
E3 ubiquitin-protein ligase RMND5A	Rmnd5a	0.330	0.006
ATP-binding cassette sub-family D member 3	Abcd3	0.333	0.049
Inositol-3-phosphate synthase 1	Isyna1	0.336	0.001
Rap guanine nucleotide exchange factor 5	Rapgef5	0.337	0.012
Zinc finger CCCH domain-containing protein 15	Zc3h15	0.339	0.014
Rho-related GTP-binding protein RhoF	Rhof	0.339	0.046
Dynein light chain 1, cytoplasmic	Dynll1;Dynll2	0.340	0.008
Ras-related protein Rap-2a	Rap2a;Rap2c	0.341	0.036
Fibroblast growth factor 1	Fgf1	0.342	0.046
Hydroxyacylglutathione hydrolase-like protein	Haghl	0.349	0.026
Calcium-binding protein 39-like	Cab39l	0.351	0.012
Mitogen-activated protein kinase 10	Mapk10;Mapk8;Mapk9	0.357	0.000
BAI1-associated protein 3	Baiap3	0.359	0.006
Autophagy-related protein 9A	Atg9a	0.359	0.003
GATOR1 complex protein DEPDC5	Depdc5	0.361	0.027
Ribosomal protein S6 kinase alpha-1	Rps6ka1	0.363	0.044
Cysteine protease ATG4C	Atg4c	0.366	0.015
Serpin H1	Serpinh1	0.366	0.002
Rho GTPase-activating protein 25	Arhgap25	0.367	0.025
Annexin A2	Anxa2	0.371	0.019
Dr1-associated corepressor	Drap1	0.373	0.031
Lysosome-associated membrane glycoprotein 2	Lamp2	0.374	0.001
Nuclear receptor-binding protein	Nrbp1	0.376	0.047
Protein diaphanous homolog 2	Diaph2	0.376	0.038
Guanine nucleotide-binding protein G(I)/G(S)/G(O) subunit gamma-5	Gng5	0.376	0.042

Ubiquitin carboxyl-terminal hydrolase 24	Usp24	0.377	0.000
Mannose-P-dolichol utilization defect 1 protein	Mpdu1	0.379	0.041
Actin-related protein 2/3 complex subunit 1B	Arpc1b	0.382	0.004
Complement C1q subcomponent subunit C	C1qc	0.385	0.010
Phosphorylase b kinase gamma catalytic chain, skeletal muscle/heart isoform	Phkg1	0.385	0.014
Heat shock protein beta-1	Hspb1	0.387	0.000
Peptidyl-prolyl cis-trans isomerase FKBP5	Fkbp5	0.388	0.002
Melanoma inhibitory activity protein 2	Mia2	0.392	0.027
DnaJ homolog subfamily C member 27	Dnajc27	0.393	0.019
Cathepsin Z	Ctsz	0.394	0.012
Transgelin-2	Tagln2	0.396	0.007
Golgi phosphoprotein 3	Golph3	0.398	0.004
T-complex protein 11-like protein 1	Tcp11l1	0.398	0.026
Heat shock 70 kDa protein 13	Hspa13	0.410	0.026
Protein tyrosine phosphatase type IVA 2	Ptp4a2	0.414	0.006
Tudor-interacting repair regulator protein	Nudt16l1	0.428	0.016
TNF receptor-associated factor 3	Traf3	0.431	0.019
Insulin receptor substrate 2	Irs2	0.438	0.034
Protein pelota homolog	Pelo	0.443	0.007
SPARC	Sparc	0.446	0.050
Ephrin type-A receptor 5	Epha5;Epha7	0.452	0.032
COMM domain-containing protein 7	Commd7	0.455	0.018
Polyisoprenoid diphosphate/phosphate phosphohydrolase PLPP6	Plpp6	0.461	0.042
Glycerol-3-phosphate dehydrogenase [NAD(+)], cytoplasmic	Gpd1;Gpd1l	0.468	0.020
Cytochrome P450 2J6	Cyp2j6	0.477	0.014
BCL2/adenovirus E1B 19 kDa protein-interacting protein 2	Bnip2	0.493	0.048
Phosphatidylinositol 4,5-bisphosphate 5-phosphatase A	Inpp5j	0.495	0.012

Peripherin	Prph;Vim	0.498	0.015
Cytochrome P450 2S1	Cyp2s1	0.499	0.034
Signal transducer and activator of transcription 1	Stat1	0.501	0.002
Fructose-bisphosphate aldolase C	Aldoa;Aldoc	0.509	0.002
N-acetylneuraminate lyase	Npl	0.515	0.006
DCN1-like protein 2	Dcun1d1;Dcun1d2	0.516	0.036
CTP synthase 2	Ctps1;Ctps2	0.522	0.020
Complement C1q subcomponent subunit B	C1qb	0.525	0.000
Inter-alpha-trypsin inhibitor heavy chain H3	Itih3	0.533	0.021
Protein-glutamine gamma-glutamyltransferase 2	Tgm2	0.534	0.000
5'-3' exoribonuclease 2	Xrn2	0.535	0.011
Synaptic vesicular amine transporter	Slc18a2	0.541	0.028
rRNA/tRNA 2'-O-methyltransferase fibrillarin-like protein 1	Fbll1	0.544	0.042
Ectonucleoside triphosphate diphosphohydrolase 6	Entpd6	0.547	0.045
LIM and SH3 domain protein 1	Lasp1;Nebl	0.563	0.046
(Lyso)-N-acylphosphatidylethanolamine lipase	Abhd4	0.567	0.017
Metal transporter CNNM1	Cnnm1	0.573	0.000
Kinesin-like protein KIFC2	Kifc2	0.576	0.010
Serine/arginine repetitive matrix protein 1	Srrm1	0.586	0.017
Macrophage-capping protein	Capg	0.589	0.022
1-phosphatidylinositol 3-phosphate 5-kinase	Pikfyve	0.595	0.021
Complement C1q subcomponent subunit A	C1qa	0.599	0.001
Proteolipid protein 2	Plp2	0.616	0.016
Lysophosphatidylcholine acyltransferase 2	Lpcat2	0.618	0.006
rRNA 2'-O-methyltransferase fibrillarin	Fbl;Fbll1	0.622	0.017
Cerebellin-1	Cbln1	0.623	0.023
Thymocyte nuclear protein 1	Thyn1	0.624	0.007
Serine protease inhibitor A3M	Serpina3m	0.626	0.023
SH3 and PX domain-containing protein 2A	Sh3pxd2a	0.632	0.011

WD repeat-containing protein 5	Wdr5	0.639	0.011
Perilipin-4	Plin4	0.659	0.013
Serine/threonine-protein phosphatase 4 catalytic subunit	Ppp4c	0.692	0.012
Tectonin beta-propeller repeat-containing protein 1	Tecpr1	0.692	0.012
Ectopic P granules protein 5 homolog	Epg5	0.706	0.000
DCN1-like protein 3	Dcun1d3	0.709	0.008
Microsomal glutathione S-transferase 1	Mgst1	0.738	0.001
Trafficking protein particle complex subunit 2	Trappc2	0.744	0.003
Electrogenic sodium bicarbonate cotransporter 4	Slc4a4;Slc4a5	0.744	0.022
Serine/threonine-protein kinase N1	Pkn1	0.747	0.006
Motile sperm domain-containing protein 2	Mospd2	0.831	0.023
GRIP and coiled-coil domain-containing protein 2	Gcc2	0.868	0.047
Phosphatidylinositol 4,5-bisphosphate 3-kinase catalytic subunit delta isoform	Pik3cb;Pik3cd	0.885	0.048
Activator of 90 kDa heat shock protein ATPase homolog 2	Ahsa2	0.891	0.037
Beta-2-microglobulin	B2m	0.926	0.001
Myelin-associated oligodendrocyte basic protein	Mobp	0.957	0.034
Keratin, type II cytoskeletal 1	Krt1	0.957	0.023
Potassium-transporting ATPase alpha chain 1	Atp1a4;Atp4a	1.052	0.007
TBC1 domain family member 1	Tbc1d1	1.146	0.027
Apolipoprotein D	Apod	1.162	0.001
Ubiquitin-like protein 7	Ubl7	1.273	0.012
Negative elongation factor B	Nelfb	1.300	0.001
Talin rod domain-containing protein 1	Tlnrd1	1.614	0.049
Cadherin-24	Cdh24	1.825	0.049
ADP-ribosylation factor GTPase-activating protein 2	Arfgap2;Arfgap3	1.933	0.013
Elongator complex protein 6	Elp6	1.947	0.031

Kinase non-catalytic C-lobe domain-containing protein 1	Kndc1;Pkd1l3	1.998	0.035
Protein CLEC16A	Clec16a	1.998	0.021
Cytochrome P450 7B1	Cyp7b1	2.078	0.044
Intraflagellar transport protein 25 homolog	Ift25	2.102	0.045
Hematopoietic lineage cell-specific protein	Hcls1	2.141	0.000
PI-PLC X domain-containing protein 2	Plcxd2	2.179	0.031
Vasodilator-stimulated phosphoprotein	Vasp	2.209	0.036
Kelch-like protein 3	Klhl3	2.366	0.003
3-keto-steroid reductase/17-beta-hydroxysteroid dehydrogenase 7	Hsd17b7	2.383	0.037
LHFPL tetraspan subfamily member 2 protein	Lhfpl2	2.384	0.017
Galactose-1-phosphate uridylyltransferase	Galt	2.432	0.021
Tapasin	Tapbp	2.466	0.000
DENN domain-containing protein 4B	Dennd4b	2.467	0.029
Interferon-induced transmembrane protein 3	Ifitm3	2.544	0.044
Rho guanine nucleotide exchange factor 1	Arhgef1	2.566	0.019
Xanthine dehydrogenase/oxidase	Xdh	2.624	0.021
H-2 class I histocompatibility antigen, D-B alpha chain	H2-D1	2.640	0.031
Sorting nexin-19	Snx19	2.676	0.017
Serine protease inhibitor A3K	Serpina3k;Serpina3m;Serpina3n	2.707	0.035
Hemopexin	Hpx	2.765	0.047
Phytanoyl-CoA dioxygenase domain-containing protein 1	Phyhd1	2.782	0.026
Neutrophil gelatinase-associated lipocalin	Lcn2	2.788	0.013
Integrin beta-5	Itgb5	2.963	0.020
	ALBU_BOVIN;ALBU_HUMAN	3.158	0.040
Glutamate receptor ionotropic, delta-2	Grid1;Grid2	3.180	0.006
Galectin-3-binding protein	Lgals3bp	3.346	0.007
Phosphatidylethanolamine-binding protein 1	Pbp2;Pebp1	3.363	0.014
Immunity-related GTPase family M protein 3	Igtp	3.386	0.002
Stefin-3	Stfa3	3.410	0.017

Ubiquitin-conjugating enzyme E2 B	Ube2b	3.542	0.013
Serine protease inhibitor A3N	Serpina3n	3.622	0.002
Guanylate-binding protein 2	Gbp2	3.645	0.004
Intercellular adhesion molecule 1	Icam1	3.914	0.000
Interferon-induced protein with tetratricopeptide repeats 3	Ifit3	3.920	0.000
Pleckstrin homology domain-containing family A member 8	Plekha8	4.187	0.016
Thrombospondin type-1 domain-containing protein 1	Thsd1	4.622	0.013
Dual serine/threonine and tyrosine protein kinase	Dstyk	4.810	0.011
H-2 class I histocompatibility antigen, K-B alpha chain	H2-K1	5.188	0.010
Haptoglobin	Hp	6.499	0.000
Macrophage colony-stimulating factor 1 receptor	Csf1r	4.040	0.000
PI-PLC X domain-containing protein 2	Plcxd2	4.283	0.000
Replication protein A 32 kDa subunit	Rpa2	4.346	0.038

7. Appendix 3: Negative control images for immunofluorescence and immunohistochemistry studies

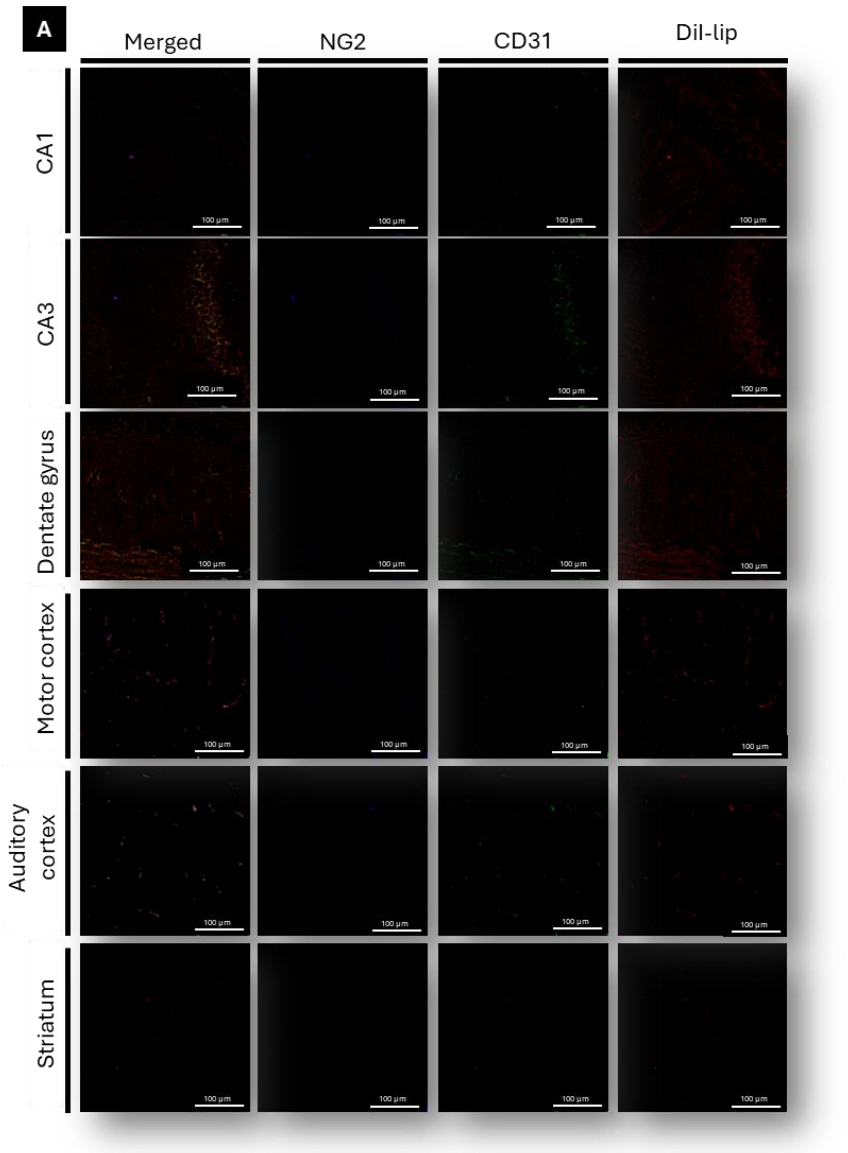

Supplementary figure 1: Immunofluorescence negative control images for NG2 in the aged cohort. Immunofluorescence staining for NG2 (blue), CD31 (green) and DiI-lip (red). All images obtained on the Leica thunder microscope at x40 magnification before LVCC. Note, negative control image is for the immunofluorescence staining (blue and green channels) and not DiI-lip so some signal may be observed in the red channel.

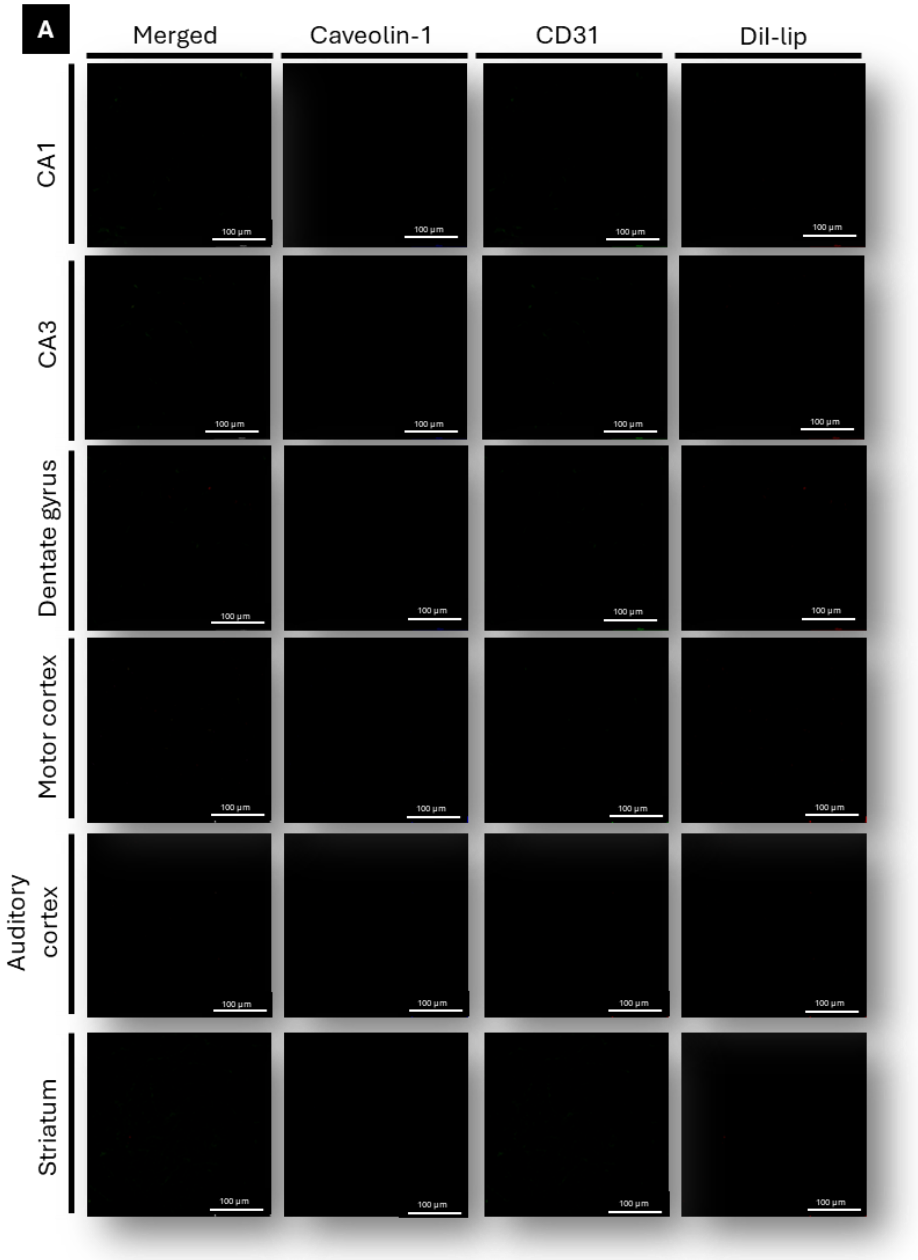

Supplementary figure 2: Immunofluorescence negative control images for Caveolin-1 in the aged and inflammation (LPS) cohorts. Immunofluorescence staining for Caveolin-1 (blue), CD31 (green) and DiI-lip (red). All images obtained on the Leica thunder microscope at x40 magnification before LVCC. Note, negative control image is for the immunofluorescence staining (blue and green channels) and not DiI-lip so some signal may be observed in the red channel.

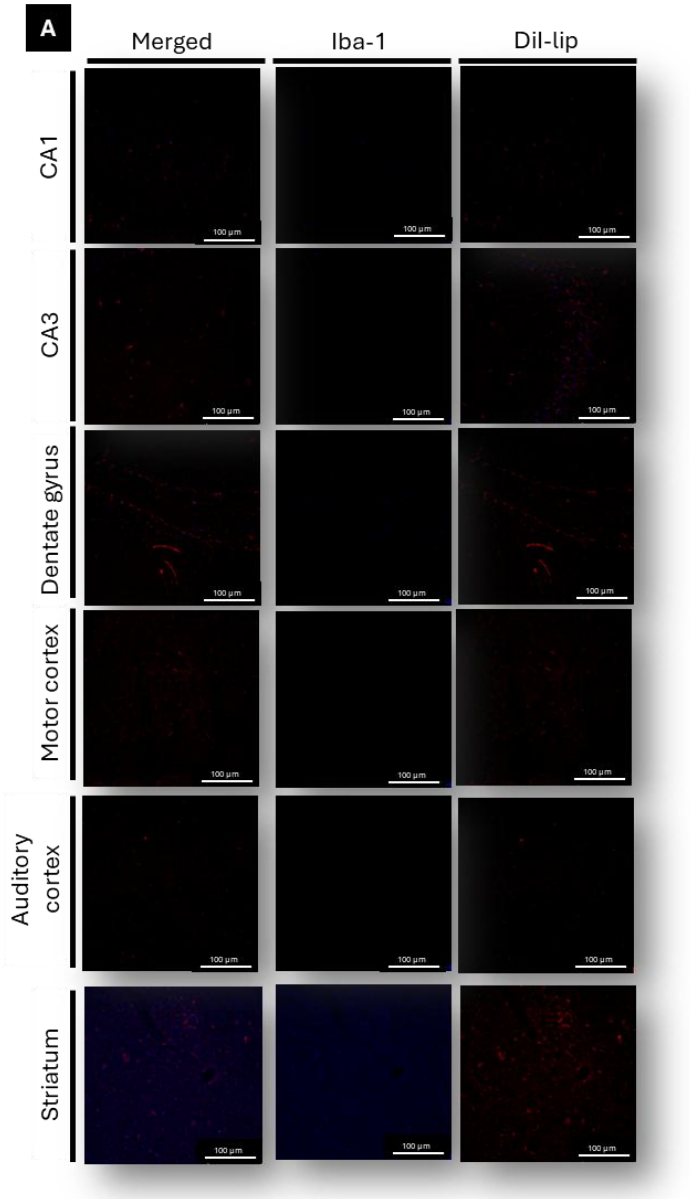

Supplementary figure 3: Immunofluorescence negative control images for Iba-1 in the aged cohort. Immunofluorescence staining for Iba-1 (blue) and DiI-lip (red). All images obtained on the Leica thunder microscope at x40 magnification before LVCC. Note, negative control image is for the immunofluorescence staining (blue channel) and not DiI-lip so some signal may be observed in the red channel.

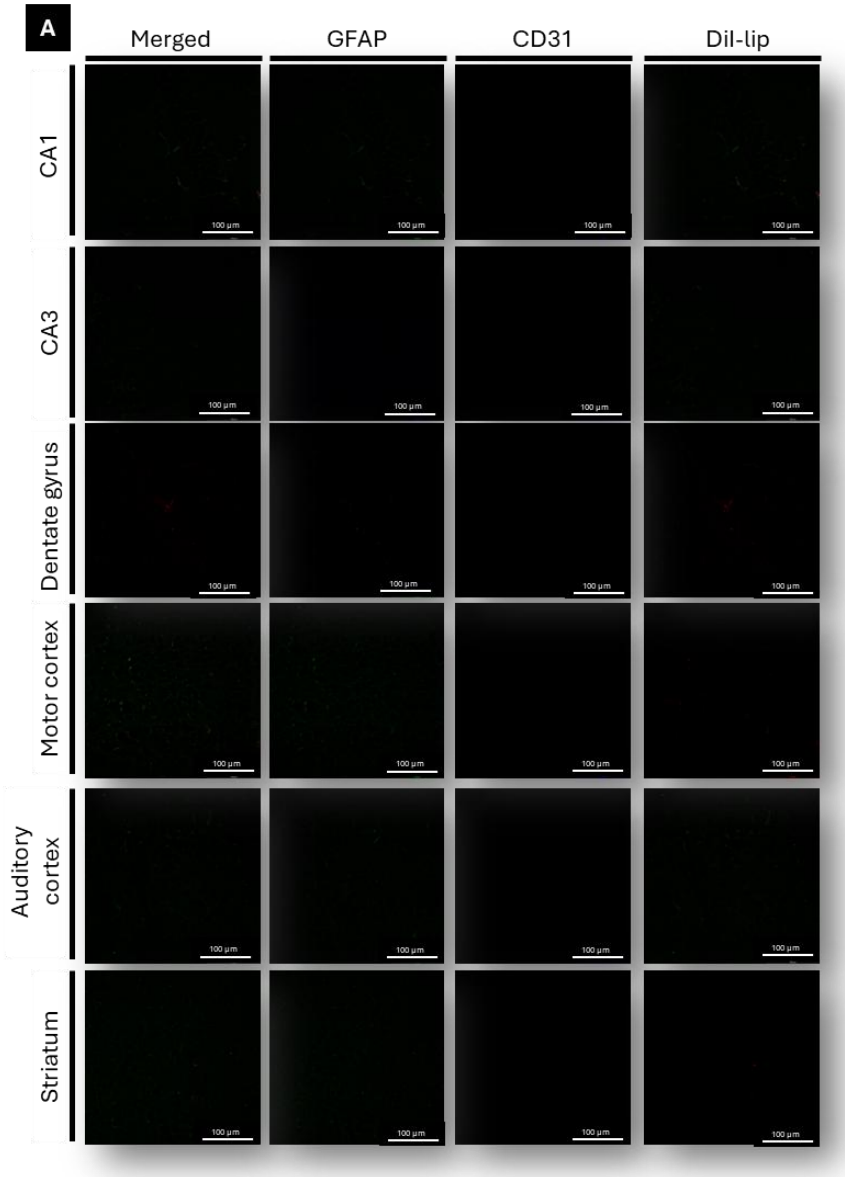

Supplementary figure 4: Immunofluorescence negative control images for GFAP in the aged and inflammation (LPS) cohorts. Immunofluorescence staining for CD31 (blue), GFAP (green) and DiI-lip (red). All images obtained on the Leica thunder microscope at x40 magnification before LVCC. Note, negative control image is for the immunofluorescence staining (blue and green channels) and not DiI-lip so some signal may be observed in the red channel.

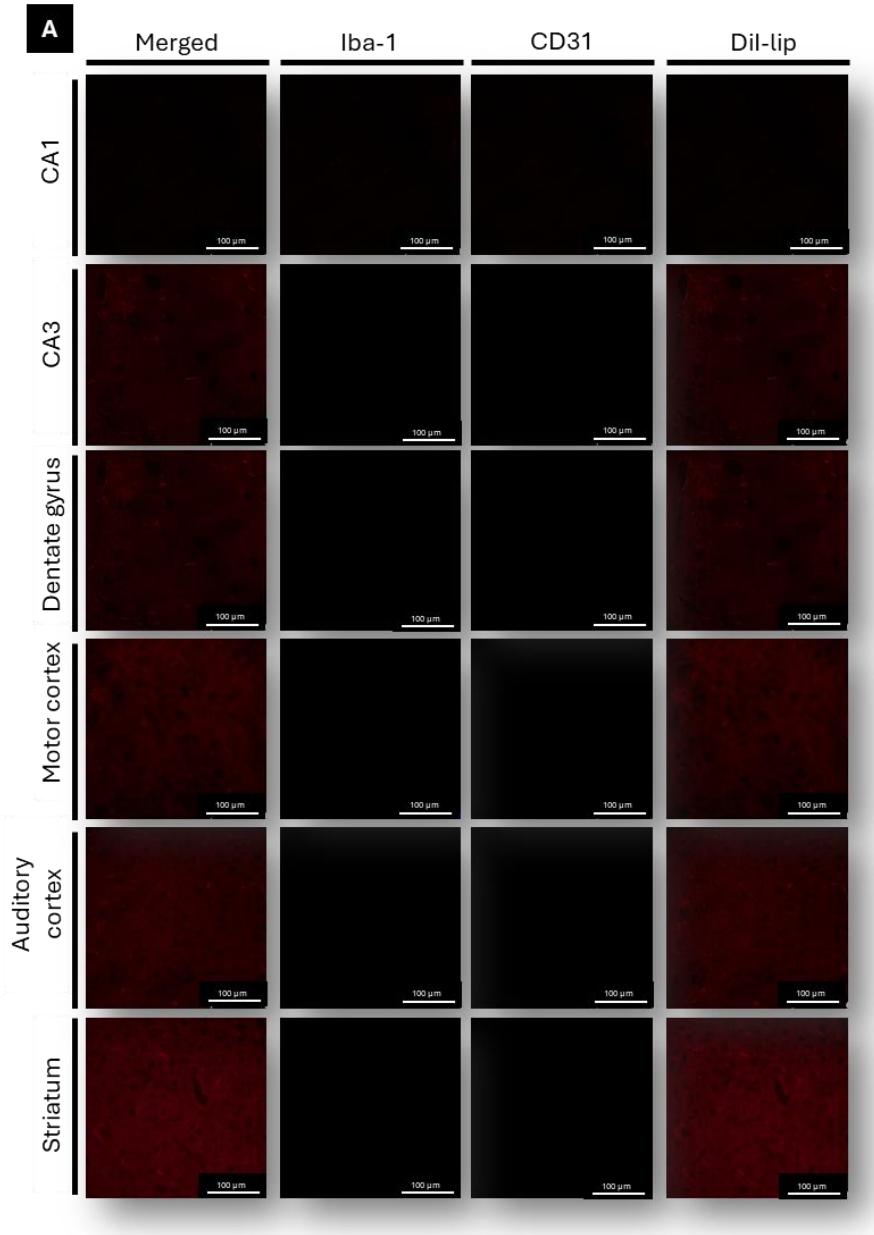

Supplementary figure 5: Immunofluorescence negative control images for Iba-1 in the inflammation (LPS) cohort. Immunofluorescence staining for Iba-1 (blue), CD31 (green) and DiI-lip (red). All images obtained on the Leica thunder microscope at x40 magnification before LVCC. Note, negative control image is for the immunofluorescence staining (blue and green channels) and not DiI-lip so some signal may be observed in the red channel.

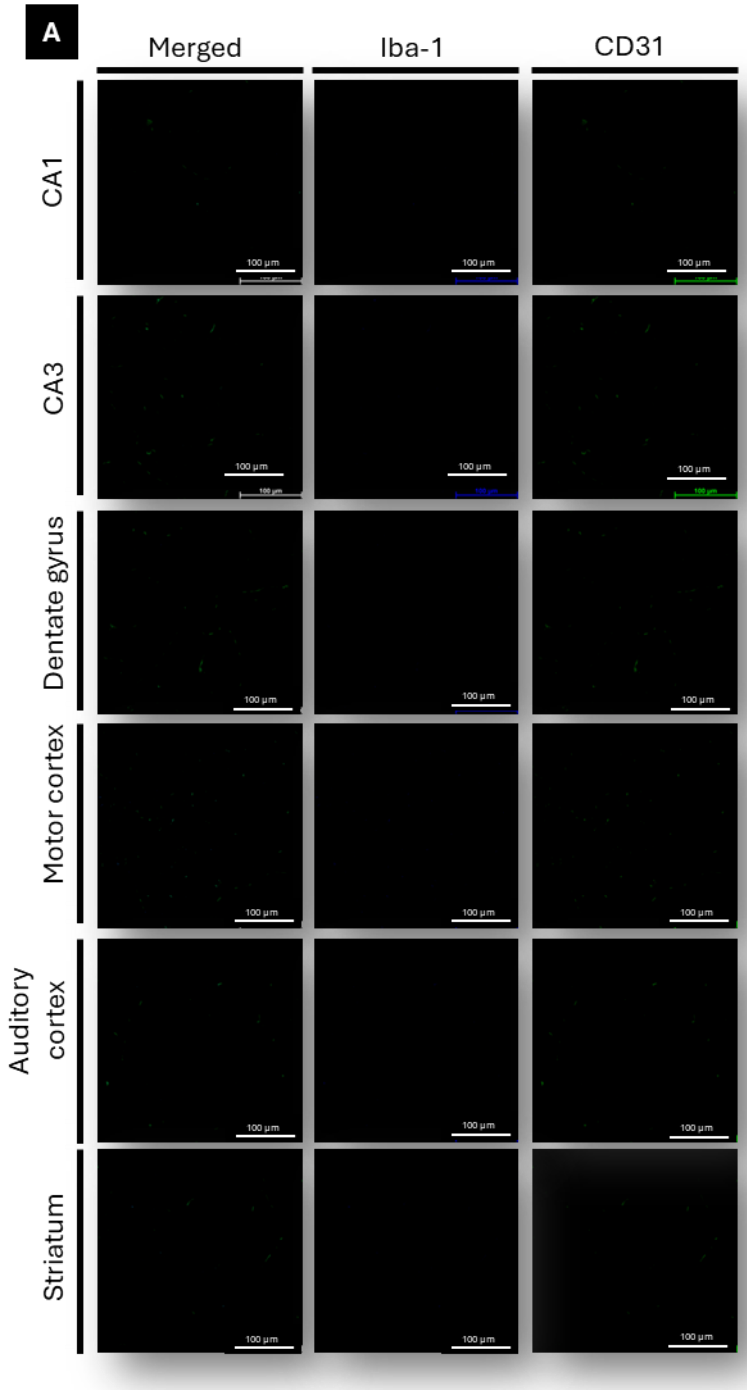

Supplementary figure 6: Immunofluorescence negative control images for Iba-1 in the IL1-ra-lip therapy cohort. Immunofluorescence staining for Iba-1 (blue), and CD31 (green) All images obtained on the Leica thunder microscope at x40 magnification before LVCC.

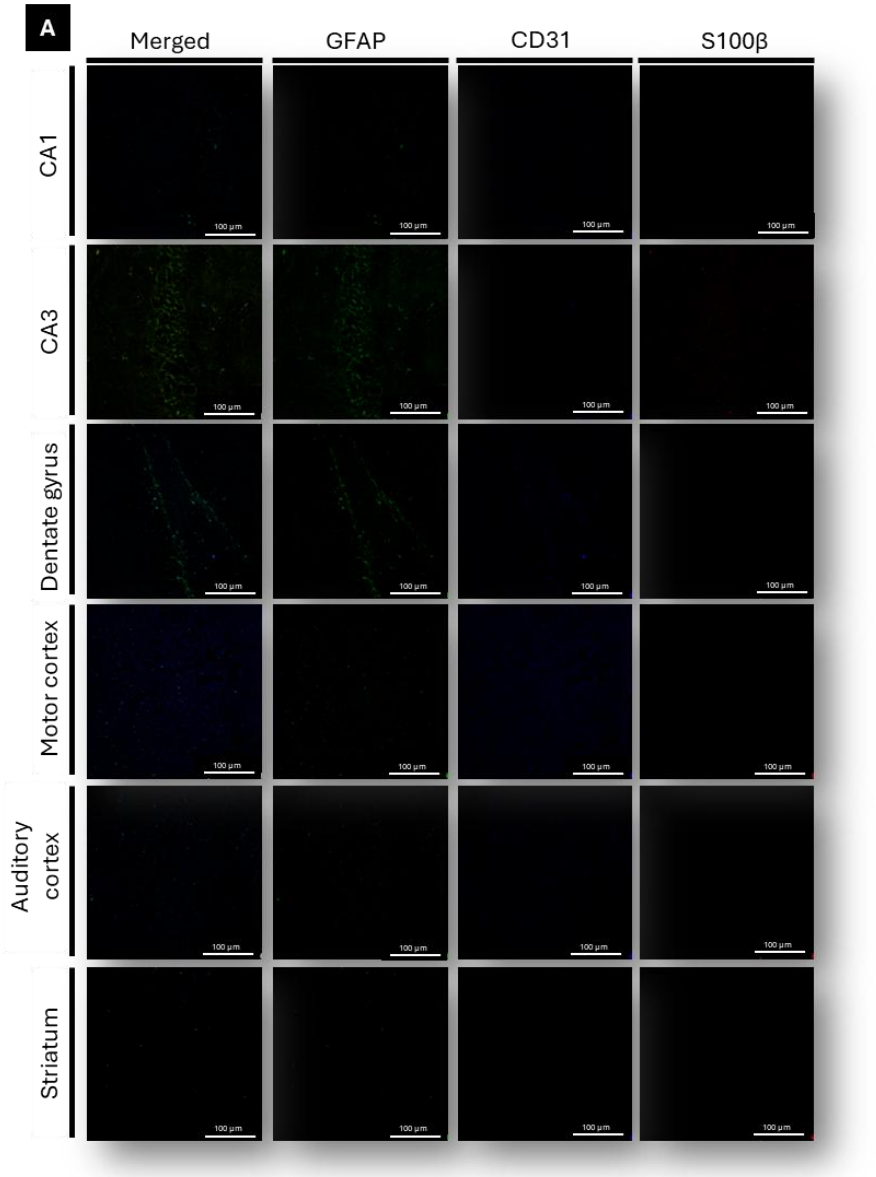

Supplementary figure 7: Immunofluorescence negative control images for GFAP and S100β in the IL1-ra-lip therapy cohort. Immunofluorescence staining for CD31 (blue), GFAP (green) and S100β (red). All images obtained on the Leica thunder microscope at x40 magnification before LVCC.

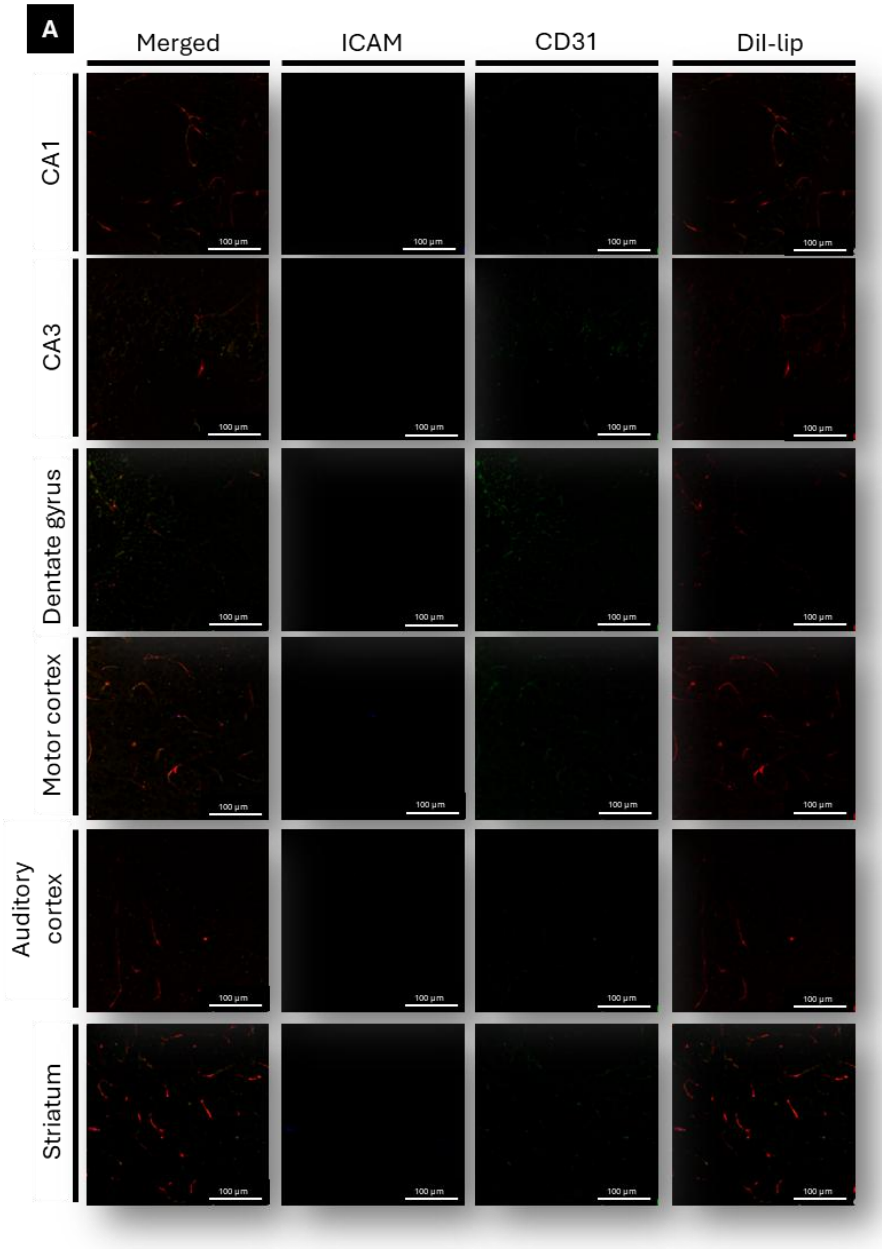

Supplementary figure 8: Immunofluorescence negative control images for ICAM-1 in the inflammation (LPS) cohorts. Immunofluorescence staining for ICAM-1 (blue), CD31 (green) and DiI-lip (red). All images obtained on the Leica thunder microscope at x40 magnification before LVCC. Note, negative control image is for the immunofluorescence staining (blue and green channels) and not DiI-lip so some signal may be observed in the red channel.

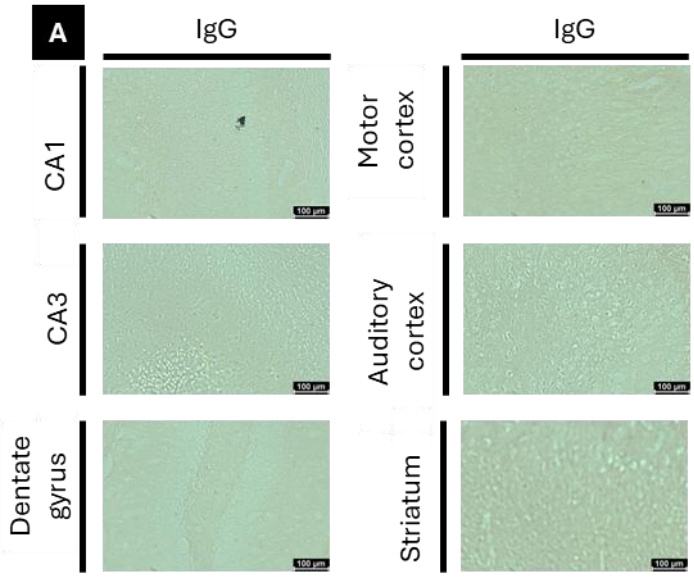

Supplementary figure 9: Immunohistochemical staining for IgG infiltration in the aged, inflammation (LPS) and Il1-ra-lip therapy cohorts. Immunohistochemical staining for IgG (brown) was imaged at x20 on Leica thunder microscope.

Appendix 4: Tissue loss log. Detailing loss of tissue for immunofluorescence and immunohistochemical studies in chapters 3, 4 and 5 and justification for this loss of data.

Figure	Figure panel	Number of samples lost	Justification
Chapter 3			
3-4	B	3 (3-month male group)	Only n=5 mice peripheral organs imaged on IVIS machine
3-7	F/G	1 (18-month group)	Tissue region loss in sample cryosectioning
3-18	B-G	1 (18-month group)	Lack of tissue available due to sample preparation issue
3-23	B-D	1 (18-month group)	Tissue region loss in sample cryosectioning
3-24	B-D	1 (18-month group)	Tissue region loss in sample cryosectioning
3-26	B-D, F-H, J-L	N/A	18-month male mice group repeated due to lack of IVIS data in first group- double n-number compared to 3-month group
3-28	B-G	1 (18-month group)	Tissue region loss in sample cryosectioning
3-36	B-D, F-H, J-L	1 (3-month group)	Slide removed from analysis due to physical damage- no spare tissue to repeat staining
3-37/3-38	B-G	X3 in -6, -12 and 22-month groups	Lack of antibody did not allow for extra 3 slides to be imaged for named groups
3-37/ 3-38	B-G	1 (3-month group)	Lack of tissue available due to sample preparation issue
3-40	B-G	1 (18 month-group)	Tissue region loss in sample cryosectioning
3-42	B-D, I-J	2 (22-month group)	Animals culled prior to behaviour experiments due to human end point reached relating to bodyweight loss.
Chapter 4			
4-27	B-G	1 (18-month 1 mg/kg LPS group)	Tissue region loss in sample cryosectioning
4-32	B-G	1 (18-month 1 mg/kg LPS group)	Tissue region loss in sample cryosectioning
4-33	B-G	1 (18-month 1 mg/kg LPS group)	Tissue region loss in sample cryosectioning
Chapter 5			

5-5	B-G	X1 in IL1-ra-lip group, x1 in IL1-ra group	Slides were damaged during immunostaining process so not able to be imaged and analysed. No further tissue was available to repeat for the entire study.

8 References

Abbott, N. J., Rönnbäck, L., & Hansson, E. (2006). Astrocyte-endothelial interactions at the blood-brain barrier. In Nature Reviews Neuroscience 7, (1) 41-53. Nature Reviews Neuroscience. https://doi.org/10.1038/nrn1824

Abcouwer, S. F., Shanmugam, S., Muthusamy, A., Lin, C. mao, Kong, D., Hager, H., Liu, X., & Antonetti, D. A. (2021). Inflammatory resolution and vascular barrier restoration after retinal ischemia reperfusion injury. *Journal of Neuroinflammation*, *18*(1), 186. https://doi.org/10.1186/S12974-021-02237-5

Abdelazim, H., Payne, L.B., Nolan, K., Paralkar, K., Bradley, V., Kanodia, R., Gude, R., Ward, R., Monavarfeshani, A., Fox, M.A., & Chappell, J.C. (2022) 'Pericyte heterogeneity identified by 3D ultrastructural analysis of the microvessel wall', Frontiers in Physiology, 13, 1016382. https://doi.org/10.3389/FPHYS.2022.1016382/BIBTEX

Abdelkarim, D., Zhao, Y., Turner, M. P., Sivakolundu, D. K., Lu, H., & Rypma, B. (2019). A neural-vascular complex of age-related changes in the human brain: Anatomy, physiology, and implications for neurocognitive aging. In Neuroscience and Biobehavioral Reviews, 107, 927–944. https://doi.org/10.1016/j.neubiorev.2019.09.005

Abrahao, A., Meng, Y., Llinas, M., Huang, Y., Hamani, C., Mainprize, T., Aubert, I., Heyn, C., Black, S. E., Hynynen, K., Lipsman, N., & Zinman, L. (2019). First-in-human trial of blood–brain barrier opening in amyotrophic lateral sclerosis using MR-guided focused ultrasound. Nature Communications, 10(1), 4373. https://doi.org/10.1038/S41467-019-12426-9

Adamson, P., Etienne, S., Couraud, P.-O., Calder, V., & Greenwood, J. (1999). Lymphocyte Migration Through Brain Endothelial Cell Monolayers Involves Signaling Through Endothelial ICAM-1 Via a Rho-Dependent Pathway. The Journal of Immunology, 162(5), 2964–2973. https://doi.org/10.4049/JIMMUNOL.162.5.2964

Ahishali, B., & Kaya, M. (2020). Evaluation of Blood-Brain Barrier Integrity Using Vascular Permeability Markers: Evans Blue, Sodium Fluorescein, Albumin-Alexa Fluor Conjugates, and Horseradish Peroxidase. In Methods in Molecular Biology 2367 (87-103)1–17. https://doi.org/10.1007/7651_2020_316

Ahn, S. I., Sei, Y. J., Park, H. J., Kim, J., Ryu, Y., Choi, J. J., Sung, H. J., MacDonald, T. J., Levey, A. I., & Kim, Y. T. (2020). Microengineered human blood–brain barrier platform for understanding nanoparticle transport mechanisms. Nature Communications, 11(1) 175. https://doi.org/10.1038/s41467-019-13896-7

Akash, M. S. H., Rehman, K., & Chen, S. (2013). IL-1Ra and its delivery strategies: inserting the association in perspective. Pharmaceutical Research, 30(11), 2951–2966. https://doi.org/10.1007/S11095-013-1118-0

Al-Ahmady, Z. S. (2018). Selective drug delivery approaches to lesioned brain through blood brain barrier disruption. In Expert Opinion on Drug Delivery 5 (4) 335–349. https://doi.org/10.1080/17425247.2018.1444601

Al-Ahmady, Z. S., Dickie, B. R., Aldred, I., Jasim, D. A., Barrington, J., Haley, M., Lemarchand, E., Coutts, G., Kaur, S., Bates, J., Curran, S., Goddard, R., Walker, M., Parry-Jones, A., Kostarelos, K., & Allan, S. M. (2022). Selective brain entry of lipid nanoparticles

in haemorrhagic stroke is linked to biphasic blood-brain barrier disruption. Theranostics, 12(10), 4477-4497. https://doi.org/10.7150/THNO.72167

Al-Ahmady, Z. S., Jasim, D., Ahmad, S. S., Wong, R., Haley, M., Coutts, G., Schiessl, I., Allan, S. M., & Kostarelos, K. (2019). Selective Liposomal Transport through Blood Brain Barrier Disruption in Ischemic Stroke Reveals Two Distinct Therapeutic Opportunities. American Chemical Society Nano, *13*(11), 12470–12486. https://doi.org/10.1021/ACSNANO.9B01808

Al-Ahmady, Z.S., Dickie, B.R., Aldred, I., Jasim, D.A., Barrington, J., Haley, M., Lemarchand, E., Coutts, G., Kaur, S., Bates, J., Curran, S., Goddard, R., Walker, M., Parry-Jones, A., Kostarelos, K., & Allan, S.M. (2022). Selective brain entry of lipid nanoparticles in haemorrhagic stroke is linked to biphasic blood-brain barrier disruption, Theranostics, 12(10), 4477-4497. https://doi.org/10.7150/THNO.72167

Al-Azzawi, S., Masheta, D., Guildford, A. L., Phillips, G., & Santin, M. (2018). Dendrimeric Poly(Epsilon-Lysine) Delivery Systems for the Enhanced Permeability of Flurbiprofen across the Blood-Brain Barrier in Alzheimer's Disease. International Journal of Molecular Sciences, 19(10), 3324. https://doi.org/10.3390/IJMS19103224

Allen, W. E., Blosser, T. R., Sullivan, Z. A., Dulac, C., & Zhuang, X. (2023). Molecular and spatial signatures of mouse brain aging at single-cell resolution. Cell, 186(1), 194-208.e18. https://doi.org/10.1016/j.cell.2022.12.010

Almanzar, N., Antony, J., Baghel, A. S., Bakerman, I., Bansal, I., Barres, B. A., Beachy, P. A., Berdnik, D., Bilen, B., Brownfield, D., Cain, C., Chan, C. K. F., Chen, M. B., Clarke, M. F., Conley, S. D., Darmanis, S., Demers, A., Demir, K., de Morree, A., … Zou, J. (2020). A single-cell transcriptomic atlas characterizes ageing tissues in the mouse. Nature, 583(7817), 590–595. https://doi.org/10.1038/s41586-020-2496-1

Alvarez, J. I., Dodelet-Devillers, A., Kebir, H., Ifergan, I., Fabre, P. J., Terouz, S., Sabbagh, M., Wosik, K., Bourbonnière, L., Bernard, M., Van Horssen, J., De Vries, H. E., Charron, F., & Prat, A. (2011). The hedgehog pathway promotes blood-brain barrier integrity and CNS immune quiescence. Science, 334(6063), 1727–1731. https://doi.org/10.1126/science.1206936

Álvarez-Rodríguez, L., López-Hoyos, M., Muñoz-Cacho, P., & Martínez-Taboada, V.M. (2012) 'Aging is associated with circulating cytokine dysregulation', Cellular Immunology, 273(2) 124–132. https://doi.org/10.1016/J.CELLIMM.2012.01.001

Amani, H., Habibey, R., Shokri, F., Hajmiresmail, S. J., Akhavan, O., Mashaghi, A., & Pazoki-Toroudi, H. (2019). Selenium nanoparticles for targeted stroke therapy through modulation of inflammatory and metabolic signaling. Scientific Reports 2019 9(1), 1–15. https://doi.org/10.1038/s41598-019-42633-9

Ammassari-Teule, M. and Passino, E. (1997) 'The dorsal hippocampus is selectively involved in the processing of spatial information even in mice with a genetic hippocampal dysfunction', Psychobiology, 25(2), 118–125. https://doi.org/10.3758/BF03331916/METRICS

Anderson, N. L., & Anderson, N. G. (2002). The Human Plasma Proteome: History, Character, and Diagnostic Prospects. Molecular & Cellular Proteomics, 1(11), 845–867. https://doi.org/10.1074/MCP.R200007-MCP200

Ando, Y., Okada, H., Takemura, G., Suzuki, K., Takada, C., Tomita, H., Zaikokuji, R., Hotta, Y., Miyazaki, N., Yano, H., Muraki, I., Kuroda, A., Fukuda, H., Kawasaki, Y., Okamoto, H., Kawaguchi, T., Watanabe, T., Doi, T., Yoshida, T., … Ogura, S. (2018). Brain-Specific Ultrastructure of Capillary Endothelial Glycocalyx and Its Possible Contribution for Blood Brain Barrier. Scientific Reports, 8(1), 17523. https://doi.org/10.1038/S41598-018-35976-2

Anlauf, E., & Derouiche, A. (2013). Glutamine synthetase as an astrocytic marker: its cell type and vesicle localization. Frontiers in Endocrinology, 4, 144. https://doi.org/10.3389/fendo.2013.00144

Arbez-Gindre, C., Steele, B. R., & Micha-Screttas, M. (2023). Dendrimers in Alzheimer's Disease: Recent Approaches in Multi-Targeting Strategies. Pharmaceutics, 15(3), 898. https://doi.org/10.3390/PHARMACEUTICS15030898

Arellano, J.I., Duque, A. and Rakic, P. (2024) A coming-of-age story: adult neurogenesis or adolescent neurogenesis in rodents? Frontiers in Neuroscience, 18, 1383728. https://doi.org/10.3389/FNINS.2024.1383728/BIBTEX

Argaw, A. T., Zhang, Y., Snyder, B. J., Zhao, M.-L., Kopp, N., Lee, S. C., Raine, C. S., Brosnan, C. F., & John, G. R. (2006). IL-1beta regulates blood-brain barrier permeability via reactivation of the hypoxia-angiogenesis program. Journal of Immunology , 177(8), 5574–5584. https://doi.org/10.4049/JIMMUNOL.177.8.5574

Aries, M., Cook, M., & Hensley-McBain, T. (2024). A Pilot Study to Investigate Peripheral Low-Level Chronic LPS Injection as a Model of Neutrophil Activation in the Periphery and Brain in Mice. International Journal of Molecular Sciences, 25(10) 5357. https://doi.org/10.3390/IJMS25105357/S1

Armulik, A., Genové, G., Mäe, M., Nisancioglu, M. H., Wallgard, E., Niaudet, C., He, L., Norlin, J., Lindblom, P., Strittmatter, K., Johansson, B. R., & Betsholtz, C. (2010). Pericytes regulate the blood-brain barrier. Nature, 468(7323), 557–561. https://doi.org/10.1038/nature09522

Aslam, M., Ahmad, N., Srivastava, R., & Hemmer, B. (2012). TNF-alpha induced NFκB signaling and p65 (RelA) overexpression repress Cldn5 promoter in mouse brain endothelial cells. Cytokine, 57(2), 269–275. https://doi.org/10.1016/J.CYTO.2011.10.016

Auriel, E., Regev, K., & Korczyn, A. D. (2014). Nonsteroidal anti-inflammatory drugs exposure and the central nervous system. Handbook of Clinical Neurology, 119, 577–584. https://doi.org/10.1016/B978-0-7020-4086-3.00038-2

Avital, A., Goshen, I., Kamsler, A., Segal, M., Iverfeldt, K., Richter-Levin, G., & Yirmiya, R. (2003). Impaired interleukin-1 signaling is associated with deficits in hippocampal memory processes and neural plasticity. Hippocampus, 13(7), 826–834. https://doi.org/10.1002/HIPO.10135

Bae, H. R., Shin, S. K., Yoo, J. H., Kim, S., Young, H. A., & Kwon, E. Y. (2023). Chronic inflammation in high-fat diet-fed mice: Unveiling the early pathogenic connection between liver and adipose tissue. Journal of Autoimmunity, 139, 103091. https://doi.org/10.1016/J.JAUT.2023.103091

Bagchi, S., Chhibber, T., Lahooti, B., Verma, A., Borse, V., & Jayant, R. D. (2019). In-vitro blood-brain barrier models for drug screening and permeation studies: An overview. Drug

Design, Development and Therapy. 13, 3591–3605. https://doi.org/10.2147/DDDT.S218708

Bake, S., & Sohrabji, F. (2004). 17beta-estradiol differentially regulates blood-brain barrier permeability in young and aging female rats. Endocrinology, 145(12), 5471–5475. https://doi.org/10.1210/EN.2004-0984

Bakhtiari, A., Vestergaard, M. B., Benedek, K., Fagerlund, B., Mortensen, E. L., Osler, M., Lauritzen, M., Larsson, H. B. W., & Lindberg, U. (2023). Changes in hippocampal volume during a preceding 10-year period do not correlate with cognitive performance and hippocampal blood–brain barrier permeability in cognitively normal late-middle-aged men. GeroScience, 45(2), 1161–1175. https://doi.org/10.1007/S11357-022-00712-2/FIGURES/4

Bamford, I.J. and Bamford, N.S. (2019) 'The Striatum's Role in Executing Rational and Irrational Economic Behaviors', The Neuroscientist : a review journal bringing neurobiology, neurology and psychiatry, 25(5), 475-490. https://doi.org/10.1177/1073858418824256

Banks, W. A. (2010). Mouse models of neurological disorders: A view from the blood-brain barrier. In Biochimica et Biophysica Acta - Molecular Basis of Disease 1802 (10) 881–888. https://doi.org/10.1016/j.bbadis.2009.10.011

Banks, W. A., & Robinson, S. M. (2010). Minimal Penetration of Lipopolysaccharide Across the Murine Blood-brain Barrier. Brain, Behavior, and Immunity, 24(1), 102-109. https://doi.org/10.1016/J.BBI.2009.09.001

Banks, W. A., Farr, S. A., & Morley, J. E. (2000). Permeability of the blood-brain barrier to albumin and insulin in the young and aged SAMP8 mouse. Journals of Gerontology - Series A Biological Sciences and Medical Sciences, 55(12), B601–B606. https://doi.org/10.1093/gerona/55.12.B601

Banks, W. A., Gray, A. M., Erickson, M. A., Salameh, T. S., Damodarasamy, M., Sheibani, N., Meabon, J. S., Wing, E. E., Morofuji, Y., Cook, D. G., & Reed, M. J. (2015). Lipopolysaccharide-induced blood-brain barrier disruption: Roles of cyclooxygenase, oxidative stress, neuroinflammation, and elements of the neurovascular unit. Journal of Neuroinflammation, 12(1)223. https://doi.org/10.1186/s12974-015-0434-1

Banks, W. A., Reed, M. J., Logsdon, A. F., Rhea, E. M., & Erickson, M. A. (2021). Healthy aging and the blood–brain barrier. Nature Aging, 1(3), 243–254. https://doi.org/10.1038/s43587-021-00043-5

Bao, M., Hofsink, N., & Plösch, T. (2022). LPS versus Poly I:C model: comparison of long-term effects of bacterial and viral maternal immune activation on the offspring. American Journal of Physiology - Regulatory, Integrative and Comparative Physiology, 322(2), R99-R111. https://doi.org/10.1152/AJPREGU.00087.2021

Barabási, B., Barna, L., Santa-Maria, A. R., Harazin, A., Molnár, R., Kincses, A., Vigh, J. P., Dukay, B., Sántha, M., Tóth, M. E., Walter, F. R., Deli, M. A., & Hoyk, Z. (2023). Role of interleukin-6 and interleukin-10 in morphological and functional changes of the blood–brain barrier in hypertriglyceridemia. Fluids and Barriers of the CNS, 20(1), 1–20. https://doi.org/10.1186/S12987-023-00418-3/FIGURES/7

Baror, R., Neumann, B., Segel, M., Chalut, K.J., Fancy, S.P.J., Schafer, D.P., & Franklin, R.J.M. (2019). Transforming growth factor-beta renders ageing microglia inhibitory to

oligodendrocyte generation by CNS progenitors, Glia, 67(7), 1374-1384. https://doi.org/10.1002/GLIA.23612

Barr, T. L., Latour, L. L., Lee, K. Y., Schaewe, T. J., Luby, M., Chang, G. S., El-Zammar, Z., Alam, S., Hallenbeck, J. M., Kidwell, C. S., & Warach, S. (2010). Blood-brain barrier disruption in humans is independently associated with increased matrix metalloproteinase-9. Stroke, 41(3) e123-128. https://doi.org/10.1161/STROKEAHA.109.570515/ASSET/89804FD0-567D-4EFC-BBD0-553511BC6509/ASSETS/GRAPHIC/6FF1.JPEG

Barton, S. M., Janve, V. A., McClure, R., Anderson, A., Matsubara, J. A., Gore, J. C., & Pham, W. (2019). Lipopolysaccharide Induced Opening of the Blood Brain Barrier on Aging 5XFAD Mouse Model. Journal of Alzheimer's Disease : JAD, 67(2), 503-513. https://doi.org/10.3233/JAD-180755

Batista, A. F., Rody, T., Forny-Germano, L., Cerdeiro, S., Bellio, M., Ferreira, S. T., Munoz, D. P., & De Felice, F. G. (2021). Interleukin-1β mediates alterations in mitochondrial fusion/fission proteins and memory impairment induced by amyloid-β oligomers. Journal of Neuroinflammation, 18(1) 54. https://doi.org/10.1186/S12974-021-02099-X

Bautista, L. E., Vera, L. M., Arenas, I. A., & Gamarra, G. (2005). Independent association between inflammatory markers (C-reactive protein, interleukin-6, and TNF-alpha) and essential hypertension. Journal of Human Hypertension, 19(2), 149–154. https://doi.org/10.1038/SJ.JHH.1001785

Bell, J. D., Rhind, S. G., Di Battista, A. P., Macdonald, R. L., & Baker, A. J. (2017). Biomarkers of Glycocalyx Injury are Associated with Delayed Cerebral Ischemia Following Aneurysmal Subarachnoid Hemorrhage: A Case Series Supporting a New Hypothesis. Neurocritical Care, 26(3), 339–347. https://doi.org/10.1007/S12028-016-0357-4

Bell, R. D., & Zlokovic, B. V. (2009). Neurovascular mechanisms and blood-brain barrier disorder in Alzheimer's disease. In Acta Neuropathologica, 118(1), 103-113. https://doi.org/10.1007/s00401-009-0522-3

Bell, R. D., Winkler, E. A., Sagare, A. P., Singh, I., LaRue, B., Deane, R., & Zlokovic, B. V. (2010a). Pericytes Control Key Neurovascular Functions and Neuronal Phenotype in the Adult Brain and during Brain Aging. Neuron, 68(3), 409–427. https://doi.org/10.1016/j.neuron.2010.09.043

Benice, T.S., Rizk, A., Kohama, S., Pfankuch, T., & Raber, J. (2006). Sex-differences in age-related cognitive decline in C57BL/6J mice associated with increased brain microtubule-associated protein 2 and synaptophysin immunoreactivity, Neuroscience, 137(2), 413–423. https://doi.org/10.1016/J.NEUROSCIENCE.2005.08.029.

Bennett, H. C., & Kim, Y. (2021). Pericytes Across the Lifetime in the Central Nervous System. In Frontiers in Cellular Neuroscience, 15, (71), 627291. https://doi.org/10.3389/fncel.2021.627291

Ben-Zvi, A., Lacoste, B., Kur, E, Andreone, B.J., Mayshar, Y., Yan, H,. & Gu, C. (2014) 'Mfsd2a is critical for the formation and function of the blood-brain barrier', Nature, 509(7501), 507–511. https://doi.org/10.1038/NATURE13324

Bettio, L.E.B., Rajendran, L. and Gil-Mohapel, J. (2017) 'The effects of aging in the hippocampus and cognitive decline', Neuroscience & Biobehavioral Reviews, 79 (1), 66–86. https://doi.org/10.1016/J.NEUBIOREV.2017.04.030

Beurel, E., & Jope, R. S. (2009). Lipopolysaccharide-induced interleukin-6 production is controlled by glycogen synthase kinase-3 and STAT3 in the brain. Journal of Neuroinflammation, 6(1), 1–11. https://doi.org/10.1186/1742-2094-6-9/FIGURES/6

Bhalerao, A., Sivandzade, F., Archie, S. R., Chowdhury, E. A., Noorani, B., & Cucullo, L. (2020). In vitro modeling of the neurovascular unit: Advances in the field. Fluids and Barriers of the CNS 17 (1) 22. https://doi.org/10.1186/s12987-020-00183-7

Bhat, N. R. (2015). Vasculoprotection as a convergent, multi-targeted mechanism of anti-AD therapeutics and interventions. In Journal of Alzheimer's Disease, 46, (3) 581–591. https://doi.org/10.3233/JAD-150098

Bhowmick, S., Malat, A., Caruso, D., Ponery, N., D'mello, V., Finn, C., & Abdul-Muneer, P. M. (2021). Intercellular Adhesion Molecule-1-Induced Posttraumatic Brain Injury Neuropathology in the Prefrontal Cortex and Hippocampus Leads to Sensorimotor Function Deficits and Psychological Stress. ENeuro, 8(4) ENEURO.0242. https://doi.org/10.1523/ENEURO.0242-21.2021

Biancardi, V. C., Son, S. J., Ahmadi, S., Filosa, J. A., & Stern, J. E. (2014). Circulating angiotensin II gains access to the hypothalamus and brain stem during hypertension via breakdown of the blood-brain barrier. Hypertension ,63(3), 572–579. https://doi.org/10.1161/HYPERTENSIONAHA.113.01743

Bien-Ly, N., Boswell, C. A., Jeet, S., Beach, T. G., Hoyte, K., Luk, W., Shihadeh, V., Ulufatu, S., Foreman, O., Lu, Y., DeVoss, J., van der Brug, M., & Watts, R. J. (2015). Lack of Widespread BBB Disruption in Alzheimer's Disease Models: Focus on Therapeutic Antibodies. Neuron, 88(2), 289–297. https://doi.org/10.1016/J.NEURON.2015.09.036

Biesmans, S., Bouwknecht, J. A., Ver Donck, L., Langlois, X., Acton, P. D., De Haes, P., Davoodi, N., Meert, T. F., Hellings, N., & Nuydens, R. (2015). Peripheral Administration of Tumor Necrosis Factor-Alpha Induces Neuroinflammation and Sickness but Not Depressive-Like Behavior in Mice. BioMed Research International, 2015 (1), 716920. https://doi.org/10.1155/2015/716920

Bitounis, D., Fanciullino, R., Iliadis, A., & Ciccolini, J. (2012). Optimizing Druggability through Liposomal Formulations: New Approaches to an Old Concept. ISRN Pharmaceutics, 738432, 1–11. https://doi.org/10.5402/2012/738432

Blair, J. A., Wang, C., Hernandez, D., Siedlak, S. L., Rodgers, M. S., Achar, R. K., Fahmy, L. M., Torres, S. L., Petersen, R. B., Zhu, X., Casadesus, G., & Lee, H. G. (2016). Individual case analysis of postmortem interval time on brain tissue preservation. PLoS ONE. 11(3), e0151615. https://doi.org/10.1371/journal.pone.0151615

Blamire, A. M., Anthony, D. C., Rajagopalan, B., Sibson, N. R., Perry, V. H., & Styles, P. (2000). Interleukin-1β-Induced Changes in Blood–Brain Barrier Permeability, Apparent Diffusion Coefficient, and Cerebral Blood Volume in the Rat Brain: A Magnetic Resonance Study. The Journal of Neuroscience, 20(21), 8153-8159. https://doi.org/10.1523/JNEUROSCI.20-21-08153.2000

Blenck, C. L., Harvey, P. A., Reckelhoff, J. F., & Leinwand, L. A. (2016). The importance of biological sex and estrogen in rodent models of cardiovascular health and disease. Circulation Research, 118(8), 1294-1312. https://doi.org/10.1161/CIRCRESAHA.116.307509

Bohannon, D. G., Okhravi, H. R., Kim, J., Kuroda, M. J., Didier, E. S., & Kim, W. K. (2020). A subtype of cerebrovascular pericytes is associated with blood-brain barrier disruption that develops during normal aging and simian immunodeficiency virus infection. Neurobiology of Aging, 96 (1), 128–136. https://doi.org/10.1016/j.neurobiolaging.2020.08.006

Boisvert, M. M., Erikson, G. A., Shokhirev, M. N., & Allen, N. J. (2018). The Aging Astrocyte Transcriptome from Multiple Regions of the Mouse Brain. Cell Reports, 22(1), 269–285. https://doi.org/10.1016/J.CELREP.2017.12.039

Bonte, S., Vandemaele, P., Verleden, S., Audenaert, K., Deblaere, K., Goethals, I., & Van Holen, R. (2017). Healthy brain ageing assessed with 18F-FDG PET and age-dependent recovery factors after partial volume effect correction. European Journal of Nuclear Medicine and Molecular Imaging, 44(5), 838–849. https://doi.org/10.1007/s00259-016-3569-0

Bony, B. A., Tarudji, A. W., Miller, H. A., Gowrikumar, S., Roy, S., Curtis, E. T., Gee, C. C., Vecchio, A., Dhawan, P., & Kievit, F. M. (2021). Claudin-1-Targeted Nanoparticles for Delivery to Aging-Induced Alterations in the Blood-Brain Barrier. American Chemical society Nano, 15(11), 18520–18531. https://doi.org/10.1021/ACSNANO.1C08432/ASSET/IMAGES/MEDIUM/NN1C08432_M005.GIF

Bors, L., Tóth, K., Tóth, E. Z., Bajza, Á., Csorba, A., Szigeti, K., Máthé, D., Perlaki, G., Orsi, G., Tóth, G. K., & Erdő, F. (2018). Age-dependent changes at the blood-brain barrier. A Comparative structural and functional study in young adult and middle aged rats. Brain Research Bulletin, 139, 269–277. https://doi.org/10.1016/j.brainresbull.2018.03.001

Bourgognon, J.-M., & Cavanagh, J. (2020). The role of cytokines in modulating learning and memory and brain plasticity. Brain and Neuroscience Advances, 4, 2398212820979802. Https://Doi.Org/10.1177/2398212820979802.

Bowyer, J. F., Sarkar, S., Burks, S. M., Hess, J. N., Tolani, S., O'Callaghan, J. P., & Hanig, J. P. (2020). Microglial activation and responses to vasculature that result from an acute LPS exposure. NeuroToxicology, 77 (1), 181–192. https://doi.org/10.1016/J.NEURO.2020.01.014

Breuer, H., Meier, M., Schneefeld, S., Härtig, W., Wittneben, A., Märkel, M., Ross, T. L., Bengel, F. M., Bankstahl, M., & Bankstahl, J. P. (2017). Multimodality imaging of blood–brain barrier impairment during epileptogenesis. Journal of Cerebral Blood Flow and Metabolism, 37(6), 2049–2061. https://doi.org/10.1177/0271678X16659672

Brezzo, G., Simpson, J., Ameen-Ali, K. E., Berwick, J., & Martin, C. (2020). Acute effects of systemic inflammation upon the neuro-glial-vascular unit and cerebrovascular function. Brain, Behavior, and Immunity – Health, 5:100074. https://doi.org/10.1016/j.bbih.2020.100074

Britton, R., Liu, A. T., Rege, S. V., Adams, J. M., Akrapongpisak, L., Le, D., Alcantara-Lee, R., Estrada, R. A., Ray, R., Ahadi, S., Gallager, I., Yang, C. F., Minami, S. S., Braithwaite, S. P., Czirr, E., & Campbell, M. K. (2022). Molecular and histological correlates of cognitive

decline across age in male C57BL/6J mice. Brain and Behavior, 12(9), e2736. https://doi.org/10.1002/BRB3.2736

Briuglia, M. L., Rotella, C., McFarlane, A., & Lamprou, D. A. (2015). Influence of cholesterol on liposome stability and on in vitro drug release. Drug Delivery and Translational Research, 5(3), 231–242. https://doi.org/10.1007/S13346-015-0220-8

Bronzuoli, M. R., Facchinetti, R., Valenza, M., Cassano, T., Steardo, L., & Scuderi, C. (2019). Astrocyte function is affected by aging and not Alzheimer's disease: A preliminary investigation in hippocampi of 3xTg-AD mice. Frontiers in Pharmacology, 10, 644. https://doi.org/10.3389/FPHAR.2019.00644/FULL

Brown, L. S., Foster, C. G., Courtney, J. M., King, N. E., Howells, D. W., & Sutherland, B. A. (2019). Pericytes and neurovascular function in the healthy and diseased brain. Frontiers in Cellular Neuroscience, 13, 282. https://doi.org/10.3389/fncel.2019.00282

Brown, W. R., & Thore, C. R. (2011). Review: Cerebral microvascular pathology in ageing and neurodegeneration. Neuropathology and Applied Neurobiology, 37(1), 56–74. https://doi.org/10.1111/j.1365-2990.2010.01139.x

Brozzi, F., Arcuri, C., Giambanco, I., & Donato, R. (2009). S100B Protein Regulates Astrocyte Shape and Migration via Interaction with Src Kinase: implications for astrocyte development, activation, and tumor growth. The Journal of Biological Chemistry, 284(13), 8797–8811. https://doi.org/10.1074/jbc.M805897200

Burton, M. D., Sparkman, N. L., & Johnson, R. W. (2011). Inhibition of interleukin-6 trans-signaling in the brain facilitates recovery from lipopolysaccharide-induced sickness behavior. Journal of Neuroinflammation, 8(1), 1–13. https://doi.org/10.1186/1742-2094-8-54/TABLES/1

Bussian, T. J., Aziz, A., Meyer, C. F., Swenson, B. L., van Deursen, J. M., & Baker, D. J. (2018). Clearance of senescent glial cells prevents tau-dependent pathology and cognitive decline. Nature, 562(7728), 578–582. https://doi.org/10.1038/s41586-018-0543-y

Buttler, L., Jordão, M. T., Fragas, M. G., Ruggeri, A., Ceroni, A., & Michelini, L. C. (2017). Maintenance of Blood-Brain Barrier Integrity in Hypertension: A Novel Benefit of Exercise Training for Autonomic Control. Frontiers in Physiology, 8(DEC), 1048. https://doi.org/10.3389/FPHYS.2017.01048

Cai, H. Q., Catts, V. S., Webster, M. J., Galletly, C., Liu, D., O'Donnell, M., Weickert, T. W., & Weickert, C. S. (2018). Increased macrophages and changed brain endothelial cell gene expression in the frontal cortex of people with schizophrenia displaying inflammation. Molecular Psychiatry, 25(4), 761–775. https://doi.org/10.1038/s41380-018-0235-x

Cai, H. Q., Weickert, T. W., Catts, V. S., Balzan, R., Galletly, C., Liu, D., O'Donnell, M., & Shannon Weickert, C. (2020). Altered levels of immune cell adhesion molecules are associated with memory impairment in schizophrenia and healthy controls. Brain, Behavior, and Immunity, 89, 200–208. https://doi.org/10.1016/J.BBI.2020.06.017

Calabrese, L. H., Nazario, M., & Parent, M. (2002). Anakinra Treatment of Patients with Rheumatoid Arthritis, 36(7–8), 1204–1209. https://doi.org/10.1345/APH.1A396

Calingasan, N. Y., & Gibson, G. E. (2000). Dietary restriction attenuates the neuronal loss, induction of heme oxygenase-1 and blood-brain barrier breakdown induced by impaired

oxidative metabolism. Brain Research, 885(1), 62–69. https://doi.org/10.1016/S0006-8993(00)02933-4

Camacho-Pereira, J., Tarragó, M. G., Chini, C. C. S., Nin, V., Escande, C., Warner, G. M., Puranik, A. S., Schoon, R. A., Reid, J. M., Galina, A., & Chini, E. N. (2016). CD38 dictates age-related NAD decline and mitochondrial dysfunction through a SIRT3-dependent mechanism. Cell Metabolism, 23(6), 1127-1139. https://doi.org/10.1016/J.CMET.2016.05.006

Campisi, M., Shin, Y., Osaki, T., Hajal, C., Chiono, V., & Kamm, R. D. (2018). 3D self-organized microvascular model of the human blood-brain barrier with endothelial cells, pericytes and astrocytes. Biomaterials, 180, 117–129. https://doi.org/10.1016/j.biomaterials.2018.07.014

Candiello, J., Cole, G. J., & Halfter, W. (2010). Age-dependent changes in the structure, composition and biophysical properties of a human basement membrane. Matrix Biology : Journal of the International Society for Matrix Biology, 29(5), 402–410. https://doi.org/10.1016/J.MATBIO.2010.03.004

Cao, Y., Xu, W. and Liu, Q. (2024). Alterations of the blood-brain barrier during aging. Journal of Cerebral Blood Flow and Metabolism [Preprint]. https://doi.org/10.1177/0271678X241240843/ASSET/IMAGES/LARGE/10.1177_0271678X241240843-FIG3.JPEG.

Cargill, R., Kohama, S. G., Struve, J., Su, W., Banine, F., Witkowski, E., Back, S. A., & Sherman, L. S. (2012). Astrocytes in aged nonhuman primate brain gray matter synthesize excess hyaluronan. Neurobiology of Aging, 33(4), 830.e13-830.e24. https://doi.org/10.1016/J.NEUROBIOLAGING.2011.07.006

Carpentier, A., Stupp, R., Sonabend, A. M., Dufour, H., Chinot, O., Mathon, B., Ducray, F., Guyotat, J., Baize, N., Menei, P., de Groot, J., Weinberg, J. S., Liu, B. P., Guemas, E., Desseaux, C., Schmitt, C., Bouchoux, G., Canney, M., & Idbaih, A. (2024). Repeated blood–brain barrier opening with a nine-emitter implantable ultrasound device in combination with carboplatin in recurrent glioblastoma: a phase I/II clinical trial. Nature Communications, 15(1), 1–12. https://doi.org/10.1038/s41467-024-45818-7

Castellani, R. J., Mojica, G., & Perry, G. (2016). The Role of the Iron Stain in Assessing Intracranial Hemorrhage. The Open Neurology Journal, 10(1), 136-142. https://doi.org/10.2174/1874205X01610010136

Cavelti-Weder, C., Babians-Brunner, A., Keller, C., Stahel, M. A., Kurz-Levin, M., Zayed, H., Solinger, A. M., Mandrup-Poulsen, T., Dinarello, C. A., & Donath, M. Y. (2012). Effects of Gevokizumab on Glycemia and Inflammatory Markers in Type 2 Diabetes. Diabetes Care, 35(8):1654-62. https://doi.org/10.2337/DC11-2219

Ceafalan, L. C., Fertig, T. E., Gheorghe, T. C., Hinescu, M. E., Popescu, B. O., Pahnke, J., & Gherghiceanu, M. (2019). Age-related ultrastructural changes of the basement membrane in the mouse blood-brain barrier. Journal of Cellular and Molecular Medicine, 23(2), 819-827. https://doi.org/10.1111/JCMM.13980

Cederholm, T., Persson, M., Andersson, P., Stenvinkel, P., Nordfors, L., Madden, J., Vedin, I., Wretlind, B., Grimble, R. F., & Palmblad, J. (2007). Polymorphisms in cytokine genes influence long-term survival differently in elderly male and female patients. Journal of Internal Medicine, 262(2), 215–223. https://doi.org/10.1111/J.1365-2796.2007.01803.X

Chakraborty, A., Tannenbaum, S., Rordorf, C., Lowe, P. J., Floch, D., Gram, H., & Roy, S. (2012). Pharmacokinetic and Pharmacodynamic Properties of Canakinumab, a Human Anti-Interleukin-1β Monoclonal Antibody. Clinical Pharmacokinetics, 51(6), e1-18. https://doi.org/10.2165/11599820-000000000-00000

Chen, A. Q., Fang, Z., Chen, X. L., Yang, S., Zhou, Y. F., Mao, L., Xia, Y. P., Jin, H. J., Li, Y. N., You, M. F., Wang, X. X., Lei, H., He, Q. W., & Hu, B. (2019). Microglia-derived TNF-α mediates endothelial necroptosis aggravating blood brain–barrier disruption after ischemic stroke. Cell Death & Disease, 10(7), 487. https://doi.org/10.1038/S41419-019-1716-9

Chen, J. P., Yang, P. C., Ma, Y. H., Tu, S. J., & Lu, Y. J. (2012). Targeted delivery of tissue plasminogen activator by binding to silica-coated magnetic nanoparticle. International Journal of Nanomedicine, 7, 5137-5149. https://doi.org/10.2147/IJN.S36197

Chen, J., Buchanan, J. B., Sparkman, N. L., Godbout, J. P., Freund, G. G., & Johnson, R. W. (2008). Neuroinflammation and disruption in working memory in aged mice after acute stimulation of the peripheral innate immune system. Brain, Behavior, and Immunity, 22(3), 301–311. https://doi.org/10.1016/J.BBI.2007.08.014

Chen, J., Dai, A. X., Tang, H. L., Lu, C. H., Liu, H. X., Hou, T., Lu, Z. J., Kong, N., Peng, X. Y., Lin, K. X., Zheng, Z. D., Xu, S. L., Ying, X. F., Ji, X. Y., Pan, H., Wu, J., Zeng, X., & Wei, N. L. (2023). Increase of ALCAM and VCAM-1 in the plasma predicts the Alzheimer's disease. Frontiers in Immunology, 13, 1097409. https://doi.org/10.3389/FIMMU.2022.1097409/FULL

Chen, J., Sivan, U., Tan, S. L., Lippo, L., de Angelis, J., Labella, R., Singh, A., Chatzis, A., Cheuk, S., Medhghalchi, M., Gil, J., Hollander, G., Marsden, B. D., Williams, R., Ramasamy, S. K., & Kusumbe, A. P. (2021). High-resolution 3D imaging uncovers organ-specific vascular control of tissue aging. Science Advances, 7(6) eabd7819. https://doi.org/10.1126/SCIADV.ABD7819

Chen, M. B., Yang, A. C., Yousef, H., Lee, D., Chen, W., Schaum, N., Lehallier, B., Quake, S. R., & Wyss-Coray, T. (2020). Brain Endothelial Cells Are Exquisite Sensors of Age-Related Circulatory Cues. Cell Reports, 30(13), 4418-4432.e4. https://doi.org/10.1016/j.celrep.2020.03.012

Chen, X., Liu, C., Muok, L., Zeng, C., & Li, Y. (2021). Dynamic 3D On-Chip BBB Model Design, Development, and Applications in Neurological Diseases. Cells, 10(11), 3183. https://doi.org/10.3390/CELLS10113183

Chen, Y., Ye, X., Escames, G., Lei, W., Zhang, X., Li, M., Jing, T., Yao, Y., Qiu, Z., Wang, Z., Acuña-Castroviejo, D., & Yang, Y. (2023). The NLRP3 inflammasome: contributions to inflammation-related diseases. Cellular & Molecular Biology Letters, 28(1), 51. https://doi.org/10.1186/S11658-023-00462-9

Chen, Z., Jalabi, W., Shpargel, K. B., Farabaugh, K. T., Dutta, R., Yin, X., Kiddds, G. J., Bergmann, C. C., Stohlman, S. A., & Trapp, B. D. (2012). Lipopolysaccharide-Induced Microglial Activation and Neuroprotection against Experimental Brain Injury Is Independent of Hematogenous TLR4. Journal of Neuroscience, 32(34), 11706–11715. https://doi.org/10.1523/JNEUROSCI.0730-12.2012

Cheng, X., Yang, Y. L., Yang, H., Wang, Y. H., & Du, G. H. (2018). Kaempferol alleviates LPS-induced neuroinflammation and BBB dysfunction in mice via inhibiting HMGB1 release

and down-regulating TLR4/MyD88 pathway. International Immunopharmacology, 56, 29–35. https://doi.org/10.1016/J.INTIMP.2018.01.002

Cheng, Y., Desse, S., Martinez, A., Worthen, R. J., Jope, R. S., & Beurel, E. (2018). TNFα disrupts blood brain barrier integrity to maintain prolonged depressive-like behavior in mice. Brain, Behavior, and Immunity, 69, 556–567. https://doi.org/10.1016/J.BBI.2018.02.003

Chew, K. S., Wells, R. C., Moshkforoush, A., Chan, D., Lechtenberg, K. J., Tran, H. L., Chow, J., Kim, D. J., Robles-Colmenares, Y., Srivastava, D. B., Tong, R. K., Tong, M., Xa, K., Yang, A., Zhou, Y., Akkapeddi, P., Annamalai, L., Bajc, K., Blanchette, M., … Kariolis, M. S. (2023). CD98hc is a target for brain delivery of biotherapeutics. *Nature Communications*, *14*(1), 1–17. https://doi.org/10.1038/s41467-023-40681-4

Chikhale, E. G., Ng, K. Y., Burton, P. S., & Borchardt, R. T. (1994). Hydrogen bonding potential as a determinant of the in vitro and in situ blood-brain barrier permeability of peptides. Pharmaceutical Research, 11(3), 412–419. https://doi.org/10.1023/A:1018969222130

Chirathaworn, C., Chansaenroj, J., Chaisuriyong, W., Lertmaharit, S., & Poovorawan, Y. (2022). IL-1Ra and sVCAM-1 in chikungunya virus infection. Acta Tropica, 233, 106548. https://doi.org/10.1016/J.ACTATROPICA.2022.106548

Chiu, C., Miller, M. C., Monahan, R., Osgood, D. P., Stopa, E. G., & Silverberg, G. D. (2015). P-glycoprotein expression and amyloid accumulation in human aging and Alzheimer's disease: Preliminary observations. Neurobiology of Aging, 36(9), 2475–2482. https://doi.org/10.1016/j.neurobiolaging.2015.05.020

Cho, E. E., Drazic, J., Ganguly, M., Stefanovic, B., & Hynynen, K. (2011). Two-photon fluorescence microscopy study of cerebrovascular dynamics in ultrasound-induced blood-brain barrier opening. Journal of Cerebral Blood Flow and Metabolism, 31(9), 1852–1862. https://doi.org/10.1038/jcbfm.2011.59

Cho, S. H., Chen, J. A., Sayed, F., Ward, M. E., Gao, F., Nguyen, T. A., Krabbe, G., Sohn, P. D., Lo, I., Minami, S., Devidze, N., Zhou, Y., Coppola, G., & Gan, L. (2015). SIRT1 Deficiency in Microglia Contributes to Cognitive Decline in Aging and Neurodegeneration via Epigenetic Regulation of IL-1β. Journal of Neuroscience, 35(2), 807–818. https://doi.org/10.1523/JNEUROSCI.2939-14.2015

Cho, S. Y., & Roh, H. T. (2022). Effects of Exercise Training on Neurotrophic Factors and Blood–Brain Barrier Permeability in Young-Old and Old-Old Women. International Journal of Environmental Research and Public Health, 19(24), 16896. https://doi.org/10.3390/IJERPH192416896

Choi, K. H., Kim, A. J., Son, I. J., Kim, K. H., Kim, K. B., Ahn, H., & Lee, E. B. (2010). Risk Factors of Drug Interaction between Warfarin and Nonsteroidal Anti-Inflammatory Drugs in Practical Setting. Journal of Korean Medical Science, 25(3), 337-341. https://doi.org/10.3346/JKMS.2010.25.3.337

Choi, S., Hill, D., Guo, L., Nicholas, R., Papadopoulos, D., & Cordeiro, M. F. (2022). Automated characterisation of microglia in ageing mice using image processing and supervised machine learning algorithms. Scientific Reports 2022 12:1, 12(1), 1–12. https://doi.org/10.1038/s41598-022-05815-6

Chu, J. J., Ji, W. B., Zhuang, J. H., Gong, B. F., Chen, X. H., Cheng, W. Bin, Liang, W. D., Li, G. R., Gao, J., & Yin, Y. (2022). Nanoparticles-based anti-aging treatment of Alzheimer's disease. Drug Delivery, 29(1), 2100-2116. https://doi.org/10.1080/10717544.2022.2094501

Chung, H. Y., Wickel, J., Hahn, N., Mein, N., Schwarzbrunn, M., Koch, P., Ceanga, M., Haselmann, H., Baade-Büttner, C., von Stackelberg, N., Hempel, N., Schmidl, L., Groth, M., Andreas, N., Götze, J., Coldewey, S. M., Bauer, M., Mawrin, C., Dargvainiene, J., … Geis, C. (2023). Microglia mediate neurocognitive deficits by eliminating C1q-tagged synapses in sepsis-associated encephalopathy. Science Advances, 9(21), eabq7806. https://doi.org/10.1126/SCIADV.ABQ7806/SUPPL_FILE/SCIADV.ABQ7806_DATA_FILES_S1_TO_S3.ZIP

Chupel, M. U., Minuzzi, L. G., Furtado, G., Santos, M. L., Hogervorst, E., Filaire, E., & Teixeira, A. M. (2018). Exercise and taurine in inflammation, cognition, and peripheral markers of blood-brain barrier integrity in older women. Applied Physiology, Nutrition, and Metabolism = Physiologie Appliquee, Nutrition et Metabolisme, 43(7), 733–741. https://doi.org/10.1139/APNM-2017-0775

Church, L. D., & McDermott, M. F. (2010). Canakinumab: a human anti-IL-1β monoclonal antibody for the treatment of cryopyrin-associated periodic syndromes. Expert Review of Clinical Immunology, 6(6), 831–841. https://doi.org/10.1586/ECI.10.66

Cibelli, M., Fidalgo, A. R., Terrando, N., Ma, D., Monaco, C., Feldmann, M., Takata, M., Lever, I. J., Nanchahal, J., Fanselow, M. S., & Maze, M. (2010). Role of Interleukin-1β in Postoperative Cognitive Dysfunction. Annals of Neurology, 68(3), 360-368. https://doi.org/10.1002/ANA.22082

Cicero, A. F. G., Ruscica, M., & Banach, M. (2019). Resveratrol and cognitive decline: a clinician perspective. Archives of Medical Science : AMS, 15(4), 936-943. https://doi.org/10.5114/AOMS.2019.85463

Ciesielska, A., Matyjek, M., & Kwiatkowska, K. (2021). TLR4 and CD14 trafficking and its influence on LPS-induced pro-inflammatory signaling. Cellular and Molecular Life Sciences: CMLS, 78(4), 1233-1261. https://doi.org/10.1007/S00018-020-03656-Y

Cipolla, M.J., Godfrey, J.A. and Wiegman, M.J. (2009) 'The effect of ovariectomy and estrogen on penetrating brain arterioles and blood-brain barrier permeability', Microcirculation (New York, N.Y. : 1994), 16(8), 685–693. https://doi.org/10.3109/10739680903164131

Clark, B. C., & Taylor, J. L. (2011). Age-Related Changes in Motor Cortical Properties and Voluntary Activation of Skeletal Muscle. Current Aging Science, 4(3), 192-199. https://doi.org/10.2174/1874609811104030192

Clarke, L. E., Liddelow, S. A., Chakraborty, C., Münch, A. E., Heiman, M., & Barres, B. A. (2018). Normal aging induces A1-like astrocyte reactivity. Proceedings of the National Academy of Sciences of the United States of America, 115(8), E1896–E1905. https://doi.org/10.1073/PNAS.1800165115/-/DCSUPPLEMENTAL

Cliteur, M. P., van der Kolk, A. G., Hannink, G., Hofmeijer, J., Jolink, W. M. T., Klijn, C. J. M., & Schreuder, F. H. B. M. (2024). Anakinra in cerebral haemorrhage to target secondary injury resulting from neuroinflammation (ACTION): Study protocol of a phase II randomised

clinical trial. European Stroke Journal, 9(1), 265–273. https://doi.org/10.1177/23969873231200686

Cluett, C., Brayne, C., Clarke, R., Evans, G., Matthews, F., Rubinsztein, D. C., Huppert, F., Llewellyn, D. J., Rice, N., Henley, W., Frayling, T. M., Murray, A., & Melzer, D. (2010). Polymorphisms in LMNA and near a SERPINA gene cluster are associated with cognitive function in older people. Neurobiology of Aging, 31(9), 1563–1568. https://doi.org/10.1016/J.NEUROBIOLAGING.2008.08.020

Cohen, J. and Torres, C. (2019) Astrocyte senescence: Evidence and significance, Aging Cell, 18(3), e12937. https://doi.org/10.1111/ACEL.12937

Cohen, S.J. and Stackman, R.W. (2015) Assessing rodent hippocampal involvement in the novel object recognition task. A review, Behavioural Brain Research, 285,105–117. https://doi.org/10.1016/J.BBR.2014.08.002

Conq, J., Joudiou, N., Ucakar, B., Vanvarenberg, K., Préat, V., & Gallez, B. (2023). Assessment of Hyperosmolar Blood–Brain Barrier Opening in Glioblastoma via Histology with Evans Blue and DCE-MRI. Biomedicines 2, 11(7), 1957. https://doi.org/10.3390/BIOMEDICINES11071957

Cortés-Ríos, J., Zárate, A. M., Figueroa, J. D., Medina, J., Fuentes-Lemus, E., Rodríguez-Fernández, M., Aliaga, M., & López-Alarcón, C. (2020). Protein quantification by bicinchoninic acid (BCA) assay follows complex kinetics and can be performed at short incubation times. Analytical Biochemistry, 608, 113904. https://doi.org/10.1016/J.AB.2020.113904

Costa, J., Martins, S., Ferreira, P. A., Cardoso, A. M. S., Guedes, J. R., Peça, J., & Cardoso, A. L. (2021). The old guard: Age-related changes in microglia and their consequences. Mechanisms of Ageing and Development, 197, 111512. https://doi.org/10.1016/J.MAD.2021.111512

Cotto, B., Natarajaseenivasan, K., & Langford, D. (2019). Astrocyte activation and altered metabolism in normal aging, age-related CNS diseases and HAND. Journal of Neurovirology, 25(5), 722-733. https://doi.org/10.1007/S13365-019-00721-6

Cox, J., Hein, M. Y., Luber, C. A., Paron, I., Nagaraj, N., & Mann, M. (2014). Accurate Proteome-wide Label-free Quantification by Delayed Normalization and Maximal Peptide Ratio Extraction, Termed MaxLFQ. Molecular & Cellular Proteomics : MCP, 13(9), 2513-2526. https://doi.org/10.1074/MCP.M113.031591

Craft, J. M., Watterson, D. M., Hirsch, E., & Van Eldik, L. J. (2005). Interleukin 1 receptor antagonist knockout mice show enhanced microglial activation and neuronal damage induced by intracerebroventricular infusion of human β-amyloid. Journal of Neuroinflammation, 2, 15. https://doi.org/10.1186/1742-2094-2-15

Crimmins, E. M. (2015). Lifespan and Healthspan: Past, Present, and Promise. The Gerontologist, 55(6), 901-911. https://doi.org/10.1093/GERONT/GNV130

Cruz, L. J., Stammes, M. A., Que, I., Van Beek, E. R., Knol-Blankevoort, V. T., Snoeks, T. J. A., Chan, A., Kaijzel, E. L., & Löwik, C. W. G. M. (2016). Effect of PLGA NP size on efficiency to target traumatic brain injury. Journal of Controlled Release, 223, 31–41. https://doi.org/10.1016/J.JCONREL.2015.12.029

Csépányi-Kömi, R., Sirokmány, G., Geiszt, M., & Ligeti, E. (2012). ARHGAP25, a novel Rac GTPase-activating protein, regulates phagocytosis in human neutrophilic granulocytes. Blood, 119(2), 573–582. https://doi.org/10.1182/BLOOD-2010-12-324053

Cummins, M. J., Cresswell, E. T., Smith, D. W., & Smith, D. (2024). Aging disrupts blood-brain and blood-spinal cord barrier homeostasis but does not increase paracellular permeability. BioRxiv (preprint), 2024.02.12.580035. https://doi.org/10.1101/2024.02.12.580035

Cyr, B., & de Rivero Vaccari, J. P. (2023). Sex Differences in the Inflammatory Profile in the Brain of Young and Aged Mice. Cells, 12(10), 1372. https://doi.org/10.3390/CELLS12101372/S1

Dagdeviren, S., Jung, D. Y., Friedline, R. H., Noh, H. L., Kim, J. H., Patel, P. R., Tsitsilianos, N., Inashima, K., Tran, D. A., Hu, X., Loubato, M. M., Craige, S. M., Kwon, J. Y., Lee, K. W., & Kim, J. K. (2017). IL-10 prevents aging-associated inflammation and insulin resistance in skeletal muscle. Federation of American Sciences for Experimental Biology Journal, 31(2), 701–710. https://doi.org/10.1096/FJ.201600832R/-/DC1

Dalla, C., Pavlidi, P., Sakelliadou, D.G., Grammatikopoulou, T. & , Kokras N. (2022) Sex Differences in Blood–Brain Barrier Transport of Psychotropic Drugs. Frontiers in Behavioral Neuroscience, 16, 844916. https://doi.org/10.3389/FNBEH.2022.844916

Damani, M. R., Zhao, L., Fontainhas, A. M., Amaral, J., Fariss, R. N., & Wong, W. T. (2011). Age-related Alterations in the Dynamic Behavior of Microglia. Aging Cell, 10(2), 263-276. https://doi.org/10.1111/J.1474-9726.2010.00660.X

Daneman, R., Zhou, L., Agalliu, D., Cahoy, J. D., Kaushal, A., & Barres, B. A. (2010). The mouse blood-brain barrier transcriptome: A new resource for understanding the development and function of brain endothelial cells. PLoS ONE, 5(10), e13741. https://doi.org/10.1371/journal.pone.0013741

Daniels, B. P., Cruz-Orengo, L., Pasieka, T. J., Couraud, P. O., Romero, I. A., Weksler, B., Cooper, J. A., Doering, T. L., & Klein, R. S. (2013). Immortalized human cerebral microvascular endothelial cells maintain the properties of primary cells in an in vitro model of immune migration across the blood brain barrier. Journal of Neuroscience Methods, 212(1), 173–179. https://doi.org/10.1016/j.jneumeth.2012.10.001

Davie, K., Janssens, J., Koldere, D., De Waegeneer, M., Pech, U., Kreft, Ł., Aibar, S., Makhzami, S., Christiaens, V., Bravo González-Blas, C., Poovathingal, S., Hulselmans, G., Spanier, K. I., Moerman, T., Vanspauwen, B., Geurs, S., Voet, T., Lammertyn, J., Thienpont, B., … Aerts, S. (2018). A Single-Cell Transcriptome Atlas of the Aging Drosophila Brain. Cell, 174(4), 982-998.e20. https://doi.org/10.1016/j.cell.2018.05.057

de Kloet, R., Wallach, G., & McEwen, B. S. (1975). Differences in Corticosterone and Dexamethasone Binding to Rat Brain and Pituitary. Endocrinology, 96(3), 598–609. https://doi.org/10.1210/ENDO-96-3-598

De Malefyt, R. W., Abrams, J., Bennett, B., Figdor, C. G., & De Vries, J. E. (1991). Interleukin 10(IL-10) inhibits cytokine synthesis by human monocytes: an autoregulatory role of IL-10 produced by monocytes. The Journal of Experimental Medicine, 174(5), 1209-1220. https://doi.org/10.1084/JEM.174.5.1209

Degl'Innocenti, E., & Dell'Anno, M. T. (2023). Human and mouse cortical astrocytes: a comparative view from development to morphological and functional characterization. *Frontiers in Neuroanatomy*, *17*, 1130729. https://doi.org/10.3389/FNANA.2023.1130729/BIBTEX

Dekkers, A. J., Miguel Amaya, J., van der Meulen, M., Biermasz, N. R., Meijer, O. C., & Pereira, A. M. (2022). Long-term effects of glucocorticoid excess on the brain. Journal of Neuroendocrinology, 34(8), e13142. https://doi.org/10.1111/JNE.13142

del Rey, A., Balschun, D., Wetzel, W., Randolf, A., & Besedovsky, H. O. (2013). A cytokine network involving brain-borne IL-1β, IL-1ra, IL-18, IL-6, and TNFα operates during long-term potentiation and learning. Brain, Behavior, and Immunity, 33, 15–23. https://doi.org/10.1016/J.BBI.2013.05.011

del Valle, J., Duran-Vilaregut, J., Manich, G., Camins, A., Pallàs, M., Vilaplana, J., & Pelegrí, C. (2009). Time-course of blood-brain barrier disruption in senescence-accelerated mouse prone 8 (SAMP8) mice. International Journal of Developmental Neuroscience, 27(1), 47–52. https://doi.org/10.1016/j.ijdevneu.2008.10.002

Deng, D., Li, X., Liu, C., Zhai, Z., Li, B., Kuang, M., Li, P., Shang, S., Song, Y., Cen, Y., Qin, R., Lu, Y., Zhao, Y., Cheng, H., Zheng, J., & Zhou, H. (2017). Systematic investigation on the turning point of over-inflammation to immunosuppression in CLP mice model and their characteristics. International Immunopharmacology, 42, 49–58. https://doi.org/10.1016/J.INTIMP.2016.11.011

Denninger, J. K., Smith, B. M., & Kirby, E. D. (2018). Novel Object Recognition and Object Location Behavioral Testing in Mice on a Budget. Journal of Visualized Experiments : JoVE, 2018(141), 10.3791/58593. https://doi.org/10.3791/58593

Denstaedt, S. J., Spencer-Segal, J. L., Newstead, M. W., Laborc, K., Zhao, A. P., Hjelmaas, A., Zeng, X., Akil, H., Standiford, T. J., & Singer, B. H. (2018). S100A8/A9 drives neuroinflammatory priming and protects against anxiety-like behavior after sepsis. Journal of Immunology (Baltimore, Md. : 1950), 200(9), 3188-3200. https://doi.org/10.4049/JIMMUNOL.1700834

Destefano, J. G., Jamieson, J. J., Linville, R. M., & Searson, P. C. (2018). Benchmarking in vitro tissue-engineered blood-brain barrier models. Fluids and Barriers of the CNS, 15(1), 32. https://doi.org/10.1186/s12987-018-0117-2

Dhingra, S., Sharma, A. K., Arora, R. C., Slezak, J., & Singal, P. K. (2009). IL-10 attenuates TNF-alpha-induced NF kappaB pathway activation and cardiomyocyte apoptosis. Cardiovascular Research, 82(1), 59–66. https://doi.org/10.1093/CVR/CVP040

Diaz-Castro, B., Bernstein, A. M., Coppola, G., Sofroniew, M. V., & Khakh, B. S. (2021). Molecular and functional properties of cortical astrocytes during peripherally induced neuroinflammation. Cell Reports, 36(6), 109508. https://doi.org/10.1016/J.CELREP.2021.109508

Dickie, B. R., Vandesquille, M., Ulloa, J., Boutin, H., Parkes, L. M., & Parker, G. J. M. (2019). Water-exchange MRI detects subtle blood-brain barrier breakdown in Alzheimer's disease rats. NeuroImage, 184, 349–358. https://doi.org/10.1016/J.NEUROIMAGE.2018.09.030

Dickie, B.R., Boutin, H., Parker, G.J.M., & Parkes, L.M. (2021) Alzheimer's disease pathology is associated with earlier alterations to blood–brain barrier water permeability compared

with healthy ageing in TgF344-AD rats, NMR in Biomedicine, 34(7), e4510. https://doi.org/10.1002/NBM.4510.

Dickie, B. R., Parker, G. J. M., & Parkes, L. M. (2020). Measuring water exchange across the blood-brain barrier using MRI. Progress in Nuclear Magnetic Resonance Spectroscopy, 116, 19–39. https://doi.org/10.1016/J.PNMRS.2019.09.002

Didusch, S., Madern, M., Hartl, M., & Baccarini, M. (2022). amica: an interactive and user-friendly web-platform for the analysis of proteomics data. BMC Genomics, 23(1), 1–9. https://doi.org/10.1186/S12864-022-09058-7/FIGURES/5

Dinarello, C. A. (2018). Overview of the IL-1 family in innate inflammation and acquired immunity. Immunological Reviews, 281(1), 8-27. https://doi.org/10.1111/IMR.12621

Dinarello, C. A., Simon, A., & Van Der Meer, J. W. M. (2012). Treating inflammation by blocking interleukin-1 in a broad spectrum of diseases. Nature Reviews. Drug Discovery, 11(8), 633-652. https://doi.org/10.1038/NRD3800

Ding, F., Yao, J., Rettberg, J. R., Chen, S., & Brinton, R. D. (2013). Early decline in glucose transport and metabolism precedes shift to ketogenic system in female aging and Alzheimer's mouse brain: Implication for bioenergetic intervention. PLoS ONE, 8(11), 79977. https://doi.org/10.1371/journal.pone.0079977

Ding, X. wei, Sun, X., Shen, X. fang, Lu, Y., Wang, J. qiang, Sun, Z. rong, Miao, C. hong, & Chen, J. wei. (2019). Propofol attenuates TNF-α-induced MMP-9 expression in human cerebral microvascular endothelial cells by inhibiting Ca2+/CAMK II/ERK/NF-κB signaling pathway. Acta Pharmacologica Sinica, 40(10), 1303-1313. https://doi.org/10.1038/S41401-019-0258-0

Diniz, D., Franze, S., & Homberg, J. (2020). Crossing the Blood-Brain-Barrier: A bifunctional liposome for BDNF gene delivery – A Pilot Study. BioRxiv, 2020.06.25.171264. https://doi.org/10.1101/2020.06.25.171264

Dion-Albert, L., Bandeira Binder, L., Daigle, B., Hong-Minh, A., Lebel, M., & Menard, C. (2022) Sex differences in the blood–brain barrier: Implications for mental health, Frontiers in Neuroendocrinology, 65, 100989. https://doi.org/10.1016/J.YFRNE.2022.100989.

Disdier, C., Awa, F., Chen, X., Dhillon, S. K., Galinsky, R., Davidson, J. O., Lear, C. A., Bennet, L., Gunn, A. J., & Stonestreet, B. S. (2020). Lipopolysaccharide-induced changes in the neurovascular unit in the preterm fetal sheep brain. Journal of Neuroinflammation, 17(1), 1–14. https://doi.org/10.1186/S12974-020-01852-Y/FIGURES/5

Dobner, S., Tóth, F. and de Rooij, L.P.M.H. (2024) A high-resolution view of the heterogeneous aging endothelium, Angiogenesis, 27(2):129-145. https://doi.org/10.1007/S10456-023-09904-6.

Dobri, S.G.J. and Ross, B. (2021) Total GABA level in human auditory cortex is associated with speech-in-noise understanding in older age, NeuroImage, 225, 117474. https://doi.org/10.1016/J.NEUROIMAGE.2020.117474.

Dockman, R. L., Carpenter, J. M., Diaz, A. N., Benbow, R. A., & Filipov, N. M. (2022). Sex differences in behavior, response to LPS, and glucose homeostasis in middle-aged mice. Behavioural Brain Research, 418, 113628. https://doi.org/10.1016/J.BBR.2021.113628

Dohgu, S., & Banks, W. A. (2008). Lipopolysaccharide-enhanced transcellular transport of HIV-1 across the blood-brain barrier is mediated by the p38 mitogen-activated protein kinase pathway. Experimental Neurology, 210(2), 740–749. https://doi.org/10.1016/J.EXPNEUROL.2007.12.028

Domínguez, A. R., Hidalgo, D. O., Garrido, R. V., & Sánchez, E. T. (2005). Liposomal cytarabine (DepoCyte) for the treatment of neoplastic meningitis. Clinical & Translational Oncology : Official Publication of the Federation of Spanish Oncology Societies and of the National Cancer Institute of Mexico, 7(6), 232–238. https://doi.org/10.1007/BF02710168

dos Santos Tramontin, N., da Silva, S., Arruda, R., Ugioni, K. S., Canteiro, P. B., de Bem Silveira, G., Mendes, C., Silveira, P. C. L., & Muller, A. P. (2020). Gold Nanoparticles Treatment Reverses Brain Damage in Alzheimer's Disease Model. Molecular Neurobiology, 57(2), 926–936. https://doi.org/10.1007/S12035-019-01780-W

Drake, J. D., Chambers, A. B., Ott, B. R., & Daiello, L. A. (2021). Peripheral Markers of Vascular Endothelial Dysfunction Show Independent but Additive Relationships with Brain-Based Biomarkers in Association with Functional Impairment in Alzheimer's Disease. Journal of Alzheimer's Disease : JAD, 80(4), 1553–1565. https://doi.org/10.3233/JAD-200759

Drake, J. D., Daiello, L. A., Chambers, A., Ott, B. R., Oliveria, J.-P., Vijayaragavan, K., Boss, M., Tebaykin, D., Montine, T. J., Angelo, M., & Bendall, S. C. (2018). P2-085: vcam-1 as a biomarker of cognitive decline in Alzheimer's disease. Alzheimer's & Dementia, 14(7S_Part_13), P700–P700. https://doi.org/10.1016/J.JALZ.2018.06.770

Drake, J.D., Chambers, A.B., Ott, B.R., & Daiello, L.A. (2021) 'Peripheral Markers of Vascular Endothelial Dysfunction Show Independent but Additive Relationships with Brain-Based Biomarkers in Association with Functional Impairment in Alzheimer's Disease', Journal of Alzheimer's Disease, 80(4), 553–1565. https://doi.org/10.3233/JAD-200759.

Duffy, C. M., Hofmeister, J. J., Nixon, J. P., & Butterick, T. A. (2019). High fat diet increases cognitive decline and neuroinflammation in a model of orexin loss. Neurobiology of Learning and Memory, 157, 41–47. https://doi.org/10.1016/j.nlm.2018.11.008

Duncombe, J., Lennen, R. J., Jansen, M. A., Marshall, I., Wardlaw, J. M., & Horsburgh, K. (2017). Ageing causes prominent neurovascular dysfunction associated with loss of astrocytic contacts and gliosis. Neuropathology and Applied Neurobiology, 43(6), 477–491. https://doi.org/10.1111/nan.12375

Elahy, M., Jackaman, C., Mamo, J. C. L., Lam, V., Dhaliwal, S. S., Giles, C., Nelson, D., & Takechi, R. (2015). Blood-brain barrier dysfunction developed during normal aging is associated with inflammation and loss of tight junctions but not with leukocyte recruitment. Immunity and Ageing, 12(1), 2. https://doi.org/10.1186/s12979-015-0029-9

Elcioğlu, H. K., Aslan, E., Ahmad, S., Alan, S., Salva, E., Elcioglu, H., & Kabasakal, L. (2016). Tocilizumab's effect on cognitive deficits induced by intracerebroventricular administration of streptozotocin in Alzheimer's model. Molecular and Cellular Biochemistry, 420(1–2), 21–28. https://doi.org/10.1007/S11010-016-2762-6

Elhaik Goldman, S., Goez, D., Last, D., Naor, S., Liraz Zaltsman, S., Sharvit-Ginon, I., Atrakchi-Baranes, D., Shemesh, C., Twitto-Greenberg, R., Tsach, S., Lotan, R., Leikin-Frenkel, A., Shish, A., Mardor, Y., Schnaider Beeri, M., & Cooper, I. (2018). High-fat diet

protects the blood–brain barrier in an Alzheimer's disease mouse model. *Aging Cell*, *17*(5), e12818. https://doi.org/10.1111/ACEL.12818

Elwood, E., Lim, Z., Naveed, H., & Galea, I. (2017). The effect of systemic inflammation on human brain barrier function. Brain, Behavior, and Immunity, 62, 35-40. https://doi.org/10.1016/J.BBI.2016.10.020

Emsley, H. C. A., Smith, C. J., Georgiou, R. F., Vail, A., Hopkins, S. J., Rothwell, N. J., & Tyrrell, P. J. (2005). A randomised phase II study of interleukin-1 receptor antagonist in acute stroke patients. Journal of Neurology, Neurosurgery, and Psychiatry, 76(10), 1366-1372. https://doi.org/10.1136/JNNP.2004.054882

Erdo, F., & Krajcsi, P. (2019). Age-related functional and expressional changes in efflux pathways at the blood-brain barrier. Frontiers in Aging Neuroscience, 10(JUL), 196 https://doi.org/10.3389/fnagi.2019.00196

Erdö, F., Denes, L. and De Lange, E. (2017) Age-associated physiological and pathological changes at the blood-brain barrier: A review. Journal of Cerebral Blood Flow and Metabolism, 37(1), 4–24. https://doi.org/10.1177/0271678X16679420

Erickson, M. A., & Banks, W. A. (2018). Neuroimmune axes of the blood-brain barriers and blood-brain interfaces: Bases for physiological regulation, disease states, and pharmacological interventions. Pharmacological Reviews, 70(2), 278–314. https://doi.org/10.1124/pr.117.014647

Erickson, M. A., & Banks, W. A. (2019). Age-associated changes in the immune system and blood–brain barrier functions. International Journal of Molecular Sciences, 20(7), 1632. https://doi.org/10.3390/ijms20071632

Erickson, M. A., Sandy Liang, W., Fernandez, E. G., Bullock, K. M., Thysell, J. A., & Banks, W. A. (2018). Genetics and sex influence peripheral and central innate immune responses and bloodbrain barrier integrity. PLoS ONE, 13(10), e0205769. https://doi.org/10.1371/journal.pone.0205769

Erickson, M. A., Wilson, M. L., & Banks, W. A. (2020). In vitro modeling of blood-brain barrier and interface functions in neuroimmune communication. In Fluids and Barriers of the CNS, 17(1), 26. https://doi.org/10.1186/s12987-020-00187-3

Fadul, M. M., Heath, P. R., Cooper-Knock, J., Kurz, J. M., Al-Azzawi, H. A., Ali, Z., Smith, T., Matthews, F. E., Brayne, C., Wharton, S. B., & Simpson, J. E. (2020). Transcriptomic analysis of age-associated periventricular lesions reveals dysregulation of the immune response. International Journal of Molecular Sciences, 21(21), 1–21. https://doi.org/10.3390/ijms21217924

Fahlström, A., Yu, Q. and Ulfhake, B. (2011) 'Behavioral changes in aging female C57BL/6 mice', Neurobiology of Aging, 32(10),1868–1880. https://doi.org/10.1016/J.NEUROBIOLAGING.2009.11.003

Falcone, C., Wolf-Ochoa, M., Amina, S., Hong, T., Vakilzadeh, G., Hopkins, W. D., Hof, P. R., Sherwood, C. C., Manger, P. R., Noctor, S. C., & Martínez-Cerdeño, V. (2019). Cortical interlaminar astrocytes across the therian mammal radiation. The Journal of Comparative Neurology, 527(10), 1654–1674. https://doi.org/10.1002/CNE.24605

Fan, X., Ma, W., Zhang, Y., & Zhang, L. (2020). P2X7 Receptor (P2X7R) of Microglia Mediates Neuroinflammation by Regulating (NOD)-Like Receptor Protein 3 (NLRP3) Inflammasome-

Dependent Inflammation After Spinal Cord Injury. Medical Science Monitor : International Medical Journal of Experimental and Clinical Research, 26, e925491-1. https://doi.org/10.12659/MSM.925491

Fensterl, V., & Sen, G. C. (2011). The ISG56/IFIT1 Gene Family. Journal of Interferon & Cytokine Research, 31(1), 71-78. https://doi.org/10.1089/JIR.2010.0101

Fernández, A., Quintana, E., Velasco, P., Moreno-Jimenez, B., de Andrés, B., Gaspar, M. L., Liste, I., Vilar, M., Mira, H., & Cano, E. (2021). Senescent accelerated prone 8 (SAMP8) mice as a model of age dependent neuroinflammation. Journal of Neuroinflammation, 18(1), 1–20. https://doi.org/10.1186/s12974-021-02104-3

Ferreira, J. (2023). Estrogen modulates cognitive function in mid-age female mice. Lab Animal, 52(11), 268–268. https://doi.org/10.1038/s41684-023-01285-z

Fetsko, A. R., Sebo, D. J., Budzynski, L. B., Scharbarth, A., & Taylor, M. R. (2024). IL-1β disrupts the initiation of blood-brain barrier development by inhibiting endothelial Wnt/β-catenin signaling. IScience, 27(5), 109651. https://doi.org/10.1016/J.ISCI.2024.109651

Fidelis, E. M., Savall, A. S. P., da Luz Abreu, E., Carvalho, F., Teixeira, F. E. G., Haas, S. E., Bazanella Sampaio, T., & Pinton, S. (2019). Curcumin-Loaded Nanocapsules Reverses the Depressant-Like Behavior and Oxidative Stress Induced by β-Amyloid in Mice. Neuroscience, 423, 122–130. https://doi.org/10.1016/J.NEUROSCIENCE.2019.09.032

Field, R., Campion, S., Warren, C., Murray, C., & Cunningham, C. (2010). Systemic challenge with the TLR3 agonist poly I:C induces amplified IFNα/β and IL-1β responses in the diseased brain and exacerbates chronic neurodegeneration. Brain, Behavior, and Immunity, 24(6), 996-1007. https://doi.org/10.1016/J.BBI.2010.04.004

Fielder, E., Tweedy, C., Wilson, C., Oakley, F., LeBeau, F. E. N., Passos, J. F., Mann, D. A., von Zglinicki, T., & Jurk, D. (2020). Anti-inflammatory treatment rescues memory deficits during aging in nfkb1−/− mice. Aging Cell, 19(10), e13188. https://doi.org/10.1111/ACEL.13188

Finch, C.E. (2014) The menopause and aging, a comparative perspective, The Journal of steroid biochemistry and molecular biology, 142, 132–141. https://doi.org/10.1016/J.JSBMB.2013.03.010.

Finger, C. E., Moreno-Gonzalez, I., Gutierrez, A., Moruno-Manchon, J. F., & McCullough, L. D. (2021). Age-related immune alterations and cerebrovascular inflammation. Molecular Psychiatry, 27(2), 803–818. https://doi.org/10.1038/s41380-021-01361-1

Flügge, G., Araya-Callis, C., Garea-Rodriguez, E., Stadelmann-Nessler, C., & Fuchs, E. (2014). NDRG2 as a marker protein for brain astrocytes. Cell and Tissue Research, 357(1), 31–41. https://doi.org/10.1007/s00441-014-1837-5

Ford, E., Greenslade, N., Paudyal, P., Bremner, S., Smith, H. E., Banerjee, S., Sadhwani, S., Rooney, P., Oliver, S., & Cassell, J. (2018). Predicting dementia from primary care records: A systematic review and meta-analysis. PLoS ONE, 13(3), e0194735. https://doi.org/10.1371/journal.pone.0194735

Franceschi, C., Capri, M., Monti, D., Giunta, S., Olivieri, F., Sevini, F., Panourgia, M. P., Invidia, L., Celani, L., Scurti, M., Cevenini, E., Castellani, G. C., & Salvioli, S. (2007). Inflammaging and anti-inflammaging: a systemic perspective on aging and longevity emerged from studies in humans. Mechanisms of Ageing and Development, 128(1), 92–105. https://doi.org/10.1016/J.MAD.2006.11.016

Francia, V., Reker-Smit, C., Boel, G., & Salvati, A. (2019) Limits and challenges in using transport inhibitors to characterize how nano-sized drug carriers enter cells, Nanomedicine, 14(12), 1533–1549. https://doi.org/10.2217/NNM-2018-0446/SUPPL_FILE/SUPPL/SUPPL_DATA.DOCX.

Frank, M. G., Fonken, L. K., Annis, J. L., Watkins, L. R., & Maier, S. F. (2018). Stress disinhibits microglia via down-regulation of CD200R: a mechanism of neuroinflammatory priming. Brain, Behavior, and Immunity, 69, 62-73. https://doi.org/10.1016/J.BBI.2017.11.001

Frank, M. G., Miguel, Z. D., Watkins, L. R., & Maier, S. F. (2010). Prior exposure to glucocorticoids sensitizes the neuroinflammatory and peripheral inflammatory responses to E. coli lipopolysaccharide. Brain, Behavior, and Immunity, 24(1), 19–30. https://doi.org/10.1016/J.BBI.2009.07.008

Frías-Anaya, E., Gromnicova, R., Kraev, I., Rogachevsky, V., Male, D. K., Crea, F., Hawkes, C. A., & Romero, I. A. (2021). Age-related ultrastructural neurovascular changes in the female mouse cortex and hippocampus. Neurobiology of Aging, 101, 273–284. https://doi.org/10.1016/j.neurobiolaging.2020.12.008

Frick, K.M. and Gresack, J.E. (2003) Sex Differences in the Behavioral Response to Spatial and Object Novelty in Adult C57BL/6 Mice, Behavioral Neuroscience, 117(6), 1283–1291. https://doi.org/10.1037/0735-7044.117.6.1283

Fu, H. Q., Yang, T., Xiao, W., Fan, L., Wu, Y., Terrando, N., & Wang, T. L. (2014). Prolonged Neuroinflammation after Lipopolysaccharide Exposure in Aged Rats. PLoS ONE, 9(8), e106331. https://doi.org/10.1371/JOURNAL.PONE.0106331

Fu, Y., Rusznák, Z., Herculano-Houzel, S., Watson C., & Paxinos, G. (2013) Cellular composition characterizing postnatal development and maturation of the mouse brain and spinal cord, Brain structure & function, 218(5), 1337–1354. https://doi.org/10.1007/S00429-012-0462-X.

Furtado, D., Björnmalm, M., Ayton, S., Bush, A. I., Kempe, K., & Caruso, F. (2018). Overcoming the Blood-Brain Barrier: The Role of Nanomaterials in Treating Neurological Diseases. Advanced Materials (Deerfield Beach, Fla.), 30(46) e1801362. https://doi.org/10.1002/ADMA.201801362

Furutama, D., Matsuda, S., Yamawaki, Y., Hatano, S., Okanobu, A., Memida, T., Oue, H., Fujita, T., Ouhara, K., Kajiya, M., Mizuno, N., Kanematsu, T., Tsuga, K., & Kurihara, H. (2020). IL-6 Induced by Periodontal Inflammation Causes Neuroinflammation and Disrupts the Blood–Brain Barrier. Brain Sciences 2020, 10(10), 679. https://doi.org/10.3390/BRAINSCI10100679

Galatro, T. F., Holtman, I. R., Lerario, A. M., Vainchtein, I. D., Brouwer, N., Sola, P. R., Veras, M. M., Pereira, T. F., Leite, R. E. P., Möller, T., Wes, P. D., Sogayar, M. C., Laman, J. D., Den Dunnen, W., Pasqualucci, C. A., Oba-Shinjo, S. M., Boddeke, E. W. G. M., Marie, S. K. N., & Eggen, B. J. L. (2017). Transcriptomic analysis of purified human cortical microglia reveals age-associated changes. Nature Neuroscience, 20(8), 1162–1171. https://doi.org/10.1038/nn.4597

Galea, I. (2021) 'The blood–brain barrier in systemic infection and inflammation', Cellular & Molecular Immunology,18(11), 2489–2501. https://doi.org/10.1038/s41423-021-00757-x.

Galea, J., Ogungbenro, K., Hulme, S., Greenhalgh, A., Aarons, L., Scarth, S., Hutchinson, P., Grainger, S., King, A., Hopkins, S. J., Rothwell, N., & Tyrrell, P. (2011). Intravenous anakinra can achieve experimentally effective concentrations in the central nervous system within a therapeutic time window: results of a dose-ranging study. Journal of Cerebral Blood Flow & Metabolism, 31(2), 439-447. https://doi.org/10.1038/JCBFM.2010.103

Gandhi, K., Barzegar-Fallah, A., Banstola, A., Rizwan, S. B., & Reynolds, J. N. J. (2022). Ultrasound-Mediated Blood–Brain Barrier Disruption for Drug Delivery: A Systematic Review of Protocols, Efficacy, and Safety Outcomes from Preclinical and Clinical Studies. Pharmaceutics, 14(4), 833. https://doi.org/10.3390/PHARMACEUTICS14040833

Gao, N., Sun, H., Dong, K., Ren, J., & Qu, X. (2015). Gold-nanoparticle-based multifunctional amyloid-β inhibitor against Alzheimer's disease. Chemistry (Weinheim an Der Bergstrasse, Germany), 21(2), 829–835. https://doi.org/10.1002/CHEM.201404562

Gao, X., Chen, H., Schwarzschild, M. A., & Ascherio, A. (2011). Use of ibuprofen and risk of Parkinson disease. Neurology, 76(10), 863-869. https://doi.org/10.1212/WNL.0B013E31820F2D79

Garces, A., Martinez, B., De La Garza, R., Roy, D., Vallee, K. A., Fields, J. A., Moore, D. J., Rodrigo, H., & Roy, U. (2023). Differential expression of interferon-induced protein with tetratricopeptide repeats 3 (IFIT3) in Alzheimer's disease and HIV-1 associated neurocognitive disorders. Scientific Reports, 13(1), 1–17. https://doi.org/10.1038/s41598-022-27276-7

Garner, K. M., Amin, R., Johnson, R. W., Scarlett, E. J., & Burton, M. D. (2018). Microglia priming by interleukin-6 signaling is enhanced in aged mice. Journal of Neuroimmunology, 324, 90-99. https://doi.org/10.1016/J.JNEUROIM.2018.09.002

Garrido, A., De La Serna, M., De La Fuente, M., Marco, E.M., & López-Gallardo,n M. (2021) Neuronal and glial region dependent changes in female mice from a model of premature aging. Experimental Gerontology, 146, 111224. https://doi.org/10.1016/J.EXGER.2020.111224.

Garwood, C. J., Ratcliffe, L. E., Simpson, J. E., Heath, P. R., Ince, P. G., & Wharton, S. B. (2017). Review: Astrocytes in Alzheimer's disease and other age-associated dementias: a supporting player with a central role. Neuropathology and Applied Neurobiology, 43(4), 281–298. https://doi.org/10.1111/nan.12338

Gaspar-Silva, F., Trigo, D., & Magalhaes, J. (2023). Ageing in the brain: mechanisms and rejuvenating strategies. Cellular and Molecular Life Sciences, 80(7), 1–21. https://doi.org/10.1007/S00018-023-04832-6

Gauberti, M., Fournier, A. P., Docagne, F., Vivien, D., & de Lizarrondo, S. M. (2018). Molecular Magnetic Resonance Imaging of Endothelial Activation in the Central Nervous System. Theranostics, 8(5), 1195-1212. https://doi.org/10.7150/THNO.22662

Gauberti, M., Montagne, A., Marcos-Contreras, O. A., Le Béhot, A., Maubert, E., & Vivien, D. (2013). Ultra-sensitive molecular MRI of vascular cell adhesion molecule-1 reveals a dynamic inflammatory penumbra after strokes. Stroke, 44(7), 1988–1996. https://doi.org/10.1161/STROKEAHA.111.000544

Gauberti, M., P. Fournier, A., Vivien, D., & de Lizarrondo, S. M. (2018). Molecular Magnetic Resonance Imaging (mMRI). Methods in Molecular Biology (Clifton, N.J.), 1718, 315–327. https://doi.org/10.1007/978-1-4939-7531-0_19

Geldenhuys, W. J., Mohammad, A. S., Adkins, C. E., & Lockman, P. R. (2015). Molecular determinants of blood–brain barrier permeation. Therapeutic Delivery, 6(7), 961-971. https://doi.org/10.4155/TDE.15.32

Georgieva, J. V., Goulatis, L. I., Stutz, C. C., Canfield, S. G., Song, H. W., Gastfriend, B. D., & Shusta, E. V. (2020). Antibody Screening Using a Human iPSC-based Blood-Brain Barrier Model Identifies Antibodies that Accumulate in the CNS. Federation of American Sciences for Experimental Biology Journal, 34(9), 12549-12564. https://doi.org/10.1096/FJ.202000851R

Germolec, D. R., Shipkowski, K. A., Frawley, R. P., & Evans, E. (2018). Markers of Inflammation. Methods in Molecular Biology (Clifton, N.J.), 1803, 57–79. https://doi.org/10.1007/978-1-4939-8549-4_5

Giacobbo, B. L., Özalay, Ö., Mediavilla, T., Ericsson, M., Axelsson, J., Rieckmann, A., Sultan, F., & Marcellino, D. (2022). The Aged Striatum: Evidence of Molecular and Structural Changes Using a Longitudinal Multimodal Approach in Mice. Frontiers in Aging Neuroscience, 14, 795132. https://doi.org/10.3389/FNAGI.2022.795132/BIBTEX

Giovannoni, F., & Quintana, F. J. (2020). The Role of Astrocytes in CNS Inflammation. Trends in Immunology, 41(9), 805-819. https://doi.org/10.1016/J.IT.2020.07.007

Giridharan, V. V., Barichello, T., & Selvaraj, S. (2019). Molecular Imaging of Blood–Brain Barrier Permeability in Preclinical Models Using PET and SPECT. In Neuromethods, 142, 329–342. https://doi.org/10.1007/978-1-4939-8946-1_19

Gliga, A. R., De Loma, J., Di Bucchianico, S., Skoglund, S., Keshavan, S., Odnevall Wallinder, I., Karlsson, H. L., & Fadeel, B. (2020). Silver nanoparticles modulate lipopolysaccharide-triggered Toll-like receptor signaling in immune-competent human cell lines. Nanoscale Advances, 2(2), 648–658. https://doi.org/10.1039/C9NA00721K

Gocmez, S. S., Gacar, N., Utkan, T., Gacar, G., Scarpace, P. J., & Tumer, N. (2016). Protective effects of resveratrol on aging-induced cognitive impairment in rats. Neurobiology of Learning and Memory, 131, 131–136. https://doi.org/10.1016/J.NLM.2016.03.022

Gold, B. T., Shao, X., Sudduth, T. L., Jicha, G. A., Wilcock, D. M., Seago, E. R., & Wang, D. J. J. (2021). Water Exchange Rate across the Blood-Brain Barrier is Associated with CSF Amyloid-β 42 in Healthy Older Adults. Alzheimer's & Dementia : The Journal of the Alzheimer's Association, 17(12), 2020. https://doi.org/10.1002/ALZ.12357

Gonzalez, P. V., Schiöth, H. B., Lasaga, M., & Scimonelli, T. N. (2009). Memory impairment induced by IL-1beta is reversed by alpha-MSH through central melanocortin-4 receptors. Brain, Behavior, and Immunity, 23(6), 817–822. https://doi.org/10.1016/J.BBI.2009.03.001

Gonzalez-Carter, D. A., Leo, B. F., Ruenraroengsak, P., Chen, S., Goode, A. E., Theodorou, I. G., Chung, K. F., Carzaniga, R., Shaffer, M. S. P., Dexter, D. T., Ryan, M. P., & Porter, A. E. (2017). Silver nanoparticles reduce brain inflammation and related neurotoxicity through induction of H2S-synthesizing enzymes. Scientific Reports, 7(1), 1–14. https://doi.org/10.1038/srep42871

González-Gualda, E., Baker, A. G., Fruk, L., & Muñoz-Espín, D. (2021). A guide to assessing cellular senescence in vitro and in vivo. The FEBS Journal, 288(1), 56–80. https://doi.org/10.1111/FEBS.15570

Goodall, E. F., Leach, V., Wang, C., Cooper-Knock, J., Heath, P. R., Baker, D., Drew, D. R., Jill Saffrey, M., Simpson, J. E., Romero, I. A., & Wharton, S. B. (2019). Age-associated mRNA and miRNA expression changes in the blood-brain barrier. International Journal of Molecular Sciences, 20(12), 3097. https://doi.org/10.3390/ijms20123097

Goodall, E. F., Wang, C., Simpson, J. E., Baker, D. J., Drew, D. R., Heath, P. R., Saffrey, M. J., Romero, I. A., & Wharton, S. B. (2018). Age-associated changes in the blood-brain barrier: comparative studies in human and mouse. Neuropathology and Applied Neurobiology, 44(3), 328–340. https://doi.org/10.1111/nan.12408

Gosselin, D., & Rivest, S. (2008). MyD88 signaling in brain endothelial cells is essential for the neuronal activity and glucocorticoid release during systemic inflammation. Molecular Psychiatry 2008 13:5, 13(5), 480–497. https://doi.org/10.1038/sj.mp.4002122

Graber, T.G., Kim J.H., Grange, R.W., McLoon, L.K., & Thompson, L.V. (2015). C57BL/6 life span study: age-related declines in muscle power production and contractile velocity, Age, 37(3), 9773. https://doi.org/10.1007/S11357-015-9773-1.

Grabert, K., Michoel, T., Karavolos, M. H., Clohisey, S., Kenneth Baillie, J., Stevens, M. P., Freeman, T. C., Summers, K. M., & McColl, B. W. (2016). Microglial brain region-dependent diversity and selective regional sensitivities to ageing. Nature Neuroscience, 19(3), 504. https://doi.org/10.1038/NN.4222

Greenhalgh, A. D., Galea, J., Dénes, A., Tyrrell, P. J., & Rothwell, N. J. (2010). Rapid brain penetration of interleukin-1 receptor antagonist in rat cerebral ischaemia: pharmacokinetics, distribution, protection. British Journal of Pharmacology, 160(1), 153-159. https://doi.org/10.1111/J.1476-5381.2010.00684.X

Groó, Z., Szenczi P., Banszegi, O., & Altbäcker V. (2013). Natal dispersal in two mice species with contrasting social systems. Behavioral Ecology and Sociobiology, 67(2), 235–242. https://doi.org/10.1007/S00265-012-1443-Z/FIGURES/5

Grossmann, R., Stence, N., Carr, J., Fuller, L., Waite, M., & Dailey, M. E. (2002). Juxtavascular microglia migrate along brain microvessels following activation during early postnatal development. Glia, 37(3), 229–240. https://doi.org/10.1002/GLIA.10031

Guarner, V., & Rubio-Ruiz, M. E. (2014). Low-grade systemic inflammation connects aging, metabolic syndrome and cardiovascular disease. Interdisciplinary Topics in Gerontology, 40, 99–106. https://doi.org/10.1159/000364934

Guerreiro, R., & Bras, J. (2015). The age factor in Alzheimer's disease. Genome Medicine, 7(1), 1–3. https://doi.org/10.1186/s13073-015-0232-5

Gundersen, G. A., Vindedal, G. F., Skare, Ø., & Nagelhus, E. A. (2014). Evidence that pericytes regulate aquaporin-4 polarization in mouse cortical astrocytes. Brain Structure and Function, 219(6), 2181–2186. https://doi.org/10.1007/s00429-013-0629-0

Guo, S., Deng, W., Xing, C., Zhou, Y., Ning, M. M., & Lo, E. H. (2019). Effects of aging, hypertension and diabetes on the mouse brain and heart vasculomes. Neurobiology of Disease, 126, 117-123. https://doi.org/10.1016/J.NBD.2018.07.021

Gupta, S., Kesarla, R., Chotai, N., Misra, A., & Omri, A. (2017). Systematic Approach for the Formulation and Optimization of Solid Lipid Nanoparticles of Efavirenz by High Pressure Homogenization Using Design of Experiments for Brain Targeting and Enhanced Bioavailability. BioMed Research International, 2017. https://doi.org/10.1155/2017/5984014

Gyoneva, S., Hosur, R., Gosselin, D., Zhang, B., Ouyang, Z., Cotleur, A. C., Peterson, M., Allaire, N., Challa, R., Cullen, P., Roberts, C., Miao, K., Reynolds, T. L., Glass, C. K., Burkly, L., & Ransohoff, R. M. (2019). Cx3cr1-deficient microglia exhibit a premature aging transcriptome. Life Science Alliance, 2(6), e201900453. https://doi.org/10.26508/LSA.201900453

Halder, S. K., & Milner, R. (2022). Exaggerated hypoxic vascular breakdown in aged brain due to reduced microglial vasculo-protection. Aging Cell, 21(11), e13720. https://doi.org/10.1111/ACEL.13720

Hamesch, k., Borkham-Kamphorst, E., Strnad, P., & Weiskirchen, R. (2015). Lipopolysaccharide-induced inflammatory liver injury in mice. Laboratory Animals, 49(1 Suppl), 37–46. https://doi.org/10.1177/0023677215570087

Hammond, R.S., Tull, L.E. and Stackman, R.W. (2004). On the delay-dependent involvement of the hippocampus in object recognition memory, Neurobiology of Learning and Memory, 82(1), 26–34. https://doi.org/10.1016/J.NLM.2004.03.005.

Hao, S., Dey, A., Yu, X., & Stranahan, A. M. (2016). Dietary obesity reversibly induces synaptic stripping by microglia and impairs hippocampal plasticity. Brain, Behavior, and Immunity, 51, 230–239. https://doi.org/10.1016/J.BBI.2015.08.023

Harmon, E., Doan, A., Bautista-Garrido, J., Jung, J. E., Marrelli, S. P., & Kim, G. S. (2022). Increased Expression of Interferon-Induced Transmembrane 3 (IFITM3) in Stroke and Other Inflammatory Conditions in the Brain. International Journal of Molecular Sciences, 23(16), 8885. https://doi.org/10.3390/IJMS23168885/S1

Hart, A. D., Wyttenbach, A., Hugh Perry, V., & Teeling, J. L. (2012). Age related changes in microglial phenotype vary between CNS regions: Grey versus white matter differences. Brain, Behavior, and Immunity, 26(5), 754-765. https://doi.org/10.1016/J.BBI.2011.11.006

Hartz, A. M. S., Bauer, B., Fricker, G., & Miller, D. S. (2006). Rapid modulation of P-glycoprotein-mediated transport at the blood-brain barrier by tumor necrosis factor-alpha and lipopolysaccharide. Molecular Pharmacology, 69(2), 462–470. https://doi.org/10.1124/MOL.105.017954

Haruwaka, K., Ikegami, A., Tachibana, Y., Ohno, N., Konishi, H., Hashimoto, A., Matsumoto, M., Kato, D., Ono, R., Kiyama, H., Moorhouse, A. J., Nabekura, J., & Wake, H. (2019). Dual microglia effects on blood brain barrier permeability induced by systemic inflammation. Nature Communications, 10(1), 5816. https://doi.org/10.1038/S41467-019-13812-Z

Hattori, Y., & Hattori, Y. (2016). Delivery of Plasmid DNA into Tumors by Intravenous Injection of PEGylated Cationic Lipoplexes into Tumor-Bearing Mice. Pharmacology & Pharmacy, 7(7), 272–282. https://doi.org/10.4236/PP.2016.77034

Hauptmann, J., Johann, L., Marini, F., Kitic, M., Colombo, E., Mufazalov, I. A., Krueger, M., Karram, K., Moos, S., Wanke, F., Kurschus, F. C., Klein, M., Cardoso, S., Strauß, J., Bolisetty, S., Lühder, F., Schwaninger, M., Binder, H., Bechman, I., … Waisman, A. (2020). Interleukin-

1 promotes autoimmune neuroinflammation by suppressing endothelial heme oxygenase-1 at the blood–brain barrier. Acta Neuropathologica, 140(4), 549–567. https://doi.org/10.1007/S00401-020-02187-X/FIGURES/6

Hayakawa, N., Kato, H. and Araki, T. (2007). Age-related changes of astorocytes, oligodendrocytes and microglia in the mouse hippocampal CA1 sector, Mechanisms of ageing and development, 128(4), 311–316. https://doi.org/10.1016/J.MAD.2007.01.005

He, Y., Taylor, N., Yao, X., & Bhattacharya, A. (2021). Mouse primary microglia respond differently to LPS and poly(I:C) in vitro. Scientific Reports, 11(1), 1–14. https://doi.org/10.1038/s41598-021-89777-1

Healy, D., Murray, C., McAdams, C., Power, R., Hollier, P. L., Lambe, J., Tortorelli, L., Lopez-Rodriguez, A. B., & Cunningham, C. (2024). Susceptibility to acute cognitive dysfunction in aged mice is underpinned by reduced white matter integrity and microgliosis. Communications Biology, 7(1), 1–15. https://doi.org/10.1038/s42003-023-05662-9

Heithoff, B.P., George, K.K., Phares, A.N., Zuidhoek, I.A., Munoz-Ballester, C., & Robel,n S. (2021). Astrocytes are necessary for blood–brain barrier maintenance in the adult mouse brain', Glia, 69(2), 436–472. https://doi.org/10.1002/GLIA.23908.

Heitzer, T., Schlinzig, T., Krohn, K., Meinertz, T., & Münzel, T. (2001). Endothelial dysfunction, oxidative stress, and risk of cardiovascular events in patients with coronary artery disease. Circulation, 104(22), 2673–2678. https://doi.org/10.1161/HC4601.099485

Helms, H. C., Abbott, N. J., Burek, M., Cecchelli, R., Couraud, P. O., Deli, M. A., Förster, C., Galla, H. J., Romero, I. A., Shusta, E. V., Stebbins, M. J., Vandenhaute, E., Weksler, B., & Brodin, B. (2015). In vitro models of the blood-brain barrier: An overview of commonly used brain endothelial cell culture models and guidelines for their use. In Journal of Cerebral Blood Flow and Metabolism, 36(5), 862-890. https://doi.org/10.1177/0271678X16630991

Hendrickx, J. O., De Moudt, S., Calus, E., De Deyn, P. P., Van Dam, D., & De Meyer, G. R. Y. (2022). Age-related cognitive decline in spatial learning and memory of C57BL/6J mice. Behavioural Brain Research, 418, 166–4328. https://doi.org/10.1016/J.BBR.2021.113649

Henry, C. B. S., & Duling, B. R. (1999). Permeation of the luminal capillary glycocalyx is determined by hyaluronan. The American Journal of Physiology, 277(2), H508-514. https://doi.org/10.1152/AJPHEART.1999.277.2.H508

Henry, C. J., Huang, Y., Wynne, A. M., & Godbout, J. P. (2009). Peripheral Lipopolysaccharide (LPS) challenge promotes microglial hyperactivity in aged mice that is associated with exaggerated induction of both pro-inflammatory IL-1β and anti-inflammatory IL-10 cytokines. Brain, Behavior, and Immunity, 23(3), 309-317. https://doi.org/10.1016/J.BBI.2008.09.002

Heye, A. K., Culling, R. D., Valdés Hernández, M. D. C., Thrippleton, M. J., & Wardlaw, J. M. (2014). Assessment of blood-brain barrier disruption using dynamic contrast-enhanced MRI. A systematic review. In NeuroImage: Clinical, 6, 262-274. (https://doi.org/10.1016/j.nicl.2014.09.002

Heye, A. K., Thrippleton, M. J., Armitage, P. A., Valdés Hernández, M. del C., Makin, S. D., Glatz, A., Sakka, E., & Wardlaw, J. M. (2016). Tracer kinetic modelling for DCE-MRI quantification of subtle blood–brain barrier permeability. NeuroImage, 125, 446–455. https://doi.org/10.1016/J.NEUROIMAGE.2015.10.018

Hill, A. R., & Spencer-Segal, J. L. (2021). Glucocorticoids and the Brain after Critical Illness. Endocrinology, 162(3), 1–14. https://doi.org/10.1210/ENDOCR/BQAA242

Hill, L. K., Hoang, D. M., Chiriboga, L. A., Wisniewski, T., Sadowski, M. J., & Wadghiri, Y. Z. (2020). Detection of Cerebrovascular Loss in the Normal Aging C57BL/6 Mouse Brain Using in vivo Contrast-Enhanced Magnetic Resonance Angiography. Frontiers in Aging Neuroscience, 12, 326. https://doi.org/10.3389/fnagi.2020.585218

Hillmer, L., Erhardt, E.B., Caprihan, A., Adair, J.C., Knoefel, J.E., Prestopnik, J., Thompson J., Hobson S., & Rosenberg G.A. (2023) 'Blood-brain barrier disruption measured by albumin index correlates with inflammatory fluid biomarkers', Journal of Cerebral Blood Flow and Metabolism, 43(5), 712–721. https://doi.org/10.1177/0271678X221146127/ASSET/IMAGES/LARGE/10.1177_0271678X221146127-FIG4.JPEG.

Hines, D. J., Choi, H. B., Hines, R. M., Phillips, A. G., & MacVicar, B. A. (2013). Prevention of LPS-Induced Microglia Activation, Cytokine Production and Sickness Behavior with TLR4 Receptor Interfering Peptides. PLoS ONE, 8(3), 60388. https://doi.org/10.1371/JOURNAL.PONE.0060388

Ho, D. H., & Kelly, G. C. (2020). Blood Serum Cytokines Induce Changes in Blood-Brain Barrier Permeability and Gene Expression in an In Vitro Blood-Brain Barrier Model. The Federation of American Sciences for Experimental Biology Journal, 34(S1), 1–1. https://doi.org/10.1096/FASEBJ.2020.34.S1.05527

Hochstrasser, T., Weiss, E., Marksteiner, J., & Humpel, C. (2010). Soluble cell adhesion molecules in monocytes of Alzheimer's disease and mild cognitive impairment. Experimental Gerontology, 45(1), 70–74. https://doi.org/10.1016/J.EXGER.2009.10.005

Hodges, S. L., Nolan, S. O., Tomac, L. A., Muhammad, I. D. A., Binder, M. S., Taube, J. H., & Lugo, J. N. (2020). Lipopolysaccharide-induced inflammation leads to acute elevations in pro-inflammatory cytokine expression in a mouse model of Fragile X syndrome. Physiology & Behavior, 215, 112776. https://doi.org/10.1016/J.PHYSBEH.2019.112776

Hoffman, J. D., Parikh, I., Green, S. J., Chlipala, G., Mohney, R. P., Keaton, M., Bauer, B., Hartz, A. M. S., & Lin, A. L. (2017a). Age drives distortion of brain metabolic, vascular and cognitive functions, and the gut microbiome. Frontiers in Aging Neuroscience, 9(SEP), 298. https://doi.org/10.3389/fnagi.2017.00298

Hogstrom, L.J., Westlye, L.T., Walhovd, K.B., & Fjell, A.M. (2013). The Structure of the Cerebral Cortex Across Adult Life: Age-Related Patterns of Surface Area, Thickness, and Gyrification, Cerebral Cortex, 23(11), 2521–2530. https://doi.org/10.1093/CERCOR/BHS231

Hoozemans, J. J. M., Rozemuller, A. J. M., van Haastert, E. S., Eikelenboom, P., & van Gool, W. A. (2011). Neuroinflammation in Alzheimer's disease wanes with age. Journal of Neuroinflammation, 8, 171. https://doi.org/10.1186/1742-2094-8-171

Horowitz, M. A., Cattaneo, A., Cattane, N., Lopizzo, N., Tojo, L., Bakunina, N., Musaelyan, K., Borsini, A., Zunszain, P. A., & Pariante, C. M. (2020). Glucocorticoids prime the inflammatory response of human hippocampal cells through up-regulation of inflammatory pathways. Brain, Behavior, and Immunity, 87, 777–794. https://doi.org/10.1016/J.BBI.2020.03.012

Hortelano, S., López-Fontal, R., Través, P. G., Villa, N., Grashoff, C., Boscá, L., & Luque, A. (2010). ILK mediates LPS-induced vascular adhesion receptor expression and subsequent leucocyte trans-endothelial migration. Cardiovascular Research, 86(2), 283–292. https://doi.org/10.1093/CVR/CVQ050

Howell, M. D., & Gottschall, P. E. (2012). Lectican proteoglycans, their cleaving metalloproteinases, and plasticity in the central nervous system extracellular microenvironment. Neuroscience, 217, 6-18. https://doi.org/10.1016/J.NEUROSCIENCE.2012.05.034

Hsieh, C. T., Lee, Y. J., Lee, J. W., Lu, S., Tucci, M. A., Dai, X., Ojeda, N. B., Lee, H. J., Fan, L. W., & Tien, L. T. (2020). Interleukin-1 receptor antagonist ameliorates the pain hypersensitivity, spinal inflammation and oxidative stress induced by systemic lipopolysaccharide in neonatal rats. Neurochemistry International, 135, 104686. https://doi.org/10.1016/J.NEUINT.2020.104686

Hsu, C., Morohashi, Y., Yoshimura, S. I., Manrique-Hoyos, N., Jung, S. Y., Lauterbach, M. A., Bakhti, M., Grønborg, M., Möbius, W., Rhee, J. S., Barr, F. A., & Simons, M. (2010). Regulation of exosome secretion by Rab35 and its GTPase-activating proteins TBC1D10A–C. The Journal of Cell Biology, 189(2), 223. https://doi.org/10.1083/JCB.200911018

Hsu, W. L., Ma, Y. L., Hsieh, D. Y., Liu, Y. C., & Lee, E. H. (2013). STAT1 Negatively Regulates Spatial Memory Formation and Mediates the Memory-Impairing Effect of Aβ. Neuropsychopharmacology, 39(3), 746–758. https://doi.org/10.1038/npp.2013.263

Hu, Y., Hu, X., He, Z., Liu, Y., Gui, Y., Zhu, S., Da, X., Liu, Y., Liu, L., Shen, Q., & Xu, G. (2024). Anesthesia/surgery activate MMP9 leading to blood-brain barrier disruption, triggering neuroinflammation and POD-like behavior in aged mice. International Immunopharmacology, 135, 112290. https://doi.org/10.1016/J.INTIMP.2024.112290

Hu, Y., Wang, Z., Pan, S., Zhang, H., Fang, M., Jiang, H., Zhang, H., Gao, Z., Xu, K., Li, Z., Xiao, J., & Lin, Z. (2017). Melatonin protects against blood-brain barrier damage by inhibiting the TLR4/ NF-κB signaling pathway after LPS treatment in neonatal rats. Oncotarget, 8(19), 31638–31654. https://doi.org/10.18632/ONCOTARGET.15780

Hu, Z., Deng, N., Liu, K., Zhou, N., Sun, Y., & Zeng, W. (2020). CNTF-STAT3-IL-6 Axis Mediates Neuroinflammatory Cascade across Schwann Cell-Neuron-Microglia. Cell Reports, 31(7), 107657. https://doi.org/10.1016/J.CELREP.2020.107657

Huang, N., Lu, S., Liu, X. G., Zhu, J., Wang, Y. J., & Liu, R. T. (2017). PLGA nanoparticles modified with a BBB-penetrating peptide co-delivering Aβ generation inhibitor and curcumin attenuate memory deficits and neuropathology in Alzheimer's disease mice. Oncotarget, 8(46), 81001. https://doi.org/10.18632/ONCOTARGET.20944

Huang, X., Guo, M., Zhang, Y., Xie, J., Huang, R., Zuo, Z., Saw, P. E., & Cao, M. (2023). Microglial IL-1RA ameliorates brain injury after ischemic stroke by inhibiting astrocytic CXCL1-mediated neutrophil recruitment and microvessel occlusion. Glia, 71(7), 1607–1625. https://doi.org/10.1002/GLIA.24359

Huang, Y., Henry, C. J., Dantzer, R., Johnson, R. W., & Godbout, J. P. (2008). Exaggerated sickness behavior and brain proinflammatory cytokine expression in aged mice in response to intracerebroventricular lipopolysaccharide. Neurobiology of Aging, 29(11), 1744. https://doi.org/10.1016/J.NEUROBIOLAGING.2007.04.012

Hughes, S., Gardiner, T., Hu, P., Baxter, L., Rosinova, E., & Chan-Ling, T. (2006). Altered pericyte-endothelial relations in the rat retina during aging: Implications for vessel stability. Neurobiology of Aging, 27(12), 1838–1847. https://doi.org/10.1016/j.neurobiolaging.2005.10.021

Hunter, J. M., Kwan, J., Malek-Ahmadi, M., Maarouf, C. L., Kokjohn, T. A., Belden, C., Sabbagh, M. N., Beach, T. G., & Roher, A. E. (2012). Morphological and pathological evolution of the brain microcirculation in aging and Alzheimer's disease. PLoS ONE, 7(5), 36893. https://doi.org/10.1371/journal.pone.0036893

Hunter, L.W., Jayachandran, M. and Miller, V.M. (2019). Sex differences in the expression of cell adhesion molecules on microvesicles derived from cultured human brain microvascular endothelial cells treated with inflammatory and thrombotic stimuli, Biology of Sex Differences, 10(1), 26. https://doi.org/10.1186/S13293-019-0241-Y

Huntley, M. A., Bien-Ly, N., Daneman, R., & Watts, R. J. (2014). Dissecting gene expression at the blood-brain barrier. Frontiers in Neuroscience, 8(OCT), 355. https://doi.org/10.3389/fnins.2014.00355

Hussein, R. M., Kandeil, M. A., Soliman, H. M., & El-Shahawy, A. A. G. (2024). Effect of quercetin-loaded poly (lactic-co-glycolic) acid nanoparticles on lipopolysaccharide-induced memory decline, oxidative stress, amyloidogenesis, neurotransmission, and Nrf2/HO-1 expression. Heliyon, 10(1), e23527. https://doi.org/10.1016/j.heliyon.2023.e23527

Hyde, S. R., Stith, R. D., & McCallum, R. E. (1990). Mortality and bacteriology of sepsis following cecal ligation and puncture in aged mice. Infection and Immunity, 58(3), 619. https://doi.org/10.1128/IAI.58.3.619-624.1990

Idris, F., Hanna Muharram, S., Zaini, Z., & Diah, S. (2018). Establishment of murine in vitro blood-brain barrier models using immortalized cell lines: co-cultures of brain endothelial cells, astrocytes, and neurons. BioRxiv, 435990. https://doi.org/10.1101/435990

Igarashi, Y., Utsumi, H., Chiba, H., Yamada-Sasamori, Y., Tobioka, H., Kamimura, Y., Furuuchi, K., Kokai, Y., Nakagawa, T., Mori, M., & Sawada, N. (1999). Glial cell line-derived neurotrophic factor induces barrier function of endothelial cells forming the blood-brain barrier. Biochemical and Biophysical Research Communications, 261(1), 108–112. https://doi.org/10.1006/bbrc.1999.0992

Imitola, J., Hollingsworth, E. W., Watanabe, F., Olah, M., Elyaman, W., Starossom, S.P., & Khoury, S. J. (2023). Stat1 is an inducible transcriptional repressor of neural stem cells self-renewal program during neuroinflammation. Frontiers in Cellular Neuroscience, 17, 1156802. https://doi.org/10.3389/FNCEL.2023.1156802/FULL

INGRAM, D.K. (1988) 'Motor Performance Variability during Aging in Rodents Assessment of Reliability and Validity of Individual Differences', Annals of the New York Academy of Sciences, 515(1), 70–96. https://doi.org/10.1111/J.1749-6632.1988.TB32969.X

Inoue, R. and Nishimune, H. (2023). Neuronal Plasticity and Age-Related Functional Decline in the Motor Cortex, Cells 2023, 12(17), 2142. https://doi.org/10.3390/CELLS12172142

Ito, K., Sanosaka, T., Igarashi, K., Ideta-Otsuka, M., Aizawa, A., Uosaki, Y., Noguchi, A., Arakawa, H., Nakashima, K., & Takizawa, T. (2016). Identification of genes associated with

the astrocyte-specific gene Gfap during astrocyte differentiation. Scientific Reports, 6(1), 1–12. https://doi.org/10.1038/srep23903

Itoh, N., Itoh, Y., Meyer, C. E., Suen, T. T., Cortez-Delgado, D., Rivera Lomeli, M., Wendin, S., Somepalli, S. S., Golden, L. C., MacKenzie-Graham, A., & Voskuhl, R. R. (2023). Estrogen receptor beta in astrocytes modulates cognitive function in mid-age female mice. Nature Communications, 14(1), 6044. https://doi.org/10.1038/S41467-023-41723-7

Jackson, S. J., Andrews, N., Ball, D., Bellantuono, I., Gray, J., Hachoumi, L., Holmes, A., Latcham, J., Petrie, A., Potter, P., Rice, A., Ritchie, A., Stewart, M., Strepka, C., Yeoman, M., & Chapman, K. (2017). Does age matter? The impact of rodent age on study outcomes. Laboratory Animals, *51*(2), 160. https://doi.org/10.1177/0023677216653984

Jaeger, L. B., Dohgu, S., Sultana, R., Lynch, J. L., Owen, J. B., Erickson, M. A., Shah, G. N., Price, T. O., Fleegal-Demotta, M. A., Butterfiled, D. A., & Banks, W. A. (2009). Lipopolysaccharide alters the blood-brain barrier transport of amyloid beta protein: a mechanism for inflammation in the progression of Alzheimer's disease. Brain, Behavior, and Immunity, 23(4), 507–517. https://doi.org/10.1016/J.BBI.2009.01.017

Janelidze, S., Hertze, J., Nägga, K., Nilsson, K., Nilsson, C.; Swedish BioFINDER Study Group; Wennström, M., van Westen, D., Blennow, K., Zetterberg H., & Hansson O. (2017). Increased blood-brain barrier permeability is associated with dementia and diabetes but not amyloid pathology or APOE genotype, Neurobiology of Aging, 51, 104-122. https://doi.org/10.1016/J.NEUROBIOLAGING.2016.11.017

Jang, M., Choi, N. and Kim, H.N. (2022). Hyperglycemic Neurovasculature-On-A-Chip to Study the Effect of SIRT1-Targeted Therapy for the Type 3 Diabetes "Alzheimer's Disease"., Advanced science (Weinheim, Baden-Wurttemberg, Germany), 9(34). e2201882. https://doi.org/10.1002/ADVS.202201882

Janota, C. S., Brites, D., Lemere, C. A., & Brito, M. A. (2015). Glio-vascular changes during ageing in wild-type and Alzheimer's disease-like APP/PS1 mice. Brain Research, 1620, 153–168. https://doi.org/10.1016/j.brainres.2015.04.056

Jeong, S. H., Jang, J. H., & Lee, Y. B. (2022). Drug delivery to the brain via the nasal route of administration: exploration of key targets and major consideration factors. Journal of Pharmaceutical Investigation 2022 53:1, 53(1), 119–152. https://doi.org/10.1007/S40005-022-00589-5

Ji, Y., Huang, W., Chen, Y., Zhang, X., Wu, F., Tang, W., Lu, Z., & Huang, C. (2023). Inhibition of MMP-2 and MMP-9 attenuates surgery-induced cognitive impairment in aged mice. Brain Research Bulletin, 204, 110810. https://doi.org/10.1016/J.BRAINRESBULL.2023.110810

Jiang, T., Yin, F., Yao, J., Brinton, R. D., & Cadenas, E. (2013). Lipoic acid restores age-associated impairment of brain energy metabolism through the modulation of Akt/JNK signaling and PGC1α transcriptional pathway. Aging Cell, 12(6), 1021–1031. https://doi.org/10.1111/acel.12127

Jing, L., Wang, J. G., Zhang, J. Z., Cao, C. X., Chang, Y., Dong, J. Da, Guo, F. Y., & Andy Li, P. (2014). Upregulation of ICAM-1 in diabetic rats after transient forebrain ischemia and reperfusion injury. Journal of Inflammation (United Kingdom), 11(1), 1–11. https://doi.org/10.1186/S12950-014-0035-2/FIGURES/7

Johnsen, K. B., Burkhart, A., Melander, F., Kempen, P. J., Vejlebo, J. B., Siupka, P., Nielsen, M. S., Andresen, T. L., & Moos, T. (2017). Targeting transferrin receptors at the blood-brain barrier improves the uptake of immunoliposomes and subsequent cargo transport into the brain parenchyma. Scientific Reports, 7(1), 1–13. https://doi.org/10.1038/s41598-017-11220-1

Joshi, B. S., & Zuhorn, I. S. (2021). Heparan sulfate proteoglycan-mediated dynamin-dependent transport of neural stem cell exosomes in an in vitro blood–brain barrier model. The European Journal of Neuroscience, 53(3), 706. https://doi.org/10.1111/EJN.14974

Juhairiyah, F. and de Lange, E.C.M. (2021). Understanding Drug Delivery to the Brain Using Liposome-Based Strategies: Studies that Provide Mechanistic Insights Are Essential. The American Association of Pharmaceutical Scientists Journal, 23(6), 114. https://doi.org/10.1208/S12248-021-00648-Z

Jung, B., Arnold, T. D., Raschperger, E., Gaengel, K., & Betsholtz, C. (2018). Visualization of vascular mural cells in developing brain using genetically labeled transgenic reporter mice. Journal of Cerebral Blood Flow and Metabolism, 38(3), 456–468. https://doi.org/10.1177/0271678X17697720

Jung, H., Lee, D., You, H., Lee, M., Kim, H., Cheong, E., & Um, J. W. (2023). LPS induces microglial activation and GABAergic synaptic deficits in the hippocampus accompanied by prolonged cognitive impairment. Scientific Reports, 13(1), 1–14. https://doi.org/10.1038/s41598-023-32798-9

Jurga, A. M., Paleczna, M., Kadluczka, J., & Kuter, K. Z. (2021). Beyond the GFAP-Astrocyte Protein Markers in the Brain. Biomolecules, 11(9), 1361. https://doi.org/10.3390/BIOM11091361

Kaddah, S., Khreich, N., Kaddah, F., Charcosset, C., & Greige-Gerges, H. (2018). Cholesterol modulates the liposome membrane fluidity and permeability for a hydrophilic molecule. Food and Chemical Toxicology, 113, 40–48. https://doi.org/10.1016/J.FCT.2018.01.017

Kadry, H., Noorani, B., & Cucullo, L. (2020). A blood–brain barrier overview on structure, function, impairment, and biomarkers of integrity. Fluids and Barriers of the CNS, 17(1), 69. https://doi.org/10.1186/s12987-020-00230-3

Kallmann, B.A., Hummel, V., Toyka, K.V., Rieckmann, P. (2004). Soluble VCAM-1 Release Indicates Inflammatory Blood-Brain Barrier Pathology and Further Modulates Adhesion, Early Indicators Early Treatments Neuroprotection in Multiple Sclerosis, Topics in Neuroscience, 115–117. https://doi.org/10.1007/978-88-470-2117-4_11

Kanashiro, A., Hiroki, C. H., da Fonseca, D. M., Birbrair, A., Ferreira, R. G., Bassi, G. S., Fonseca, M. D., Kusuda, R., Cebinelli, G. C. M., da Silva, K. P., Wanderley, C. W., Menezes, G. B., Alves-Filho, J. C., Oliveira, A. G., Cunha, T. M., Pupo, A. S., Ulloa, L., & Cunha, F. Q. (2020). The role of neutrophils in neuro-immune modulation. Pharmacological Research, 151, 104580. https://doi.org/10.1016/J.PHRS.2019.104580

Kang, J. Bin, Park, D. J., Shah, M. A., Kim, M. O., & Koh, P. O. (2019). Lipopolysaccharide induces neuroglia activation and NF-κB activation in cerebral cortex of adult mice. Laboratory Animal Research, 35(1), 1–8. https://doi.org/10.1186/S42826-019-0018-9/FIGURES/5

Kang, Y. K., Min, B., Eom, J., & Park, J. S. (2022). Different phases of aging in mouse old skeletal muscle. *Aging (Albany NY)*, *14*(1), 143. https://doi.org/10.18632/AGING.203812

Kaushik, W., & Moots, R. J. (2005). CDP-870 (certolizumab) in rheumatoid arthritis. Expert Opinion on Biological Therapy, 5(4), 601–606. https://doi.org/10.1517/14712598.5.4.601

Keane, T. M., Goodstadt, L., Danecek, P., White, M. A., Wong, K., Yalcin, B., Heger, A., Agam, A., Slater, G., Goodson, M., Furlotte, N. A., Eskin, E., Nellåker, C., Whitley, H., Cleak, J., Janowitz, D., Hernandez-Pliego, P., Edwards, A., Belgard, T. G., … Adams, D. J. (2011). Mouse genomic variation and its effect on phenotypes and gene regulation. *Nature*, *477*(7364), 289-294. https://doi.org/10.1038/NATURE10413

Kenkhuis, B., Somarakis, A., de Haan, L., Dzyubachyk, O., IJsselsteijn, M. E., de Miranda, N. F. C. C., Lelieveldt, B. P. F., Dijkstra, J., van Roon-Mom, W. M. C., Höllt, T., & van der Weerd, L. (2021). Iron loading is a prominent feature of activated microglia in Alzheimer's disease patients. Acta Neuropathologica Communications, 9(1), 1–15. https://doi.org/10.1186/S40478-021-01126-5/FIGURES/6

Kenkhuis, B., van Eekeren, M., Parfitt, D. A., Ariyurek, Y., Banerjee, P., Priller, J., van der Weerd, L., & van Roon-Mom, W. M. C. (2022). Iron accumulation induces oxidative stress, while depressing inflammatory polarization in human iPSC-derived microglia. Stem Cell Reports, 17(6), 1351. https://doi.org/10.1016/J.STEMCR.2022.04.006

Khabour, O. F., & Barnawi, J. M. (2010). Association of longevity with IL-10 −1082 G/A and TNF-α−308 G/A polymorphisms. International Journal of Immunogenetics, 37(4), 293–298. https://doi.org/10.1111/J.1744-313X.2010.00925.X

Khan, S.R., Yaqub A., Ikram, M.K., van Hagen, P.M., Peeters, P., Dalm, V.A.S.H., Chaker, L. &, Ikram, M.A. (2023) 'The association of serum immunoglobulins with cognition and dementia: the Rotterdam Study', Journal of Neurology, 270(1), 423. https://doi.org/10.1007/S00415-022-11374-7.

Khani, E., Shahrabi, M., Rezaei, H., Pourkarim, F., Afsharirad, H., & Solduzian, M. (2022). Current evidence on the use of anakinra in COVID-19. International Immunopharmacology, 111, 109075. https://doi.org/10.1016/J.INTIMP.2022.109075

Kiessling, C.J. (2024). Age- and Sex-Dependent Caveolar Gene Expression in Normoxic and Post-Ischemic Mouse Hearts, bioRxiv, p. 2024.03.01.582960. https://doi.org/10.1101/2024.03.01.582960

Kim, H., Leng, K., Park, J., Sorets, A. G., Kim, S., Shostak, A., Embalabala, R. J., Mlouk, K., Katdare, K. A., Rose, I. V. L., Sturgeon, S. M., Neal, E. H., Ao, Y., Wang, S., Sofroniew, M. V., Brunger, J. M., McMahon, D. G., Schrag, M. S., Kampmann, M., & Lippmann, E. S. (2022). Reactive astrocytes transduce inflammation in a blood-brain barrier model through a TNF-STAT3 signaling axis and secretion of alpha 1-antichymotrypsin. Nature Communications, 13(1), 1–18. https://doi.org/10.1038/s41467-022-34412-4

Kim, J. Y., Kim, J. K., Park, J. S., Byun, Y., & Kim, C. K. (2009). The use of PEGylated liposomes to prolong circulation lifetimes of tissue plasminogen activator. Biomaterials, 30(29), 5751–5756. https://doi.org/10.1016/J.BIOMATERIALS.2009.07.021

Kim, Y. S., & Joh, T. H. (2006). Microglia, major player in the brain inflammation: their roles in the pathogenesis of Parkinson's disease. Experimental & Molecular Medicine, 38(4), 333–347. https://doi.org/10.1038/EMM.2006.40

Kip, E., & Parr-Brownlie, L. C. (2023). Healthy lifestyles and wellbeing reduce neuroinflammation and prevent neurodegenerative and psychiatric disorders. Frontiers in Neuroscience, 17, 1092537. https://doi.org/10.3389/FNINS.2023.1092537

Kiss, T., Nyúl-Tóth, Á., Balasubramanian, P., Tarantini, S., Ahire, C., DelFavero, J., Yabluchanskiy, A., Csipo, T., Farkas, E., Wiley, G., Garman, L., Csiszar, A., & Ungvari, Z. (2020). Single-cell RNA sequencing identifies senescent cerebromicrovascular endothelial cells in the aged mouse brain. GeroScience, 42(2), 429–444. https://doi.org/10.1007/s11357-020-00177-1

Kitazawa, M., Cheng, D., Tsukamoto, M. R., Koike, M. A., Wes, P. D., Vasilevko, V., Cribbs, D. H., & LaFerla, F. M. (2011). Blocking IL-1 Signaling Rescues Cognition, Attenuates Tau Pathology, and Restores Neuronal β-Catenin Pathway Function in an Alzheimer's Disease Model. The Journal of Immunology, 187(12), 6539–6549. https://doi.org/10.4049/JIMMUNOL.1100620

Klein, A. L., Imazio, M., Cremer, P., Brucato, A., Abbate, A., Fang, F., Insalaco, A., LeWinter, M., Lewis, B. S., Lin, D., Luis, S. A., Nicholls, S. J., Pano, A., Wheeler, A., & Paolini, J. F. (2021). Phase 3 Trial of Interleukin-1 Trap Rilonacept in Recurrent Pericarditis. The New England Journal of Medicine, 384(1), 31–41. https://doi.org/10.1056/NEJMOA2027892

Knopp, R. C., Banks, W. A., & Erickson, M. A. (2022). Physical associations of microglia and the vascular blood-brain barrier and their importance in development, health, and disease. Current Opinion in Neurobiology, 77, 102648. https://doi.org/10.1016/J.CONB.2022.102648

Knopp, R. C., Baumann, K. K., Wilson, M. L., Banks, W. A., & Erickson, M. A. (2022). Amyloid Beta Pathology Exacerbates Weight Loss and Brain Cytokine Responses following Low-Dose Lipopolysaccharide in Aged Female Tg2576 Mice. International Journal of Molecular Sciences, 23(4), 2377. https://doi.org/10.3390/IJMS23042377/S1

Knox, E. G., Aburto, M. R., Clarke, G., Cryan, J. F., & O'Driscoll, C. M. (2022). The blood-brain barrier in aging and neurodegeneration. Molecular Psychiatry, 27(6), 2659–2673. https://doi.org/10.1038/s41380-022-01511-z

Koh, M.T., Spiegel, A.M. and Gallagher, M. (2014). Age-Associated Changes in Hippocampal-Dependent Cognition in Diversity Outbred Mice, Hippocampus, 24(11),1300-1307. https://doi.org/10.1002/HIPO.2231

Kõks, S., Dogan, S., Tuna, B. G., González-Navarro, H., Potter, P., & Vandenbroucke, R. E. (2016). Mouse models of ageing and their relevance to disease. Mechanisms of Ageing and Development, 160, 41-53. https://doi.org/10.1016/j.mad.2016.10.001

Kong, L., Li, X. T., Ni, Y. N., Xiao, H. H., Yao, Y. J., Wang, Y. Y., Ju, R. J., Li, H. Y., Liu, J. J., Fu, M., Wu, Y. T., Yang, J. X., & Cheng, L. (2020). Transferrin-Modified Osthole PEGylated Liposomes Travel the Blood-Brain Barrier and Mitigate Alzheimer’s Disease-Related Pathology in APP/PS-1 Mice. International Journal of Nanomedicine, 15, 2841–2858. https://doi.org/10.2147/IJN.S239608

Konsman, J. P. (2022). Cytokines in the Brain and Neuroinflammation: We Didn't Starve the Fire! Pharmaceuticals, 15(2), 140. https://doi.org/10.3390/PH15020140

Kudara, M. Kato-Ishikura, E., Ikegaya, Y., & Matsumoto, N. (2023). Ramelteon administration enhances novel object recognition and spatial working memory in mice,

Journal of Pharmacological Sciences, 152(2), 128–135. https://doi.org/10.1016/J.JPHS.2023.04.002

Kuhn, S., Gritti, L., Crooks, D., & Dombrowski, Y. (2019). Oligodendrocytes in Development, Myelin Generation and Beyond. Cells, 8(11), 1424. https://doi.org/10.3390/CELLS8111424

Kuhnline Sloan, C. D., Nandi, P., Linz, T. H., Aldrich, J. V., Audus, K. L., & Lunte, S. M. (2012). Analytical and Biological Methods for Probing the Blood-Brain Barrier. Annual Review of Analytical Chemistry (Palo Alto, Calif.), 5, 505-531. https://doi.org/10.1146/ANNUREV-ANCHEM-062011-143002

Kulczar, C., Lubin, K. E., Lefebvre, S., Miller, D. W., & Knipp, G. T. (2017). Development of a direct contact astrocyte-human cerebral microvessel endothelial cells blood–brain barrier coculture model. Journal of Pharmacy and Pharmacology, 69(12), 1684–1696. https://doi.org/10.1111/jphp.12803

Kumar, A., Gibbs, J. R., Beilina, A., Dillman, A., Kumaran, R., Trabzuni, D., Ryten, M., Walker, R., Smith, C., Traynor, B. J., Hardy, J., Singleton, A. B., & Cookson, M. R. (2013). Age-associated changes in gene expression in human brain and isolated neurons. Neurobiology of Aging, 34(4), 1199–1209. https://doi.org/10.1016/j.neurobiolaging.2012.10.021

Kuo, Y. C., & Wang, C. T. (2014). Protection of SK-N-MC cells against β-amyloid peptide-induced degeneration using neuron growth factor-loaded liposomes with surface lactoferrin. Biomaterials, 35(22), 5954–5964. https://doi.org/10.1016/J.BIOMATERIALS.2014.03.082

Kuo, Y. C., Lou, Y. I., & Rajesh, R. (2020). Dual functional liposomes carrying antioxidants against tau hyperphosphorylation and apoptosis of neurons. Journal of Drug Targeting, 28(9), 949–960. https://doi.org/10.1080/1061186X.2020.1761819

Kuruca, S. E., Karadenizli, S., Akgun-Dar, K., Kapucu, A., Kaptan, Z., & Uzum, G. (2017). The effects of 17β-estradiol on blood brain barrier integrity in the absence of the estrogen receptor alpha; an in-vitro model. Acta Histochemica, 119(6), 638–647. https://doi.org/10.1016/J.ACTHIS.2017.07.005

Kutuzov, N., Flyvbjerg, H., & Lauritzen, M. (2018). Contributions of the glycocalyx, endothelium, and extravascular compartment to the blood–brain Barrier. Proceedings of the National Academy of Sciences of the United States of America, 115(40), E9429–E9438. https://doi.org/10.1073/PNAS.1802155115/-/DCSUPPLEMENTAL

Labus, J., Häckel, S., Lucka, L., & Danker, K. (2014). Interleukin-1β induces an inflammatory response and the breakdown of the endothelial cell layer in an improved human THBMEC-based in vitro blood-brain barrier model. Journal of Neuroscience Methods, 228, 35–45. https://doi.org/10.1016/J.JNEUMETH.2014.03.002

Lacy, P. (2006). Mechanisms of Degranulation in Neutrophils. Allergy, Asthma, and Clinical Immunology : Official Journal of the Canadian Society of Allergy and Clinical Immunology, 2(3), 98-108. https://doi.org/10.1186/1710-1492-2-3-98

Lam, D., Enright, H. A., Cadena, J., Peters, S. K. G., Sales, A. P., Osburn, J. J., Soscia, D. A., Kulp, K. S., Wheeler, E. K., & Fischer, N. O. (2019). Tissue-specific extracellular matrix accelerates the formation of neural networks and communities in a neuron-glia co-culture on a multi-electrode array. Scientific Reports, 9(1), 1–15. https://doi.org/10.1038/s41598-019-40128-1

Lamson, N. G., Pickering, A. J., Wyckoff, J., Ganesh, P., Calle, E. A., Straehla, J. P., & Hammond, P. T. (2024). Trafficking through the blood–brain barrier is directed by core and outer surface components of layer-by-layer nanoparticles. Bioengineering & Translational Medicine, 9(4), e10636. https://doi.org/10.1002/BTM2.10636

Langeh, U., & Singh, S. (2021). Targeting S100B Protein as a Surrogate Biomarker and its Role in Various Neurological Disorders. Current Neuropharmacology, 19(2), 265-277. https://doi.org/10.2174/1570159X18666200729100427

Latham, A. S., Moreno, J. A., & Geer, C. E. (2023). Biological agents and the aging brain: glial inflammation and neurotoxic signaling. Frontiers in Aging, 4, 1244149. https://doi.org/10.3389/FRAGI.2023.1244149

Lawson, L. J., Perry, V. H., Dri, P., & Gordon, S. (1990). Heterogeneity in the distribution and morphology of microglia in the normal adult mouse brain. Neuroscience, 39(1), 151–170. https://doi.org/10.1016/0306-4522(90)90229-W

Lazar, A. N., Mourtas, S., Youssef, I., Parizot, C., Dauphin, A., Delatour, B., Antimisiaris, S. G., & Duyckaerts, C. (2013). Curcumin-conjugated nanoliposomes with high affinity for Aβ deposits: Possible applications to Alzheimer disease. Nanomedicine: Nanotechnology, Biology and Medicine, 9(5), 712–721. https://doi.org/10.1016/J.NANO.2012.11.004

Le, T. T., Kuplicki, R., Yeh, H. W., Aupperle, R. L., Khalsa, S. S., Simmons, W. K., & Paulus, M. P. (2018). Effect of Ibuprofen on BrainAGE: A Randomized, Placebo-Controlled, Dose-Response Exploratory Study. Biological Psychiatry. Cognitive Neuroscience and Neuroimaging, 3(10), 836-843. https://doi.org/10.1016/J.BPSC.2018.05.002

Lécuyer, M. A., Kebir, H., & Prat, A. (2016). Glial influences on BBB functions and molecular players in immune cell trafficking. Biochimica et Biophysica Acta - Molecular Basis of Disease, 1862(3), 472–482. https://doi.org/10.1016/j.bbadis.2015.10.004

Lee, B. K., Lee, W. J., & Jung, Y. S. (2017). Chrysin Attenuates VCAM-1 Expression and Monocyte Adhesion in Lipopolysaccharide-Stimulated Brain Endothelial Cells by Preventing NF-κB Signaling. International Journal of Molecular Sciences 2017, 18(7), 1424. https://doi.org/10.3390/IJMS18071424

Lee, C. S., & Leong, K. W. (2020). Advances in microphysiological blood-brain barrier (BBB) models towards drug delivery. Current Opinion in Biotechnology, 66, 78-87. Elsevier Ltd. https://doi.org/10.1016/j.copbio.2020.06.009

Lee, H. M., Kim, J. J., Kim, H. J., Shong, M., Ku, B. J., & Jo, E. K. (2013). Upregulated NLRP3 inflammasome activation in patients with type 2 diabetes. Diabetes, 62(1), 194–204. https://doi.org/10.2337/DB12-0420/-/DC1

Lee, K. M., Kim, J. M., Baik, E. J., Ryu, J. H., & Lee, S. H. (2015). Isobavachalcone attenuates lipopolysaccharide-induced ICAM-1 expression in brain endothelial cells through blockade of toll-like receptor 4 signaling pathways. European Journal of Pharmacology, 754, 11–18. https://doi.org/10.1016/J.EJPHAR.2015.02.013

Lee, S. W. L., Campisi, M., Osaki, T., Possenti, L., Mattu, C., Adriani, G., Kamm, R. D., & Chiono, V. (2020). Modeling Nanocarrier Transport across a 3D In Vitro Human Blood-Brain–Barrier Microvasculature. Advanced Healthcare Materials, 9(7), e1901486. https://doi.org/10.1002/adhm.201901486

Lee, S., Kang, B. M., Kim, J. H., Min, J., Kim, H. S., Ryu, H., Park, H., Bae, S., Oh, D., Choi, M., & Suh, M. (2018). Real-time in vivo two-photon imaging study reveals decreased cerebrovascular volume and increased blood-brain barrier permeability in chronically stressed mice. Scientific Reports, 8(1), 13064. https://doi.org/10.1038/s41598-018-30875-y

Levi, S., Ripamonti, M., Moro, A. S., & Cozzi, A. (2024). Iron imbalance in neurodegeneration. Molecular Psychiatry 2024 29:4, 29(4), 1139–1152. https://doi.org/10.1038/s41380-023-02399-z

Lewis, A. J., Seymour, C. W., & Rosengart, M. R. (2016). Current Murine Models of Sepsis. Surgical Infections, 17(4), 385-393. https://doi.org/10.1089/SUR.2016.021

Li, S., Yue-Hong, G., Deng-Ke, T., Jian-Pu, Z., Zhu, C.-Y., Yan, K. E., & Ka, B. (2006). Inflammation of different tissues in spontaneously hypertensive rats. Acta Physiologica Sinica, 58(4), 318–323. http://www.actaps.com.cn

Li, X., Li, C., Zhang, W., Wang, Y., Qian, P., & Huang, H. (2023). Inflammation and aging: signaling pathways and intervention therapies. Signal Transduction and Targeted Therapy, 8(1), 1–29. https://doi.org/10.1038/s41392-023-01502-8

Li, Y., & Wang, J. (2023). Site-specifically radiolabeled nanobodies for imaging blood-brain barrier penetration and targeting in the brain. Journal of Labelled Compounds and Radiopharmaceuticals, 66(14), 444–451. https://doi.org/10.1002/JLCR.4069

Li, Y., Ruan, X., Sun, M., Yuan, M., Song, J., Zhou, Z., Li, H., Ma, Y., Mi, W., & Zhang, X. (2024). Iron deposition participates in LPS-induced cognitive impairment by promoting neuroinflammation and ferroptosis in mice. Experimental Neurology, 379, 114862. https://doi.org/10.1016/J.EXPNEUROL.2024.114862

Liddelow, S. A., Guttenplan, K. A., Clarke, L. E., Bennett, F. C., Bohlen, C. J., Schirmer, L., Bennett, M. L., Münch, A. E., Chung, W. S., Peterson, T. C., Wilton, D. K., Frouin, A., Napier, B. A., Panicker, N., Kumar, M., Buckwalter, M. S., Rowitch, D. H., Dawson, V. L., Dawson, T. M., … Barres, B. A. (2017). Neurotoxic reactive astrocytes are induced by activated microglia. Nature, 541(7638), 481. https://doi.org/10.1038/NATURE21029

Lin, W. W., Lu, Y. C., Huang, B. C., Chuang, C. H., Cheng, Y. A., Chen, I. J., Liu, H. J., Ho, K. W., Liao, T. Y., Liu, E. S., Wu, T. Y., Chang, L. Sen, Hong, S. T., & Cheng, T. L. (2021). Selective activation of pro-anti-IL-1β antibody enhances specificity for autoinflammatory disorder therapy. Scientific Reports, 11(1), 1–10. https://doi.org/10.1038/s41598-021-94298-y

Lindbergh, C. A., Casaletto, K. B., Staffaroni, A. M., Elahi, F., Walters, S. M., You, M., Neuhaus, J., Contreras, W. R., Wang, P., Karydas, A., Brown, J., Wolf, A., Rosen, H., Cobigo, Y., & Kramer, J. H. (2020). Systemic Tumor Necrosis Factor-Alpha Trajectories Relate to Brain Health in Typically Aging Older Adults. The Journals of Gerontology Series A: Biological Sciences and Medical Sciences, 75(8), 1558-1565. https://doi.org/10.1093/GERONA/GLZ209

Lindsberg, P. J., Carpén, O., Paetau, A., Karjalainen-Lindsberg, M. L., & Kaste, M. (1996). Endothelial ICAM-1 expression associated with inflammatory cell response in human ischemic stroke. Circulation, 94(5), 939–945. https://doi.org/10.1161/01.CIR.94.5.939/ASSET/423D1001-425B-4EAA-957E-88100744AD76/ASSETS/GRAPHIC/0030F3.JPEG

Lindwall, C., Olsson, M., Osman, A. M., Kuhn, H. G., & Curtis, M. A. (2013). Selective expression of hyaluronan and receptor for hyaluronan mediated motility (Rhamm) in the adult mouse subventricular zone and rostral migratory stream and in ischemic cortex. Brain Research, 1503, 62–77. https://doi.org/10.1016/J.BRAINRES.2013.01.045

Linville, R. M., & Searson, P. C. (2021). Next-generation in vitro blood–brain barrier models: benchmarking and improving model accuracy. Fluids and Barriers of the CNS, 18(1), 1–7. https://doi.org/10.1186/S12987-021-00291-Y/FIGURES/2

Linville, R. M., DeStefano, J. G., Sklar, M. B., Xu, Z., Farrell, A. M., Bogorad, M. I., Chu, C., Walczak, P., Cheng, L., Mahairaki, V., Whartenby, K. A., Calabresi, P. A., & Searson, P. C. (2019). Human iPSC-derived blood-brain barrier microvessels: validation of barrier function and endothelial cell behavior. Biomaterials, 190–191, 24–37. https://doi.org/10.1016/j.biomaterials.2018.10.023

Lippens, R. J. J. (1999). Liposomal daunorubicin (DaunoXome) in children with recurrent or progressive brain tumors. Pediatric Hematology and Oncology, 16(2), 131–139. https://doi.org/10.1080/088800199277452

Lippmann, E. S., Al-Ahmad, A., Azarin, S. M., Palecek, S. P., & Shusta, E. V. (2014). A retinoic acid-enhanced, multicellular human blood-brain barrier model derived from stem cell sources. Scientific Reports, 4(1), 1–10. https://doi.org/10.1038/srep04160

Lipsman, N., Meng, Y., Bethune, A. J., Huang, Y., Lam, B., Masellis, M., Herrmann, N., Heyn, C., Aubert, I., Boutet, A., Smith, G. S., Hynynen, K., & Black, S. E. (2018). Blood–brain barrier opening in Alzheimer's disease using MR-guided focused ultrasound. Nature Communications, 9(1), 2336. https://doi.org/10.1038/S41467-018-04529-6

Lister, J.P. and Barnes, C.A. (2009) 'Neurobiological Changes in the Hippocampus During Normative Aging', Archives of Neurology, 66(7), 829–833. https://doi.org/10.1001/ARCHNEUROL.2009.125

Liu, B., Liu, J., & Shi, J.-S. (2020). SAMP8 Mice as a Model of Age-Related Cognition Decline with Underlying Mechanisms in Alzheimer's Disease. Journal of Alzheimer's Disease, 75(2), 385–395. https://doi.org/10.3233/jad-200063

Liu, C., Zhang, S., Shi, H., Zhou, H., Zhuang, J., Cao, Y., Ward, N., & Wang, J. (2022). Atp11b Deletion Affects the Gut Microbiota and Accelerates Brain Aging in Mice. Brain Sciences, 12(6), 709. https://doi.org/10.3390/BRAINSCI12060709/S1

Liu, C., Zhang, S., Shi, H., Zhou, H., Zhuang, J., Cao, Y., Ward, N., & Wang, J. (2022). Atp11b Deletion Affects the Gut Microbiota and Accelerates Brain Aging in Mice. Brain Sciences, 12(6), 709. https://doi.org/10.3390/BRAINSCI12060709/S1

Liu, M., Wu, E., Pan, F., Tian, K., Fu, J., Yu, Y., Guo, Z., Ma, Y., Wei, A., Yu, X., Zhan, C., & Qian, J. (2024). Effects of drug-induced liver injury on the in vivo fate of liposomes. European Journal of Pharmaceutics and Biopharmaceutics, 201, 114389. https://doi.org/10.1016/J.EJPB.2024.114389

Liu, P., Zhang, T., Chen, Q., Li, C., Chu, Y., Guo, Q., Zhang, Y., Zhou, W., Chen, H., Zhou, Z., Wang, Y., Zhao, Z., Luo, Y., Li, X., Song, H., Su, B., Li, C., Sun, T., & Jiang, C. (2021). Biomimetic Dendrimer-Peptide Conjugates for Early Multi-Target Therapy of Alzheimer's Disease by Inflammatory Microenvironment Modulation. Advanced Materials (Deerfield Beach, Fla.), 33(26), e2100746. https://doi.org/10.1002/ADMA.202100746

Liu, S., Grigoryan, M. M., Vasilevko, V., Sumbria, R. K., Paganini-Hill, A., Cribbs, D. H., & Fisher, M. J. (2014). Comparative Analysis of H&E and Prussian Blue Staining in a Mouse Model of Cerebral Microbleeds. Journal of Histochemistry and Cytochemistry, 62(11), 767. https://doi.org/10.1369/0022155414546692

Liu, T., Zhang, L., Joo, D., & Sun, S. C. (2017). NF-κB signaling in inflammation. Signal Transduction and Targeted Therapy, 2(1), 1–9. https://doi.org/10.1038/sigtrans.2017.23

Liu, W. Y., Yu, Y., Zang, J., Liu, Y., Li, F. R., Zhang, L., Guo, R. B., Kong, L., Ma, L. Y., & Li, X. T. (2024). Menthol-Modified Quercetin Liposomes with Brain-Targeting Function for the Treatment of Senescent Alzheimer's Disease. American Chemical Society Chemical Neuroscience, 15(11), 2283–2295. https://doi.org/10.1021/ACSCHEMNEURO.4C00109/ASSET/IMAGES/MEDIUM/CN4C00109_0011.GIF

Liu, X., & Quan, N. (2018). Microglia and CNS Interleukin-1: Beyond Immunological Concepts. Frontiers in Neurology, 9(JAN), 1. https://doi.org/10.3389/FNEUR.2018.00008

Liu, Y. C., Gao, X. X., Chen, L., & You, X. qing. (2017). Rapamycin suppresses Aβ25-35- or LPS-induced neuronal inflammation via modulation of NF-κB signaling. Neuroscience, 355, 188–199. https://doi.org/10.1016/J.NEUROSCIENCE.2017.05.005

Logsdon, A. F., Rhea, E. M., Reed, M., Banks, W. A., & Erickson, M. A. (2021). The neurovascular extracellular matrix in health and disease. Experimental Biology and Medicine, 246(7), 835–844. https://doi.org/10.1177/1535370220977195

Loomis, K., Smith, B., Feng, Y., Garg, H., Yavlovich, A., Campbell-Massa, R., Dimitrov, D. S., Blumenthal, R., Xiao, X., & Puri, A. (2010). Specific targeting to B cells by lipid-based nanoparticles conjugated with a novel CD22-ScFv. Experimental and Molecular Pathology, 88(2), 238–249. https://doi.org/10.1016/J.YEXMP.2010.01.006

Lopes-Paciencia, S., Saint-Germain, E., Rowell, M. C., Ruiz, A. F., Kalegari, P., & Ferbeyre, G. (2019). The senescence-associated secretory phenotype and its regulation. Cytokine, 117, 15–22. https://doi.org/10.1016/J.CYTO.2019.01.013

Louveau, A., Harris, T. H., & Kipnis, J. (2015). Revisiting the concept of CNS immune privilege. Trends in Immunology, 36(10), 569-577. https://doi.org/10.1016/J.IT.2015.08.006

Lu, S., Wang, J., Huang, J., Sun, F., Zhu, J., Que, Y., Li, H., Guo, Y., Cai, R., Zhen, Z., Sun, X., & Zhang, Y. (2024). Pegylated liposomal doxorubicin combined with cyclophosphamide and vincristine in pediatric patients with relapsed/refractory solid tumor: a single-arm, open-label, phase I study. eClinicalMedicine, 73, 102701 https://doi.org/10.1016/j.eclinm.2024.102701

Luan, W., Qi, X., Liang, F., Zhang, X., Jin, Z., Shi, L., Luo, B., & Dai, X. (2021). Microglia Impede Oligodendrocyte Generation in Aged Brain. Journal of Inflammation Research, 14, 6813-6831. https://doi.org/10.2147/JIR.S338242

Lueptow, L.M. (2017). Novel Object Recognition Test for the Investigation of Learning and Memory in Mice, Journal of Visualized Experiments : JoVE, 2017(126), 55718. https://doi.org/10.3791/55718.

Lukic, L., Lalic, N. M., Rajkovic, N., Jotic, A., Lalic, K., Milicic, T., Seferovic, J. P., Macesic, M., & Gajovic, J. S. (2014). Hypertension in Obese Type 2 Diabetes Patients is Associated with Increases in Insulin Resistance and IL-6 Cytokine Levels: Potential Targets for an

Efficient Preventive Intervention. International Journal of Environmental Research and Public Health, 11(4), 3586-3698. https://doi.org/10.3390/IJERPH110403586

Lukic-Panin, V., Deguchi, K., Yamashita, T., Shang, J., Zhang, X., Tian, F., Liu, N., Kawai, H., Matsuura, T., & Abe, K. (2012). Free Radical Scavenger Edaravone Administration Protects against Tissue Plasminogen Activator Induced Oxidative Stress and Blood Brain Barrier Damage. Current Neurovascular Research, 7(4), 319–329. https://doi.org/10.2174/156720210793180747

Lundström, Y., Lundström, P., Popova, S. N., Lindblom, R. P. F., & Alafuzoff, I. (2019). Detection of Changes in Immunohistochemical Stains Caused by Postmortem Delay and Fixation Time. Applied Immunohistochemistry and Molecular Morphology, 27(3), 238-245. https://doi.org/10.1097/PAI.0000000000000658

Lv, S., Song, H. L., Zhou, Y., Li, L. X., Cui, W., Wang, W., & Liu, P. (2010). Tumour necrosis factor-α affects blood-brain barrier permeability and tight junction-associated occludin in acute liver failure. Liver International, 30(8), 1198–1210. https://doi.org/10.1111/j.1478-3231.2010.02211.x

Lv, W., Xu, J., Wang, X., Li, X., Xu, Q., & Xin, H. (2018). Bioengineered Boronic Ester Modified Dextran Polymer Nanoparticles as Reactive Oxygen Species Responsive Nanocarrier for Ischemic Stroke Treatment. American Chemical Society Nano, 12(6), 5417–5426. https://doi.org/10.1021/ACSNANO.8B00477/ASSET/IMAGES/LARGE/NN-2018-004776_0005.JPEG

Lyons, A., Downer, E. J., Crotty, S., Nolan, Y. M., Mills, K. H. G., & Lynch, M. A. (2007). CD200 Ligand–Receptor Interaction Modulates Microglial Activation In Vivo and In Vitro: A Role for IL-4. The Journal of Neuroscience, 27(31), 8309-1313. https://doi.org/10.1523/JNEUROSCI.1781-07.2007

M Leite, D., Matias, D., & Battaglia, G. (2020). The Role of BAR Proteins and the Glycocalyx in Brain Endothelium Transcytosis. Cells, 9(12), 2685. https://doi.org/10.3390/CELLS9122685

Machin, D. R., Bloom, S. I., Campbell, R. A., Phuong, T. T. T., Gates, P. E., Lesniewski, L. A., Rondina, M. T., & Donato, A. J. (2018). Vascular Biology and Microcirculation: Advanced age results in a diminished endothelial glycocalyx. American Journal of Physiology - Heart and Circulatory Physiology, 315(3), H531- H539. https://doi.org/10.1152/AJPHEART.00104.2018

Mackic, J. B., Bading, J., Ghiso, J., Walker, L., Wisniewski, T., Frangione, B., & Zlokovic, B. V. (2002). Circulating amyloid-β peptide crosses the blood-brain barrier in aged monkeys and contributes to Alzheimer's disease lesions. Vascular Pharmacology, 38(6), 303–313. https://doi.org/10.1016/S1537-1891(02)00198-2

Maggioli, E., McArthur, S., Mauro, C., Kieswich, J., Kusters, D. H. M., Reutelingsperger, C. P. M., Yaqoob, M., & Solito, E. (2016). Estrogen protects the blood–brain barrier from inflammation-induced disruption and increased lymphocyte trafficking. Brain, Behavior, and Immunity, 51, 212–222. https://doi.org/10.1016/j.bbi.2015.08.020

Malenfant, J. H., & Batsis, J. A. (2019). Obesity in the geriatric population – a global health perspective. Journal of Global Health Reports, 3, e2019045. https://doi.org/10.29392/JOGHR.3.E2019045

Manda-Handzlik, A., & Demkow, U. (2019). The Brain Entangled: The Contribution of Neutrophil Extracellular Traps to the Diseases of the Central Nervous System. Cells, 8(12), 1477. https://doi.org/10.3390/CELLS8121477

Manglani, M., Rua, R., Hendricksen, A., Braunschweig, D., Gao, Q., Tan, W., Houser, B., McGavern, D. B., & Oh, K. (2019). Method to Quantify Cytokines and Chemokines in Mouse Brain Tissue Using Bio-Plex Multiplex Immunoassays. Methods (San Diego, Calif.), 158, 22-26. https://doi.org/10.1016/J.YMETH.2019.02.007

Mangold, C.A., Wronowski, B., Du, M., Masser, D.R., Hadad, N., Bixler, G.V., Brucklacher, R.M., Ford, M.M., Sonntag, W.E., & Freeman, W.M. (2017). Sexually divergent induction of microglial-associated neuroinflammation with hippocampal aging. Journal of Neuroinflammation, 14(1), 141. https://doi.org/10.1186/S12974-017-0920-8.

Marcum, Z. A., & Hanlon, J. T. (2010). Recognizing the Risks of Chronic Nonsteroidal Anti-Inflammatory Drug Use in Older Adults. The Annals of Long-Term Care : The Official Journal of the American Medical Directors Association, 18(9), 24-27. https://pubmed.ncbi.nlm.nih.gov/21857795/

Marschallinger, J., Iram, T., Zardeneta, M., Lee, S. E., Lehallier, B., Haney, M. S., Pluvinage, J. V., Mathur, V., Hahn, O., Morgens, D. W., Kim, J., Tevini, J., Felder, T. K., Wolinski, H., Bertozzi, C. R., Bassik, M. C., Aigner, L., & Wyss-Coray, T. (2020). Lipid droplet accumulating microglia represent a dysfunctional and pro-inflammatory state in the aging brain. Nature Neuroscience, 23(2), 194-208. https://doi.org/10.1038/S41593-019-0566-1

Martano, S., De Matteis, V., Cascione, M., & Rinaldi, R. (2022). Inorganic Nanomaterials versus Polymer-Based Nanoparticles for Overcoming Neurodegeneration. Nanomaterials, 12(14), 2337. https://doi.org/10.3390/NANO12142337

Martens, R. J. H., Vink, H., Van Oostenbrugge, R. J., & Staals, J. (2013). Sublingual microvascular glycocalyx dimensions in lacunar stroke patients. Cerebrovascular Diseases (Basel, Switzerland), 35(5), 451–454. https://doi.org/10.1159/000348854

Mason McClatchey, P., Schafer, M., Hunter, K. S., & Reusch, J. E. B. (2016). The endothelial glycocalyx promotes homogenous blood flow distribution within the microvasculature. American Journal of Physiology - Heart and Circulatory Physiology, 311(1), H168–H176. https://doi.org/10.1152/AJPHEART.00132.2016/ASSET/IMAGES/LARGE/ZH401116196200 06.JPEG

Mathew, A., Fukuda, T., Nagaoka, Y., Hasumura, T., Morimoto, H., Yoshida, Y., Maekawa, T., Venugopal, K., & Kumar, D. S. (2012). Curcumin loaded-PLGA nanoparticles conjugated with Tet-1 peptide for potential use in Alzheimer's disease. PloS One, 7(3), e32616. https://doi.org/10.1371/JOURNAL.PONE.0032616

Matthews, F.E., Arthur, A., Barnes, L.E., Bond, J., Jagger, C., Robinson, L., & Brayne, C. (2013). A two-decade comparison of prevalence of dementia in individuals aged 65 years and older from three geographical areas of England: results of the Cognitive Function and Ageing Study I and II' Lancet (London, England), 382(9902), 1405-1412. https://doi.org/10.1016/S0140-6736(13)61570-6

Mayor, S., & Pagano, R. E. (2007). Pathways of clathrin-independent endocytosis. Nature Reviews Molecular Cell Biology, 8(8), 603–612. https://doi.org/10.1038/nrm2216

Mbagwu, S. I., & Filgueira, L. (2020). Differential expression of CD31 and von willebrand factor on endothelial cells in different regions of the human brain: Potential implications for cerebral malaria pathogenesis. Brain Sciences, 10(1), 31. https://doi.org/10.3390/brainsci10010031

McAteer, M. A., Sibson, N. R., Von Zur Muhlen, C., Schneider, J. E., Lowe, A. S., Warrick, N., Channon, K. M., Anthony, D. C., & Choudhury, R. P. (2007). In vivo magnetic resonance imaging of acute brain inflammation using microparticles of iron oxide. Nature Medicine, 13(10), 1253-1258. https://doi.org/10.1038/NM1631

McHale, J.F., Harari, O.A., Marshall, D., & Haskard, D.O. (1999) 'TNF-α and IL-1 Sequentially Induce Endothelial ICAM-1 and VCAM-1 Expression in MRL/lpr Lupus-Prone Mice', The Journal of Immunology, 163(7), 3993–4000. https://doi.org/10.4049/JIMMUNOL.163.7.3993

McIntosh, A., Mela, V., Harty, C., Minogue, A. M., Costello, D. A., Kerskens, C., & Lynch, M. A. (2019). Iron accumulation in microglia triggers a cascade of events that leads to altered metabolism and compromised function in APP/PS1 mice. Brain Pathology, 29(5), 606-621. https://doi.org/10.1111/BPA.12704

McMahon, D., & Hynynen, K. (2017). Acute Inflammatory Response Following Increased Blood-Brain Barrier Permeability Induced by Focused Ultrasound is Dependent on Microbubble Dose. Theranostics, 7(16), 3989-4000. https://doi.org/10.7150/THNO.21630

McNamara, K. M., Harwood, D. T., Simanainen, U., Walters, K. A., Jimenez, M., & Handelsman, D. J. (2010). Measurement of sex steroids in murine blood and reproductive tissues by liquid chromatography-tandem mass spectrometry. The Journal of Steroid Biochemistry and Molecular Biology, 121(3–5), 611–618. https://doi.org/10.1016/J.JSBMB.2010.02.001

Mecca, C., Giambanco, I., Donato, R., & Arcuri, C. (2018). Microglia and Aging: The Role of the TREM2–DAP12 and CX3CL1-CX3CR1 Axes. International Journal of Molecular Sciences, 19(1), 318. https://doi.org/10.3390/IJMS19010318

Meier, H. C. S., Mitchell, C., Karadimas, T., & Faul, J. D. (2023). Systemic inflammation and biological aging in the Health and Retirement Study. GeroScience, 45(6), 3257-3265. https://doi.org/10.1007/S11357-023-00880-9

Melzer, L., Freiman, T. M., & Derouiche, A. (2021). Rab6A as a Pan-Astrocytic Marker in Mouse and Human Brain, and Comparison with Other Glial Markers (GFAP, GS, Aldh1L1, SOX9). Cells, 10(1), 72. https://doi.org/10.3390/cells10010072

Meng, F., Asghar, S., Gao, S., Su, Z., Song, J., Huo, M., Meng, W., Ping, Q., & Xiao, Y. (2015). A novel LDL-mimic nanocarrier for the targeted delivery of curcumin into the brain to treat Alzheimer's disease. Colloids and Surfaces B: Biointerfaces, 134, 88–97. https://doi.org/10.1016/J.COLSURFB.2015.06.025

Menna, E., Zambetti, S., Morini, R., Donzelli, A., Disanza, A., Calvigioni, D., Braida, D., Nicolini, C., Orlando, M., Fossati, G., Cristina Regondi, M., Pattini, L., Frassoni, C., Francolini, M., Scita, G., Sala, M., Fahnestock, M., & Matteoli, M. (2013). Eps8 controls dendritic spine density and synaptic plasticity through its actin-capping activity. EMBO Journal, 32(12), 1730–1744. https://doi.org/10.1038/EMBOJ.2013.107/SUPPL_FILE/EMBJ2013107.REVIEWER_COMMENTS.PDF

Mi, X. J., Le, H. M., Lee, S., Park, H. R., & Kim, Y. J. (2022). Silymarin-Functionalized Selenium Nanoparticles Prevent LPS-Induced Inflammatory Response in RAW264.7 Cells through Downregulation of the PI3K/Akt/NF-κB Pathway. ACS Omega, 7(47), 42723–42732. https://doi.org/10.1021/ACSOMEGA.2C04140/ASSET/IMAGES/LARGE/AO2C04140_0006.JPEG

Michael, B. D., Griffiths, M. J., Granerod, J., Brown, D., Keir, G., Wnęk, G., Cox, D. J., Vidyasagar, R., Borrow, R., Parkes, L. M., & Solomon, T. (2016). The Interleukin-1 Balance During Encephalitis Is Associated With Clinical Severity, Blood-Brain Barrier Permeability, Neuroimaging Changes, and Disease Outcome. The Journal of Infectious Diseases, 213(10), 1651-1660. https://doi.org/10.1093/INFDIS/JIV771

Miguel-Hidalgo, J. J., Nithuairisg, S., Stockmeier, C., & Rajkowska, G. (2007). Distribution of ICAM-1 immunoreactivity during aging in the human orbitofrontal cortex. Brain, Behavior, and Immunity, 21(1), 100–111. https://doi.org/10.1016/J.BBI.2006.05.001

Minogue, A. M., Barrett, J. P., & Lynch, M. A. (2012). LPS-induced release of IL-6 from glia modulates production of IL-1β in a JAK2-dependent manner. Journal of Neuroinflammation, 9, 126. https://doi.org/10.1186/1742-2094-9-126

Mitoma, H., Horiuchi, T., Hatta, N., Tsukamoto, H., Harashima, S. I., Kikuchi, Y., Otsuka, J., Okamura, S., Fujita, S., & Harada, M. (2005). Infliximab induces potent anti-inflammatory responses by outside-to-inside signals through transmembrane TNF-α. Gastroenterology, 128(2), 376–392. https://doi.org/10.1053/j.gastro.2004.11.060

Mittal, K. R., Pharasi, N., Sarna, B., Singh, M., Rachana, Haider, S., Singh, S. K., Dua, K., Jha, S. K., Dey, A., Ojha, S., Mani, S., & Jha, N. K. (2022). Nanotechnology-based drug delivery for the treatment of CNS disorders. Translational Neuroscience, 13(1), 527-546. https://doi.org/10.1515/TNSCI-2022-0258

Moiseeva, O., Deschênes-Simard, X., St-Germain, E., Igelmann, S., Huot, G., Cadar, A. E., Bourdeau, V., Pollak, M. N., & Ferbeyre, G. (2013). Metformin inhibits the senescence-associated secretory phenotype by interfering with IKK/NF-κB activation. Aging Cell, 12(3), 489–498. https://doi.org/10.1111/ACEL.12075

Mol, S., Hafkamp, F. M. J., Varela, L., Simkhada, N., Taanman-Kueter, E. W., Tas, S. W., Wauben, M. H. M., Kormelink, T. G., & de Jong, E. C. (2021). Efficient neutrophil activation requires two simultaneous activating stimuli. International Journal of Molecular Sciences, 22(18), 10106. https://doi.org/10.3390/IJMS221810106/S1

Molino, Y., Jabès, F., Lacassagne, E., Gaudin, N., & Khrestchatisky, M. (2014). Setting-up an in vitro model of rat blood-brain barrier (BBB): A focus on BBB impermeability and receptor-mediated transport. Journal of Visualized Experiments, 88(88), 51278. https://doi.org/10.3791/51278

Mondal, S., & Ghosh, S. (2023). Liposome-Mediated Anti-Viral Drug Delivery Across Blood–Brain Barrier: Can Lipid Droplet Target Be Game Changers? Cellular and Molecular Neurobiology, 44(1), 1–22. https://doi.org/10.1007/S10571-023-01443-4

Monge-Fuentes, V., Biolchi Mayer, A., Lima, M.R., Geraldes, L.R., Zanotto, L.N., Moreira, K.G., Martins, O.P., Piva, H.L., Felipe, M.S.S., Amaral, A.C., Bocca, A.L., Tedesco, A.C., & Mortari, M.R. (2021). Dopamine-loaded nanoparticle systems circumvent the blood–brain barrier restoring motor function in mouse model for Parkinson's Disease, Scientific Reports, 11(1), 15185. https://doi.org/10.1038/S41598-021-94175-8.

Monif, M., Reid, C. A., Powell, K. L., Drummond, K. J., O'Brien, T. J., & Williams, D. A. (2016). Interleukin-1β has trophic effects in microglia and its release is mediated by P2X7R pore. Journal of Neuroinflammation, 13(1), 1–15. https://doi.org/10.1186/S12974-016-0621-8/FIGURES/7

Montagne, A., Barnes, S. R., Sweeney, M. D., Halliday, M. R., Sagare, A. P., Zhao, Z., Toga, A. W., Jacobs, R. E., Liu, C. Y., Amezcua, L., Harrington, M. G., Chui, H. C., Law, M., & Zlokovic, B. V. (2015). Blood-Brain barrier breakdown in the aging human hippocampus. Neuron, 85(2), 296–302. https://doi.org/10.1016/j.neuron.2014.12.032

Montagne, A., Gauberti, M., Macrez, R., Jullienne, A., Briens, A., Raynaud, J. S., Louin, G., Buisson, A., Haelewyn, B., Docagne, F., Defer, G., Vivien, D., & Maubert, E. (2012). Ultra-sensitive molecular MRI of cerebrovascular cell activation enables early detection of chronic central nervous system disorders. NeuroImage, 63(2), 760–770. https://doi.org/10.1016/J.NEUROIMAGE.2012.07.018

Montagne, A., Zhao, Z., & Zlokovic, B. V. (2017). Alzheimer's disease: A matter of blood-brain barrier dysfunction? In Journal of Experimental Medicine, 214(11). 3151-3169. https://doi.org/10.1084/jem.20171406

Montizaan, D., Yang, K., Reker-Smit, C., & Salvati, A. (2020). Comparison of the uptake mechanisms of zwitterionic and negatively charged liposomes by HeLa cells, Nanomedicine: Nanotechnology, Biology and Medicine, 30, 102300. https://doi.org/10.1016/J.NANO.2020.102300.

Moon, Y., Lim, C., Kim, Y., & Moon, W.J. (2021). Sex-Related Differences in Regional Blood–Brain Barrier Integrity in Non-Demented Elderly Subjects, International Journal of Molecular Sciences, 22(6), 1–15. https://doi.org/10.3390/IJMS22062860

Mooradian, A. D., Haas, M. J., & Chehade, J. M. (2003). Age-related changes in rat cerebral occludin and zonula occludens-1 (ZO-1). Mechanisms of Ageing and Development, 124(2), 143–146. https://doi.org/10.1016/S0047-6374(02)00041-6

Morris, A. W. J., Carare, R. O., Schreiber, S., & Hawkes, C. A. (2014). The Cerebrovascular Basement Membrane: Role in the Clearance of β-amyloid and Cerebral Amyloid Angiopathy. Frontiers in Aging Neuroscience, 6(SEP), 251. https://doi.org/10.3389/FNAGI.2014.00251

Morse, S. V., Mishra, A., Chan, T. G., T. M. de Rosales, R., & Choi, J. J. (2022). Liposome delivery to the brain with rapid short pulses of focused ultrasound and microbubbles. Journal of Controlled Release, 341, 605–615. https://doi.org/10.1016/J.JCONREL.2021.12.005

Mota, B. C., & Kelly, A. M. (2020). Exercise alters LPS-induced glial activation in the mouse brain. Neuronal Signaling, 4(4), 1–14. https://doi.org/10.1042/NS20200003

Mourtas, S., Lazar, A. N., Markoutsa, E., Duyckaerts, C., & Antimisiaris, S. G. (2014). Multifunctional nanoliposomes with curcumin–lipid derivative and brain targeting functionality with potential applications for Alzheimer disease. European Journal of Medicinal Chemistry, 80, 175–183. https://doi.org/10.1016/J.EJMECH.2014.04.050

Mouton, P.R., Long, J.M., Lei, D.L., Howard, V., Jucker, M., Calhoun M.E., & Ingram D.K. (2002) 'Age and gender effects on microglia and astrocyte numbers in brains of mice', Brain Research, 956(1), 30–35. https://doi.org/10.1016/S0006-8993(02)03475-3

Moynagh, P. N., Williams, D. C., & O'Neill, L. A. (1994). Activation of NF-kappa B and induction of vascular cell adhesion molecule-1 and intracellular adhesion molecule-1 expression in human glial cells by IL-1. Modulation by antioxidants. The Journal of Immunology, 153(6), 2681–2690. https://doi.org/10.4049/JIMMUNOL.153.6.2681

Muldoon, L. L., Alvarez, J. I., Begley, D. J., Boado, R. J., Del Zoppo, G. J., Doolittle, N. D., Engelhardt, B., Hallenbeck, J. M., Lonser, R. R., Ohlfest, J. R., Prat, A., Scarpa, M., Smeyne, R. J., Drewes, L. R., & Neuwelt, E. A. (2013). Immunologic privilege in the central nervous system and the blood-brain barrier. In Journal of Cerebral Blood Flow and Metabolism, 33 (1), 13-21, https://doi.org/10.1038/jcbfm.2012.153

Murali, K., Kenesei, K., Li, Y., Demeter, K., Környei, Z., & Madarász, E. (2015). Uptake and bio-reactivity of polystyrene nanoparticles is affected by surface modifications, ageing and LPS adsorption: in vitro studies on neural tissue cells. Nanoscale, 7(9), 4199–4210. https://doi.org/10.1039/C4NR06849A

Murman, D.L. (2015). The Impact of Age on Cognition, Seminars in Hearing, 36(3), 111. https://doi.org/10.1055/S-0035-1555115

Murray, K. N., Parry-Jones, A. R., & Allan, S. M. (2015). Interleukin-1 and acute brain injury. Frontiers in Cellular Neuroscience, 9(FEB), 123775. https://doi.org/10.3389/FNCEL.2015.00018/BIBTEX

Murtaj, V., Belloli, S., Di Grigoli, G., Pannese, M., Ballarini, E., Rodriguez-Menendez, V., Marmiroli, P., Cappelli, A., Masiello, V., Monterisi, C., Bellelli, G., Panina-Bordignon, P., & Moresco, R. M. (2019). Age and Sex Influence the Neuro-inflammatory Response to a Peripheral Acute LPS Challenge. Frontiers in Aging Neuroscience, 11, 299. https://doi.org/10.3389/FNAGI.2019.00299/BIBTEX

Murugesan, N., Demarest, T. G., Madri, J. A., & Pachter, J. S. (2012). Brain regional angiogenic potential at the neurovascular unit during normal aging. Neurobiology of Aging, 33(5), 1004.e1-1004.e16. https://doi.org/10.1016/J.NEUROBIOLAGING.2011.09.022

Musafargani, S., Mishra, S., Gulyás, M., Mahalakshmi, P., Archunan, G., Padmanabhan, P., & Gulyás, B. (2020). Blood brain barrier: A tissue engineered microfluidic chip. Journal of Neuroscience Methods, 331, 108525. https://doi.org/10.1016/J.JNEUMETH.2019.108525

Muscetti, O., Blal, N., Mollo, V., Netti, P. A., & Guarnieri, D. (2023). Intracellular Localization during Blood–Brain Barrier Crossing Influences Extracellular Release and Uptake of Fluorescent Nanoprobes. Nanomaterials, 13(13), 1999. https://doi.org/10.3390/NANO13131999

Nahirney, P. C., Reeson, P., & Brown, C. E. (2016). Ultrastructural analysis of blood-brain barrier breakdown in the peri-infarct zone in young adult and aged mice. Journal of Cerebral Blood Flow and Metabolism, 36(2), 413–425. https://doi.org/10.1177/0271678X15608396

Nakagomi, T., Kubo, S., Nakano-Doi, A., Sakuma, R., Lu, S., Narita, A., Kawahara, M., Taguchi, A., & Matsuyama, T. (2015). Brain vascular pericytes following ischemia have multipotential stem cell activity to differentiate into neural and vascular lineage cells. Stem Cells, 33(6), 1962–1974. https://doi.org/10.1002/stem.1977

Nakata, M., Nakagomi, T., Maeda, M., Nakano-Doi, A., Momota, Y., & Matsuyama, T. (2017). Induction of Perivascular Neural Stem Cells and Possible Contribution to Neurogenesis

Following Transient Brain Ischemia/Reperfusion Injury. Translational Stroke Research, 8(2), 131–143. https://doi.org/10.1007/s12975-016-0479-1

Naler, L. B., Hsieh, Y. P., Geng, S., Zhou, Z., Li, L., & Lu, C. (2022). Epigenomic and transcriptomic analyses reveal differences between low-grade inflammation and severe exhaustion in LPS-challenged murine monocytes. Communications Biology, 5(1), 102. https://doi.org/10.1038/S42003-022-03035-2

Nassrally, M. S., Lau, A., Wise, K., John, N., Kotecha, S., Lee, K. L., & Brooks, R. F. (2019). Cell cycle arrest in replicative senescence is not an immediate consequence of telomere dysfunction. Mechanisms of Ageing and Development, 179, 11–22. https://doi.org/10.1016/J.MAD.2019.01.009

Nation, D. A., Sweeney, M. D., Montagne, A., Sagare, A. P., D'Orazio, L. M., Pachicano, M., Sepehrband, F., Nelson, A. R., Buennagel, D. P., Harrington, M. G., Benzinger, T. L. S., Fagan, A. M., Ringman, J. M., Schneider, L. S., Morris, J. C., Chui, H. C., Law, M., Toga, A. W., & Zlokovic, B. V. (2019). Blood–brain barrier breakdown is an early biomarker of human cognitive dysfunction. Nature Medicine, 25(2), 270–276. https://doi.org/10.1038/s41591-018-0297-y

Nelson, J. F., Felicio, L. S., Osterburg, H. H., & Finch, C. E. (1981). Altered profiles of estradiol and progesterone associated with prolonged estrous cycles and persistent vaginal cornification in aging C57BL/6J mice. Biology of Reproduction, 24(4), 784–794. https://doi.org/10.1095/BIOLREPROD24.4.784

Neves, A. R., Queiroz, J. F., & Reis, S. (2016a). Brain-targeted delivery of resveratrol using solid lipid nanoparticles functionalized with apolipoprotein E. Journal of Nanobiotechnology, 14(1), 27. https://doi.org/10.1186/S12951-016-0177-X

Nikodemova, M., Small, A. L., Kimyon, R. S., & Watters, J. J. (2016). Age-dependent differences in microglial responses to systemic inflammation are evident as early as middle age. Physiological Genomics, 48(5), 336-344. https://doi.org/10.1152/PHYSIOLGENOMICS.00129.2015

Nikolakopoulou, A. M., Zhao, Z., Montagne, A., & Zlokovic, B. V. (2017). Regional early and progressive loss of brain pericytes but not vascular smooth muscle cells in adult mice with disrupted platelet-derived growth factor receptor-β signaling. PLoS ONE, 12(4), e0176225. https://doi.org/10.1371/journal.pone.0176225

Noh, B., Blasco-Conesa, M. P., Rahman, S. M., Monga, S., Ritzel, R., Guzman, G., Lai, Y. J., Ganesh, B. P., Urayama, A., McCullough, L. D., & Moruno-Manchon, J. F. (2023). Iron overload induces cerebral endothelial senescence in aged mice and in primary culture in a sex-dependent manner. Aging Cell, 22(11), e13977. https://doi.org/10.1111/ACEL.13977

Nonaka, N., Farr, S. A., Kageyama, H., Shioda, S., & Banks, W. A. (2008). Delivery of Galanin-Like Peptide to the Brain: Targeting with Intranasal Delivery and Cyclodextrins. Journal of Pharmacology and Experimental Therapeutics, 325(2), 513–519. https://doi.org/10.1124/JPET.107.132381

Noori, M. S., Courreges, M. C., Bergmeier, S. C., McCall, K. D., & Goetz, D. J. (2020). Modulation of LPS-induced inflammatory cytokine production by a novel glycogen synthase kinase-3 inhibitor. European Journal of Pharmacology, 883, 173340. https://doi.org/10.1016/J.EJPHAR.2020.173340

Nyúl-Tóth, Á., Tarantini, S., DelFavero, J., Yan, F., Balasubramanian, P., Yabluchanskiy, A., Ahire, C., Kiss, T., Csipo, T., Lipecz, A., Farkas, A. E., Wilhelm, I., Krizbai, I. A., Tang, Q., Csiszar, A., & Ungvari, Z. (2021). Demonstration of age-related blood-brain barrier disruption and cerebromicrovascular rarefaction in mice by longitudinal intravital two-photon microscopy and optical coherence tomography. American Journal of Physiology - Heart and Circulatory Physiology, 320(4), H1370–H1392. https://doi.org/10.1152/AJPHEART.00709.2020

O'Brown, N. M., Pfau, S. J., & Gu, C. (2018). Bridging barriers: A comparative look at the blood-brain barrier across organisms. Genes and Development, 32(7-8), 466-478. https://doi.org/10.1101/gad.309823.117

O'Carroll, S. J., Kho, D. T., Wiltshire, R., Nelson, V., Rotimi, O., Johnson, R., Angel, C. E., & Graham, E. S. (2015). Pro-inflammatory TNFαα and IL-1β differentially regulate the inflammatory phenotype of brain microvascular endothelial cells. Journal of Neuroinflammation, 12(1), 1–18. https://doi.org/10.1186/S12974-015-0346-0/FIGURES/8

O'Leary, L. A., Davoli, M. A., Belliveau, C., Tanti, A., Ma, J. C., Farmer, W. T., Turecki, G., Murai, K. K., & Mechawar, N. (2020). Characterization of Vimentin-Immunoreactive Astrocytes in the Human Brain. Frontiers in Neuroanatomy, 14, 31. https://doi.org/10.3389/fnana.2020.00031

O'Neil, S. M., Witcher, K. G., McKim, D. B., & Godbout, J. P. (2018). Forced turnover of aged microglia induces an intermediate phenotype but does not rebalance CNS environmental cues driving priming to immune challenge. Acta Neuropathologica Communications, 6(1), 129. https://doi.org/10.1186/S40478-018-0636-8/FIGURES/9

Ogrodnik, M. (2021a). Cellular aging beyond cellular senescence: Markers of senescence prior to cell cycle arrest in vitro and in vivo. Aging Cell, 20(4), e13338. https://doi.org/10.1111/ACEL.13338

Ohara, Y., McCarron, R.M., Hoffman, T.T., Sugano, H., Bembry, J., Lenz, F.A., & Spatz, M. (2000) 'Adrenergic mediation of TNF alpha-stimulated ICAM-1 expression on human brain microvascular endothelial cells', Acta neurochirurgica. Supplement, 76,117–120. https://doi.org/10.1007/978-3-7091-6346-7_24

Ohene, Y., Harrison, I. F., Evans, P. G., Thomas, D. L., Lythgoe, M. F., & Wells, J. A. (2021). Increased blood–brain barrier permeability to water in the aging brain detected using noninvasive multi-TE ASL MRI. Magnetic Resonance in Medicine, 85(1), 326–333. https://doi.org/10.1002/MRM.28496

Ohmori, Y., & Hamilton, T. A. (2001). Requirement for STAT1 in LPS-induced gene expression in macrophages. Journal of Leukocyte Biology, 69(4), 598–604. https://doi.org/10.1189/JLB.69.4.598

Ohta, S., Kikuchi, E., Ishijima, A., Azuma, T., Sakuma, I., & Ito, T. (2020). Investigating the optimum size of nanoparticles for their delivery into the brain assisted by focused ultrasound-induced blood–brain barrier opening. Scientific Reports, 10(1), 1–13. https://doi.org/10.1038/s41598-020-75253-9

Oike, H., Ogawa, Y., & Azami, K. (2020). Long-Term Feeding of a High-Fat Diet Ameliorated Age-Related Phenotypes in SAMP8 Mice. Nutrients, 12(5), 1416. https://doi.org/10.3390/NU12051416

Oliveira, A.M., Hawk, J.D., Abel, T., & Havekes, R. (2010). Post-training reversible inactivation of the hippocampus enhances novel object recognition memory. Learning & Memory, 17(3), 155-160. https://doi.org/10.1101/LM.1625310.

Oria, M., Figueira, R. L., Scorletti, F., Sbragia, L., Owens, K., Li, Z., Pathak, B., Corona, M. U., Marotta, M., Encinas, J. L., & Peiro, J. L. (2018). CD200-CD200R imbalance correlates with microglia and pro-inflammatory activation in rat spinal cords exposed to amniotic fluid in retinoic acid-induced spina bifida. Scientific Reports, 8(1), 1–12. https://doi.org/10.1038/s41598-018-28829-5

Orre, M., Kamphuis, W., Osborn, L. M., Melief, J., Kooijman, L., Huitinga, I., Klooster, J., Bossers, K., & Hol, E. M. (2014). Acute isolation and transcriptome characterization of cortical astrocytes and microglia from young and aged mice. Neurobiology of Aging, 35(1), 1–14. https://doi.org/10.1016/j.neurobiolaging.2013.07.008

Osgood, D., Miller, M. C., Messier, A. A., Gonzalez, L., & Silverberg, G. D. (2017). Aging alters mRNA expression of amyloid transporter genes at the blood-brain barrier. Neurobiology of Aging, 57, 178–185. https://doi.org/10.1016/j.neurobiolaging.2017.05.011

Osipova, E. D., Komleva, Y. K., Morgun, A. V., Lopatina, O. L., Panina, Y. A., Olovyannikova, R. Ya., Vais, E. F., Salmin, V. V., & Salmina, A. B. (2018). Designing in vitro Blood-Brain Barrier Models Reproducing Alterations in Brain Aging. Frontiers in Aging Neuroscience, 10, 234. https://doi.org/10.3389/fnagi.2018.00234

Otgongerel, D., Lee, H. J., & Jo, S. A. (2023). Induction of ICAM1 in Brain Vessels is Implicated in an Early AD Pathogenesis by Modulating Neprilysin. Neuromolecular Medicine, 25(2), 193–204. https://doi.org/10.1007/S12017-022-08726-X

Palmer, A. L., & Ousman, S. S. (2018a). Astrocytes and aging. Frontiers in Aging Neuroscience, 10, 337. https://doi.org/10.3389/fnagi.2018.00337

Pan, J., Ma, N., Zhong, J., Yu, B., Wan, J., & Zhang, W. (2021) 'Age-associated changes in microglia and astrocytes ameliorate blood-brain barrier dysfunction', Molecular Therapy: Nucleic Acid, 26, 970–986. https://doi.org/10.1016/j.omtn.2021.08.030

Pandit, R., Koh, W.K., Sullivan, R.K.P., Palliyaguru, T., Parton R.G., & Götz J. (2020). Role for caveolin-mediated transcytosis in facilitating transport of large cargoes into the brain via ultrasound , Journal of Controlled Release, 327, 667–675. https://doi.org/10.1016/J.JCONREL.2020.09.015

Pardridge, W. M. (2005). The Blood-Brain Barrier: Bottleneck in Brain Drug Development. NeuroRx, 2(1), 3-14. https://doi.org/10.1602/NEURORX.2.1.3

Pardridge, W. M. (2012). Drug transport across the blood–brain barrier. Journal of Cerebral Blood Flow & Metabolism, 32(11), 1959. https://doi.org/10.1038/JCBFM.2012.126

Park, L., Koizumi, K., El Jamal, S., Zhou, P., Previti, M. Lou, Van Nostrand, W. E., Carlson, G., & Iadecola, C. (2014). Age-dependent neurovascular dysfunction and damage in a mouse model of cerebral amyloid angiopathy. Stroke, 45(6), 1815–1821. https://doi.org/10.1161/STROKEAHA.114.005179

Park, M. H., Lee, J. Y., Park, K. H., Jung, I. K., Kim, K. T., Lee, Y. S., Ryu, H. H., Jeong, Y., Kang, M., Schwaninger, M., Gulbins, E., Reichel, M., Kornhuber, J., Yamaguchi, T., Kim, H. J., Kim, S. H., Schuchman, E. H., Jin, H. K., & Bae, J. sung. (2018). Vascular and Neurogenic

Rejuvenation in Aging Mice by Modulation of ASM. Neuron, 100(1), 167-182.e9. https://doi.org/10.1016/j.neuron.2018.09.010

Parkhurst, C. N., Yang, G., Ninan, I., Savas, J. N., Yates, J. R., Lafaille, J. J., Hempstead, B. L., Littman, D. R., & Gan, W. B. (2013). Microglia promote learning-dependent synapse formation through BDNF. Cell, 155(7), 1596-1609. https://doi.org/10.1016/J.CELL.2013.11.030

Parks, E. E., Logan, S., Yeganeh, A., Farley, J. A., Owen, D. B., & Sonntag, W. E. (2020). Interleukin 6 reduces allopregnanolone synthesis in the brain and contributes to age-related cognitive decline in mice. Journal of Lipid Research, 61(10), 1308-1319. https://doi.org/10.1194/JLR.RA119000479

Parrott, J. M., Oster, T., & Lee, H. Y. (2021). Altered inflammatory response in FMRP-deficient microglia. IScience, 24(11), 103293. https://doi.org/10.1016/J.ISCI.2021.103293

Parry-Jones, A. R., Stocking, K., MacLeod, M. J., Clarke, B., Werring, D. J., Muir, K. W., & Vail, A. (2023). Phase II randomised, placebo-controlled, clinical trial of interleukin-1 receptor antagonist in intracerebral haemorrhage: BLOcking the Cytokine IL-1 in ICH (BLOC-ICH). European Stroke Journal, 8(3), 819–827. https://doi.org/10.1177/23969873231185208

Partridge, L., Deelen, J., & Slagboom, P. E. (2018). Facing up to the global challenges of ageing. Nature, 561 (7721), 45–56. https://doi.org/10.1038/s41586-018-0457-8

Pas, S. P. (2018). The rise of three-dimensional human brain cultures. Nature, 553 (7689), 437–445. https://doi.org/10.1038/nature25032

Pascovici, D., Handler, D. C. L., Wu, J. X., & Haynes, P. A. (2016). Multiple testing corrections in quantitative proteomics: A useful but blunt tool. Proteomics, 16(18), 2448–2453. https://doi.org/10.1002/PMIC.201600044

Patil, C. G., Lad, S. P., Katznelson, L., & Laws, E. R. (2007). Brain atrophy and cognitive deficits in Cushing's disease. Neurosurgical Focus, 23(3), 1–4. https://doi.org/10.3171/FOC.2007.23.3.13

Patrick, M.B., Preveza, N.J., Kincaid, S.E., Setenet, G., Abraham, J.R., Cummings, A., Banani S., Ray, W.K., Helm, R.F., Trask, S., & Jarome, T.J. (2024). Dysregulation of baseline and learning-dependent protein degradation in the aged hippocampus, Brain Research Bulletin, 215, 111015. https://doi.org/10.1016/J.BRAINRESBULL.2024.111015

Paul, J., Strickland, S., & Melchor, J. P. (2007). Fibrin deposition accelerates neurovascular damage and neuroinflammation in mouse models of Alzheimer's disease. Journal of Experimental Medicine, 204(8), 1999–2008. https://doi.org/10.1084/jem.20070304

Peinado, M. A., Quesada, A., Pedrosa, J. A., Torres, M. I., Martinez, M., Esteban, F. J., Del Moral, M. L., Hernandez, R., Rodrigo, J., & Peinado, J. M. (1998). Quantitative and Ultrastructural Changes in Glia and Pericytes in the Parietal Cortex of the Aging Rat. Microscopy Research Techniques, 43(1):34-42. 10.1002/(SICI)1097-0029(19981001)43:1<34::AID-JEMT6>3.0.CO;2-G

Pelegrí, C., Canudas, A. M., del Valle, J., Casadesus, G., Smith, M. A., Camins, A., Pallàs, M., & Vilaplana, J. (2007). Increased permeability of blood-brain barrier on the hippocampus of a murine model of senescence. Mechanisms of Ageing and Development, 128(9), 522–528. https://doi.org/10.1016/j.mad.2007.07.002

Pelvig, D. P., Pakkenberg, H., Stark, A. K., & Pakkenberg, B. (2008). Neocortical glial cell numbers in human brains. Neurobiology of Aging, 29(11), 1754–1762. https://doi.org/10.1016/J.NEUROBIOLAGING.2007.04.013

Peng, X., Luo, Z., He, S., Zhang, L., & Li, Y. (2021). Blood-Brain Barrier Disruption by Lipopolysaccharide and Sepsis-Associated Encephalopathy. Frontiers in Cellular and Infection Microbiology, 11, 768108. https://doi.org/10.3389/FCIMB.2021.768108

Peters, A., Josephson, K., & Vincent, S. L. (1991). Effects of aging on the neuroglial cells and pericytes within area 17 of the rhesus monkey cerebral cortex. The Anatomical Record, 229(3), 384–398. https://doi.org/10.1002/ar.1092290311

Peters, R. (2006). Ageing and the brain. In Postgraduate Medical Journal, 82(964), 84-88 https://doi.org/10.1136/pgmj.2005.036665

Petersen, M. A., Ryu, J. K., & Akassoglou, K. (2018). Fibrinogen in neurological diseases: Mechanisms, imaging and therapeutics. Nature Reviews Neuroscience, 19(5), 283–301. https://doi.org/10.1038/nrn.2018.13

Pieper, C., Marek, J. J., Unterberg, M., Schwerdtle, T., & Galla, H. J. (2014). Brain capillary pericytes contribute to the immune defense in response to cytokines or LPS in vitro. Brain Research, 1550, 1–8. https://doi.org/10.1016/j.brainres.2014.01.004

Piirsalu, M., Taalberg, E., Lilleväli, K., Tian, L., Zilmer, M., & Vasar, E. (2020). Treatment With Lipopolysaccharide Induces Distinct Changes in Metabolite Profile and Body Weight in 129Sv and Bl6 Mouse Strains. Frontiers in Pharmacology, 11, 525770. https://doi.org/10.3389/FPHAR.2020.00371/BIBTEX

Pikkarainen, M., Martikainen, P., & Alafuzoff, I. (2010). The effect of prolonged fixation time on immunohistochemical staining of common Neurodegenerative disease markers. Journal of Neuropathology and Experimental Neurology, 69(1), 40–52. https://doi.org/10.1097/NEN.0b013e3181c6c13d

Pinosanu, L. R., Capitanescu, B., Glavan, D., Godeanu, S., Cadenas, I. F., Doeppner, T. R., Hermann, D. M., Balseanu, A. T., Bogdan, C., & Popa-Wagner, A. (2023). Neuroglia Cells Transcriptomic in Brain Development, Aging and Neurodegenerative Diseases. Aging and Disease, 14(1), 63-83. https://doi.org/10.14336/AD.2022.0621

Pires, P. C., Rodrigues, M., Alves, G., & Santos, A. O. (2022). Strategies to Improve Drug Strength in Nasal Preparations for Brain Delivery of Low Aqueous Solubility Drugs. Pharmaceutics, 14(3), 588. https://doi.org/10.3390/PHARMACEUTICS14030588

Popov, A., Brazhe A., Denisov, P., Sutyagina, O., Li L., Lazareva, N., Verkhratsky, A., & Semyanov, A. (2021). Astrocyte dystrophy in ageing brain parallels impaired synaptic plasticity, Aging Cell, 20(3), e13334. https://doi.org/10.1111/ACEL.13334.

Porcher, L., Bruckmeier, S., Burbano, S. D., Finnell, J. E., Gorny, N., Klett, J., Wood, S. K., & Kelly, M. P. (2021). Aging triggers an upregulation of a multitude of cytokines in the male and especially the female rodent hippocampus but more discrete changes in other brain regions. Journal of Neuroinflammation, 18(1), 1–19. https://doi.org/10.1186/S12974-021-02252-6

Porro, C., Cianciulli, A., & Panaro, M. A. (2020). The Regulatory Role of IL-10 in Neurodegenerative Diseases. Biomolecules, 10(7), 1–15. https://doi.org/10.3390/BIOM10071017

Powers, N. E., Swartzwelter, B., Marchetti, C., De Graaf, D. M., Lerchner, A., Schlapschy, M., Datar, R., Binder, U., Edwards, C. K., Skerra, A., & Dinarello, C. A. (2020). PASylation of IL-1 receptor antagonist (IL-1Ra) retains IL-1 blockade and extends its duration in mouse urate crystal-induced peritonitis. The Journal of Biological Chemistry, 295(3), 868-882. https://doi.org/10.1074/JBC.RA119.010340

Pradillo, J. M., Murray, K. N., Coutts, G. A., Moraga, A., Oroz-Gonjar, F., Boutin, H., Moro, M. A., Lizasoain, I., Rothwell, N. J., & Allan, S. M. (2017). Reparative effects of interleukin-1 receptor antagonist in young and aged/co-morbid rodents after cerebral ischemia. Brain, Behavior, and Immunity, 61, 117-126. https://doi.org/10.1016/J.BBI.2016.11.013

Prashanth, A., Donaghy, H., Stoner, S. P., Hudson, A. L., Wheeler, H. R., Diakos, C. I., Howell, V. M., Grau, G. E., & McKelvey, K. J. (2021). Are in vitro human blood–brain–tumor-barriers suitable replacements for in vivo models of brain permeability for novel therapeutics? Cancers, 13(5), 1–20. https://doi.org/10.3390/cancers13050955

Pulgar, V. M. (2019). Transcytosis to cross the blood brain barrier, new advancements and challenges. Frontiers in Neuroscience, 13(JAN), 1019. https://doi.org/10.3389/FNINS.2018.01019/BIBTEX

Qin, L., Wu, X., Block, M. L., Liu, Y., Breese, G. R., Hong, J. S., Knapp, D. J., & Crews, F. T. (2007). Systemic LPS Causes Chronic Neuroinflammation and Progressive Neurodegeneration. Glia, 55(5), 453-462. https://doi.org/10.1002/GLIA.20467

Quick, J. D., Silva, C., Wong, J. H., Lim, K. L., Reynolds, R., Barron, A. M., Zeng, J., & Lo, C. H. (2023). Lysosomal acidification dysfunction in microglia: an emerging pathogenic mechanism of neuroinflammation and neurodegeneration. Journal of Neuroinflammation, 20(1), 1–13. https://doi.org/10.1186/S12974-023-02866-Y/FIGURES/3

Rafiyan, M., Sadeghmousavi, S., Akbarzadeh, M., & Rezaei, N. (2023). Experimental animal models of chronic inflammation. Current Research in Immunology, 4, 100063. https://doi.org/10.1016/J.CRIMMU.2023.100063

Raju, R., Abuwatfa, W. H., Pitt, W. G., & Husseini, G. A. (2023). Liposomes for the Treatment of Brain Cancer—A Review. Pharmaceuticals, 16(8), 1056. https://doi.org/10.3390/PH16081056

Rakhimbaeva, G. S., & Abdurakhmonova, K. B. kizi. (2023). ICAM-1 and CRP as biomarkers of 3-month outcome in acute ischaemic stroke. BMJ Neurology Open, 5(2), 516, e000516. https://doi.org/10.1136/BMJNO-2023-000516

Ralvenius, W. T., Andresen, J. L., Huston, M. M., Penney, J., Bonner, J. M., Fenton, O. S., Langer, R., & Tsai, L. H. (2024). Nanoparticle-Mediated Delivery of Anti-PU.1 siRNA via Localized Intracisternal Administration Reduces Neuroinflammation. Advanced Materials, 36(8), 2309225. https://doi.org/10.1002/ADMA.202309225

Ramos-Zaldívar, H. M., Polakovicova, I., Salas-Huenuleo, E., Corvalán, A. H., Kogan, M. J., Yefi, C. P., & Andia, M. E. (2022). Extracellular vesicles through the blood–brain barrier: a review. Fluids and Barriers of the CNS, *19*(1), 1–15. https://doi.org/10.1186/S12987-022-00359-3/FIGURES/3

Rapoport, S. I., Ohno, K., & Pettigrew, K. D. (1979). Blood-brain barrier permeability in senescent rats. Journals of Gerontology, 34(2), 162–169. https://doi.org/10.1093/geronj/34.2.162

Rasmussen, R. N., & Smith, N. A. (2022). The elusive varicose astrocytes. *Trends in Neurosciences*, *45*(2), 94–95. https://doi.org/10.1016/J.TINS.2021.11.003

Rathore, K. I., Redensek, A., & David, S. (2012). Iron homeostasis in astrocytes and microglia is differentially regulated by TNF-α and TGF-β1. Glia, 60(5), 738–750. https://doi.org/10.1002/GLIA.22303

Raulin, A. C., Doss, S. V., Trottier, Z. A., Ikezu, T. C., Bu, G., & Liu, C. C. (2022). ApoE in Alzheimer's disease: pathophysiology and therapeutic strategies. Molecular Neurodegeneration, 17(1), 1–26. https://doi.org/10.1186/S13024-022-00574-4

Reed, M. J., Damodarasamy, M., & Banks, W. A. (2019). The extracellular matrix of the blood–brain barrier: structural and functional roles in health, aging, and Alzheimer's disease. Tissue Barriers, 7(4), 1651157. https://doi.org/10.1080/21688370.2019.1651157

Reed, M. J., Damodarasamy, M., Pathan, J. L., Erickson, M. A., Banks, W. A., & Vernon, R. B. (2018). The Effects of Normal Aging on Regional Accumulation of Hyaluronan and Chondroitin Sulfate Proteoglycans in the Mouse Brain. Journal of Histochemistry and Cytochemistry, 66(10), 697-707. https://doi.org/10.1369/0022155418774779

Reginald-Opara, J. N., Svirskis, D., Paek, S. Y., Tang, M., O'Carroll, S. J., Dean, J. M., Chamley, L. W., & Wu, Z. (2022). The involvement of extracellular vesicles in the transcytosis of nanoliposomes through brain endothelial cells, and the impact of liposomal pH-sensitivity. Materials Today Bio, 13, 100212. https://doi.org/10.1016/J.MTBIO.2022.100212

Rehman, F. U., Bao, J., Muhammad, P., He, W., Hanif, S., & Rauf, M. A. (2020). Blood-brain barrier amenable gold nanoparticles biofabrication in aged cell culture medium. Materials Today. Bio, 8, 100072. https://doi.org/10.1016/J.MTBIO.2020.100072

Ren, B., Lu, J., Li, M., Zou, X., Liu, Y., Wang, C., & Wang, L. (2021). Anti-inflammatory effect of IL-1ra-loaded dextran/PLGA microspheres on Porphyromonas gingivalis lipopolysaccharide-stimulated macrophages in vitro and in vivo in a rat model of periodontitis. Biomedicine & Pharmacotherapy, 134, 111171. https://doi.org/10.1016/J.BIOPHA.2020.111171

Rezaei, S., Prévot, T. D., Vieira, E., & Sibille, E. (2024). LPS-induced inflammation reduces GABAergic interneuron markers and brain-derived neurotrophic factor in mouse prefrontal cortex and hippocampus. Brain, Behavior, & Immunity - Health, 38, 100761. https://doi.org/10.1016/J.BBIH.2024.100761

Richter, M., Vidovic, N., Biber, K., Dolga, A., Culmsee, C., & Dodel, R. (2020). The neuroprotective role of microglial cells against amyloid beta-mediated toxicity in organotypic hippocampal slice cultures. Brain Pathology, 30(3), 589-602. https://doi.org/10.1111/BPA.12807

Ridker, P. M., Everett, B. M., Thuren, T., MacFadyen, J. G., Chang, W. H., Ballantyne, C., Fonseca, F., Nicolau, J., Koenig, W., Anker, S. D., Kastelein, J. J. P., Cornel, J. H., Pais, P., Pella, D., Genest, J., Cifkova, R., Lorenzatti, A., Forster, T., Kobalava, Z., … Glynn, R. J. (2017). Antiinflammatory Therapy with Canakinumab for Atherosclerotic Disease. New England Journal of Medicine, 377(12), 1119–1131. https://doi.org/10.1056/NEJMOA1707914/SUPPL_FILE/NEJMOA1707914_DISCLOSURES.PDF

Rim, C., You, M. J., Nahm, M., & Kwon, M. S. (2024). Emerging role of senescent microglia in brain aging-related neurodegenerative diseases. Translational Neurodegeneration, 13(1), 1–14. https://doi.org/10.1186/S40035-024-00402-3

Roboon, J., Hattori, T., Ishii, H., Takarada-Iemata, M., Nguyen, D. T., Heer, C. D., O'Meally, D., Brenner, C., Yamamoto, Y., Okamoto, H., Higashida, H., & Hori, O. (2021). Inhibition of CD38 and supplementation of nicotinamide riboside ameliorate lipopolysaccharide-induced microglial and astrocytic neuroinflammation by increasing NAD. Journal of Neurochemistry, 158(2), 311–327. https://doi.org/10.1111/JNC.15367

Rodrigues, B. D. S., Kanekiyo, T., & Singh, J. (2020). Nerve Growth Factor Gene Delivery across the Blood-Brain Barrier to Reduce Beta Amyloid Accumulation in AD Mice. Molecular Pharmaceutics, 17(6), 2054–2063. https://doi.org/10.1021/ACS.MOLPHARMACEUT.0C00218/ASSET/IMAGES/LARGE/MP0C00218_0005.JPEG

Rodríguez, J. J., Yeh, C. Y., Terzieva, S., Olabarria, M., Kulijewicz-Nawrot, M., & Verkhratsky, A. (2014). Complex and region-specific changes in astroglial markers in the aging brain. Neurobiology of Aging, 35(1), 15–23. https://doi.org/10.1016/j.neurobiolaging.2013.07.002

Rodríguez-Callejas, J. de D., Cuervo-Zanatta, D., Rosas-Arellano, A., Fonta, C., Fuchs, E., & Perez-Cruz, C. (2019). Loss of ferritin-positive microglia relates to increased iron, RNA oxidation, and dystrophic microglia in the brains of aged male marmosets. American Journal of Primatology, 81(2), e22956. https://doi.org/10.1002/AJP.22956

Rogers, C.S., Jones, M.S., McConkey, S., Spehar, B., Van Engen, K.J., Sommers, M.S., & Peelle, J.E. (2020). Age-Related Differences in Auditory Cortex Activity During Spoken Word Recognition, Neurobiology of Language, 1(4), 452-473. https://doi.org/10.1162/NOL_A_00021

Rohm, T. V., Meier, D. T., Olefsky, J. M., & Donath, M. Y. (2022). Inflammation in Obesity, Diabetes and related Disorders. Immunity, 55(1), 31-55. https://doi.org/10.1016/J.IMMUNI.2021.12.013

Ross, C., Taylor, M., Fullwood, N., & Allsop, D. (2018). Liposome delivery systems for the treatment of Alzheimer's disease. International Journal of Nanomedicine, 13, 8507-8522. https://doi.org/10.2147/IJN.S183117

Rothaug, M., Stroobants, S., Schweizer, M., Peters, J., Zunke, F., Allerding, M., D'Hooge, R., Saftig, P., & Blanz, J. (2015). LAMP-2 deficiency leads to hippocampal dysfunction but normal clearance of neuronal substrates of chaperone-mediated autophagy in a mouse model for Danon disease. Acta Neuropathologica Communications, 3, 6. https://doi.org/10.1186/S40478-014-0182-Y

Rothhammer, V., & Quintana, F. J. (2015). Control of autoimmune CNS inflammation by astrocytes. Seminars in Immunopathology, 37(6), 625-638. https://doi.org/10.1007/S00281-015-0515-3

Roux, G. Le, Jarray, R., Guyot, A. C., Pavoni, S., Costa, N., Théodoro, F., Nassor, F., Pruvost, A., Tournier, N., Kiyan, Y., Langer, O., Yates, F., Deslys, J. P., & Mabondzo, A. (2019). Proof-of-Concept Study of Drug Brain Permeability Between in Vivo Human Brain and an in Vitro iPSCs-Human Blood-Brain Barrier Model. Scientific Reports, 9(1), 1–11. https://doi.org/10.1038/s41598-019-52213-6

Sadick, J. S., & Liddelow, S. A. (2019). Don't forget astrocytes when targeting Alzheimer's disease. In British Journal of Pharmacology, 176(18):3585-3598. https://doi.org/10.1111/bph.14568

Safaiyan, S., Kannaiyan, N., Snaidero, N., Brioschi, S., Biber, K., Yona, S., Edinger, A. L., Jung, S., Rossner, M. J., & Simons, M. (2016). Age-related myelin degradation burdens the clearance function of microglia during aging. Nature Neuroscience, 19(8), 995-998. https://doi.org/10.1038/NN.4325

Salahuddin, t. S., Johansson, b. B., Kalimo, h., & Olsson, y. (1988). Structural changes in the rat brain after carotid infusions of hyperosmolar solutions: a light microscopic and immunohistochemical study. In Neuropathology and Applied Neurobiology, 14(6), 467-482 https://doi.org/10.1111/j.1365-2990.1988.tb01338.x

Salas, I. H., Burgado, J., & Allen, N. J. (2020). Glia: victims or villains of the aging brain? Neurobiology of Disease, 143, 105008. https://doi.org/10.1016/J.NBD.2020.105008

Salkeni, M. A., Lynch, J. L., Otamis-Price, T., & Banks, W. A. (2009). Lipopolysaccharide Impairs Blood–Brain Barrier P-glycoprotein Function in Mice Through Prostaglandin- and Nitric Oxide-Independent Pathways. Journal of Neuroimmune Pharmacology : The Official Journal of the Society on NeuroImmune Pharmacology, 4(2), 276-282. https://doi.org/10.1007/S11481-008-9138-Y

Sama, M. A., Mathis, D. M., Furman, J. L., Abdul, H. M., Artiushin, I. A., Kraner, S. D., & Norris, C. M. (2008). Interleukin-1β-dependent Signaling between Astrocytes and Neurons Depends Critically on Astrocytic Calcineurin/NFAT Activity. The Journal of Biological Chemistry, 283(32), 21953-21964. https://doi.org/10.1074/JBC.M800148200

Santos, S. D., Xavier, M., Leite, D. M., Moreira, D. A., Custódio, B., Torrado, M., Castro, R., Leiro, V., Rodrigues, J., Tomás, H., & Pêgo, A. P. (2018). PAMAM dendrimers: blood-brain barrier transport and neuronal uptake after focal brain ischemia. Journal of Controlled Release, 291, 65–79. https://doi.org/10.1016/J.JCONREL.2018.10.006

Saraiva, M., Christensen, J. R., Veldhoen, M., Murphy, T. L., Murphy, K. M., & O'Garra, A. (2009). Interleukin-10 Production by Th1 Cells Requires Interleukin-12-Induced STAT4 Transcription Factor and ERK MAP Kinase Activation by High Antigen Dose. Immunity, 31(2–3), 209-219. https://doi.org/10.1016/J.IMMUNI.2009.05.012

Sarin, H. (2009). Recent progress towards development of effective systemic chemotherapy for the treatment of malignant brain tumors. Journal of Translational Medicine, 7, 77. https://doi.org/10.1186/1479-5876-7-77

Sartori, A. C., Vance, D. E., Slater, L. Z., & Crowe, M. (2012). The Impact of Inflammation on Cognitive Function in Older Adults: Implications for Health Care Practice and Research. The Journal of Neuroscience Nursing, 44(4), 206. https://doi.org/10.1097/JNN.0B013E3182527690

Sartorius, T., Peter, A., Heni, M., Maetzler, W., Fritsche, A., Häring, H. U., & Hennige, A. M. (2015). The brain response to peripheral insulin declines with age: A contribution of the blood-brain barrier? PLoS ONE, 10(5), e0126804. https://doi.org/10.1371/journal.pone.0126804

Saunders, N. R., Dziegielewska, K. M., Møllgård, K., & Habgood, M. D. (2015). Markers for blood-brain barrier integrity: How appropriate is Evans blue in the twenty-first century and

what are the alternatives? In Frontiers in Neuroscience, 9 (OCT), 385. https://doi.org/10.3389/fnins.2015.00385

Schädlich, I. S., Vienhues, J. H., Jander, A., Piepke, M., Magnus, T., Lambertsen, K. L., Clausen, B. H., & Gelderblom, M. (2022). Interleukin-1 Mediates Ischemic Brain Injury via Induction of IL-17A in γδ T Cells and CXCL1 in Astrocytes. Neuromolecular Medicine, 24(4), 437–451. https://doi.org/10.1007/S12017-022-08709-Y

Schaffenrath, J., Huang, S. F., Wyss, T., Delorenzi, M., & Keller, A. (2021). Characterization of the blood–brain barrier in genetically diverse laboratory mouse strains. Fluids and Barriers of the CNS, 18(1), 34. https://doi.org/10.1186/S12987-021-00269-W

Schnoor, M., Alcaide, P., Voisin, M. B., & Van Buul, J. D. (2015). Crossing the Vascular Wall: Common and Unique Mechanisms Exploited by Different Leukocyte Subsets during Extravasation. Mediators of Inflammation, 2015, 946509. https://doi.org/10.1155/2015/946509

Schuitemaker, A., van der Doef, T. F., Boellaard, R., van der Flier, W. M., Yaqub, M., Windhorst, A. D., Barkhof, F., Jonker, C., Kloet, R. W., Lammertsma, A. A., Scheltens, P., & van Berckel, B. N. M. (2012). Microglial activation in healthy aging. Neurobiology of Aging, 33(6), 1067–1072. https://doi.org/10.1016/J.NEUROBIOLAGING.2010.09.016

Seemann, S., Zohles, F., & Lupp, A. (2017). Comprehensive comparison of three different animal models for systemic inflammation. Journal of Biomedical Science, 24(1), 1–17. https://doi.org/10.1186/S12929-017-0370-8/FIGURES/9

Senatorov, V. V., Friedman, A. R., Milikovsky, D. Z., Ofer, J., Saar-Ashkenazy, R., Charbash, A., Jahan, N., Chin, G., Mihaly, E., Lin, J. M., Ramsay, H. J., Moghbel, A., Preininger, M. K., Eddings, C. R., Harrison, H. V., Patel, R., Shen, Y., Ghanim, H., Sheng, H., … Kaufer, D. (2019). Blood-brain barrier dysfunction in aging induces hyperactivation of TGFβ signaling and chronic yet reversible neural dysfunction. Science Translational Medicine, 11(521):eaaw8283 https://doi.org/10.1126/scitranslmed.aaw8283

Shahidehpour, R. K., Higdon, R. E., Crawford, N. G., Neltner, J. H., Ighodaro, E. T., Patel, E., Price, D., Nelson, P. T., & Bachstetter, A. D. (2021). Dystrophic microglia are associated with neurodegenerative disease and not healthy aging in the human brain. Neurobiology of Aging, 99, 19-27. https://doi.org/10.1016/J.NEUROBIOLAGING.2020.12.003

Shao, X., Shou, Q., Felix, K., Ojogho, B., Jiang, X., Gold, B.T., Herting, M.M., Goldwaser, E.L., Kochunov, P., Hong, L.E., Pappas, I., Braskie, M., Kim, H., Cen, S., Jann, K., & Wang, D.J. (2024). Age-Related Decline in BBB Function is More Pronounced in Males than Females, eLife, 13. https://doi.org/10.7554/ELIFE.96155.1

Shao, X., Jann, K., Ma, S. J., Yan, L., Montagne, A., Ringman, J. M., Zlokovic, B. V., & Wang, D. J. J. (2020). Comparison Between Blood-Brain Barrier Water Exchange Rate and Permeability to Gadolinium-Based Contrast Agent in an Elderly Cohort. Frontiers in Neuroscience, 14, 571480. https://doi.org/10.3389/fnins.2020.571480

Sharma, A., Sanjay, Jaiswal, V., Park, M., & Lee, H. J. (2023). Biogenic silver NPs alleviate LPS-induced neuroinflammation in a human fetal brain-derived cell line: Molecular switch to the M2 phenotype, modulation of TLR4/MyD88 and Nrf2/HO-1 signaling pathways, and molecular docking analysis. Biomaterials Advances, 148, 213363. https://doi.org/10.1016/J.BIOADV.2023.213363

Shawahna, R., Decleves, X., & Scherrmann, J.-M. (2013). Hurdles with Using In Vitro Models to Predict Human Blood-brain Barrier Drug Permeability: A Special Focus on Transporters and Metabolizing Enzymes. Current Drug Metabolism, 14(1), 120–136. https://doi.org/10.2174/1389200211309010120

Shayan, G., Choi, Y. S., Shusta, E. V., Shuler, M. L., & Lee, K. H. (2011). Murine in vitro model of the blood-brain barrier for evaluating drug transport. European Journal of Pharmaceutical Sciences, 42(1–2), 148–155. https://doi.org/10.1016/j.ejps.2010.11.005

Sheng, W. S., Hu, S., Feng, A., & Rock, R. B. (2013). Reactive Oxygen Species From Human Astrocytes Induced Functional Impairment and Oxidative Damage. Neurochemical Research, 38(10), 2148-2159. https://doi.org/10.1007/S11064-013-1123-Z

Shimizu, F., Sano, Y., Saito, K., Abe, M. A., Maeda, T., Haruki, H., & Kanda, T. (2012). Pericyte-derived glial cell line-derived neurotrophic factor increase the expression of claudin-5 in the blood-brain barrier and the blood-nerve barrier. Neurochemical Research, 37(2), 401–409. https://doi.org/10.1007/s11064-011-0626-8

Shin, J., Kong, C., Cho, J. S., Lee, J., Koh, C. S., Yoon, M. S., Na, Y. C., Chang, W. S., & Chang, J. W. (2018). Focused ultrasound-mediated noninvasive blood-brain barrier modulation: preclinical examination of efficacy and safety in various sonication parameters. Neurosurgical Focus, 44(2), e15. https://doi.org/10.3171/2017.11.FOCUS17627

Shin, Y., Choi, S. H., Kim, E., Bylykbashi, E., Kim, J. A., Chung, S., Kim, D. Y., Kamm, R. D., & Tanzi, R. E. (2019). Blood–Brain Barrier Dysfunction in a 3D In Vitro Model of Alzheimer's Disease. Advanced Science, 6(20), 1900962. https://doi.org/10.1002/advs.201900962

Shobin, E., Bowley, M. P., Estrada, L. I., Heyworth, N. C., Orczykowski, M. E., Eldridge, S. A., Calderazzo, S. M., Mortazavi, F., Moore, T. L., & Rosene, D. L. (2017). Microglia activation and phagocytosis: relationship with aging and cognitive impairment in the rhesus monkey. GeroScience, 39(2), 199-220. https://doi.org/10.1007/S11357-017-9965-Y

Shu, H., Wang, M., Song, M., Sun, Y., Shen, X., Zhang, J., & Jin, X. (2020). Acute Nicotine Treatment Alleviates LPS-Induced Impairment of Fear Memory Reconsolidation Through AMPK Activation and CRTC1 Upregulation in Hippocampus. The International Journal of Neuropsychopharmacology, 23(10), 687–699. https://doi.org/10.1093/IJNP/PYAA043

Sierra, A., Gottfried-Blackmore, A. C., Mcewen, B. S., & Bulloch, K. (2007). Microglia derived from aging mice exhibit an altered inflammatory profile. Glia, 55(4), 412–424. https://doi.org/10.1002/GLIA.20468

Şik, A., van Nieuwehuyzen, P., Prickaerts, J., & Blokland, A. (2003). Performance of different mouse strains in an object recognition task, Behavioural Brain Research, 147(1–2), 49–54. https://doi.org/10.1016/S0166-4328(03)00117-7.

Simoncic, U., Leibfarth, S., Welz, S., Schwenzer, N., Schmidt, H., Reischl, G., Pfannenberg, C., Fougere, C., Nikolaou, K., Zips, D., & Thorwarth, D. (2017). Comparison of DCE-MRI kinetic parameters and FMISO-PET uptake parameters in head and neck cancer patients. Medical Physics, 44(6), 2358–2368. https://doi.org/10.1002/mp.12228

Simpson, J. E., Ince, P. G., Shaw, P. J., Heath, P. R., Raman, R., Garwood, C. J., Gelsthorpe, C., Baxter, L., Forster, G., Matthews, F. E., Brayne, C., & Wharton, S. B. (2011). Microarray analysis of the astrocyte transcriptome in the aging brain: relationship to Alzheimer's

pathology and APOE genotype. Neurobiology of Aging, 32(10), 1795–1807. https://doi.org/10.1016/j.neurobiolaging.2011.04.013

Singer, B. H., Newstead, M. W., Zeng, X., Cooke, C. L., Thompson, R. C., Singer, K., Ghantasala, R., Parent, J. M., Murphy, G. G., Iwashyna, T. J., & Standiford, T. J. (2016). Cecal Ligation and Puncture Results in Long-Term Central Nervous System Myeloid Inflammation. PLoS ONE, 11(2). https://doi.org/10.1371/JOURNAL.PONE.0149136

Singer, B. H., Newstead, M. W., Zeng, X., Cooke, C. L., Thompson, R. C., Singer, K., Ghantasala, R., Parent, J. M., Murphy, G. G., Iwashyna, T. J., & Standiford, T. J. (2016). Cecal Ligation and Puncture Results in Long-Term Central Nervous System Myeloid Inflammation. PLoS ONE, 11(2), e0149136. https://doi.org/10.1371/JOURNAL.PONE.0149136

Sittig, L. J., Carbonetto, P., Engel, K. A., Krauss, K. S., Barrios-Camacho, C. M., & Palmer, A. A. (2016). Genetic background limits generalizability of genotype-phenotype relationships. *Neuron*, *91*(6), 1253-1259. https://doi.org/10.1016/J.NEURON.2016.08.013

Sjöstedt, N., Kortejärvi, H., Kidron, H., Vellonen, K. S., Urtti, A., & Yliperttula, M. (2014). Challenges of using in vitro data for modeling P-glycoprotein efflux in the blood-brain barrier. Pharmaceutical Research, 31(1), 1-19. https://doi.org/10.1007/s11095-013-1124-2

Sjöström, E. O., Culot, M., Leickt, L., Åstrand, M., Nordling, E., Gosselet, F., & Kaiser, C. (2021). Transport study of interleukin-1 inhibitors using a human in vitro model of the blood-brain barrier. Brain, Behavior, & Immunity - Health, 16, 100307. https://doi.org/10.1016/J.BBIH.2021.100307

Skaria, T., Bachli, E., & Schoedon, G. (2017). Wnt5A/Ryk signaling critically affects barrier function in human vascular endothelial cells. Cell Adhesion & Migration, 11(1), 24–38. https://doi.org/10.1080/19336918.2016.1178449

Skrzypczak-Wiercioch, A., & Sałat, K. (2022). Lipopolysaccharide-Induced Model of Neuroinflammation: Mechanisms of Action, Research Application and Future Directions for Its Use. Molecules, 27(17), 5481. https://doi.org/10.3390/MOLECULES27175481

Sochocka, M., Diniz, B. S., & Leszek, J. (2017). Inflammatory Response in the CNS: Friend or Foe? Molecular Neurobiology, 54(10), 8071- 8089. https://doi.org/10.1007/S12035-016-0297-1

Soenen, S. J., Rivera-Gil, P., Montenegro, J. M., Parak, W. J., De Smedt, S. C., & Braeckmans, K. (2011). Cellular toxicity of inorganic nanoparticles: Common aspects and guidelines for improved nanotoxicity evaluation. Nano Today, 6(5), 446–465. https://doi.org/10.1016/J.NANTOD.2011.08.001

Sofroniew, M. V, & Vinters, H. V. (2010). Astrocytes: biology and pathology. Acta Neuropathologica, 119(1), 7–35. https://doi.org/10.1007/s00401-009-0619-8

Soles, A., Selimovic, A., Sbrocco, K., Ghannoum, F., Hamel, K., Moncada, E. L., Gilliat, S., & Cvetanovic, M. (2023). Extracellular Matrix Regulation in Physiology and in Brain Disease. International Journal of Molecular Sciences, 24(8), 7049. https://doi.org/10.3390/IJMS24087049

Song, H. W., Foreman, K. L., Gastfriend, B. D., Kuo, J. S., Palecek, S. P., & Shusta, E. V. (2020). Transcriptomic comparison of human and mouse brain microvessels. *Scientific Reports 2020 10:1*, *10*(1), 1–14. https://doi.org/10.1038/s41598-020-69096-7

Sorets, A. G., Rosch, J. C., Duvall, C. L., & Lippmann, E. S. (2020). Caveolae-mediated transport at the injured blood–brain barrier as an underexplored pathway for central nervous system drug delivery. *Current Opinion in Chemical Engineering*, *30*, 86–95. https://doi.org/10.1016/j.coche.2020.08.009

Soto, I., Graham, L. C., Richter, H. J., Simeone, S. N., Radell, J. E., Grabowska, W., Funkhouser, W. K., Howell, M. C., & Howell, G. R. (2015). APOE Stabilization by Exercise Prevents Aging Neurovascular Dysfunction and Complement Induction. PLOS Biology, 13(10), e1002279. https://doi.org/10.1371/JOURNAL.PBIO.1002279

Stamatakou, E., Marzo, A., Gibb, A., & Salinas, P. C. (2013). Activity-Dependent Spine Morphogenesis: A Role for the Actin-Capping Protein Eps8. The Journal of Neuroscience, 33(6), 2661-2170. https://doi.org/10.1523/JNEUROSCI.0998-12.2013

Stamatovic, S. M., Martinez-Revollar, G., Hu, A., Choi, J., Keep, R. F., & Andjelkovic, A. V. (2019). Decline in Sirtuin-1 expression and activity plays a critical role in blood-brain barrier permeability in aging. In Neurobiology of Disease, 126, 105-116. https://doi.org/10.1016/j.nbd.2018.09.006

Starr, M. E., Saito, M., Evers, B. M., & Saito, H. (2015). Age-Associated Increase in Cytokine Production During Systemic Inflammation—II: The Role of IL-1β in Age-Dependent IL-6 Upregulation in Adipose Tissue. The Journals of Gerontology Series A: Biological Sciences and Medical Sciences, 70(12), 1508-1515. https://doi.org/10.1093/GERONA/GLU197

Starr, M. E., Ueda, J., Takahashi, H., Weiler, H., Esmon, C. T., Evers, B. M., & Saito, H. (2010). Age-dependent vulnerability to endotoxemia is associated with reduction of anticoagulant factors activated protein C and thrombomodulin. Blood, 115(23), 4886–4893. https://doi.org/10.1182/BLOOD-2009-10-246678

Stewart, P. A., Magliocco, M., Hayakawa, K., Farrell, C. L., Del Maestro, R. F., Girvin, J., Kaufmann, J. C. E., Vinters, H. V., & Gilbert, J. (1987). A quantitative analysis of blood-brain barrier ultrastructure in the aging human. Microvascular Research, 33(2), 270–282. https://doi.org/10.1016/0026-2862(87)90022-7

Sticozzi, C., Belmonte, G., Meini, A., Carbotti, P., Grasso, G., & Palmi, M. (2013). IL-1β induces GFAP expression in vitro and in vivo and protects neurons from traumatic injury-associated apoptosis in rat brain striatum via NFκB/Ca2+-calmodulin/ERK mitogen-activated protein kinase signaling pathway. Neuroscience, 252, 367–383. https://doi.org/10.1016/J.NEUROSCIENCE.2013.07.061

Stolp, H. B., Dziegielewska, K. M., Ek, C. J., Potter, A. M., & Saunders, N. R. (2005). Long-term changes in blood–brain barrier permeability and white matter following prolonged systemic inflammation in early development in the rat. European Journal of Neuroscience, 22(11), 2805–2816. https://doi.org/10.1111/J.1460-9568.2005.04483.X

Stone, N. L., England, T. J., & O'Sullivan, S. E. (2019). A novel transwell blood brain barrier model using primary human cells. Frontiers in Cellular Neuroscience, 13, 230. https://doi.org/10.3389/fncel.2019.00230

Stopsack K.H., Tyekucheva S., Wang M., Gerke T.A., Vaselkiv J.B., Penney K.L., Kantoff P.W., Finn S.P., Fiorentino M., Loda M., Lotan T.L., Parmigiani G., Mucci LA. (2021). Extent, impact, and mitigation of batch effects in tumor biomarker studies using tissue microarrays. Elife.;10:e71265. https://10.7554/eLife.71265.

Storck, S. E., Hartz, A. M. S., Bernard, J., Wolf, A., Kachlmeier, A., Mahringer, A., Weggen, S., Pahnke, J., & Pietrzik, C. U. (2018). The concerted amyloid-beta clearance of LRP1 and ABCB1/P-gp across the blood-brain barrier is linked by PICALM. Brain, Behavior, and Immunity, 73, 21–33. https://doi.org/10.1016/j.bbi.2018.07.017

Storck, S. E., Kurtyka, M., & Pietrzik, C. U. (2021). Brain endothelial LRP1 maintains blood–brain barrier integrity. *Fluids and Barriers of the CNS*, *18*(1), 1–7. https://doi.org/10.1186/S12987-021-00260-5/FIGURES/4

Stringer, M. S., Heye, A. K., Armitage, P. A., Chappell, F., Valdés Hernández, M. del C., Makin, S. D. J., Sakka, E., Thrippleton, M. J., & Wardlaw, J. M. (2021). Tracer kinetic assessment of blood–brain barrier leakage and blood volume in cerebral small vessel disease: Associations with disease burden and vascular risk factors. NeuroImage: Clinical, 32, 102883. https://doi.org/10.1016/J.NICL.2021.102883

Su, M. Y., Head, E., Brooks, W. M., Wang, Z., Muggenburg, B. A., Adam, G. E., Sutherland, R., Cotman, C. W., & Nalcioglu, O. (1998). Magnetic resonance imaging of anatomic and vascular characteristics in a canine model of human aging. Neurobiology of Aging, 19(5), 479–485. https://doi.org/10.1016/S0197-4580(98)00081-5

Subhash, S., Kalmbach, N., Wegner, F., Petri, S., Glomb, T., Dittrich-Breiholz, O., Huang, C., Bali, K. K., Kunz, W. S., Samii, A., Bertalanffy, H., Kanduri, C., & Kar, S. (2019). Transcriptome-wide Profiling of Cerebral Cavernous Malformations Patients Reveal Important Long noncoding RNA molecular signatures. Scientific Reports, 9(1), 18203. https://doi.org/10.1038/S41598-019-54845-0

Sumbria, R. K., Grigoryan, M. M., Vasilevko, V., Paganini-Hill, A., Kilday, K., Kim, R., Cribbs, D. H., & Fisher, M. J. (2018). Aging exacerbates development of cerebral microbleeds in a mouse model. Journal of Neuroinflammation, 15(1), 69. https://doi.org/10.1186/S12974-018-1092-X

Sun, H., Hu, H., Liu, C., Sun, N., & Duan, C. (2021). Methods used for the measurement of blood-brain barrier integrity. In Metabolic Brain Disease, 36(5), 723-725. https://doi.org/10.1007/s11011-021-00694-8

Sun, Y., Coppé, J. P., & Lam, E. W. F. (2018). Cellular Senescence: The Sought or the Unwanted? Trends in Molecular Medicine, 24(10), 871–885. https://doi.org/10.1016/J.MOLMED.2018.08.002

Swartzlander, D. B., Propson, N. E., Roy, E. R., Saito, T., Saido, T., Wang, B., & Zheng, H. (2018). Concurrent cell type–specific isolation and profiling of mouse brains in inflammation and Alzheimer's disease. Journal of Clinical Investigation Insight, 3(13), e121109. https://doi.org/10.1172/JCI.INSIGHT.121109

Swindell, W. R., Johnston, A., Xing, X., Little, A., Robichaud, P., Voorhees, J. J., Fisher, G., & Gudjonsson, J. E. (2013). Robust shifts in S100a9 expression with aging: A novel mechanism for chronic inflammation. Scientific Reports, 3(1), 1–13. https://doi.org/10.1038/srep01215

Syvänen, S., Lindhe, Ö., Palner, M., Kornum, B. R., Rahman, O., Långström, B., Knudsen, G. M., & Hammarlund-Udenaes, M. (2009). Species differences in blood-brain barrier transport of three positron emission tomography radioligands with emphasis on P-

glycoprotein transport. Drug Metabolism and Disposition, 37(3), 635–643. https://doi.org/10.1124/dmd.108.024745

Tachibana, K., Hirayama, R., Sato, N., Hattori, K., Kato, T., Takeda, H., & Kondoh, M. (2024). Association of Plasma Claudin-5 with Age and Alzheimer Disease. International Journal of Molecular Sciences, 25(3), 1419. https://doi.org/10.3390/IJMS25031419/S1

Takemiya, T., Fumizawa, K., Yamagata, K., Iwakura, Y., & Kawakami, M. (2017). Brain interleukin-1 facilitates learning of a water maze spatial memory task in Young Mice. Frontiers in Behavioral Neuroscience, 11, 258496. https://doi.org/10.3389/FNBEH.2017.00202/BIBTEX

Tan, Y. L., Yuan, Y., & Tian, L. (2019). Microglial regional heterogeneity and its role in the brain. Molecular Psychiatry 2019 25:2, 25(2), 351–367. https://doi.org/10.1038/s41380-019-0609-8

Tarbell, J. M. (2010). Shear stress and the endothelial transport barrier. Cardiovascular Research, 87(2), 320-330. https://doi.org/10.1093/CVR/CVQ146

Tateda, K., Matsumoto, T., Miyazaki, S., & Yamaguchi, K. (1996). Lipopolysaccharide-induced lethality and cytokine production in aged mice. Infection and Immunity, 64(3), 769-764. https://doi.org/10.1128/IAI.64.3.769-774.1996

Tay, T. L., Mai, D., Dautzenberg, J., Fernández-Klett, F., Lin, G., Sagar, S., Datta, M., Drougard, A., Stempfl, T., Ardura-Fabregat, A., Staszewski, O., Margineanu, A., Sporbert, A., Steinmetz, L. M., Pospisilik, J. A., Jung, S., Priller, J., Grün, D., Ronneberger, O., & Prinz, M. (2017). A new fate mapping system reveals context-dependent random or clonal expansion of microglia. Nature Neuroscience, 20(6), 793–803. https://doi.org/10.1038/nn.4547

Teixeira, M. I., Lopes, C. M., Amaral, M. H., & Costa, P. C. (2023). Surface-modified lipid nanocarriers for crossing the blood-brain barrier (BBB): A current overview of active targeting in brain diseases. Colloids and Surfaces B: Biointerfaces, 221, 112999. https://doi.org/10.1016/J.COLSURFB.2022.112999

Teleanu, R. I., Preda, M. D., Niculescu, A. G., Vladâcenco, O., Radu, C. I., Grumezescu, A. M., & Teleanu, D. M. (2022). Current Strategies to Enhance Delivery of Drugs across the Blood–Brain Barrier. Pharmaceutics, 14(5), 987. https://doi.org/10.3390/PHARMACEUTICS14050987

Tichauer, J. E., Flores, B., Soler, B., Eugenín-von Bernhardi, L., Ramírez, G., & Von Bernhardi, R. (2014). Age-dependent changes on TGFβ1 Smad3 pathway modify the pattern of microglial cell activation. Brain, Behavior, and Immunity, 37, 187–196. https://doi.org/10.1016/J.BBI.2013.12.018

Tincu, C. E., Andrițoiu, C. V., Popa, M., & Ochiuz, L. (2023). Recent Advancements and Strategies for Overcoming the Blood–Brain Barrier Using Albumin-Based Drug Delivery Systems to Treat Brain Cancer, with a Focus on Glioblastoma. Polymers, 15(19), 3969. https://doi.org/10.3390/POLYM15193969/S1

To, X. V., Donnelly, P., Maclachlan, L., Mahady, K., Apellaniz, E. M., Cumming, P., Winter, C., & Nasrallah, F. (2023). Anti-inflammatory interleukin 1 receptor antagonist concentration in plasma correlates with blood-brain barrier integrity in the primary lesion area in

traumatic brain injury patients. Brain, Behavior, & Immunity - Health, 31, 100653. https://doi.org/10.1016/J.BBIH.2023.100653

Tomita, H., Vawter, M. P., Walsh, D. M., Evans, S. J., Choudary, P. V., Li, J., Overman, K. M., Atz, M. E., Myers, R. M., Jones, E. G., Watson, S. J., Akil, H., & Bunney, W. E. (2004). Effect of agonal and postmortem factors on gene expression profile: Quality control in microarray analyses of postmortem human brain. In Biological Psychiatry, 55(4), 346-352. https://doi.org/10.1016/j.biopsych.2003.10.013

Tong Ong, D. S., Wang, L., Zhu, Y., Ho, B., & Ding, J. L. (2005). The response of ferritin to LPS and acute phase of Pseudomonas infection. Journal of Endotoxin Research, 11(5), 267–280. https://doi.org/10.1179/096805105X58698

Tracy, G. C., Huang, K. Y., Hong, Y. T., Ding, S., Noblet, H. A., Lim, K. H., Kim, E. C., Chung, H. J., & Kong, H. (2023). Intracerebral Nanoparticle Transport Facilitated by Alzheimer Pathology and Age. Nano Letters, 23(23), 10971–10982. https://doi.org/10.1021/ACS.NANOLETT.3C03222/SUPPL_FILE/NL3C03222_SI_001.PDF

Traschütz, A., Kummer, M.P., Schwartz, S., & Heneka, M.T. (2018). Variability and temporal dynamics of novel object recognition in aging male C57BL/6 mice, Behavioural Processes, 157, 711–716. https://doi.org/10.1016/J.BEPROC.2017.11.009

Tsai, H. C., Tsai, C. H., Chen, W. S., Inserra, C., Wei, K. C., & Liu, H. L. (2018). Safety evaluation of frequent application of microbubble-enhanced focused ultrasound blood-brain-barrier opening. Scientific Reports, 8(1), 17720. https://doi.org/10.1038/S41598-018-35677-W

Tsakiri, N., Kimber, I., Rothwell, N. J., & Pinteaux, E. (2008). Mechanisms of interleukin-6 synthesis and release induced by interleukin-1 and cell depolarisation in neurones. Molecular and Cellular Neuroscience, 37(1), 110–118. https://doi.org/10.1016/J.MCN.2007.09.001

Tylawsky, D.E., Kiguchi, H., Vaynshteyn, J., Gerwin, J., Shah, J., Islam, T., Boyer, J.A., Boué, D.R., Snuderl, M., Greenblatt, M.B., Shamay, Y., Raju, G.P., & Heller, D.A. (2023) 'P-selectin-targeted nanocarriers induce active crossing of the blood–brain barrier via caveolin-1-dependent transcytosis', Nature Materials, 22(3), 391–399. https://doi.org/10.1038/s41563-023-01481-9.

Tyrrell, D. J., Blin, M. G., Song, J., Wood, S. C., & Goldstein, D. R. (2020). Aging Impairs Mitochondrial Function and Mitophagy and Elevates Interleukin 6 Within the Cerebral Vasculature. Journal of the American Heart Association, 9(23), e017820. https://doi.org/10.1161/JAHA.120.017820

Ueno, M., Shinnou, M., Sakamoto, H., Akiguchi, I., Hosokawa, M., & Vorbrodt, A. W. (1996). Age-related changes in blood-brain barrier (BBB) on senescence accelerated mouse (SAM). Neurobiology of Aging, 17(4), S64. https://doi.org/10.1016/s0197-4580(96)80256-9

Urrutia, P., Aguirre, P., Esparza, A., Tapia, V., Mena, N. P., Arredondo, M., González-Billault, C., & Núñez, M. T. (2013). Inflammation alters the expression of DMT1, FPN1 and hepcidin, and it causes iron accumulation in central nervous system cells. Journal of Neurochemistry, 126(4), 541–549. https://doi.org/10.1111/JNC.12244

Uspenskaia, O., Liebetrau, M., Herms, J., Danek, A., & Hamann, G. F. (2004). Aging is associated with increased collagen type IV accumulation in the basal lamina of human cerebral microvessels. BMC Neuroscience, 5, 37. https://doi.org/10.1186/1471-2202-5-37

Van Assema, D. M. E., Lubberink, M., Boellaard, R., Schuit, R. C., Windhorst, A. D., Scheltens, P., Lammertsma, A. A., & Van Berckel, B. N. M. (2012). P-glycoprotein function at the blood-brain barrier: Effects of age and gender. Molecular Imaging and Biology, 14(6), 771–776. https://doi.org/10.1007/s11307-012-0556-0

Van Tassell, B. W., Toldo, S., Mezzaroma, E., & Abbate, A. (2013). Targeting Interleukin-1 in Heart Disease. Circulation, 128(17), 1910-1923. https://doi.org/10.1161/CIRCULATIONAHA.113.003199

VanGuilder, H.D., Bixler, G.V., Brucklacher, R.M., Farley, J.A., Yan, H., Warrington, J.P., Sonntag, W.E., & Freeman, W.M. (2011). Concurrent hippocampal induction of MHC II pathway components and glial activation with advanced aging is not correlated with cognitive impairment, Journal of Neuroinflammation, 8, 138. https://doi.org/10.1186/1742-2094-8-138.

Vanlandewijck, M., He, L., Mäe, M. A., Andrae, J., Ando, K., Del Gaudio, F., Nahar, K., Lebouvier, T., Laviña, B., Gouveia, L., Sun, Y., Raschperger, E., Räsänen, M., Zarb, Y., Mochizuki, N., Keller, A., Lendahl, U., & Betsholtz, C. (2018). A molecular atlas of cell types and zonation in the brain vasculature. Nature, 554(7693), 475–480. https://doi.org/10.1038/nature25739

Varatharaj, A., & Galea, I. (2017). The blood-brain barrier in systemic inflammation. Brain, Behavior, and Immunity, 60, 1–12. https://doi.org/10.1016/J.BBI.2016.03.010

Varatharaj, A., Liljeroth, M., Darekar, A., Larsson, H. B. W., Galea, I., & Cramer, S. P. (2019). Blood–brain barrier permeability measured using dynamic contrast-enhanced magnetic resonance imaging: a validation study. Journal of Physiology, 597(3), 699–709. https://doi.org/10.1113/JP276887

Veksler, R., Shelef, I., & Friedman, A. (2014). Blood-Brain Barrier Imaging in Human Neuropathologies. In Archives of Medical Research, 45(8), 646-652. https://doi.org/10.1016/j.arcmed.2014.11.016

Venugopal, J., Wang, J., Mawri, J., Guo, C., & Eitzman, D. T. (2021). Interleukin-1 receptor inhibition reduces stroke size in a murine model of sickle cell disease. Haematologica, 106(9), 2469–2477. https://doi.org/10.3324/HAEMATOL.2020.252395

Verheggen, I. C. M., de Jong, J. J. A., van Boxtel, M. P. J., Gronenschild, E. H. B. M., Palm, W. M., Postma, A. A., Jansen, J. F. A., Verhey, F. R. J., & Backes, W. H. (2020). Increase in blood–brain barrier leakage in healthy, older adults. GeroScience, 42(4), 1183–1193. https://doi.org/10.1007/s11357-020-00211-2

Verheggen, I. C. M., de Jong, J. J. A., van Boxtel, M. P. J., Postma, A. A., Jansen, J. F. A., Verhey, F. R. J., & Backes, W. H. (2020). Imaging the role of blood–brain barrier disruption in normal cognitive ageing. GeroScience, 42(6), 1751–1764. https://doi.org/10.1007/s11357-020-00282-1

Verkerke, M., Hol, E.M. and Middeldorp, J. (2021). Physiological and Pathological Ageing of Astrocytes in the Human Brain, Neurochemical Research, 46(10), 2662-2675. https://doi.org/10.1007/s11064-021-03256-7

Verscheijden, L. F. M., Koenderink, J. B., de Wildt, S. N., & Russel, F. G. M. (2021). Differences in P-glycoprotein activity in human and rodent blood–brain barrier assessed by mechanistic modelling. *Archives of Toxicology,* 95(9):3015-3029. https://doi.org/10.1007/S00204-021-03115-Y

Versele, R., Sevin, E., Gosselet, F., Fenart, L., & Candela, P. (2022). TNF-α and IL-1β Modulate Blood-Brain Barrier Permeability and Decrease Amyloid-β Peptide Efflux in a Human Blood-Brain Barrier Model. International Journal of Molecular Sciences, 23(18), 10235. https://doi.org/10.3390/IJMS231810235

Veszelka, S., Pásztói, M., Farkas, A. E., Krizbai, I., Dung, N. T. K., Niwa, M., Ábrahám, C. S., & Deli, M. A. (2007). Pentosan polysulfate protects brain endothelial cells against bacterial lipopolysaccharide-induced damages. Neurochemistry International, 50(1), 219–228. https://doi.org/10.1016/J.NEUINT.2006.08.006

Viggars, A. P., Wharton, S. B., Simpson, J. E., Matthews, F. E., Brayne, C., Savva, G. M., Garwood, C., Drew, D., Shaw, P. J., & Ince, P. G. (2011). Alterations in the blood brain barrier in ageing cerebral cortex in relationship to Alzheimer-type pathology: A study in the MRC-CFAS population neuropathology cohort. Neuroscience Letters, 505(1), 25–30. https://doi.org/10.1016/j.neulet.2011.09.049

Villaseñor, R., & Collin, L. (2017). High-resolution Confocal Imaging of the Blood-brain Barrier: Imaging, 3D Reconstruction, and Quantification of Transcytosis. Journal of Visualized Experiments : *JoVE*, *2017*(129), 56407. https://doi.org/10.3791/56407

Vizuete, A. F. K., Fróes, F., Seady, M., Zanotto, C., Bobermin, L. D., Roginski, A. C., Wajner, M., Quincozes-Santos, A., & Gonçalves, C. A. (2022). Early effects of LPS-induced neuroinflammation on the rat hippocampal glycolytic pathway. Journal of Neuroinflammation, 19(1), 255. https://doi.org/10.1186/S12974-022-02612-W

Vutukuri, R., Brunkhorst, R., Kestner, R. I., Hansen, L., Bouzas, N. F., Pfeilschifter, J., Devraj, K., & Pfeilschifter, W. (2018). Alteration of sphingolipid metabolism as a putative mechanism underlying LPS-induced BBB disruption. Journal of Neurochemistry, 144(2), 172–185. https://doi.org/10.1111/JNC.14236

Waller, R., Baxter, L., Fillingham, D.J., Coelho, S., Pozo, J.M., Mozumder, M., Frangi, A.F., Ince, P.G., Simpson, J.E., & Highley, J.R. (2019). Iba-1-/CD68+ microglia are a prominent feature of age-associated deep subcortical white matter lesions, PLoS ONE, 14(1), e0210888. https://doi.org/10.1371/JOURNAL.PONE.0210888.

Waller, R., Woodroofe, M. N., Wharton, S. B., Ince, P. G., Francese, S., Heath, P. R., Cudzich-Madry, A., Thomas, R. H., Rounding, N., Sharrack, B., & Simpson, J. E. (2016). Gene expression profiling of the astrocyte transcriptome in multiple sclerosis normal appearing white matter reveals a neuroprotective role. Journal of Neuroimmunology, 299, 139–146. https://doi.org/10.1016/j.jneuroim.2016.09.010

Walther, K., Bendlin, B. B., Glisky, E. L., Trouard, T. P., Lisse, J. R., Posever, J. O., & Ryan, L. (2011). Anti-inflammatory drugs reduce age-related decreases in brain volume in cognitively normal older adults. Neurobiology of Aging, 32(3), 497–505. https://doi.org/10.1016/J.NEUROBIOLAGING.2009.03.006

Wang, C., Iashchishyn, I. A., Pansieri, J., Nyström, S., Klementieva, O., Kara, J., Horvath, I., Moskalenko, R., Rofougaran, R., Gouras, G., Kovacs, G. G., Shankar, S. K., & Morozova-Roche, L. A. (2018). S100A9-Driven Amyloid-Neuroinflammatory Cascade in Traumatic

Brain Injury as a Precursor State for Alzheimer's Disease. Scientific Reports, 8(1), 1–16. https://doi.org/10.1038/s41598-018-31141-x

Wang, H. M., Huang, P., Li, Q., Yan, L. L., Sun, K., Yan, L., Pan, C. S., Wei, X. H., Liu, Y. Y., Hu, B. H., Wang, C. S., Fan, J. Y., & Han, J. Y. (2019). Post-treatment With Qing-Ying-Tang, a Compound Chinese Medicine Relives Lipopolysaccharide-Induced Cerebral Microcirculation Disturbance in Mice. Frontiers in Physiology, 10, 472387. https://doi.org/10.3389/FPHYS.2019.01320/BIBTEX

Wang, H., Xu, Z., Xia, Z., Rallo, M., Duffy, A., & Matise, M. P. (2021). Inactivation of Hedgehog signal transduction in adult astrocytes results in region-specific blood–brain barrier defects. Proceedings of the National Academy of Sciences of the United States of America, 118(34), e2017779118. https://doi.org/10.1073/PNAS.2017779118/SUPPL_FILE/PNAS.2017779118.SAPP.PDF

Wang, J., Li, W., Zhou, F., Feng, R., Wang, F., Zhang, S., Li, J., Li, Q., Wang, Y., Xie, J., & Wen, T. (2019). ATP11B deficiency leads to impairment of hippocampal synaptic plasticity. Journal of Molecular Cell Biology, 11(8), 688-702. https://doi.org/10.1093/JMCB/MJZ042

Wang, Q., Du, F., Qian, Z. M., Xiao, H. G., Zhu, L., Wing, H. Y., Yang, L., & Ke, Y. (2008). Lipopolysaccharide Induces a Significant Increase in Expression of Iron Regulatory Hormone Hepcidin in the Cortex and Substantia Nigra in Rat Brain. Endocrinology, 149(8), 3920-3925. https://doi.org/10.1210/EN.2007-1626

Wang, X. Y., Hurme, M., Jylh, M., & Hervonen, A. (2001). Lack of association between human longevity and polymorphisms of IL-1 cluster, IL-6, IL-10 and TNF-α genes in Finnish nonagenarians. Mechanisms of Ageing and Development, 123(1), 29–38. https://doi.org/10.1016/S0047-6374(01)00338-4

Wang, X., Xue, G. X., Liu, W. C., Shu, H., Wang, M., Sun, Y., Liu, X., Sun, Y. E., Liu, C. F., Liu, J., Liu, W., & Jin, X. (2017). Melatonin alleviates lipopolysaccharide-compromised integrity of blood-brain barrier through activating AMP-activated protein kinase in old mice. Aging Cell, 16(2), 414–421. https://doi.org/10.1111/ACEL.12572

Wang, Y., Jin, S., Sonobe, Y., Cheng, Y., Horiuchi, H., Parajuli, B., Kawanokuchi, J., Mizuno, T., Takeuchi, H., & Suzumura, A. (2014). Interleukin-1β Induces Blood–Brain Barrier Disruption by Downregulating Sonic Hedgehog in Astrocytes, PLoS ONE, 9(10), 110024. https://doi.org/10.1371/JOURNAL.PONE.0110024

Wang, Y., Du, W., Sun, Y., Zhang, J., Ma, C., & Jin, X. (2023). CRTC1 is a potential target to delay aging-induced cognitive deficit by protecting the integrity of the blood-brain barrier via inhibiting inflammation. Journal of Cerebral Blood Flow & Metabolism, 43(7), 1042. https://doi.org/10.1177/0271678X231169133

Wang, Y., Jin, S., Sonobe, Y., Cheng, Y., Horiuchi, H., Parajuli, B., Kawanokuchi, J., Mizuno, T., Takeuchi, H., & Suzumura, A. (2014). Interleukin-1β Induces Blood–Brain Barrier Disruption by Downregulating Sonic Hedgehog in Astrocytes. PLoS ONE, 9(10), 110024. https://doi.org/10.1371/JOURNAL.PONE.0110024

Wang, Y., Ni, J., Zhai, L., Gao, C., Xie, L., Zhao, L., & Yin, X. (2019). Inhibition of activated astrocyte ameliorates lipopolysaccharide- induced depressive-like behaviours. Journal of Affective Disorders, 242, 52–59. https://doi.org/10.1016/J.JAD.2018.08.015

Wang, Y., Wang, N., Cai, B., Wang, G. Y., Li, J., & Piao, X. X. (2015). In vitro model of the blood-brain barrier established by co-culture of primary cerebral microvascular endothelial and astrocyte cells. Neural Regeneration Research, 10(12), 2011–2017. https://doi.org/10.4103/1673-5374.172320

Wang, Z. M., Liu, C., Wang, Y. Y., Deng, Y. Sen, He, X. C., Du, H. Z., Liu, C. M., & Teng, Z. Q. (2020). SerpinA3N deficiency deteriorates impairments of learning and memory in mice following hippocampal stab injury. Cell Death Discovery, 6(1), 1–11. https://doi.org/10.1038/s41420-020-00325-8

Weiss, N., Miller, F., Cazaubon, S., & Couraud, P. O. (2009). The blood-brain barrier in brain homeostasis and neurological diseases. Biochimica et Biophysica Acta (BBA) - Biomembranes, 1788(4), 842–857. https://doi.org/10.1016/J.BBAMEM.2008.10.022

Weksler, B., Romero, I. A., & Couraud, P. O. (2013). The hCMEC/D3 cell line as a model of the human blood brain barrier. In Fluids and Barriers of the CNS, 10(1), 16. https://doi.org/10.1186/2045-8118-10-16

Wilkinson, M. J., Selman, C., Mclaughlin, L., Horan, L., Hamilton, L., Gilbert, C., Chadwick, C., & Flynn, N. (2020). Progressing the care, husbandry and management of ageing mice used in scientific studies. Laboratory Animals, 54(3), 225–238. https://doi.org/10.1177/0023677219865291

Williams-Medina, A., Deblock, M., & Janigro, D. (2021). In vitro Models of the Blood–Brain Barrier: Tools in Translational Medicine. Frontiers in Medical Technology, 2, 623950. https://doi.org/10.3389/fmedt.2020.623950

Wilson, A.C., Clemente, L., Liu, T., Bowen, R.L., Meethal, S.V., & Atwood, C.S. (2008) 'Reproductive hormones regulate the selective permeability of the blood-brain barrier', Biochimica et biophysica acta, 1782(6), 401–407. https://doi.org/10.1016/J.BBADIS.2008.02.011

Wimmer, I., Tröscher, A. R., Brunner, F., Rubino, S. J., Bien, C. G., Weiner, H. L., Lassmann, H., & Bauer, J. (2018). Systematic evaluation of RNA quality, microarray data reliability and pathway analysis in fresh, fresh frozen and formalin-fixed paraffin-embedded tissue samples. Scientific Reports, 8(1), 1–17. https://doi.org/10.1038/s41598-018-24781-6

Wimmer, M.E., Hernandez, P.J., Blackwell, J., Abel, T. (2012). Aging impairs hippocampus-dependent long-term memory for object location in mice, Neurobiology of Aging, 33(9), 2220-2224. https://doi.org/10.1016/J.NEUROBIOLAGING.2011.07.007

Windener, F., Grewing, L., Thomas, C., Dorion, M. F., Otteken, M., Kular, L., Jagodic, M., Antel, J., Albrecht, S., & Kuhlmann, T. (2024). Physiological aging and inflammation-induced cellular senescence may contribute to oligodendroglial dysfunction in MS. Acta Neuropathologica, 147(1), 1–19. https://doi.org/10.1007/S00401-024-02733-X/FIGURES/5

Winkler, E. A., Bell, R. D., & Zlokovic, B. V. (2011). Central nervous system pericytes in health and disease. In Nature Neuroscience, 14(11), 1398-1405. https://doi.org/10.1038/nn.2946

Witte, A. V., Fobker, M., Gellner, R., Knecht, S., & Flöel, A. (2009). Caloric restriction improves memory in elderly humans. Proceedings of the National Academy of Sciences of the United States of America, 106(4), 1255–1260. https://doi.org/10.1073/PNAS.0808587106/SUPPL_FILE/0808587106SI.PDF

Wolfe, H., Minogue, A. M., Rooney, S., & Lynch, M. A. (2018). Infiltrating macrophages contribute to age-related neuroinflammation in C57/BL6 mice. Mechanisms of Ageing and Development, 173, 84–91. https://doi.org/10.1016/J.MAD.2018.05.003

Wong, D., & Dorovini-Zis, K. (1992). Upregulation of intercellular adhesion molecule-1 (ICAM-1) expression in primary cultures of human brain microvessel endothelial cells by cytokines and lipopolysaccharide. Journal of Neuroimmunology, 39(1–2), 11–21. https://doi.org/10.1016/0165-5728(92)90170-P

Wu, B., Ueno, M., Onodera, M., Kusaka, T., Huang, C., Hosomi, N., Kanenishi, K., & Sakamoto, H. (2010). Age-Related Changes in P-Glycoprotein Expression in Senescence-Accelerated Mouse. Current Aging Sciencee, 2(3), 187–192. https://doi.org/10.2174/1874609810902030187

Wu, D. mei, Liu, J. ping, Liu, J., Ge, W. hong, Wu, S. zhen, Zeng, C. jia, Liang, J., Liu, K. J., Lin, Q., Hong, X. wu, Sun, Y. E., & Lu, J. (2023). Immune pathway activation in neurons triggers neural damage after stroke. Cell Reports, 42(11), 113368. https://doi.org/10.1016/J.CELREP.2023.113368

Wu, F., Chen, X., Zhai, L., Wang, H., Sun, M., Song, C., Wang, T., & Qian, Z. (2020). CXCR2 antagonist attenuates neutrophil transmigration into brain in a murine model of LPS induced neuroinflammation. Biochemical and Biophysical Research Communications, 529(3), 839–845. https://doi.org/10.1016/J.BBRC.2020.05.124

Wynne, A. M., Henry, C. J., Huang, Y., Cleland, A., & Godbout, J. P. (2010). Protracted downregulation of CX3CR1 on microglia of aged mice after lipopolysaccharide challenge. Brain, Behavior, and Immunity, 24(7), 1190–1201. https://doi.org/10.1016/J.BBI.2010.05.011

Xia, Y. peng, He, Q. wei, Li, Y. nan, Chen, S. cai, Huang, M., Wang, Y., Gao, Y., Huang, Y., Wang, M. die, Mao, L., & Hu, B. (2013a). Recombinant Human Sonic Hedgehog Protein Regulates the Expression of ZO-1 and Occludin by Activating Angiopoietin-1 in Stroke Damage. PLoS ONE, 8(7), 68891. https://doi.org/10.1371/JOURNAL.PONE.0068891

Xia, Y. Y., Song, S. W., Min, Y., Zhong, Y., Sheng, Y. C., Li, R. P., & Liu, Q. H. (2014). The Effects of Anakinra on Focal Cerebral Ischemic Injury in Rats. CNS Neuroscience & Therapeutics, 20(9), 879-881. https://doi.org/10.1111/CNS.12310

Xiang, P., Chew, W. S., Seow, W. L., Lam, B. W. S., Ong, W. Y., & Herr, D. R. (2021). The S1P2 receptor regulates blood-brain barrier integrity and leukocyte extravasation with implications for neurodegenerative disease. Neurochemistry International, 146, 105018. https://doi.org/10.1016/J.NEUINT.2021.105018

Xie, X., Gao, Y., Zeng, M., Wang, Y., Wei, T. F., Lu, Y. B., & Zhang, W. P. (2019). Nicotinamide ribose ameliorates cognitive impairment of aged and Alzheimer's disease model mice. Metabolic Brain Disease, 34(1), 353–366. https://doi.org/10.1007/S11011-018-0346-8

Ximerakis, M., Lipnick, S. L., Innes, B. T., Simmons, S. K., Adiconis, X., Dionne, D., Mayweather, B. A., Nguyen, L., Niziolek, Z., Ozek, C., Butty, V. L., Isserlin, R., Buchanan, S. M., Levine, S. S., Regev, A., Bader, G. D., Levin, J. Z., & Rubin, L. L. (2019). Single-cell transcriptomic profiling of the aging mouse brain. Nature Neuroscience, 22(10), 1696–1708. https://doi.org/10.1038/s41593-019-0491-3

Xing, G., Zhao, T., Zhang, X., Li, H., Li, X., Cui, P., Li, M., Li, D., Zhang, N., & Jiang, W. (2020). Astrocytic Sonic Hedgehog Alleviates Intracerebral Hemorrhagic Brain Injury via Modulation of Blood-Brain Barrier Integrity. Frontiers in Cellular Neuroscience, 14, 364. https://doi.org/10.3389/FNCEL.2020.575690/BIBTEX

Xingi, E., Koutsoudaki, P. N., Thanou, I., Phan, M. S., Margariti, M., Scheller, A., Tinevez, J. Y., Kirchhoff, F., & Thomaidou, D. (2023). LPS-Induced Systemic Inflammation Affects the Dynamic Interactions of Astrocytes and Microglia with the Vasculature of the Mouse Brain Cortex. Cells, 12(10), 1418. https://doi.org/10.3390/CELLS12101418

Xu, T., Liu, C., Deng, S., Gan, L., Zhang, Z., Yang, G. Y., Tian, H., & Tang, Y. (2023). The roles of microglia and astrocytes in myelin phagocytosis in the central nervous system. Journal of Cerebral Blood Flow & Metabolism, 43(3), 325-340. https://doi.org/10.1177/0271678X221137762

Xu, Y. Z., Nygård, M., Kristensson, K., & Bentivoglio, M. (2010). Regulation of cytokine signaling and T-cell recruitment in the aging mouse brain in response to central inflammatory challenge. Brain, Behavior, and Immunity, 24(1), 138–152. https://doi.org/10.1016/J.BBI.2009.09.006

Xu, Y., Jia, B., Li, J., Li, Q., & Luo, C. (2024b). The Interplay between Ferroptosis and Neuroinflammation in Central Neurological Disorders. Antioxidants, 13(4), 395. https://doi.org/10.3390/ANTIOX13040395

Yadav, S., Gandham, S. K., Panicucci, R., & Amiji, M. M. (2016). Intranasal Brain Delivery of Cationic Nanoemulsion-Encapsulated TNFα siRNA in Prevention of Experimental Neuroinflammation. Nanomedicine : Nanotechnology, Biology, and Medicine, 12(4), 987. https://doi.org/10.1016/J.NANO.2015.12.374

Yamazaki, Y., Baker, D. J., Tachibana, M., Liu, C. C., Van Deursen, J. M., Brott, T. G., Bu, G., & Kanekiyo, T. (2016). Vascular cell senescence contributes to blood-brain barrier breakdown. Stroke, 47(4), 1068–1077. https://doi.org/10.1161/STROKEAHA.115.010835

Yan, P., Xue, Z., Li, D., Ni, S., Wang, C., Jin, X., Zhou, D., Li, X., Zhao, X., Chen, X., Cui, W., Xu, D., Zhou, W., & Zhang, J. (2021). Dysregulated CRTC1-BDNF signaling pathway in the hippocampus contributes to Aβ oligomer-induced long-term synaptic plasticity and memory impairment. Experimental Neurology, 345, 113812. https://doi.org/10.1016/J.EXPNEUROL.2021.113812

Yan, Z., Cai, M., Han, X., Chen, Q., & Lu, H. (2023). The Interaction Between Age and Risk Factors for Diabetes and Prediabetes: A Community-Based Cross-Sectional Study. Diabetes, Metabolic Syndrome and Obesity, 16, 85-93. https://doi.org/10.2147/DMSO.S390857

Yanai, S. and Endo, S. (2021). Functional Aging in Male C57BL/6J Mice Across the Life-Span: A Systematic Behavioral Analysis of Motor, Emotional, and Memory Function to Define an Aging Phenotype. Frontiers in Aging Neuroscience, 13, 697621. https://doi.org/10.3389/FNAGI.2021.697621/BIBTEX

Yang, A. C., Stevens, M. Y., Chen, M. B., Lee, D. P., Stähli, D., Gate, D., Contrepois, K., Chen, W., Iram, T., Zhang, L., Vest, R. T., Chaney, A., Lehallier, B., Olsson, N., du Bois, H., Hsieh, R., Cropper, H. C., Berdnik, D., Li, L., … Wyss-Coray, T. (2020). Physiological blood–brain transport is impaired with age by a shift in transcytosis. Nature, 583(7816), 425–430. https://doi.org/10.1038/s41586-020-2453-z

Yang, I., Han, S. J., Kaur, G., Crane, C., & Parsa, A. T. (2010). The Role of Microglia in Central Nervous System Immunity and Glioma Immunology. Journal of Clinical Neuroscience : Official Journal of the Neurosurgical Society of Australasia, 17(1), 6-10. https://doi.org/10.1016/J.JOCN.2009.05.006

Yang, J., Ran, M., Li, H., Lin, Y., Ma, K., Yang, Y., Fu, X., & Yang, S. (2022). New insight into neurological degeneration: Inflammatory cytokines and blood–brain barrier. Frontiers in Molecular Neuroscience, 15, 1013933. https://doi.org/10.3389/FNMOL.2022.1013933/BIBTEX

Yang, K., Yang, X., Jin, C., Ding, S., Liu, T., Ma, B., Sun, H., Zhang, J., & Li, Y. (2024). Global burden of type 1 diabetes in adults aged 65 years and older, 1990-2019: population based study. British Medical Journal, 385, e078432. https://doi.org/10.1136/BMJ-2023-078432

Yang, M., Jin, L., Wu, Z., Xie, Y., Zhang, P., Wang, Q., Yan, S., Chen, B., Liang, H., Naman, C. B., Zhang, J., He, S., Yan, X., Zhao, L., & Cui, W. (2021). PLGA-PEG Nanoparticles Facilitate in Vivo Anti-Alzheimer's Effects of Fucoxanthin, a Marine Carotenoid Derived from Edible Brown Algae. Journal of Agricultural and Food Chemistry, 69(34), 9764–9777. https://doi.org/10.1021/ACS.JAFC.1C00569/ASSET/IMAGES/LARGE/JF1C00569_0008.JPEG

Yang, T., Roder, K. E., & Abbruscato, T. J. (2007). Evaluation of bEnd5 cell line as an in vitro model for the blood-brain barrier under normal and hypoxic/aglycemic conditions. Journal of Pharmaceutical Sciences, 96(12), 3196–3213. https://doi.org/10.1002/jps.21002

Yang, W., Zhou, X. and Ma, T. (2019). Memory Decline and Behavioral Inflexibility in Aged Mice Are Correlated With Dysregulation of Protein Synthesis Capacity, Frontiers in Aging Neuroscience, 11, 246. https://doi.org/10.3389/FNAGI.2019.00246/FULL.

Yang, X., Li, X., Liu, L., Chen, Y. H., You, Y., Gao, Y., Liu, Y. Y., Yang, L., Tong, K., Chen, D. S., Hao, J. R., Sun, N., Zhao, Z. M., & Gao, C. (2021). Transferrin-Pep63-liposomes accelerate the clearance of Aβ and rescue impaired synaptic plasticity in early Alzheimer's disease models. Cell Death Discovery, 7(1), 256. https://doi.org/10.1038/S41420-021-00639-1

Yang, Y., Vidensky, S., Jin, L., Jie, C., Lorenzini, I., Frankl, M., & Rothstein, J. D. (2011). Molecular comparison of GLT1+ and ALDH1L1+ astrocytes in vivo in astroglial reporter mice. Glia, 59(2), 200–207. https://doi.org/10.1002/glia.21089

Yao, M., Wei, Z., Nielsen, J. S., Kakazu, A., Ouyang, Y., Li, R., Chu, T., Scafidi, S., Lu, H., Aggarwal, M., & Duan, W. (2024). Senolytic therapy preserves blood-brain barrier integrity and promotes microglia homeostasis in a tauopathy model. BioRxiv, 2024.03.25.586662. https://doi.org/10.1101/2024.03.25.586662

Ye, S. M., & Johnson, R. W. (1999). Increased interleukin-6 expression by microglia from brain of aged mice. Journal of Neuroimmunology, 93(1–2), 139–148. https://doi.org/10.1016/S0165-5728(98)00217-3

Ye, Z., Gastfriend, B. D., Umlauf, B. J., Lynn, D. M., & Shusta, E. V. (2022). Antibody-targeted liposomes for enhanced targeting of the blood-brain barrier. Pharmaceutical Research, 39(7), 1523-1534. https://doi.org/10.1007/S11095-022-03186-1

Yegla, B., Boles, J., Kumar, A., & Foster, T.C. (2021). Partial microglial depletion is associated with impaired hippocampal synaptic and cognitive function in young and aged rats. Glia, 69(6), 1494-1514. https://doi.org/10.1002/GLIA.23975

Yeon, J. H., Na, D., Choi, K., Ryu, S. W., Choi, C., & Park, J. K. (2012). Reliable permeability assay system in a microfluidic device mimicking cerebral vasculatures. Biomedical Microdevices, 14(6), 1141–1148. https://doi.org/10.1007/s10544-012-9680-5

You, L. H., Yan, C. Z., Zheng, B. J., Ci, Y. Z., Chang, S. Y., Yu, P., Gao, G. F., Li, H. Y., Dong, T. Y., & Chang, Y. Z. (2017). Astrocyte hepcidin is a key factor in LPS-induced neuronal apoptosis. Cell Death & Disease, 8(3), e2676–e2676. https://doi.org/10.1038/cddis.2017.93

Yousef, H., Czupalla, C.J., Lee, D., Chen, M.B., Burke, A.N., Zera, K.A., Zandstra, J., Berber, E., Lehallier, B., Mathur, V., Nair, R.V., Bonanno, L.N., Yang, A.C., Peterson, T., Hadeiba, H., Merkel, T., Körbelin. J., Schwaninger, M., Buckwalter, M.S., Quake, S.R., Butcher, E.C., & Wyss-Coray, T. (2019). Aged blood impairs hippocampal neural precursor activity and activates microglia via brain endothelial cell VCAM1, Nature Medicine, 25(6), 988–1000. https://doi.org/10.1038/s41591-019-0440-4

Yuan, H., Sun, D., Ji, Y., Meng, B., Lu, B., Liu, R., Xing, X., Wang, R., & Chen, J. (2023). Pericyte loss impairs the blood–brain barrier and cognitive function in aged mice after anesthesia/surgery. Brain Research Bulletin, 204, 110799. https://doi.org/10.1016/J.BRAINRESBULL.2023.110799

Yuan, R., Peters, L. L., & Paigen, B. (2011). Mice as a mammalian model for research on the genetics of aging. In ILAR Journal, 52(1), 4-15. https://doi.org/10.1093/ilar.52.1.4

Zakharova, M. V., Dyomina, A. V., Kovalenko, A. A., Zubareva, O. E., Ischenko, A. M., & Zaitsev, A. V. (2024). Anakinra Promotes M2 Microglia Activation during the Latent Phase of the Lithium-Pilocarpine Model of Temporal Lobe Epilepsy. Journal of Evolutionary Biochemistry and Physiology, 60(2), 672–689. https://doi.org/10.1134/S0022093024020182

Zemse, S. M., Chiao, C. W., Hilgers, R. H. P., & Webb, R. C. (2010). Interleukin-10 inhibits the in vivo and in vitro adverse effects of TNF-α on the endothelium of murine aorta. American Journal of Physiology - Heart and Circulatory Physiology, 299(4), H1160-H1167. https://doi.org/10.1152/AJPHEART.00763.2009

Zeng, J., Zhào, H., Liu, Z., Zhang, W., & Huang, Y. (2018). Lipopolysaccharide Induces Subacute Cerebral Microhemorrhages with Involvement of Nitric Oxide Synthase in Rats. Journal of Stroke and Cerebrovascular Diseases, 27(7), 1905–1913. https://doi.org/10.1016/J.JSTROKECEREBROVASDIS.2018.02.044

Zeng, J., Zhào, H., Liu, Z., Zhang, W., & Huang, Y. (2018). Lipopolysaccharide Induces Subacute Cerebral Microhemorrhages with Involvement of Nitric Oxide Synthase in Rats. Journal of Stroke and Cerebrovascular Diseases, 27(7), 1905–1913. https://doi.org/10.1016/J.JSTROKECEREBROVASDIS.2018.02.044

Zeppenfeld, D. M., Simon, M., Haswell, J. D., D'Abreo, D., Murchison, C., Quinn, J. F., Grafe, M. R., Woltjer, R. L., Kaye, J., & Iliff, J. J. (2017). Association of Perivascular Localization of Aquaporin-4 With Cognition and Alzheimer Disease in Aging Brains. JAMA Neurology, 74(1), 91-99. https://doi.org/10.1001/jamaneurol.2016.4370

Zhang, D. D., Jin, C., Zhang, Y. T., Gan, X. D., Zou, M. J., Wang, Y. Y., Fu, W. L., Xu, T., Xing, W. W., Xia, W. R., & Xu, D. G. (2018). A novel IL-1RA-PEP fusion protein alleviates blood-brain barrier disruption after ischemia-reperfusion in male rats. Journal of Neuroinflammation, 15(1), 16. https://doi.org/10.1186/S12974-018-1058-Z

Zhang, F., Nance, E., Zhang, Z., Jasty, V., Kambhampati, S. P., Mishra, M. K., Burd, I., Romero, R., Kannan, S., & Kannan, R. M. (2016). Surface functionality affects the biodistribution and microglia-targeting of intra-amniotically delivered dendrimers. Journal of Controlled Release : Official Journal of the Controlled Release Society, 237, 61-70. https://doi.org/10.1016/J.JCONREL.2016.06.046

Zhang, H. (2017). Thin-Film Hydration Followed by Extrusion Method for Liposome Preparation. Methods in Molecular Biology, 1522, 17–22. https://doi.org/10.1007/978-1-4939-6591-5_2

Zhang, H., Shang, J., Li, W., Gao, D., & Zhang, J. (2024). Increased Expression of VCAM1 on Brain Endothelial Cells Drives Blood-Brain Barrier Impairment Following Chronic Cerebral Hypoperfusion. American Chemical Society Chemical Neuroscience, 15(10), 2028–2041. https://doi.org/10.1021/ACSCHEMNEURO.4C00039/ASSET/IMAGES/LARGE/CN4C00039_0006.JPEG

Zhang, J., Liu, H., Du, X., Guo, Y., Chen, X., Wang, S., Fang, J., Cao, P., Zhang, B., Liu, Z., & Zhang, W. (2017). Increasing of blood-brain tumor barrier permeability through transcellular and paracellular pathways by microbubble-enhanced diagnostic ultrasound in a C6 glioma model. Frontiers in Neuroscience, 11(FEB), 86. https://doi.org/10.3389/fnins.2017.00086

Zhang, J., Sadowska, G. B., Chen, X., Park, S. Y., Kim, J. E., Bodge, C. A., Cummings, E., Lim, Y. P., Makeyev, O., Besio, W. G., Gaitanis, J., Banks, W. A., & Stonestreet, B. S. (2015). Anti-IL-6 neutralizing antibody modulates blood-brain barrier function in the ovine fetus. FASEB Journal : Official Publication of the Federation of American Societies for Experimental Biology, 29(5), 1739–1753. https://doi.org/10.1096/FJ.14-258822

Zhang, W., Liu, Q. Y., Haqqani, A. S., Leclerc, S., Liu, Z., Fauteux, F., Baumann, E., Delaney, C. E., Ly, D., Star, A. T., Brunette, E., Sodja, C., Hewitt, M., Sandhu, J. K., & Stanimirovic, D. B. (2020). Differential expression of receptors mediating receptor-mediated transcytosis (RMT) in brain microvessels, brain parenchyma and peripheral tissues of the mouse and the human. Fluids and Barriers of the CNS, *17*(1), 47. https://doi.org/10.1186/S12987-020-00209-0

Zhang, X., Li, Y., & Hu, Y. (2020). Green synthesis of silver nanoparticles and their preventive effect in deficits in recognition and spatial memory in sporadic Alzheimer's rat model. Colloids and Surfaces A: Physicochemical and Engineering Aspects, 605, 125288. https://doi.org/10.1016/J.COLSURFA.2020.125288

Zhang, Y., Sloan, S. A., Clarke, L. E., Caneda, C., Plaza, C. A., Blumenthal, P. D., Vogel, H., Steinberg, G. K., Edwards, M. S. B., Li, G., Duncan, J. A., Cheshier, S. H., Shuer, L. M., Chang, E. F., Grant, G. A., Gephart, M. G. H., & Barres, B. A. (2016). Purification and Characterization of Progenitor and Mature Human Astrocytes Reveals Transcriptional and Functional Differences with Mouse. Neuron, 89(1), 37–53. https://doi.org/10.1016/j.neuron.2015.11.013

Zhang, Z., Ma, Z., Zou, W., Guo, H., Liu, M., Ma, Y., & Zhang, L. (2019). The Appropriate Marker for Astrocytes: Comparing the Distribution and Expression of Three Astrocytic Markers in Different Mouse Cerebral Regions. BioMed Research International, 2019, 1–15. https://doi.org/10.1155/2019/9605265

Zhao, J., Bi, W., Xiao, S., Lan, X., Cheng, X., Zhang, J., Lu, D., Wei, W., Wang, Y., Li, H., Fu, Y., & Zhu, L. (2019). Neuroinflammation induced by lipopolysaccharide causes cognitive

impairment in mice. Scientific Reports 2019 9:1, 9(1), 1–12. https://doi.org/10.1038/s41598-019-42286-8

Zhao, L., Li, Z., Vong, J. S. L., Chen, X., Lai, H. M., Yan, L. Y. C., Huang, J., Sy, S. K. H., Tian, X., Huang, Y., Chan, H. Y. E., So, H. C., Ng, W. L., Tang, Y., Lin, W. J., Mok, V. C. T., & Ko, H. (2020). Pharmacologically reversible zonation-dependent endothelial cell transcriptomic changes with neurodegenerative disease associations in the aged brain. Nature Communications, 11(1), 4413. https://doi.org/10.1038/s41467-020-18249-3

Zhao, X., Li, J., & Sun, H. (2019). CD200-CD200R interaction: An important regulator after stroke. Frontiers in Neuroscience, 13(JUL), 468717. https://doi.org/10.3389/FNINS.2019.00840/BIBTEX

Zhao, Y., Ma, C., Chen, C., Li, S., Wang, Y., Yang, T., Stetler, R. A., Bennett, M. V. L., Dixon, C. E., Chen, J., & Shi, Y. (2022). STAT1 Contributes to Microglial/Macrophage Inflammation and Neurological Dysfunction in a Mouse Model of Traumatic Brain Injury. The Journal of Neuroscience, 42(39), 7466-7481. https://doi.org/10.1523/JNEUROSCI.0682-22.2022

Zhong, H., Lin, H., Pang, Q., Zhuang, J., Liu, X., Li, X., Liu, J., & Tang, J. (2021). Macrophage ICAM-1 functions as a regulator of phagocytosis in LPS induced endotoxemia. Inflammation Research, 70(2), 193-203. https://doi.org/10.1007/S00011-021-01437-2

Zhou, S., Du, X., Xie, J., & Wang, J. (2017). Interleukin-6 regulates iron-related proteins through c-Jun N-terminal kinase activation in BV2 microglial cell lines. PLoS ONE, 12(7), e0180464. https://doi.org/10.1371/JOURNAL.PONE.0180464

Zhu, J., Li, X., Yin, J., Hu, Y., Gu, Y., & Pan, S. (2018). Glycocalyx degradation leads to blood-brain barrier dysfunction and brain edema after asphyxia cardiac arrest in rats. Journal of Cerebral Blood Flow and Metabolism : Official Journal of the International Society of Cerebral Blood Flow and Metabolism, 38(11), 1979–1992. https://doi.org/10.1177/0271678X17726062

Zhu, J., Li, Z., Ji, Z., Wu, Y., He, Y., Liu, K., Chang, Y., Peng, Y., Lin, Z., Wang, S., Wang, D., Huang, K., & Pan, S. (2022). Glycocalyx is critical for blood-brain barrier integrity by suppressing caveolin1-dependent endothelial transcytosis following ischemic stroke. Brain Pathology, 32(1), e13006. https://doi.org/10.1111/BPA.13006

Zhu, L., Liu, X., Nemeth, D. P., DiSabato, D. J., Witcher, K. G., Mckim, D. B., Oliver, B., Le, X., Gorantla, G., Berdysz, O., Li, J., Ramani, A. D., Chen, Z., Wu, D., Godbout, J. P., & Quan, N. (2019). Interleukin-1 causes CNS inflammatory cytokine expression via endothelia-microglia bi-cellular signaling. Brain, Behavior, and Immunity, 81, 292-304. https://doi.org/10.1016/J.BBI.2019.06.026

Zhu, M., Wang, Y., Park, J., Gong, S., & Guo, F. (2024). Dispensable regulation of brain development and myelination by Serpina3n. BioRxiv (preprint). https://doi.org/10.1101/2024.02.06.579239

Zhu, W., Cao, F. S., Feng, J., Chen, H. W., Wan, J. R., Lu, Q., & Wang, J. (2017). Nlrp3 inflammasome activation contributes to long-term behavioural alterations in mice injected with lipopolysaccharide. Neuroscience, 343, 77-84. https://doi.org/10.1016/J.NEUROSCIENCE.2016.11.037

Zhu, W., London, N. R., Gibson, C. C., Davis, C. T., Tong, Z., Sorensen, L. K., Shi, D. S., Guo, J., Smith, M. C. P., Grossmann, A. H., Thomas, K. R., & Li, D. Y. (2012). Interleukin receptor

activates a MYD88-ARNO-ARF6 cascade to disrupt vascular stability. Nature, 492(7428):252-5. https://doi.org/10.1038/nature11603

Zotova, N., Zhuravleva, Y., Chereshnev, V., & Gusev, E. (2023). Acute and Chronic Systemic Inflammation: Features and Differences in the Pathogenesis, and Integral Criteria for Verification and Differentiation. International Journal of Molecular Sciences, 24(2), 1144. https://doi.org/10.3390/IJMS24021144/S1